ADVANCEMENTS IN METASTATIC BREAST CANCER: PREDICTIVE AND PROGNOSTIC BIOMARKERS, AND MOLECULAR MECHANISMS

EDITED BY: Masakazu Toi and San-Gang Wu
PUBLISHED IN: Frontiers in Oncology

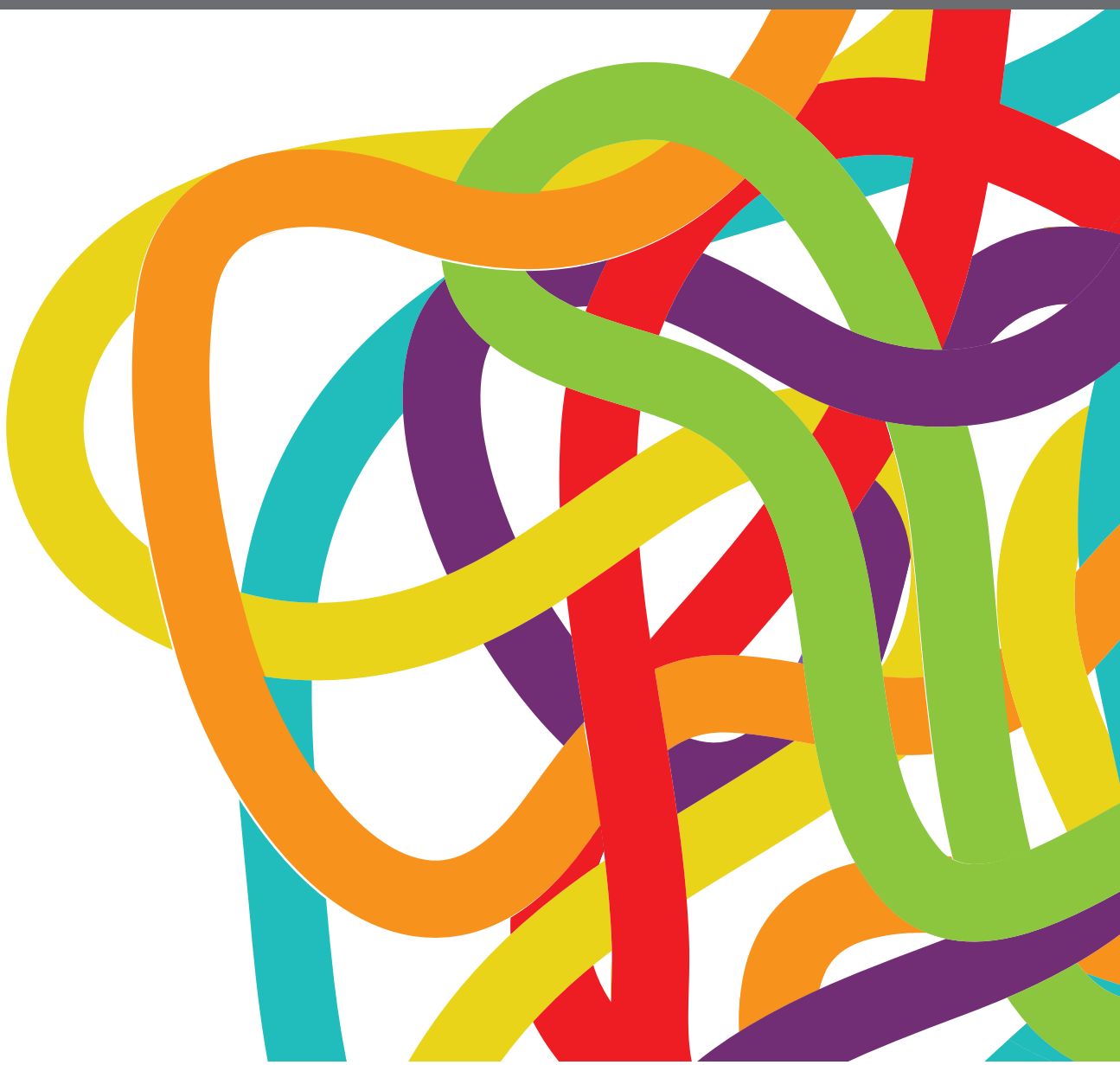

frontiers Research Topics

ISSN 1664-8714
ISBN 978-2-83250-085-9
DOI 10.3389/978-2-83250-085-9

About Frontiers

Frontiers is more than just an open-access publisher of scholarly articles: it is a pioneering approach to the world of academia, radically improving the way scholarly research is managed. The grand vision of Frontiers is a world where all people have an equal opportunity to seek, share and generate knowledge. Frontiers provides immediate and permanent online open access to all its publications, but this alone is not enough to realize our grand goals.

Frontiers Journal Series

The Frontiers Journal Series is a multi-tier and interdisciplinary set of open-access, online journals, promising a paradigm shift from the current review, selection and dissemination processes in academic publishing. All Frontiers journals are driven by researchers for researchers; therefore, they constitute a service to the scholarly community. At the same time, the Frontiers Journal Series operates on a revolutionary invention, the tiered publishing system, initially addressing specific communities of scholars, and gradually climbing up to broader public understanding, thus serving the interests of the lay society, too.

Dedication to Quality

Each Frontiers article is a landmark of the highest quality, thanks to genuinely collaborative interactions between authors and review editors, who include some of the world's best academicians. Research must be certified by peers before entering a stream of knowledge that may eventually reach the public - and shape society; therefore, Frontiers only applies the most rigorous and unbiased reviews.
Frontiers revolutionizes research publishing by freely delivering the most outstanding research, evaluated with no bias from both the academic and social point of view. By applying the most advanced information technologies, Frontiers is catapulting scholarly publishing into a new generation.

What are Frontiers Research Topics?

Frontiers Research Topics are very popular trademarks of the Frontiers Journals Series: they are collections of at least ten articles, all centered on a particular subject. With their unique mix of varied contributions from Original Research to Review Articles, Frontiers Research Topics unify the most influential researchers, the latest key findings and historical advances in a hot research area! Find out more on how to host your own Frontiers Research Topic or contribute to one as an author by contacting the Frontiers Editorial Office: frontiersin.org/about/contact

ADVANCEMENTS IN METASTATIC BREAST CANCER: PREDICTIVE AND PROGNOSTIC BIOMARKERS, AND MOLECULAR MECHANISMS

Topic Editors:
Masakazu Toi, Kyoto University, Japan
San-Gang Wu, First Affiliated Hospital of Xiamen University, China

Citation: Toi, M., Wu, S.-G., eds. (2022). Advancements in Metastatic Breast Cancer: Predictive and Prognostic Biomarkers, and Molecular Mechanisms. Lausanne: Frontiers Media SA. doi: 10.3389/978-2-83250-085-9

Table of Contents

frontiers in Oncology

ORIGINAL RESEARCH
published: 26 April 2021
doi: 10.3389/fonc.2021.665240

Preoperative Nomogram for Predicting Sentinel Lymph Node Metastasis Risk in Breast Cancer: A Potential Application on Omitting Sentinel Lymph Node Biopsy

Xi'E Hu[1], Jingyi Xue[2], Shujia Peng[1], Ping Yang[1], Zhenyu Yang[1], Lin Yang[1], Yanming Dong[1], Lijuan Yuan[1], Ting Wang[3] and Guoqiang Bao[1]**

[1] Department of General Surgery, The Second Affiliated Hospital of Air Force Medical University, Xi'an, China, [2] The Second Clinical Medical College, Shaanxi University of Chinese Medicine, Xianyang, China, [3] Department of Vascular Surgery and Thyroid-Breast Surgery, The First Affiliated Hospital of Air Force Medical University, Xi'an, China

OPEN ACCESS

Edited by:
Masakazu Toi,
Kyoto University, Japan

Reviewed by:
Han-Byoel Lee,
Seoul National University Hospital, South Korea
Kosuke Kawaguchi,
Kyoto University, Japan

***Correspondence:**
Guoqiang Bao
guoqiang@fmmu.edu.cn
Ting Wang
ting_w100@126.com

Specialty section:
This article was submitted to Women's Cancer, a section of the journal Frontiers in Oncology

Received: *07 February 2021*
Accepted: *06 April 2021*
Published: *26 April 2021*

Citation:
Hu X, Xue J, Peng S, Yang P, Yang Z, Yang L, Dong Y, Yuan L, Wang T and Bao G (2021) Preoperative Nomogram for Predicting Sentinel Lymph Node Metastasis Risk in Breast Cancer: A Potential Application on Omitting Sentinel Lymph Node Biopsy. Front. Oncol. 11:665240. doi: 10.3389/fonc.2021.665240

Background: Sentinel lymph node (SLN) biopsy is feasible for breast cancer (BC) patients with clinically negative axillary lymph nodes; however, complications develop in some patients after surgery, although SLN metastasis is rarely found. Previous predictive models contained parameters that relied on postoperative data, thus limiting their application in the preoperative setting. Therefore, it is necessary to find a new model for preoperative risk prediction for SLN metastasis to help clinicians facilitate individualized clinical decisions.

Materials and Methods: BC patients who underwent SLN biopsy in two different institutions were included in the training and validation cohorts. Demographic characteristics, preoperative tumor pathological features, and ultrasound findings were evaluated. Multivariate logistic regression was used to develop the nomogram. The discrimination, accuracy, and clinical usefulness of the nomogram were assessed using Harrell's C-statistic and ROC analysis, the calibration curve, and the decision curve analysis, respectively.

Results: A total of 624 patients who met the inclusion criteria were enrolled, including 444 in the training cohort and 180 in the validation cohort. Young age, high BMI, high Ki67, large tumor size, indistinct tumor margins, calcifications, and an aspect ratio ≥1 were independent predictive factors for SLN metastasis of BC. Incorporating these parameters, the nomogram achieved a robust predictive performance with a C-index and accuracy of 0.92 and 0.85, and 0.82 and 0.80 in the training and validation cohorts, respectively. The calibration curves also fit well, and the decision curve analysis revealed that the nomogram was clinically useful.

Conclusions: We established a nomogram to preoperatively predict the risk of SLN metastasis in BC patients, providing a non-invasive approach in clinical practice and serving as a potential tool to identify BC patients who may omit unnecessary SLN biopsy.

Keywords: breast cancer, nomogram, SLN, metastasis, ultrasound, external validation

INTRODUCTION

Breast cancer (BC) is the most frequently diagnosed malignant tumor among women worldwide. There were approximately 2.1 million new cases of BC worldwide in 2018, and 627 000 mortalities, seriously threatening women's life and health (1). The presence of lymph node (LN) metastasis is one of the most important prognostic factors in BC patients; thus, the intervention on axillary lymph nodes (ALNs) has been the focus in the field of surgical treatment of BC (2). Identified as the first station of LN metastasis in BC, sentinel lymph nodes (SLNs) play a significant role in breast tumor invasion (3). SLN biopsy (SLNB) is a standard method for determining the metastatic status of ALN and assists clinicians in developing individualized treatment regimens. However, SLNB is not a completely benign procedure, as it is invasive and carries a risk of long-term comorbidities, such as sensory neuropathy, lymphedema, motor neuropathy, and pain (4, 5). In addition, it was reported that the SLN metastasis rate was 28.9-42.0% in clinically LN-negative BC patients, indicating that nearly half of these patients do not need SLNB (6). Therefore, an appropriate predictive nomogram is required to distinguish BC patients with a lower risk of SLN metastases from those at higher risk preoperatively to help doctors determine whether their patients could avoid SLNB.

Several previous studies have reported various risk factors associated with LN metastasis of BC, such as histological grade, lymphovascular invasion (LVI), and molecular indexes (7–10); however, whether they are sufficiently accurate to determine SLNB omission remains uncertain. Moreover, these predictive models are based on postoperative histopathological findings, which restrict their potential for non-invasive or preoperative applications. Thus, the development of a nomogram for preoperative use can help clinicians make more individualized clinical decisions.

Ultrasonography is a traditional medical imaging method that plays a significant role in BC detection, image-guided biopsy, and LN diagnosis (11). It has apparent advantages in breast assessments (12). It is a non-invasive diagnostic tool that is convenient, radiation-free, inexpensive, reusable, and has great potential for accurately evaluating the size and location of tumors, delineating the internal structure of LNs, and even diagnosing early metastatic lesions. Therefore, ultrasound imaging could provide a promising approach for predicting SLN metastasis in patients with BC.

Hence, this study aimed to establish a nomogram that combines clinicopathological characteristics and ultrasound findings to predict the SLN-metastasis risk of BC patients in a preoperative setting. We hope to explore a robust tool to help make a more favorable diagnosis of SLN in BC patients and contribute to assisting clinicians in selecting those who have the opportunity to avoid unnecessary SLNB, thereby allowing more individualized treatment for BC patients.

MATERIALS AND METHODS

Patients

Female patients with pathologically confirmed BC, clinically negative LN metastasis, and who underwent SLNB were retrospectively included in this study. The training cohort comprised of BC patients from Xijing Hospital (the First Affiliated Hospital of Air Force Medical University) from January 1st, 2016, to January 1st, 2019 and BC patients from Tangdu Hospital (the Second Affiliated Hospital of Air Force Medical University) between January 1st, 2017, and January 1st, 2018. Clinicopathological data were obtained from medical records of the institutional database, and the ultrasound findings were collected from the Picture Archiving and Communication Systems (PACS), which is a database for medical images.

The inclusion criteria were as follows: (1) female patients with breast tumors diagnosed for the first time by pathological or clinical examinations; (2) had clinically negative LN metastasis (detected by medical imaging examination or puncture pathology); (3) underwent SLNB surgery in Xijing or Tangdu Hospital; and (4) had complete clinicopathological data, including breast and ALN ultrasound findings. Patients who were male, had distant metastases, bilateral lesions, or had previously received neoadjuvant therapies or breast surgeries were excluded. Ethical approval for this retrospective study was obtained (K202101-06), and informed consent was waived.

Ultrasonography and Image Analysis

Ultrasound detection was performed in all patients using the Acuson S2000 system (Siemens Medical Solutions, Mountain View, CA, USA) with a transducer frequency of 5-12 MHz. In order for each quadrant of the breast to be examined thoroughly, the patients were kept in the supine, left-lateral, and right-lateral positions. Two sonographers with more than 5 years of experience in breast ultrasound examined the breast and ALNs using two-dimensional images and color Doppler spectra features. On the condition that the sonographers disagreed in assessing any parameters, the third sonographer with a 10-year experience of breast ultrasound would review the images and make the final decision. All the confirmed information, including both ultrasound images and reporting descriptions, was stored in the PACS database. The specific ultrasound characteristics collected were tumor size, tumor shape (regular or irregular, such as microlobulated, angular, or spiculated), tumor margin (distinct or indistinct), color Doppler flow (rich or poor), aspect ratio (<1 or ≥1; when under the ultrasound probe, the diameter of the tumor that is parallel to the skin is the horizontal line, and the diameter perpendicular to the skin is the vertical line; the aspect ratio refers to the ratio of the vertical line to the horizontal line of the tumor, which on the ultrasonic images is the ratio of the width of the tumor to its height), calcification (present or absent), whether ALNs are visible or enlarged, and Breast Imaging Reporting and Data System (BI-RADS) grade. All breast and LN information on B-mode and color Doppler flow were extracted and collected from the PACS. Upon extraction of the data from the PACS database, we assigned three breast ultrasound specialists to review and confirm the ultrasound images again, and then recorded the report results based on the ultrasound lexicon of the BI-RADS 5th edition (13) and the color Doppler flow grading methods of Adler et al. (14) to avoid the subjectivity of the ultrasound findings in different centers as much as possible.

Preoperative Pathologic and Immunohistochemical Analyses

The pathologic type, histologic grade, and status of ALN metastases were confirmed. The estrogen receptor (ER), progesterone receptor (PR), human epidermal growth factor receptor 2 (HER2), and Ki-67 status were evaluated by immunohistochemistry (IHC) in a preoperative pathological puncture. The cutoff point for ER- and PR-positive expression levels was 1% based on IHC results (15). HER2 positivity was defined as IHC staining of 3+ or fluorescence *in situ* hybridization (ISH) proliferation greater than 2 (15). The detailed ISH detection criteria for HER2 can be found in the NCCN guidelines (16). Ki67 scores were evaluated using the percentage of tumor cell nuclei with positive immunostaining above background, with greater than 30% showing elevated expression (17). BC molecular subtypes were categorized as luminal A, luminal B, HER2 amplified type and hormone receptor- (HR-) negative, HER2 amplified type and HR-positive, and triple-negative type according to the status of ER, PR, HER2, and Ki-67.

SLNB and LN Histopathology

The patient was anesthetized and subsequently injected with 0.5 mL of 1% methylene blue or nano-carbon into the subcutaneous tissue at 3 o'clock, 6 o'clock, 9 o'clock, and 12 o'clock of the edge of the areola of the patient, followed by a light massage for 5 minutes. A radial incision was made at the lateral border of the pectoralis major muscle. The skin, subcutaneous, and adipose tissues were cut layer by layer. We separated and traced the lymphatic vessels, and the blue- and black-stained LNs were regarded as SLNs. The enlarged LNs palpated intraoperatively were also removed as SLNs. All SLNs were sent for rapid frozen pathological detection during the operation. If any of them were found to be positive for metastasis, further axillary lymph node dissection would be subsequently performed.

According to the AJCC 8th edition BC staging criteria (18), our main evaluation criteria for the final status of LN metastases were based on the postoperative pathologic diagnosis (pN). Negative LNs (pN0) were defined as no tumor cells or only isolated tumor cells that could be seen in histopathology (the maximum diameter of metastasis foci was less than 0.2 mm and the number of tumor cells in one section was less than 200), and positive LNs (pN[+]) were defined as the presence of macro-metastasis (maximum diameter of metastasis foci >2.0 mm) and micro-metastasis (maximum diameter of metastasis foci was 0.2-2.0 mm) of isolated tumor cells.

Statistical Analyses

Descriptive statistics were used to delineate the clinicopathological characteristics of the study population. Continuous variables were presented as mean ± standard deviation (SD) or median and interquartile range and were compared using an unpaired two-independent-simple Student's t-test or Mann-Whitney U test. Categorical variables were expressed as counts and percentages and compared using the Chi-square test or Fisher's exact test.

Univariate logistic regression analysis was used to select the candidate variables of the training cohort, and variables with a p-value <0.2 were included in the multivariable regression model as independent predictive factors associated with SLN metastasis of BC (19). Backward stepwise selection was applied using the likelihood ratio test with Akaike's information criterion (AIC) as the stopping rule. To provide the clinician with a quantitative tool to predict the individual probability of SLN metastasis, we established a nomogram based on the multivariate logistic regression analysis in the training cohort, using the rms package of R (R Project for Statistical Computing, RRID: SCR_001905; version 4.0.3; http://www.r-project.org). The predictive performance was measured by both internal and external validation by plotting the calibration curve of 1000 bootstrap samples and calculating the concordance index (C-index) to reduce the overfitting bias. Sensitivity, specificity, predictive value, and likelihood ratios with their 95% confidence intervals (CIs) were evaluated to assess the accuracy of the model using the receiver operation characteristic curve (ROC) analysis. Decision curve analysis (DCA) was conducted to estimate the potential clinical usefulness of the nomogram by quantitative analysis of the net benefits at different threshold probabilities (20). Our research data were processed in Stata (Stata, RRID: SCR_012763) version 15.0 for Windows (StataCorp, Texas, USA) and R version 4.0.3. Statistical significance was defined as a two-sided P value <.05.

RESULTS

Clinicopathologic Characteristics

During the study period, 1205 consecutive patients diagnosed with BC based on preoperative pathology underwent SLNB. Of these, 624 patients who met the inclusion criteria were enrolled (**Figure 1**). The training set consisted of 444 patients from Xijing Hospital (positive vs. negative SLN metastasis: 103 vs. 341), and the validation set included 180 patients from Tangdu Hospital (positive vs. negative SLN metastasis: 44 vs. 136). The sample size of this study met the standard of 10 outcome events per predictor variable (EPV) (21, 22). The comparison between patients with positive and negative final SLN status showed statistically significant differences in BMI, overall TNM stage, clinical T classification, tumor size, presence of tumor calcification, and aspect ratio of the tumor (**Table S1**).

Patients' baseline characteristics in the training (mean age, 51.19 ± 0.52 years; range, 23 to 80 years) and validation cohort (mean age, 51.31 ± 0.82 years; range, 23 to 82 years) are given in **Table 1**. The positive rate of SLN metastasis was 23.2% and 24.4%, respectively, in these two cohorts, with no significant differences in SLN prevalence (P=0.74). There were also no significant differences in age, BMI, menstrual status, lesion position, LN stage, histological type, ER status, PR status, Ki67, BI-RADS, tumor shape, and color Doppler flow between the training and validation cohorts; however, differences in some clinicopathologic characteristics were observed in patients of these two cohorts owing to the spatial span of the different institutions, according to our study. In terms of clinicopathological features, the tumor stage and pathological stage were lower in the training set than in the validation set. Based on the pathological evaluation, approximately

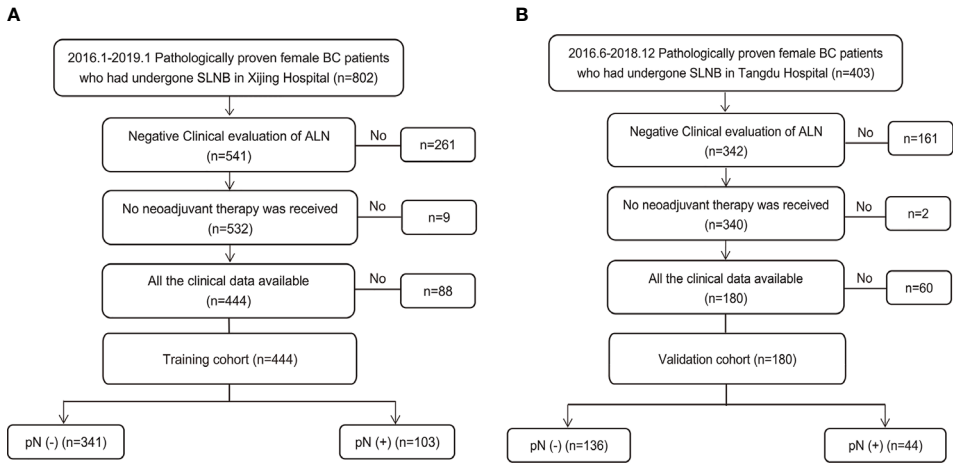

FIGURE 1 | Study population enrolment in the training and validation cohort. **(A)** Study population enrolment in the training cohort; **(B)** Study population enrolment in the validation cohort. SLNB, sentinel lymph node biopsy; BC, breast cancer; pN(-), negative lymph node metastasis confirmed by pathology; pN(+), positive lymph node metastasis confirmed by pathology.

two-thirds of the patients in the training cohort were in stage T1 (62.4%), but in the validation cohort were in stage T2 (65.6%). More patients in the training set had primary tumors at histological grade 1 than in the validation set (21.1% vs. 6.1%; P<.001).

Moreover, more patients were diagnosed with the HER2 positive subtype in the validation cohort than in the training cohort (22.8% vs. 12.1%; P=.001). Similarly, according to the preoperative ultrasound examination results, both training and validation cohorts had more patients with a single lesion, but fewer patients with multifocal BC tumors in the former (P=0.01). In addition, compared with the patients in the validation set, the primary tumor in the training set was generally more extensive, with indistinct margins, more uneven internal echoes, more calcifications, and more lesions with an aspect ratio <1 (P<.001, <.001, <0.05, =.001, and =.001, respectively). The variety in these different baseline characteristics in the two cohorts may be caused by differences in the studied population from the two centers after excluding those who received neoadjuvant therapy. These differences can better indicate the generalizability and predictive capacity of the model application.

Nomogram Development of SLN-Metastasis Risk

Univariate Logistic Analysis and Candidate Factors Selection

All variables incorporated in the model were based on the data obtained preoperatively; therefore, postoperative indicators such as pathological T and N classifications, pathological TNM stage, and histological grade were not included. The results of the univariate logistic analysis are presented in **Table 2**. Variables with p-values <0.2 were age (P=0.04), BMI (P=0.02), PR status (P=0.15), Ki67 (P=0.04), tumor size (P<0.001), inner echo of tumor (P=0.09), tumor calcification (P<0.001), color Doppler flow (P=0.17), and aspect ratio (P<0.001). These variables were included in the multivariable regression model as the candidate predictive factors associated with SLN metastasis risk.

Multivariate Logistic Analysis Nomogram Development

In the multivariate analysis, with results reported as odds ratio (95% CI), young age (0.97 [0.94-1.00]), high BMI (1.14 [0.99-1.31]), high Ki67 (1.02 [1.00-1.04]), large tumor size (4.29 [2.88-6.39]), indistinct tumor margins (0.29 [0.10-0.79]), calcified tumor (14.79 [6.45-33.94]), and an aspect ratio ≥1 (0.05 [0.02-0.13]) were independent predictive factors associated with the risk of SLN metastasis (**Table 3**). These independent predictors were used to form the SLN metastasis risk estimation nomogram, as shown in **Figure 2**.

Nomogram Validation of SLN-Metastasis Risk

Calibration of the Nomogram

The resulting model was validated both internally and externally using bootstrap validation. The nomogram demonstrated good accuracy in estimating the risk of SLN metastasis with a C-index of 0.92 (95% CI, 0.89-0.95). In addition, calibration plots graphically showed good agreement on the presence of SLN metastasis between the risk estimation by the nomogram and histopathologic confirmation on surgical specimens (**Figure 3A**). In the validation cohort, the nomogram displayed a C index of 0.82 (95% CI, 0.74-0.89) to estimate SLN metastasis risk. There was also a good calibration curve for risk estimation (**Figure 3B**).

Accuracy of the Nomogram

The area under the ROC curve (AUC) for internal and external validation was 0.92 (**Figure 4A**) and 0.82 (**Figure 4B**), respectively. The cutoff score was 55 when the Youden index was at the maximum. Patients with a score of 55 or more were at a high risk of SLN metastasis. Using 55 as a cutoff score, the sensitivity, specificity, accuracy, positive predictive value, and

TABLE 1 | Participant baseline characteristics in two cohorts.

Characteristics	Training data (n=444) (%)	Validation data (n=180) (%)	P Value
Age, media (IQR), years	49.0 (44.0, 58.5)	49.5 (44.0, 58.5)	0.90
BMI, media (IQR), kg/m^2	23.3 (21.6, 24.8)	23.4 (21.5, 25.4)	0.06
Menstrual status			0.13
Pre-	237 (53.4)	84 (46.7)	
Post-	207 (46.6)	96 (53.3)	
Lesion position			0.89
OUQ	255 (57.4)	109 (60.6)	
OLQ	69 (15.5)	26 (14.4)	
IUQ	83 (18.7)	29 (16.1)	
ILQ	26 (5.9)	10 (5.6)	
Center	11 (2.5)	6 (3.3)	
T classification			**<0.001**
Tis	67 (15.1)	1 (0.6)	
T1	277 (62.4)	59 (32.8)	
T2	100 (22.5)	118 (65.6)	
T3	0 (0.0)	2 (1.1)	
N classification			0.21
N0	344 (77.5)	136 (75.6)	
N1	97 (21.8)	39 (21.7)	
N2	2 (0.5)	3 (1.7)	
N3	1 (0.2)	2 (1.1)	
Overall TNM stage			**<0.001**
Ia	246 (55.4)	48 (26.7)	
Ib	68 (15.3)	11 (6.1)	
IIa	71 (16.0)	86 (47.8)	
IIb	29 (6.5)	28 (15.6)	
III	2 (0.5)	6 (3.3)	
Histological type			0.96
Ductal	353 (79.5)	144 (80.0)	
Lobular	35 (7.9)	13 (7.2)	
Others	56 (12.6)	23 (12.8)	
Histological grade			**<0.001**
I	94 (21.1)	11 (6.1)	
II	314 (70.0)	153 (85.0)	
III	36 (8.1)	16 (8.9)	
Subtype			**0.001**
Luminal A	264 (59.5)	92 (51.1)	
Luminal B	77 (17.3)	23 (12.8)	
HER2+ (HR-)	29 (6.5)	14 (7.8)	
HER2+ (HR+)	25 (5.6)	27 (15.0)	
TNBC	49 (11.0)	24 (13.3)	
ER			0.23
Negative	80 (18.8)	40 (22.2)	
Positive	364 (82.0)	140 (77.8)	
PR			0.53
Negative	122 (27.5)	45 (25.0)	
Positive	322 (72.5)	135 (75)	
HER2			**0.001**
Negative	390 (87.8)	139 (77.2)	
Positive	54 (12.2)	41 (22.8)	
Ki67, media (IQR), %	18 (10, 30)	20 (10, 30)	0.17
US Findings			
BI-RADS			0.70
4A	65 (14.6)	23 (12.8)	
4B	74 (16.7)	35 (19.4)	
4C	112 (25.2)	52 (28.9)	
5	87 (19.6)	32 (17.8)	
6	106 (23.9)	38 (21.1)	
Multifocality			**0.01**
yes	96 (21.6)	23 (12.8)	
no	348 (78.4)	157 (87.2)	
Tumor size, media (IQR), cm	1.6 (1.2, 2.1)	2.1 (1.7, 2.7)	**<0.001**
Tumor shape			0.44
regular	27 (6.1)	14 (7.8)	
irregular	417 (93.9)	166 (92.2)	
Tumor Margin			**<0.001**
distinct	46 (10.4)	52 (28.9)	
indistinct	398 (89.6)	128 (71.1)	
Inner echo			**0.03**
even	72 (16.2)	17 (9.4)	
uneven	372 (83.8)	163 (90.6)	
Calcification			**<0.001**
present	209 (47.1)	52 (28.9)	
absent	235 (52.9)	128 (71.1)	
Color Doppler flow			0.18
rich	424 (95.5)	176 (97.8)	
poor	20 (4.5)	4 (2.2)	
Aspect ratio			**<0.001**
≥1	34 (7.7)	66 (36.7)	
<1	410 (92.3)	114 (63.3)	

OUQ, outer upper quadrant; OLQ, outer lower quadrant; IUQ, inner upper quadrant; ILQ, inner lower quadrant; HR, hormone receptor; TNBC, triple-negative breast cancer; ER, estrogen receptor; PR, progesterone receptor; US, ultrasound.
Bold value indicates statistical significance.

negative predictive value were 66%, 91%, 85%, 71%, and 89% in the training cohort and 93%, 77%, 80%, 55%, and 97% in the validation cohort, respectively (**Table 4**).

Clinical Usefulness Evaluation of the Nomogram

DCA is used to assess the benefits of diagnostic models covering a range of patient preferences for the risks of under- and overtreatment to facilitate more reasonable decisions regarding the model selection and use (23). The net benefit in DCA was calculated by subtracting the proportion of all false-positive patients from the ratio of true positives and weighing the relative harm of abandoning treatment and the adverse outcomes of unnecessary treatment. The DCA in the current study showed that the nomogram of the SLN metastasis model used in our study was more effective than all-patient treatment or no treatment if the threshold probability ranged from 2% to 92% in the training cohort (**Figure 5A**), and from 6% to 50% in the validation cohort (**Figure 5B**).

DISCUSSION

Among the currently available prediction tools, the nomogram has high accuracy and good discriminability, as well as convenient and important in clinical use (24), which can change the treatment pattern of BC patients (25). Previous nomograms of breast tumors mainly focused on the risk of non-SLN metastasis (26–28) or total LN metastasis (10, 29–31) to predict the possibility of axillary lymph node dissection omission to appropriately minimize the scope of axillary surgery. However, few studies have focused on the omission of

TABLE 2 | Univariate Logistic Regression Analysis of SLN Metastasis Based on Preoperative Data in the Training Cohort.

Variables	P Value	OR (95% CI)
Age (years)	**0.04**	0.98 (0.96-1.00)
BMI (kg/m^2)	**0.02**	1.12 (1.02-1.22)
Menstrual status (post- vs. pre-)	0.50	0.86 (0.55-1.34)
Lesion position		
OLQ vs. OUQ	0.62	0.88 (0.53-1.46)
IUQ vs. OUQ	0.41	0.82 (0.51-1.32)
ILQ vs. OUQ	0.79	0.90 (0.42-1.93)
Center vs. OUQ	0.64	1.28 (0.46-3.54)
Histological type		
lobular vs. ductal	0.78	0.91 (0.47-1.77)
others vs. ductal	0.98	1.01 (0.60-1.70)
Subtype		
Luminal B vs. Luminal A	0.56	0.86 (0.51-1.45)
HER2+ (HR-) vs. Luminal A	0.35	1.39 (0.70-2.74)
HER2+ (HR+) vs. Luminal A	**<0.001**	3.10 (1.71-5.61)
TNBC vs. Luminal A	0.22	1.41 (0.82-2.42)
ER (negative vs. positive)	0.32	0.76 (0.44-1.31)
PR (negative vs. positive)	**0.15**	0.71 (0.44-1.14)
HER2 (negative vs. positive)	**0.06**	1.79 (0.97-3.32)
Ki67	**0.04**	1.01 (1.00-1.02)
US Findings		
Multifocality (multiple vs. single)	0.25	0.71 (0.41-1.26)
Tumor size (cm)	**<0.001**	3.33 (2.42-4.59)
Tumor shape (irregular vs. regular)	0.73	0.85 (0.35-2.08)
Margin (indistinct vs. distinct)	0.22	0.66 (0.34-1.29)
Inner echo (uneven vs. even)	**0.09**	1.82 (0.92-3.61)
Calcification (present vs. absent)	**<0.001**	8.97 (5.10-15.78)
Color Doppler flow (rich vs. poor)	**0.17**	2.81 (0.64-12.34)
Aspect ratio (<1 vs. ≥1)	**<0.001**	0.10 (0.05-0.22)

CI, confidence interval; OUQ, outer upper quadrant; OLQ, outer lower quadrant; IUQ, inner upper quadrant; ILQ, inner lower quadrant; HR, hormone receptor; TNBC, triple-negative breast cancer; ER, estrogen receptor; PR, progesterone receptor; US, ultrasound.

Bold value are variables with P <0.2 which are candidate variables in multivariable regression analysis.

TABLE 3 | Multivariate logistic regression analysis of SLN metastasis based on preoperative data in the training cohort.

Variables	β[#]	P value	OR (95% CI)
Age (per 1-year increase)	-0.03	0.059	0.97 (0.94-1.00)
BMI (per 0.1kg/m^2 increase)	0.14	0.071	1.14 (0.99-1.31)
Ki67 (per 1% increase)	0.02	0.016	1.02 (1.00-1.04)
Tumor size* (per 0.1cm increase)	1.46	<.001	4.29 (2.88-6.39)
Tumor margin* (distinct vs. indistinct)	-1.25	0.015	0.29 (0.10-0.79)
Calcification* (present vs. absent)	2.69	<.001	14.79 (6.45-33.94)
Aspect ratio* (<1 vs. ≥1)	-3.06	<.001	0.05 (0.02-0.13)
Constant	0.19	0.937	1.20 (0.01-107.65)

[#]*Unstandardized β coefficients were calculated from the multivariate logistic regression analysis based on stepwise regression (AIC: 267.85).*

**Variables based on US results.*

CI, confidence interval.

SLNB. Additionally, most of the parameters included in these models were pathological indicators obtained postoperatively, such as tumor molecular subtypes, tumor grade, and LVI, which were difficult to accurately obtain before surgery, thus restricting their usage in the preoperative setting. In addition, some studies have attempted to introduce radiomics examinations and pathological indicators to predict breast malignancy or LN metastasis (32–35), but further clinical validation is required.

In this study, we included two cohorts of BC patients from different centers to develop and validate a predictive nomogram of SLN-metastasis risk, combining various indicators that were easily available preoperatively, including clinicopathological characteristics and detailed ultrasound diagnostic results. Seven preoperative parameters were identified as independent predictive risk factors. Although the spatial disconnection existed between the two study cohorts, the nomogram achieved a robust predictive performance with a C-index and accuracy of 0.92, 0.85, 0.82, and 0.80 in the training and validation cohorts, respectively. In addition, the calibration curves also fit well. For clinical use of the nomogram, we adopted 55 as the cutoff value and summarized the sensitivity, specificity, accuracy, positive predictive value, and negative predictive value to evaluate the quality of the model. The nomogram might enable 91% and 77% (**Table 4**) of patients in the training and validation sets, respectively, in our study, to avoid unnecessary SLNB. It provides a new method for preoperative and non-invasive prediction of SLN metastasis in BC patients, which has a potential predictive reference value for the omission of SLNB in the clinic.

Currently, two ongoing clinical trials, the SOUND trial (ClinicalTrials.gov identifier NCT02167490) (36) and the NAUTILUS trial (ClinicalTrials.gov identifier NCT04303715), have some similarities to this study. A detailed comparison of the three studies is presented in **Table S2**. The aim of the three studies was similar, which was to establish a minimally invasive treatment omitting SLNB of BC; however, these two clinical trials have strict inclusion criteria. Among these criteria, tumor size is the only one that is associated with the risk of LN metastasis. However, this study was designed to build a prediction system in which a variety of indicators probably associated with lymph node metastasis were retrospectively analyzed, and seven of them were selected and developed a nomogram to predict the risk of SLN metastasis. Patients with a low risk evaluated by the model may omit SLNB.

In the LN metastasis predictive nomogram, young age, large tumor size, tumor calcifications, high BMI, and Ki67 status were associated with an increase in LN metastasis in BC (7, 10, 30, 31, 37–40). Likewise, our study showed that these factors were also related to an increased probability of SLN metastasis in BC. In addition, we found that an indistinct margin and the aspect ratio of the tumor based on ultrasonography were independent predictive factors for SLN metastasis.

Ultrasound imaging is a promising tool for predicting LN metastasis in patients with BC and is an important imaging method for preoperative BC screening and evaluation (34). In this study, the tumor size (the maximum diameter of the tumor) based on ultrasound imaging was the most significant predictive factor for SLN metastasis. This significantly contributed to the model with an OR of 4.29, which suggested that patients were 4.29 times more likely to have SLN metastasis with every 0.1 cm increase in tumor size. Tumor size is easily and quickly measured by ultrasonography, which enables the model to be more applicable in the clinic.

Calcification is a deposit of calcium in the breast that appears as white, opaque spots, and scattered or partial agglutination on ultrasound images. Currently, calcification in breast imaging is

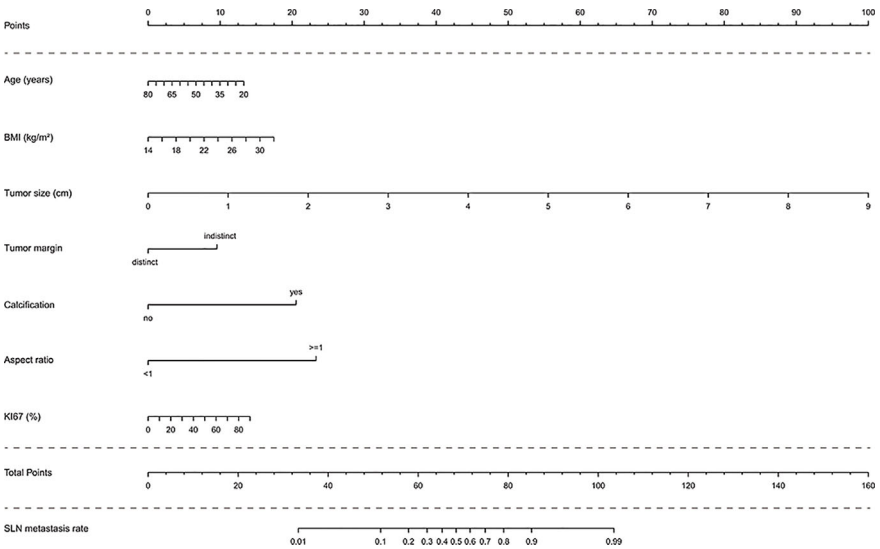

FIGURE 2 | Nomogram to predict the rate of SLN metastasis in clinically LN-negative breast cancer patients. The nomogram to predict SLN-metastasis-risk was created based on the above seven predictive factors. To use the nomogram, the value of each patient is placed on each variable axis and a line is drawn upward to determine the number of received points for each variable value. The sum of these numbers is located on the total point axis and a line down the bottom axis is drawn to determine the probability of SLN metastasis.

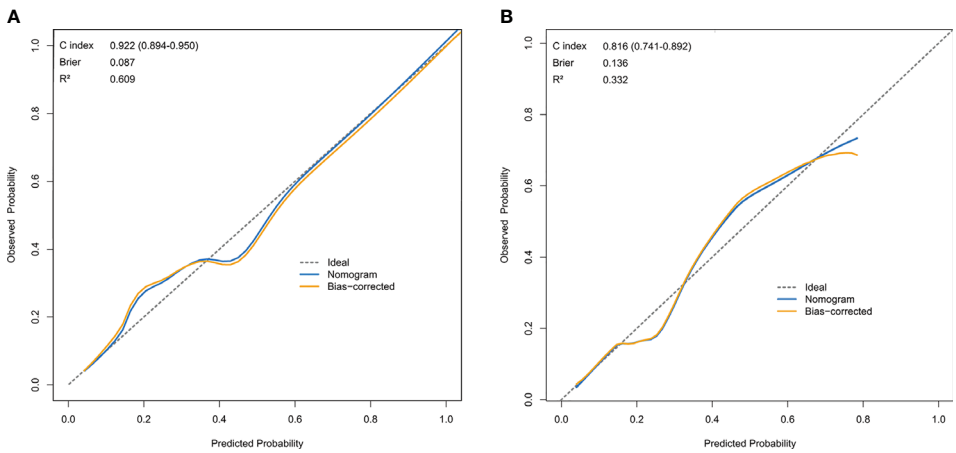

FIGURE 3 | Calibration curve comparing predicted and actual SLN-metastasis-risk probabilities. **(A)** Calibration curve of the nomogram in the training cohort. **(B)** Calibration curve of the nomogram in the validation cohort. The calibration curve describes the calibration of the model according to the consistency between the predicted risk of SLN metastasis and the observed results of SLN metastasis. The x-axis represents the predicted probability of SLN metastasis. T The y-axis represents the actual SLN metastasis probability. he gray dotted line represents the perfect prediction of the ideal model. The solid blue line represents the prediction of the nomogram, and the solid orange line represents the bootstrap-corrected estimates. A well calibrated curve of a nomogram would be near the ideal line.

primarily used in the diagnosis of cancer, noting that calcification is associated with invasive BC or ductal carcinoma *in situ* (41). When the tumor is rapidly growing with an active metabolism, the lack of oxygen and nutrients results in ischemic necrosis and calcium deposition, leading to calcifications appearing on the ultrasound image (42). It has been reported that calcifications not only play a crucial role in BC diagnosis but also have prognostic value, due to their correlation with high histological grade (43, 44), LN-positive status (44), HR-negative status (45), and HER2-positive status (46). Similarly, the calcification in breast tumors was also found to be associated with SLN-metastasis according to our research, with a 13.79-fold increased risk compared with uncalcified BC lesions, suggesting that clinicians should be alert about calcified breast tumors.

To the best of our knowledge, this is the first forecasting model consisting of tumor margin and aspect ratio for predicting SLN metastasis. Previous studies revealed that breast tumors with a non-circumscribed margin had a higher probability of LVI

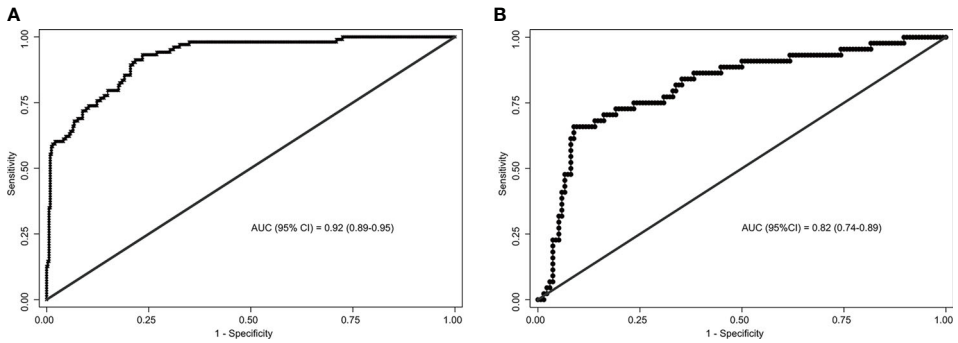

FIGURE 4 | Receiver operating characteristics (ROC) curves of the nomograms in training and validation cohort. **(A)** The ROC curve of the training cohort; **(B)** The ROC curve of the validation cohort. The nomogram had a good discriminative performance with Area under ROC curve (AUC) (95% confidence interval) of 0.92 (95% CI: 0.89-0.95) and 0.82 (95% CI: 0.74-0.89) in the training and validation cohort, respectively.

TABLE 4 | Accuracy of the prediction score of the nomogram for estimating the risk of SLN metastasis.

Variables	P Value (95% CI)	
	Training Cohort	Validation Cohort
AUC/C-Index	0.92 (0.89-0.95)	0.82 (0.74-0.89)
Cutoff score	55	55
Sensitivity	0.66 (0.50-0.79)	0.93 (0.86-0.97)
Specificity	0.91 (0.85-0.95)	0.77 (0.72-0.81)
Accuracy	0.85 (0.79-0.90)	0.80 (0.76-0.84)
Positive predictive value	0.71 (0.54-0.83)	0.55 (0.47-0.62)
Negative predictive value	0.89 (0.83-0.94)	0.97 (0.94-0.99)

CI, confidence interval; AUC, the area under the receiver operating curve; C-Index, concordance index.

(47), noting that the indistinct margin of the tumor may provide important information regarding neoplasm invasion. According to our study, SLN-positive BC tumors were more likely to have an aspect ratio greater than 1. For patients with invasive BC, the tumor does not routinely grow in the plane but grows vertically or away from the horizontal direction, so the overall volume of the tumor will expand, resulting in a larger aspect ratio.

According to our study, younger patients were more likely to develop SLN metastases. Several studies have demonstrated that age at diagnosis is an independent prognostic factor in patients with metastatic BC (48–51). In most cases, breast tumors in younger women behave more aggressively than those in older women and have a higher rate of local recurrence (52, 53). The exact definition of young women in breast oncology settings varies, with most articles identifying women <35, 40, or 45 years as young (54). However, several studies support that premenopausal women with BC should be further subdivided into very early stages of disease (<40 years) and relatively early stages (40-49 years) (55). To discover a more subtle effect, we incorporated age as a continuous variable in our model. The result implied that for each 1-year younger age at BC diagnosis, the risk of SLN metastasis would increase by 3%.

High BMI is associated with tumor invasiveness, shorter disease recurrence, and more significant mortality in patients with BC. The POSH study following 2 956 young British patients from 2001 to 2007 reported a positive association between BMI and larger tumor size, higher tumor histological grade, and positive LN involvement (56). The American Cancer Society's

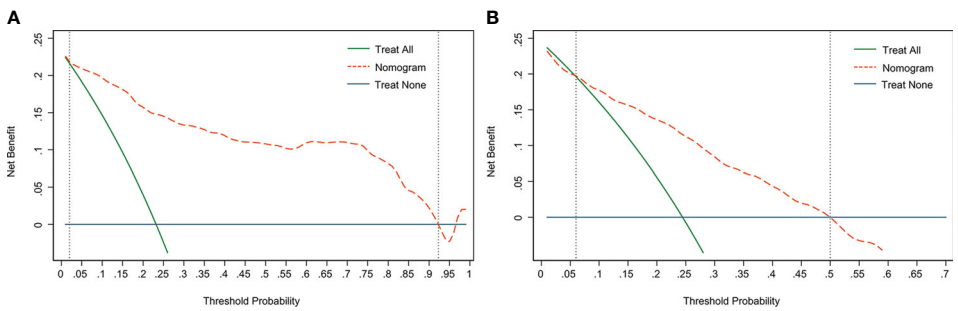

FIGURE 5 | Decision curve analysis (DCA) of the nomogram. **(A)** The DCA curve of the training cohort; **(B)** The DCA curve of the validation cohort. The orange line shows the nomogram. The green line represents the assumption that all patients have undergone SLNB. The dark blue line represents the assumption that no patients have undergone SLNB. The decision curve revealed that it was more benefit to use the nomogram in our study to predict SLN metastasis than the treat-all-patients scheme or the treat-none scheme, when the threshold probability of a patient is 2%-92%, and 6%-50% in the training cohort and validation cohort, respectively.

Cancer Prevention Study II, which followed 495 477 women from 1982 to 1998, reported a positive association between BMI and BC mortality: women with a BMI of 40 kg/m^2 had more than a two-fold increased risk of death compared with those with a BMI of 18 to 24.9 kg/m^2 (57). Moreover, a meta-analysis of 52 904 subjects showed that BMI increased the LN metastasis risk of BC, and for every 1 kg/m^2 increment in BMI, the risk of LN metastasis increased by 0.89 (58). This may be attributed to the increase in pro-inflammatory cytokines in the local and circulation caused by the high BMI, which promotes tumor growth, angiogenesis, invasion, and metastasis (59). Our study also revealed that high BMI was more likely to cause SLN metastasis, and for each 0.1 kg/m^2 increase in BMI, the risk of SLN metastasis increased by 14%, which indicated that losing weight and maintaining a healthy lifestyle intervention would be beneficial to BC patients.

As a biomarker of tumor proliferation, Ki67, which is a prognostic indicator that provides a rapid method to assess the proportion of proliferating cells in a tumor, and a higher level of Ki67 indicates more proliferating tumor cells (60). A previous study reported that BC patients with higher expression of Ki67 had significantly poorer 10-year disease-free survival than those with lower expression (61). In most studies concerning the association between Ki67 and metastasis of breast tumors, Ki67 was frequently treated as a classification variable; hence, the relationship between them could only be roughly estimated. In this study, we included Ki67 as a continuous variable, and the results showed that every 1% increase in the expression level of Ki67 increased the risk of SLN-metastasis by 1.02 times.

This study explored the probability of omitting SLNB from the perspective of retrospective observation and analysis. Based on the preoperative predictions, the nomogram may also serve as a useful tool to select BC patients for further randomized clinical trials of omission of SLNB. Additionally, the nomogram may also be used in clinical trials to evaluate the efficacy of breast-conserving surgery in patients with early BC and other subgroups with different risks of SLN metastasis.

However, this study has several limitations. First, this retrospective study excluded males, patients who had undergone neoadjuvant therapy, and those with incomplete clinical data; therefore, this model may not be applicable to them. Second, ultrasound findings, including tumor size, aspect ratio, and tumor margin, were assessed by the radiologist in a subjective manner. For the aspect ratio, a 0.1-difference in the measurement can add approximately 25 points. In addition, differences in the assessment of tumor margins can result in various tumor sizes. Compared to other objective factors (age, BMI, calcification), these subjective factors are the primary factors that may influence the results of the final nomogram, which could be a critical issue to consider when being applied in the clinic to evaluate patients who would potentially be able to omit SLNB. Third, although the nomogram achieved a favorable predictive performance, it still had a 34% and 7% false-negative-rate in the training and validation cohorts, respectively. Therefore, it is necessary to establish more accurate and uniform ultrasound assessment criteria for BC in the future, and prospective cohort studies in terms of SLNB omitting with more subgroups, larger samples, and more centers are still required.

CONCLUSIONS

In summary, we established a nomogram combining clinicopathological characteristics and ultrasound features, including age, BMI, Ki67, tumor size, tumor margin, calcifications, and aspect ratio, to predict SLN-metastasis risk in BC patients before surgery. The nomogram provides a non-invasive approach in preoperative clinical decision-making and individualized treatment, which also has the potential to serve as a helpful and convenient tool to identify BC patients who have an opportunity to omit SLNB.

DATA AVAILABILITY STATEMENT

The raw data supporting the conclusions of this article will be made available by the authors, without undue reservation.

AUTHOR CONTRIBUTIONS

Xi'eH: data collection, data analysis and interpretation, and drafting the article. GB and TW: conception of the work, critical revision of the article and final approval of the version to be published. JX, SP, PY, ZY and LYa: data collection. LYu, JX and YD: critical revision of the article. All authors contributed to the article and approved the submitted version.

FUNDING

This work was supported by the National Natural Science Foundation of China (NO: 81572916, 81502424).

ACKNOWLEDGMENTS

The authors would like to acknowledge all the ultrasonographers and pathologists for their assistance, patients involved in this study, and Editage (www.editage.com) for English language editing.

SUPPLEMENTARY MATERIAL

The Supplementary Material for this article can be found online at: https://www.frontiersin.org/articles/10.3389/fonc.2021.665240/full#supplementary-material

REFERENCES

1. Bray F, Ferlay J, Soerjomataram I, Siegel RL, Torre LA, Jemal A. Global Cancer Statistics 2018: GLOBOCAN Estimates of Incidence and Mortality Worldwide for 36 Cancers in 185 Countries. *CA Cancer J Clin* (2018) 68:394–424. doi: 10.3322/caac.21492
2. Sopik V, Narod SA. The Relationship Between Tumour Size, Nodal Status and Distant Metastases: On the Origins of Breast Cancer. *Breast Cancer Res Treat* (2018) 170:647–56. doi: 10.1007/s10549-018-4796-9
3. Giuliano AE, Kirgan DM, Guenther JM, Morton DL. Lymphatic Mapping and Sentinel Lymphadenectomy for Breast Cancer. *Ann Surg* (1994) 220:391–8. doi: 10.1097/00000658-199409000-00015
4. Wilke LG, McCall LM, Posther KE, Whitworth PW, Reintgen DS, Leitch AM, et al. Surgical Complications Associated With Sentinel Lymph Node Biopsy: Results From a Prospective International Cooperative Group Trial. *Ann Surg Oncol* (2006) 13:491–500. doi: 10.1245/ASO.2006.05.013
5. Jalalian A, Mashohor SB, Mahmud HR, Saripan MI, Ramli AR, Karasfi B. Computer-Aided Detection/Diagnosis of Breast Cancer in Mammography and Ultrasound: A Review. *Clin Imaging* (2013) 37:420–6. doi: 10.1016/j.clinimag.2012.09.024
6. Galimberti V, Cole BF, Viale G, Veronesi P, Vicini E, Intra M, et al. Axillary Dissection Versus No Axillary Dissection in Patients With Breast Cancer and Sentinel-Node Micrometastases (IBCSG 23-01): 10-Year Follow-Up of a Randomised, Controlled Phase 3 Trial. *Lancet Oncol* (2018) 19:1385–93. doi: 10.1016/S1470-2045(18)30380-2
7. Verheuvel NC, Ooms HW, Tjan-Heijnen VC, Roumen RM, Voogd AC. Predictors for Extensive Nodal Involvement in Breast Cancer Patients With Axillary Lymph Node Metastases. *Breast* (2016) 27:175–81. doi: 10.1016/j.breast.2016.02.006
8. Bevilacqua JL, Kattan MW, Fey JV, Cody HS3, Borgen PI, Van Zee KJ. Doctor, What are My Chances of Having a Positive Sentinel Node? A Validated Nomogram for Risk Estimation. *J Clin Oncol* (2007) 25:3670–9. doi: 10.1200/JCO.2006.08.8013
9. Nos C, Harding-MacKean C, Fréneaux P, Trie A, Falcou MC, Sastre-Garau X, et al. Prediction of Tumour Involvement in Remaining Axillary Lymph Nodes When the Sentinel Node in a Woman With Breast Cancer Contains Metastases. *Br J Surg* (2003) 90:1354–60. doi: 10.1002/bjs.4325
10. Rivadeneira DE, Simmons RM, Christos PJ, Hanna K, Daly JM, Osborne MP. Predictive Factors Associated With Axillary Lymph Node Metastases in T1a and T1b Breast Carcinomas: Analysis in More Than 900 Patients. *J Am Coll Surg* (2000) 191:1–6; discussion 6-8. doi: 10.1016/s1072-7515(00)00310-0
11. Guo R, Lu G, Qin B, Fei B. Ultrasound Imaging Technologies for Breast Cancer Detection and Management: A Review. *Ultrasound Med Biol* (2018) 44:37–70. doi: 10.1016/j.ultrasmedbio.2017.09.012
12. Sigrist R, Liau J, Kaffas AE, Chammas MC, Willmann JK. Ultrasound Elastography: Review of Techniques and Clinical Applications. *Theranostics* (2017) 7:1303–29. doi: 10.7150/thno.18650
13. Spak DA, Plaxco JS, Santiago L, Dryden MJ, Dogan BE. Bi-RADS® Fifth Edition: A Summary of Changes. *Diagn Interv Imaging* (2017) 98:179–90. doi: 10.1016/j.diii.2017.01.001
14. Adler DD, Carson PL, Rubin JM, Quinn-Reid D. Doppler Ultrasound Color Flow Imaging in the Study of Breast Cancer: Preliminary Findings. *Ultrasound Med Biol* (1990) 16:553–9. doi: 10.1016/0301-5629(90)90020-d
15. Guerra I, Algorta J, Díaz de Otazu R, Pelayo A, Fariña J. Immunohistochemical Prognostic Index for Breast Cancer in Young Women. *Mol Pathol* (2003) 56:323–7. doi: 10.1136/mp.56.6.323
16. Gradishar WJ, Anderson BO, Abraham J, Aft R, Agnese D, Allison KH, et al. Breast Cancer, Version 3.2020, NCCN Clinical Practice Guidelines in Oncology. *J Natl Compr Canc Netw* (2020) 18:452–78. doi: 10.6004/jnccn.2020.0016
17. Howell SJ, Wardley AM, Armstrong AC. Re: Ki67 Index, HER2 Status, and Prognosis of Patients With Luminal B Breast Cancer. *J Natl Cancer Inst* (2009) 101:1730; author reply 1730–1. doi: 10.1093/jnci/djp390
18. *AJCC Cancer Staging Manual Eighth Edition*. (2017). Available at: https://cancerstaging.org/About/news/Pages/Updated-Breast-Chapter-for-8th-Edition.aspx (Accessed January 23, 2021).
19. Kang SJ, Cho YR, Park GM, Ahn JM, Han SB, Lee JY, et al. Predictors for Functionally Significant in-Stent Restenosis: An Integrated Analysis Using Coronary Angiography, IVUS, and Myocardial Perfusion Imaging. *JACC Cardiovasc Imaging* (2013) 6:1183–90. doi: 10.1016/j.jcmg.2013.09.006
20. Vickers AJ, Cronin AM, Elkin EB, Gonen M. Extensions to Decision Curve Analysis, a Novel Method for Evaluating Diagnostic Tests, Prediction Models and Molecular Markers. *BMC Med Inform Decis Mak* (2008) 8:53. doi: 10.1186/1472-6947-8-53
21. Peduzzi P, Concato J, Feinstein AR, Holford TR. Importance of Events Per Independent Variable in Proportional Hazards Regression Analysis. II. Accuracy and Precision of Regression Estimates. *J Clin Epidemiol* (1995) 48:1503–10. doi: 10.1016/0895-4356(95)00048-8
22. Concato J, Peduzzi P, Holford TR, Feinstein AR. Importance of Events Per Independent Variable in Proportional Hazards Analysis. I. Background, Goals, and General Strategy. *J Clin Epidemiol* (1995) 48:1495–501. doi: 10.1016/0895-4356(95)00510-2
23. Vickers AJ, Elkin EB. Decision Curve Analysis: A Novel Method for Evaluating Prediction Models. *Med Decis Making* (2006) 26:565–74. doi: 10.1177/0272989X06295361
24. Shariat SF, Capitanio U, Jeldres C, Karakiewicz PI. Can Nomograms be Superior to Other Prediction Tools. *BJU Int* (2009) 103:492–5; discussion 495-7. doi: 10.1111/j.1464-410X.2008.08073.x
25. Park J, Fey JV, Naik AM, Borgen PI, Van Zee KJ, Cody HS3. A Declining Rate of Completion Axillary Dissection in Sentinel Lymph Node-Positive Breast Cancer Patients is Associated With the Use of a Multivariate Nomogram. *Ann Surg* (2007) 245:462–8. doi: 10.1097/01.sla.0000250439.86020.85
26. Wang XY, Wang JT, Guo T, Kong XY, Chen L, Zhai J, et al. Risk Factors and a Predictive Nomogram for non-Sentinel Lymph Node Metastases in Chinese Breast Cancer Patients With One or Two Sentinel Lymph Node Macrometastases and Mastectomy. *Curr Oncol* (2019) 26:e210–210e215. doi: 10.3747/co.26.4295
27. Houvenaeghel G, Bannier M, Nos C, Giard S, Mignotte H, Jacquemier J, et al. Non Sentinel Node Involvement Prediction for Sentinel Node Micrometastases in Breast Cancer: Nomogram Validation and Comparison With Other Models. *Breast* (2012) 21:204–9. doi: 10.1016/j.breast.2011.09.013
28. Wang NN, Yang ZJ, Wang X, Chen LX, Zhao HM, Cao WF, et al. A Mathematical Prediction Model Incorporating Molecular Subtype for Risk of non-Sentinel Lymph Node Metastasis in Sentinel Lymph Node-Positive Breast Cancer Patients: A Retrospective Analysis and Nomogram Development. *Breast Cancer* (2018) 25:629–38. doi: 10.1007/s12282-018-0863-7
29. Qiu SQ, Aarnink M, van Maaren MC, Dorrius MD, Bhattacharya A, Veltman J, et al. Validation and Update of a Lymph Node Metastasis Prediction Model for Breast Cancer. *Eur J Surg Oncol* (2018) 44:700–7. doi: 10.1016/j.ejso.2017.12.008
30. Houvenaeghel G, Lambaudie E, Classe JM, Mazouni C, Giard S, Cohen M, et al. Lymph Node Positivity in Different Early Breast Carcinoma Phenotypes: A Predictive Model. *BMC Cancer* (2019) 19:45. doi: 10.1186/s12885-018-5227-3
31. Sandoughdaran S, Malekzadeh M, Mohammad Esmaeil ME. Frequency and Predictors of Axillary Lymph Node Metastases in Iranian Women With Early Breast Cancer. *Asian Pac J Cancer Prev* (2018) 19:1617–20. doi: 10.22034/APJCP.2018.19.6.1617
32. Luo WQ, Huang QX, Huang XW, Hu HT, Zeng FQ, Wang W. Predicting Breast Cancer in Breast Imaging Reporting and Data System (Bi-Rads) Ultrasound Category 4 or 5 Lesions: A Nomogram Combining Radiomics and BI-RADS. *Sci Rep* (2019) 9:11921. doi: 10.1038/s41598-019-48488-4
33. Dong Y, Feng Q, Yang W, Lu Z, Deng C, Zhang L, et al. Preoperative Prediction of Sentinel Lymph Node Metastasis in Breast Cancer Based on Radiomics of T2-weighted Fat-Suppression and Diffusion-Weighted MRI. *Eur Radiol* (2018) 28:582–91. doi: 10.1007/s00330-017-5005-7
34. Guo Q, Dong Z, Zhang L, Ning C, Li Z, Wang D, et al. Ultrasound Features of Breast Cancer for Predicting Axillary Lymph Node Metastasis. *J Ultrasound Med* (2018) 37:1354–3. doi: 10.1002/jum.14469
35. Tan H, Gan F, Wu Y, Zhou J, Tian J, Lin Y, et al. Preoperative Prediction of Axillary Lymph Node Metastasis in Breast Carcinoma Using Radiomics Features Based on the Fat-Suppressed T2 Sequence. *Acad Radiol* (2020) 27:1217–25. doi: 10.1016/j.acra.2019.11.004
36. Gentilini O, Veronesi U. Abandoning Sentinel Lymph Node Biopsy in Early Breast Cancer? A New Trial in Progress At the European Institute of Oncology

of Milan (Sound: Sentinel Node vs Observation After Axillary Ultrasound). *Breast* (2012) 21:678–81. doi: 10.1016/j.breast.2012.06.013
37. Kondo T, Hayashi N, Ohde S, Suzuki K, Yoshida A, Yagata H, et al. A Model to Predict Upstaging to Invasive Carcinoma in Patients Preoperatively Diagnosed With Ductal Carcinoma in Situ of the Breast. *J Surg Oncol* (2015) 112:476–80. doi: 10.1002/jso.24037
38. Wang K, Zhang X, Zheng K, Yin XD, Xing L, Zhang AJ, et al. Predictors of Internal Mammary Lymph Nodes (IMLN) Metastasis and Disease-Free Survival Comparison Between IMLN-positive and IMLN-negative Breast Cancer Patients: Results From Western China Clinical Cooperation Group (WCCCG) Database (CONSORT). *Med (Baltimore)* (2018) 97:e11296. doi: 10.1097/MD.0000000000011296
39. Jin X, Jiang YZ, Chen S, Shao ZM, Di GH. A Nomogram for Predicting the Pathological Response of Axillary Lymph Node Metastasis in Breast Cancer Patients. *Sci Rep* (2016) 6:32585. doi: 10.1038/srep32585
40. Liu C, Zhao Z, Gu X, Sun L, Chen G, Zhang H, et al. Establishment and Verification of a Bagged-Trees-Based Model for Prediction of Sentinel Lymph Node Metastasis for Early Breast Cancer Patients. *Front Oncol* (2019) 9:282. doi: 10.3389/fonc.2019.00282
41. Venkatesan A, Chu P, Kerlikowske K, Sickles EA, Smith-Bindman R. Positive Predictive Value of Specific Mammographic Findings According to Reader and Patient Variables. *Radiology* (2009) 250:648–57. doi: 10.1148/radiol.2503080541
42. Nagashima T, Hashimoto H, Oshida K, Nakano S, Tanabe N, Nikaido T, et al. Ultrasound Demonstration of Mammographically Detected Microcalcifications in Patients With Ductal Carcinoma in Situ of the Breast. *Breast Cancer* (2005) 12:216–20. doi: 10.2325/jbcs.12.216
43. James JJ, Evans AJ, Pinder SE, Macmillan RD, Wilson AR, Ellis IO. Is the Presence of Mammographic Comedo Calcification Really a Prognostic Factor for Small Screen-Detected Invasive Breast Cancers. *Clin Radiol* (2003) 58:54–62. doi: 10.1053/crad.2002.1110
44. Tabar L, Tony Chen HH, Amy Yen MF, Tot T, Tung TH, Chen LS, et al. Mammographic Tumor Features can Predict Long-Term Outcomes Reliably in Women With 1-14-mm Invasive Breast Carcinoma. *Cancer* (2004) 101:1745–59. doi: 10.1002/cncr.20582
45. Shin HJ, Kim HH, Huh MO, Kim MJ, Yi A, Kim H, et al. Correlation Between Mammographic and Sonographic Findings and Prognostic Factors in Patients With Node-Negative Invasive Breast Cancer. *Br J Radiol* (2011) 84:19–30. doi: 10.1259/bjr/92960562
46. Månsson E, Bergkvist L, Christenson G, Persson C, Wärnberg F. Mammographic Casting-Type Calcifications is Not a Prognostic Factor in Unifocal Small Invasive Breast Cancer: A Population-Based Retrospective Cohort Study. *J Surg Oncol* (2009) 100:670–4. doi: 10.1002/jso.21405
47. Tamaki K, Ishida T, Miyashita M, Amari M, Ohuchi N, Tamaki N, et al. Correlation Between Mammographic Findings and Corresponding Histopathology: Potential Predictors for Biological Characteristics of Breast Diseases. *Cancer Sci* (2011) 102:2179–85. doi: 10.1111/j.1349-7006.2011.02088.x
48. Chen MT, Sun HF, Zhao Y, Fu WY, Yang LP, Gao SP, et al. Comparison of Patterns and Prognosis Among Distant Metastatic Breast Cancer Patients by Age Groups: A SEER Population-Based Analysis. *Sci Rep* (2017) 7:9254. doi: 10.1038/s41598-017-10166-8
49. Rossi L, Mazzara C, Pagani O. Diagnosis and Treatment of Breast Cancer in Young Women. *Curr Treat Options Oncol* (2019) 20:86. doi: 10.1007/s11864-019-0685-7
50. Wang R, Zhu Y, Liu X, Liao X, He J, Niu L. The Clinicopathological Features and Survival Outcomes of Patients With Different Metastatic Sites in Stage IV Breast Cancer. *BMC Cancer* (2019) 19:1091. doi: 10.1186/s12885-019-6311-z
51. Shoemaker ML, White MC, Wu M, Weir HK, Romieu I. Differences in Breast Cancer Incidence Among Young Women Aged 20-49 Years by Stage and Tumor Characteristics, Age, Race, and Ethnicity, 2004-2013. *Breast Cancer Res Treat* (2018) 169:595–606. doi: 10.1007/s10549-018-4699-9
52. Radecka B, Litwiniuk M. Breast Cancer in Young Women. *Ginekol Pol* (2016) 87:659–63. doi: 10.5603/GP.2016.0062
53. Lee HB, Han W. Unique Features of Young Age Breast Cancer and its Management. *J Breast Cancer* (2014) 17:301–7. doi: 10.4048/jbc.2014.17.4.301
54. Reyna C, Lee MC. Breast Cancer in Young Women: Special Considerations in Multidisciplinary Care. *J Multidiscip Healthc* (2014) 7:419–29. doi: 10.2147/JMDH.S49994
55. Kroman N, Jensen MB, Wohlfahrt J, Mouridsen HT, Andersen PK, Melbye M. Factors Influencing the Effect of Age on Prognosis in Breast Cancer: Population Based Study. *BMJ* (2000) 320:474–8. doi: 10.1136/bmj.320.7233.474
56. Copson ER, Cutress RI, Maishman T, Eccles BK, Gerty S, Stanton L, et al. Obesity and the Outcome of Young Breast Cancer Patients in the UK: The POSH Study. *Ann Oncol* (2015) 26:101–12. doi: 10.1093/annonc/mdu509
57. Calle EE, Rodriguez C, Walker-Thurmond K, Thun MJ. Overweight, Obesity, and Mortality From Cancer in a Prospectively Studied Cohort of U.s. *Adults N Engl J Med* (2003) 348:1625–38. doi: 10.1056/NEJMoa021423
58. Wang J, Cai Y, Yu F, Ping Z, Liu L. Body Mass Index Increases the Lymph Node Metastasis Risk of Breast Cancer: A Dose-Response Meta-Analysis With 52904 Subjects From 20 Cohort Studies. *BMC Cancer* (2020) 20:601. doi: 10.1186/s12885-020-07064-0
59. Picon-Ruiz M, Morata-Tarifa C, Valle-Goffin JJ, Friedman ER, Slingerland JM. Obesity and Adverse Breast Cancer Risk and Outcome: Mechanistic Insights and Strategies for Intervention. *CA Cancer J Clin* (2017) 67:378–97. doi: 10.3322/caac.21405
60. Gerdes J, Schwab U, Lemke H, Stein H. Production of a Mouse Monoclonal Antibody Reactive With a Human Nuclear Antigen Associated With Cell Proliferation. *Int J Cancer* (1983) 31:13–20. doi: 10.1002/ijc.2910310104
61. Ono M, Tsuda H, Yunokawa M, Yonemori K, Shimizu C, Tamura K, et al. Prognostic Impact of Ki-67 Labeling Indices With 3 Different Cutoff Values, Histological Grade, and Nuclear Grade in Hormone-Receptor-Positive, HER2-negative, Node-Negative Invasive Breast Cancers. *Breast Cancer* (2015) 22:141–52. doi: 10.1007/s12282-013-0464-4

Conflict of Interest: The authors declare that the research was conducted in the absence of any commercial or financial relationships that could be construed as a potential conflict of interest.

frontiers in Oncology

REVIEW
published: 17 June 2021
doi: 10.3389/fonc.2021.643155

Role of the Combination of Cyclin-Dependent Kinase Inhibitors (CDKI) and Radiotherapy (RT) in the Treatment of Metastatic Breast Cancer (MBC): Advantages and Risks in Clinical Practice

*Ambrogio Gagliano, Angela Prestifilippo, Ornella Cantale, Gianluca Ferini, Giacomo Fisichella, Paolo Fontana, Dorotea Sciacca and Dario Giuffrida**

Department of Medical Oncology, The Mediterranean Institute of Oncology, Viagrande, Italy

OPEN ACCESS

Edited by:
San-Gang Wu, First Affiliated Hospital of Xiamen University, China

Reviewed by:
Miguel J. Gil Gil, Catalan Institute of Oncology, Spain
Zhou Zhu, Pfizer, United States

***Correspondence:**
Dario Giuffrida
dario.giuffrida@grupposamed.com

Specialty section:
This article was submitted to Women's Cancer, a section of the journal Frontiers in Oncology

Received: *17 December 2020*
Accepted: *07 May 2021*
Published: *17 June 2021*

Citation:
Gagliano A, Prestifilippo A, Cantale O, Ferini G, Fisichella G, Fontana P, Sciacca D and Giuffrida D (2021) Role of the Combination of Cyclin-Dependent Kinase Inhibitors (CDKI) and Radiotherapy (RT) in the Treatment of Metastatic Breast Cancer (MBC): Advantages and Risks in Clinical Practice. Front. Oncol. 11:643155. doi: 10.3389/fonc.2021.643155

Targeting cell cycle has become the gold standard for metastatic breast cancer (MBC), being cyclin-dependent kinase inhibitors (CDKIs) cornerstones of its treatment, alongside radiotherapy (RT). To date, no definite evidence regarding safety and efficacy of the combination of CDKIs plus radiotherapy (RT) is currently available. Purpose of this review is to collect data in favor or against the feasibility of the association of CDKIs + RT, describing its potential adverse events. Our review shows how CDKI + RT allows an overall satisfying disease control, proving to be effective and causing a grade of toxicity mainly influenced by the site of irradiation, leaning to favourable outcomes for sites as liver, spine or brain and to poorer outcomes for thoracic lesions or sites close to viscera; controversial evidence is instead for bone treatment. Toxicity also varies from patient to patient. To sum up, our contribution enriches and enlightens a still indefinite field regarding the feasibility of CDKIs + RT, giving cues for innovative clinical management of hormone-responsive MBC.

Keywords: metastatic breast cancer (mbc), cyclin-dependent kinase inhibitors (CDKi), palbociclib, radiotherapy, toxicity, ribociclib, abemaciclib

INTRODUCTION

Up-to-date therapy of hormone-responsive metastatic breast cancer (MBC) is mainly based on cyclin-dependent kinase inhibitors (CDKI), nowadays considered cornerstones of its treatment. Examples of such agents are palbociclib, ribociclib and abemaciclib. These drugs CDKIs have been approved through three pivotal trials, namely PALOMA, MONALEESA and MONARCH for palbociclib, ribociclib, and abemaciclib, respectively. The main characteristics of such approving studies are summarized in **Supplementary Table 1** (1, 2), **Supplementary Table 2** (3, 4) and **Supplementary Table 3** (5, 6). CDKIs mechanism of action consists of the blockage of cyclin-dependent kinases 4 and 6, allowing the activation of RB oncosuppressor, thus halting tumor cell

cycle in phase G1; main features regarding targets, use and toxicities recorded in a pivotal trial of theirs, are shown in **Supplementary Table 4** (1–3, 5, 7–15).

CDKIs, as **Supplementary Tables** show, are associated to endocrine therapy (ET) as best standard therapy for MBC HR+/HER2−, without visceral crisis or substantial organ impairment. Indeed, ET + CDKI provides better survival than ChT, with better RR than ChT, lesser toxicities and higher quality of life. Aromatase Inhibitors (AI) are currently preferred to tamoxifen as first line therapy in post-menopausal women, showing better TTP/PFS. OS was not proved to be higher than tamoxifen though. Recently, fulvestrant resulted more efficient than AIs as first line therapy in patients who did not receive any line of therapy. The combination of AI + CDKI showed higher efficacy than AI alone for hormone-sensitive patients. As second line therapy, for those who already received AI, CDKI + fulvestrant combination therapy showed better results than ET alone (16).

All the above given, no definite evidence regarding safety and efficacy of the combination of CDKIs plus radiotherapy (RT) is currently available. For instance, PALOMA trial encountered in the first place the issue of combining palliative RT with CDKIs: it was here indicated to suspend palbociclib from the day prior to RT to the seventh day following RT. Our purpose is to review available literature to collect data in favor or against the feasibility of the combination of CDKIs + RT, evaluating its efficacy and describing its potential toxicity.

METHODS

This review is based on clinical records collected across several cancer centers with scope of assessing possible advantages or disadvantages of CDKI + RT combination therapy. To select the relevant papers for the analysis, we performed a literature search on PubMed, updated until year 2020, with the following keywords: "RT + Palbociclib + metastatic breast cancer"; "RT + CDKI + metastatic breast cancer". Overall, two letters to the editor, one review, five retrospective analyses and three case reports were selected and reviewed.

RESULTS

In all PALOMA studies patients who had bone lesions at the time of their enrolment benefited from palliative RT to improve pain, stopping palbociclib from the day prior to RT to the seventh day following RT. Patients who received such treatment were one in PALOMA 1, 16 in PALOMA 2 and nine in PALOMA 3 trials. Following the above-mentioned scheme, the time windows of the two treatments did not overlap ever, so no data were reported describing the interaction of Palbociclib + RT. Toxicities reported in literature hereby reviewed, are listed in **Table 1** below.

The analysis conducted by Hans et al. (17) explored the interaction of palbociclib + fulvestrant + RT in five patients with MBC, whose median age was 57.2. RT was here used to control pain and compression symptoms. Four patients received a dose of 20 Gy in five fractions to treat bone metastases, one patient underwent radiosurgery, receiving a dose of 60 Gy in 10 fractions for the treatment of liver metastases. All five patients obtained a symptoms control, and no significant skin toxicity was reported. Two patients developed grade 1/2 mucositis, two developed grade 3 neutropenia, one grade 3 anemia, and two grade 3 thrombocytopenia.

Another study was conducted by Kalash et al. (18) on three patients with MBC who received palbociclib + letrozole + RT. Two patients received RT on lung and one on chest wall. All three patients developed a severe pulmonary fibrosis. In addition, patients who received RT on lung developed a severe corticosteroid-resistant radiation pneumonia. Noteworthy, toxicity remitted after palbociclib suspension.

Kawamoto et al. (19) published a case report of a 58-year old woman with MBC and bone lesions who received palbociclib + RT combination therapy. The patient received palbociclib 100 mg every day for three weeks with one week stop and fulvestrant 500 mg every 14 days for the first three administrations, then every 4 weeks; subsequently, she received palbociclib and RT (30 Gy in 10 fractions) addressed to treat metastases on the iliac bone and on the first sacral vertebra. Reported adverse events were an episode of grade 1 diarrhea, left abdominal pain, swelling and bloody stool 3 days after last RT fraction. A CT scan and colonoscopy allowed to identify a radio-induced enterocolitis, responsive to a 3-week conservative management.

A further study addressed at evaluating the effects of CDKI + RT was conducted by Figura et al. (20) in patients with hormone-responsive MBC and brain metastases (BMs). The primary end point was brain toxicity during or after stereotactic RT, while control over BMs and overall survival (OS) were secondary end points. The final sample consisted of 15 patients, 10 treated with palbociclib and five with abemaciclib. Overall, 42 BMs were treated, 18 concurrently with CDKI, nine before and 15 afterwards, with a 9-month follow-up after stereotactic RT. Results showed that the combination of CDKI + cranial RT was well tolerated and effective in controlling BMs, displaying a survival benefit compared to conventional therapies.

In a study conducted by Ippolito et al. (21), a sample of 16 patients with hormone-responsive MBC was examined, 13 treated with palbociclib and three with ribociclib. RT treatment was administered to all of them, mainly with scope of palliation to bone disease, exception made for five patients who received RT at higher doses for local control of the lesion. Toxicities were mainly hematological, with neutropenia occurring the most: 12.5% of patients developed grade 2, 25% grade 3, and 6.3% grade 4 neutropenia. This study showed that the combination therapy seems to be safe, since adverse events consequent to either CDKI + RT or CDKI monotherapy were similar. Furthermore, it is of paramount importance to keep track of each patient's history of adverse events, so to approach them appropriately in case of recurrence. In conclusion, since toxicities were mostly handled successfully, treatment was not modified.

Messer et al. (22), presented a case report of a woman with MBC who received RT on a metastatic supraclavicular lymph

TABLE 1 | Main studies regarding CDKIs + RT interaction.

Reference study design	No. of patients	Combination therapy	RT dose fraction and target	Type of toxicity	G1	G2	G3	G4
Hans et al., Radiother. Oncol (17).; Letter to the editor	5	Palbociclib + fulvestrant + RT	four backbone: **20 Gy/5** one liver: **60 Gy/10**	Mucositis Neutropenia Anemia Thrombocytopenia	1	1	 2 1 2	
Kalash et al., Int J Radiat Oncol Biol Phys (18); Review	3	Palbociclib + letrozole + RT	two lung (dose missing) one liver (dose missing)	two Irradiation pneumonitis three Pulmonary fibrosis				
Kawamoto et al., Radiother. Oncol (19).; Letter to the editor	1	Palbociclib + fulvestrant + RT	Left iliac bone First sacral vertebra **30 Gy/10**	Diarrhea (during RT) Bloody diarrhea, bloating, abdominal pain (after RT)	1			
Figura et al., J. Neurooncol (20).; Retrospective analysis	15	10 Palbociclib + RT 5 Abemaciclib + RT	42 Brain mets **Median dose: 21 Gy (18–30 Gy)** 5: **18 Gy/1** 9: **20 Gy/1** 8: **21 Gy/1** 4: **24 Gy/1** 3: **20 Gy/5** 8: **25 Gy/5** 5: **30 Gy/5**	-				
Ippolito et al., Breast (21); Retrospective analysis	16	13 Palbociclib + RT 3 Ribociclib + RT	68.7% patients have bone mets **(median dose: 30 Gy [8–36])** 31.2% patients have other site mets **(median dose: 50 Gy [39.6–60])**	Neutropenia		2	4	1
Messer et al., Reports Pract. Oncol. Radiother (22).; Case report	1	Palbociclib + fulvestrant + RT	Supraclavicular metastatic node **(60 Gy/30)**	Esophagitis Dermatitis				
Chowdhary et al., Adv. Radiat. Oncol (23).; Retrospective analysis	16	Palbociclib + letrozole (10)/ fulvestrant (6) + RT	11 Back bone four Pelvis three Extremities (16/18 bone mets: **30–37.5 Gy/10–15**; 1/18 bone mets: **18 Gy/1**; 1/18 bone mets: **30 Gy/3**) four Brain **(30–35 Gy/10–14** for WBRT; **25 Gy/5** for fSRS) Mediastinum: **36 Gy/18 fractions**	Leucopenia Neutropenia Thrombocytopenia	8 5 4	1 1		
Guerini et al., Sci. Rep (24).; Retrospective analysis	18	9 Palbociclib + RT 6 Ribociclib + RT 3 Abemaciclib + RT + letrozole (8/18)/fulvestrant (10/18)	32 bone mets: 13/32: **30 Gy/10** 12/32: **20 Gy/5** 5/32: **8 Gy/1** 2/32: **30 Gy/3**	Ileitis Neutropenia			1 11	
Ratosa et al., Clin. Breast Cancer (25); Retrospective analysis	46	30 Palbociclib + RT 15 Ribociclib + RT 1 Abemaciclib + RT	50 Bone mets seven Visceral mets three Brain mets two Primary breast tumours **(median dose: 20 Gy [8–63]/5 [1–28])**	–				
Dasgupta et al., J. Med. Radiat. Sci (26).; Case report	1	Palbociclib + letrozole + RT	Left pelvis and femur **30 Gy/10**	Pancolitis				

(Continued)

TABLE 1 | Continued

Reference study design	No. of patients	Combination therapy	RT dose fraction and target	Type of toxicity	G1	G2	G3	G4
Nasir et al., Anticancer Res (27).; Case report	1	Palbociclib + letrozole + RT	10th thoracic vertebra (T10): **2 Gy/5** Right iliac crest: **2 Gy/5**	Esophagitis				
Meattini et al., The Breast (28)	5	Ribociclib + letrozole + RT	Bone (8) and visceral (2 lung, 1 liver) mets five bone mets: 4/5: 20 Gy/5 1/5: 30 Gy/5	Neutropenia Diarrhea + Vomiting				1 1
Total No. 128			**RT localization** **Total 199** Bone mets 101 Liver mets 2 Lung mets 4 Brain mets 49 Primary breast tumors 2 Other (unknown site) 41	**Type of toxicity** Mucositis 2 Neutropenia 26 Anemia 1 Leucopenia 9 Thrombocytopenia 6 Diarrhea 1 Irradiation pneumonitis 2 Pulmonary fibrosis 3 Esophagitis 2 Dermatitis 1 Ileitis 1	**G1** 1 5 8 4	**G2** 1 3 1 	**G3** 18 1 2 1	**G4**

CDKI, Cycline-Dependent Kinase Inhibitor; Gy, Gray; MBC, Metastatic Breast Cancer; Mets, Metastases; No., Number; RTm Radiotherapy.
Bold values regard radiotherapy and display erogated dose fraction and median dose fraction.

node with a total dose of 60 Gy in 30 fractions during palbociclib treatment. The patient reported early and severe side effects, such as esophagitis and dermatitis, heavily harming the left neck and requiring hospitalization. Therefore, palbociclib was suspended and RT completed, obtaining control over the neoplastic node. This study strongly underpins the importance of patients' assessment prior to palbociclib + RT combination therapy, with timely treatment suspension where needed.

6A retrospective study conducted by Chowdhary et al. (23) collected cases ranging from 2015 to 2018 and evaluated the efficacy and toxicity of palbociclib + RT combination therapy. Overall, 16 patients were examined, four received palbociclib before RT, five concurrently and seven afterwards, for bone lesions (11 axial skeleton, four pelvis, three limbs), BMs (three whole brain RT and one stereotactic radiosurgery), and mediastinal lesions, respectively. It succeeded in relieving pain in every patient and detected adverse events were mainly haematological. Authors reported four cases of leukopenia, five of neutropenia and one of thrombocytopenia prior to RT, and five cases of leukopenia, one of neutropenia and three of thrombocytopenia after RT. Two grade 2 cases aside, all haematological toxicities were mainly grade 1. No grade 2 dermatological, neurological or gastrointestinal toxicities were notified, either in acute or afterwards. No differences were found based on either the timing of palbociclib + RT administration, or the number and anatomical site of irradiated lesions.

A recent retrospective study published by Guerini et al. (24) analyzed a group of patients with MBC treated with CDKI + RT. Toxicities were measured according to the Common Terminology Criteria for Adverse Events (CTCAE) 4.0, whilst local response was measured according to RECIST 1.1 or PERCIST 1.0, and pain control using a verbal numerical scale. Enrolled patients were 18, with 32 treated sites: they received palbociclib (50%) ribociclib (33.3%) and abemaciclib (16.7%). Acute non-haematological toxicity was not significant, exception made for a grade 3 ileitis. During the third month following RT, 61.1% of patients developed grade 3/4 neutropenia; however, no patient required permanent discontinuation of treatment. Pain control was fully achieved in 88.2% of patients three months after RT; 94.4% of patients obtained and maintained local disease control.

Another retrospective study was recently published by Ratosa et al. (25). On a sample of 46 patients with MBC treated with CDKI + RT, 30 receiving palbociclib, 15 ribociclib and one abemaciclib, with a total number of 62 sites treated with RT, for 50 bone lesions, seven visceral metastases, three BMs and two primary breast tumors. Overall, grade 3 or higher adverse events rates were 6.5% prior to RT, 4.3% during RT, 15.2% at 2nd week and 23.9% at 6th week after RT.

A case report presented by Dasgupta et al. (26) described a 77-year-old woman with hormone-dependent MBC treated with palbociclib and palliative RT on left pelvis and femur. Five days after RT, she developed pancolitis which required hospitalization.

Another case report was recently published by Nasir et al. (27) describing the visceral toxicity of CDKI + RT association. A 63-year-old patient receiving palbociclib and RT developed

odynophagia and dysphagia due to the presence of grade 2/3 esophageal ulcers. Symptoms improved after discontinuation of the association, allowing the patient to continue palbociclib therapy.

In 2018, Meattini et al. (28) published preliminary data regarding five patients suffering from MBC treated with ribociclib plus letrozole and concomitant palliative RT as first-line treatment. Three patients had both bone and visceral disease and two patients had bone disease only. RT was never interrupted, and the palliative intent was achieved. Letrozole was also not suspended. Ribociclib was discontinued for two weeks in two cases: firstly, a G3-G4 neutropenia and secondly, a case of G3-G4 diarrhea and vomiting. At 3-month follow up, three stable disease and two partial response were observed, showing encouraging results regarding the combination of ribociclib, letrozole and RT.

In 2020, Meattini et al. (29) published a retrospective analysis, in form of abstract, of direct administration of RT to metastases in combination with first or second-line treatment with CDKIs for MBC.

The study involved 85 consecutive patients treated with CDKI between 2017 and 2019, 22 of these received ribociclib and 63 palbociclib. Overall, 29.4% of patients (n = 25) received metastases-directed RT during CDKI administration: specifically, 16.5% (n = 14) were treated concurrently, 12.9% (n = 11) subsequently.

The main endpoints of the analysis were the impact of RT on CDKI treatment, such as dose reduction or discontinuation, adverse events of any grade plus grade ≥2, and grade ≥2 neutropenia according to CTCAE (Common Terminology Criteria for Adverse Events) scale version 5.0.

Finally, they observed that metastases-directed RT did not cause dose reduction or discontinuation of CDKI, as proved by the stationary rate of adverse events: indeed, there was no difference in terms of CDKI dose reduction or treatment discontinuation, toxicity of any grade or grade ≥2, neutropenia grade ≥2 between patients receiving RT vs. no RT and between groups receiving concomitant RT vs. sequential RT vs. no RT.

DISCUSSION

As previously mentioned, PALOMA trials in the first place encountered the issue of combining palliative RT with CDKIs. In this instance, it was indicated to suspend palbociclib from the day prior to RT to the seventh day following RT, as authors recommend doing for other CDKI agents too. According to **Table 1**, it is possible to compare grade 1/2 toxicities to grade 3/4 toxicities; two mucositis all fall in grade 1/2 events; 26 neutropenia fall mainly instead in the grade 3/4 category (18), than in the grade 1/2 category (8); a reported anemia event was of grade 3; nine cases of leukopenia are all of grade 1/2; among six cases of thrombocytopenia, four were grade 1/2, two grade 3; the only reported ileitis was of grade 3; overall, among 45 overall cases of reported degree toxicities, 22 were of grade 3/4 (18 (82%) of them were all represented by neutropenia events), while 23 were of grade 1/2.

First off, an evidence emerging from this analysis concerns the not yet clarified correlation between anatomical site of treated lesions and toxicity degree induced by CDKI + RT. Evidence in support is provided by the study conducted by Hans et al., highlighting satisfying symptoms control alongside low-grade blood toxicity and mild mucositis in MBC patients treated with CDKI + RT for spine or liver metastases. Conversely, as backed by Kalash et al., MBC patients treated alike, though for chest wall or lung lesions, suffered from severe adverse events, such as pulmonary fibrosis and radiation pneumonia, ultimately determining treatment suspension. Thoraco-pulmonary lesions seem to show higher risk of more severe adverse events than bone or liver localization when treated with RT. However, it still is contradictory whether RT treatment on bone lesions spares the patient severe toxicities: as described by Kawamoto et al. in their case report, where irradiation regarded the iliac bone involving part of the bowel, it caused diarrhea and acute radiation-induced enteritis. Similar considerations apply to the case report published by Dasgupta et al. on a 77-year-old woman who developed a severe pancolitis following RT to pelvis and femur in combination with palbociclib. The authors warn to record patient's gastrointestinal history and to adopt the best RT techniques to reduce the dose of radiation, thus minimizing any potential side effect.

Therefore, on one hand, RT seems safer on spine than on chest wall or lung; on the other hand, the site of targeted metastasis is crucially relevant: if it is close to viscera, such as bowels, side effects could be so severe that stopping the combination therapy might be mandatory. According to Figura et al, as far as palbociclib + RT on BMs is regarded, evidence shows that it is more effective in symptoms and disease control than palbociclib monotherapy, positively affecting the survival too and not causing any extra toxicity than palbociclib only. Increase in toxicity due to palbociclib + RT combination therapy was instead claimed by the case report of Messer et al., in which RT on superficial lesions determined esophagitis and acute dermatitis, requiring hospitalization. Same combination therapy was used in the case report of Nasir et al., which caused severe esophagitis with grade 2/3 ulcers, alongside odynophagia and dysphagia. In both cases treatments were suspended. From all the evidence above, it can be said that oncologists should be able to foresee and manage in advance any mucositis and dermatitis in case of administration of CDKI + RT combination therapy. The study conducted by Ippolito et al., underpins the relevance of assessing potential toxicities of palbociclib + RT association based on patient's personal history. Indeed, adverse events are highly associated to pre-treatment conditions and individual features, in both this regimen and palbociclib alone. Therefore, it is highly recommended for oncologists to predict and prevent toxicity before even combining a CDKI with RT. Latest retrospective analyses seem to confirm the efficacy and safety of CDKI + RT. For instance, the study conducted by Guerini et al., shows that the main adverse event was neutropenia; moreover grade 3/4 neutropenia rate was comparable to the one detected with CDKI monotherapy. The most interesting aspect concerns pain

improvement and disease local control. Data provided by the retrospective study conducted by Ratosa et al., highlighted the improvement of pain symptoms in an 80% of patients.

Finally, we found that several ongoing studies are focussed on proving the potential radiosensitizing effect of palbociclib, to make cancer cells more susceptible to RT. We here report the experimental study of a Spanish research team carrying out an analysis exploring palbociclib as a radiosensitizer on lung, colorectal and breast cancer cells (30). The results showed that wild type p53 is strictly needed for palbociclib to act as a radiosensitizer; oppositely, palbociclib loses any radiosensitizing efficacy when p53 is functionally blocked, reacquiring it when p53 is restored. These data provide cues for a more patient-tailored therapy, in which responders to CDKI + RT would only be those with a normally functioning p53 pathway (30).

CONCLUSIONS

According to collected data, it can be concluded that the combination of CDKI + RT allows an overall satisfying disease control, proving to be effective and causing a grade of toxicity influenced by some factors as the site of irradiation, leaning to favourable outcomes for sites as liver, spine or brain and to poorer outcomes for thoracic lesions or sites close to viscera; controversial evidence is instead for bone treatment. Toxicity also varies from patient to patient: in this context, the acknowledgment of toxicity and comorbidities history becomes of crucial importance. Therefore, according to our analysis we believe that the association of CDKI + RT might be effective and safe, and it is surely deserving more deepening through further analyses.

AUTHOR CONTRIBUTIONS

Conception and design: AG and AP. Administrative support: OC. Provision of study materials: AG, AP, GFe, GFi, PF, DS, and DG. Collection and assembly of data: AG and AP. Data interpretation: AG and OC. All authors contributed to the article and approved the submitted version.

SUPPLEMENTARY MATERIAL

The Supplementary Material for this article can be found online at: https://www.frontiersin.org/articles/10.3389/fonc.2021.643155/full#supplementary-material

REFERENCES

1. Rugo HS, Finn RS, Diéras V, Etti J, Lipatov O, Joy AA, et al. Palbociclib Plus Letrozole as First-Line Therapy in Estrogen Receptor-Positive/Human Epidermal Growth Factor Receptor 2-Negative Advanced Breast Cancer With Extended Follow-Up. *Breast Cancer Res Treat* (2019) 174(3):719–29. doi: 10.1007/s10549-018-05125-4
2. Loibl S, Turner NC, Ro J, Cristofanilli M, Iwata H, Ah Im S, et al. Palbociclib Combined With Fulvestrant in Premenopausal Women With Advanced Breast Cancer and Prior Progression on Endocrine Therapy: PALOMA-3 Results. *Oncologist* (2017) 22(9):1028–38. doi: 10.1634/theoncologist.2017-0072
3. Hortobagyi GN, Stemmer SM, Burris HA, Yap YS, Sonke GS, Paluch-Shimon S, et al. Updated Results From MONALEESA-2, a Phase III Trial of First-Line Ribociclib Plus Letrozole Versus Placebo Plus Letrozole in Hormone Receptor-Positive, HER2-negative Advanced Breast Cancer. *Ann Oncol* (2018) 29(7):1541–7. doi: 10.1093/annonc/mdy155
4. Tripathy D, Ah Im S, Colleoni M, Franke F, Bardia A, Harbeck N, et al. Ribociclib Plus Endocrine Therapy for Premenopausal Women With Hormone-Receptor-Positive, Advanced Breast Cancer (MONALEESA-7): A Randomised Phase 3 Trial. *Lancet Oncol* (2018) 19(7):904–15. doi: 10.1016/S1470-2045(18)30292-4
5. Sledge GWJr, Toi M, Neven P, Sohn J, Inoue K, Pivot X, et al. Monarch 2: Abemaciclib in Combination With Fulvestrant in Women With HR+/HER2- Advanced Breast Cancer Who had Progressed While Receiving Endocrine Therapy. *J Clin Oncol* (2017) 35(25):2875–84. doi: 10.1200/JCO.2017.73.7585
6. Goetz MP, Toi M, Campone M, Sohn J, Paluch-Shimon S, Huober J, et al. Monarch 3: Abemaciclib as Initial Therapy for Advanced Breast Cancer. *J Clin Oncol* (2017) 35(32):3638–46. doi: 10.1200/JCO.2017.75.6155
7. DeMichele A, Clark AS, Tan KS, Heitjan DF, Gramlich K, Gallagher M, et al. Cdk 4/6 Inhibitor Palbociclib (PD0332991) in Rb+ Advanced Breast Cancer: Phase Ii Activity, Safety and Predictive Biomarker Assessment. *Clin Cancer Res* (2015) 21:995–1001. doi: 10.1158/1078-0432
8. Hamilton E, Infante JR. Targeting CDK4/6 in Patients With Cancer. *Cancer Treat Rev* (2016) 45:129–38. doi: 10.1016/j.ctrv.2016.03.002
9. Costa R, Carneiro BA, Wainwright DA, Santa-Maria CA, Kumthekar P, Chae YK, et al. Developmental Therapeutics for Patients With Breast Cancer and Central Nervous System Metastasis: Current Landscape and Future Perspectives. *Ann Oncol* (2017) 28:44–56. doi: 10.1093/annonc/mdw532
10. Infante JR, Cassier PA, Gerecitano JF, Witteveen PO, Chugh R, Ribrag V, et al. Phase I Study of the Cyclin-Dependent Kinase 4/6 Inhibitor Ribociclib (LEE011) in Patients With Advanced Solid Tumors and Lymphomas. *Clin Cancer Res* (2016) 22:5696–705. doi: 10.1158/1078-0432.CCR-16-1248
11. Barroso-Sousa R, Shapiro GI, Tolaney SM. Clinical Development of the CDK4/6 Inhibitors Ribociclib and Abemaciclib in Breast Cancer. *Breast Care* (2016) 11:167–73. doi: 10.1159/000447284
12. Dickler MN, Tolaney SM, Rugo HS, Cortés J, Diéras V, Patt D, et al. Correction: MONARCH 1, A Phase II Study of Abemaciclib, a CDK4 and CDK6 Inhibitor, as a Single Agent, in Patients With Refractory Hr+/Her2- Metastatic Breast Cancer. *Clin Cancer Res* (2018). 24(21):5485. doi: 10.1158/1078-0432.CCR-18-3193
13. Slamon DJ, Neven P, Chia S, Fasching PA, De Laurentis M, Ah Im S, et al. Phase III Randomized Study of Ribociclib and Fulvestrant in Hormone Receptor-Positive, Human Epidermal Growth Factor Receptor 2-Negative Advanced Breast Cancer: Monaleesa-3. *J Clin Oncol* (2018) 36(24):2465–72. doi: 10.1200/JCO.2018.78.9909
14. Dickler MN, Tolaney SM, Rugo HS, Cortés J, Diéras V, Patt D, et al. Monarch 1, A Phase II Study of Abemaciclib, a CDK4 and CDK6 Inhibitor, as a Single Agent, in Patients With Refractory Hr +/Her2 - Metastatic Breast Cancer. *Clin Cancer Res* (2017) 23(17):5218–24. doi: 10.1158/1078-0432.CCR-17-0754
15. Finn RS, Martin M, Rugo HS, Jones S, Ah Im S, Gelmon K, et al. Palbociclib and Letrozole in Advanced Breast Cancer. *N Engl J Med* (2016) 375(20):1925–1936. doi: 10.1056/NEJMoa1607303
16. Gori S, Dieci MV, Biganzoli L, Calabrese M, Cortesi L, Criscitiello C, et al. Linee Guida AIOM 2020 Neoplasie della Mammella. (aggiornato 30 Ottobre 2020).
17. Hans S, Cottu P, Kirova YM. Preliminary Results of the Association of Palbociclib and Radiotherapy in Metastatic Breast Cancer Patients. *Radiother Oncol* (2018) 126(1):181. doi: 10.1016/j.radonc.2017.09.010

18. Kalash R, Iarrobino NA, Beriwal S, Sun M, Glaser SM, Champ CE, et al. Palbociclib Enhances Pulmonary Fibrosis in Patients Undergoing Thoracic Radiation Therapy: A Case Series and Review of the Literature. *Int J Radiat Oncol* (2018) 102:e610. doi: 10.1016/j.ijrobp.2018.07.1673
19. Kawamoto T, Shikama N, Sasai K. Severe Acute Radiation-Induced Enterocolitis After Combined Palbociclib and Palliative Radiotherapy Treatment. *Radiother Oncol* (2019) 131:240–1. doi: 10.1016/j.radonc.2018.09.020
20. Figura NB, Potluri TK, Mohammadi H, Oliver DE, Arrington JA, Robinson TJ, et al. CDK 4/6 Inhibitors and Stereotactic Radiation in the Management of Hormone Receptor Positive Breast Cancer Brain Metastases. *J Neurooncol* (2019) 144:583–9. doi: 10.1007/s11060-019-03260-6
21. Ippolito E, Greco C, Silipigni S, Dell'Aquila E, Petrianni GM, Tonini G, et al. Concurrent Radiotherapy With Palbociclib or Ribociclib for Metastatic Breast Cancer Patients: Preliminary Assessment of Toxicity. *Breast* (2019) 46:70–4. doi: 10.1016/j.breast.2019.05.001
22. Messer JA, Ekinci E, Patel TA, Teh BS. Enhanced Dermatologic Toxicity Following Concurrent Treatment With Palbociclib and Radiation Therapy: A Case Report. *Rep Pract Oncol Radiother* (2019) 24:276–80. doi: 10.1016/j.rpor.2019.03.001
23. Chowdhary M, Sen N, Chowdhary A, Usha L, Cobleigh MA, Wang D, et al. Safety and Efficacy of Palbociclib and Radiation Therapy in Patients With Metastatic Breast Cancer: Initial Results of a Novel Combination. *Adv Radiat Oncol* (2020) 4:453–7. doi: 10.1016/j.adro.2019.03.011
24. Guerini AE, Pedretti S, Salah E, Simoncini EL, Maddalo M, Pegurri L, et al. A Single-Center Retrospective Safety Analysis of Cyclin-Dependent Kinase 4/6 Inhibitors Concurrent With Radiation Therapy in Metastatic Breast Cancer Patients. *Sci Rep* (2020) 10(1):13589. doi: 10.1038/s41598-020-70430-2
25. Ratosa I, Orazem M, Scoccimarro E, Steinacher M, Dominici L, Aquilano M, et al. Cyclin-Dependent Kinase 4/6 Inhibitors Combined With Radiotherapy for Patients With Metastatic Breast Cancer. *Clin Breast Cancer* (2020) 20:495–502. doi: 10.1016/j.clbc.2020.05.013
26. Dasgupta A, Sahgal A, Warner E, Czarnota GJ. Safety of Palbociclib Concurrent With Palliative Pelvic Radiotherapy: Discussion of a Case of Increased Toxicity and Brief Review of Literature. *J Med Radiat Sci* (2020) 68:96–102 doi: 10.1002/jmrs.435
27. Nasir UM, Mozeika AM, Sayan M, Jan I, Kowal N, Haffty B, et al. Severe Gastrointestinal Mucositis Following Concurrent Palbociclib and Palliative Radiation Therapy. *Anticancer Res* (2020) 40:5291–4. doi: 10.21873/anticanres.14534
28. Meattini I, Desideri I, Scotti V, Simontacchi G, Livi L. Ribociclib Plus Letrozole and Concomitant Palliative Radiotherapy for Metastatic Breast Cancer. *Breast* (2018) 42:1–2. doi: 10.1016/j.breast.2018.08.096
29. Meattini I, Scoccimarro E, Saieva C, Desideri I, Visani L, Dominici L. Impact of Metastases Directed Radiation Therapy on CDK4/6 Inhibitors Dose Reduction and Treatment Discontinuation for Metastatic HR+/HER2- Breast Cancer (MBC). *J Clin Oncol* (2020) 38:562–2. doi: 10.1200/JCO.2020.38.15_suppl.562
30. Fernández-Aroca DM, Roche O, Sabater S, Pascual-Serra R, Ortega-Muelas M, Sánchez Pérez I, et al. (2019). P53 Pathway is a Major Determinant in the Radiosensitizing Effect of Palbociclib: Implication in Cancer Therapy. *Cancer Lett* (2019) 451:23–33. doi: 10.1016/j.canlet.2019.02.049

Conflict of Interest: The authors declare that the research was conducted in the absence of any commercial or financial relationships that could be construed as a potential conflict of interest.

frontiers in Oncology

STUDY PROTOCOL
published: 25 June 2021
doi: 10.3389/fonc.2021.653370

INSTIGO Trial: Evaluation of a Plasma Protein Profile as a Predictive Biomarker for Metastatic Relapse of Triple Negative Breast Cancer

Hugo Veyssière[1,2,3]*, *Sejdi Lusho*[1,2,3], *Ioana Molnar*[1,2,3], *Myriam Kossai*[1,4], *Maureen Bernadach*[1,2], *Catherine Abrial*[1,2,3], *Yannick Bidet*[1,5†], *Nina Radosevic-Robin*[1,4†] *and Xavier Durando*[1,2,3†]

[1] Université Clermont Auvergne, INSERM UMR 1240 « Imagerie Moléculaire et Stratégies Théranostiques », Centre Jean PERRIN, Clermont-Ferrand, France, [2] Division de Recherche Clinique, Délégation Recherche Clinique & Innovation, Centre Jean PERRIN, Clermont-Ferrand, France, [3] Centre d'Investigation Clinique, UMR501, Clermont-Ferrand, France, [4] Département d'anatomie et de cytologie pathologiques, Centre Jean PERRIN, Clermont-Ferrand, France, [5] Département d'oncogénétique, Laboratoire d'Oncologie Moléculaire, Centre Jean PERRIN, Clermont-Ferrand, France

OPEN ACCESS

Edited by:
San-Gang Wu,
First Affiliated Hospital of Xiamen University, China

Reviewed by:
Charles Cox,
University of South Florida, United States
Juan Zhou,
Xiamen University, China

***Correspondence:**
Hugo Veyssière
hugo.veyssiere@clermont.unicancer.fr
orcid.org/0000-0003-2202-7362

†These authors have contributed equally to this work

Specialty section:
This article was submitted to Breast Cancer, a section of the journal Frontiers in Oncology

Received: 01 April 2021
Accepted: 09 June 2021
Published: 25 June 2021

Citation:
Veyssière H, Lusho S, Molnar I, Kossai M, Bernadach M, Abrial C, Bidet Y, Radosevic-Robin N and Durando X (2021) INSTIGO Trial: Evaluation of a Plasma Protein Profile as a Predictive Biomarker for Metastatic Relapse of Triple Negative Breast Cancer. Front. Oncol. 11:653370. doi: 10.3389/fonc.2021.653370

Background: Triple negative breast cancer (TNBC) accounts for 10-20% of breast cancers but has no specific therapy. While TNBC may be more sensitive to chemotherapy than other types of breast cancer, it has a poor prognosis. Most TNBC relapses occur during the five years following treatment, however predictive biomarkers of metastatic relapse are still lacking. High tumour-infiltrating lymphocytes (TILs) levels before and after neo-adjuvant chemotherapy (NAC) are associated with lower relapse risk and longer survival but TILs assessment is highly error-prone and still not introduced into the clinic. Therefore, having reliable biomarker of relapse, but easier to assess, remains essential for TNBC management. Searching for such biomarkers among serum/plasma proteins, circulating tumoral DNA (ctDNA) and blood cells appear relevant.

Methods: This single-centre and prospective study aims to discover predictive biomarkers of TNBC relapse and particularly focuses on plasma proteins. Blood samples will be taken at diagnosis, on the day of first-line or post-NAC surgery, on the day of radiotherapy start, then 6 months and one year after radiotherapy. A blood sample will be taken at the time of metastatic relapse diagnosis. Blood samples will be used for circulating protein quantification, blood cell counts and circulating tumour DNA quantification. A tumour RNA signature, based on the analysis of the RNA expression of 6 genes, will also be tested from the initial biopsy taken routinely. In NAC patients, TILs quantity will be assessed on TNBC pre-treatment biopsy and surgical specimen.

Ethics and Dissemination: INSTIGO belongs to category 2 interventional research on humans. This study has been approved by the SUD-EST IV ethics committee and is conducted in accordance with the Declaration of Helsinki and General Data Protection Regulation (GDPR). Study findings will be published in peer-reviewed medical journals.

Clinical Trial Registration: ClinicalTrials.gov, identifier NCT04438681.

Keywords: triple negative breast cancer, predictive biomarker, plasma proteins, metastatic relapse, ctDNA, TILs, RNA signature, blood cells

INTRODUCTION

Triple negative breast cancer accounts for approximately 10-20% of breast cancers and is characterized by the lack -or by very low - expression of oestrogen and progesterone receptors and the lack of amplification of the gene coding for HER2 (Human Epidermal Growth Factor Receptor 2) (1). TNBC has no specific therapy; chemotherapy, radiotherapy and surgery remain preferred modalities. While TNBC may be more sensitive to chemotherapy than other types of breast cancer, it has a poor prognosis due to its heterogeneity (2–4). Predictive biomarkers of metastatic relapse and type of relapse need to be discovered. Among these predictive biomarkers, it has been shown that a high level of TILs before and after NAC is associated with lower recurrence risk and longer recurrence-free survival (5, 6). However, TIL assessment is error-prone and subject to high inter-evaluator variability despite the existence of standardized recommendations (7, 8). It is also known that a complete pathological response to NAC is associated with a low risk of metastatic relapse in TNBC (9). The determination of biomarkers that are easily quantifiable at diagnosis is essential. The search for predictive biomarkers of metastatic progression among circulating molecules seems relevant (10, 11). It has been shown that high concentrations of proteins involved in inflammation, such as interleukins 6 and 8, or involved in angiogenesis, such as angiopoietin-like protein, are associated with a high risk of metastatic progression of breast cancer (12–14). In TNBC, high blood levels of transforming growth factor-β (TGF-β) and vascular endothelial growth factor-A (VEGF-A) are associated with a high risk of relapse (15). Circulating proteins assays are part of routine clinical testing and have a high sensitivity. Targeted analysis of the blood proteome (serum/plasma), using high throughput techniques such as multiplex ELISA, appears to be an interesting approach for the discovery of new biomarkers. In this context, we propose to conduct a study that measures the concentrations of a set of plasma proteins to evaluate their ability to predict metastatic relapse in patients with TNBC.

The interest in circulating biomarkers also leads us to focus on blood cells which are easily quantifiable and accessible. Blood cells and their ratios [Platelet-to-lymphocyte Ratio (PLR) and Neutrophil-to-lymphocyte Ratio (NLR)] are predictive and prognostic biomarkers of breast cancer (16, 17). In patients with TNBC, a high NLR, reflecting a weak immune response, is associated with a poor response to NAC and a poor survival (18, 19). In addition, plasma from cancer patients contains circulating tumoral DNA (ctDNA) carrying tumour mutations. ctDNA is proving to be another biomarker of interest to study. ctDNA levels make it possible to anticipate the response to treatment and to predict the risk of metastatic relapse (20, 21). They are also a predictive and prognostic biomarker in patients with metastatic breast cancer (22). Combining the characteristics of a plasma protein profile, blood cells levels (PLR, NLR) and ctDNA would provide information on the metastatic potential of a given tumour.

Finally, analyses of tumour RNA expression of a wide range of genes by PAM50 tests, EndoPredict tests, MammaPrint tests or even BluePrint tests allow clinicians to classify breast cancers into molecular subtypes, each corresponding to a specific prognosis and treatment proposal (23–27). However, no such tests exist for TNBCs. The validation of an RNA signature of triple negative breast tumours, established at the Centre Jean Perrin by the analysis of the RNA expression of 6 genes, could provide us an indication on the treatments to be preferred.

Abbreviations: ctDNA, circulating tumoral DNA; HER2, Human Epidermal Growth Factor Receptor 2; NAC, Neoadjuvant chemotherapy; NLR, Neutrophil-to-lymphocyte Ratio; PLR, Platelet-to-lymphocyte Ratio; TILs, Tumour infiltrating lymphocytes; TNBC, Triple negative breast cancer.

METHODS AND STUDY DESIGN

Study Design

This is a single-centre prospective trial designed to evaluate a plasma protein profile as a predictive biomarker for metastatic relapse of TNBC. The estimated duration of patients' enrolment is 3 years: 90 patients will be enrolled and followed from the patient inclusion until the first metastatic relapse or up to 5 years after the end of treatment if no relapse occurs. Study design is presented in **Figure 1**. TNBC patients will have blood samples taken at diagnosis, on the day of first-line surgery or post-NAC surgery, on the day of radiotherapy start, and 6 months and one year after the end of radiotherapy. Patients receiving neoadjuvant radiation will not be included in the trial. In case of recurrence, a blood sample will be taken at the time of diagnosis of metastatic relapse. Blood samples will be used for the quantification of plasma proteins, for the determination of blood cells and for the quantification of ctDNA. TILs rate evaluation will be performed on tumour tissue from the biopsy and from the operating specimen. The quantification of proteins will be done by multiplex ELISA. The identification of tumoral DNA mutations will be made from extracted DNA from tumour tissue from the operating specimen or from the biopsy. All coding regions, including exons borders and splicing sites, of the ten most frequently muted genes in breast tumours (including TP53, PTEN, PIK3CA, etc) will be captured from sample genomes. Then, targeted regions will be analysed by high throughput sequencing. Targeting several genes will ensure to discover at least one tumour-specific mutation. This mutation will later be quantified in peripheral blood samples. The RNA signature will be generated from transcripts extracted from tumour tissue from the surgical specimen or from the biopsy. A multiplex RT-qPCR will quantify the expression levels of the 6 genes of interest. The expression level of each gene will be multiplied by the corresponding coefficient in order to generate a prognostic score.

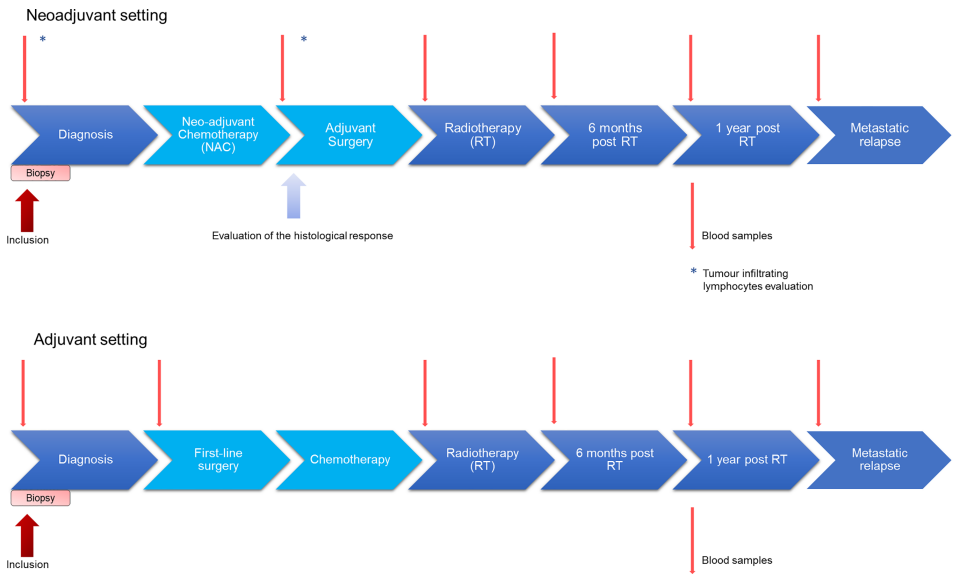

FIGURE 1 | Design of the INSTIGO study. Patients will have blood samples taken at diagnosis, on the day of first-line surgery or post-NAC surgery, on the day of the start of radiotherapy, and 6 months and one year after radiotherapy. If necessary, a blood sample will be taken at the time of diagnosis of metastatic relapse. Blood samples will be used for circulating proteins quantification, blood cells assay and circulating tumour DNA quantification. In neoadjuvant setting, TILs rate will be evaluated from tumour tissue from the biopsy and from the operating room.

Study Objectives

The primary objective of the INSTIGO trial is to discover a baseline plasma protein profile predictive of metastatic relapse in patients with TNBC (**Table 1**). It also aims to identify a plasma protein profile at different times during patient follow-up that could be predictive of metastatic relapse. Based on a review of the literature INSTIGO focuses on a specific group of proteins: Matrix metalloproteinase 9, tissue inhibitor of metalloproteinase 1, interleukin-6, interleukin-8, interleukin-10, programmed death-ligand 1, stromal cell-derived factor 1, GM-CSF, tyrosine kinase with immunoglobulin and epidermal growth factor-homology domains 2, TGF-β, VEGF-A, hepatocyte growth factor, fibroblast growth factor, CXCL5, CXCL12. Moreover, the INSTIGO study takes interest in others potential biomarkers such as ctDNA, blood cells, TILS, or tumour RNA expression (**Table 1**). Briefly, the objective is to evaluate the ability of those potential biomarkers to predict metastatic relapse in patients with triple-negative breast cancers.

Patient Selection

Inclusion and exclusion criteria are presented in **Table 2**. Briefly, women (18 years or older) with newly diagnosed, histologically proven and never treated primary triple negative breast cancer, and non-metastatic (M0) at diagnosis, will be included.

Recruitment and Consent

Eligible patients will be offered the opportunity to participate in the study by their oncologist or their surgeon. Patients who agree to participate in this study will provide written informed consent

TABLE 1 | Primary and secondary objectives.

Primary objective	• To discover a baseline plasma protein profile predictive of metastatic relapse in patients with TNBC
Secondary objectives	• To discover plasma protein profiles predictive of metastatic relapse in patients with TNBC, assessed at - the day of first surgery or post-CTNA surgery - the day of the radiotherapy start - 6 months and one year after radiotherapy • To study the relationship between the quantity of tumour infiltrating lymphocytes at diagnosis and metastatic relapse • To study the relationship between NLR and PLR and metastatic relapse, when those 2 parameters are assessed at - diagnosis - the day of first surgery or post-CTNA surgery • To study the relationship between plasma levels of circulating tumoral DNA and metastatic relapse - at diagnosis - at the day of first surgery or post-CTNA surgery - at the day of the start radiotherapy start - 6 months and one year after radiotherapy • To verify prognostic value of a baseline RNA signature
In neoadjuvant setting	• To identify a baseline plasma protein profile predictive of histological response to neoadjuvant chemotherapy (NAC) • To study the relationship between variation in protein concentration, between diagnosis and end of NAC, and histological response to NAC • To study the relationship between TIL quantity before and after NAC, as well as between the relationship between the baseline TIL level and the level of histological response to NAC • To study the relationship between the variation of the PLR and the NLR before and after NAC, as well as between the relationship between the baseline PLR and NLR levels and the level of histological response to NAC

TABLE 2 | Inclusion and non-inclusion criteria.

Inclusion criteria	• Female • Age ≥ 18 years • Newly diagnosed, histologically proven and never treated primary triple negative breast cancer, and non-metastatic (M0) at diagnosis • Speaking and understanding French • Affiliated to the French Social Security System • Able to give informed consent.
Non-inclusion criteria	• Patient deprived of liberty by court or administration decision • In neoadjuvant situation: neoadjuvant treatment by radiotherapy or hormone therapy • Refusal to participate to the study

for enrolment. Data obtained will be retained with consent, and any reasons given for withdrawal will be recorded. Participants can withdraw at any time.

Sample Size Calculation

Given the exploratory nature of the study, and the lack of sufficient data to provide hypotheses in order to perform sample size calculation, the objective is to recruit a maximum of patients. The recruitment capacity for this study is estimated at 90 patients (30 patients per year). An interim analysis at 30 patients will allow us to re-evaluate the recruitment capacity, and to assess the interest of extending the recruitment period, and to re-estimate the number of subjects needed in view of the amount of missing data and the variability of the protein data. A rough estimation allows us to evaluate that with a sample size of 90 patients we would obtain a 95% (Wilson's) confidence interval for the sensitivity of a 90% predictive score, with a precision of +/- 12%, assuming that the proportion of metastatic relapses at 5 years will be 1/3.

Data Collections

Data collected are the patient's age (month and year of birth), pathology, treatments received, response to NAC, clinical and molecular characteristics of the tumour on biopsy and surgical specimen and blood tests at diagnosis, on the day of the first-line surgery, before the start of radiotherapy, 6 months and 1 year after the end of radiotherapy and at the time of metastatic relapse. Data collected will be pseudonymized. Thus, study data will not contain any names or other personal identifiers such as addresses. Patients included in the trial will be identified by a code specific to this trial. The investigator will have access to the correspondence table between the patient's last name, first name, date of birth and the code assigned in the trial.

Statistical Analysis

Primary Analysis

The predictive plasma profile of metastatic relapse will be investigated using an approach based on the elastic-net method. Firstly, univariate analyses (Wilcoxon-Mann-Whitney tests with p-value correction for FDR control) will be performed to evaluate the relationship between the concentration of each protein and the occurrence of relapse. Then, a multivariate logistic regression model with elastic-net regularization will be constructed to allow an intrinsic selection of predictive variables (proteins). If necessary, a selection stabilization algorithm will also be applied. The results of the analysis will therefore be the set of predictive variables selected by the selected model, their regression coefficients, as well as an estimation of the model performance (with associated confidence intervals). However, in the absence of a test dataset the performance of the model can only be estimated by cross-validation.

Secondary Analysis

To identify a plasma protein profile that is predictive of metastatic relapse, the same approach as for the main objective will be used.

The relationship between TILs, NLR and PLR levels measured at different times, or ctDNA plasma levels and metastatic relapse will be studied by Wilcoxon-Mann-Whitney tests and logistic regressions. Mixed models will be used to account for repeated data.

The relationship between, on the one hand, the variation in protein concentration, the variation in TILs, or the variation in PLR and NLR levels, between diagnosis and end of NAC, and, on the other hand, the histological response to NAC, will be studied as in the previous point. These aspects are also concerned by an intermediate analysis on the first 30 patients.

An RNA signature predictive of metastatic relapse will be assessed by applying a previously constructed model on the data obtained in the INSTIGO study. The classical indices for the evaluation of a classification (sensitivity, specificity, and precision, among others) will be calculated.

Trial Status

As of this day 2 patients has been recruited in the INSTIGO trial. Participant recruitment began on 9th November 2020 and is expected to finish in November 2023. The approved protocol is version 15, 04/09/2020.

Patient and Public Involvement

Neither patients nor the public were involved in the design of this research.

Ethics and Dissemination

The INSTIGO trial has been approved by an ethics committee (SUD-EST IV – Léon Bérard) on September 2020 (ID-RCB number: 2020-A01423-36). It is conducted notably in accordance with the Declaration of Helsinki and General Data Protection Regulation (GDPR). Study data and finding will be published in peer-reviewed medical journals. We plan to present the study and all data at national congresses and conferences.

DISCUSSION

The discovery of new inexpensive and reliable biomarkers to predict treatment response and metastatic recurrence in TNBC patients remain an important medical need. Such biomarkers would allow oncologists to offer an alternative treatment to TNBC patients with a high risk of metastatic recurrence. During the last years, many proteins appeared to predict clinical behaviour and new biomarkers have been proposed to predict survival and response to chemotherapy in many cases. The INSTIGO trial explores a group of blood proteins expected

to be reliable biomarkers. Thus, this study would allow us to determine whether a group of plasma proteins can predict response to neo-adjuvant chemotherapy and metastatic relapse in TNBC. Proteins are easily quantifiable and accessible biomarkers that could be used routinely.

Moreover, as many studies have demonstrated, the strength of a liquid biopsy is based on the association of several biomarkers (20). Thus, in the long term, this study and the discovery of various biomarkers such as plasma proteins, ctDNA, and blood cells would help clinicians choosing the best adapted treatment to each patient. More interestingly, the association of these biomarkers could provide a more reliable and powerful composite biomarker in TNBC.

AUTHOR'S NOTE

The trial is managed by the Jean Perrin Centre, in Clermont-Ferrand, France.

ETHICS STATEMENT

This study has been approved by the SUD-EST IV ethics committee and is conducted in accordance with the Declaration of Helsinki and General Data Protection Regulation (GDPR).

AUTHOR CONTRIBUTIONS

HV, XD, SL, YB, NR-R, IM, CA, and MB participated in the developing and conception of the study, and drafted the manuscript. XD is the coordinator of the study. XD and MB are medical leads. IM is the statistical lead, designed and will perform statistical analyses. HV is the project manager of the study and is involved in aspects of the day-to-day running of the trial. HV wrote the first draft of this manuscript. All authors contributed to the article and approved the submitted version.

REFERENCES

1. Lee J, Kim D-M, Lee A. Prognostic Role and Clinical Association of Tumor-Infiltrating Lymphocyte, Programmed Death Ligand-1 Expression With Neutrophil-Lymphocyte Ratio in Locally Advanced Triple-Negative Breast Cancer. *Cancer Res Treat* (2019) 51:649–63. doi: 10.4143/crt.2018.270
2. Dent R, Trudeau M, Pritchard KI, Hanna WM, Kahn HK, Sawka CA, et al. Triple-Negative Breast Cancer: Clinical Features and Patterns of Recurrence. *Clin Cancer Res* (2007) 13:4429–34. doi: 10.1158/1078-0432.CCR-06-3045
3. Foulkes WD, Smith IE, Reis-Filho JS. Triple-Negative Breast Cancer. *N Engl J Med* (2010) 363:1938–48. doi: 10.1056/NEJMra1001389
4. Garrido-Castro AC, Lin NU, Polyak K. Insights Into Molecular Classifications of Triple-Negative Breast Cancer: Improving Patient Selection for Treatment. *Cancer Discov* (2019) 9:176–98. doi: 10.1158/2159-8290.CD-18-1177
5. Loi S, Drubay D, Adams S, Pruneri G, Francis PA, Lacroix-Triki M, et al. Tumor-Infiltrating Lymphocytes and Prognosis: A Pooled Individual Patient Analysis of Early-Stage Triple-Negative Breast Cancers. *J Clin Oncol* (2019) 37:559–69. doi: 10.1200/JCO.18.01010
6. Luen SJ, Salgado R, Dieci MV, Vingiani A, Curigliano G, Gould RE, et al. Prognostic Implications of Residual Disease Tumor-Infiltrating Lymphocytes and Residual Cancer Burden in Triple-Negative Breast Cancer Patients After Neoadjuvant Chemotherapy. *Ann Oncol* (2019) 30:236–42. doi: 10.1093/annonc/mdy547
7. Dieci MV, Radosevic-Robin N, Fineberg S, van den Eynden G, Ternes N, Penault-Llorca F, et al. Update on Tumor-Infiltrating Lymphocytes (Tils) in Breast Cancer, Including Recommendations to Assess TILs in Residual Disease After Neoadjuvant Therapy and in Carcinoma in Situ: A Report of the International Immuno-Oncology Biomarker Working Group on Breast Cancer. *Semin Cancer Biol* (2018) 52:16–25. doi: 10.1016/j.semcancer.2017.10.003
8. Salgado R, Denkert C, Demaria S, Sirtaine N, Klauschen F, Pruneri G, et al. The Evaluation of Tumor-Infiltrating Lymphocytes (Tils) in Breast Cancer: Recommendations by an International Tils Working Group 2014. *Ann Oncol* (2015) 26:259–71. doi: 10.1093/annonc/mdu450
9. von Minckwitz G, Untch M, Blohmer J-U, Costa SD, Eidtmann H, Fasching PA, et al. Definition and Impact of Pathologic Complete Response on Prognosis After Neoadjuvant Chemotherapy in Various Intrinsic Breast Cancer Subtypes. *J Clin Oncol* (2012) 30:1796–804. doi: 10.1200/JCO.2011.38.8595
10. Ghajar CM. Metastasis Prevention by Targeting the Dormant Niche. *Nat Rev Cancer* (2015) 15:238–47. doi: 10.1038/nrc3910
11. Redig AJ, McAllister SS. Breast Cancer as a Systemic Disease: A View of Metastasis. *J Intern Med* (2013) 274:113–26. doi: 10.1111/joim.12084
12. Benoy IH, Salgado R, Dam PV, Geboers K, Marck EV, Scharpé S, et al. Increased Serum Interleukin-8 in Patients With Early and Metastatic Breast Cancer Correlates With Early Dissemination and Survival. *Clin Cancer Res* (2004) 10:7157–62. doi: 10.1158/1078-0432.CCR-04-0812
13. Endo M, Yamamoto Y, Nakano M, Masuda T, Odagiri H, Horiguchi H, et al. Serum ANGPTL2 Levels Reflect Clinical Features of Breast Cancer Patients: Implications for the Pathogenesis of Breast Cancer Metastasis. *Int J Biol Markers* (2014) 29:239–45. doi: 10.5301/jbm.5000080
14. Noman AS, Uddin M, Chowdhury AA, Nayeem MJ, Raihan Z, Rashid MI, et al. Serum Sonic Hedgehog (SHH) and Interleukin-(IL-6) as Dual Prognostic Biomarkers in Progressive Metastatic Breast Cancer. *Sci Rep* (2017) 7. doi: 10.1038/s41598-017-01268-4
15. Bahhnassy A, Mohanad M, Shaarawy S, Ismail MF, El-Bastawisy A, Ashmawy AM, et al. Transforming Growth Factor-β, Insulin-Like Growth Factor I/insulin-like Growth Factor I Receptor and Vascular Endothelial Growth Factor-a: Prognostic and Predictive Markers in Triple-Negative and non-Triple-Negative Breast Cancer. *Mol Med Rep* (2015) 12:851–64. doi: 10.3892/mmr.2015.3560
16. Ethier J-L, Desautels D, Templeton A, Shah PS, Amir E. Prognostic Role of Neutrophil-to-Lymphocyte Ratio in Breast Cancer: A Systematic Review and Meta-Analysis. *Breast Cancer Res BCR* (2017) 19. doi: 10.1186/s13058-016-0794-1
17. Huszno J, Kołosza Z, Mrochem-Kwarciak J, Zajusz A. Prognostic Value of the Neutrophil-Lymphocyte, Platelet-Lymphocyte, and Monocyte-Lymphocyte Ratios in Male Breast Cancer Patients. *Oncology* (2020) 98:1–6. doi: 10.1159/000505627
18. Chae S, Kang KM, Kim HJ, Kang E, Park SY, Kim JH, et al. Neutrophil–Lymphocyte Ratio Predicts Response to Chemotherapy in Triple-Negative Breast Cancer. *Curr Oncol* (2018) 25:e113–9. doi: 10.3747/co.25.3888
19. Patel DA, Xi J, Luo J, Hassan B, Thomas S, Ma CX, et al. Neutrophil-to-Lymphocyte Ratio as a Predictor of Survival in Patients With Triple-Negative Breast Cancer. *Breast Cancer Res Treat* (2019) 174:443–52. doi: 10.1007/s10549-018-05106-7
20. Alix-Panabières C, Pantel K. Clinical Applications of Circulating Tumor Cells and Circulating Tumor DNA as Liquid Biopsy. *Cancer Discov* (2016) 6:479–91. doi: 10.1158/2159-8290.CD-15-1483
21. Beddowes E, Sammut SJ, Gao M, Caldas C. Predicting Treatment Resistance and Relapse Through Circulating DNA. *Breast* (2017) 34:S31–5. doi: 10.1016/j.breast.2017.06.024
22. Fernandez-Garcia D, Hills A, Page K, Hastings RK, Toghill B, Goddard KS, et al. Plasma Cell-Free DNA (cfDNA) as a Predictive and Prognostic Marker

in Patients With Metastatic Breast Cancer. *Breast Cancer Res BCR* (2019) 21. doi: 10.1186/s13058-019-1235-8
23. Chia SK, Bramwell VH, Tu D, Shepherd LE, Jiang S, Vickery T, et al. A 50-Gene Intrinsic Subtype Classifier for Prognosis and Prediction of Benefit From Adjuvant Tamoxifen. *Clin Cancer Res* (2012) 18:4465–72. doi: 10.1158/1078-0432.CCR-12-0286
24. Vieira AF, Schmitt F. An Update on Breast Cancer Multigene Prognostic Tests—Emergent Clinical Biomarkers. *Front Med* (2018) 5:248. doi: 10.3389/fmed.2018.00248
25. Wallden B, Storhoff J, Nielsen T, Dowidar N, Schaper C, Ferree S, et al. Development and Verification of the PAM50-based Prosigna Breast Cancer Gene Signature Assay. *BMC Med Genomics* (2015) 8:54. doi: 10.1186/s12920-015-0129-6
26. Soliman H, Shah V, Srkalovic G, Mahtani R, Levine E, Mavromatis B, et al. MammaPrint Guides Treatment Decisions in Breast Cancer: Results of the IMPACt Trial. *BMC Cancer* (2020) 20:81. doi: 10.1186/s12885-020-6534-z
27. Mittempergher L, Delahaye LJ, Witteveen AT, Snel MH, Mee S, Chan BY, et al. Performance Characteristics of the BluePrint® Breast Cancer Diagnostic Test. *Transl Oncol* (2020) 13:100756. doi: 10.1016/j.tranon.2020.100756

Conflict of Interest: The authors declare that the research was conducted in the absence of any commercial or financial relationships that could be construed as a potential conflict of interest.

frontiers in Oncology

ORIGINAL RESEARCH
published: 16 July 2021
doi: 10.3389/fonc.2021.661184

Pinocembrin Inhibits the Proliferation and Metastasis of Breast Cancer *via* Suppression of the PI3K/AKT Signaling Pathway

*Xinbing Zhu[1], Rongnian Li[2], Chen Wang[1], Shuo Zhou[1], Yujia Fan[1], Shuang Ma[1], Didi Gao[1], Nian Gai[1] and Jing Yang[3]**

[1] Department of Breast Surgery, The First Affiliated Hospital of Jinzhou Medical University, Jinzhou, China, [2] Department of General Surgery, Panjin Liaohe Oilfield Gem Flower Hospital, Panjin, China, [3] Department of Otolaryngology Head and Neck Surgery, Shengjing Hospital of China Medical University, Shenyang City, China

The survival rate of breast cancer (BC) patients remains poor, thus the identification of safe and effective new drugs is crucial to improve therapeutic outcomes and overall survival. Pinocembrin (PCB), a pharmacologically active ingredient of Pinus heartwood, Eucalyptus, Euphorbia, Populus, and Sparattosperma leucanthum, has been widely applied for the treatment of various diseases and possesses anticancer activities. In vitro assays were performed to investigate the antiproliferation and antimetastasis activities of PCB in BC cells. A tumorigenesis assay with the use of murine BC models was performed to assess the antiproliferation activities of PCB *in vivo*. Moreover, the molecular mechanisms underlying the anticancer activities of PCB in BC cells were explored. The results showed that the anti-inhibitory and antiproliferation activities of PCB in BC might involve cell cycle (G2/M phase) arrest and apoptosis. PCB downregulated the expression levels of proteins involved in cell cycle progression and apoptosis, including cyclinB1, Cdc2, PARP1, Bcl-2, and survivin, and upregulated protein levels of cleaved PARP1, cleaved caspase3, cleaved caspase9, and BAX. In a murine subcutaneous tumor model, PCB suppressed the growth of MCF-7 cells *in vivo*. Low concentrations of PCB also significantly inhibited the migration and invasion abilities of BC cells. Mechanistically, PCB administration was correlated to suppression of the PI3K/AKT signaling pathway. Inhibition of the proliferation of BC cells by PCB involved cell cycle (G2/M phase) arrest and apoptosis *in vitro* and *in vivo*. Low concentrations of PCB also significantly inhibited the migration and invasion abilities of BC cells. These findings suggest that PCB might be an effective agent for treatment of BC patients.

Keywords: pinocembrin, breast cancer, cell cycle, apoptosis, PI3K/AKT signaling pathway

OPEN ACCESS

Edited by:
Dhivya R. Sudhan, University of Texas Southwestern Medical Center, United States

Reviewed by:
Xiaoyu Chen, Binzhou Medical University, China
Christiana Michael Neophytou, European University Cyprus, Cyprus
Nikhil Baban Ghate, University of Southern California, United States
Shankar Suman, The Ohio State University, United States

****Correspondence:***
Jing Yang
yangjing7694@126.com

Specialty section:
This article was submitted to Breast Cancer, a section of the journal Frontiers in Oncology

Received: *13 April 2021*
Accepted: *30 June 2021*
Published: *16 July 2021*

Citation:
Zhu X, Li R, Wang C, Zhou S, Fan Y, Ma S, Gao D, Gai N and Yang J (2021) Pinocembrin Inhibits the Proliferation and Metastasis of Breast Cancer via Suppression of the PI3K/AKT Signaling Pathway. Front. Oncol. 11:661184. doi: 10.3389/fonc.2021.661184

HIGHLIGHTS

1. Pinocembrin (PCB) inhibited the proliferation of breast cancer cells *in vitro* and *in vivo*.
2. PCB at non-cytotoxic concentrations inhibited the migration and invasion abilities of breast cancer cells.
3. PCB treatment inhibited activity of the PI3K/AKT signaling pathway through up-regulation the expression of PTEN in breast cancer cells.

INTRODUCTION

Breast cancer (BC) accounts for about 30% of female cancers and is the second most common cause of cancer-related death among women worldwide (1, 2). BC treatment strategies including surgery, chemotherapy, radiotherapy, hormone therapy, and biological targeted therapies (3). However, due to tumor heterogeneity and multidrug resistance, the overall survival of BC patients remains less than optimal (4, 5), Thus exploring safe and effective drugs is crucial to improve the therapeutic outcomes and overall survival of BC patients.

Pinocembrin (PCB; 5,7-dihydroxyflavanone) is a pharmacologically active ingredient of Pinus heartwood, Populus, Sparattosperma leucanthum, Eucalyptus, and Euphorbia with diverse pharmacological effects (6) that has been extensively applied for the treatment of microbial infection (7), inflammation (8), ischemia-reperfusion injury (9), and atherosclerosis (10). In addition, numerous recent studies have reported that PCB has anticancer activities by targeting the cell cycle, apoptosis, and the metastatic potential of various solid tumors (11–14). However, the effect of PCB for the treatment of BC remains unclear.

Therefore, the aim of the present study was to explore the antitumor activities of PCB in BC cells and to reveal possible underlying mechanisms. The results showed that PCB had antiproliferative and antimetastatic effects *in vitro*, as well as inhibited tumorigenesis in mouse model of BC. Moreover, PCB may be function as anticancer agent *via* regulation of the PI3K/AKT pathway in BC cells.

MATERIALS AND METHODS

Reagents and Kit

PCB was obtained from the National Institutes for Food and Drug Control (Beijing, China). Antibodies (Abs) against Cdc2 (catalog no. 10762-1-AP), cyclinA2 (18202-1-AP), cyclinB1 (55004-1-AP), cyclinD1 (26939-1-AP), cyclinE1 (11554-1-AP), Bcl-2 (12789-1-AP), BAX (50599-2-Ig), PARP1 (66520-1-Ig), survivin (10508-1-AP), PI3K (20584-1-AP), PTEN (22034-1-AP), caspase9 (10380-1-AP), and GAPDH (60004-1-Ig) were obtained from Proteintech Group, Inc. (Rosemont, IL, USA), while caspase3 (#14220), cleaved caspase3 (#9664), cleaved caspase9 (#9509), phosphorylated AKT ser473 (#4060), total AKT (#4691), LC3B (#3868), and P62 (#16177) were acquired from Cell Signaling Technology, Inc. (Danvers, MA, USA). A Cell Counting Kit-8 (CCK-8; CK04) was obtained from Dojindo Laboratories Co., Ltd. (Kumamoto, Japan). Cell cycle and cell apoptosis detection kits were purchased from Nanjing KeyGen Biotech Co., Ltd. (Nanjing, China).

Cell Culture

Normal immortalized breast epithelial MCF-10A cells and the BC cell lines MCF-7, SKBR3, and MDA-MB-231 were obtained from the Cell Bank of the Chinese Academy of Sciences (Shanghai, China) and maintained in Dulbecco's minimum essential medium (Gibco, Carlsbad, CA, USA) supplemented with 10% fetal bovine serum. The complexity of genetic alteration in MCF-7, MDA-MB-231, and SKBR3 cells has been shown (**Table S1**).

CCK-8 Assay

The CCK-8 assay was used to examine the antiproliferation effects of PCB in immortalized breast epithelial cells and BC cells. Briefly, MCF-7, SKBR3, and MDA-MB-231 cells, and immortalized epithelial MCF-10A cells were seeded in the wells of 96-well plates at 2 × 104 cells/well and treated with 0, 20, 40, 80, 120, 160, 200, or 240 μM PCB for 48 or 72 h. Control cells were treated with an equal volume of vehicle (dimethyl sulfoxide). After PCB treatment for 48 or 72 h, 10 μL of CCK-8 solution was added to the wells and the plates were incubated for an additional 3 h at 37°C. Afterward, the optical density at 450 nm (OD 450) of the wells was measured with a microplate reader.

Colony Formation Assay

Following treatment with 0, 80, 160, or 240 μM PCB for 72 h, the MCF-7 and MDA-MB-231 cells were subcultured for 2 weeks. Then, the surviving colonies were washed twice, fixed, stained with 0.5% crystal violet, photographed, and counted.

Cell Cycle Analysis

The proportions of MCF-7 and MDA-MB-231 cells at each phase of the cell cycle were determined by flow cytometry. Briefly, the cells were seeded and cultured overnight at 37°C, and then treated with 0, 80, 160, or 240 μM PCB for 72 h. Afterward, viable MCF-7 and MDA-MB-231 cells were collected, fixed with 70% ethanol at 4°C overnight, then washed twice and treated with RNase A and propidium iodide in the dark at room temperature for 30 min. The DNA contents of the different treatment groups were determined using a flow cytometer.

Apoptosis Analysis

The proportions of apoptotic MCF-7 and MDA-MB-231 cells were determined using an Annexin V-fluorescein isothiocyanat apoptosis detection kit. Briefly, MCF-7 and MDA-MB-231 cells were treated with 0, 80, 160, or 240 μM PCB for 72 h and then incubated with propidium iodide and Annexin V-fluorescein isothiocyanate in the dark for 30 min. A flow cytometer was used to detect apoptotic cells.

Transfection With Small Interfering RNA (siRNA)

siRNA-PTEN and siRNA-control were synthesized by GenePharma Co., Ltd. (Shanghai, China). MCF-7 and MDA-

MB-231 cells were seeded into the wells of 6-well plates at a density of 2 × 105 cells/well in Dulbecco's minimum essential medium and then transfected with siRNA-control or siRNA targeting PTEN using Lipofectamine 2000 reagent (Invitrogen Corporation, Carlsbad, CA, USA) in accordance with the manufacturer's instructions. After transfection for 24 h, the medium was discarded and the cells were washed and then treated with 240 μM PCB for 72 h. Downregulation of PTEN was confirmed by western blot analysis.

The transfections were conducted using the following siRNA sequences: siRNA-control: (forward) GAT CCA CTA CCG TTG TTA TAG GTG TTC AAG AGA CAC CTA TAA CAA CGG TAG TTT TTT GGA AA/(reverse) AGC TTT TCC AAA AAA CTA CCG TTG TTA TAG GTG TCT CTT GAA CAC CTA TAA CAA CGG TAGG; and siRNA-PTEN (forward) GGC GCU AUG UGU AUU AUU AdT dT/(reverse) dTd TCC GCG AUA CAC AUA AUA AU. Afterward, the cells were harvested and assayed.

Wound Healing Assay

The migration of BC cells treated with 0, 20, 40, or 60 μM PCB for 24 h was evaluated with the wound healing assay. In brief, when the cell density reached 95%, a wound was created and the MCF-7 and MDA-MB-231 cells were seeded and incubated in serum-free medium with 0, 20, 40, or 60 μM PCB for 24 h. Images were captured under a microscope at 100× magnification. The incision width at different time points was measured and calculated. The experiment was performed independently in triplicate.

Transwell Migration and Invasion Assay

The migration and invasion abilities of MCF-7 and MDA-MB-231 cells treated with 0, 20, 40, or 60 μM PCB for 24 h was evaluated with the transwell assay. The filter inserts of the transwell apparatus were coated with or without Matrigel. Then, 2 × 10^5 MCF-7 and MDA-MB-231 cells were respectively seeded into the upper chamber and treated with 0, 20, 40, or 60 μM PCB in serum-free medium. After 24 h of incubation, the cells were carefully removed from the upper chamber using a cotton swab and fixed with 70% methanol, stained with 0.5% crystal violet, counted, and the permeating cells were photographed at 200× magnification.

Western Blot Analysis

Total protein was extracted from MCF-7 and MDA-MB-231 cells using radioimmunoprecipitation assay buffer containing protease inhibitors (Proteintech, Wuhan, China). The concentrations of the protein samples were measured using the bicinchoninic acid assay. Total protein samples were separated by electrophoresis and transferred to polyvinylidene difluoride membranes, which were blocked with 5% bovine serum albumin at room temperature for 2 h and then incubated with primary Abs at 4°C overnight. The next day, the membranes were washed twice and then incubated with the secondary Abs at room temperature for 2 h. Finally, the protein bands were detected with the ChemiDoc XRS+ System (Bio-Rad Laboratories, Hercules, CA, USA).

Animal Studies

BALB/C nude mice (age, 5–7 weeks; body weight, 15–20 g) were obtained from Beijing Vital River Laboratory Animal Technology Co., Ltd. (Beijing China) and housed in a pathogen-free facility at the Experimental Animal Center of Dalian Medical University (Dalian, China). All animal procedures were conducted in accordance with the guidelines of the Animal Care and Use Committee of Dalian Medical University. Briefly, the flank of each nude mice was subcutaneously injected with 2 × 106 MCF-7 cells. After 7 days, the mice were randomly assigned to the PCB treatment group or the control group (6 mice/group) and orally administered either 30 mg/kg of PCB in saline solution per day (PCB group) or the same volume of saline solution (control group) for 30 days. The subcutaneous tumors were measured with a caliper once every 3 days and the tumor volumes were calculated as volume = length × width2/2.

Immunohistochemical (IHC) Analysis

IHC analysis was performed to evaluate Ki67 expression in the subcutaneous tumors. Paraffin-embedded tumor sections were deparaffinized in xylene and then rehydrated in a descending series of ethanol. For antigen retrieval, the paraffin-embedded sections were heated in citrate buffer (pH 6.0), then blocked with 3.0% hydrogen peroxide and 10% goat serum, and incubated with rabbit anti-Ki67 Ab (dilution, 1:200; Proteintech) at 4°C overnight. After incubation with the biotinylated secondary Ab, the sections were counterstained with hematoxylin, dehydrated, mounted on glass slides, and imaged under a microscope (Microphot-FX; Nikon Corporation, Tokyo, Japan) at 200× magnification.

Statistical Analysis

Statistical analyses were performed using GraphPad Prism software (GraphPad Software Inc., La Jolla, CA, USA). Data of at least three independent experiments are presented in bar graphs as the mean ± standard deviation (SD). A probability (p) value of < 0.05 was considered statistically significant.

RESULTS

PCB Inhibited the Proliferation of BC Cells *In Vitro*

The chemical structure of PCB is shown in **Figure 1A**. The cytotoxic effects of PCB at 0, 20, 40, 80, 120, 160, 200, or 240 μM for 48 or 72 h were measured in normal immortalized breast epithelial cells (MCF-10A) and BC cells (MCF-7, SKBR3, and MDA-MB-231). The viability of cells treated with various concentrations PCB for 48 or 72 h was detected with the CCK-8 assay. The OD values of MCF-10A, MCF-7, SKBR3, and MDA-MB-231 cells incubated with various concentrations of PCB for 48 and 72 h are shown in **Figure 1B**. The CCK-8 assay results show that PCB inhibited the proliferation of BC cells in a concentration- and time-dependent manner. After incubation with PCB for 48 and 72 h, the half maximal inhibitory

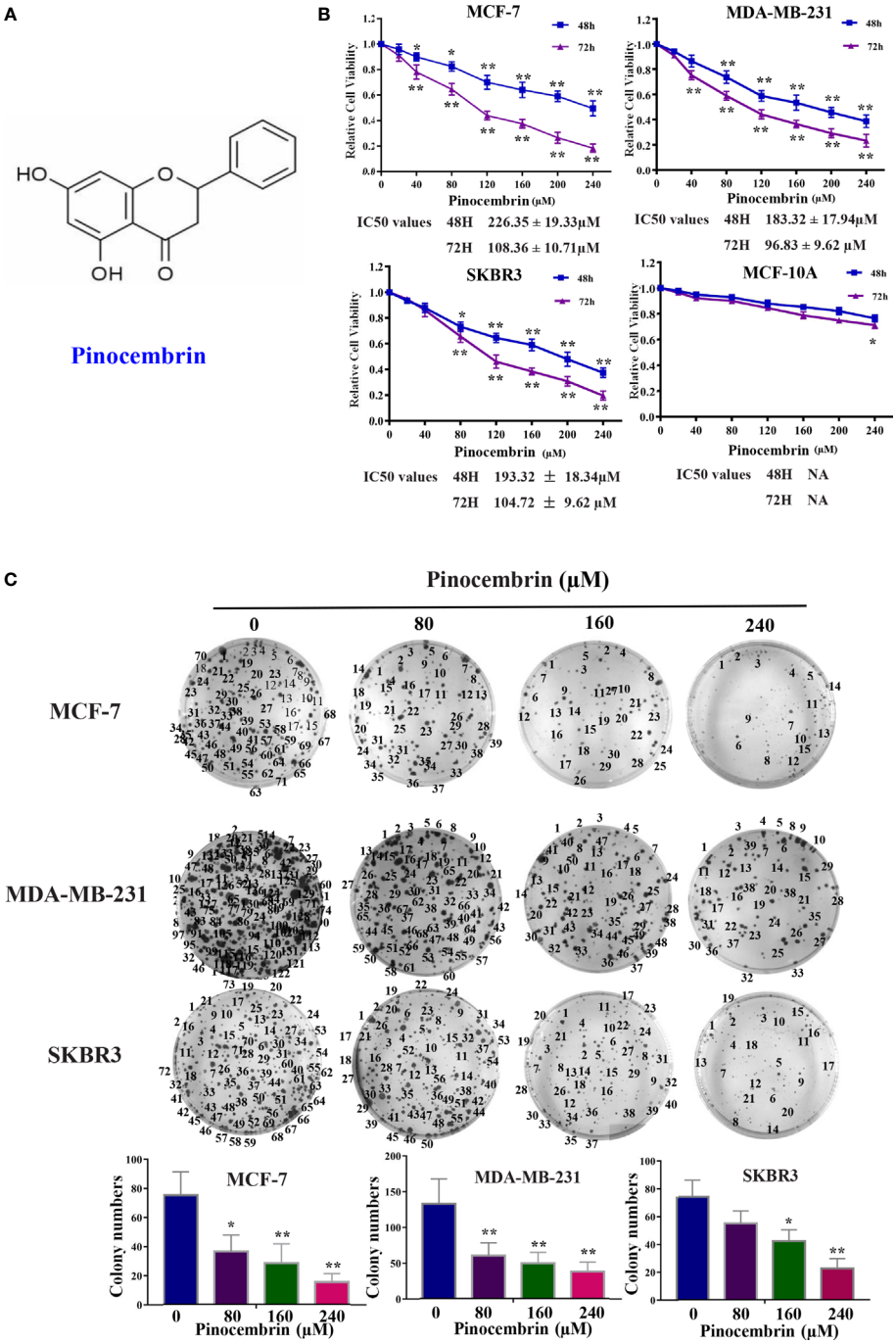

FIGURE 1 | Antiproliferation effect of Pinocembrin (PCB) on breast cancer (BC) cells. **(A)** The chemical structure of PCB. **(B)** BC cells (MCF-7, MDA-MB-231, and SKBR3) and breast epithelial cells (MCF-10A) were incubated with 0, 20, 40, 80, 120, 160, 200, or 240 μM PCB for 48 or 72 h. The viabilities of cells in the different treatment groups were measured with the CCK-8 assay. **(C)** PCB treatment inhibited colony formation of MCF-7, MDA-MB-231, and SKBR3 cells. *$p < 0.05$, **$p < 0.01$ *vs*. the control group.

concentration values (IC50) were 226.35 ± 19.33 and 108.36 ± 10.71 μM, respectively, for MCF-7 cells, 183.32 ± 17.94 and 96.83 ± 9.62 μM for MDA-MB-231 cells, and 193.32 ± 18.34 and 104.72 ± 9.62 μM for SKBR3 cells. Notably, PCB was relatively less cytotoxic to normal immortalized breast epithelial MCF-10A cells than the three BC cell lines (**Table 1**). The colony formation assay was performed to further confirm that PCB inhibited the proliferation of BC cells. As shown in **Figure 1C**, treatment with

TABLE 1 | The IC50 values of MCF-7, MDA-MB-231, SKBR3 and MCF-10A incubated with Pinocembrin for 48 and 72 h.

	48H	72H
MCF-7	226.35 ± 19.33μM	108.36 ± 10.71μM
MDA-MB-231	183.32 ± 17.94μM	96.83 ± 9.62μM
SKBR3	193.32 ± 18.34μM	104.72 ± 9.62μM
MCF-10A	NA	NA

PCB (80, 160, or 240 μM) for 72 h significantly suppressed the colony formation abilities of MCF-7, MDA-MB-231 and SKBR3 cells.

PCB Induces Cell Cycle (G2/M Phase) Arrest and Apoptosis of BC Cells

The cell cycle distribution of BC cells treated with PCB (0, 80, 160, or 240 μM) for 72 h was analyzed by flow cytometry. The proportions of MCF-7 and MDA-MB-231 cells treated with PCB at concentrations of 0, 80, 160, or 240 μM in the G2/M phase were significantly increased. The proportion of MCF-7 cells in the G2/M phase increased from 14.43% ± 1.34% at 0 μM PCB to 23.76% ± 1.87% at 80 μM, 36.14% ± 2.86% at 160 μM, and 42.04% ± 3.98% at 240 μM PCB. The proportion of MDA-MB-231 cells in the G2/M phase increased from 13.91% ± 1.23% at 0 μM PCB to 22.1% ± 2.04% at 80 μM, 27.94% ± 2.08% at 160 μM, and 40.66% ± 3.96% at 240 μM PCB. Meanwhile, the proportions of cells in the G0/G1 phase were decreased (**Figure 2A**). To verify the anti-proliferation effect of PCB, the proportions of apoptotic MCF-7 and MDA-MB-231 cells treated with PCB (0, 80, 160, or 240 μM) for 72 h were determined with the Annexin V/PI assay. The results showed that PCB treatment dramatically increased the proportions of apoptotic MCF-7 and MDA-MB-231 cells (control, 9.2% ± 0.87% and 5.0% ± 0.32%; 80 μM PCB, 13.6% ± 1.28% and 18.6% ± 1.53%; 160 μM PCB, 24.8% ± 4.27% and 30.0% ± 2.13%; 240 μM PCB, 47.4% ± 4.38% and 38.2% ± 3.26%, respectively; **Figure 2B**), suggesting that the anti-proliferation activity of PCB might be associated with G2/M phase arrest and apoptosis of BC cells.

Effects of PCB on the Expression Patterns of Proteins Related to the Cell Cycle and Apoptosis of BC Cells

CyclinB1 and Cdc2 play important roles in the switch from the G2 to M phase (15, 16). To explore the possible molecular mechanisms underlying G2/M phase arrest in response to PCB treatment, the protein expression levels of Cdc2, cyclinB1, cyclinA2, cyclinE1, and cyclinD1 in BC cells were measured. The results revealed that the Cdc2 and cyclinB1 protein expression levels of MCF-7 and MDA-MB-231 were significantly decreased after treatment with 80, 160, or 240 μM PCB (**Figure 3A**). PCB treatment also increased the proportion of apoptotic BC cells. Bax and Bcl-2 are known or well established to be involved in the apoptotic process (17). So, the BAX and Bcl-2 expression levels were assessed in MCF-7 and MDA-MB-231 cells after PCB treatment. The results showed that PCB treatment upregulated BAX and downregulated Bcl-2 in MCF-7 and MDA-MB-231 cells. In regard to other apoptosis-related proteins cleaved PARP1, cleaved caspase 3/9 were upregulated in MCF-7 and MDA-MB-231 cells in response to PCB treatment, while PARP1, caspase 3/9, and survivin were downregulated (**Figure 3B**). Collectively, these results showed that PCB regulated the expression levels of proteins related to the cell cycle and apoptosis in MCF-7 and MDA-MB-231 cells. Autophagy also plays an important role in tumorigenesis and development. In order to investigate whether autophagy is involved in the anticancer activity of PCB in breast cancer cells, we detected the expression levels of LC3B and p62 after 0, 80, 160, or 240 μM PCB treatment for 72 hours. The results showed that PCB treatment did not affect the autophagy process of breast cancer cells (**Figure S1**).

Low Concentrations of PCB Suppressed the Migration and Invasion Abilities of BC Cells

To investigate the antimetastatic potential of PCB, the wound healing and transwell assays(with or without Matrigel) were performed to assess the effects of PCB on the migration and invasion abilities of MCF-7 and MDA-MB-231 cells. The results of the wound healing and transwell assays revealed that treatment with low concentrations (20, 40, or 60 μM) of PCB for 24 h did not induce apoptosis, but did suppress the migration and invasion abilities of BC cells in a dose-dependent manner (**Figures 4A, B**).

PCB Suppressed Tumorigenesis of BC Cells *In Vivo*

A mouse model was used to investigate the antiproliferation activities of PCB *in vivo*. In brief, 2×106 MCF-7 cells were injected subcutaneously to the flanks of nude mice. After 7 days, the mice were randomly assigned to the PCB group (orally administered PCB at 30 mg/kg in saline solution per day for 30 days) or the control group (equal volume of saline solution per day for 30 days). As shown in **Figure 5A**, the weights of the excised tumors of the PCB-treated group were lower than those of the control group. Meanwhile, the growth curves of the excised subcutaneous tumors demonstrated that PCB treatment inhibited the growth of MCF-7 cells *in vivo* (**Figure 5B**). IHC analysis showed that KI67 expression was lower in the tumors of the PCB-treated groups than the control group (**Figure 5C**).

PCB Treatment Inhibited Activity of the PI3K/AKT Signaling Pathway in BC Cells

The PI3K/AKT pathway is involved in the proliferation, differentiation, and metastasis of various tumor cells (18). Accumulated evidence indicates that active constituents of plants used in traditional Chinese medicine, including PCB, have the ability to regulate the PI3K pathway (19). Therefore, the expression levels of PI3K, phosphorylated AKT, and total AKT were measured to investigate the activity of the PI3K/AKT signaling pathway in BC cells after PCB treatment. The results showed that PCB decreased the expression levels of PI3K and phosphorylated AKT, while total AKT protein levels remained

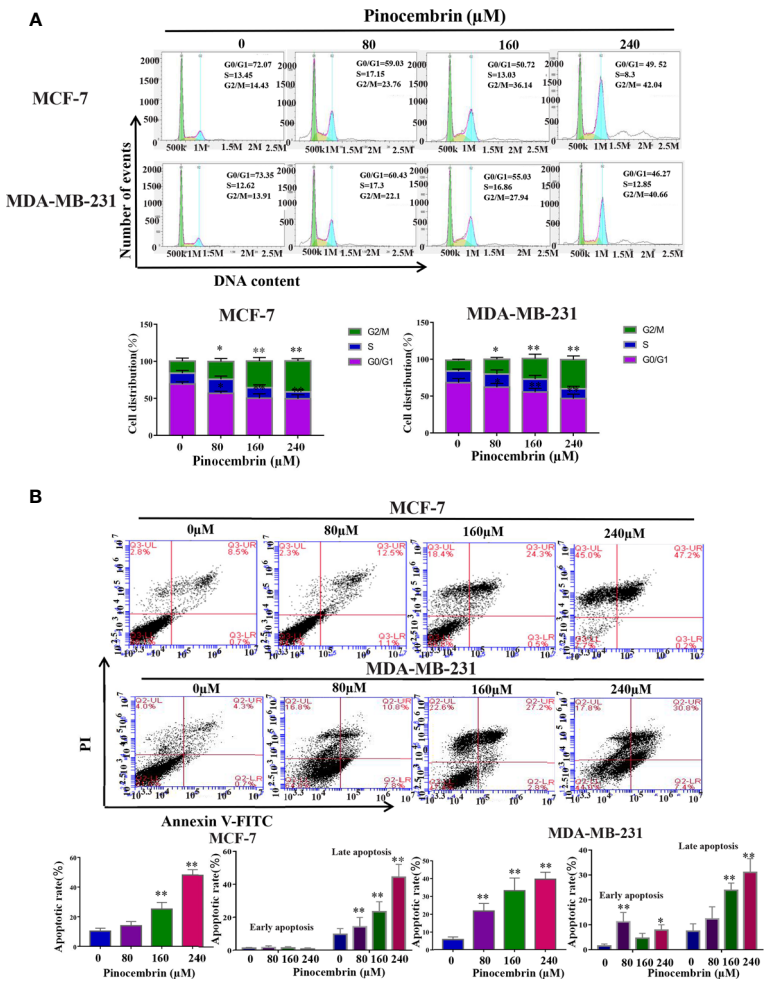

FIGURE 2 | Effect of Pinocembrin (PCB) on cell cycle distribution and apoptosis in breast cancer (BC) cells. **(A)** MCF-7 and MDA-MB-231 cells were incubated with PCB (0, 80, 160, or 240 μM) for 72 h. Cell cycle distribution of MCF-7 and MDA-MB-231 cells was analyzed by flow cytometry, representative images were shown. The proportions of MCF-7 and MDA-MB-231 cells in G0/G1, S, and G2/M phases are presented in the histograms. *p < 0.05, **p < 0.01 *vs*. the control group. **(B)** MCF-7 and MDA-MB-231 cells were incubated with 0, 80, 160, or 240 μM PCB for 72 h. Annexin V/PI flow cytometry analysis was used to assess the proportions of apoptotic cells, which are presented in histograms. *p < 0.05, **p < 0.01 *vs*. the control group.

constant. PTEN is an upstream suppressor of the PI3K/AKT signaling pathway (20). As shown in **Figure 6**, treatment with 80, 160, or 240 μM PCB for 72 h upregulated PTEN protein levels, thereby inhibiting the PI3K/AKT pathway in MCF-7 and MDA-MB-231 cells (**Figure 6**). Collectively, these findings suggest that the anticancer activities of PCB might result from inhibition of the PI3K/AKT pathway.

Knockdown of PTEN Expression Rescued Down-Regulate the Activity of PI3K/AKT Pathway by PCB Treatment in MCF-7 and MDA-MB-231 Cells

In order to validate the role of PTEN in the anti-tumor activity of PCB,We knockdown the expression of PTEN in MCF-7 and MDA-MB-231 cells (**Figure 7A**) and investigated the protein levels of PI3K, phosphorylated AKT, and total AKT after PCB treatment. Our data showed that Knockdown of PTEN expression rescued down-regulate the activity of PI3K/AKT pathway after PCB treatment (**Figure 7B**).

DISCUSSION

Patients with BC still face the challenges of drug resistance and side effects of chemotherapy. Monomer active constituents of plants used in traditional Chinese medicine have potential for treatment of malignant tumors (21). Therefore, the anticancer activities of PCB in BC cells were explored as an attempt to identify effective agents with lower toxicity for treatment of BC patients. PCB, an active component extracted from Pinus heartwood, Euphorbia, Eucalyptus, Populus, and Sparattosperma leucanthum, has been extensively applied for

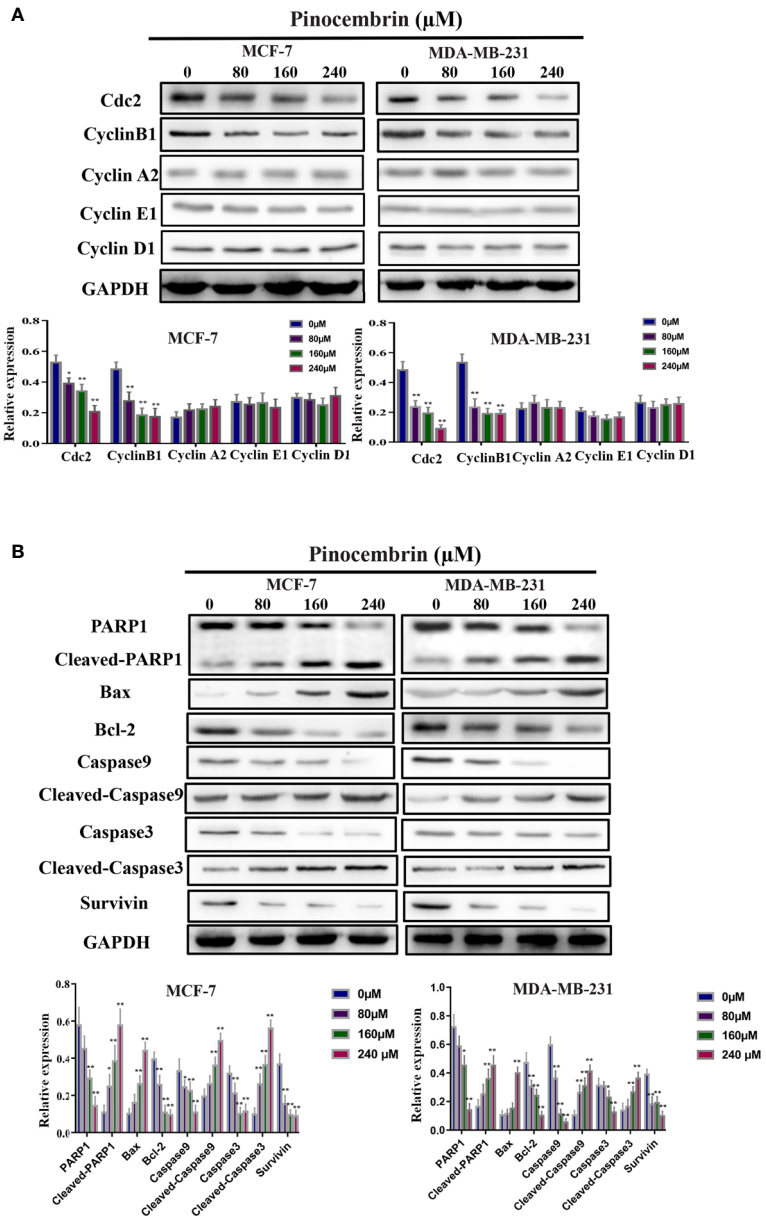

FIGURE 3 | Effects of Pinocembrin (PCB) on proteins involved in the cell cycle and apoptosis of breast cancer cells. MCF-7 and MDA-MB-231 cells were incubated with 0, 80, 160, or 240 μM PCB for 72 h. **(A)** Expression of cyclinB1, Cdc2, cyclinA2, cyclinE1, and cyclinD1 were examined after PCB treatment for 72 h. **(B)** Expression of Bax, Bcl-2, PARP1, cleaved PARP1, caspase 3, cleaved caspase 3, caspase 9, cleaved caspase 9, and survivin were examined after PCB treatment for 72 h. GAPDH served as an internal control. Bands were quantified using Image J software. Each bar represents the mean ± SD of three independent experiments. *$p < 0.05$, **$p < 0.01$ *vs*. the control group.

the treatment of microbial infection (7), inflammation (8), ischemia-reperfusion injury (9), and atherosclerosis. In addition, recent studies have demonstrated the antitumor activities of PCB (11–14). Therefore, the aim of the present study was to investigate the effects of PCB on BC and to identify potential underlying molecular mechanisms.

Various monomer plant extracts have been demonstrated to inhibit the proliferation of cancer cells by inducing cell cycle arrest and/or apoptosis (22–24). Cdc2 and cyclinB1 are involved in initiating a switch from the G2 to M phase of the cell cycle (25), and some antineoplastic agents can induce G2/M arrest in cancer cells by downregulating cyclinB1 and Cdc2 protein levels (26, 27). The results of the present study showed that PCB treatment increased G2/M phase arrest *via* downregulation of cyclinB1 and Cdc2 protein levels in MCF-7 and MDA-MB-231 cells. In addition, apoptosis plays a crucial role in the regulation

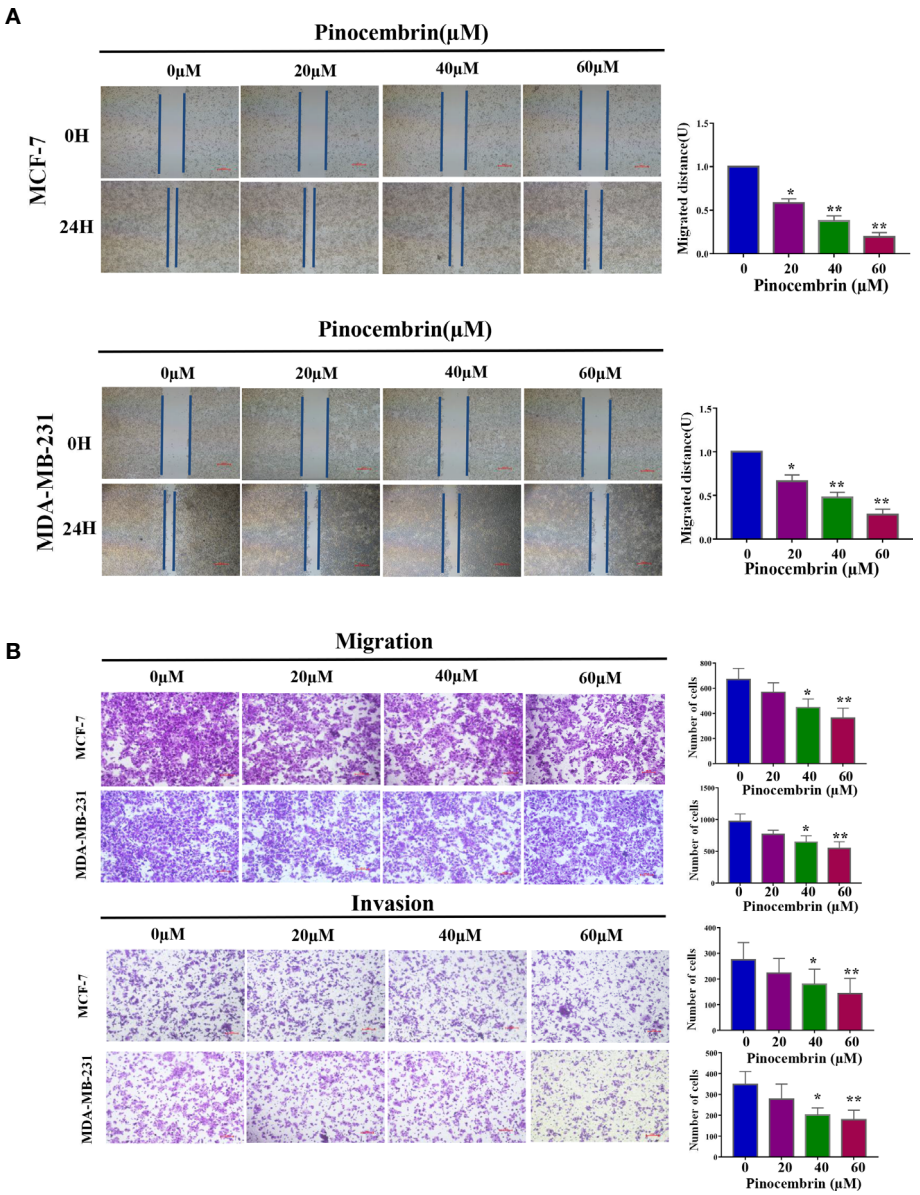

FIGURE 4 | Effect of Pinocembrin (PCB) on the migration and invasion abilities of MCF-7 and MDA-MB-231 cells. **(A)** Representative images of the wound healing assay under a microscope are shown and migrated distances of MCF-7 and MDA-MB-231 cells were quantified. **(B)** The photos represent cells migrating or invading the underside of the transwell membrane. All photos were captured at 200× magnification. The cell number of each field was counted. The numbers of migrating and invading cells are shown in the histograms. *$p < 0.05$, **$p < 0.01$ *vs*. the control group.

of cell proliferation. The induction of apoptosis of cancer cells is a common mechanism of antineoplastic agents (28). Previous studies have demonstrated that PCB inhibits the proliferation of colorectal cancer and ovarian cancer cells *via* the induction of apoptosis (11, 13, 14).

Our data also demonstrated that the proportion of apoptotic cells was increased following PCB treatment. Mitochondrial proteins reportedly directly regulate apoptosis (29). Bax and Bcl-2 have been implicated in caspase-associated apoptosis (30, 31). An increase in the Bax/Bcl-2 ratio can trigger apoptotic events, including activation of caspase3/9 and the subsequent degradation of intracellular substrates. In the present study, PCB treatment up-regulated cleaved PARP1, cleaved caspase3, and cleaved caspase9, while downregulating caspase3, caspase9, PARP1. Survivin is a member of the inhibitor of apoptosis (IAP) protein family, it inhibits apoptosis and regulates cell division (32–34). Silencing of survivin expression inhibited proliferation and induced cell cycle arrest in hela cells (35). Accordingly, our data showed PCB

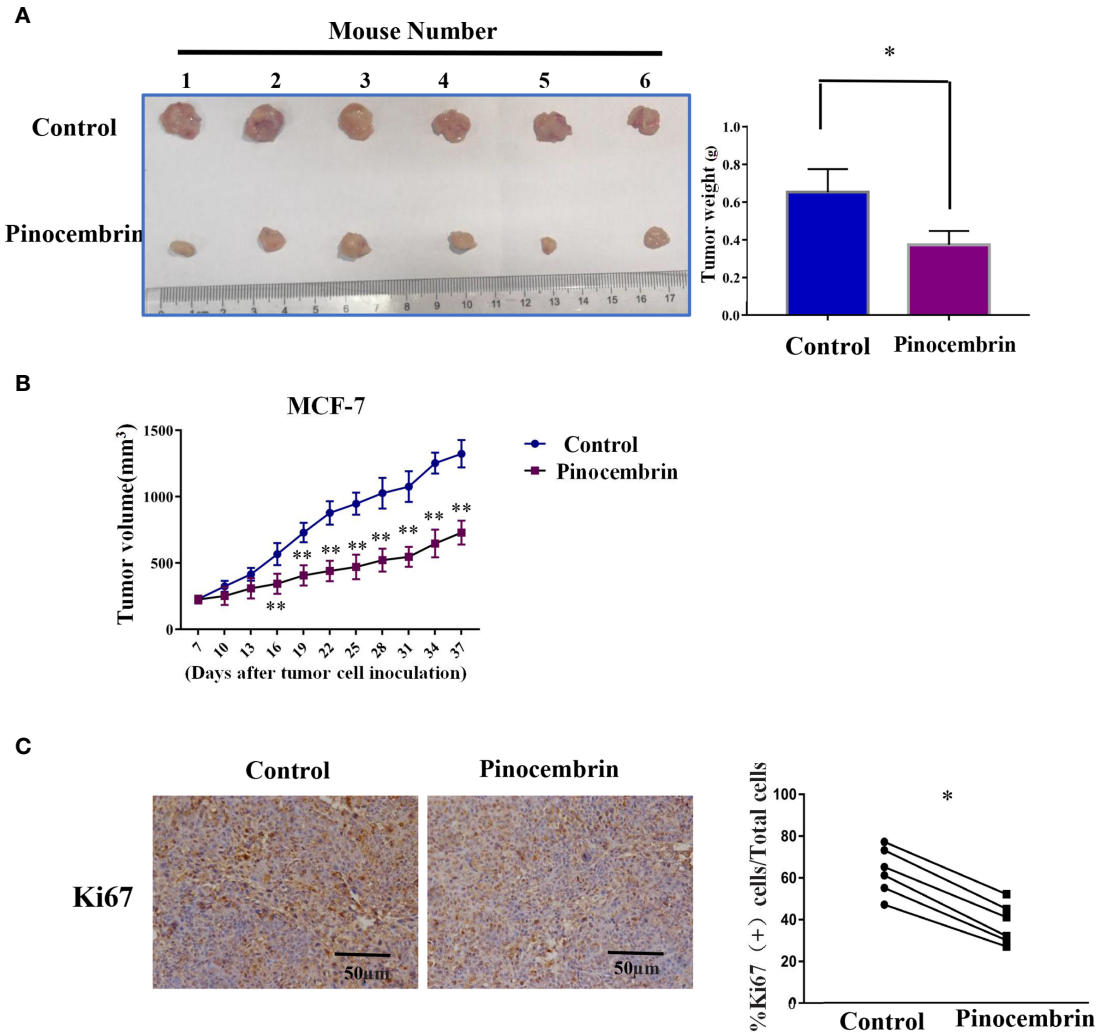

FIGURE 5 | Pinocembrin (PCB) inhibits proliferation of xenografted MCF-7 cells *in vivo*. **(A)** Photograph of excised tumors from the PCB and control groups. Histogram illustrating the weight of the excised tumors. **(B)** Growth curves of subcutaneous tumors. **(C)** Ki67 expression in xenografts of the two groups by IHC analysis. *p < 0.05, **p < 0.01 *vs*. the control group.

treatment remarkably decreased the protein lever of survivin. To date, few studies have investigated the anti-metastatic effects of PCB on tumor cells (13). To the best of our knowledge, the present study is the first to demonstrate that PCB at non-cytotoxic concentrations inhibited the migration and invasion abilities of MCF-7 and MDA-MB-231 cells.

To further investigate the possible mechanisms of the effects of PCB on cell cycle arrest, apoptosis, and cell migration/invasion, the activities of related pathways were examined. It has been reported that the PI3K/AKT signaling pathway plays important roles in the proliferation, apoptosis, and metastasis of various cancers, including BC (36, 37). Phosphorylated Akt is crucial to multiple physiological functions, such as cell proliferation, the cell cycle, apoptosis, and metastasis (38). PCB was previously reported to participate in the regulation of the PI3K/AKT signaling pathway (19). Consistent with previous studies, our data demonstrated that PCB treatment decreased the protein expression levels of phosphorylated AKT and PI3K, and increased protein expression of PTEN, while total AKT protein levels remained constant. Regulation of the PI3K/AKT signal pathway may be a potential mechanism of the anticancer effect of PCB in BC cells. In the present study, PCB downregulated the expression levels of PI3K and p-Akt, inhibited the activities of the PI3K signaling pathway, and subsequently attenuated the proliferation, migration, and metastasis abilities of MCF-7 and MDA-MB-231 cells. Meanwhile, PCB upregulated the expression of PTEN, which is upstream of the PI3K signaling pathway, similar to the common mechanism of many Chinese herbal medicines (39, 40). PTEN, as a negative upstream regulator, inhibits the activity of the PI3K signaling pathway, which may be a novel mechanism of PCB as an anticancer drug.

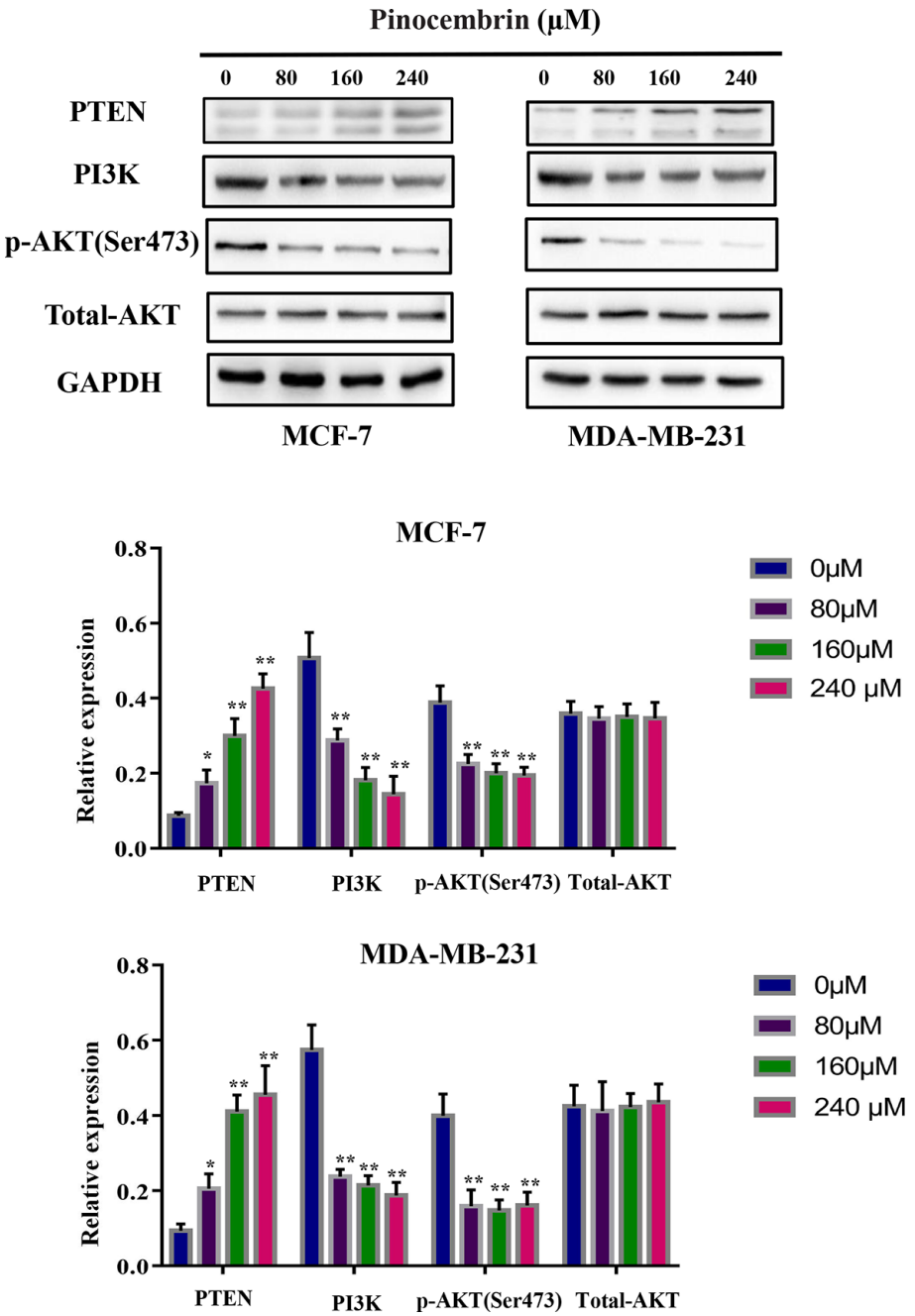

FIGURE 6 | Pinocembrin (PCB) regulates the PI3K/AKT pathway. MCF-7 and MDA-MB-231 cells were incubated with PCB (0, 80, 160, or 240 μM) for 72 h. The expression levels of PTEN, PI3K, total AKT, and phosphorylated AKT were measured. GAPDH was used as an internal control. Protein bands were quantified using Image J software. Each bar represents the mean ± SD of three independent experiments. *$p < 0.05$, **$p < 0.01$ *vs*. the control group.

The anti-tumor activities of plant extracts used in traditional Chinese medicine may involve multiple mechanisms and signaling pathways, especially in different cell lines. The same drug may have different pharmacological effects on tumor cells with different backgrounds. The results of the present study suggest that the inhibitory effect of PCB on MCF-7 and MDA-MB-231 cells may be achieved by down-regulating the activities of the PI3K signaling pathway. In future studies, we plan to use whole transcriptome sequencing (RNA-Seq) and pathway analysis to assess the effects of PCB on the activities of tumor-related signaling pathways in MCF-7 and MDA-MB-231 cells in order to comprehensively and objectively elucidate the exact mechanisms underlying the anticancer activities of PCB.

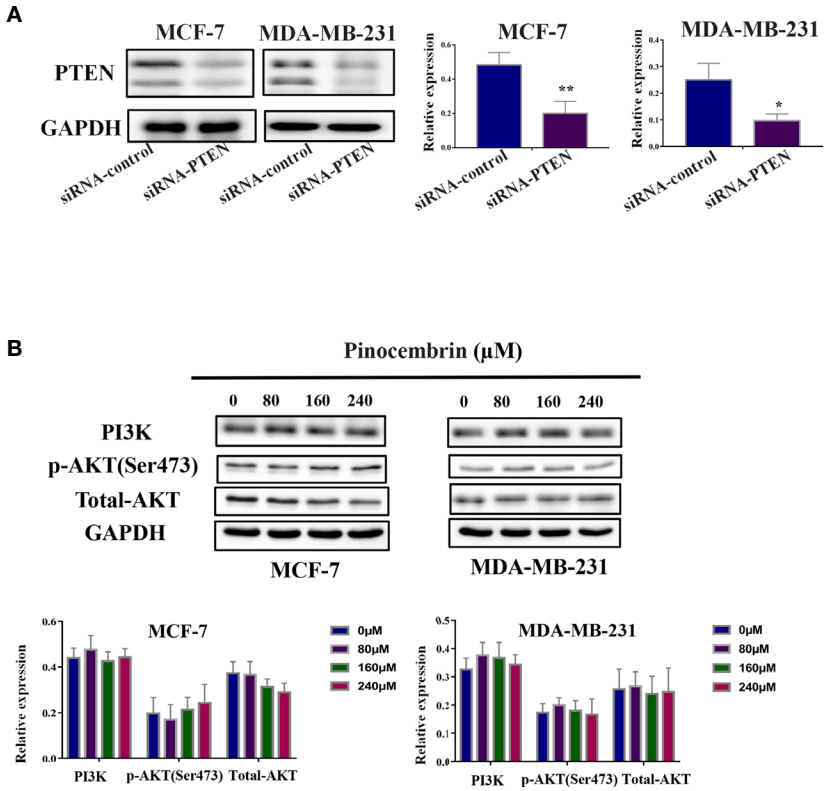

FIGURE 7 | Knockdown of PTEN expression rescued down-regulate the activity of PI3K/AKT pathway by PCB treatment in MCF-7 and MDA-MB-231 cells. **(A)** Knockdown of PTEN in MCF-7 and MDA-MB-231 cells was confirmed by western blot analysis. **(B)** After PTEN protein knockdown, MCF-7 and MDA-MB-231 cells were treatment with PCB (0, 80, 160, or 240 μM) for 72 h and the expression of PI3K, total AKT, phosphorylated AKT were examined. GAPDH served as an internal control. Bands were quantified using Image J software. Each bar represents the mean ± SD of three independent experiments. *$p < 0.05$, **$p < 0.01$ *vs*. the control group.

The results of the present study demonstrated that PCB suppressed the growth and metastasis of BC cells both *in vitro* and *in vivo*, indicating the potential as a novel anticancer agent for the treatment of BC. PCB treatment induced cell cycle (G2M phase) arrest and apoptosis *via* regulation of the expression of proteins associated with apoptosis and the cell cycle. Also, PCB at non-cytotoxic concentrations inhibited the migration and invasion abilities of MCF-7 and MDA-MB-231 cells. Mechanistically, in response to PCB treatment, PTEN expression was upregulated, phosphorylated AKT and PI3K expression was downregulated, and the activities of the PI3K/AKT signaling pathway were suppressed. Collectively, these findings demonstrate that PCB might have beneficial applications for the treatment of BC patients.

DATA AVAILABILITY STATEMENT

The original contributions presented in the study are included in the article/**Supplementary Material**. Further inquiries can be directed to the corresponding author.

ETHICS STATEMENT

The animal study was reviewed and approved by Animal Care and Use Committee of Dalian Medical University.

AUTHOR CONTRIBUTIONS

XZ, RL, JY, and CW contributed to conception and design of the study. SZ performed the statistical analysis. XZ wrote the first draft of the manuscript. YF, SM, DG, JY, and NG wrote sections of the manuscript. All authors contributed to the article and approved the submitted version.

FUNDING

This present study was supported by Natural Science Foundation of Liaoning (2019-ZD-0581) and shenyang science and technology planning project (19-112-4-084).

SUPPLEMENTARY MATERIAL

The Supplementary Material for this article can be found online at: https://www.frontiersin.org/articles/10.3389/fonc.2021.661184/full#supplementary-material

Supplementary Figure 1 | The expression levels of LC3B and P62 were measured after incubated with PCB (0, 80, 160, or 240 μM) for 72 h. GAPDH was used as an internal control. Protein bands were quantified using Image J software. Each bar represents the mean ± SD of three independent experiments.

Supplementary Table 1 | The complexity of genetic alteration in MCF-7, MDA-MB-231, and SKBR3 cells has been shown.

REFERENCES

1. DeSantis C, Ma J, Bryan L, Jemal A. Breast Cancer Statistics, 2013. *CA Cancer J Clin* (2014) 64:52–62. doi: 10.3322/caac.21203
2. Torre LA, Siegel RL, Ward EM, Jemal A. Global Cancer Incidence and Mortality Rates and Trends–An Update. *Cancer Epidemiol Biomarkers Prev* (2016) 25(1):16–27. doi: 10.1158/1055-9965.EPI-15-0578
3. Tong CWS, Wu M, Cho WCS, To KKW. Recent Advances in the Treatment of Breast Cancer. *Front Oncol* (2018) 8:227. doi: 10.3389/fonc.2018.00227
4. Strobl S, Korkmaz B, Devyatko Y, Schuetz M, Exner R, Dubsky PC, et al. Adjuvant Bisphosphonates and Breast Cancer Survival. *Annu Rev Med* (2016) 1-10:67. doi: 10.1146/annurev-med-053014-103600
5. Clarke R, Leonessa F, Trock B. Multidrug Resistance/P-Glycoprotein and Breast Cancer: Review and Meta-Analysis. *Semin Oncol* (2005) 32:S9–15. doi: 10.1053/j.seminoncol.2005.09.009
6. Rasul A, Millimouno FM, Ali Eltayb W, Ali M, Li J, Li XM. Pinocembrin: A Novel Natural Compound With Versatile Pharmacological and Biological Activities. *BioMed Res Int* (2013) 2013:379850. doi: 10.1155/2013/379850
7. Arslan S, Ozbilge H, Kaya EG, Er O. In Vitro Antimicrobial Activity of Propolis, BioPure MTAD, Sodium Hypochlorite, and Chlorhexidine on Enterococcus Faecalis and Candida Albicans. *Saudi Med J* (2011) 32:479–83.
8. Soromou LW, Chu X, Jiang LX, Wei MM, Huo M, Chen N, et al. In Vitro and In Vivo Protection Provided by Pinocembrin Against Lipopolysaccharide-Induced Inflammatory Responses. *Int Immunopharmacol* (2012) 14:66–74. doi: 10.1016/j.intimp.2012.06.009
9. Shi LL, Chen BN, Gao M, Zhang HA, Li YJ, Wang L, et al. The Characteristics of Therapeutic Effect of Pinocembrin in Transient Global Brain Ischemia/Reperfusion Rats. *Life Sci* (2011) 88:521–8. doi: 10.1016/j.lfs.2011.01.011
10. Sang H, Yuan N, Yao ST, Li FR, Wang JF, Fang YQ, et al. Inhibitory Effect of the Combination Therapy of Simvastatin and Pinocembrin on Atherosclerosis in ApoE-Deficient Mice. *Lipids Health Dis* (2012) 11:166. doi: 10.1186/1476-511X-11-166
11. Kumar MA, Nair M, Hema PS, Mohan J, Santhoshkumar TR. Pinocembrin Triggers Bax-Dependent Mitochondrial Apoptosis in Colon Cancer Cells. *Mol Carcinog* (2007) 46:231–41. doi: 10.1002/mc.20272
12. Punvittayagul C, Pompimon W, Wanibuchi H, Fukushima S, Wongpoomchai R. Effects of Pinocembrin on the Initiation and Promotion Stages of Rat Hepatocarcinogenesis. *Asian Pac J Cancer Prev* (2012) 13:2257–61. doi: 10.7314/APJCP.2012.13.5.2257
13. Gao J, Lin S, Gao Y, Zou X, Zhu J, Chen M, et al. Pinocembrin Inhibits the Proliferation and Migration and Promotes the Apoptosis of Ovarian Cancer Cells Through Down-Regulating the mRNA Levels of N-Cadherin and GABAB Receptor. *BioMed Pharmacother* (2019) 120:109505. doi: 10.1016/j.biopha.2019.109505
14. Kumar N, Biswas S, Hosur Shrungeswara A, Basu Mallik S, Hipolith Viji M, Elizabeth Mathew J, et al. Pinocembrin Enriched Fraction of Elytranthe Parasitica (L.) Danser Induces Apoptosis in HCT 116 Colorectal Cancer Cells. *J Infect Chemother* (2017) 23:354–9. doi: 10.1016/j.jiac.2017.02.009
15. Smits VA, Medema RH. Checking Out the G(2)/M Transition. *Biochim Biophys Acta* (2001) 1519:1–12. doi: 10.1016/S0167-4781(01)00204-4
16. Greenbaum LE. Cell Cycle Regulation and Hepatocarcinogenesis. *Cancer Biol Ther* (2004) 3:1200–7. doi: 10.4161/cbt.3.12.1392
17. Czabotar PE, Lessene G, Strasser A, Adams JM. Control of Apoptosis by the BCL-2 Protein Family: Implications for Physiology and Therapy. *Nat Rev Mol Cell Biol* (2014) 15:49–63. doi: 10.1038/nrm3722
18. Hemmings BA, Restuccia DF. PI3K-PKB/Akt Pathway. *Cold Spring Harb Perspect Biol* (2012) 4:a011189. doi: 10.1101/cshperspect.a011189
19. Zhou LT, Wang KJ, Li L, Li H, Geng M. Pinocembrin Inhibits Lipopolysaccharide-Induced Inflammatory Mediators Production in BV2 Microglial Cells Through Suppression of PI3K/Akt/NF-KappaB Pathway. *Eur J Pharmacol* (2015) 761:211–6. doi: 10.1016/j.ejphar.2015.06.003
20. Song MS, Salmena L, Pandolfi PP. The Functions and Regulation of the PTEN Tumour Suppressor. *Nat Rev Mol Cell Biol* (2012) 13:283–96. doi: 10.1038/nrm3330
21. Zhu DM, Xue WL, Tao W, Li JC. Biological Effects of Ray Cartilage Extract on Human Breast Cancer Cell Line MCF-7 and Its Mechanism. *Int J Clin Exp Med* (2015) 8:7425–9.
22. Gudarzi H, Salimi M, Irian S, Amanzadeh A, Kandelous HM, Azadmanesh K, et al. Ethanolic Extract of Ferula Gummosa Is Cytotoxic Against Cancer Cells by Inducing Apoptosis and Cell Cycle Arrest. *Nat Prod Res* (2015) 29:546–50. doi: 10.1080/14786419.2014.951854
23. Kwon SB, Kim MJ, Yang JM, Lee HP, Hong JT, Jeong HS, et al. Cudrania Tricuspidata Stem Extract Induces Apoptosis via the Extrinsic Pathway in SiHa Cervical Cancer Cells. *PloS One* (2016) 11:e0150235. doi: 10.1371/journal.pone.0150235
24. Bai Y, Chen B, Hong W, Liang Y, Zhou M, Zhou L. Sedum Sarmentosum Bunge Extract Induces Apoptosis and Inhibits Proliferation in Pancreatic Cancer Cells via the Hedgehog Signaling Pathway. *Oncol Rep* (2016) 35:2775–84. doi: 10.3892/or.2016.4679
25. Kong WH, Zheng G, Lu JN, Tso JK. Temperature Dependent Expression of Cdc2 and Cyclin B1 in Spermatogenic Cells During Spermatogenesis. *Cell Res* (2000) 10:289–302. doi: 10.1038/sj.cr.7290056
26. Xu XY, Song GQ, Yu YQ, Ma HY, Ma L, Jin YN. Apoptosis and G2/M Arrest Induced by Allium Ursinum (Ramson) Watery Extract in an AGS Gastric Cancer Cell Line. *Onco Targets Ther* (2013) 6:779–83. doi: 10.2147/OTT.S45865
27. Chou WM, Chen CN, Hsieh HT, Lo TY, Juan PY, Mai FD. G2/M Arrest and Apoptosis of Human Colorectal Cancer Cells Induced by Water Extract From Residues of Jelly Fig Achene. *Technol Health Care* (2015) 24(Suppl 1):S147–53. doi: 10.3233/THC-151063
28. Crowley LC, Marfell BJ, Scott AP, Waterhouse NJ. Triggering Apoptosis in Hematopoietic Cells With Cytotoxic Drugs. *Cold Spring Harb Protoc* (2016) 2016(7). doi: 10.1101/pdb.prot087130
29. Alenzi FQ. Cell Type Specific Expression of the Apoptosis Stimulating Protein (ASPP-2) in Human Tissues. *Acta Microbiol Immunol Hung* (2010) 57:419–29. doi: 10.1556/AMicr.57.2010.4.8
30. Hu J, Xu ML, Dai YJ, Ding XL, Xiao C, Ji HJ, et al. Exploration of Bcl-2 Family and Caspases-Dependent Apoptotic Signaling Pathway in Zearalenone-Treated Mouse Endometrial Stromal Cells. *Biochem Biophys Res Commun* (2016) 476:553–9. doi: 10.1016/j.bbrc.2016.05.161
31. Salvador-Gallego R, Mund M, Cosentino K, Schneider J, Unsay J, Schraermeyer U, et al. Bax Assembly Into Rings and Arcs in Apoptotic Mitochondria is Linked to Membrane Pores. *EMBO J* (2016) 35:389–401. doi: 10.15252/embj.201593384
32. Srinivasula SM, Ashwell JD. IAPs: What's in a Name? *Mol Cell* (2008) 30:123–35. doi: 10.1016/j.molcel.2008.03.008
33. Dohi T, Okada K, Xia F, Wilford CE, Samuel T, Welsh K, et al. An IAP-IAP Complex Inhibits Apoptosis. *J Biol Chem* (2004) 279:34087–90. doi: 10.1074/jbc.C400236200
34. Mita AC, Mita MM, Nawrocki ST, Giles FJ. Survivin: Key Regulator of Mitosis and Apoptosis and Novel Target for Cancer Therapeutics. *Clin Cancer Res* (2008) 14:5000–5. doi: 10.1158/1078-0432.CCR-08-0746
35. Yuhuan L, Da L, Yulin Z, Yujing L, Jing X, Lee1 RJ, et al. Silencing of Survivin Expression Leads to Reduced Proliferation and Cell Cycle Arrest in Cancer Cells. *J Cancer* (2015) 6(11):1187–94. doi: 10.7150/jca.12437
36. Hatem R, El Botty R, Chateau-Joubert S, Servely JL, Labiod D, Plater LD, et al. Targeting mTOR Pathway Inhibits Tumor Growth in Different Molecular

Subtypes of Triple-Negative Breast Cancers. *Oncotarget* (2016) 7:48206–19. doi: 10.18632/oncotarget.10195
37. Zhang YQ, Kwok-Shing Ng P, Kucherlapati M, Chen FJ, Liu YX, Tsang YH, et al. A Pan-Cancer Proteogenomic Atlas of PI3K/AKT/mTOR Pathway Alterations. *Cancer Cell* (2017) 31:820–32. doi: 10.1016/j.ccell.2017.04.013
38. Guertin DA, Sabatini DM. Defining the Role of mTOR in Cancer. *Cancer Cell* (2007) 12:9–22. doi: 10.1016/j.ccr.2007.05.008
39. Xiao-Yu L, Shan-Shan W, Zhe H, Fei H, Yun-Peng C, Yang Y, et al. Triptolide Restores Autophagy to Alleviate Diabetic Renal Fibrosis Through the miR-141-3p/PTEN/Akt/mTOR Pathway. *Mol Ther: Nucleic Acids* (2017) 9:48–56. doi: 10.1016/j.omtn.2017.08.011
40. Xinbing Z, Zhengzheng L, Tongtong L, Fei L, Yuesheng Lv, Lei L, et al. Osthole Inhibits the PI3K/AKT Signaling Pathway *via* Activation of PTEN and Induces Cell Cycle Arrest and Apoptosis in Esophageal Squamous Cell Carcinoma. *Biomed Pharmacother* (2018) 102:502–9. doi: 10.1016/j.biopha.2018.03.106

Conflict of Interest: The authors declare that the research was conducted in the absence of any commercial or financial relationships that could be construed as a potential conflict of interest.

frontiers in Oncology

ORIGINAL RESEARCH
published: 10 January 2022
doi: 10.3389/fonc.2021.818869

Breast Cancer Classification Based on Tumor Budding and Stem Cell-Related Signatures Facilitate Prognosis Evaluation

Zhenxian Xiang[1,2,3,4†], *Qiuming He*[1,2,3,4†], *Li Huang*[5], *Bin Xiong*[1,2,3,4*] *and Qingming Xiang*[3,4,6*]

[1] Department of Gastrointestinal Surgery, Zhongnan Hospital of Wuhan University, Wuhan, China, [2] Department of Gastric and Colorectal Surgical Oncology, Zhongnan Hospital of Wuhan University, Wuhan, China, [3] Hubei Key Laboratory of Tumor Biological Behaviors, Wuhan, China, [4] Hubei Cancer Clinical Study Center, Wuhan, China, [5] Department of Pathology, Tongji Hospital, Tongji Medical College, Huazhong University of Science and Technology, Wuhan, China, [6] Department of Radiation and Medical Oncology, Zhongnan Hospital of Wuhan University, Hubei Key Laboratory of Tumor Biological Behaviors & Hubei Cancer Clinical Study Center, Wuhan, China

OPEN ACCESS

Edited by:
San-Gang Wu,
First Affiliated Hospital of Xiamen University, China

Reviewed by:
Jun Wang,
Sichuan University, China
Guiying Wang,
The Third Hospital of Hebei Medical University, China

***Correspondence:**
Bin Xiong
Tony126liu@126.com
Qingming Xiang
15327105188@163.com

[†]These authors have contributed equally to this work

Specialty section:
This article was submitted to Breast Cancer, a section of the journal Frontiers in Oncology

Received: 20 November 2021
Accepted: 13 December 2021
Published: 10 January 2022

Citation:
Xiang Z, He Q, Huang L, Xiong B and Xiang Q (2022) Breast Cancer Classification Based on Tumor Budding and Stem Cell-Related Signatures Facilitate Prognosis Evaluation. Front. Oncol. 11:818869. doi: 10.3389/fonc.2021.818869

Background: Tumor budding (TB) is emerging as a prognostic factor in multiple cancers. Likewise, the stemness of cancer cells also plays a vital role in cancer progression. However, nearly no research has focused on the interaction of TB and tumor stemness in cancer.

Methods: Tissue microarrays including 229 cases of invasive breast cancer (BC) were established and subjected to pan-cytokeratin immunohistochemical staining to evaluate molecular expression. Univariate and multivariate analyses were applied to identify prognostic factors of BC, and the Chi-square test was used for comparison of categorical variables.

Results: High-grade TB was significantly associated with T stage, lymph node metastasis, tumor node metastasis (TNM) stage, epithelial-mesenchymal transition, and poor disease-free survival (DFS) of BC patients. We also found that the prognostic value of TB varied widely among different subtypes and subgroups. Cox regression analysis then showed that TB grade was an independent prognostic factor. Moreover, cancer stem cell (CSC) markers CD44 and ALDH1A1 were significantly higher in high-grade TB tumors. Consequently, patients were classified into high CSC score subgroup and low CSC score subgroups. Further research found that CSC scores correlated with clinicopathological features and DFS of BC patients. Based on TB grade and CSC scores, we classified BC patients into TB_{low}-$CSCs_{low}$ (type I), TB_{low}-$CSCs_{high}$ (type II), TB_{high}-$CSCs_{low}$ (type III), and TB_{high}-$CSCs_{high}$ (type IV) subgroups. Survival analysis showed that patients in the type I subgroup had the best DFS, whereas those in the type IV subgroup had the worst DFS. Finally, a TB-CSC-based nomogram for use in BC was established. The nomogram was well calibrated to predict the probability of 5-year DFS, and the C-index was 0.837.

Finally, the area under the curve value for the nomogram (0.892) was higher than that of the TNM staging system (0.713).

Conclusion: The combination of TB grade with CSC score improves the prognostic evaluation of BC patients. A novel nomogram containing TB grade and CSC score provides doctors with a candidate tool to guide the individualized treatment of cancer patients.

Keywords: CSCs, ALDH1A1, CD24, CD44, breast cancer, tumor budding, prognosis, EMT

INTRODUCTION

Breast cancer (BC), which has the highest incidence of any female cancer worldwide, is one of the significant risk factors affecting women's health (1). Owing to cancer heterogeneity and individual differences, BC patients show variation in prognosis. That is to say, despite a favorable overall survival rate, the recurrence rate of BC within 15 years exceeds 40% (2). Therefore, individualized cancer therapy appears to be important to maximize therapeutic effects and improve quality of life. Standardized and reproducible biomarkers, which could be applied to predict tumor progression, are a cornerstone of individualized cancer therapy.

Tumor budding (TB), first introduced in colorectal cancer and typically defined as the formation of single malignant cells or cell clusters of fewer than five malignant cells at the invasive tumor front (3), is an emerging prognostic biomarker in solid cancers (4, 5). The 2019 World Health Organization (WHO) classification of colorectal cancer introduce TB as a second major grading criterion (6). Additionally, the prognostic value of TB in CRC is emphasized by the inclusion of this feature as an additional prognostic factor for this disease in the tumor-node-metastasis (TNM) classification of 2017 and WHO classification of 2019 (3, 6, 7). Besides, TB is also a novel prognostic indicator independent of tumor stage and grade in esophageal, gastric (8), bladder (9), and pancreatic tumors (10, 11). Owing to the lack of standardized scoring systems and large-scale studies, whether TB represents an additional prognostic factor in BC requires further research.

The concept of cancer stem cells (CSCs) was first formulated in 1800 (12) and refers to a unique subset of cells with elevated self-renewal, differentiation, and proliferation abilities (13). Because of their "stem-like" properties commonly shared with normal tissue stem cells, these cells are termed CSCs. In acute myeloid leukemia, researchers first found the clear evidence of CSCs being an essential tumor-initiating subset of cancer cells (14, 15). Since then, similar tumor-initiating subpopulations have been identified in various types of cancers *via* different CSC cell surface markers or side population (SP) analysis (16–18). Accumulating evidence demonstrates that breast CSCs originate from either normal mammary stem cells or mammary epithelial cells by epithelial-mesenchymal transition (EMT) (19). In addition, CSCs have been shown to maintain the dormant state of BC during chemotherapy and confer resistance to anoikis, causing BC recurrence, metastasis, and therapy resistance (20, 21). Numerous CSC surface markers (CD44, CD24, and ALDH1A1) (22) that can be used to assess prognosis have been identified in BC (23). As is known to all, TB is a complex biological phenomenon that is closely related to increased tumor cell dissociation, migration, and infiltration. EMT, which is the first step of TB (24, 25), has been shown to play a prominent role in tumor cell dissociation. Subsequently, some detached cancer cells could acquire stem cell phenotype to adapt to a hypoxic environment (26, 27). Thus, TB cells may acquire CSC phenotype to realize distant metastasis and colonization (28). However, whether a combination of TB and CSC markers could be used to estimate the outcomes of BC more precisely remains to be explored.

This study found that high-grade TB was correlated with the TNM stage, lymph node metastasis (LNM), and EMT of BC. Furthermore, we identified TB as an independent prognostic factor and showed that high-grade TB was correlated with worse disease-free survival (DFS) of cancer patients. Subsequently, we verified that CSC scores were correlated with tumor progression and TB. A novel nomogram based on TB and CSC score was constructed and shown to improve the prognostic evaluation of BC. The defined subtype may provide guidance for individualized treatment of cancer patients.

MATERIALS AND METHODS

Patients and Tissue Arrays

Tumor tissue microarrays (TMAs), containing 240 cases of formalin-fixed paraffin-embedded invasive BC tissues from Hubei Cancer Hospital, were constructed (January 2002–December 2006). Eleven cases of tumor tissues were excluded due to substandard quality or incomplete information. Finally, 229 cases of specimens were enrolled in our research. Major pathological parameters, including tumor size, location, LNM, estrogen receptor (ER) status, progesterone receptor (PR) status, human epidermal growth factor receptor 2 (HER2) status,

Abbreviations: BC, breast cancer; TB, tumor budding; LNM, lymph node metastasis; TNM, tumor node metastasis; EMT, epithelial-mesenchymal transition; DFS, disease-free survival; CSCs, cancer stem cells; ER, estrogen receptor; PR, progesterone receptor; HER2, human epidermal growth factor receptor 2; AJCC, American Joint Committee on Cancer; TNBC, triple-negative BC; CMT, chemotherapy; hormone receptor positive, estrogen receptor positive or progesterone receptor positive; hormone receptor negative, estrogen receptor negative and progesterone receptor negative; TMAs, tissue microarrays; CMT +R, chemotherapy + radiotherapy.

neoadjuvant therapy, and postoperative treatment, were collected from the medical record. The Research Ethics Committee of Wuhan University (Wuhan, Hubei, China) approved this study. Informed consent was obtained from all participating patients.

Immunohistochemistry

Slides were baked in a 65°C oven for 2 h. Slides were then deparaffinized by xylene. After rehydration, we used the citrate buffer to retrieve the antigen. Being incubated with 3% hydrogen peroxide (Merck, Darmstadt, Germany) for 20 min, slides were blocked with 0.5% BSA (Beyotime, China) for 20 mins at 37°C. Next, sections were incubated overnight with primary antibody rabbit anti-pankeratin, anti-CD44 (1:100, CST 37259S), anti-ALDH1A1 (1:400, CST 36671S), and anti-CD24 (1:300, CST 9705S), anti-E-cadherin (1:400, CST 3195S, China), and anti-vimentin (1:300, CST 5741S, China). The next day, sections were incubated with secondary antibody labeled with horseradish peroxidase (HPR) for 30 min. Finally, slides were stained with diaminobenzidine and hematoxylin.

TB Assessment and IHC Score

According to the International TB Consensus Conference (ITBCC) 2016 (29), standard criteria for TB assessment was made in colorectal cancer. Pan-cytokeratin immunohistochemistry (IHC), which could highlight tumor buds and improve the interobserver agreement, was chosen to assess TB (3). In brief, TB is assessed in one 0.785 mm^2 hotspot at the invasive front. The TB was evaluated and scored by pathologist (Qingming Xiang and Li Huang). CD44, ALDH1A1, CD24, E-cadherin, and vimentin expressions were calculated as the product of percentage expressing cells (calculated by counting the number of positive tumor cells among at least 1,000 tumor cells for each tissue section manually) multiplied by mean intensity (0 to 2+). All IHC results were independently scored by two pathologists (Qingming Xiang and Li Huang). The X-tile software was used to select the best cutoff value for E-cadherin expression, vimentin expression, and TB numbers.

Statistical Analysis

IBM SPSS 24.0 (Chicago, IL, USA) was used to perform statistical analyses. Univariate and multivariate analyses were used to identify prognostic factors, and the Chi-square test was used to calculate significant differences between categorical variables. R 3.6.3 software (https://cran.r-project.org/) was used to construct heatmap and the nomogram ("DynNom" package). *p*-values less than 0.05 were considered statistically significant.

RESULT

Patient Characteristics and Pathological Examination

After screening, 229 patients with invasive BC were enrolled in the present research. The clinicopathological features of these 229 patients are shown in **Table 1**. The details of the study design and a flow chart are shown in **Figure 1**. We divided the participants into two groups: those that had tumor recurrence (86 patients) and those that did not have tumor recurrence. In addition, 62% of participants were under 50 and 100 (44%) had gone through menopause. Neoadjuvant therapy had been conducted in 44% of participants, and 190 patients had undergone postoperative chemoradiotherapy.

ER-positive and PR-positive patients were found in 102 (55%) and 102 (55%) cancer patients, respectively. In addition, there were 58 (25%) cases of HER2-positive cancer patients. Of the 229 tumors, 192 were classified as showing moderate differentiation or poor differentiation. A total of 127 tumors were LNM positive, and the T stage of most tumors (68%) was T2. TNM stage was classified according to the American Joint Committee on Cancer guidelines, and 64% of patients were classified as stage II. Finally,

TABLE 1 | Basal characteristics of 229 patients with invasive BC.

Characteristics	Total cohort	Without recurrence *N* (%)	With recurrence *N* (%)
Total cases	229	143 (100%)	86 (100%)
Age (years)			
≤50	142 (62%)	89 (62%)	53 (62%)
>50	87 (38%)	54 (38%)	33 (38%)
Menopausal status			
Premenopausal	129 (56%)	86 (60%)	43 (50%)
Postmenopausal	100 (44%)	57 (40%)	43 (50%)
T stage			
T1	30 (13%)	27 (19%)	3 (3%)
T2	156 (68%)	100 (70%)	56 (65%)
T3	43 (19%)	16 (11%)	27 (31%)
LNM			
N (–)	102 (45%)	86 (60%)	16 (19%)
N (+)	127 (55%)	57 (40%)	70 (81%)
Tumor differentiation			
Well	37 (16%)	34 (24%)	3 (3%)
Moderate	134 (59%)	97 (68%)	37 (43%)
Poor	58 (25%)	12 (8%)	46 (53%)
ER			
Negative	127 (55%)	65 (45%)	62 (72%)
Positive	102 (45%)	78 (55%)	24 (28%)
PR			
Negative	127 (55%)	70 (49%)	57 (66%)
Positive	102 (45%)	73 (51%)	29 (34%)
TNM stage			
I	14 (6%)	14 (10%)	0 (0%)
II	147 (64%)	107 (75%)	40 (47%)
III	68 (30%)	22 (15%)	46 (53%)
HER2 status			
Negative	171 (75%)	115 (80%)	56 (65%)
Positive	58 (25%)	28 (20%)	30 (35%)
Neoadjuvant therapy			
CMT	101 (44%)	51 (36%)	50 (58%)
No treatment	28 (56%)	92 (64%)	36 (42%)
Postoperative treatment			
CMT	141 (62%)	97 (68%)	44 (51%)
CMT+R	49 (21%)	20 (14%)	29 (34%)
No treatment	39 (17%)	26 (18%)	13 (15%)
TB			
Low-grade TB	150	109	41
High-grade TB	79	34	45

LNM, lymph node metastasis; ER, estrogen receptor; PR, progesterone receptor; TNM, tumor node metastasis; HER2, human epidermal growth factor receptor 2; CMT, chemotherapy; CMT+R, chemotherapy + radiotherapy.

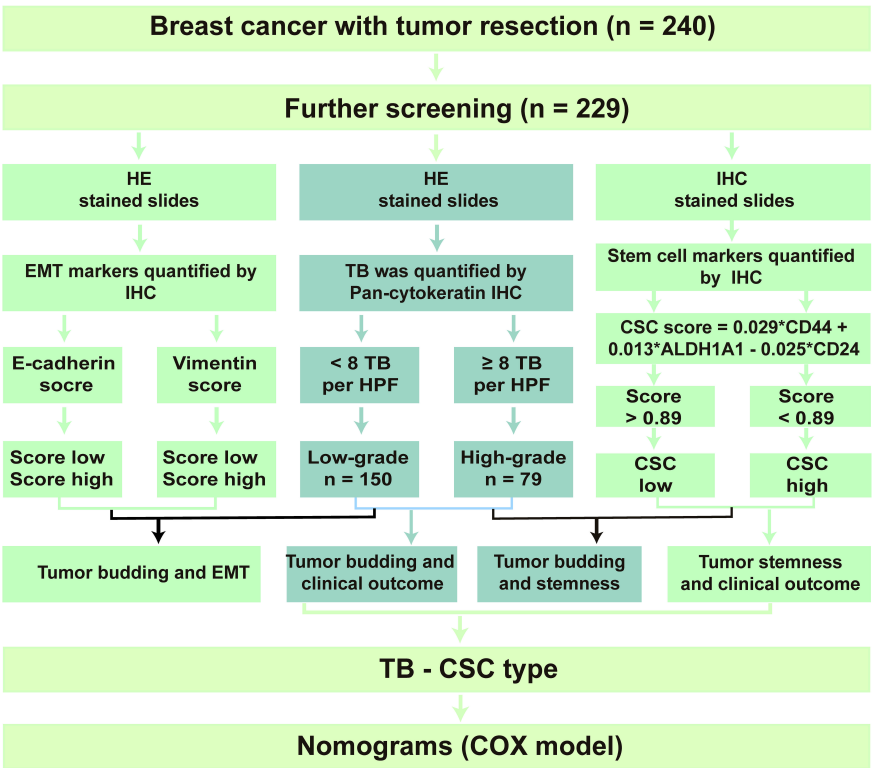

FIGURE 1 | Flow chart of the study design.

79 cases of tumors were identified as high-grade TB, and 150 cases were identified as low-grade TB.

Budding Quantification and Its Relationship With Patients' Clinical Outcome

As shown in **Figure 2A**, we observed a wide variability of TB numbers in BC, ranging from 0 to 30. The median value and mean value of TB numbers in the recurrence cohort were 7 and 8.2, respectively. Also, the median value and mean value of TB numbers in the no-recurrence cohort were 4 and 5.2, respectively. In addition, we found that the number of TB was larger in the recurrence group than the no-recurrence group, and the difference between the two groups was statistically significant (**Figure 2B**).

All possible cutoff values obtained from X-Tile (version 3.6.1) were examined with respect to their ability to predict tumor progression (30), and a budding count of eight was defined as the optimal cutoff value (**Figure 2C**). As shown in **Figure 2D**, we found that the rate of high-grade TB in the recurrence group was higher than the no-recurrence group. This result indicated that tumors with high-grade TB were more likely to recur. Representative pan-cytokeratin IHC images of low-grade TB and high-grade TB are shown in **Figures 2E, F**, respectively. TB was significantly associated with age and menopausal status (**Table 2**). Importantly, the rate of high-grade TB was significantly higher in tumors with higher T stage, LNM positivity, and advanced TNM stage (**Table 2**). However, no significant association was found between TB (high- or low-grade) and tumor differentiation, ER expression, PR expression, HER2 status, neoadjuvant therapy, or postoperative treatment (**Table 2**). These results demonstrate that TB might involve in cancer progression.

Follow-up data were available for all 229 patients. After a mean and median follow-up of 27 and 60 months, respectively, disease progression was observed in 37.2% of patients. Survival analysis was performed to compare DFS between patients with low-grade TB and those with high-grade TB. The 5-year DFS rate for patients with low-grade or high-grade TB was 72.7% and 40.0%, respectively. Thus, high-grade TB was associated with worse DFS of cancer patients (**Figure 2G**). In molecular subgroup analyses, high-grade TB was related to poor outcomes in patients with HER2-positive tumors ($p < 0.001$) (**Figure 2H**), luminal A tumors ($p = 0.038$) (**Figure 2I**), and triple-negative BC (TNBC) tumors ($p = 0.028$) (**Figure 2J**), but not in luminal B subtypes ($p = 0.237$) (**Supplementary Figure S1**). After adjusting confounding factors, multivariate analysis revealed that T stage (T2: hazard ratio [HR] = 3.256, 95% CI = 1.013–10.462; T3: HR = 4.016, 95% CI = 1.195–13.492), LNM status (HR = 3.276, 95% CI = 1.857–5.778), tumor differentiation (poor: HR = 8.402, 95% CI = 2.403–26.926), HER2 (HR = 1.725; 95% CI = 1.083–2.748), and TB (HR = 1.871, 95% CI = 1.197–2.924) were independent prognostic factors of BC patients (**Table 3**).

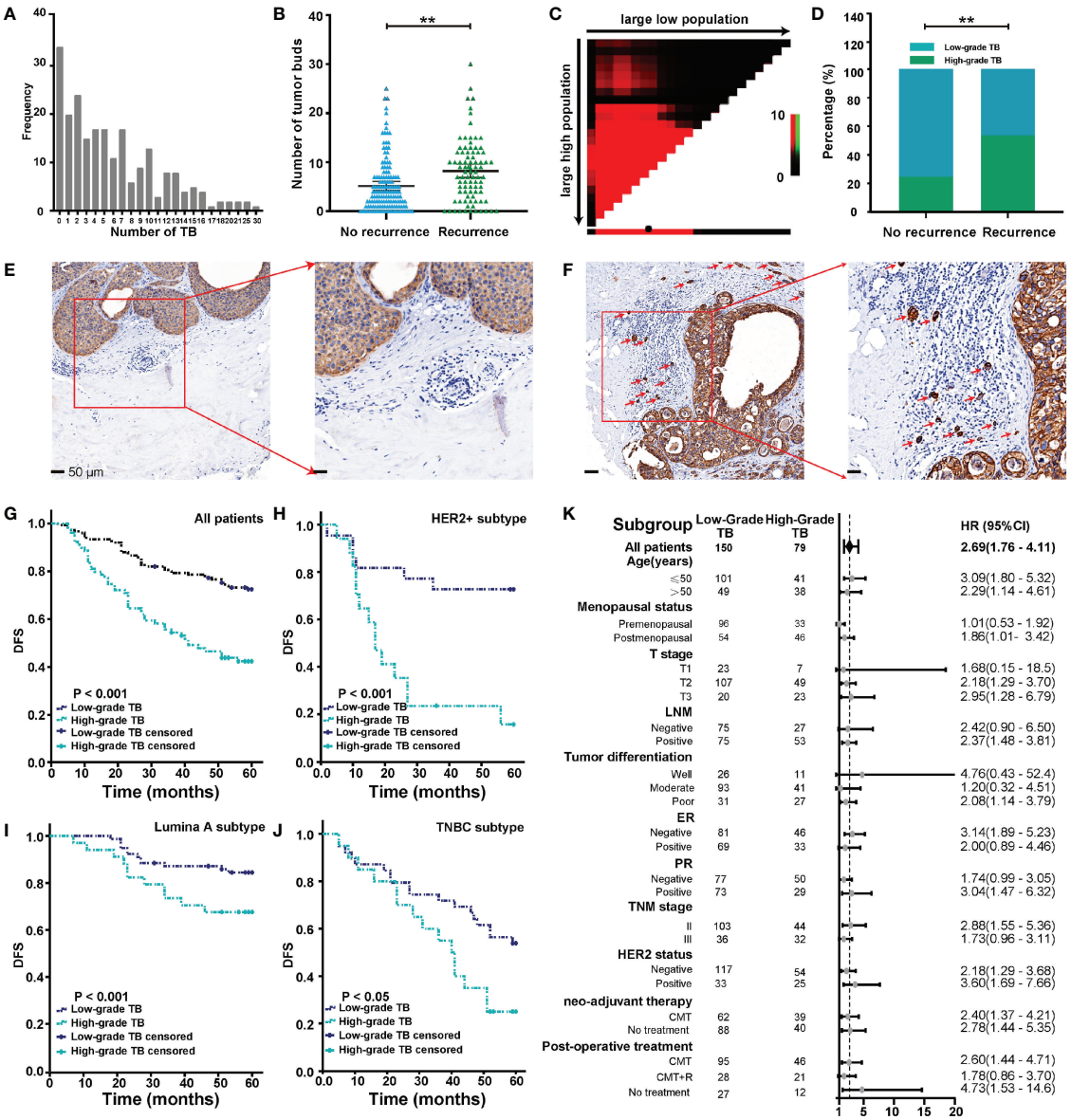

FIGURE 2 | Budding quantification and its relationship with clinical outcome. **(A)** Distribution of tumor buds in 229 cases of BC. **(B)** TB score in recurrent and nonrecurrent groups. **(C)** Analyses to define the optimal cutoff value for TB. **(D)** TB grade in recurrent and nonrecurrent groups. **(E, F)** Representative images of low-grade TB **(E)** and high-grade TB **(F)**. Red arrows point to tumor buds. **(G)** The Kaplan-Meier survival curve shows the DFS of BC after stratification by TB grade. **(H–J)** The Kaplan-Meier survival curve shows DFS of different BC subtypes after stratification by TB. **(K)** The forest map shows the prognostic significance of TB in different subgroups. $^{**}p < 0.01$.

Subgroup Analysis of the Association of TB With DFS in BC Patients

The prognostic significance of TB for 5-year DFS was analyzed in each subgroup (**Figure 2K**). High-grade TB predicted a worse DFS of BC patients (HR = 2.69, 95% CI = 1.76–4.11). High-grade TB also significantly predicted a worse DFS in subgroups based on age (≤50 years) (HR = 3.09, 95% CI = 1.80–5.32), age (>50 years) (HR = 2.29, 95% CI = 1.14–4.61), postmenopausal status (HR = 1.86, 95% CI = 1.01–3.42), T2 (HR = 2.18, 95% CI = 1.29–3.70), T3 (HR = 2.95, 95% CI = 1.28–6.79), LNM positivity (HR = 2.37, 95% CI = 1.48–3.81), poor differentiation (HR = 2.08, 95% CI = 1.14–3.79), PR-positive group (HR = 3.04, 95% CI = 1.47–6.32), stage II (HR = 2.88, 95% CI = 1.55–5.36), HER2 negativity (HR = 2.18, 95% CI = 1.29–3.68), HER2 positivity (HR = 3.60, 95% CI = 1.69–7.66), neoadjuvant chemotherapy (CMT) (HR = 2.4, 95% CI = 1.37–4.21), no neoadjuvant therapy (HR = 2.78, 95% CI = 1.44–5.35), postoperative CMT (HR = 2.6, 95% CI = 1.44–4.71), and no postoperative treatment (HR = 4.73,

TABLE 2 | The relationship between TB, CSC score, and major clinicopathological characteristics of BC patients.

Characteristics	Low-grade TB *N* (%)	High-grade TB *N* (%)	*p*-value	Low CSC score *N* (%)	High CSC score *N* (%)	*p*-value
Total cases	150	79		114 (100%)	115 (100%)	
Age (years)						
≤50	101 (67%)	41 (52%)		75 (66%)	67 (58%)	
>50	49 (33%)	38 (48%)	***0.022***	39 (34%)	48 (42%)	0.241
Menopausal status						
Premenopausal	96 (64%)	33 (42%)		71 (62%)	58 (50%)	
Postmenopausal	54 (36%)	46 (58%)	***0.001***	43 (38%)	57 (50%)	0.071
T stage						
T1	23 (15%)	7 (9%)		21 (18%)	9 (8%)	
T2	107 (71%)	49 (62%)		79 (69%)	77 (67%)	
T3	20 (13%)	23 (29%)	***0.027***	14 (13%)	29 (25%)	***0.007***
LNM						
N (–)	75 (50%)	27 (34%)		62 (54%)	40 (35%)	
N (+)	75 (50%)	53 (67%)	***0.01***	52 (46%)	75 (65%)	***0.003***
Tumor differentiation						
Well	26 (17%)	11 (14%)		26 (23%)	11 (10%)	
Moderate	93 (62%)	41 (52%)		71 (62%)	63 (55%)	
Poor	31 (21%)	27 (34%)	0.082	17 (15%)	41 (35%)	***<0.001***
ER						
Negative	81 (54%)	46 (58%)		49 (43%)	78 (68%)	
Positive	69 (46%)	33 (42%)	0.541	65 (57%)	37 (32%)	***<0.001***
PR						
Negative	77 (51%)	50 (63%)		49 (43%)	78 (68%)	
Positive	73 (49%)	29 (37%)	0.084	65 (57%)	37 (32%)	***<0.001***
TNM stage						
I	29 (7%)	3 (4%)		21 (18%)	9 (8%)	
II	103 (69%)	44 (56%)		79 (69%)	77 (67%)	
III	36 (24%)	32 (41%)	***0.028***	14 (12%)	29 (25%)	***0.007***
HER2 status						
Negative	117 (78%)	54 (68%)		91 (80%)	80 (70%)	
Positive	33 (22%)	25 (32%)	0.111	23 (20%)	35 (30%)	0.074
Neoadjuvant therapy						
CMT	62 (41%)	39 (49%)		50 (44%)	51 (44%)	
No treatment	88 (59%)	40 (51%)	0.244	64 (56%)	64 (56%)	0.941
Postoperative treatment						
CMT	95 (63%)	46 (58%)		19 (17%)	68 (59%)	
CMT+R	28 (19%)	21 (27%)		73 (64%)	30 (26%)	
No treatment	27 (18%)	12 (15%)	0.373	22 (19%)	17 (15%)	***<0.001***

LNM, lymph node metastasis; ER, estrogen receptor; PR, progesterone receptor; TNM, tumor node metastasis; HER2, human epidermal growth factor receptor 2; CMT, chemotherapy; CMT+R, chemotherapy + radiotherapy. Boldface indicates P < 0.05.

TABLE 3 | Multivariable analysis for 5-DFS.

Parameters	HR	95% CI	*p*-value	Parameters	HR	95% CI	*p*-value
T stage				**T stage**			
T1	1.000			T1	1.000		
T2	3.256	1.013–10.462	**0.048**	T2	3.170	0.987–10.186	0.053
T3	4.016	1.195–13.492	**0.025**	T3	3.866	1.153–12.969	0.029
Tumor differentiation				**Tumor differentiation**			
Well	1			Well	1		
Moderate	2.252	0.684–7.411	0.182	Moderate	2.18	0.665–7.151	0.199
Poor	8.042	2.403–26.926	**0.001**	Poor	7.23	2.169–24.102	***0.001***
LNM				**LNM**			
Negative	1.000			Negative	1.000		
Positive	3.276	1.857–5.778	**0.001**	Positive	3.122	1.776-5.488	0.001
HER2				**HER2**			
Negative	1.000			Negative	1.000		
Positive	1.725	1.083–2.748	**0.022**	Positive	1.725	1.083-2.748	***0.028***
TB				**TB-CSC type**			
Low grade	1.000			Type I. vs type II and III	0.316	0.164-0.608	***0.001***
High grade	1.871	1.197–2.924	**0.006**	Type IV vs. type II and III	1.776	1.085-2.907	***0.022***

LNM, Lymph node metastasis; HER2, human epidermal growth factor receptor-2; TB, tumor budding; CSCs, cancer stem cells. Boldface indicates P < 0.05.

95% CI = 1.53–14.6) subgroup. However, no significant association was found in the other subgroups (**Figure 2K**).

High-Grade TB Was Correlated With EMT and Stemness of Cancer

IHC analysis of 229 cases of BC revealed that high-grade TB was significantly associated with low expression of E-cadherin (**Figure 3A**). As expected, vimentin was more likely to be upregulated in high-grade TB tissues (**Figure 3B**). These results demonstrate that TB is associated with the EMT process in BC patients.

Through the process of EMT, some detached cancer cells can adapt to a hypoxic environment and acquire resistance to anoikis to realize survival and metastasis (11, 12). Based on previous research, TB cells may acquire stem cell phenotypes to allow the colonization (3). Thus, expression of classic CSC markers, CD44, CD24, and ALDH1A1 was detected by IHC in TAMs (**Figure 3C**). As shown in **Figures 3D–F**, CD44 and CD24 were mainly located in the cell membrane, while ALDH1A1 was mainly located in the cytoplasm. We also found that CD44 and ALDH1A1 were more likely upregulated in high-grade TB tissues (**Figures 3D, E**). No significant association was found between TB and CD24 expression (**Figure 3F**). We performed Cox regression analysis to establish a CSC score, consisting of three parameters (CD44, ALDH1A1, and CD24). The Cox regression coefficient of CD44, ALDH1A1, and CD24 are 0.029,

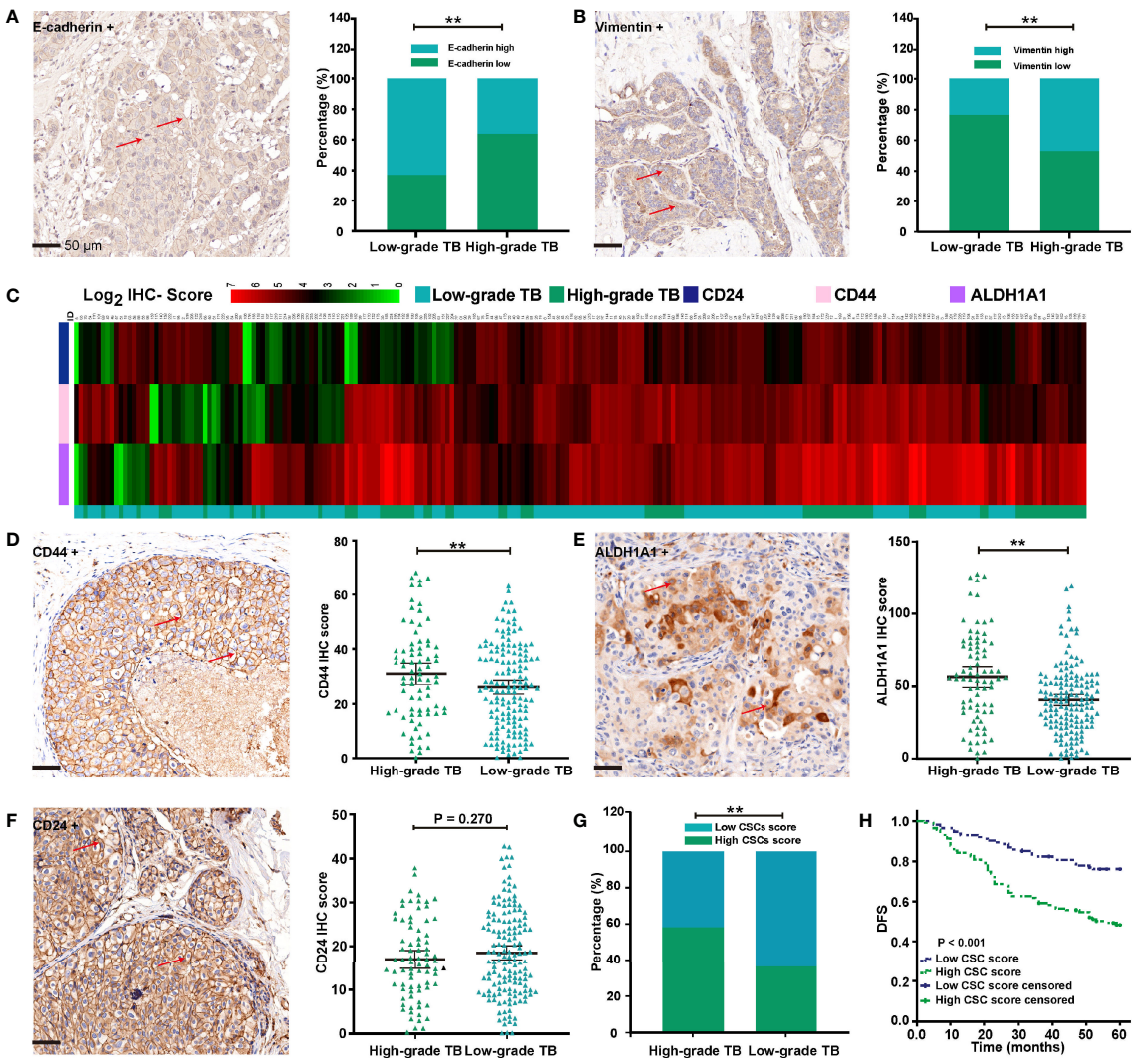

FIGURE 3 | Associations of TB with EMT and tumor stemness. **(A)** Representative IHC images of E-cadherin and its associations with TB grade. **(B)** Representative IHC images of vimentin and its associations with TB grade. **(C)** Heatmap showed CSC marker expression in 229 cases of BC patients. **(D)** Representative IHC images of CD44 and its associations with TB grade. **(E)** Representative IHC images of ALDH1A1 and its associations with TB grade. **(F)** Representative IHC images of CD24 and its associations with TB grade. **(G)** Association between TB grade and CSC score. **(H)** The Kaplan-Meier survival curve shows disease-free survival of BC after stratification by CSC score. $^{**}p < 0.01$.

0.013, and −0.025, respectively. A formula, which is based on Cox regression coefficient of three CSC markers and IHC score of three CSC markers, was established to calculate CSC score. The CSC score is = 0.029 × (CD44 IHC score) + 0.013 × (ALDH1A1 IHC score) − 0.025 × (CD24 IHC score). According to the median value (0.89) of the CSC score, we classified BC patients into high and low CSC score groups. Among 229 patients, the CSC score was high in 115 patients (49%), and 114 patients (51%) were defined as low CSC score. Further research revealed that CSC score was significantly associated with T stage, LNM, tumor differentiation, ER positivity, PR positivity, and TB of BC (**Table 2** and **Figure 3G**). In contrast, no significant association was found between CSC score and other clinicopathological factors. Kaplan-Meier survival analysis showed that the duration of DFS of BC patients with low CSC scores was significantly longer than that of those with high CSC scores ($p < 0.001$) (**Figure 3H**).

Combination of TB Grade and CSC Score Improves Prognostic Evaluation

Our data show that TB is an independent prognostic factor for BC, and that this complex biological behavior is closely related to CSC characteristics. Here, we also assessed the predictive value of the combination of TB grade and CSC score for 5-year DFS in BC patients.

Based on TB and CSC score, we classified patients into TB_{low}-$CSCs_{low}$ (type I), TB_{low}-$CSCs_{high}$ (type II), TB_{high}-$CSCs_{low}$ (type III), and TB_{high}-$CSCs_{high}$ (type IV) subgroups. Survival analysis revealed that patients in the type I group had the best DFS, while the worst DFS was found in the type IV group (**Figure 4A**). As the type II and type III groups had similar survival, we grouped these two types together for multivariable analysis. Multivariable Cox regression analysis of the relevant clinical variables and TB-CSC type revealed that TB-CSC type was an independent prognostic factor (**Table 3**).

A nomogram, integrating the TB-CSC type and clinicopathological risk variables was established to predict the probability of 1-year, 3-year, and 5-year DFS in BC patients (**Figure 4B**). The predictive accuracy of the nomogram for DFS is displayed in **Figure 4C**. The detailed points of each variable were provided in the following, T stage (T1: 0.0, T2: 55.2, T3: 48.8), N status (N0: 0.0, N1: 36.5, N2:61.9, N3: 91.9), histological grade (G1: 0.0, G2: 35.2, G3: 100.0), HER-2 status (negative: 0.0, positive: 20.2), and TB-CSC type (type 1: 0.0, type 2 or type 3: 35.8, type 4: 59.3). The c-index of this nomogram for 5-year DFS was 0.837 (95% CI = 0.76–0.92). Calibration curves showed that the models performed well compared with ideal models' performance in both cohorts (**Figure 4C**). The nomograms also had better predictive ability than the TNM staging system, with area under the curve values of 0.892 (95% CI = 0.850–0.935) and 0.713 (95% CI = 0.644-0.783) (**Figure 4D**).

DISCUSSION

BC is a highly heterogeneous disease, with wide variation in prognosis among different molecular subtypes (31). Disease risk assessment to guide individualized treatment of cancer patients is particularly essential and urgent for precision medicine (32). As two different aspects of the tumor microenvironment, TB and CSCs are promising prognostic indicators for risk assessment. For its simple evaluation method and enormous clinical significance, TB is an emerging prognostic biomarker in solid cancers (33, 34). Likewise, the independent predictive significance of CSC markers in the prognosis of cancer has been documented (35–37). The current study revealed that

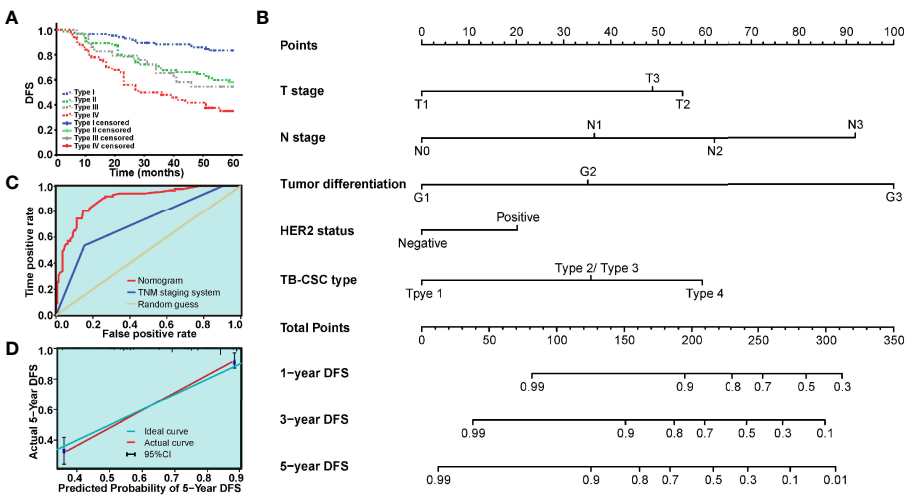

FIGURE 4 | The model based on TB-CSC type for predicting tumor recurrence in patients with BC. **(A)** The Kaplan-Meier survival curve shows DFS after stratification by TB-CSC type. **(B)** The nomogram based on TB-CSC type predicting DFS probability of BC patients. **(C)** Calibration plot showing favorable agreement between the predicted rate (red line) and actual rate (green line). **(D)** The ROC curve shows a better prognostic value of nomogram on recurrence than TNM staging system.

high-grade TB was correlated with the TNM stage, LNM, EMT, and CSC score of BC patients. Furthermore, we demonstrated that TB was an independent prognostic factor, and that high-grade TB was correlated with worse DFS of cancer patients. Finally, a novel nomogram based on TB grade and CSC score was constructed and shown to improve the prognostic evaluation of BC patients.

Accurate assessment of the TB is the key to fully exploiting its prognostic value. Hematoxylin and eosin staining of specimens is typically used to assess TB; however, it is challenging to accurately identify TB by this method against a background of peritumoral inflammation. Pan-cytokeratin IHC, a powerful approach that can highlight tumor buds and reduce observed differences, has been adopted to assess TB (38). In our study, TB was verified to be an independent prognostic factor in BC. We also demonstrated that TB was associated with age, menopausal status, T stage, TNM stage, and LNM status. Consistent with previous studies (39), our study showed that TB was an independent prognostic factor of BC patients. In BC, which is highly heterogeneous, prognosis varies widely among different subtypes. Our research verified that high-grade TB predicted a worse DFS in patients with HER2+ tumors, luminal A tumors, and TNBC tumors. However, no significant association was found between TB and luminal B subtypes. Subgroup analysis also demonstrated that the prognostic value of TB varies widely among different subgroups. Thus, the prognostic value of TB may be different in different subtypes and subgroups.

The EMT process, which provides tumor cells with several prometastatic traits (40, 41), has also been implicated in the metastatic process (42). Generally, epithelial-type cells can gain more mesenchymal traits to increase their invasive ability *via* EMT (43), thereby overcoming antimetastatic bottlenecks and achieving the great potential for metastasis. In our research, diminished expression of E-cadherin was found in the high-grade TB sample and aberrantly expressed vimentin was observed in the low-grade TB samples. High-grade TB was also associated with EMT of BC patients. TB correlates with EMT confirmed the hypothesis that TB may represent the EMT process. Through EMT, some detached cancer cells from the primary site could acquire stem cell phenotype to adapt to a hypoxic environment (26, 27). Thus, TB cells might acquire stem cell phenotypes to realize distant metastasis and colonization (28). As expected, we demonstrated that high-grade TB was highly correlated with overexpression of CSC markers in BC. Furthermore, we found that CD44 and ALDH1A1 were strongly expressed in tumor buds. No significant association was found between TB grade and CD24 expression.

Our study of TB and CSC markers inspires us a new understanding of molecular and pathogenetic mechanisms of TB, which could be a potential target of "antibudding therapies". As part of the invasive tumor front, TB should be integrated into the biological context for better characterized. The role of CSC score as a prognostic factor is emerging. In esophageal cancer (44), high CSC score predicted a worse overall survival of cancer patients. In the current research, the CSC score integrated three types of CSC markers (CD24+, CD44+, ALDH1A1+). For the first time, we found that a high CSC score predicted worse DFS of BC patients. A retrospective analysis found that a CSC-related signature could facilitate the prognostic prediction in pancreatic ductal adenocarcinoma (45), consistent with our results. However, almost no study has explored the interaction between TB and CSC score. For the first time, we verified that high-grade TB was correlated with high CSC score. We also revealed that CSC score was significantly associated with tumor sizes, LNM, tumor differentiation, ER, PR, and TB. Consequently, tumor classification based on TB and CSC score revealed that TB_{low}-$CSCs_{low}$ (type I) patients had the best 5-year DFS, whereas TB_{high}-$CSCs_{high}$ group had the worst 5-year DFS. For the first time, we combined TB and CSC score to evaluate prognosis. This method paves a new way to potential new tumor therapies.

Due to the limitations of a single prognostic factor, an integrated prognostic system was needed for a better prognostic evaluation. In previous research, autophagy-, EMT-, and immune-related gene signatures of cancers have been extensively reported (46–48), while few studies have combined CSC expression profile and TB to conduct risk assessment. The nomogram is a comprehensive predictive model, which assigns a score to each risk factor based on its contribution to the prognosis. The incidence rate was then evaluated through the scoring system. Here, we developed a novel predictive nomogram (49) for recurrence in invasive BC; the first TB-CSC-based nomogram in BC was established. The result demonstrated that TB-CSC-based nomograms could provide a more accurate prognostic assessment than the TNM staging system.

However, this study had some limitations. Firstly, as it was a retrospective study with a relatively small sample size, it was difficult to exclude heterogeneity and define optimal cutoff value. In the same cancer type, cutoff value of TB often varies widely in different researchers (50, 51). Thus, further validation is needed in large-scale multicenter randomized controlled trials. We also hope that further results about TB will be uploaded to a public database (such as The Cancer Genome Atlas), which could provide doctors with global dataset and optimal cutoff value of TB and CSCs to evaluate prognosis. Second, although pan-cytokeratin IHC exhibited its excellent score ability, more accurate and convenient methods are needed to be combined to assess TB, such as artificial intelligence tools (52). Third, although tissue cores from different areas were used to construct the TMAs, not every core of the TMAs could completely represent the optimal site for TB assessment. In this sense, slides of the whole tumor will be of great importance to assess TB. Fourth, the size of the TB needs to be strictly uniformly characterized in future research. In some studies, TB was defined as a cell cluster of less than four cells, whereas other studies used a threshold of five or more cells.

Despite the aforementioned limitations, this study found high-grade TB was correlated with TNM stage, LNM, and EMT of BC. Furthermore, we found that TB was an independent prognostic factor, and that high-grade TB correlated with worse DFS of cancer patients. We then revealed that CSC score (based on CD44, CD24, and ALDH1A1) was correlated with tumor progression and TB. A novel nomogram based on TB and CSC score, which improved the prognostic evaluation of BC, was constructed. The defined subtype

may provide doctors a candidate guideline for individualized treatment of cancer patients.

DATA AVAILABILITY STATEMENT

The original contributions presented in the study are included in the article/**Supplementary Material**. Further inquiries can be directed to the corresponding authors.

ETHICS STATEMENT

Written informed consent was obtained from the individual(s) for the publication of any potentially identifiable images or data included in this article.

AUTHOR CONTRIBUTIONS

Participated in research design: ZX, QH, QX, and BX. Performed data analysis: ZX, QH, and QX. Experimental operation: ZX, QH, and QX. Wrote or contributed to the writing of the manuscript: QH, ZX, and BX. All authors contributed to the article and approved the submitted version.

FUNDING

This work was supported by the National Natural Science Foundation of China (No. 82103005, No. 81872376).

ACKNOWLEDGMENTS

The authors appreciate Sze Ka Lun for his helpful language revisions.

SUPPLEMENTARY MATERIAL

The Supplementary Material for this article can be found online at: https://www.frontiersin.org/articles/10.3389/fonc.2021.818869/full#supplementary-material

REFERENCES

1. Sung H, Ferlay J, Siegel RL, Laversanne M, Soerjomataram I, Jemal A, et al. Global Cancer Statistics 2020: GLOBOCAN Estimates of Incidence and Mortality Worldwide for 36 Cancers in 185 Countries. *CA: Cancer J Clin* (2021) 71(3):209–49. doi: 10.3322/caac.21660
2. Torre LA, Bray F, Siegel RL, Ferlay J, Lortet-Tieulent J, Jemal A. Global Cancer Statistics, 2012. *CA: Cancer J Clin* (2015) 65(2):87–108. doi: 10.3322/caac.21262
3. Lugli A, Zlobec I, Berger MD, Kirsch R, Nagtegaal ID. Tumour Budding in Solid Cancers. *Nat Rev Clin Oncol* (2021) 18(2):101–15. doi: 10.1038/s41571-020-0422-y
4. Niwa Y, Yamada S, Koike M, Kanda M, Fujii T, Nakayama G, et al. Epithelial to Mesenchymal Transition Correlates With Tumor Budding and Predicts Prognosis in Esophageal Squamous Cell Carcinoma. *J Surg Oncol* (2014) 110 (6):764–9. doi: 10.1002/jso.23694
5. Gujam FJ, McMillan DC, Mohammed ZM, Edwards J, Going JJ. The Relationship Between Tumour Budding, the Tumour Microenvironment and Survival in Patients With Invasive Ductal Breast Cancer. *Br J Cancer* (2015) 113(7):1066–74. doi: 10.1038/bjc.2015.287
6. Nagtegaal ID, Odze RD, Klimstra D, Paradis V, Rugge M, Schirmacher P, et al. The 2019 WHO Classification of Tumours of the Digestive System. *Histopathology* (2020) 76(2):182–8. doi: 10.1111/his.13975
7. Weiser MR. AJCC 8th Edition: Colorectal Cancer. *Ann Surg Oncol* (2018) 25 (6):1454–5. doi: 10.1245/s10434-018-6462-1
8. Kucuk S. Prognostic Value of Tumour Budding in Stomach Cancers. *Int J Clin Pract* (2021) 75(12):e14922. doi: 10.1111/ijcp.14922
9. Eckstein M, Kimmel C, Bruendl J, Weber F, Denzinger S, Gierth M, et al. Tumor Budding Correlates With Tumor Invasiveness and Predicts Worse Survival in Pt1 non-Muscle-Invasive Bladder Cancer. *Sci Rep* (2021) 11 (1):17981. doi: 10.1038/s41598-021-97500-3
10. Sadozai H, Acharjee A, Gruber T, Gloor B, Karamitopoulou E. Pancreatic Cancers With High Grade Tumor Budding Exhibit Hallmarks of Diminished Anti-Tumor Immunity. *Cancers (Basel)* (2021) 13(5):1090. doi: 10.3390/cancers13051090
11. Zlobec I, Lugli A, Baker K, Roth S, Minoo P, Hayashi S, et al. Role of APAF-1, E-Cadherin and Peritumoral Lymphocytic Infiltration in Tumour Budding in Colorectal Cancer. *J Pathol* (2007) 212(3):260–8. doi: 10.1002/path.2164
12. Virchow R. Archiv für pathologische Anatomie und Physiologie und für klinische Medicin. *Cellular-Pathologie* (1861) 27(53):52–65.
13. Reya T, Morrison SJ, Clarke MF, Weissman IL. Stem Cells, Cancer, and Cancer Stem Cells. *Nature* (2001) 414(6859):105–11. doi: 10.1038/35102167
14. Bonnet D, Dick JE. Human Acute Myeloid Leukemia is Organized as a Hierarchy That Originates From a Primitive Hematopoietic Cell. *Nat Med* (1997) 3(7):730–7. doi: 10.1038/nm0797-730
15. Lapidot T, Sirard C, Vormoor J, Murdoch B, Hoang T, Caceres-Cortes J, et al. A Cell Initiating Human Acute Myeloid Leukaemia After Transplantation Into SCID Mice. *Nature* (1994) 367(6464):645–8. doi: 10.1038/367645a0
16. Ricci-Vitiani L, Lombardi DG, Pilozzi E, Biffoni M, Todaro M, Peschle C, et al. Identification and Expansion of Human Colon-Cancer-Initiating Cells. *Nature* (2007) 445(7123):111–5. doi: 10.1038/nature05384
17. Singh SK, Hawkins C, Clarke ID, Squire JA, Bayani J, Hide T, et al. Identification of Human Brain Tumour Initiating Cells. *Nature* (2004) 432 (7015):396–401. doi: 10.1038/nature03128
18. Schatton T, Murphy GF, Frank NY, Yamaura K, Waaga-Gasser AM, Gasser M, et al. Identification of Cells Initiating Human Melanomas. *Nature* (2008) 451(7176):345–9. doi: 10.1038/nature06489
19. Dittmer J, Rody A. Cancer Stem Cells in Breast Cancer. *Histol Histopathol* (2013) 28(7):827–38. doi: 10.14670/hh-28.827
20. Kim SY, Hong SH, Basse PH, Wu C, Bartlett DL, Kwon YT, et al. Cancer Stem Cells Protect Non-Stem Cells From Anoikis: Bystander Effects. *J Cell Biochem* (2016) 117(10):2289–301. doi: 10.1002/jcb.25527
21. Butti R, Gunasekaran VP, Kumar TVS, Banerjee P, Kundu GC. Breast Cancer Stem Cells: Biology and Therapeutic Implications. *Int J Biochem Cell Biol* (2019) 107:38–52. doi: 10.1016/j.biocel.2018.12.001
22. Li J, Qi D, Hsieh TC, Huang JH, Wu JM, Wu E. Trailblazing Perspectives on Targeting Breast Cancer Stem Cells. *Pharmacol Ther* (2021) 223:107800. doi: 10.1016/j.pharmthera.2021.107800
23. Dionísio MR, Vieira AF, Carvalho R, Conde I, Oliveira M, Gomes M, et al. BR-BCSC Signature: The Cancer Stem Cell Profile Enriched in Brain Metastases That Predicts a Worse Prognosis in Lymph Node-Positive Breast Cancer. *Cells* (2020) 9(11):2442. doi: 10.3390/cells9112442
24. Kohler I, Bronsert P, Timme S, Werner M, Brabletz T, Hopt UT, et al. Detailed Analysis of Epithelial-Mesenchymal Transition and Tumor Budding Identifies Predictors of Long-Term Survival in Pancreatic Ductal Adenocarcinoma. *J Gastroenterol Hepatol* (2015) 30(Suppl 1):78–84. doi: 10.1111/jgh.12752

25. Koyuncuoglu M, Okyay E, Saatli B, Olgan S, Akin M, Saygili U. Tumor Budding and E-Cadherin Expression in Endometrial Carcinoma: Are They Prognostic Factors in Endometrial Cancer? *Gynecol Oncol* (2012) 125(1):208–13. doi: 10.1016/j.ygyno.2011.12.433
26. Dawson H, Grundmann S, Koelzer VH, Galván JA, Kirsch R, Karamitopoulou E, et al. Tyrosine Kinase Receptor B (TrkB) Expression in Colorectal Cancers Highlights Anoikis Resistance as a Survival Mechanism of Tumour Budding Cells. *Histopathology* (2015) 66(5):715–25. doi: 10.1111/his.12603
27. Righi A, Sarotto I, Casorzo L, Cavalchini S, Frangipane E, Risio M. Tumour Budding is Associated With Hypoxia at the Advancing Front of Colorectal Cancer. *Histopathology* (2015) 66(7):982–90. doi: 10.1111/his.12602
28. Charpentier M, Martin S. Interplay of Stem Cell Characteristics, EMT, and Microtentacles in Circulating Breast Tumor Cells. *Cancers (Basel)* (2013) 5 (4):1545–65. doi: 10.3390/cancers5041545
29. Lugli A, Kirsch R, Ajioka Y, Bosman F, Cathomas G, Dawson H, et al. Recommendations for Reporting Tumor Budding in Colorectal Cancer Based on the International Tumor Budding Consensus Conference (ITBCC) 2016. *Mod Pathol: Off J United States Can Acad Pathol Inc* (2017) 30(9):1299–311. doi: 10.1038/modpathol.2017.46
30. Wang JB, Li P, Liu XL, Zheng QL, Ma YB, Zhao YJ, et al. An Immune Checkpoint Score System for Prognostic Evaluation and Adjuvant Chemotherapy Selection in Gastric Cancer. *Nat Commun* (2020) 11 (1):6352. doi: 10.1038/s41467-020-20260-7
31. Perou CM, Sørlie T, Eisen MB, van de Rijn M, Jeffrey SS, Rees CA, et al. Molecular Portraits of Human Breast Tumours. *Nature* (2000) 406 (6797):747–52. doi: 10.1038/35021093
32. Britt KL, Cuzick J, Phillips KA. Key Steps for Effective Breast Cancer Prevention. *Nat Rev Cancer* (2020) 20(8):417–36. doi: 10.1038/s41568-020-0266-x
33. Ueno H, Ishiguro M, Nakatani E, Ishikawa T, Uetake H, Matsuda C, et al. Prospective Multicenter Study on the Prognostic and Predictive Impact of Tumor Budding in Stage II Colon Cancer: Results From the SACURA Trial. *J Clin Oncol: Off J Am Soc Clin Oncol* (2019) 37(22):1886–94. doi: 10.1200/jco.18.02059
34. Bosch SL, Teerenstra S, de Wilt JH, Cunningham C, Nagtegaal ID. Predicting Lymph Node Metastasis in Pt1 Colorectal Cancer: A Systematic Review of Risk Factors Providing Rationale for Therapy Decisions. *Endoscopy* (2013) 45 (10):827–34. doi: 10.1055/s-0033-1344238
35. Wang JL, Guo CR, Su WY, Chen YX, Xu J, Fang JY. CD24 Overexpression Related to Lymph Node Invasion and Poor Prognosis of Colorectal Cancer. *Clin Lab* (2018) 64(4):497–505. doi: 10.7754/Clin.Lab.2017.171012
36. Kaufmann M, Heider KH, Sinn HP, von Minckwitz G, Ponta H, Herrlich P. CD44 Isoforms in Prognosis of Breast Cancer. *Lancet* (1995) 346(8973):502. doi: 10.1016/s0140-6736(95)91350-5
37. Liu WT, Liu WB, Gao M, Zhang YY, Gu KS. Expression of ALDH1A1 and CD133 is Associated With the Prognosis and Effect of Different Chemotherapeutic Regimens in Gastric Cancer. *Oncol Lett* (2019) 18 (5):4573–82. doi: 10.3892/ol.2019.10798
38. Koelzer VH, Zlobec I, Berger MD, Cathomas G, Dawson H, Dirschmid K, et al. Tumor Budding in Colorectal Cancer Revisited: Results of a Multicenter Interobserver Study. *Virchows Archiv: Int J Pathol* (2015) 466(5):485–93. doi: 10.1007/s00428-015-1740-9
39. Okcu O, Öztürk Ç, Şen B, Arpa M, Bedir R. Tumor Budding is a Reliable Predictor for Death and Metastasis in Invasive Ductal Breast Cancer and Correlates With Other Prognostic Clinicopathological Parameters. *Ann Diagn Pathol* (2021) 54:151792. doi: 10.1016/j.anndiagpath.2021.151792
40. Mani SA, Guo W, Liao MJ, Eaton EN, Ayyanan A, Zhou AY, et al. The Epithelial-Mesenchymal Transition Generates Cells With Properties of Stem Cells. *Cell* (2008) 133(4):704–15. doi: 10.1016/j.cell.2008.03.027
41. Yang J, Mani SA, Donaher JL, Ramaswamy S, Itzykson RA, Come C, et al. Twist, a Master Regulator of Morphogenesis, Plays an Essential Role in Tumor Metastasis. *Cell* (2004) 117(7):927–39. doi: 10.1016/j.cell.2004.06.006
42. Yang J, Weinberg RA. Epithelial-Mesenchymal Transition: At the Crossroads of Development and Tumor Metastasis. *Dev Cell* (2008) 14(6):818–29. doi: 10.1016/j.devcel.2008.05.009
43. Ferreira MM, Ramani VC, Jeffrey SS. Circulating Tumor Cell Technologies. *Mol Oncol* (2016) 10(3):374–94. doi: 10.1016/j.molonc.2016.01.007
44. Yi L, Huang P, Zou X, Guo L, Gu Y, Wen C, et al. Integrative Stemness Characteristics Associated With Prognosis and the Immune Microenvironment in Esophageal Cancer. *Pharmacol Res* (2020) 161:105144. doi: 10.1016/j.phrs.2020.105144
45. Feng Z, Shi M, Li K, Ma Y, Jiang L, Chen H, et al. Development and Validation of a Cancer Stem Cell-Related Signature for Prognostic Prediction in Pancreatic Ductal Adenocarcinoma. *J Trans Med* (2020) 18(1):360. doi: 10.1186/s12967-020-02527-1
46. Cao R, Yuan L, Ma B, Wang G, Qiu W, Tian Y. An EMT-Related Gene Signature for the Prognosis of Human Bladder Cancer. *J Cell Mol Med* (2020) 24(1):605–17. doi: 10.1111/jcmm.14767
47. Zeng F, Liu X, Wang K, Zhao Z, Li G. Transcriptomic Profiling Identifies a DNA Repair-Related Signature as a Novel Prognostic Marker in Lower Grade Gliomas. *Cancer Epidemiol Biomarkers Prev* (2019) 28(12):2079–86. doi: 10.1158/1055-9965.Epi-19-0740
48. Yang S, Wu Y, Deng Y, Zhou L, Yang P, Zheng Y, et al. Identification of a Prognostic Immune Signature for Cervical Cancer to Predict Survival and Response to Immune Checkpoint Inhibitors. *Oncoimmunology* (2019) 8(12): e1659094. doi: 10.1080/2162402x.2019.1659094
49. He C, Sun S, Zhang Y, Lin X, Li S. A Novel Nomogram to Predict Survival in Patients With Recurrence of Pancreatic Ductal Adenocarcinoma After Radical Resection. *Front Oncol* (2020) 10:1564. doi: 10.3389/fonc.2020.01564
50. Salhia B, Trippel M, Pfaltz K, Cihoric N, Grogg A, Ladrach C, et al. High Tumor Budding Stratifies Breast Cancer With Metastatic Properties. *Breast Cancer Res Treat* (2015) 150(2):363–71. doi: 10.1007/s10549-015-3333-3
51. Liang F, Cao W, Wang Y, Li L, Zhang G, Wang Z. The Prognostic Value of Tumor Budding in Invasive Breast Cancer. *Pathol Res Pract* (2013) 209 (5):269–75. doi: 10.1016/j.prp.2013.01.009
52. Weis CA, Kather JN, Melchers S, Al-Ahmdi H, Pollheimer MJ, Langner C, et al. Automatic Evaluation of Tumor Budding in Immunohistochemically Stained Colorectal Carcinomas and Correlation to Clinical Outcome. *Diagn Pathol* (2018) 13(1):64. doi: 10.1186/s13000-018-0739-3

Conflict of Interest: The authors declare that the research was conducted in the absence of any commercial or financial relationships that could be construed as a potential conflict of interest.

frontiers in Oncology

ORIGINAL RESEARCH
published: 13 January 2022
doi: 10.3389/fonc.2021.784096

Screening and Identification of Novel Potential Biomarkers for Breast Cancer Brain Metastases

Lulu Wang[1,2,3], *Dan Zeng*[1], *Qi Wang*[1], *Li Liu*[4], *Tao Lu*[1] *and Yan Gao*[1,2,3]*

[1] Department of Human Anatomy, School of Basic Medical Sciences, Capital Medical University, Beijing, China, [2] Beijing Key Laboratory of Cancer Invasion and Metastasis Research, Beijing, China, [3] Cancer Institute of Capital Medical University, Beijing, China, [4] Department of Experimental Center for Basic Medical Teaching, School of Basic Medical Sciences, Capital Medical University, Beijing, China

OPEN ACCESS

Edited by:
San-Gang Wu,
First Affiliated Hospital of Xiamen University, China

Reviewed by:
Kshama Gupta,
Mayo Clinic, United States
Xixian Ke,
Affiliated Hospital of Zunyi Medical College, China

***Correspondence:**
Yan Gao
gy1003@ccmu.edu.cn

Specialty section:
This article was submitted to Breast Cancer, a section of the journal Frontiers in Oncology

Received: 27 September 2021
Accepted: 09 December 2021
Published: 13 January 2022

Citation:
Wang L, Zeng D, Wang Q, Liu L, Lu T and Gao Y (2022) Screening and Identification of Novel Potential Biomarkers for Breast Cancer Brain Metastases. Front. Oncol. 11:784096. doi: 10.3389/fonc.2021.784096

Brain metastases represent a major cause of mortality among patients with breast cancer, and few effective targeted treatment options are currently available. Development of new biomarkers and therapeutic targets for breast cancer brain metastases (BCBM) is therefore urgently needed. In this study, we compared the gene expression profiles of the brain metastatic cell line MDA-MB-231-BR (231-BR) and its parental MDA-MB-231, and identified a total of 84 genes in the primary screening through a series of bioinformatic analyses, including construction of protein-protein interaction (PPI) networks by STRING database, identification of hub genes by applying of MCODE and Cytohubba algorithms, identification of leading-edge subsets of Gene Set Enrichment Analysis (GSEA), and identification of most up-regulated genes. Eight genes were identified as candidate genes due to their elevated expression in brain metastatic 231-BR cells and prognostic values in patients with BCBM. Then we knocked down the eight individual candidate genes in 231-BR cells and evaluated their impact on cell migration through a wound-healing assay, and four of them (KRT19, FKBP10, GSK3B and SPANXB1) were finally identified as key genes. Furthermore, the expression of individual key genes showed a correlation with the infiltration of major immune cells in the brain tumor microenvironment (TME) as analyzed by Tumor Immune Estimation Resource (TIMER) and Gene Expression Profiling Interactive Analysis (GEPIA), suggesting possible roles of them in regulation of the tumor immune response in TME. Therefore, the present work may provide new potential biomarkers for BCBM. Additionally, using GSEA, Gene Ontology (GO) and Kyoto Encyclopedia of Genes and Genomes (KEGG) Enrichment Analysis, we determined the top enriched cellular functions or pathways in 231-BR cells, which may help better understand the biology governing the development and progression of BCBM.

Keywords: breast cancer, brain metastases, KRT19, FKBP10, GSK3B, SPANXB1

INTRODUCTION

Brain metastases are the most common malignant brain tumors and are the next frontier for the management of metastatic cancer patients (1, 2). Even small lesions can cause neurological disability, and the median survival of patients with brain metastases is less than 1 year (3–5). Breast cancer is the second most frequent cause of brain metastases (3–5), and recently it has surpassed lung cancer as the leading cause of global cancer incidence (6). Despite major advances over past decades in prolonging breast cancer survival, breast cancer brain metastases (BCBM) remain incurable with current therapies, and the incidence is steadily increasing (6, 7). The cumulative incidence of identified brain metastases among patients with breast cancer (all stages at diagnosis) was not high (about 5.1%); however, it varies by subtype. Patients with HER2-positive (34% to 55%) or triple-negative (22% to 46%) subtypes experience significantly higher brain metastasis occurrence than patients with other subtypes (8–10). Moreover, prognosis after brain metastases is also subtype-dependent, and triple-negative breast cancer (TNBC) patients showed the shortest survival time after brain metastasis than other subtypes, which is only 4.9 months (9, 11).

Currently, treatment options for brain metastases include surgery, whole-brain radiotherapy, stereotactic radiosurgery, and systemic drug therapy, such as chemotherapy, targeted therapies, and immunotherapy (12–15). While systemic chemotherapy has limited efficacy, targeted therapies have recently shown promise for BCBM management (16–21). HER2-targeted therapies have been shown to increase the time to development of brain metastases and improved survival following brain metastases (16, 18–21), and patients with estrogen receptor-positive BCBM can be treated with endocrine agents, cyclin-dependent kinases 4/6 (CDK4/6) inhibitors, and the mechanistic target of rapamycin kinase (mTOR) inhibitors (17). Unfortunately, there is no effective targeted therapy for TNBC brain metastases (5, 9, 22). It is desirable to identify potential therapeutic targets or molecular risk factors or early biomarkers for this lethal disease.

Several brain metastasis-related genes and signaling pathways have been identified, such as COX2, PTGS2, HBEGF, ST6GALNAC5, CXCR4, GABA, heparinase, etc. (23–26). However, the molecular basis for BCBM remains largely unknown. The human MDA-MB-231-BR "brain-seeking" breast cancer cell line (hereafter referred to as 231-BR cells) was initially established from the TNBC cell line MDA-MB-231 (27, 28). It metastasizes with 100% frequency to the brain and has been used as an established preclinical model of brain metastatic breast cancer (29–31). In this study, we compared the gene expression profiles of the two cell lines with RNA-sequencing, and carried out a series of bioinformatic analyses and wet-lab experiments to identify the potential genes that may serve as prognostic biomarkers or therapeutic targets for BCBM.

There are many approaches to identify key genes. To be as comprehensive as possible, here we integrate different bioinformatic approaches and obtained a total of 84 differentially expressed genes (DEGs) from the primary screening. Among them, we selected 8 genes that have not been reported to be associated with BCBM in previous studies, and validated their expression levels using quantitative RT-PCR. Following this, we knocked down the 8 genes in 231-BR cells to evaluate their effects on cell migration, and finally 4 genes were identified as key genes for further exploration in our study. The key genes identified here are screened from TNBC cells and showed an impact on migration of the brain metastatic cell line 231-BR. In addition, the overexpression of the above genes was associated with worse distant metastasis–free survival (DMFS) of TNBC patients on data from Gene Expression Omnibus (GEO) database. All these pieces of evidence point to our key genes as potential therapeutic targets in TNBC brain metastases.

To establish a better understanding of the function of the selected genes, we further evaluated their RNA expression on data from The Cancer Genome Atlas (TCGA), evaluated their protein expression on data from the Clinical Proteomic Tumor Analysis Consortium (CPTAC) and HPA database, investigated the relationship between their expression and immune cell infiltration through Tumor Immune Estimation Resource (TIMER) and Gene Expression Profiling Interactive Analysis (GEPIA). It is hoped that these multiple investigative approaches could help decipher the underlying mechanisms of the specific functions of these genes in BCBM. Along with the above, we determined the top differentially regulated pathways using Gene Set Enrichment Analysis (GSEA), Gene Ontology (GO) and Kyoto Encyclopedia of Genes and Genomes (KEGG) Enrichment Analysis to better understand the biology governing the development and progression of BCBM (for a list of abbreviations used in the main text, see **Supplementary Table 1**).

MATERIALS AND METHODS

Cell Culture

The 231-BR cell line was a generous gift from Dr. Patricia Steeg (National Cancer Institute, Bethesda, MD, USA) (27). It was maintained in Dulbecco's Modified Eagle Medium (DMEM), supplemented with 200 μg/mL G418 (Sigma-Aldrich), 10% Fetal Bovine Serum (FBS), and 1% penicillin-streptomycin. MDA-MB-231 was purchased from ATCC and maintained in DMEM supplemented with 10% FBS and 1% penicillin-streptomycin.

Transwell Cell Migration and Invasion Assay

Cell migration and invasion assay were performed using 24-well transwell chambers and BioCoat Matrigel invasion chambers (BD Biosciences), respectively. For this, 2×10^4 cells were suspended in 0.1 ml medium without FBS and added to the upper compartment of the Transwell chamber. Next, 0.6 ml medium with 1% FBS was added to the lower compartment as a chemoattractant. After incubation at 37°C and 5% CO_2 for 12 h, the cells on the upper surface of the membrane were carefully removed using a cotton bud; and cells on the lower surface were fixed with 70% ethanol for 10 minutes and stained with 0.2% crystal violet. Six fields were randomly selected of each insert at a

magnification of 200× with a light microscope (Olympus, Japan). Student's t-test was used to test for significance. P values of < 0.05 were defined as significant.

RNA Extraction

Total RNA from 231-BR and MDA-MB-231 cells was extracted using TRIzol reagent (Qiagen, CA, USA) according to the manufacturer's instructions. Each group was prepared with three parallel replicates. RNA quantity and purity were assessed by a NanoDrop spectrophotometer (Thermo Fisher Scientific, Wilmington, DE, USA).

RNA Sequencing

RNA sequencing library preparation and sequencing were conducted in BGI Tech (Shenzhen, China) *via* BGISEQ-500 sequencer. The sequencing data was filtered with SOAPnuke (v1.5.2) (https://github.com/BGI-flexlab/SOAPnuke) (32) by removing reads containing sequencing adapter, removing reads whose low-quality base ratio (base quality less than or equal to 5) is more than 20%, and removing reads whose unknown base ('N' base) ratio is more than 5%. After this, clean reads were obtained and stored in FASTQ format. The clean reads were mapped to the reference genome using HISAT2 (v2.0.4). Bowtie2 (v2.2.5) was applied to align the clean reads to the gene set, a database built by BGI Tech, with known and novel coding transcripts included (33). The expression level of gene was measured in the normalized read count (given by Fragments Per Kilobase of transcript per Million mapped reads, FPKM). The gene expression heatmap was drawn by pheatmap (v1.0.8). Differential expression analysis was performed using the DESeq2 (v1.4.5) (34). False discovery rate (FDR) adjusted P values (Q value) of < 0.05 were defined as significant. The RNA sequencing data have been uploaded to the GEO with accession number: GSE183862.

GO and KEGG Enrichment Analysis

In order to gain a better insight to the change of phenotype, GO (including biological processes (BP), molecular functions (MF), and cellular components (CC)) and KEGG enrichment analysis of DEGs were performed using DR.TOM system of BGI Tech as previously described (35). The significant terms and pathways were obtained with a criterion of Bonferroni adjusted P value (Q value) < 0.05. Only the top twenty terms for each category were shown.

PPI Network Construction and Module Analysis

The PPI (Protein-Protein Interaction) Network of DEGs was constructed using STRING database (version 11.0), and the minimum required interaction score was 0.4 (36). Cytoscape (version 3.7.2) was employed to visualize the molecular interaction networks (37). The MCODE algorithm was used to determine the most significant clusters of highly interacting nodes within the PPI network. The criteria for cluster finding were as follows: MCODE scores > 5, degree cutoff = 2, node score cutoff = 0.2, k-score = 2, and max. depth=100 (38). The CytoHubba algorithm was used to determine the top 30 nodes ranked by Degree in the PPI network (39).

GSEA

GSEA on RNA-seq expression data was performed using GSEA official software package (https://www.gsea-msigdb.org/gsea/index.jsp). Analyses were performed to identify gene sets that were enriched in 231-BR cells relative to 231 cells. GSEA statistical significance was assessed using GSEA software that calculated FDR. Gene sets were considered significantly enriched if their FDR adjusted P values were less than 0.25, as defined by the publishers of the GSEA tool (40, 41).

Quantitative RT-PCR

After total RNA was extracted, quantitative RT-PCR was performed using SuperReal PreMix Plus (SYBR Green) (TIGANGEN, Beijing, China) in a final volume of 20 μl containing 10 μM each of the forward and reverse primers as described by the manufacture. Relative levels of transcript expression were measured using CFX96 Real-time System, C1000 Thermal Cycler (BioRad). The relative expression was calculated using the 2−ddct method with GAPDH as endogenous controls. The following primers were used: see **Supplementary Table 2**. Student's t-test was used to test for significance. P values of < 0.05 were defined as significant.

RNA Interference Assay

To knock down each candidate gene in 231-BR cells, the lentiviral vector (U6-MCS-Ubiquitin-Cherry-IRES-puromycin) containing the short-hairpin RNA (shRNA) specifically targeting each gene was constructed (GeneChem, China). For lentivirus infection, three individual shRNA oligos targeting each gene were pooled together: see **Supplementary Table 3**, and the HitransG (Genechem) was used according to the manufacturer's instructions. Student's t-test was used to test for significance. P values of < 0.05 were defined as significant.

Wound Healing Assay

The monolayer culture growth rate was determined using a Cellomics Arrayscan (Genechem). Briefly, after infected by lentivirus, cells of the same density were seeded into flat-bottom 96-well plates and grown under normal conditions. Images of the same area were captured at 0, 16 and 24 hours after the scratch using a Cellomics Arrayscan according to the manufacturer's instructions (GeneChem). The migration area was measured on the images using ImageJ. The wound healing rate was calculated as the area of original wound minus the area of wound during healing divided by the area of original wound. Student's t-test was used to test for significance. P values of < 0.05 were defined as significant.

Metastasis-Free Survival Analysis

The metastasis-free survival in breast cancer patients was analyzed on datasets obtained from GEO database through PROGgene Version 2, a comprehensive survival analysis tool (42). Patients were divided into two groups based on the cutoff of

median or 25th percentile. Survival analysis was performed using cox proportional hazards analysis. The two groups were compared by a Kaplan-Meier survival plot, and the HR and log rank P value were calculated. The P value was calculated by log rank test. P values of < 0.05 were defined as significant.

UALCAN Analysis

RNA-Seq-derived gene expression levels from TCGA and protein expression levels from CPTAC were acquired and analyzed by UALCAN portal (http://ualcan.path.uab.edu). The expression levels of the genes were analyzed based on sample types and tumor stages (43). Student's t-test was used to test for significance. P values of < 0.05 were defined as significant.

Receiver Operating Characteristic Analysis

ROC analyses were performed in TCGA data using the function "roc" in the R package pROC.

TIMER Analysis

Correlations between the key genes (KRT19, FKBP10 and GSK3B) expression level and infiltration of immune cells and tumor purity based on TCGA database were calculated and plotted using TIMER2.0 (44, 45). The "Immune-Gene" module were selected, and the TIMER, EPIC, quanTIseq, xCell, MCP-counter, CIBERSORT and CIBERSORT-ABS algorithms were applied for immune infiltration estimations. The correlation coefficient was determined by the Spearman method. P values for the Kaplan-Meier analyses are based on log rank tests.

GEPIA Analysis

The correlations between gene expression and different immune cell biomarkers were analyzed though GEPIA (http://gepia.cancer-pku.cn/), which is a newly developed interactive web server for analyzing the RNA sequencing expression data of tumors and normal samples from the TCGA and the GTEx projects, using a standard processing pipeline (46). The correlation coefficient was determined by the Spearman method.

Statistical Analysis

Statistical analyses are described in detail in the respective *Materials and Methods* sections above and in the figure legends. The statistical test is also indicated whenever a P value is reported in the text. Unless specified otherwise, statistical comparisons were performed using GraphPad Prism 7 software.

RESULTS

Screening and Identifying of DEGs Based on RNA Sequencing

To study the characteristics of the brain metastatic variant 231-BR cells, transwell cell migration and invasion assay were performed. As a "brain-seeking" breast cancer cell line, 231-BR cells exhibited an increased invasion and migration capacities as compared with its parental MDA-MB-231 cells, especially the former (**Figure 1A**). In the search for novel genes related to the pathogenesis of breast cancer brain metastasis, DEGs between 231-BR and MDA-MB-231 cells were screened and identified by

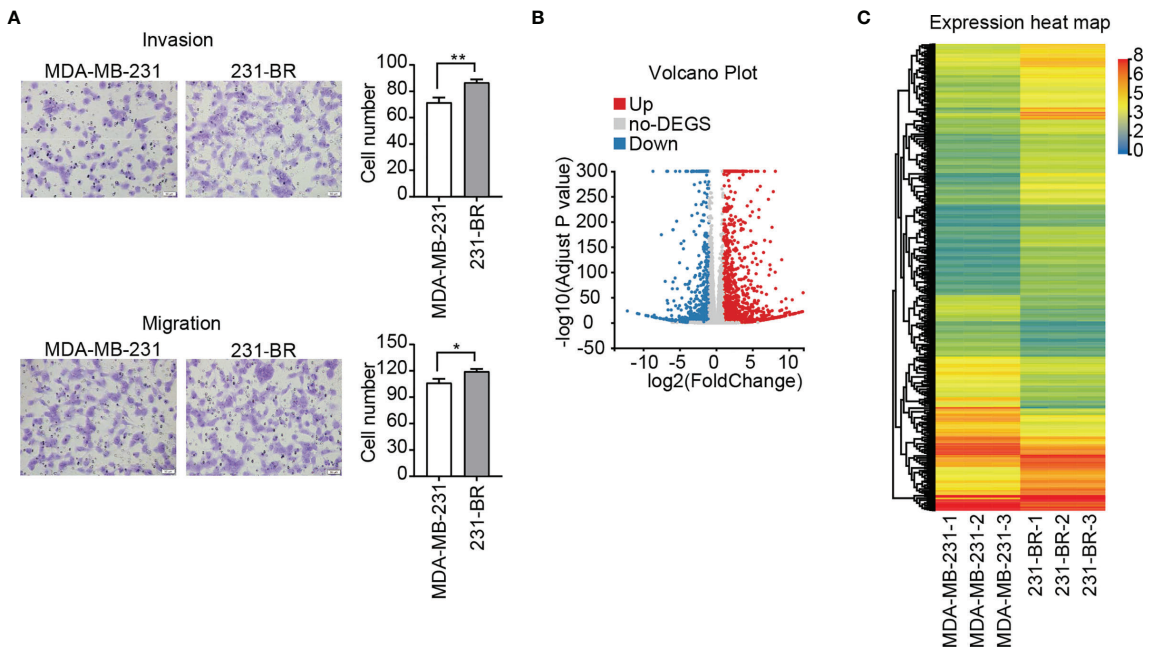

FIGURE 1 | Invasion, migration and gene expression of MDA-MB-231 and 231-BR cells. **(A)** Representative images of invasion and migration assays are shown on the left and quantified data on the right. Bar, 50μm. Student's t-test was used for statistical analysis: *P < 0.05, **P < 0.01. **(B)** Volcano plot of DEGs. **(C)** The heatmap represents the expression values (FPKM) of DEGs.

RNA sequencing. Expression was measured using FPKM. The mRNAs were identified as DEGs if they met the following criteria: the FPKM values≥ 1, FDR adjusted P value (Q value) < 0.05 and |Log2 (fold-change)| > 1. On the basis of this definition, 545 upregulated genes and 315 downregulated genes were identified and shown in volcano plot and heatmap (**Figures 1B, C**).

KEGG and GO Enrichment Analysis of DEGs

To gain a better insight of the potential mechanisms underlying brain metastases of breast cancer cells, GO and KEGG enrichment analysis of DEGs was performed. The pathway with a criterion of Bonferroni adjusted P value (Q value) < 0.05 was identified as significant. The most significant KEGG pathways are shown in **Figure 2A**. Among the twenty involved pathways, eleven of them were related to Cancers (KEGG Pathway Term Level 2), including Pathways in cancer, Proteoglycans in cancer, Small cell lung cancer, Chronic myeloid leukemia, Choline metabolism in cancer, Pancreatic cancer, Colorectal cancer, Glioma, Non-small cell lung cancer, Hepatocellular carcinoma, Breast cancer and Bladder cancer; four were related to Signal transduction (KEGG Pathway Term Level 2), including ErbB signaling pathway, Ras signaling

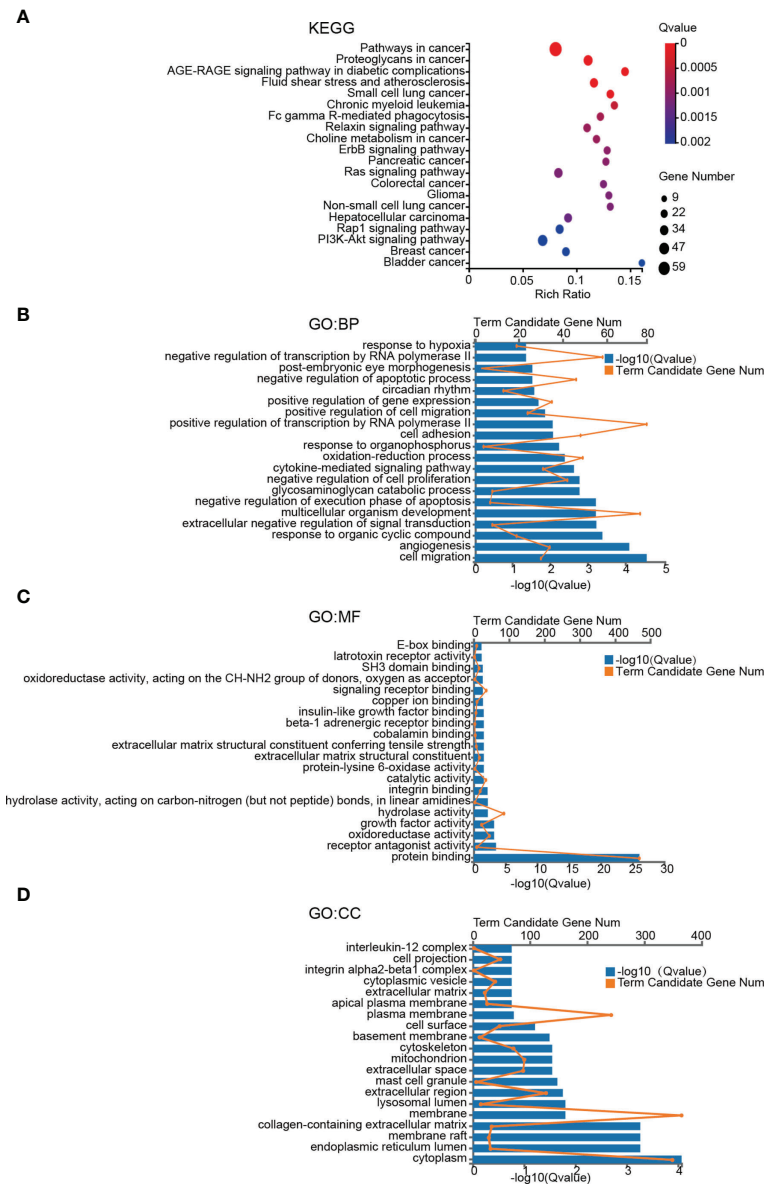

FIGURE 2 | KEGG pathway and GO term enrichment analyses of DEGs. **(A)** KEGG pathway analysis of DEGs. **(B–D)** Enriched GO-terms for BP, MF, and CC. The top twenty terms for each category are shown. The significant pathways and terms were obtained with a criterion of Bonferroni adjusted P value (Q value) < 0.05.

pathway, Rap1 signaling pathway and PI3K-Akt signaling pathway; two were related to Endocrine system, including AGE-RAGE signaling pathway in diabetic complications and Relaxin signaling pathway; Fluid shear stress and atherosclerosis that was related to Cardiovascular diseases (KEGG Pathway Term Level 2) and Fc gamma R-mediated phagocytosis that was related to Organismal Systems (KEGG Pathway Term Level 2).

GO functional annotation analysis including biological process (BP), molecular function (MF), cellular component (CC) was used to further investigate functional differences of the DEGs. The top 20 most enriched terms of BP, MF and CC were presented in **Figures 2B–D**. Cell migration, angiogenesis and response to organic cyclic compound in BP category, protein binding, receptor antagonist activity and oxidoreductase activity in MF category, and plasma membrane, membrane and integral component of plasma membrane in CC category were the top 3 most significant terms in the 3 categories of GO, respectively (**Figures 2B–D**).

PPI Network Construction and Module Analysis

Hub genes defined as highly interconnected genes in the network have been considered functionally significant. To find the hub genes and clarify the interactions between the DEGs, the PPI network of the 860 DEGs was constructed using STRING database (**Figure 3A**). Two plug-ins of Cytoscape were employed to identify the hub genes: (1) The core network modules of the PPI network were identified by plug-in MCODE of Cytoscape, and the top one significant module with 13 nodes and 68 edges were extracted (Score=11.333). These 13 hub genes were identified and assigned to MCODE Group (**Figure 3B** and **Table 1**). (2) The top 30 nodes ranked by Degree in the PPI network were calculated by the plug-in CytoHubba, and these 30 genes were selected and assigned to CytoHubba Group (**Figure 3C** and **Table 1**).

Pathway Enrichment Assessed by GSEA

GSEA is a computational method to determine the statistical significance of *a priori* defined set of genes and the existence of concordant differences between two biological states (40, 41). Upon performing the GSEA analysis, Axon guidance was the only significant signaling pathway identified by the default setting in the GSEA tool, with FDR P value = 0.114, Nominal P value < 0.0001, Normalized Enrichment Score (NES) = 1.715, ES = 0.523, Leading edge: tags=29%, list=13%, signal=32%, FWER P value: 0.129 (**Figure 4A**). The elevated expression of the 36 leading edge subsets in 231-BR groups was shown (**Figure 4B**), and these genes were assigned to the GSEA Group (**Table 1**).

Identification of Candidate Genes

From the primary screening, genes that may be related to brain metastatic potential were determined through the following approaches and assigned to four groups accordingly: (1) MCODE Group: the 13 hub genes identified by MCODE (**Figure 3B**, **Table 1** and **Supplementary Table 4**); (2) Cytohubba Group: the 30 hub genes identified by Cytohubba (**Figure 3C**, **Table 1** and **Supplementary Table 5**); (3) GSEA group: the 36 leading edge subsets of GSEA (**Figure 4B**, **Table 1** and **Supplementary Tables 6**, **7**); (4) TOP DEGs group: the 10 most up-regulated DEGs in 231-BR group determined by Log2 (fold-change) (**Table 1** and **Supplementary Table 8**). Accordingly, a total of 84 unique genes were identified (**Table 1**).

To analyze the prognostic value of the genes, the correlation between gene expression and metastasis-free survival, which was defined as time from diagnosis to distant metastasis as first event, was assessed using datasets from GEO (**Figure 5**). Patients were divided into two groups based on the cutoff of median or 25th percentile. High expression of combined expression of the 8 genes, KRT19, FKBP10, GSK3B, SPANXB1, FN1, MYO1D, ANO8 and ESM1 in breast cancer patients was associated with worse metastasis-free survival in breast cancer patients (combined expression: log rank P = 0.0159, HR = 1; KRT19: log rank P = 0.0075, HR = 1.45; FKBP10: log rank P = 0.0061, HR = 3.5; GSK3B: log rank P = 0.0130, HR = 2.15; SPANXB1: log rank P = 0.0306, HR = 1; FN1: log rank P = 0.0003, HR = 1.62; MYO1D: log rank P = 0.0245, HR = 2.36; ANO8: log rank P = 0.0415, HR = 1; ESM1: log rank P = 0.0049, HR = 1.71) (**Figure 5**). Meanwhile, their roles in BCBM have not been thoroughly investigated in previous studies. Therefore, the above 8 genes were identified as our candidate genes (**Figure 5**).

The PPI network of the candidate genes was built with STRING and showed in **Figure 6A**. They were annotated using KEGG pathway annotations and GO terms (**Figure 6B** and **Supplementary Figure 1**). The expression levels of the candidate genes were verified using quantitative RT-PCR (**Figure 6C**). These genes all showed a higher expression in 231-BR cells as compared with MDA-MB-231 cells.

The Prognostic Values of the Candidate Genes in BCBM and Effects of Them on 231-BR Cell Migration

To explore the prognostic values of the candidate genes in BCBM, we analyzed the relationship of the gene expression with brain-metastasis survival in breast cancer patients using data from a public dataset GSE12276, which contain the brain relapse information of a total of 204 patients. We assessed the prognostic value using Cox proportional hazards analysis, with risk group as covariate and brain metastasis-free survival as endpoint. The candidate gene set showed a significantly correlation with brain metastasis-free survival of breast cancer patients [log rank P = 0.011, hazard ratio (HR) = 3.781, CI = 1.257 − 11.368], indicating a prognostic value of the gene set in predicting brain metastasis (**Figure 7A**).

Next, Each gene was analyzed individually for its effect on 231-BR cell migration. The 8 candidate genes were individually knocked down in 231-BR cells, and cell migration was evaluated using the wound healing assay (**Figures 7B, C**). Knockdown efficiency was verified by quantitative RT-PCR (**Figure 7D**). As shown, among the above-mentioned 8 genes, knockdown of four

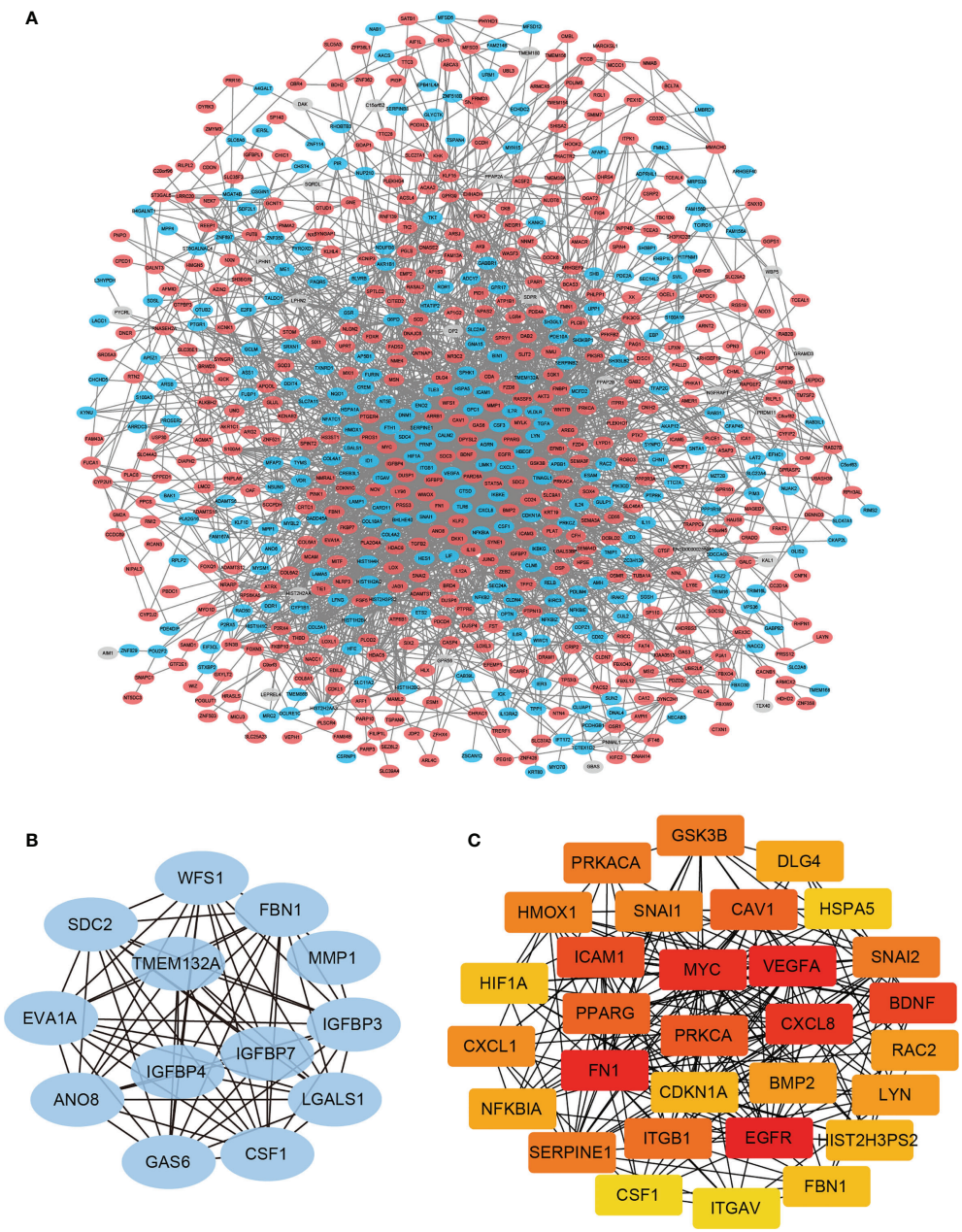

FIGURE 3 | PPI network construction and module analysis. **(A)** The PPI Network of DEGs was constructed using STRING database, and visualized with Cytoscape. **(B)** The most significant cluster of highly interacting nodes within the PPI network as determined by MCODE algorithm. **(C)** The top 30 nodes ranked by degree in the PPI network determined by CytoHubba algorithm.

genes: KRT19, FKBP10, GSK3B, and SPANXB1 significantly inhibited the migration of 231-BR cells. Arising from this, these four genes were determined as the final key genes in our study.

Expression of the Key Genes in Breast Cancer Patients

In the results section above, the candidate gene set showed a significantly correlation with brain metastasis-free survival of breast cancer patients, and each individual candidate genes appear to have an impact on metastasis-free survival of breast cancer patients. In addition, each individual key genes showed an effect on the migration of 231-BR cells (**Figure 7**). These data indicated these genes may serve as potential biomarkers in BCBM. To better understand the functions of the genes in breast cancer, we next evaluated the expression of the key genes in breast cancer patients using Samples from the public databases, including TCGA, CPTAC, and HPA Databases (**Figures 8A–E**).

TABLE 1 | Candidate genes from the primary screen.

Group names	Number of genes	Gene symbols
MCODE group	13	CSF1 FBN1 MMP1 IGFBP3 IGFBP4 ANO8 GAS6 LGALS1 WFS1 TMEM132A SDC2 EVA1A IGFBP7
CYTOHUBBA group	30	CSF1 FBN1 GSK3B BDNF LYN NFKBIA HSPA5 CXCL1 PPARG SERPINE1 SNAI1 HIF1A PRKCA PRKACA RAC2 HMOX1 VEGFA DLG4 CXCL8 HIST2H3PS2 EGFR ICAM1 MYC FN1 CAV1 CDKN1A ITGB1 BMP2 SNAI2 ITGAV
GSEA group	36	GSK3B SEMA3A EPHA5 NTN4 NGEF SEMA6D CFL2 EPHA7 EFNB1 NFATC4 SEMA3E DCC CXCR4 EPHA4 FES SLIT2 ROBO2 EFNA3 EPHA6 SEMA4G EPHA3 ROBO3 PLXNC1 EPHB1 SEMA3B SRGAP3 SEMA3G GNAI1 ABLIM1 EPHA1 SEMA3F SEMA4D FYN DPYSL2 UNC5C SRGAP1
TOP DEGs group	10	MMP1 SEMA3A KRT19 SOCS2 SPANXB1 FST KCNAB2 FKBP10 MYO1D ESM1

The RNA and protein expression of the key genes in breast cancer patients based on sample types and individual cancer stages was evaluated using TCGA and CPTAC databases, respectively (**Figures 8A–D**). Elevated expression of KRT19, FKBP10 and GSK3B at both transcriptional and translational levels in BRCA were observed as compared with normal breast tissue, while the transcript per million (TPM) values of SPANXB1 were extremely low (TPM < 1) and not shown. Moreover, HPA database was applied to validate the expression of the key genes at protein level. The similar result was obtained, that is, KRT19, FKBP10 and GSK3B protein all showed elevated expression in BRCA tissue compared with normal breast tissue, whereas SPANXB1 was not detected (**Figure 8E**). The expression levels of the four key genes were also evaluated in human cancer cell lines, particularly in breast cancer cell lines, and overexpression of KRT19, FKBP10 and GSK3B in TCGA breast cancer patients and breast cancer cell lines were observed (**Supplementary Figure 2**). In addition, relationships between KRT19, FKBP10 and GSK3B expression and clinicopathological features from TCGA breast cancer cohort (n = 1083) were also explored (**Supplementary Table 9**). It should be noted that although the expression level of SPANXB1 was very low in breast cancer patients as well as in most of the human cancer cell lines (**Supplementary Figure 2**), it showed a very high expression in the brain metastatic 231-BR cells as compared with its parental MDA-MD-231. In light of its pro-migratory effect on 231-BR cells as well as its prognostic value in metastasis-free survival of breast cancer patients (**Figures 5E**, **7**), SPANXB1 was therefore also considered as a key gene in the present study.

To assess the predictive performance of the key genes in breast cancer, we performed ROC analysis and used the area

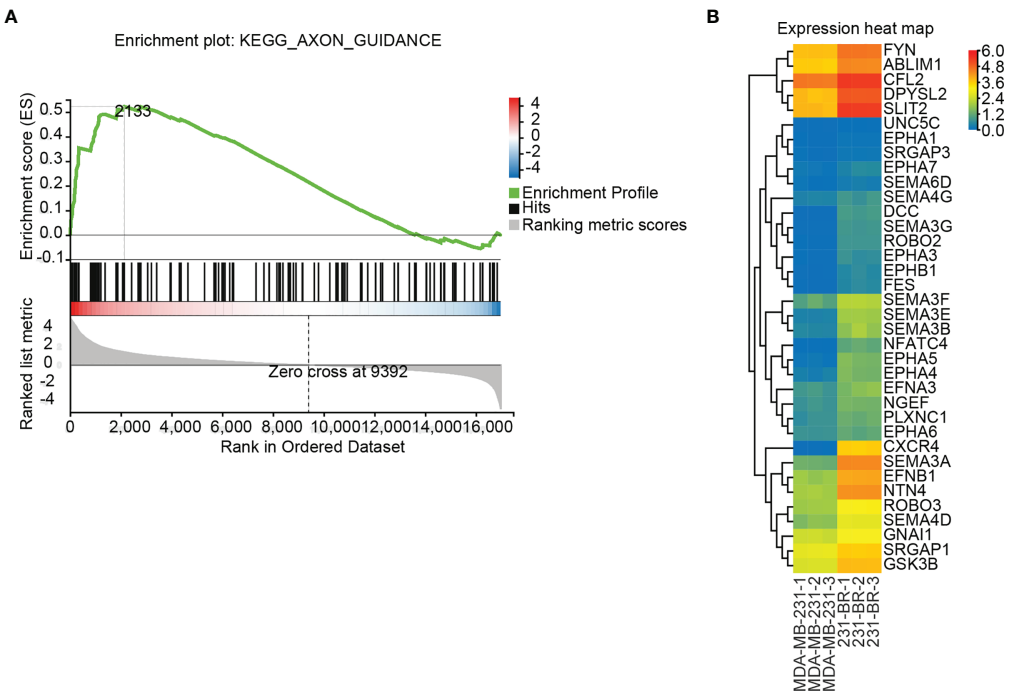

FIGURE 4 | Differentially regulated pathways determined using GSEA. **(A)** GSEA identified the "Axon guidance" signaling pathway as significant (FDR adjusted P value < 0.25). **(B)** Expression values (FPKM) of the 36 leading edge subsets of "Axon guidance" pathway are shown in a heatmap.

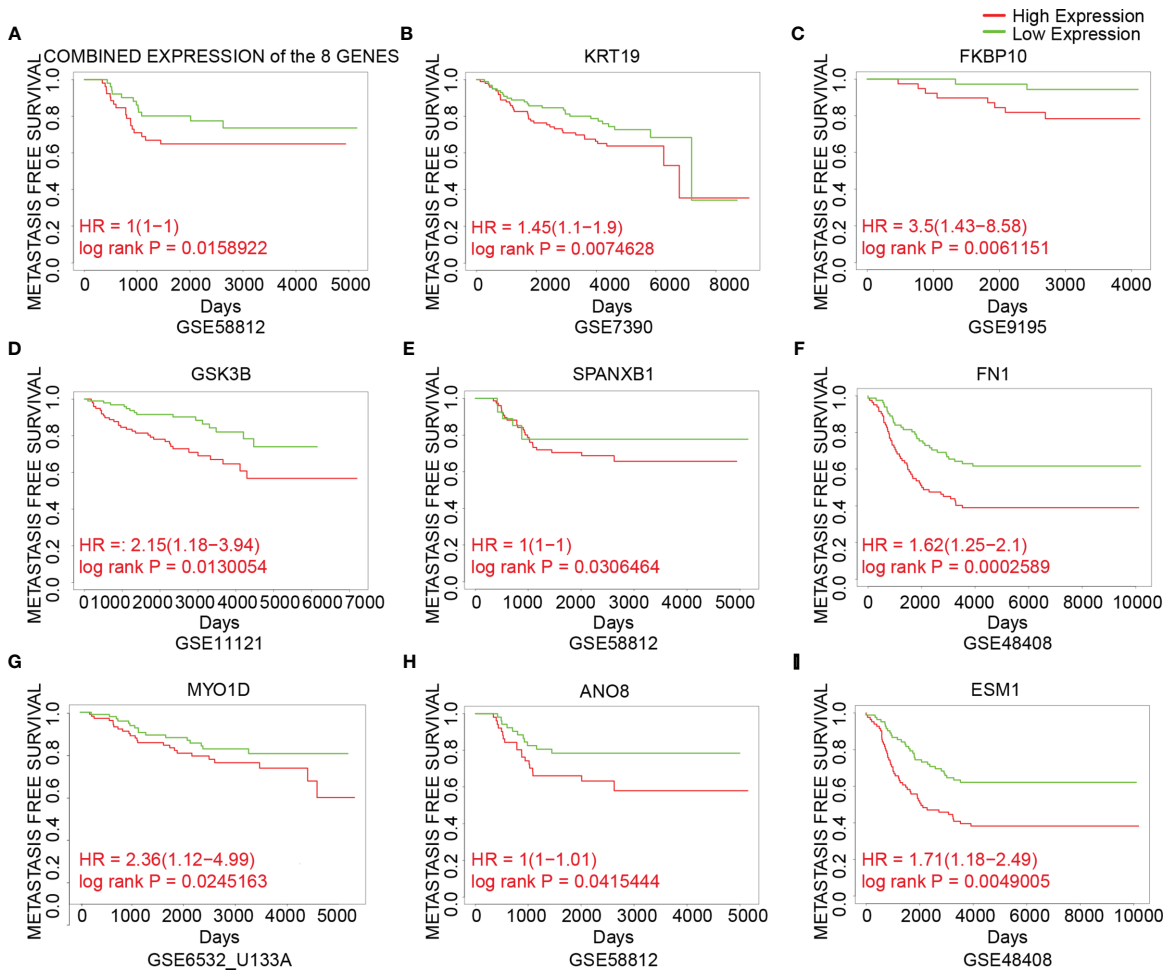

FIGURE 5 | The association between expression of the candidate genes and metastasis-free survival in breast cancer. **(A)** The association between the combined expression of the 8 candidate genes and metastasis-free survival in breast cancer cohorts. **(B–I)** The association between expression of individual genes and metastasis-free survival in breast cancer cohorts. Samples were obtained from the GEO database. The P value was calculated by log rank test.

under the ROC curve (AUC) as an assessment of the prediction accuracy. A total of 1,083 breast tumor samples and 111 normal breast samples were obtained from TCGA. As shown in **Figure 8F**, KRT19 (AUC = 0.855, CI = 0.825 - 0.885) and FKBP10 (AUC = 0.836, CI = 0.808 - 0.864) had a certain accuracy in predicting cancer and normal, and the predictive abilities of GSK3B (AUC = 0.654, CI = 0.613 - 0.696) and SPANXB1 (AUC = 0.682, CI = 0.650 - 0.714) were less accurate.

Correlation Between Gene Expression and Infiltration of Immune Cells in Breast Cancer

The tumor microenvironment (TME) landscape in brain metastases was analyzed recently, which revealed that breast brain metastases showed the highest neutrophil infiltration of myeloid cells compared with non-tumor, glioma, melanoma brain metastases and lung cancer brain metastases (47). Meanwhile, CD4+ and CD8+ T cells are the major immune cells of lymphocytes in breast brain metastases (47).

Herein, we used TIMER, EPIC, quanTIseq, xCell, MCP-counter, CIBERSORT and CIBERSORT-ABS algorithms to investigate the potential correlations between key gene expression and immune infiltration levels of neutrophils, CD4+ and CD8+ T cells in 1,100 breast cancer samples from TCGA through the TIMER 2.0 web server. The correlation coefficients (Spearman's Rho values) between the expression of the key genes and the abundance of the immune cell type as well as its subtypes were shown in heatmaps (**Figures 9A–C**). A positive correlation of GSK3B expression with neutrophil infiltration was observed based on most algorithms (**Figure 9A**). The correlations of the above gene with tumor purity and infiltration level of neutrophil in breast cancer estimated by TIMER algorithm were shown in **Figure 9D** (Rho value = 0.19, P value = 1.70e-09).

Negative correlations of KRT19, FKBP10 and SPANXB1 expression with CD8+ T cell infiltration were observed (**Figure 9B**). The correlations of KRT19, FKBP10 and SPANXB1 expression with tumor purity and infiltration level of CD8+ T cell in breast cancer estimated by EPIC algorithm

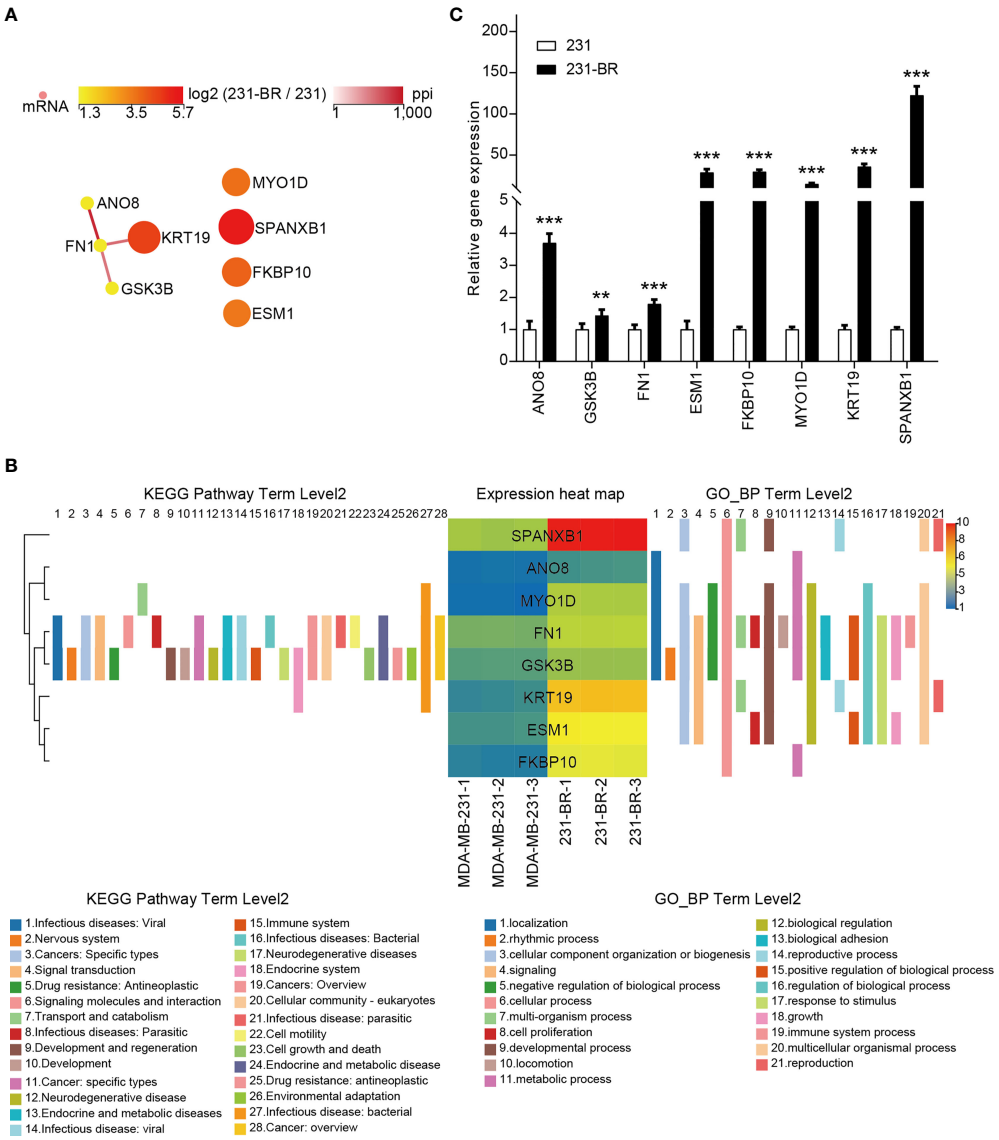

FIGURE 6 | The 8 candidate genes selected from the screening. **(A)** The PPI network of the 8 candidate genes. **(B)** The KEGG pathway annotations and GP_BP terms of the 8 candidate genes. **(C)** The mRNA levels of all candidates were validated by quantitative RT-PCR. Student's t-test was used for statistical analysis: **P < 0.01, ***P < 0.001 compared with 231 group.

were shown in **Figure 9E** (Rho value = -0.158, P value = 5.16e-07), 9F (Rho value = -0.319, P value = 5.42e-25) and 9G (Rho value = -0.153, P value = 1.33e-06), respectively. Furthermore, how the expression level (high versus low) of the immune cells and the key genes are associated with patient survival on Kaplan–Meier curves were explored (**Figures 9H–K**). Low GSK3B expression with low neutrophil infiltration group has a better survival as compared with low GSK3B expression with high neutrophil infiltration group (**Figure 9H**). Low KRT19, FKBP10 and SPANXB1 expression with low CD8+ T cell infiltration group has a poorer survival as compared with low KRT19, FKBP10 and SPANXB1 expression with high CD8+ T cell infiltration group, whereas high KRT19, FKBP10 and SPANXB1 expression with low CD8+ T cell infiltration group has a poorer survival as compared with high KRT19, FKBP10 and SPANXB1 expression with high CD8+ T cell infiltration group (**Figures 9I–K**).

Correlation Between Gene Expression and Biomarkers of Different Immune Cell Subsets in Breast Cancer

As microglia (MG), monocyte-derived macrophages (MDMs), neutrophils, and CD8+ and CD4+ T cells have been confirmed to be the major immune cell determinants of the brain TME landscape (47), we investigated the association between the key genes and the above immune cells based on immune biomarkers

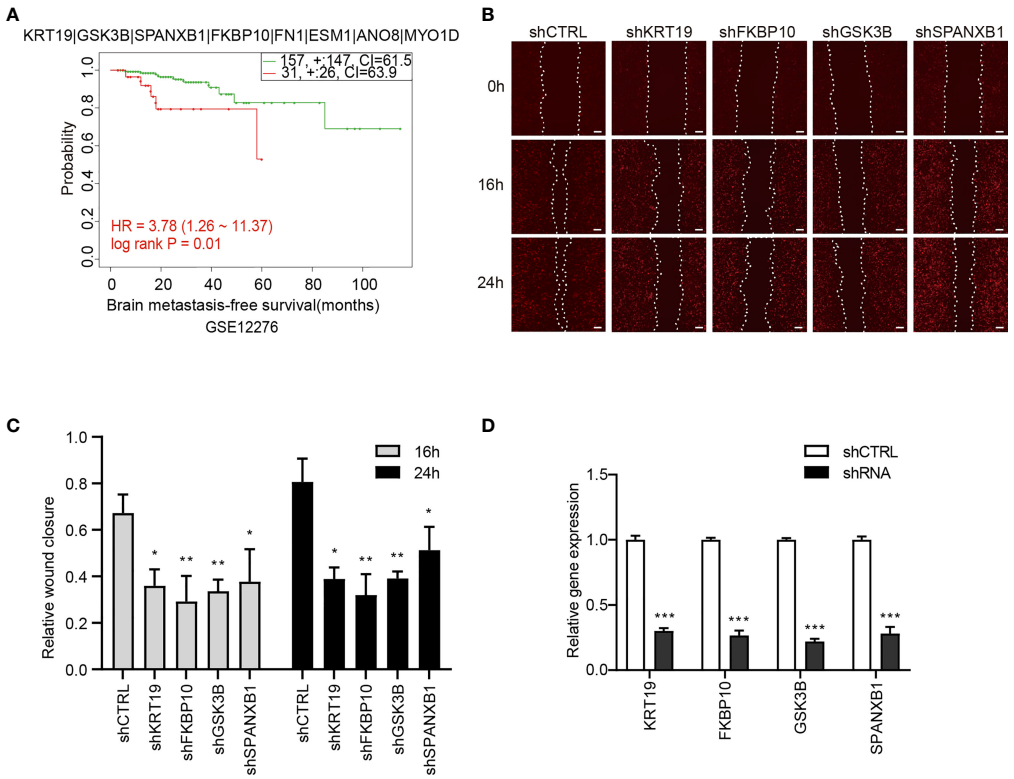

FIGURE 7 | The association of the candidate gene set with brain metastasis-free survival of breast cancer patients and effects of the genes on migration of 231-BR cells. **(A)** The association between the candidate gene set and brain metastasis-free survival in breast cancer patients. Samples were obtained from the GEO database. The P value was calculated by log rank test. **(B)** Knockdown of KRT19, FKBP10, GSK3B and SPANXB1 inhibited the migration of 231-BR cells as determined by wound healing assay, and the representative images are shown. Bar, 200μm. **(C)** The quantified data of wound healing assay are shown. Student's t-test was used for statistical analysis: *P < 0.05, **P < 0.01, ***P < 0.001 compared with corresponding control (shCTRL) at the same time point. **(D)** Knockdown efficiency of shRNAs was verified by quantitative RT-PCR. Student's t-test was used for statistical analysis: ***P < 0.001 compared with shCTRL.

expression in breast cancer *via* GEPIA. The results indicated a negative correlation between KRT19 expression and expression of CD8+ T cells (biomarkers: CD8A and CD8B), CD4+ T cells (biomarker: CD4), neutrophils (biomarkers: CD66b, CD11b and CCR7), and MDMs (biomarkers: AHR, FCGR2B, CLEC10A, CD1C, CD1B, CD207 and CD209); a negative correlation between FKBP10 expression and expression of CD8+ T cells (biomarkers: CD8A and CD8B); a positive correlation between GSK3B expression and expression of neutrophils (biomarker: CD11b); a negative correlation between SPANXB1 expression and expression of CD8+ T cells (biomarkers: CD8A, CD8B), neutrophils (biomarkers: CD11b and CCR7) and MDMs (biomarkers: AHR, FCGR2B, CLEC10A, CD1C, CD1B, CD207 and CD209) (**Table 2**).

To better understand the possible functional states of the key genes in breast cancer, we explored the expression characteristics of the key genes at the single-cell level through CancerSEA, (http://biocc.hrbmu.edu.cn/CancerSEA/), a database that aims to comprehensively decode distinct functional states of cancer cells at single-cell resolution (48). As shown in **Supplementary Figure 3**, KRT19, FKBP10, GSK3B, and SPANXB1 have been investigated at the single-cell level in 9, 10, 16 and 3 types of cancer, respectively (**Supplementary Figures 3A–D**). Correlations between the gene and functional state in different single-cell datasets were filtered by the correlation > 0.3 and P value < 0.05 (Spearman's rank correlation test with Benjamini & Hochberg FDR correction for multiple comparisons). In breast cancer (GSE77308) (49), KRT19 and SPANXB1 were shown to be correlated with several functional states. KRT19 was positively correlated with metastasis, hypoxia and stemness, and negatively correlated with DNA repair, inflammation, cell cycle, proliferation (**Supplementary Figure 3E**). SPANXB1 was positively correlated with inflammation and proliferation (**Supplementary Figure 3F**).

DISCUSSION

Attempts to identity new therapeutic targets for BCBM are emerging (23–26). In the present study, we focused on mining RNA-seq data of brain metastatic breast cancer cell lines and multiple clinical cohorts, by utilizing an integrated bioinformatic analyses approach and leveraging a comprehensive collection of databases, we identified potential biomarkers, validated their functions in brain metastatic breast cancer cell migration, and

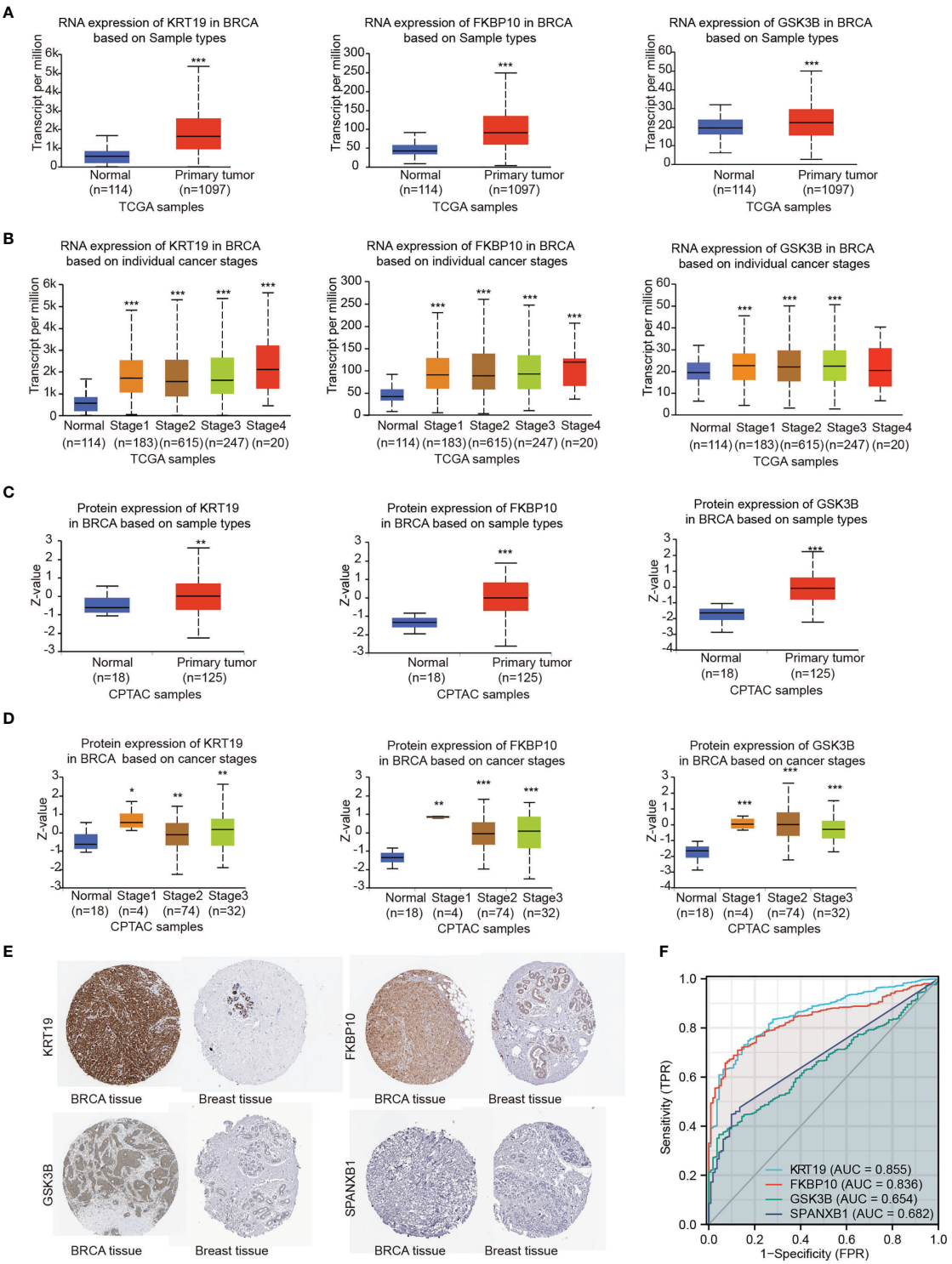

FIGURE 8 | Gene expression levels were explored by TCGA, CPTAC and HPA databases. **(A)** RNA expression levels of KRT19, FKBP10 and GSK3B were explored by TCGA based on sample types. **(B)** RNA expression levels of KRT19, FKBP10 and GSK3B were explored by TCGA based on cancer stages. **(C)** Protein expression levels of KRT19, FKBP10 and GSK3B were explored by CPTAC based on sample types. **(D)** Protein expression levels of KRT19, FKBP10 and GSK3B were explored by CPTAC based on cancer stages. **(E)** Protein expression levels of KRT19, FKBP10 GSK3B and SPANXB1 as detected by immunohistochemistry staining from the HPA database. **(F)** ROC curves of the key genes using data from TCGA. Expression values were compared using Student's t-test: *P < 0.05, **P < 0.01, ***P < 0.001 compared with Normal.

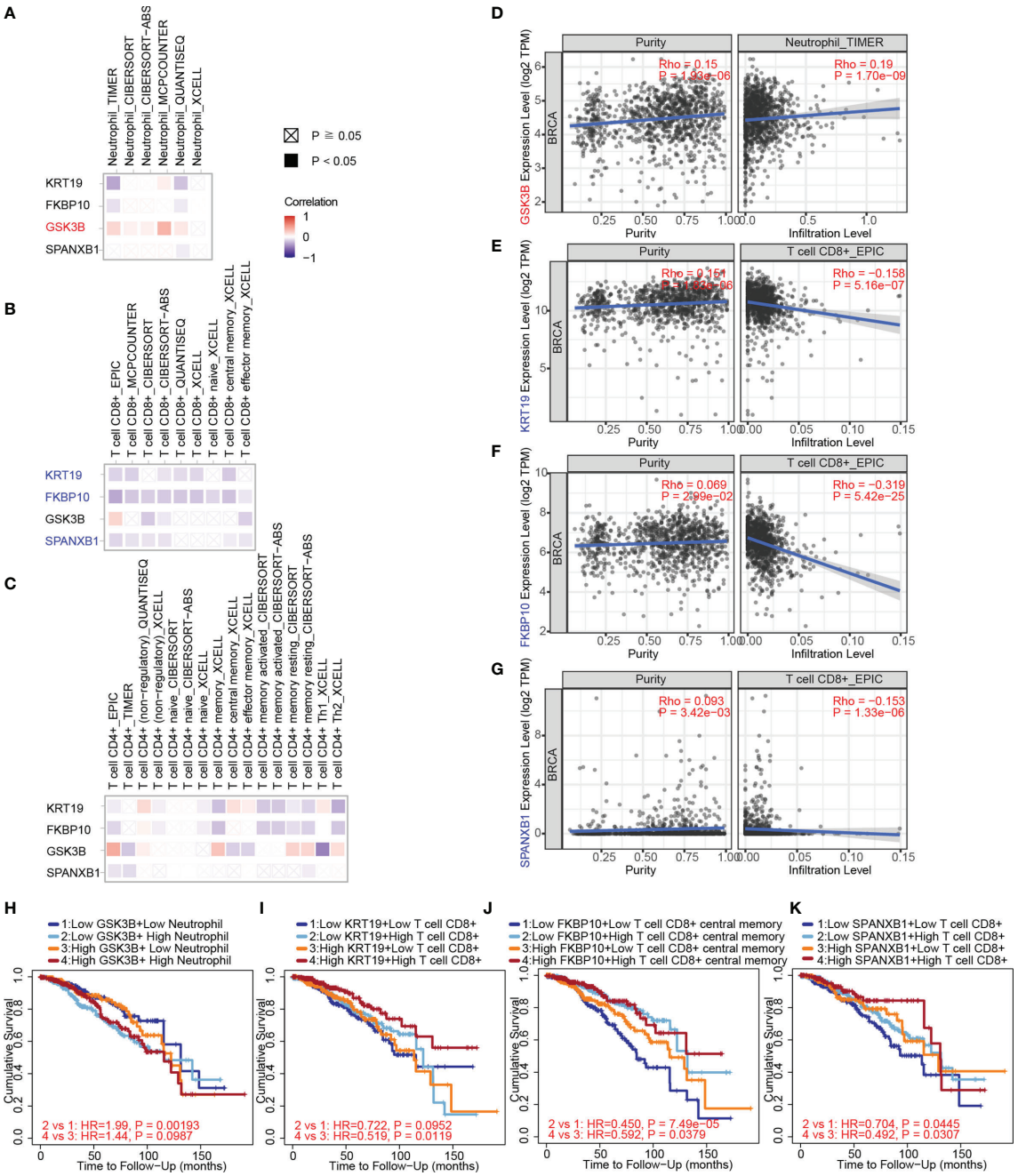

FIGURE 9 | The correlation between key gene expression and immune cell infiltration in breast cancer samples from TCGA through TIMER. **(A)** The correlations between key gene expression and immune infiltration levels of neutrophils are shown in a heatmap. **(B)** The correlations between gene expression and immune infiltration levels of CD8+ T cells. **(C)** The correlations between gene expression and immune infiltration levels of CD4+ T cells. **(D)** The correlations of GSK3B with tumor purity (left) and infiltration level (right) of neutrophils in breast cancer estimated by TIMER. **(E)** The correlations of KRT19 expression with tumor purity and infiltration level of CD8+ T cells in breast cancer estimated by EPIC algorithm. **(F)** The correlations of FKBP10 expression with tumor purity and infiltration level of CD8+ T cells in breast cancer estimated by EPIC algorithm. **(G)** The correlations of SPANXB1 expression with tumor purity and infiltration level of CD8+ T cells in breast cancer estimated by EPIC algorithm. **(H)** The associations of the neutrophil and GSK3B expression levels (high versus low) with patient survival on Kaplan–Meier curves. **(I)** The associations of the CD8+ T cells and KRT19 expression levels (high versus low) with patient survival on Kaplan–Meier curves. **(J)** The associations of the CD8+ T cells and FKBP10 expression levels (high versus low) with patient survival on Kaplan–Meier curves. **(K)** The associations of the CD8+ T cells and SPANXB1 expression levels (high versus low) with patient survival on Kaplan–Meier curves. The correlation coefficient was determined by the Spearman method in **(A–G)**. P values for the Kaplan-Meier analyses are based on log rank tests in **(H–K)**.

TABLE 2 | Correlation between gene expression and biomarkers of different immune cell subsets in breast cancer.

Description	Gene Markers	KRT19		FKBP10		GSK3B		SPANXB1	
		Cor	P value	Cor	P value	Cor	P value	Cor	P value
CD8+ T cell	CD8A	**-0.20**	**2.30e-11**	**-0.19**	**1.40e-10**	-0.05	1.40e-01	**-0.13**	**1.70e-05**
	CD8B	**-0.22**	**1.80e-13**	**-0.20**	**3.10e-11**	**-0.09**	**5.30e-03**	**-0.15**	**8.10e-07**
CD4+ T cell	CD4	**-0.21**	**2.60e-12**	**-0.07**	**2.00e-02**	**0.09**	**2.60e-03**	**-0.09**	**2.30e-03**
Neutrophil	CD66b(CEACAM8)	**-0.08**	**1.20e-02**	-0.05	1.20e-01	0.01	8.20e-01	0.04	1.70e-01
	CD11b(ITGAM)	**-0.11**	**1.80e-04**	0.02	4.40e-01	**0.15**	**1.40e-06**	**-0.06**	**3.60e-02**
	CCR7	**-0.14**	**2.40e-06**	**-0.17**	**1.80e-08**	-0.06	6.60e-02	**-0.13**	**1.40e-05**
MG	P2RY12	**-0.10**	**6.50e-04**	-0.05	1.40e-01	**0.06**	**4.60e-02**	**-0.12**	**6.60e-05**
	TMEM119	-0.05	9.70e-02	**0.10**	**1.40e-03**	-0.03	4.00e-01	**-0.06**	**4.10e-02**
	TAL1	-0.03	3.30e-01	**0.08**	**5.50e-03**	-0.05	1.30e-01	**-0.08**	**1.20e-02**
	SALL1	0.03	3.10e-01	**0.19**	**5.20e-10**	**0.27**	**4.90e-19**	**0.17**	**1.10e-08**
MDMs	AHR	**-0.09**	**1.90e-03**	0.03	3.00e-01	**0.44**	**1.10e-53**	**-0.07**	**2.80e-02**
	FCGR2B	**-0.16**	**1.50e-07**	-0.01	7.50e-01	**0.11**	**4.20e-04**	**-0.07**	**2.10e-02**
	CLEC10A	**-0.16**	**1.40e-07**	**-0.14**	**6.20e-06**	**-0.12**	**1.10e-04**	**-0.18**	**2.7e–09**
	CD1C	**-0.15**	**3.80e-07**	**-0.09**	**2.30e-03**	**-0.11**	**1.70e-04**	**-0.15**	**4.1e–07**
	CD1B	**-0.19**	**1.90e-10**	**-0.17**	**2.50e-08**	**-0.06**	**4.90e-02**	**-0.10**	**1.50e-03**
	CD207	**-0.14**	**1.70e-06**	-0.02	5.50e-01	0.003	9.30e-01	**-0.09**	**3.20e-03**
	CD209	**-0.20**	**6.50e-11**	-0.03	3.40e-01	**0.16**	**1.10e-07**	**-0.14**	**7.5e–06**

Cor, R value of Spearman's correlation. Bold values indicate P value < 0.05.

showed their clinical relevance to breast cancer metastasis. Our study not only provided unprecedented insights into BCBM, but also showcased the bioinformatics analytical pipeline that could be applied to other cancers.

Enrichments of Proteoglycans in cancer signaling pathway and Collagen-containing ECM can be observed in our KEGG and GO-CC analyses (**Figures 2A–D**). Therefore, as two main components of the extracellular matrix, which played critical roles in malignant cell behavior and cancer metastasis (50), proteoglycans and collagens may play roles in regulating 231-BR cellular functions. For the latter, collagen fibers can lay tracks for cells to migrate (51, 52), and the remodeled stiff collagens might be exploited as invasion "highways" by cancer cells (51–53). Among the identified key genes in our study, FKBP10 is a molecular chaperone able to pro-collagen maturation in fibroblasts and contributes to high-collagenous ECM (54, 55). For Proteoglycans in cancer pathway, it enables a mesenchymal phenotype with increased cellular motility. Proteoglycans in the ECM can make the extracellular space more compliant for migration, and cell-surface proteoglycans receive signals triggered by interactions with ECM components and modulate cellular behavior such as migration (56–58). There was not much evidence highlighting the relationships between Proteoglycans in cancer pathway and the 4 key genes. However, as one of the 8 candidate genes (**Figures 5**, **6**), which showed a significantly correlation with brain metastasis-free survival as a gene set (**Figure 7A**), FN1 contributes to the "proteoglycans in cancer" pathway (KEGG Pathway Map: 05205). Although FN1 was not identified as key genes in our study because it did not affect 231-BR cell migration in wound healing assay, its possible role in BCBM through Proteoglycans in cancer signaling pathway should not be ignored. This requires investigation in future studies.

GSEA is a computational method to determine whether a predefined set of genes shows statistical difference between two sets of processes or phenotypes (40, 41). Based on our RNA seq data, Axon guidance was the only signaling pathway identified through GSEA (**Figure 4**), indicating a role of it in phenotype determination of 231-BR cells. Axon guidance is a specialized form of cell migratory phenomenon (59) and has been implicated in tumor cell migration (60). Meanwhile, as one of the identified key genes, GSK3B is a member of the above pathway (KEGG Pathway Map: 04360). The emergence of this pathway indicates the regulation of Axon guidance by GSK3B may thereby affect the promigratory phenotype of 231-BR cells. This needs to be demonstrated in future studies.

The brain has been considered previously to be an immune privileged site. Indeed, it had remained uncertain for a long time whether immune cells exist and function in the brain TME (61). Recently, it has been reported that various types of immune cells can be recruited into the brain TME when the blood-brain barrier is compromised by metastatic cancer cells (61). The co-evolution of metastatic cancer cells with the brain microenvironment is critical for metastatic cells' escaping dormancy and colonizing the brain. The TME landscape in brain metastases was analyzed and MG, MDMs, neutrophils, and CD8+ and CD4+ T cells have been confirmed to be the major immune cell determinants of the brain TME landscape (47, 62). To better predict the functions of the above genes in breast cancer, we explored the correlations between gene expression level and infiltration of immune cells. Meanwhile, correlation between gene expression and biomarkers of different immune cell subsets in breast cancer were explored. As one of the identified key genes, GSK3B positively correlated with neutrophil infiltration (**Figure 9A**). Neutrophils play important and contradictory roles in cancer development. In the TME, they may inhibit tumor progression by generating anti-tumor factors (63). However, more frequently, they are reported as tumor accomplices to promote cancer metastasis (64–67) and seems to be an indicator of poor outcome (68, 69). A common mechanism of how tumors can induce neutrophilia seems to be the production by tumors of cytokines that influence

granulopoiesis (70). In breast cancer, neutrophils have been shown to drive metastatic establishment within the lung TME (65), meanwhile, they represented a major immune compartment and showed a high infiltration in the brain TME (47). Therefore, the positive correlation of GSK3B and neutrophil infiltration may suggest a metastasis-promoting effect or a prognostic role or of this gene in BCBM (**Figure 9**).

Three of the identified key genes (FKBP10, KRT19, and SPANXB1) negatively correlated with the infiltration of CD8+ T cells, which is the lymphocytes primarily responsible for immune-mediated tumor cell death (**Figure 9B**). One possible cause of the immunosuppression caused by FKBP10 is that collagen can act as a regulator for tumor associated immune infiltration (71–73). High-fibrillar collagens could act as barrier to immune infiltration, and stop the production of chemokines, that lead to suppression of the anti-tumor immune response in the TME (71–74). Higher collagen deposition resulted in tumor immune suppression characterized by decreased total CD8+ T cells and increased exhausted CD8+ T cell subpopulations due to the leukocyte-specific collagen receptor LAIR1, which suppresses lymphocytic activity and is expressed on CD8+ T cells following integrin beta 2 binding to collagen (71–77). Few studies have explored the effects of the other two (KRT19, and SPANXB1) in immunoregulation. However, interrupting expression of KRT19 in mouse tumors prevented the formation of the CXCL12–KRT19 coating, allowed the accumulation of T cells (78), suggesting a possible role of KRT19 in immunoregulation. Considering low CD8+ T cell infiltration often associated with poor outcome and CD8+ T cell is one of the major immune cell determinants of the brain TME (47, 71, 74), the negative correlation between the identified genes (KRT19, FKBP10 and SPANXB1) and CD8+ T cell infiltration suggests the immunosuppressive and metastasis-promoting effects in BCBM.

To the best of our knowledge, the effects of our key genes on BCBM have not been reported so far. Some previous studies have shown effects of these genes on cell migration or metastasis to other sites in some malignant tumors. KRT19 encodes a protein belonging to the keratin family, which are integrated in the cellular framework and interact with a range of cellular proteins (14, 15). It has been shown to exhibit tumor-promoting effects in breast, hepatocellular carcinoma, oral squamous cell carcinomas and lung cancers (79–81). However, studies in breast cancer cells have shown that modulation of KRT19 expression led to contrasting effects on cell behaviors. It can either suppress cell proliferation, migration and invasion (14, 15, 82), or promote oncogenesis, tumor growth and metastasis (83, 84). MARIA et al. reported that KRT19 was only detected in circulating tumor cells of breast cancer patients, but not in healthy donors. The KRT19-positive detections correlated with the diagnosis and high proliferation rate of breast cancer (85), and the combined positive detection of PTHRP-plus-KRT19 correlated with the presence of distant metastasis, especially with bone metastasis (85). These results also asked whether KRT19 could be a marker in breast cancer bone metastasis, which need further investigation. In addition, KRT19 is involved in Estrogen signaling pathway (KEGG Pathway Map: 04915), which has been shown to stimulate cell migration and contribute to brain metastases of breast cancer (86–89). MDA-MB-231 cells also express estrogen receptors, including wild-type ERα, ERα variants (ERα Δ5 and Δ7) and ERβ variants (ERβ1 and ERβ2) (90–93). Moreover, although not in the top 20, Estrogen signaling pathway was enriched in our KEGG analysis (Term Candidate Gene Num = 20, Q value = 0.02). These findings may help explain why KRT19 was identified as key genes in this study.

FKBP10 is a gene encoding FKBP65, which belongs to the FKBP-type peptidyl-prolyl cis/trans isomerase family. This protein localizes to the endoplasmic reticulum and acts as a molecular chaperone (RefSeq database). FKBP family members are involved in multiple cellular processes, including receptor signaling, protein folding, transcription, chaperone activity and immunosuppression (94). A growing body of evidence has suggested that FKBPs play important roles in cancer (95, 96). FKBP10 has been studied in some cancers and its role is currently controversial (97–101), while few studies have investigated FKBP10 in breast cancer. FKBP10 has been reported to be an intracellular regulatory factor for ECM reconstruction and directly interact with collagen I (54, 55). Combined with our GO-CC results that showed an enrichment of Collagen-containing extracellular matrix (**Figures 2A, D**), the role of FKBP10 in 231-BR cellular behavior may partly be explained.

The protein encoded by GSK3B is a serine-threonine kinase belonging to the glycogen synthase kinase subfamily. It is one of the few signaling mediators that play central roles in a diverse range of signaling pathways, and it has been shown to be involved in energy metabolism, inflammation, apoptotic pathways, ER-stress, and mitochondrial dysfunction (102). Multiple roles have been suggested for GSK3B in different cancers, and even after years of study they remain complex and controversial (103). Due to its ability to phosphorylate and thereby target some pro-oncogenic molecules for ubiquitin-dependent proteosomal degradation, GSK3B has been thought of potential tumor suppressor in some cancers (104–106). However, recent reports have suggested that GSK3B is a positive regulator of cancer progression (107–111). In breast cancer, GSK3B knockdown has been shown to inhibit cell proliferation, and GSK3B overexpression has been shown to correlate with poor prognosis in TNBC patients (112–114).

SPANXB1 is a member of the SPANX family, which consists of five members all located in a gene cluster at Xq27.1 (115). SPANX family encompasses cancer-testis antigens that are epigenetically silenced in normal tissue except testes, while expressed in several human tumors (116, 117). SPANXB1 has been reported to be expressed in melanoma and carcinomas of breast, lung, ovary, colon, and bladder (118–120). In TNBC, SPANXB1 has been shown to promote lung and liver metastasis and be traceable in the circulating extracellular vesicles (120). These data support our findings, and suggest a utility of SPANXB1 as a prognostic biomarker in breast cancer metastasis (120).

Combining the previous studies with insights from our work, we believe that the candidate gene set and individual key genes

identified here may be implicated in brain metastasis of breast cancer. The present study may provided new potential biomarkers for BCBM. However, this study has several limitations. Firstly, the screening conducted by us was performed in two TNBC cell lines and the effect of the identified genes on cell migration was only validated in the brain metastatic cell line 231-BR. Although some evidence points to the key genes as potential biomarkers of BCBM, further biological experimental validation and clinical verification along with extensive mechanistic studies are necessary for more accurate and reliable conclusions. Indeed, this is an on-going study in our laboratory with the aim to better clarify and ultimately decipher the underlying mechanism of various key genes. Secondly, although the candidate gene set showed a significantly correlation with brain metastasis-free survival of breast cancer patients from a public dataset, the prognostic value of each individual candidate genes requires further investigation in clinical studies. Since we have not gotten enough brain metastases samples of breast cancer patients from public databases, we have already set up a reliable clinical source in collaboration with some local hospitals and proposed a future study to further investigate the effects of our selected genes from a clinical perspective.

CONCLUSION

In the present study, we identified candidate genes that may play roles in BCBM through a series of bioinformatic analyses and wet-lab experiments. The identified genes showed an elevated expression in brain metastatic 231-BR and a prognostic value in patients with BCBM. Among them, KRT19, FKBP10, GSK3B and SPANXB1 were identified as key genes based on their roles in migration of 231-BR. Furthermore, the key genes showed a correlation with the infiltration of major immune cells in the brain TME, suggesting possible roles of them in regulation of immune response in brain TME. Therefore, the present work may provide new potential biomarkers for BCBM.

FUTURE DIRECTIONS

Several future directions can be envisioned. The involvement of the identified genes in BCBM demonstrated utility for the identification of biomarkers or potential drug targets for BCBM treatment. Screening brain penetrable compounds targeting these genes may be a promising way for BCBM drug discovery. For example, GSK3B has been studied as a target for drug discovery in the treatment of nervous system disorders (121, 122), and a brain penetrable and orally active GSK3 inhibitor has been reported as a clinical candidate for Alzheimer's disease and progressed into Phase 1 clinical trials (122). These findings in conjunction with our findings, suggest new indications for such compounds in BCBM.

DATA AVAILABILITY STATEMENT

The datasets presented in this study can be found in online repositories. The names of the repository/repositories and accession number(s) can be found in the article/**Supplementary Material**.

AUTHOR CONTRIBUTIONS

The experiment was designed by all authors. LW and YG performed the bioinformatics analysis and wrote the manuscript. DZ, QW, LL, and TL conducted the experimental part. All authors contributed to the article and approved the submitted version.

FUNDING

The present study was supported by National Natural Science Foundation of China (grant no. 81602532); Beijing Natural Science Foundation (grant no.5202004 and 5214022). Support Project of High-level Teachers in Beijing Municipal Universities in the Period of 13th Five-year Plan (grant no. IDHT20170516).

ACKNOWLEDGMENTS

We thank Eng-Ang Ling (National University of Singapore, Singapore) for assistance with the manuscript. We thank Dr. Patricia Steeg (National Cancer Institute, Bethesda, MD, USA) for the kind gift of 231-BR cell line.

SUPPLEMENTARY MATERIAL

The Supplementary Material for this article can be found online at: https://www.frontiersin.org/articles/10.3389/fonc.2021.784096/full#supplementary-material

REFERENCES

1. Lowery FJ, Yu D. Brain Metastasis: Unique Challenges and Open Opportunities. *Biochim Biophys Acta Rev Cancer* (2017) 1867(1):49–57. doi: 10.1016/j.bbcan.2016.12.001
2. Preusser M, Capper D, Ilhan-Mutlu A, Berghoff AS, Birner P, Bartsch R, et al. Brain Metastases: Pathobiology and Emerging Targeted Therapies. *Acta Neuropathol* (2012) 123(2):205–22. doi: 10.1007/s00401-011-0933-9
3. Cagney DN, Martin AM, Catalano PJ, Redig AJ, Lin NU, Lee EQ, et al. Incidence and Prognosis of Patients With Brain Metastases at Diagnosis of Systemic Malignancy: A Population-Based Study. *Neuro Oncol* (2017) 19 (11):1511–21. doi: 10.1093/neuonc/nox077
4. Suh JH, Kotecha R, Chao ST, Ahluwalia MS, Sahgal A, Chang EL. Current Approaches to the Management of Brain Metastases. *Nat Rev Clin Oncol* (2020) 17(5):279–99. doi: 10.1038/s41571-019-0320-3

5. Ren D, Cheng H, Wang X, Vishnoi M, Teh BS, Rostomily R, et al. Emerging Treatment Strategies for Breast Cancer Brain Metastasis: From Translational Therapeutics to Real-World Experience. *Ther Adv Med Oncol* (2020) 12:1758835920936151. doi: 10.1177/1758835920936151
6. Sung H, Ferlay J, Siegel RL, Laversanne M, Soerjomataram I, Jemal A, et al. Global Cancer Statistics 2020: GLOBOCAN Estimates of Incidence and Mortality Worldwide for 36 Cancers in 185 Countries. *CA Cancer J Clin* (2021) 71(3):209–49. doi: 10.3322/caac.21660
7. Custodio-Santos T, Videira M, Brito MA. Brain Metastasization of Breast Cancer. *Biochim Biophys Acta Rev Cancer* (2017) 1868(1):132–47. doi: 10.1016/j.bbcan.2017.03.004
8. Martin AM, Cagney DN, Catalano PJ, Warren LE, Bellon JR, Punglia RS, et al. Brain Metastases in Newly Diagnosed Breast Cancer: A Population-Based Study. *JAMA Oncol* (2017) 3(8):1069–77. doi: 10.1001/jamaoncol.2017.0001
9. Lin NU, Claus E, Sohl J, Razzak AR, Arnaout A, Winer EP. Sites of Distant Recurrence and Clinical Outcomes in Patients With Metastatic Triple-Negative Breast Cancer: High Incidence of Central Nervous System Metastases. *Cancer* (2008) 113(10):2638–45. doi: 10.1002/cncr.23930
10. Kennecke H, Yerushalmi R, Woods R, Cheang MC, Voduc D, Speers CH, et al. Metastatic Behavior of Breast Cancer Subtypes. *J Clin Oncol* (2010) 28 (20):3271–7. doi: 10.1200/JCO.2009.25.9820
11. Niwinska A, Murawska M, Pogoda K. Breast Cancer Brain Metastases: Differences in Survival Depending on Biological Subtype, RPA RTOG Prognostic Class and Systemic Treatment After Whole-Brain Radiotherapy (WBRT). *Ann Oncol* (2010) 21(5):942–8. doi: 10.1093/annonc/mdp407
12. Nabors LB, Portnow J, Ahluwalia M, Baehring J, Brem H, Brem S, et al. Central Nervous System Cancers, Version 3.2020, NCCN Clinical Practice Guidelines in Oncology. *J Natl Compr Canc Netw* (2020) 18(11):1537–70. doi: 10.6004/jnccn.2020.0052
13. Lin X, DeAngelis LM. Treatment of Brain Metastases. *J Clin Oncol* (2015) 33 (30):3475–84. doi: 10.1200/JCO.2015.60.9503
14. Saha SK, Choi HY, Kim BW, Dayem AA, Yang GM, Kim KS, et al. KRT19 Directly Interacts With Beta-Catenin/RAC1 Complex to Regulate NUMB-Dependent NOTCH Signaling Pathway and Breast Cancer Properties. *Oncogene* (2017) 36(3):332–49. doi: 10.1038/onc.2016.221
15. Ju JH, Yang W, Lee KM, Oh S, Nam K, Shim S, et al. Regulation of Cell Proliferation and Migration by Keratin19-Induced Nuclear Import of Early Growth Response-1 in Breast Cancer Cells. *Clin Cancer Res* (2013) 19 (16):4335–46. doi: 10.1158/1078-0432.CCR-12-3295
16. Dawood S, Broglio K, Esteva FJ, Ibrahim NK, Kau SW, Islam R, et al. Defining Prognosis for Women With Breast Cancer and CNS Metastases by HER2 Status. *Ann Oncol* (2008) 19(7):1242–8. doi: 10.1093/annonc/mdn036
17. Costa R, Carneiro BA, Wainwright DA, Santa-Maria CA, Kumthekar P, Chae YK, et al. Developmental Therapeutics for Patients With Breast Cancer and Central Nervous System Metastasis: Current Landscape and Future Perspectives. *Ann Oncol* (2017) 28(1):44–56. doi: 10.1093/annonc/mdw532
18. Ramakrishna N, Temin S, Chandarlapaty S, Crews JR, Davidson NE, Esteva FJ, et al. Recommendations on Disease Management for Patients With Advanced Human Epidermal Growth Factor Receptor 2-Positive Breast Cancer and Brain Metastases: American Society of Clinical Oncology Clinical Practice Guideline. *J Clin Oncol* (2014) 32(19):2100–8. doi: 10.1200/JCO.2013.54.0955
19. Eichler AF, Kuter I, Ryan P, Schapira L, Younger J, Henson JW. Survival in Patients With Brain Metastases From Breast Cancer: The Importance of HER-2 Status. *Cancer* (2008) 112(11):2359–67. doi: 10.1002/cncr.23468
20. Petrelli F, Ghidini M, Lonati V, Tomasello G, Borgonovo K, Ghilardi M, et al. The Efficacy of Lapatinib and Capecitabine in HER-2 Positive Breast Cancer With Brain Metastases: A Systematic Review and Pooled Analysis. *Eur J Cancer* (2017) 84:141–8. doi: 10.1016/j.ejca.2017.07.024
21. Freedman RA, Gelman RS, Anders CK, Melisko ME, Parsons HA, Cropp AM, et al. TBCRC 022: A Phase II Trial of Neratinib and Capecitabine for Patients With Human Epidermal Growth Factor Receptor 2-Positive Breast Cancer and Brain Metastases. *J Clin Oncol* (2019) 37(13):1081–9. doi: 10.1200/JCO.18.01511
22. Lin NU, Vanderplas A, Hughes ME, Theriault RL, Edge SB, Wong YN, et al. Clinicopathologic Features, Patterns of Recurrence, and Survival Among Women With Triple-Negative Breast Cancer in the National Comprehensive Cancer Network. *Cancer* (2012) 118(22):5463–72. doi: 10.1002/cncr.27581
23. Bos PD, Zhang XH, Nadal C, Shu W, Gomis RR, Nguyen DX, et al. Genes That Mediate Breast Cancer Metastasis to the Brain. *Nature* (2009) 459 (7249):1005–9. doi: 10.1038/nature08021
24. Neman J, Termini J, Wilczynski S, Vaidehi N, Choy C, Kowolik CM, et al. Human Breast Cancer Metastases to the Brain Display GABAergic Properties in the Neural Niche. *Proc Natl Acad Sci USA* (2014) 111 (3):984–9. doi: 10.1073/pnas.1322098111
25. Lee BC, Lee TH, Avraham S, Avraham HK. Involvement of the Chemokine Receptor CXCR4 and its Ligand Stromal Cell-Derived Factor 1alpha in Breast Cancer Cell Migration Through Human Brain Microvascular Endothelial Cells. *Mol Cancer Res* (2004) 2(6):327–38.
26. Zhang L, Sullivan PS, Goodman JC, Gunaratne PH, Marchetti D. MicroRNA-1258 Suppresses Breast Cancer Brain Metastasis by Targeting Heparanase. *Cancer Res* (2011) 71(3):645–54. doi: 10.1158/0008-5472.CAN-10-1910
27. Gril B, Palmieri D, Bronder JL, Herring JM, Vega-Valle E, Feigenbaum L, et al. Effect of Lapatinib on the Outgrowth of Metastatic Breast Cancer Cells to the Brain. *J Natl Cancer Inst* (2008) 100(15):1092–103. doi: 10.1093/jnci/djn216
28. Yoneda T, Williams PJ, Hiraga T, Niewolna M. Nishimura R. A Bone-Seeking Clone Exhibits Different Biological Properties From the MDA-MB-231 Parental Human Breast Cancer Cells and a Brain-Seeking Clone *In Vivo* and *In Vitro*. *J Bone Miner Res* (2001) 16(8):1486–95. doi: 10.1359/jbmr.2001.16.8.1486
29. Dun MD, Chalkley RJ, Faulkner S, Keene S, Avery-Kiejda KA, Scott RJ, et al. Proteotranscriptomic Profiling of 231-BR Breast Cancer Cells: Identification of Potential Biomarkers and Therapeutic Targets for Brain Metastasis. *Mol Cell Proteomics* (2015) 14(9):2316–30. doi: 10.1074/mcp.M114.046110
30. Eichler AF, Chung E, Kodack DP, Loeffler JS, Fukumura D, Jain RK. The Biology of Brain Metastases-Translation to New Therapies. *Nat Rev Clin Oncol* (2011) 8(6):344–56. doi: 10.1038/nrclinonc.2011.58
31. Fitzgerald DP, Subramanian P, Deshpande M, Graves C, Gordon I, Qian Y, et al. Opposing Effects of Pigment Epithelium-Derived Factor on Breast Cancer Cell Versus Neuronal Survival: Implication for Brain Metastasis and Metastasis-Induced Brain Damage. *Cancer Res* (2012) 72(1):144–53. doi: 10.1158/0008-5472.CAN-11-1904
32. Fitzgerald DP, Palmieri D, Hua E, Hargrave E, Herring JM, Qian Y, et al. Reactive Glia are Recruited by Highly Proliferative Brain Metastases of Breast Cancer and Promote Tumor Cell Colonization. *Clin Exp Metastasis* (2008) 25(7):799–810. doi: 10.1007/s10585-008-9193-z
33. Langmead B, Salzberg SL. Fast Gapped-Read Alignment With Bowtie 2. *Nat Methods* (2012) 9(4):357–9. doi: 10.1038/nmeth.1923
34. Love MI, Huber W, Anders S. Moderated Estimation of Fold Change and Dispersion for RNA-Seq Data With Deseq2. *Genome Biol* (2014) 15(12):550. doi: 10.1186/s13059-014-0550-8
35. Geng P, Zhang S, Liu J, Zhao C, Wu J, Cao Y, et al. MYB20, MYB42, MYB43, and MYB85 Regulate Phenylalanine and Lignin Biosynthesis During Secondary Cell Wall Formation. *Plant Physiol* (2020) 182(3):1272–83. doi: 10.1104/pp.19.01070
36. Szklarczyk D, Gable AL, Lyon D, Junge A, Wyder S, Huerta-Cepas J, et al. STRING V11: Protein-Protein Association Networks With Increased Coverage, Supporting Functional Discovery in Genome-Wide Experimental Datasets. *Nucleic Acids Res* (2019) 47(D1):D607–13. doi: 10.1093/nar/gky1131
37. Shannon P, Markiel A, Ozier O, Baliga NS, Wang JT, Ramage D, et al. Cytoscape: A Software Environment for Integrated Models of Biomolecular Interaction Networks. *Genome Res* (2003) 13(11):2498–504. doi: 10.1101/gr.1239303
38. Bader GD, Hogue CW. An Automated Method for Finding Molecular Complexes in Large Protein Interaction Networks. *BMC Bioinf* (2003) 4:2. doi: 10.1186/1471-2105-4-2
39. Chin CH, Chen SH, Wu HH, Ho CW, Ko MT, Lin CY. Cytohubba: Identifying Hub Objects and Sub-Networks From Complex Interactome. *BMC Syst Biol* (2014) 8(Suppl 4):S11. doi: 10.1186/1752-0509-8-S4-S11
40. Subramanian A, Tamayo P, Mootha VK, Mukherjee S, Ebert BL, Gillette MA, et al. Gene Set Enrichment Analysis: A Knowledge-Based Approach for

Interpreting Genome-Wide Expression Profiles. *Proc Natl Acad Sci USA* (2005) 102(43):15545–50. doi: 10.1073/pnas.0506580102
41. Mootha VK, Lindgren CM, Eriksson KF, Subramanian A, Sihag S, Lehar J, et al. PGC-1alpha-Responsive Genes Involved in Oxidative Phosphorylation are Coordinately Downregulated in Human Diabetes. *Nat Genet* (2003) 34 (3):267–73. doi: 10.1038/ng1180
42. Goswami CP, Nakshatri H. PROGgeneV2: Enhancements on the Existing Database. *BMC Cancer* (2014) 14(1):970. doi: 10.1186/1471-2407-14-970
43. Chandrashekar DS, Bashel B, Balasubramanya SAH, Creighton CJ, Ponce-Rodriguez I, Chakravarthi B, et al. UALCAN: A Portal for Facilitating Tumor Subgroup Gene Expression and Survival Analyses. *Neoplasia* (2017) 19(8):649–58. doi: 10.1016/j.neo.2017.05.002
44. Li T, Fu J, Zeng Z, Cohen D, Li J, Chen Q, et al. TIMER2.0 for Analysis of Tumor-Infiltrating Immune Cells. *Nucleic Acids Res* (2020) 48(W1):W509–W14. doi: 10.1093/nar/gkaa407
45. Li T, Fan J, Wang B, Traugh N, Chen Q, Liu JS, et al. TIMER: A Web Server for Comprehensive Analysis of Tumor-Infiltrating Immune Cells. *Cancer Res* (2017) 77(21):e108–e10. doi: 10.1158/0008-5472.CAN-17-0307
46. Tang Z, Li C, Kang B, Gao G, Li C, Zhang Z. GEPIA: A Web Server for Cancer and Normal Gene Expression Profiling and Interactive Analyses. *Nucleic Acids Res* (2017) 45(W1):W98–102. doi: 10.1093/nar/gkx247
47. Klemm F, Maas RR, Bowman RL, Kornete M, Soukup K, Nassiri S, et al. Interrogation of the Microenvironmental Landscape in Brain Tumors Reveals Disease-Specific Alterations of Immune Cells. *Cell* (2020) 181 (7):1643–60.e17. doi: 10.1016/j.cell.2020.05.007
48. Yuan H, Yan M, Zhang G, Liu W, Deng C, Liao G, et al. CancerSEA: A Cancer Single-Cell State Atlas. *Nucleic Acids Res* (2019) 47(D1):D900–8. doi: 10.1093/nar/gky939
49. Braune EB, Tsoi YL, Phoon YP, Landor S, Silva Cascales H, Ramskold D, et al. Loss of CSL Unlocks a Hypoxic Response and Enhanced Tumor Growth Potential in Breast Cancer Cells. *Stem Cell Rep* (2016) 6(5):643–51. doi: 10.1016/j.stemcr.2016.03.004
50. Walker C, Mojares E, Del Rio Hernandez A. Role of Extracellular Matrix in Development and Cancer Progression. *Int J Mol Sci* (2018) 19(10):3028. doi: 10.3390/ijms19103028
51. Wyckoff JB, Wang Y, Lin EY, Li JF, Goswami S, Stanley ER, et al. Direct Visualization of Macrophage-Assisted Tumor Cell Intravasation in Mammary Tumors. *Cancer Res* (2007) 67(6):2649–56. doi: 10.1158/0008-5472.CAN-06-1823
52. Giese A, Kluwe L, Laube B, Meissner H, Berens ME, Westphal M. Migration of Human Glioma Cells on Myelin. *Neurosurgery* (1996) 38(4):755–64. doi: 10.1227/00006123-199604000-00026
53. Nissen NI, Karsdal M, Willumsen N. Collagens and Cancer Associated Fibroblasts in the Reactive Stroma and its Relation to Cancer Biology. *J Exp Clin Cancer Res* (2019) 38(1):115. doi: 10.1186/s13046-019-1110-6
54. Ishikawa Y, Vranka J, Wirz J, Nagata K, Bachinger HP. The Rough Endoplasmic Reticulum-Resident FK506-Binding Protein FKBP65 Is a Molecular Chaperone That Interacts With Collagens. *J Biol Chem* (2008) 283(46):31584–90. doi: 10.1074/jbc.M802535200
55. Liang X, Chai B, Duan R, Zhou Y, Huang X, Li Q. Inhibition of FKBP10 Attenuates Hypertrophic Scarring Through Suppressing Fibroblast Activity and Extracellular Matrix Deposition. *J Invest Dermatol* (2017) 137(11):2326–35. doi: 10.1016/j.jid.2017.06.029
56. Theocharis AD, Skandalis SS, Tzanakakis GN, Karamanos NK. Proteoglycans in Health and Disease: Novel Roles for Proteoglycans in Malignancy and Their Pharmacological Targeting. *FEBS J* (2010) 277 (19):3904–23. doi: 10.1111/j.1742-4658.2010.07800.x
57. Karamanos NK, Piperigkou Z, Theocharis AD, Watanabe H, Franchi M, Baud S, et al. Proteoglycan Chemical Diversity Drives Multifunctional Cell Regulation and Therapeutics. *Chem Rev* (2018) 118(18):9152–232. doi: 10.1021/acs.chemrev.8b00354
58. Multhaupt HA, Leitinger B, Gullberg D, Couchman JR. Extracellular Matrix Component Signaling in Cancer. *Adv Drug Deliv Rev* (2016) 97:28–40. doi: 10.1016/j.addr.2015.10.013
59. Aberle H. Axon Guidance and Collective Cell Migration by Substrate-Derived Attractants. *Front Mol Neurosci* (2019) 12:148. doi: 10.3389/fnmol.2019.00148
60. Mehlen P, Delloye-Bourgeois C, Chedotal A. Novel Roles for Slits and Netrins: Axon Guidance Cues as Anticancer Targets? *Nat Rev Cancer* (2011) 11(3):188–97. doi: 10.1038/nrc3005
61. Engelhardt B, Vajkoczy P, Weller RO. The Movers and Shapers in Immune Privilege of the CNS. *Nat Immunol* (2017) 18(2):123–31. doi: 10.1038/ni.3666
62. Lou W, Wang W, Chen J, Wang S, Huang Y. ncRNAs-Mediated High Expression of SEMA3F Correlates With Poor Prognosis and Tumor Immune Infiltration of Hepatocellular Carcinoma. *Mol Ther Nucleic Acids* (2021) 24:845–55. doi: 10.1016/j.omtn.2021.03.014
63. Catena R, Bhattacharya N, El Rayes T, Wang S, Choi H, Gao D, et al. Bone Marrow-Derived Gr1+ Cells Can Generate a Metastasis-Resistant Microenvironment *via* Induced Secretion of Thrombospondin-1. *Cancer Discov* (2013) 3(5):578–89. doi: 10.1158/2159-8290.CD-12-0476
64. Zhuang X, Zhang H, Li X, Li X, Cong M, Peng F, et al. Differential Effects on Lung and Bone Metastasis of Breast Cancer by Wnt Signalling Inhibitor DKK1. *Nat Cell Biol* (2017) 19(10):1274–85. doi: 10.1038/ncb3613
65. Wculek SK, Malanchi I. Neutrophils Support Lung Colonization of Metastasis-Initiating Breast Cancer Cells. *Nature* (2015) 528(7582):413–7. doi: 10.1038/nature16140
66. Coffelt SB, Kersten K, Doornebal CW, Weiden J, Vrijland K, Hau CS, et al. IL-17-Producing Gammadelta T Cells and Neutrophils Conspire to Promote Breast Cancer Metastasis. *Nature* (2015) 522(7556):345–8. doi: 10.1038/nature14282
67. Xiao Y, Cong M, Li J, He D, Wu Q, Tian P, et al. Cathepsin C Promotes Breast Cancer Lung Metastasis by Modulating Neutrophil Infiltration and Neutrophil Extracellular Trap Formation. *Cancer Cell* (2021) 39(3):423–37 e7. doi: 10.1016/j.ccell.2020.12.012
68. Sionov RV, Fridlender ZG, Granot Z. The Multifaceted Roles Neutrophils Play in the Tumor Microenvironment. *Cancer Microenviron* (2015) 8 (3):125–58. doi: 10.1007/s12307-014-0147-5
69. Schmidt H, Bastholt L, Geertsen P, Christensen IJ, Larsen S, Gehl J, et al. Elevated Neutrophil and Monocyte Counts in Peripheral Blood are Associated With Poor Survival in Patients With Metastatic Melanoma: A Prognostic Model. *Br J Cancer* (2005) 93(3):273–8. doi: 10.1038/sj.bjc.6602702
70. Lechner MG, Liebertz DJ, Epstein AL. Characterization of Cytokine-Induced Myeloid-Derived Suppressor Cells From Normal Human Peripheral Blood Mononuclear Cells. *J Immunol* (2010) 185(4):2273–84. doi: 10.4049/jimmunol.1000901
71. Peng DH, Rodriguez BL, Diao L, Chen L, Wang J, Byers LA, et al. Collagen Promotes Anti-PD-1/PD-L1 Resistance in Cancer Through LAIR1-Dependent CD8(+) T Cell Exhaustion. *Nat Commun* (2020) 11(1):4520. doi: 10.1038/s41467-020-18298-8
72. Kamphorst AO, Pillai RN, Yang S, Nasti TH, Akondy RS, Wieland A, et al. Proliferation of PD-1+ CD8 T Cells in Peripheral Blood After PD-1-Targeted Therapy in Lung Cancer Patients. *Proc Natl Acad Sci USA* (2017) 114(19):4993–8. doi: 10.1073/pnas.1705327114
73. Chen L, Diao L, Yang Y, Yi X, Rodriguez BL, Li Y, et al. CD38-Mediated Immunosuppression as a Mechanism of Tumor Cell Escape From PD-1/PD-L1 Blockade. *Cancer Discov* (2018) 8(9):1156–75. doi: 10.1158/2159-8290.CD-17-1033
74. Chen Y, Kim J, Yang S, Wang H, Wu CJ, Sugimoto H, et al. Type I Collagen Deletion in alphaSMA(+) Myofibroblasts Augments Immune Suppression and Accelerates Progression of Pancreatic Cancer. *Cancer Cell* (2021) 39 (4):548–65.e6. doi: 10.1016/j.ccell.2021.02.007
75. Lebbink RJ, de Ruiter T, Kaptijn GJ, Bihan DG, Jansen CA, Lenting PJ, et al. Mouse Leukocyte-Associated Ig-Like Receptor-1 (mLAIR-1) Functions as an Inhibitory Collagen-Binding Receptor on Immune Cells. *Int Immunol* (2007) 19(8):1011–9. doi: 10.1093/intimm/dxm071
76. Lebbink RJ, Raynal N, de Ruiter T, Bihan DG, Farndale RW, Meyaard L. Identification of Multiple Potent Binding Sites for Human Leukocyte Associated Ig-Like Receptor LAIR on Collagens II and III. *Matrix Biol* (2009) 28(4):202–10. doi: 10.1016/j.matbio.2009.03.005
77. Meyaard L. The Inhibitory Collagen Receptor LAIR-1 (Cd305). *J Leukoc Biol* (2008) 83(4):799–803. doi: 10.1189/jlb.0907609
78. Fearon DT, Janowitz T. AMD3100/Plerixafor Overcomes Immune Inhibition by the CXCL12-KRT19 Coating on Pancreatic and Colorectal

Cancer Cells. *Br J Cancer* (2021) 125(2):149–51. doi: 10.1038/s41416-021-01315-y
79. Tang F, Li W, Chen Y, Wang D, Han J, Liu D. Downregulation of hnRNP K by RNAi Inhibits Growth of Human Lung Carcinoma Cells. *Oncol Lett* (2014) 7(4):1073–7. doi: 10.3892/ol.2014.1832
80. Crowe DL, Milo GE, Shuler CF. Keratin 19 Downregulation by Oral Squamous Cell Carcinoma Lines Increases Invasive Potential. *J Dent Res* (1999) 78(6):1256–63. doi: 10.1177/00220345990780061001
81. Ohtsuka T, Sakaguchi M, Yamamoto H, Tomida S, Takata K, Shien K, et al. Interaction of Cytokeratin 19 Head Domain and HER2 in the Cytoplasm Leads to Activation of HER2-Erk Pathway. *Sci Rep* (2016) 6:39557. doi: 10.1038/srep39557
82. Bambang IF, Lu D, Li H, Chiu LL, Lau QC, Koay E, et al. Cytokeratin 19 Regulates Endoplasmic Reticulum Stress and Inhibits ERp29 Expression *via* P38 MAPK/XBP-1 Signaling in Breast Cancer Cells. *Exp Cell Res* (2009) 315 (11):1964–74. doi: 10.1016/j.yexcr.2009.02.017
83. Bhagirath D, Zhao X, West WW, Qiu F, Band H, Band V. Cell Type of Origin as Well as Genetic Alterations Contribute to Breast Cancer Phenotypes. *Oncotarget* (2015) 6(11):9018–30. doi: 10.18632/oncotarget.3379
84. Ju JH, Oh S, Lee KM, Yang W, Nam KS, Moon HG, et al. Cytokeratin19 Induced by HER2/ERK Binds and Stabilizes HER2 on Cell Membranes. *Cell Death Differ* (2015) 22(4):665–76. doi: 10.1038/cdd.2014.155
85. Skondra M, Gkioka E, Kostakis ID, Pissimissis N, Lembessis P, Pectasides D, et al. Detection of Circulating Tumor Cells in Breast Cancer Patients Using Multiplex Reverse Transcription-Polymerase Chain Reaction and Specific Primers for MGB, PTHRP and KRT19 Correlation With Clinicopathological Features. *Anticancer Res* (2014) 34(11):6691–9. doi: 10.1093/annonc/mdu358.49
86. Li Y, Wang JP, Santen RJ, Kim TH, Park H, Fan P, et al. Estrogen Stimulation of Cell Migration Involves Multiple Signaling Pathway Interactions. *Endocrinology* (2010) 151(11):5146–56. doi: 10.1210/en.2009-1506
87. Xue J, Peng G, Yang JS, Ding Q, Cheng J. Predictive Factors of Brain Metastasis in Patients With Breast Cancer. *Med Oncol* (2013) 30(1):337. doi: 10.1007/s12032-012-0337-2
88. Iyer V, Klebba I, McCready J, Arendt LM, Betancur-Boissel M, Wu MF, et al. Estrogen Promotes ER-Negative Tumor Growth and Angiogenesis Through Mobilization of Bone Marrow-Derived Monocytes. *Cancer Res* (2012) 72 (11):2705–13. doi: 10.1158/0008-5472.CAN-11-3287
89. Spence RD, Hamby ME, Umeda E, Itoh N, Du S, Wisdom AJ, et al. Neuroprotection Mediated Through Estrogen Receptor-Alpha in Astrocytes. *Proc Natl Acad Sci USA* (2011) 108(21):8867–72. doi: 10.1073/pnas.1103833108
90. Al-Bader M, Ford C, Al-Ayadhy B, Francis I. Analysis of Estrogen Receptor Isoforms and Variants in Breast Cancer Cell Lines. *Exp Ther Med* (2011) 2 (3):537–44. doi: 10.3892/etm.2011.226
91. Leygue E, Dotzlaw H, Watson PH, Murphy LC. Expression of Estrogen Receptor Beta1, Beta2, and Beta5 Messenger RNAs in Human Breast Tissue. *Cancer Res* (1999) 59(6):1175–9. doi: 10.1186/bcr30
92. Poola I, Abraham J, Liu A. Estrogen Receptor Beta Splice Variant mRNAs are Differentially Altered During Breast Carcinogenesis. *J Steroid Biochem Mol Biol* (2002) 82(2-3):169–79. doi: 10.1016/s0960-0760(02)00185-1
93. Girault I, Andrieu C, Tozlu S, Spyratos F, Bieche I, Lidereau R. Altered Expression Pattern of Alternatively Spliced Estrogen Receptor Beta Transcripts in Breast Carcinoma. *Cancer Lett* (2004) 215(1):101–12. doi: 10.1016/j.canlet.2004.05.006
94. Bonner JM, Boulianne GL. Diverse Structures, Functions and Uses of FK506 Binding Proteins. *Cell Signal* (2017) 38:97–105. doi: 10.1016/j.cellsig.2017.06.013
95. Solassol J, Mange A, Maudelonde T. FKBP Family Proteins as Promising New Biomarkers for Cancer. *Curr Opin Pharmacol* (2011) 11(4):320–5. doi: 10.1016/j.coph.2011.03.012
96. Yao YL, Liang YC, Huang HH, Yang WM. FKBPs in Chromatin Modification and Cancer. *Curr Opin Pharmacol* (2011) 11(4):301–7. doi: 10.1016/j.coph.2011.03.005
97. Ge Y, Xu A, Zhang M, Xiong H, Fang L, Zhang X, et al. FK506 Binding Protein 10 Is Overexpressed and Promotes Renal Cell Carcinoma. *Urol Int* (2017) 98(2):169–76. doi: 10.1159/000448338
98. Cai HQ, Zhang MJ, Cheng ZJ, Yu J, Yuan Q, Zhang J, et al. FKBP10 Promotes Proliferation of Glioma Cells *via* Activating AKT-CREB-PCNA Axis. *J BioMed Sci* (2021) 28(1):13. doi: 10.1186/s12929-020-00705-3
99. Quinn MC, Wojnarowicz PM, Pickett A, Provencher DM, Mes-Masson AM, Davis EC, et al. FKBP10/FKBP65 Expression in High-Grade Ovarian Serous Carcinoma and its Association With Patient Outcome. *Int J Oncol* (2013) 42 (3):912–20. doi: 10.3892/ijo.2013.1797
100. Gong LB, Zhang C, Yu RX, Li C, Fan YB, Liu YP, et al. FKBP10 Acts as a New Biomarker for Prognosis and Lymph Node Metastasis of Gastric Cancer by Bioinformatics Analysis and *in Vitro* Experiments. *Onco Targets Ther* (2020) 13:7399–409. doi: 10.2147/OTT.S253154
101. Sun Z, Dong J, Zhang S, Hu Z, Cheng K, Li K, et al. Identification of Chemoresistance-Related Cell-Surface Glycoproteins in Leukemia Cells and Functional Validation of Candidate Glycoproteins. *J Proteome Res* (2014) 13 (3):1593–601. doi: 10.1021/pr4010822
102. Wu D, Pan W. GSK3: A Multifaceted Kinase in Wnt Signaling. *Trends Biochem Sci* (2010) 35(3):161–8. doi: 10.1016/j.tibs.2009.10.002
103. McCubrey JA, Steelman LS, Bertrand FE, Davis NM, Sokolosky M, Abrams SL, et al. GSK-3 as Potential Target for Therapeutic Intervention in Cancer. *Oncotarget* (2014) 5(10):2881–911. doi: 10.18632/oncotarget.2037
104. Rubinfeld B, Albert I, Porfiri E, Fiol C, Munemitsu S, Polakis P. Binding of GSK3beta to the APC-Beta-Catenin Complex and Regulation of Complex Assembly. *Science* (1996) 272(5264):1023–6. doi: 10.1126/science.272.5264.1023
105. Diehl JA, Cheng M, Roussel MF, Sherr CJ. Glycogen Synthase Kinase-3beta Regulates Cyclin D1 Proteolysis and Subcellular Localization. *Genes Dev* (1998) 12(22):3499–511. doi: 10.1101/gad.12.22.3499
106. Sears R, Nuckolls F, Haura E, Taya Y, Tamai K, Nevins JR. Multiple Ras-Dependent Phosphorylation Pathways Regulate Myc Protein Stability. *Genes Dev* (2000) 14(19):2501–14. doi: 10.1101/gad.836800
107. Ougolkov AV, Fernandez-Zapico ME, Savoy DN, Urrutia RA, Billadeau DD. Glycogen Synthase Kinase-3beta Participates in Nuclear Factor kappaB-Mediated Gene Transcription and Cell Survival in Pancreatic Cancer Cells. *Cancer Res* (2005) 65(6):2076–81. doi: 10.1158/0008-5472.CAN-04-3642
108. Bilim V, Ougolkov A, Yuuki K, Naito S, Kawazoe H, Muto A, et al. Glycogen Synthase Kinase-3: A New Therapeutic Target in Renal Cell Carcinoma. *Br J Cancer* (2009) 101(12):2005–14. doi: 10.1038/sj.bjc.6605437
109. Naito S, Bilim V, Yuuki K, Ugolkov A, Motoyama T, Nagaoka A, et al. Glycogen Synthase Kinase-3beta: A Prognostic Marker and a Potential Therapeutic Target in Human Bladder Cancer. *Clin Cancer Res* (2010) 16 (21):5124–32. doi: 10.1158/1078-0432.CCR-10-0275
110. Cao Q, Lu X, Feng YJ. Glycogen Synthase Kinase-3beta Positively Regulates the Proliferation of Human Ovarian Cancer Cells. *Cell Res* (2006) 16(7):671–7. doi: 10.1038/sj.cr.7310078
111. Zhu Q, Yang J, Han S, Liu J, Holzbeierlein J, Thrasher JB, et al. Suppression of Glycogen Synthase Kinase 3 Activity Reduces Tumor Growth of Prostate Cancer *In Vivo*. *Prostate* (2011) 71(8):835–45. doi: 10.1002/pros.21300
112. Shin S, Wolgamott L, Tcherkezian J, Vallabhapurapu S, Yu Y, Roux PP, et al. Glycogen Synthase Kinase-3beta Positively Regulates Protein Synthesis and Cell Proliferation Through the Regulation of Translation Initiation Factor 4E-Binding Protein 1. *Oncogene* (2014) 33(13):1690–9. doi: 10.1038/onc.2013.113
113. Vijay GV, Zhao N, Den Hollander P, Toneff MJ, Joseph R, Pietila M, et al. GSK3beta Regulates Epithelial-Mesenchymal Transition and Cancer Stem Cell Properties in Triple-Negative Breast Cancer. *Breast Cancer Res* (2019) 21(1):37. doi: 10.1186/s13058-019-1125-0
114. Ugolkov A, Gaisina I, Zhang JS, Billadeau DD, White K, Kozikowski A, et al. GSK-3 Inhibition Overcomes Chemoresistance in Human Breast Cancer. *Cancer Lett* (2016) 380(2):384–92. doi: 10.1016/j.canlet.2016.07.006
115. Westbrook VA, Schoppee PD, Diekman AB, Klotz KL, Allietta M, Hogan KT, et al. Genomic Organization, Incidence, and Localization of the SPAN-X Family of Cancer-Testis Antigens in Melanoma Tumors and Cell Lines. *Clin Cancer Res* (2004) 10(1 Pt 1):101–12. doi: 10.1158/1078-0432.ccr-0647-3
116. Yilmaz-Ozcan S, Sade A, Kucukkaraduman B, Kaygusuz Y, Senses KM, Banerjee S, et al. Epigenetic Mechanisms Underlying the Dynamic Expression of Cancer-Testis Genes, PAGE2, -2B and SPANX-B, During Mesenchymal-to-Epithelial Transition. *PloS One* (2014) 9(9):e107905. doi: 10.1371/journal.pone.0107905

117. Maine EA, Westcott JM, Prechtl AM, Dang TT, Whitehurst AW, Pearson GW. The Cancer-Testis Antigens SPANX-A/C/D and CTAG2 Promote Breast Cancer Invasion. *Oncotarget* (2016) 7(12):14708–26. doi: 10.18632/oncotarget.7408
118. Almanzar G, Olkhanud PB, Bodogai M, Dell'agnola C, Baatar D, Hewitt SM, et al. Sperm-Derived SPANX-B Is a Clinically Relevant Tumor Antigen That is Expressed in Human Tumors and Readily Recognized by Human CD4+ and CD8+ T Cells. *Clin Cancer Res* (2009) 15(6):1954–63. doi: 10.1158/1078-0432.CCR-08-1290
119. Chen Y, Xu T, Xie F, Wang L, Liang Z, Li D, et al. Evaluating the Biological Functions of the Prognostic Genes Identified by the Pathology Atlas in Bladder Cancer. *Oncol Rep* (2021) 45(1):191–201. doi: 10.3892/or.2020.7853
120. Kannan A, Philley JV, Hertweck KL, Ndetan H, Singh KP , Sivakumar S, et al. Cancer Testis Antigen Promotes Triple Negative Breast Cancer Metastasis and is Traceable in the Circulating Extracellular Vesicles. *Sci Rep-Uk* (2019) 9 (1):11632. ARTN 11632 doi: 10.1038/s41598-019-48064-w
121. Jope RS, Cheng Y, Lowell JA, Worthen RJ, Sitbon YH, Beurel E. Stressed and Inflamed, Can GSK3 Be Blamed? *Trends Biochem Sci* (2017) 42(3):180–92. doi: 10.1016/j.tibs.2016.10.009
122. Georgievska B, Sandin J, Doherty J, Mortberg A, Neelissen J, Andersson A, et al. AZD1080, a Novel GSK3 Inhibitor, Rescues Synaptic Plasticity Deficits in Rodent Brain and Exhibits Peripheral Target Engagement in Humans. *J Neurochem* (2013) 125(3):446–56. doi: 10.1111/jnc.12203

Conflict of Interest: The authors declare that the research was conducted in the absence of any commercial or financial relationships that could be construed as a potential conflict of interest.

Publisher's Note: All claims expressed in this article are solely those of the authors and do not necessarily represent those of their affiliated organizations, or those of the publisher, the editors and the reviewers. Any product that may be evaluated in this article, or claim that may be made by its manufacturer, is not guaranteed or endorsed by the publisher.

frontiers in Oncology

ORIGINAL RESEARCH
published: 13 January 2022
doi: 10.3389/fonc.2021.802177

Path to Clonal Theranostics in Luminal Breast Cancers

Nawale Hajjaji[1,2*†], *Soulaimane Aboulouard*[1], *Tristan Cardon*[1], *Delphine Bertin*[1,2], *Yves-Marie Robin*[1,2], *Isabelle Fournier*[1,3*] and *Michel Salzet*[1,3*]

[1] Univ. Lille, Inserm, CHU Lille, U1192, Laboratoire Protéomique, Réponse Inflammatoire et Spectrométrie de Masse (PRISM), Lille, France, [2] Breast Cancer Unit, Oscar Lambret Center, Lille, France, [3] Institut universitaire de France, Paris, France

OPEN ACCESS

Edited by:
San-Gang Wu,
First Affiliated Hospital of Xiamen University, China

Reviewed by:
Yong-Yu Liu,
University of Louisiana at Monroe, United States
Saverio Alberti,
University of Messina, Italy

***Correspondence:**
Nawale Hajjaji
n-hajjaji@o-lambret.fr
Isabelle Fournier
isabelle.fournier@univ-lille.fr
Michel Salzet
michel.salzet@univ-lille.fr

†Lead contact:
Nawale Hajjaji
n-hajjaji@o-lambret.fr

Specialty section:
This article was submitted to Breast Cancer, a section of the journal Frontiers in Oncology

Received: 26 October 2021
Accepted: 06 December 2021
Published: 13 January 2022

Citation:
Hajjaji N, Aboulouard S, Cardon T, Bertin D, Robin Y-M, Fournier I and Salzet M (2022) Path to Clonal Theranostics in Luminal Breast Cancers. Front. Oncol. 11:802177. doi: 10.3389/fonc.2021.802177

Integrating tumor heterogeneity in the drug discovery process is a key challenge to tackle breast cancer resistance. Identifying protein targets for functionally distinct tumor clones is particularly important to tailor therapy to the heterogeneous tumor subpopulations and achieve clonal theranostics. For this purpose, we performed an unsupervised, label-free, spatially resolved shotgun proteomics guided by MALDI mass spectrometry imaging (MSI) on 124 selected tumor clonal areas from early luminal breast cancers, tumor stroma, and breast cancer metastases. 2868 proteins were identified. The main protein classes found in the clonal proteome dataset were enzymes, cytoskeletal proteins, membrane-traffic, translational or scaffold proteins, or transporters. As a comparison, gene-specific transcriptional regulators, chromatin related proteins or transmembrane signal receptor were more abundant in the TCGA dataset. Moreover, 26 mutated proteins have been identified. Similarly, expanding the search to alternative proteins databases retrieved 126 alternative proteins in the clonal proteome dataset. Most of these alternative proteins were coded mainly from non-coding RNA. To fully understand the molecular information brought by our approach and its relevance to drug target discovery, the clonal proteomic dataset was further compared to the TCGA breast cancer database and two transcriptomic panels, BC360 (nanoString®) and CDx (Foundation One®). We retrieved 139 pathways in the clonal proteome dataset. Only 55% of these pathways were also present in the TCGA dataset, 68% in BC360 and 50% in CDx. Seven of these pathways have been suggested as candidate for drug targeting, 22 have been associated with breast cancer in experimental or clinical reports, the remaining 19 pathways have been understudied in breast cancer. Among the anticancer drugs, 35 drugs matched uniquely with the clonal proteome dataset, with only 7 of them already approved in breast cancer. The number of target and drug interactions with non-anticancer drugs (such as agents targeting the cardiovascular system, metabolism, the musculoskeletal or the nervous systems) was higher in the clonal proteome dataset (540 interactions) compared to TCGA (83 interactions), BC360 (419 interactions), or CDx (172 interactions). Many of the protein targets identified and drugs screened were clinically relevant to breast cancer and are in

clinical trials. Thus, we described the non-redundant knowledge brought by this clone-tailored approach compared to TCGA or transcriptomic panels, the targetable proteins identified in the clonal proteome dataset, and the potential of this approach for drug discovery and repurposing through drug interactions with antineoplastic agents and non-anticancer drugs.

Keywords: functional tumor heterogeneity, spatially resolved MALDI mass spectrometry imaging, microproteomics, spatially resolved proteome, luminal breast cancers, clonal theranostics, mutated and alternative proteomes, drug repurposing and drug target discovery

HIGHLIGHTS

- Spatially resolved mass spectrometry guided by MALDI mass spectrometry imaging allows an in-depth proteomic screening for drug targets in luminal breast cancers.
- This unsupervised and unlabeled technology performed on intact tumors provides a multidimensional analysis of the clonal proteome including conventional proteins, mutated proteins, and alternative proteins.
- The rich clonal proteomic information generated was not redundant with TCGA or transcriptomic panels, and showed pathways exclusively found in the proteomic analysis.
- A large proportion of the proteins in the clonal proteome dataset were druggable with both antineoplastic agents and non-anticancer drugs, showing the potential application to drug repurposing.
- A significant number of the proteins detected had partially or not yet known drug interactions, showing the potential for discovery.
- Many of the protein targets identified and drugs screened were clinically relevant to breast cancer.

INTRODUCTION

Breast cancer remains the most frequent cancer and the leading cause of cancer-related death among women in Europe (globocan iarc). The rational development of targeted drugs based on molecular knowledge of cancer is a major therapeutic progress that brought substantial hope to improving patients' outcome. However, the complex biological features of this disease, especially the existence of multiple heterogeneous tumor subclones (1), have prevented its eradication, driven drug resistance, including to targeted therapies (2), and has been identified as a marker of poor prognosis in breast cancer patients (3, 4). Integrating tumor heterogeneity in the target discovery process to tailor therapies to the clones present within the tumor is a paradigm shift to reach clonal theranostics. However, technological limitations and breast tumors molecular features have prevented this breakthrough. In fact, this implies the ability to isolate and screen tumor clones separately to understand their biology, find vulnerabilities and identify potential druggable targets.

Historically, sequencing methods revealed genomic alterations driving the emergence of clonal cancer cell subpopulations (5, 6). Beside this genomic heterogeneity, non-genetic mechanisms, such as dynamic transcriptional, translational and metabolic adaptations also contribute to tumor heterogeneity and drug resistance or tolerance (7, 8). Thus, beside the technologies used to detect gene mutations or single nucleotide polymorphisms, technics exploring transcript expression (9), proteins (10), or metabolites (11) also showed significant tumor heterogeneity, demonstrating that heterogeneity is constantly present from the structural to the functional levels of the tumor. Therefore, approaches complementary to genomics are necessary to comprehensively analyze tumor heterogeneity.

Yielding large molecular information on tumor clones from small samples for biomarker or drug target discovery represents a technical challenge despite the advent of single cell technologies (12). Current single-cell sequencing methods require suspensions of cells for isolation, whereas in routine clinical practice the majority of tumors after surgery or biopsy are fixed in formalin and embedded in paraffin blocks. Moreover, analyzing isolated cells does not capture cell-cell interaction in the microenvironment. Spatial transcriptomics represent a powerful tool to access *in situ* functional information about tumor subpopulations (13), and offers the possibility to be multiplexed to fluorescence *in situ* hybridization (14, 15). However, some limitations include the poor prediction of protein expression from RNA expression (16) or transcriptional errors (17) that may hamper drug target inference. Moreover, transcriptome measurements may not necessarily capture adaptive responses that involve post-transcriptional mechanisms such as translation

Abbreviations: ABC, advanced breast cancer; ACN, acetonitrile; AGC, automatic gain control; AltProt, alternative proteins; Amu, atomic mass unit; ANOVA, analysis of variance; ATC, anatomical therapeutic chemical; BC, breast cancer; Da, Dalton; DMFS, distant metastases free survival; EBC, early breast cancer; EMA, European medicines agency; FDA, food and drug administration; FDR, false discovery rate; FFPE, formalin-fixed paraffin-embedded; HCCA, hydroxycinnamic acid; HER2, human epidermal growth factor receptor-2; HR, hazard ratio; HUGO, human genome organization; ID, identification; IDG, illuminating the druggable genome; IDG-KMC, illuminating the druggable genome knowledge management center; ITO, indium tin oxide; LC, liquid chromatography; LESA, liquid extraction surface analysis; LFQ, label-free quantification; MALDI, matrix assisted laser desorption ionization; MeOH, methanol; Meta metastases; MS mass spectrometry; MSI mass spectrometry imaging; OS, overall survival; PMDA, pharmaceuticals and medical devices agency; PSM, peptide spectrum matches; SNP, single nucleotide polymorphism; TDL, target development level; TFA, trifluoroacetic acid; TIC, total ion count.

or metabolic reprogramming (18–20). Focusing on tumor proteomic landscape has the advantage of recapitulating both the expressed genomic landscape and the non-genetic processes. This could be of particular interest in tumors with a relatively low mutational burden such as breast cancers (21). Besides, given that the vast majority of drug targets are proteins (22), a proteomic approach allows direct target detection. Technologies specifically dedicated to study the spatial proteomic heterogeneity of tumors, combined or not with transcriptomics are scarce. Most rely on selected and labeled markers, limited in number, for instance with multiplexed pathology methods (23–25), which is not suited for discovery.

We asked whether matrix-assisted laser desorption/ionization (MALDI) mass spectrometry imaging (MSI) combined with microproteomics could screen for relevant druggable protein targets from breast cancer clones to guide clonal theranostics. MALDI MSI enables the spatially resolved label-free imaging of different molecular classes, including proteins, in their histological context (26–28), thus revealing functionally heterogeneous tumor subpopulations in solid tumors (29, 30). The selected subclones are further extracted *in situ* using a semi-automated standardized microproteomic technology to perform a full proteomic profiling with LC-MS/MS (31) comprising identification of referenced proteins but also proteins presenting mutations or alternative proteins issued from the non-coding parts of RNA or non-coding RNA. This approach constitutes a unique tool to characterize the proteomic profile of functionally distinct tumor subpopulations, which we denoted the clonal proteome. Our aims were (i) to map and characterize luminal breast cancers' functional clones using MALDI MSI combined with microproteomics, and (ii) determine the potential of this approach to identify clinically relevant druggable protein targets in luminal tumors.

TABLE 1 | Clinico-pathological parameters for the breast cancer patients' series.

	Early stage BC n=51 pts	Advanced BC n=12 pts
Age (median, range)	55 (29-80)	64 (47-82)
Initial Tumor size		
T1	18	7
T2	29	3
T3	4	1
unknown	_	1
Histology		
ductal	40	7
lobular	7	3
other	4	2
Tumor grade		
1	5	2
2	44	5
3	2	3
unknown	_	2
Initial nodal involvement		
node positive	26	6
node negative	25	6
Metastases		
yes	0	12
no	51	0
Hormone receptors positive	50	10
unknown	1	2
HER2 expression negative	50	9
unknown	1	3
Metastatic sites at diagnosis of metastases		
node	_	2
liver	_	3
bone	_	6
skin	_	4
lung/pleura	_	4

BC, breast cancer; pts, patients.

METHODS

Patient Samples and Consent

We carried out a retrospective single center study at Centre Oscar Lambret (Lille, France) to analyze the spatial heterogeneity of primary breast tumors and breast cancer metastases. Eligible patients were women with early breast cancer or metastatic luminal breast cancer with available FFPE tumor tissue after a surgical procedure or a fine needle biopsy. Our pathologists selected 52 primary tumors and 24 metastases from 51 and 12 patients respectively. All patients still alive gave their informed consent. This retrospective study was approved by the local institutional clinical research committee. The clinico-pathological data of both patient series were listed in **Table 1** (**Supplementary Table 1**).

MALDI Mass Spectrometry Imaging

For each tumor sample, 2 consecutive sections of 8 micrometers were cut of off the block. The first section was used to perform the MALDI MSI analysis (27, 32–34). The tumor tissue section was deposited on ITO-coated glass slides (LaserBio Labs, Valbonne, France) and vacuum-dried during 15 min. Protein demasking was performed with washing with NH4HCO3 10mM for 5 min twice, then TRIS HCl 20mM pH9 for 30 min at 95°C. Tryptic digestion was performed (40µg/mL, dissolved in NH4HCO3 50mM) by micro-spraying trypsin on the section surface using an HTX TM sprayer (HTX technologies, LLC), and incubation overnight at 56°C. The slide was dried in a dessicator prior to deposition of a solid ionic matrix HCCA-aniline using an HTX TM sprayer (HTX technologies, LLC). Briefly, 36 µL of aniline were added to 5 mL of a solution of 10 mg/mL HCCA dissolved in ACN/0.1% TFA aqueous (7:3, v/v). A real-time control of the deposition was performed by monitoring scattered light to obtain a uniform layer of matrix. The MALDI mass spectrometry images were performed on a RapifleX Tissuetyper MALDI TOF/TOF instrument (Bruker Daltonics, Germany) equipped with a smartbeam 3D laser. The MSI mass spectra were acquired in the positive delayed extraction reflectron mode using the 500-3000 m/z range, and averaged from 200 laser shots per pixel, using a 70µm spatial resolution raster.

MALDI MSI Data Processing and Analysis

The MALDI-MSI data were analyzed using SCiLS Lab software (SCiLS Lab 2019, SCiLS GmbH). Common processing methods for MALDI MSI were applied with a baseline removal using a

convolution method and data were normalized using Total Ion Count (TIC) method (35, 36). Then, the resulting pre-processing data were clustered to obtain a spatial segmentation using the bisecting k means algorithm (37). Different spatial segmentations were performed. First, an individual segmentation was applied to each tissue separately. Then, the data from all tissues were clustered together to obtain a global segmentation. Briefly, the spatial segmentation consists of grouping all spectra according to their similarity using a clustering algorithm that apply a color code to all pixels of a same cluster. Colors are arbitrarily assigned to clusters; several disconnected regions can have the same color if they share the same molecular content. To limit the pixel-to-pixel variability, edge-preserving image denoising was applied. The segmentation results were represented on a dendrogram resulting from a hierarchical clustering. The branches of the dendrogram were defined based on a distance calculation between each cluster. The manual selection of different branches of the dendrogram allows further segmentation of selected clusters to visualize more regions with distinct molecular composition. Each color-coded region identified a proteomic tumor clone. The regions/clones of interest were then subjected to on-tissue microproteomics, i.e. microdigestion and microextraction, to perform nanoLC-MS & MS/MS analysis of the extract for in-depth protein identification.

Microproteomic Analysis

Superimposing the molecular image with the immunochemistry image allowed selection of the subclonal areas to be submitted to microproteomics using the second consecutive 8 µm tumor sections. The tissue sections were deposited on polylysine glass slides, and microdigested with a trypsin solution deposited with a microspotter. On-tissue trypsin digestion was performed using a Chemical Inkjet Printer (CHIP-100, Shimadzu, Kyoto, Japan). The trypsin solution (40µg/mL, 50mM NH4HCO3 buffer) was deposited on a region defined to 1mm² for 2h. During this time, the trypsin was changed every half-hour. With 350 cycles and 450pl per spot, a total of 6.3µg was deposited. After microdigestion, the spot content was micropextracted by liquid microjunction using the TriVersa Nanomate (Advion Biosciences Inc., Ithaca, NY, USA) using Liquid Extraction and Surface Analysis (LESA) settings. With 3 different solvent mixtures composed of 0.1% TFA, ACN/0.1% TFA (8:2, v/v), and MeOH/0.1% TFA (7:3, v/v). A complete LESA sequence run 2 cycles for each mixture composed of an aspiration (2µL), a mixing onto the tissue, and a dispensing into low-binding tubes. For each tumor area of interest, 2 microextraction sequences were run and pooled (38).

NanoLC-MS and MS/MS Analysis

After liquid extraction, samples were freeze-dried in a SpeedVac concentrator (SPD131DPA, ThermoScientific, Waltham, Massachusetts, USA), reconstituted with 10µL 0.1% TFA and subjected to solid-phase extraction to remove salts and concentrate the peptides. This was done using a C-18 Ziptip (Millipore, Saint-Quentin-en-Yvelines, France), eluted with ACN/0.1% TFA (8:2, v/v) and then the samples were dried for storage. Before analysis, samples were suspended in 20µL ACN/0.1% FA (2:98, v/v), deposited in vials and 10µL were injected for analysis. The separation prior to the MS used online reversed-phase chromatography coupled with a Proxeon Easy-nLC-1000 system (Thermo Scientific) equipped with an Acclaim PepMap trap column (75 µm ID x 2 cm, Thermo Scientific) and C18 packed tip Acclaim PepMap RSLC column (75 µm ID x 50 cm, Thermo Scientific). Peptides were separated using an increasing amount of acetonitrile (5%-40% over 140 minutes) and a flow rate of 300 nL/min. The LC eluent was electrosprayed directly from the analytical column and a voltage of 2 kV was applied *via* the liquid junction of the nanospray source. The chromatography system was coupled to a Thermo Scientific Q-Exactive mass spectrometer. The mass spectrometer was programmed to acquire in a data-dependent mode. The survey scans were acquired in the Orbitrap mass analyzer operated at 70,000 (FWHM) resolving power. A mass range of 200 to 2000 m/z and a target of 3E6 ions were used for the survey scans. Precursors observed with an intensity over 500 counts were selected "on the fly" for ion trap collision-induced dissociation (CID) fragmentation with an isolation window of 4 amu and a normalized collision energy of 30%. A target of 5000 ions and a maximum injection time of 120 ms were used for CID MS2 spectra. The method was set to analyze the top 10 most intense ions from the survey scan and a dynamic exclusion was enabled for 20 s. Extracts were sequenced randomly to avoid batch effect.

Data Analysis

All MS data were processed with MaxQuant (39, 40) (Version 1.5.6.5) using the Andromeda (41) search engine. The proteins were identified by searching MS and MS/MS data against the Decoy version of the complete proteome for Homo sapiens in the UniProt database (Release March 2017, 70941 entries) combined with 262 commonly detected contaminants. Trypsin specificity was used for digestion mode, with N-terminal acetylation and methionine oxidation selected as a variable. We allowed up to two missed cleavages. Initial mass accuracy of 6 ppm was selected for MS spectra, and the MS/MS tolerance was set to 20 ppm for the HCD data. False discovery rate (FDR) at the peptide spectrum matches (PSM) and protein level was set to 1%. Relative, label-free quantification of the proteins was conducted into MaxQuant using the MaxLFQ algorithm (42) with default parameters. Analysis of the identified proteins was performed using Perseus software (http://www.perseus-framework.org/) (version 1.6.12.0). The file containing the information from the identification was filtered to remove hits from the reverse database, proteins with only modified peptides and potential contaminants. The LFQ intensity was logarithmized (log2[x]). Categorical annotation of the rows was used to define the different groups. Principal component analysis (PCA) was done to compare the protein content of each sample. Multiple-sample tests were performed using ANOVA with a p-value of 1%. Normalization was achieved using a Z-score with matrix access by rows. Only proteins that were significant by ANOVA were retained. The hierarchical clustering and profile plots of the statistically significant proteins were performed and visualized with Perseus. Functional annotation and characterization of the identified

proteins were performed using FunRich software (version 3) and STRING (version 9.1, http://stringdb.org) (43). Pearson's correlation coefficient and matrix representation were generated in R software using corrplot package. Gene Set Enrichment Analysis (GSEA) and Cytoscape software (version 3.6.1) were used for the biological process analysis of the clusters selected from the heatmap. The data sets were deposited at the ProteomeXchange Consortium (http://proteomecentral.proteomexchange.org) *via* the PRIDE partner repository (44) with Data available *via* ProteomeXchange with identifier PXD024134.

Subnetwork Enrichment Pathway Analyses and Statistical Testing

The Elsevier's Pathway Studio version 10.0 (Ariadne Genomics/Elsevier) was used to deduce relationships among differentially expressed proteomics protein candidates using the Ariadne ResNet database (45, 46). "Subnetwork Enrichment Analysis" (SNEA) algorithm was selected to extract statistically significant altered biological and functional pathways pertaining to each identified set of protein hits among the different groups. SNEA utilizes Fisher's statistical test set to determine if there are nonrandom associations between two categorical variables organized by specific relationships. Integrated Venn diagram analysis was performed using "the InteractiVenn": a web-based tool for the analysis of complex data sets (47). Annotation analysis of gene ontology terms for the identified proteins was performed using PANTHER Classification System (version 15.0, http://www.pantherdb.org) (48). Interaction network analyses were performed with Cytoscape (version 3.7.2) and the Cluego application (version 2.5.5) to interpret the lists of genes and proteins by selecting representative Gene Ontology terms and pathways from multiple ontologies and visualize them into functionally organized networks (49). The ontologies used included GO_BiologicalProcess-EBI-UniProt-GOA_27.02.2019, GO_CellularComponent-EBI-UniProt-GOA_27.02.2019, GO_ImmuneSystemProcess-EBI-UniProt-GOA_27.02.2019, GO_MolecularFunction-EBI-UniProt-GOA_27.02.2019, KEGG_27.02.2019, REACTOME_Pathways_27.02.2019, REACTOME_Reactions_27.02.2019, and WikiPathways_27.02.2019. The GO level range was 3 to 8, and groups with more than 50% overlap were merged. The statistical test used was enrichment/depletion (two-sided hypergeometric test) with a Bonferroni step down correction method.

Mutated Protein Identification

Protein identification was also performed using the mutation-specific database (50). XMan v2 database contains 2 539 031 mutated peptide sequences from 17 599 Homo sapiens proteins (2 377 103 are missense and 161 928 are nonsense mutations). The interrogation was performed by Proteome Discoverer 2.3 software and Sequest HT package, using an iterative method. The precursor mass tolerance was set to 15 ppm and the fragment mass tolerance was set to 0.02 Da. For high confidence result, the FDR values were specified to 1%. A filter with a minimum Xcorr of 2 was applied. The generated result file was filtered using a Python script to remove unmutated peptides. All mutations were then manually checked based on MS/MS spectra profile.

Alternative Proteins Identification

RAW data obtained by nanoLC-MS/MS analysis were processed using Proteome Discoverer V2.3 (Thermo Scientific) with the following parameters: Trypsin as an enzyme, 2 missed cleavages, methionine oxidation as a variable modification, Precursor Mass Tolerance: 10 ppm and Fragment mass tolerance: 0.6 Da. The validation was performed using Percolator with an FDR set to 0.001%. A consensus workflow was then applied for the statistical arrangement, using the high confidence protein identification. The protein database was uploaded from Openprot (https://openprot.org/) and included reference proteins, novel isoforms, and alternative proteins predicted from both Ensembl and RefSeq annotations (GRCh38.83, GRCh38.p7) (51).

TCGA, BC360, CDx Datasets

To compare our proteomic data with genomic and transcriptomic datasets used in breast cancer, the reference genes of the proteins were contrasted to publically available TCGA, BC360 (nanoString®) and CDx (Foundation One®) datasets. Breast cancer genomic alterations were collected from the TCGA web portal using "breast cancer" as keyword in the search engine. The TCGA gene list is in **Supplementary Material 1**. The gene list of the BC360 and CDx panels were obtained from nanoString and Foundation One websites. The gene lists are in **Supplementary Materials 2** and **3** respectively.

Druggable Genome Database

DrugCentral (http://drugcentral.org) is an online drug information resource created and maintained by the Division of Translational Informatics at University of New Mexico in collaboration with the IDG Illuminating the Druggable Genome (IDG) (https://druggablegenome.net/index) (52). DrugCentral provides information on active ingredients, chemical entities, pharmaceutical products, the mode of action of drugs, indications, and pharmacologic action. Data is monitored on FDA, EMA, and PMDA for new drug approval on regular basis. Supported target search terms are HUGO gene symbols, Uniprot accessions and target names, and Swissprot identifiers. We used the WHO anatomical therapeutic chemical (ATC) classification to categorize drugs.

Druggability Level of the Targets

The druggability level of the targets was classified using the definition of the Illuminating the Druggable Genome Knowledge Management Center (IDG-KMC) based on four target development levels (TDLs) categorized as follows: (i) Tclin: targets with activities in DrugCentral (i.e., approved drugs) and known mechanism of action, (ii) Tchem: targets with activities in ChEMBL or DrugCentral that satisfy the activity thresholds detailed in https://druggablegenome.net/ProteinFam, (iii) Tbio: targets with no known drug or small molecule activities that satisfy the activity thresholds and criteria (detailed in https://druggablegenome.net/ProteinFam), (iv) Tdark: targets with

virtually no known drug or small molecule activities that satisfy the criteria defined by IDG-KMC.

Clinical Trial Database

ClinicalTrials.gov is a web-based resource that provides information on publicly and privately supported clinical studies on a wide range of diseases and conditions (https://clinicaltrials.gov/ct2/home). The web site is maintained by the National Library of Medicine at the National Institutes of Health (US). Information on ClinicalTrials.gov is provided and updated by the sponsor or principal investigator of the clinical study. 6159 studies corresponding to interventional clinical trials conducted in breast cancer patients were retrieved using "breast cancer" as the medical condition and "drug" as other condition. Results were also filtered to select "Adult" and "Older Adult", and "Interventional Studies".

Statistical Analyses

Descriptive analyses used frequency of distribution, median, quartiles and extremes. Survival analyses were performed using the breast cancer Kaplan-Meier plotter online tool (https://kmplot.com; n=3955). The database sources included GEO, EGA, and TCGA (53). A multiple gene testing was run using available cohorts of patients with estrogen receptor positive and HER2 negative disease to analyze the reference genes association with distant metastases free survival (DMFS) and overall survival (OS). A logrank $p<0.05$ was considered significant.

RESULTS

Workflow for Breast Cancer Clonal Proteome Analysis

The workflow described in **Figure 1A** was applied to two FFPE tumor slides to provide a spatially resolved unsupervised and unlabeled visualization of breast cancer spatial heterogeneity, and an in-depth proteomic profiling. The MALDI MSI on-tissue spatial analysis mapped high molecular weight peptide composition on the first tumor slide. The spectral data obtained were clustered by the bisecting k-means method, which attributed color-coded groups to tumors areas according to the similarity of their proteomic signature. Manual group splitting (group segmentation) was limited to 3 in order to map only main functional differences between tumor subpopulations. Imaging revealed distinct proteomic clones, as illustrated in **Figure 1B** showing representative MALDI MS images of a primary tumor and a metastasis sample among the 76 luminal tumors analyzed (52 primary breast tumors and 24 metastases in (**Supplementary Materials 4**, **5**). From the MSI data, 124 MSI clonal areas were retrieved corresponding to 52 areas of primary tumors, 48 areas of primary tumor stroma and 24 areas of metastases. Each of these 124 MSI clones were individually analyzed by spatially resolved shotgun proteomic. MaxLFQ algorithm was used to perform label-free quantification of proteins and resulted in a total of 2868 proteins from the 124 clonal areas (**Figure 2A**). The number of proteins identified did not significantly differ between tissue types (**Supplementary Material 6A**), or according to the sampling method, *i.e.* mastectomy, surgical biopsy or fine needle core biopsy (**Supplementary Material 6B**). Panther analysis showed that the main protein classes found in the clonal proteome dataset were enzymes, cytoskeletal proteins, membrane-traffic, translational or scaffold proteins, or transporters (**Figure 2B**). As a comparison, gene-specific transcriptional regulators, chromatin related proteins or transmembrane signal receptor were more abundant in the TCGA dataset (**Figure 2B**). Differences between primary tumors and stroma, or between primary tumors and metastases were mild among the main protein classes (**Supplementary Material 7**). We also detected modified proteins, specifically mutated proteins and alternative proteins. Mutations-missense at a protein-level were identified by expanding the search of the raw mass spectrometry files of our proteomic dataset against a mutated peptide database. The search identified 26 mutated proteins, 18 in primary tumors, 20 in stroma and 12 in metastases, with various frequencies (**Figure 2C**). Similarly, expanding the search to alternative proteins databases retrieved 126 alternative proteins in the clonal proteome dataset (**Figure 2D**): 79 were identified in primary tumors, 69 in stroma and 50 in metastases. The majority of these alternative proteins had a length ranging from 29 to 150 amino acids (**Figures 2E–G**). They were coded mainly from non-coding RNA (**Figures 2H–J**). These proteins were infrequent and found mostly in less than 25% of the patients (**Figures 2K–M**).

Luminal Tumors Clonal Proteome Landscape Among Classic and Modified Proteins

To fully understand the molecular information brought by our approach and its relevance to drug target discovery, the clonal proteomic dataset was further compared to the TCGA breast cancer database and two transcriptomic panels, BC360 (nanoString®) and CDx (Foundation One®). The Venn diagram in **Figure 3A** showed that only few proteins of the clonal proteomic dataset (identified by their reference gene) were shared with TCGA, BC360 or CDx panels, both in primary tumors and metastases. 2264 and 1562 proteins were exclusively found in the clonal proteome dataset of primary tumors and metastases respectively (**Supplementary Material 8**). Enrichment analysis using Panther software identified 139 pathways in the clonal proteome dataset. Only 55% of these pathways were also present in the TCGA dataset, 68% in BC360 and 50% in CDx. The pathways and processes identified were differentially distributed across the datasets as depicted in the heatmap in **Figure 3B**. Pathways over-represented in the clonal proteome dataset were integrin or inflammation mediated by chemokine and cytokine signaling pathways, cytoskeletal regulation by Rho GTPase, the ubiquitin proteasome pathway, glycolysis, *de novo* purine biosynthesis or DNA replication. Under-represented processes were mainly signaling pathways or the oxidative stress response. 41 pathways were exclusive to

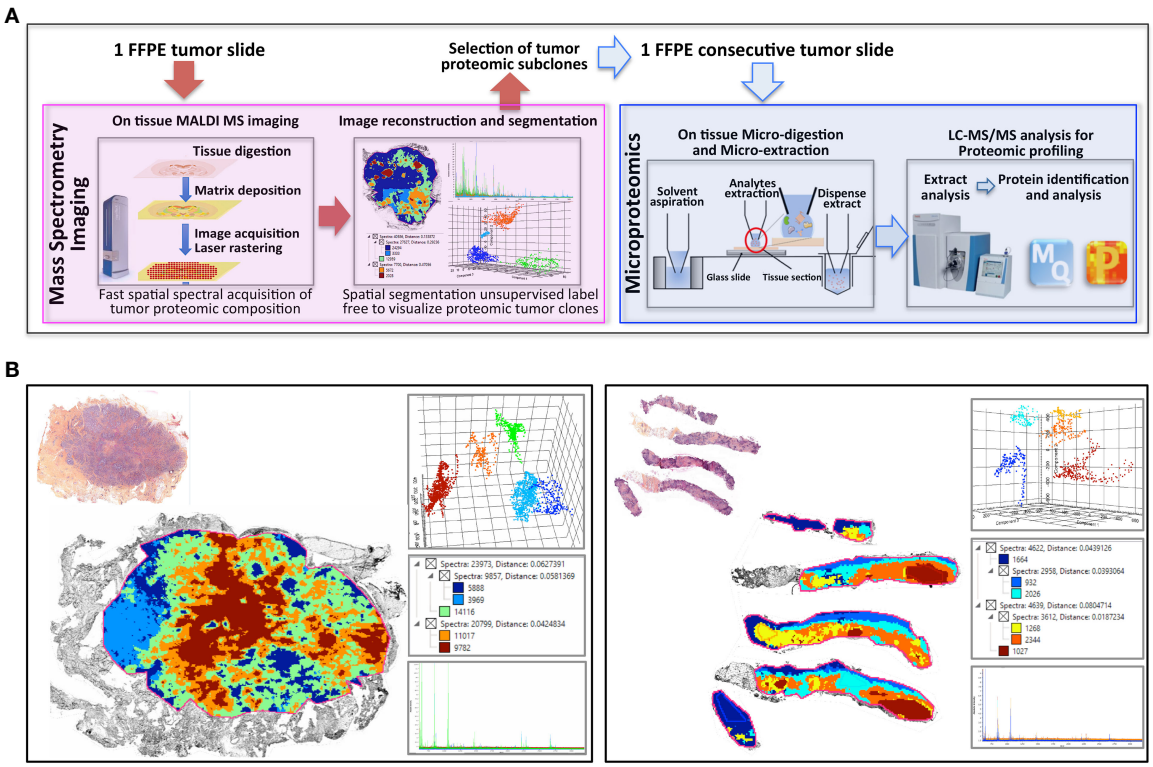

FIGURE 1 | Clonal proteome analysis in breast cancer. **(A)** Workflow for on tissue analysis of tumor proteomic heterogeneity using spatially resolved microproteomics guided by MALDI MSI **(B)** The presence of tumor proteomic clones revealed by MSI was illustrated in a primary tumor (left) from a surgical resection (case 42) and a metastatic sample (right) collected with a fine needle biopsy (case 22). In each sample vignette, the MALDI MS imaging is displayed with the histological HPS picture (upper left), the principal component analysis of the proteomic clones (upper right), the segmentation tree (middle right), and the spectra of the clones (bottom right).

the clonal proteome (**Table 2**), mainly metabolic pathways involved in amino acid, lipid or nucleic acid synthesis. Seven of these pathways have been suggested as candidate for drug targeting, 22 have been associated with breast cancer in experimental or clinical reports, the remaining 19 pathways have been understudied in breast cancer (**Table 2**) (54–86). The mutated proteins identified have been reported in a variety of human tissues; only mutated polyubiquitin-C has been reported in breast tissue with an impact on proteasome degradation and DNA replication. The other mutated proteins may affect hemostasis, complement and coagulation cascades, hormone biosynthesis, metabolism, EGFR1 signaling, signaling in the immune system, apoptosis, cell junction organization, or integrin signaling (**Figure 2C**). Enrichment analyses performed on the identified mutated proteins using their reference genes showed three main biological processes: expression of interferon gamma genes, apoptosis, and senescence (**Figures 3C, D**). Only 4 of the reference genes (COL6A3, COL1A1, HBB, HLA-A) were also found in TCGA or BC360 datasets (none in CDx). The functions of the alternative proteins identified are not known yet. Among their known reference genes, only 8 (ARNT, CD79B, KAT6B, LMO1, PBX1, CD276, ELF3, HDAC2) were also present in TCGA, BC360 or CDx panels.

Clonal Proteome Druggability and Interactions With Approved Drugs

The clonal proteome dataset was reviewed against DrugCentral database to determine the number of proteins targetable, their level of druggability and their interaction with approved drugs. Among the proteins identified in the clonal proteome dataset, 1495 proteins were targetable with a level of druggability high for 52% of them (known mechanism of action and drug interaction, Tclin), while 39% had a lower level of knowledge (Tchem), and 9% had no known drug or small molecule interaction (Tbio) (**Figure 4A**). The highest number of druggable targets was observed in the clonal proteome compared to the genomic and transcriptomic datasets. The proportion of less known targets was also greater in the clonal proteome dataset (47%) compared to TCGA (18%), BC360 (23%) or CDx (25%) (**Figure 4A**). The main target classes in the clonal proteome dataset were enzymes (60%), kinases (23%) and transporters (7%), whereas kinases were dominant in the other datasets (46% to 77%) (**Figure 4B**). The number of protein and drug interactions with antineoplastic and immunomodulating agents were up to 309 in the clonal proteome dataset, 485 in TCGA, 506 in BC360, and 647 in CDx (**Figure 4C** and **Supplementary Material 9**). Among the anticancer drugs, 35 drugs matched uniquely with the clonal

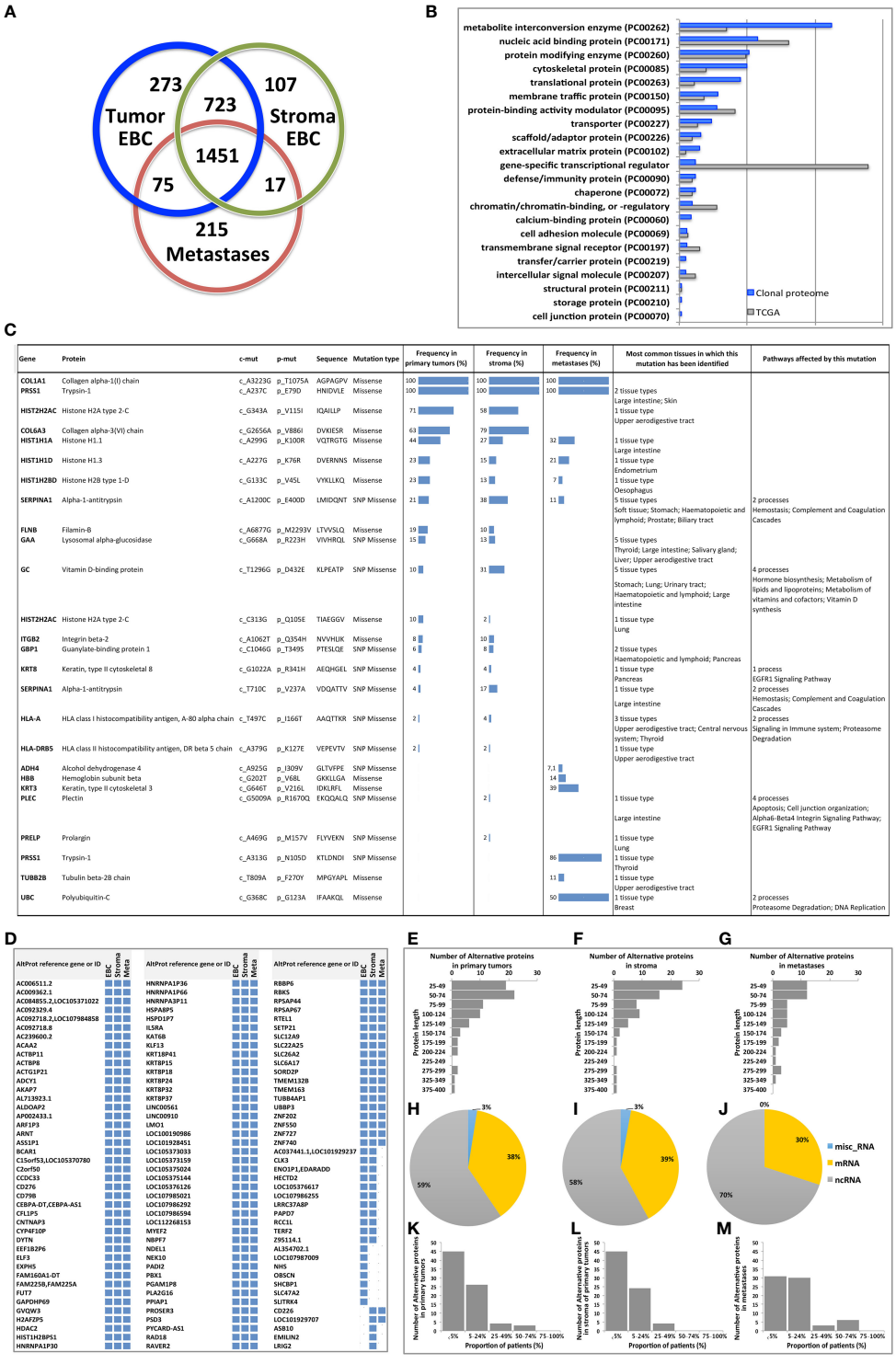

Gene	Protein	c-mut	p-mut	Sequence	Mutation type	Frequency in primary tumors (%)	Frequency in stroma (%)	Frequency in metastases (%)	Most common tissues in which this mutation has been identified	Pathways affected by this mutation
COL1A1	Collagen alpha-1(I) chain	c_A3223G	p_T1075A	AGPAGPV	Missense	100	100	100		
PRSS1	Trypsin-1	c_A237C	p_E79D	HNIDVLE	Missense	100	100	100	2 tissue types	
									Large intestine; Skin	
HIST2H2AC	Histone H2A type 2-C	c_G343A	p_V115I	IQAILLP	Missense	71	58		1 tissue type	
									Upper aerodigestive tract	
COL6A3	Collagen alpha-3(VI) chain	c_G2656A	p_V886I	DVKIESR	Missense	63	79			
HIST1H1A	Histone H1.1	c_A299G	p_K100R	VQTRGTG	Missense	44	27	32	1 tissue type	
									Large intestine	
HIST1H1D	Histone H1.3	c_A227G	p_K76R	DVERNNS	Missense	23	15	21	1 tissue type	
									Endometrium	
HIST1H2BD	Histone H2B type 1-D	c_G133C	p_V45L	VYKLLKQ	Missense	23	13	7	1 tissue type	
									Oesophagus	
SERPINA1	Alpha-1-antitrypsin	c_A1200C	p_E400D	LMIDQNT	SNP Missense	21	38	11	5 tissue types	2 processes
									Soft tissue; Stomach; Haematopoietic and lymphoid; Prostate; Biliary tract	Hemostasis; Complement and Coagulation Cascades
FLNB	Filamin-B	c_A6877G	p_M2293V	LTVVSLQ	Missense	19	10			
GAA	Lysosomal alpha-glucosidase	c_G668A	p_R223H	VIVHRQL	SNP Missense	15	13		5 tissue types	
									Thyroid; Large intestine; Salivary gland; Liver; Upper aerodigestive tract	
GC	Vitamin D-binding protein	c_T1296G	p_D432E	KLPEATP	SNP Missense	10	31		5 tissue types	4 processes
									Stomach; Lung; Urinary tract; Haematopoietic and lymphoid; Large intestine	Hormone biosynthesis; Metabolism of lipids and lipoproteins; Metabolism of vitamins and cofactors; Vitamin D synthesis
HIST2H2AC	Histone H2A type 2-C	c_C313G	p_Q105E	TIAEGGV	Missense	10	2		1 tissue type	
									Lung	
ITGB2	Integrin beta-2	c_A1062T	p_Q354H	NVVHLIK	Missense	8	10			
GBP1	Guanylate-binding protein 1	c_C1046G	p_T349S	PTESLQE	SNP Missense	6	8		2 tissue types	
									Haematopoietic and lymphoid; Pancreas	
KRT8	Keratin, type II cytoskeletal 8	c_G1022A	p_R341H	AEQHGEL	SNP Missense	4	4		1 tissue type	1 process
									Pancreas	EGFR1 Signaling Pathway
SERPINA1	Alpha-1-antitrypsin	c_T710C	p_V237A	VDQATTV	SNP Missense	4	17		1 tissue type	2 processes
									Large intestine	Hemostasis; Complement and Coagulation Cascades
HLA-A	HLA class I histocompatibility antigen, A-80 alpha chain	c_T497C	p_I166T	AAQTTKR	SNP Missense	2	4		3 tissue types	2 processes
									Upper aerodigestive tract; Central nervous system; Thyroid	Signaling in Immune system; Proteasome Degradation
HLA-DRB5	HLA class II histocompatibility antigen, DR beta 5 chain	c_A379G	p_K127E	VEPEVTV	SNP Missense	2	2		1 tissue type	
									Upper aerodigestive tract	
ADH4	Alcohol dehydrogenase 4	c_A925G	p_I309V	GLTVFPE	SNP Missense			7,1		
HBB	Hemoglobin subunit beta	c_G202T	p_V68L	GKKLLGA	Missense			14		
KRT3	Keratin, type II cytoskeletal 3	c_G646T	p_V216L	IDKLRFL	Missense			39		
PLEC	Plectin	c_G5009A	p_R1670Q	EKQQALQ	SNP Missense		2		1 tissue type	4 processes
										Apoptosis; Cell junction organization; Alpha6-Beta4 Integrin Signaling Pathway; EGFR1 Signaling Pathway
									Large intestine	
PRELP	Prolargin	c_A469G	p_M157V	FLYVEKN	SNP Missense		2		1 tissue type	
									Lung	
PRSS1	Trypsin-1	c_A313G	p_N105D	KTLDNDI	SNP Missense			86	1 tissue type	
									Thyroid	
TUBB2B	Tubulin beta-2B chain	c_T809A	p_F270Y	MPGYAPL	Missense			11	1 tissue type	
									Upper aerodigestive tract	
UBC	Polyubiquitin-C	c_G368C	p_G123A	IFAAKQL	Missense			50	1 tissue type	2 processes
									Breast	Proteasome Degradation; DNA Replication

AltProt reference gene or ID	EBC	Stroma	Meta
AC006511.2			
AC009362.1			
AC084855.2,LOC105371022			
AC092329.4			
AC092718.2,LOC107984858			
AC092718.8			
AC239600.2			
ACAA2			
ACTBP11			
ACTBP8			
ACTG1P21			
ADCY1			
AKAP7			
AL713923.1			
ALDOAP2			
AP002433.1			
ARF1P3			
ARNT			
AS51P1			
BCAR1			
C15orf53,LOC105370780			
C2orf50			
CCDC33			
CD276			
CD79B			
CEBPA-DT,CEBPA-AS1			
CFL1P5			
CNTNAP3			
CYP4F10P			
DYTN			
EEF1B2P6			
ELF3			
EXPH5			
FAM160A1-DT			
FAM225B,FAM225A			
FUT7			
GAPDHP69			
GVQW3			
H2AFZP5			
HDAC2			
HIST1H2BP51			
HNRNPA1P30			
HNRNPA1P36			
HNRNPA1P66			
HNRNPA3P11			
HSPA8P5			
HSPD1P7			
IL9RA			
KAT6B			
KLF13			
KRT18P41			
KRTBP15			
KRTBP18			
KRTBP24			
KRTBP32			
KRTBP37			
LINC00561			
LINC00910			
LMO1			
LOC100190986			
LOC101928451			
LOC105373033			
LOC105373159			
LOC105375024			
LOC105375144			
LOC105376126			
LOC107985021			
LOC107986292			
LOC107986594			
LOC112268153			
MYEF2			
NBPF7			
NDEL1			
NEK10			
PADI2			
PBX1			
PGAM1P8			
PLA2G16			
PPIAP1			
PROSER3			
PSD3			
PYCARD-AS1			
RAD18			
RAVER2			
RBBP6			
RBKS			
RPSAP44			
RPSAP67			
RTEL1			
SETP21			
SLC12A9			
SLC22A25			
SLC26A2			
SLC6A17			
SORD2P			
TMEM132B			
TMEM163			
TUBB4AP1			
UBBP3			
ZNF202			
ZNF550			
ZNF727			
ZNF740			
AC037441.1,LOC101929237			
CLK3			
ENO1P1,LEDARADD			
HECTD2			
LOC105376617			
LOC107986255			
LRRC37A8P			
PAPD7			
RCC1L			
TERF2			
Z95114.1			
AL354702.1			
LOC107987009			
NHS			
OBSCN			
SHCBP1			
SLC47A2			
SLITRK4			
CD226			
LOC101929707			
ASB10			
ENKUN2			
LRIG2			

FIGURE 2 | **(A)** The Venn diagram showing the number of proteins specific or shared among primary tumors (blue), stroma (green) and metastases (red). **(B)** Distribution of protein classes (in %) in the clonal proteome dataset (in blue) compared with TCGA dataset (in grey). **(C)** Mutated proteins identified using mass spectrometry, with their frequency in primary tumors, stroma and metastases, and the tissues in which they have been reported, along with the processes they affected. **(D)** 126 Alternative proteins identified by mass spectrometry; their length is indicated in **(E)** primary tumor samples, **(F)** stroma samples and **(G)** metastases. Their coding RNA distribution is shown in **(H–J)**, respectively. The frequency of alternative proteins among patients is shown in **(K)** primary tumors, **(L)** stroma and **(M)** metastases. AltProt, alternative proteins; EBC, early breast cancer; ID, identification; Meta, metastases; SNP, single nucleotide polymorphism.

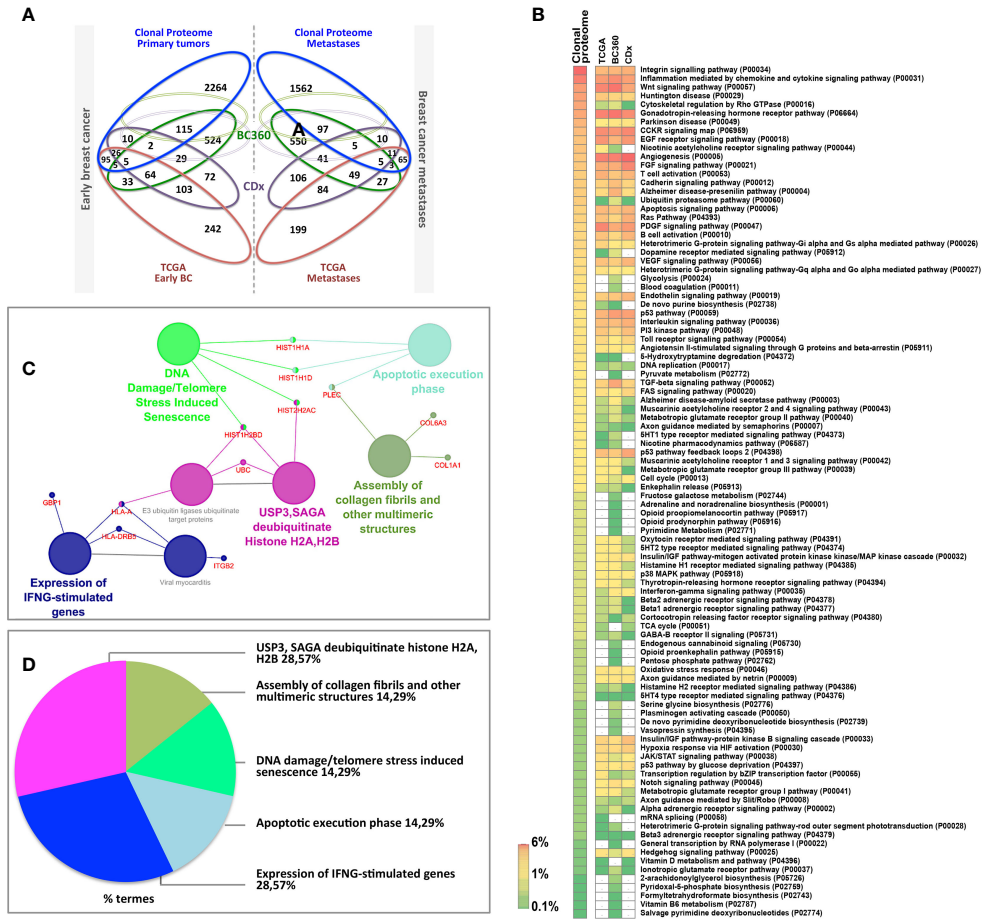

FIGURE 3 | **(A)** Venn diagram comparing the clonal proteome dataset with TCGA, BC360 and CDx panels, in primary breast cancer (left) or metastases (right). **(B)** Panther pathways heatmap showing gene distribution between the datasets. Pathways over-represented are colored in orange and those underrepresented in green. **(C)** Mutated protein networks and **(D)** biological processes distribution analyzed using Cytoscape and Cluego.

proteome dataset, with only 7 of them already approved in breast cancer. The number of target and drug interactions with non-anticancer drugs (such as agents targeting the cardiovascular system, metabolism, the musculoskeletal or the nervous systems) was higher in the clonal proteome dataset (540 interactions) compared to TCGA (83 interactions), BC360 (419 interactions), or CDx (172 interactions) (**Figure 4C**).

Proteins and Processes of Interest in the Clonal Proteome Dataset for Target Discovery

In the clonal proteome dataset, proteins shared among samples or specific to primary tumors, stroma or metastases, or differentially expressed may associate with biological processes intrinsic to breast cancer stage, tumor microenvironment, or progression. These proteins may therefore be of interest, especially if they also associate with breast cancer survival. Protein distribution among patients showed that 200 proteins were found in all primary tumor samples (**Figure 5A**), 65 proteins were shared among all the stromal samples (**Figure 5B**), 98 proteins were found in all the metastases samples (**Figure 5C**), and 37 proteins were present in all the 124 clonal samples (**Figure 5D**). Enrichment analyses for specific pathways showed as main biological processes in primary tumors AUF1, DNA-PK, S193-KSRP, or CDK5 related activities (**Figure 5E**), in stroma BGN activity, keratin sulfate cleavage, AUF1 ubiquitinoylation, and C5 pathway activity (**Figure 5F**), and in metastases DCN, HSP90, and MAP2Ks related activities (**Figure 5G**). In addition, ficolin-rich granule exocytosis and cellular response to heat stress were among the main processes found in all samples (**Figure 5H**). Enrichment analyses of proteins specific to primary tumors (n=273), stroma (n=107) or metastases (n=215) showed biological processes related to membrane components of the endoplasmic reticulum, RAS or MAPK signaling in primary tumors (**Figure 6A**), AP-2, clathrin, or PP2A activities or ketone body metabolism in stroma (**Figure 6B**), oxidation, contractile fibers processes, and drug metabolism in metastases (**Figure 6C**).

TABLE 2 | Pathways exclusive to the clonal proteomic dataset.

Pathway exclusive to the clonal proteomic dataset	Panther pathway ID	Proteins (gene ID)	Involvement in BC and potentially druggable	Reference
5HT3 type receptor mediated signaling pathway	P04375	SNAP23, VAT1	_	
Acetate utilization	P02722	ACSS3	Nutrient	(54)
Adenine and hypoxanthine salvage pathway	P02723	HPRT1, ADA	_	(55)
Alanine biosynthesis	P02724	BCAT2	Alters cell migration and proliferation; sensitivity to doxorubicin	(56)
Aminobutyrate degradation	P02726	ALDH5A1, ABAT	Connection to p53/apoptosis pathway; chemotherapeutic efficacy of doxorubicin	(57)
Androgen/estrogen/progesterone biosynthesis	P02727	ACAT1, ACAT2, HSD17B6	Tumor growth*	(58)
Arginine biosynthesis	P02728	ASL, CPS1, CAD, ASS1	Metabolic starvation therapy; estrogen signaling connection*	(59)
Asparagine and aspartate biosynthesis	P02730	GOT2, GOT1	_	
ATP synthesis	P02721	CYC1, HAO1	oncosphere formation; regulation of cancer driver genes	(60)
Cholesterol biosynthesis	P00014	HMGCS1	Cancer stem cell propagation; mechanism of resistance to endocrine therapy*	(61–63)
Coenzyme A biosynthesis	P02736	PPCS, PANK4	_	
Cysteine biosynthesis	P02737	CBS	_	
De novo pyrimidine ribonucleotides biosynthesis	P02740	CPS1, CTPS2, CTPS1, NME2, CAD	Metabolic reprogramming; synthetic lethality with DNA damaging chemotherapy	(64)
Gamma-aminobutyric acid synthesis	P04384	ALDH5A1, ABAT	Hormonal regulation and BC pathogenesis	(65)
General transcription regulation	P00023		Inflammatory BC	(66)
Glutamine glutamate conversion	P02745	GLUD1	Cell growth; mTOR connection; stress response pathway*	(67)
Heme biosynthesis	P02746	EPRS, FECH, CPOX, HMBS, ALAD, QARS	Cancer stem cells mammosphere formation	(68)
Histidine biosynthesis	P02747	TAT	_	
Isoleucine biosynthesis	P02748	BCAT2, ILVBL	_	
Leucine biosynthesis	P02749	IDH3B, BCAT2	_	
Mannose metabolism	P02752	GMPPB, PMM2, GMDS, GMPPA	_	
Methionine biosynthesis	P02753	CTH	Altered methylation	(69)
Methylcitrate cycle	P02754	ACSS3, ACO1	_	
Methylmalonyl pathway	P02755	PCCB, MCCC2	_	
N-acetylglucosamine metabolism	P02756	GNPDA2, GNPDA1, GFPT1	DNA repair regulation; tumorigenesis; metabolic reprograming; survival stress signaling; epigenetics*	(70–78)
Nicotine degradation	P05914	FMO3, CYP2A6, UGT2B7	_	
O-antigen biosynthesis	P02757	GFPT1, MAT2B	_	
Ornithine degradation	P02758	ALDH16A1	Synthetic lethality*	(79)
Phenylethylamine degradation	P02766	ALDH16A1, AOC3	_	
Proline biosynthesis	P02768	PYCR1	Proline biosynthesis activated in ER negative tumors*	(80)
Purine metabolism	P02769	MTAP	BC cell lines differentiation; pathway genetic interactions	(81, 82)
Pyridoxal phosphate salvage pathway	P02770	PNPO	_	
S-adenosylmethionine biosynthesis	P02773	MAT2A, MAT1A	Cancer stem cells*	(83)
Salvage pyrimidine ribonucleotides	P02775	NME2	_	
Succinate to proprionate conversion	P02777	PCCB, ECHDC1, ECHS1, MCCC2	_	
Sulfate assimilation	P02778	PAPSS2, PAPSS1	_	
Synaptic vesicle trafficking	P05734	UNC13D, NSF	Intercellular communication	(84)
Threonine biosynthesis	P02781		BC cell lines differentiation	(82)
Tyrosine biosynthesis	P02784	TAT	Differentially expressed in BC cancer	(85)
Valine biosynthesis	P02785	BCAT2, ILVBL	Associated with BC subtypes	(86)
Xanthine and guanine salvage pathway	P02788	HPRT1	_	

**Pathways potentially druggable.*

Proteins differentially expressed among primary tumors, stroma and metastases were identified using a multiple sample test ANOVA with a $p<0.01$. A total of 662 proteins showed a significant difference in expression among the 3 groups. Two clusters have been identified separating the stroma (Cluster 1) from the primary tumor and the metastases (Cluster 2) (**Figure 6D**). String analysis of Cluster 1 revealed two separated networks linked by VCAN *i.e.* one centered on immune response inhibition and one on collagen proteins and protein in interaction with the extracellular matrix

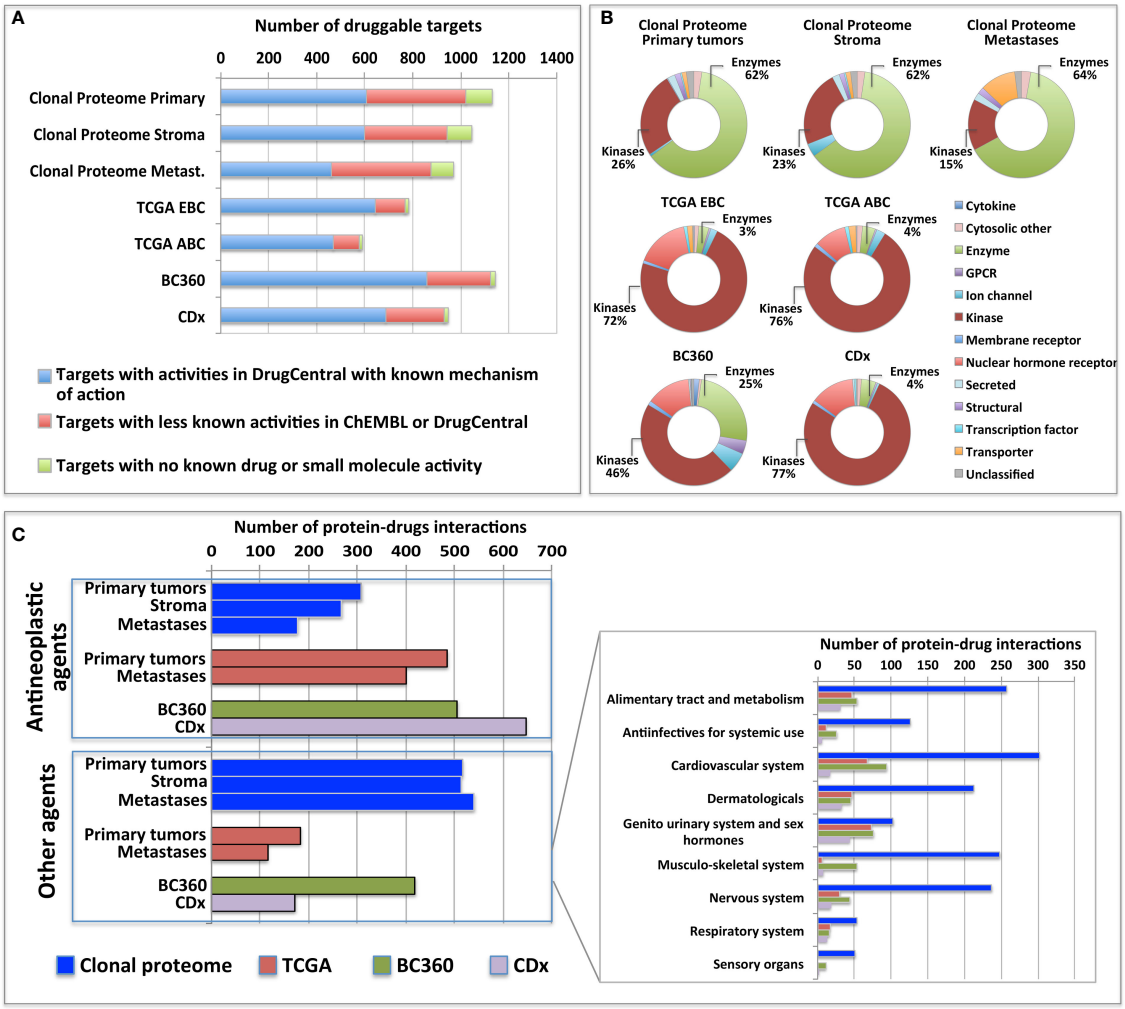

FIGURE 4 | Druggable targets identified **(A)** in the clonal proteome, TCGA, CDx, and BC360 datasets using DrugCentral, and the druggability level as defined by IDG-KMC (https://druggablegenome.net/ProteinFam). Known targets (Tclin) are in blue, less known targets are in orange (Tchem) and targets with no known drug are in red (Tbio). **(B)** Target class distribution among the datasets, and **(C)** matching drugs, both approved antineoplastic drugs or other drugs (non-anticancer drugs) described using the ATC classification. ABC, advanced breast cancer; EBC, early breast cancer; Metas, metastases.

(**Supplementary Material 10**). In Cluster 2, gene ontology reflects the presence of paraspeckles, VCP-NSFL1C complex, cytosolic small ribosomal subunit, cytosolic and polysomal ribosome, SNP and RNP complexes networks. KEGG Pathways identify as major networks the ones related to metabolism (lipids, glycosgelysis, pyruvate, proteins, carbon, butanoate, amino acid residues), antigen processing and presentation (**Supplementary Material 10**). The relationship between the proteins of interest in the clonal proteome (shared, specific or differentially expressed) with TCGA, BC360 or CDx datasets on the one hand, and with survival on the other hand was detailed in **Figure 7**. Less than 5% of these proteins of interest were shared with the genomic/transcriptomic datasets, and 25% were associated with distant metastases free survival (DMFS) (n=222) or overall survival (OS) (n=227). Enrichment analyses of genes associated with both breast cancer DMFS and OS showed their involvement in natural killer cell mediated cytotoxicity, drug metabolism, muscle filament, ERBB2 and leptin signaling, aminoacid synthesis and B cell receptor signaling (**Figures 8A–C**). Among the proteins of interest, 48 (5%) had interactions with known drugs, mostly non-anticancer agents such as colchicine, acemetacin, aceclofenac (musculo-skeletal system), astemizole (respiratory system), eptifibatide (blood system), or acetyldigitoxin (cardiovascular system), which have shown anti-tumor activity experimentally in breast cancer (**Figure 8D**) (**Supplementary Table 2**). Among the mutated proteins, 10 reference genes were associated with breast cancer DMFS (**Figure 9A**) or OS (**Figure 9B**) and were involved in the response to interferon gamma.

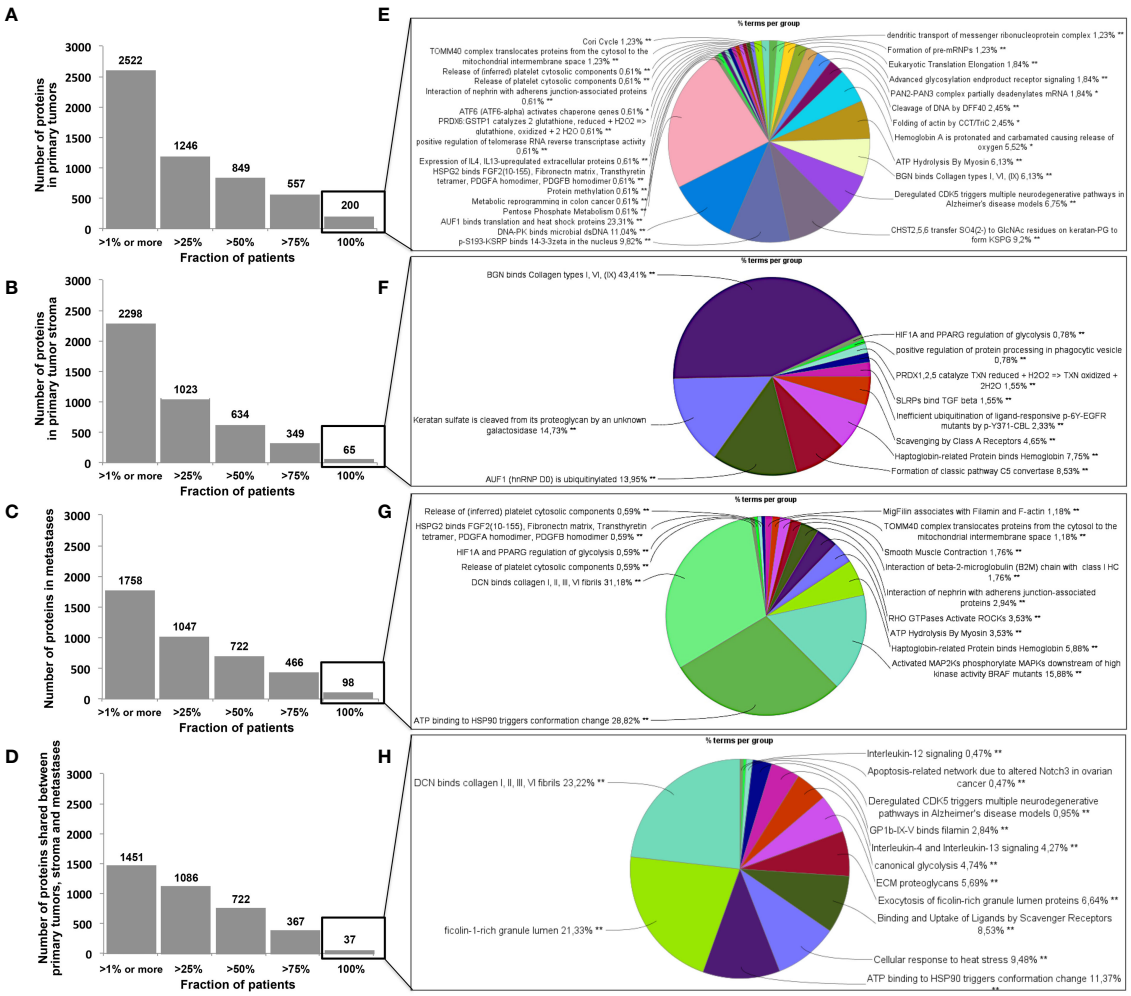

FIGURE 5 | Distribution of proteins among patients in **(A)** primary tumors, **(B)** in stroma, **(C)** in metastases, and **(D)** shared in all samples. Biological processes enriched (in %) from proteins shared by all patients in **(A–D)** are represented as pie charts in **(E–H)**, respectively. Analyses were performed with Cytoscape and ClueGo. *p < 0.05, **p < 0.01, ***p < 0.001.

Clinical Relevance of the Drugs Identified With the Clonal Proteome Approach

To show the clinical usefulness of the drugs identified through their interactions with protein targets of the clonal proteomic dataset, the clinicaltrial.gov database was searched to determine the proportion of these drugs that reached clinical investigation for breast cancer treatment. Among the 721 drugs accessible through the clonal proteome, 107 drugs were investigated in at least one breast cancer clinical trial: only 26 were drugs already used to treat breast cancer, 49 were antineoplastic drugs not yet approved for breast cancer and 32 were non-anticancer drugs. As expected, the 26 drugs used in breast cancer were chemotherapy molecules (taxanes, doxorubicin, eribulin, methotrexate, gemcitabine, etoposide, platinum, vinorelbine), endocrine therapy, targeted therapies such as everolimus and olaparib, and anti-HER2 therapies (trastuzumab, pertuzumab, trastuzumab emtansine, lapatinib), and steroids and zoledronic acid. Our approach identified 49 antineoplastic drugs already under clinical investigation to explore their value for repositioning in breast cancer, either in monotherapy or in combination. Their known protein targets were detailed in **Table 3** along with identification number of the clinical trials and the trials phase. A majority of these drugs were investigated in phase 1 or 2 trials. Our approach also identified 32 non-anticancer drugs in trial for repurposing in breast cancer. The drugs were mainly anti-infective agents, or were involved in metabolism, the cardiovascular system or the nervous system. The ATC category of the drugs was indicated in **Table 4** with the protein targets, trials ID and trial phase.

DISCUSSION

The present study showed that MALDI MSI combined with microproteomics can be used as a precision oncology tool to map

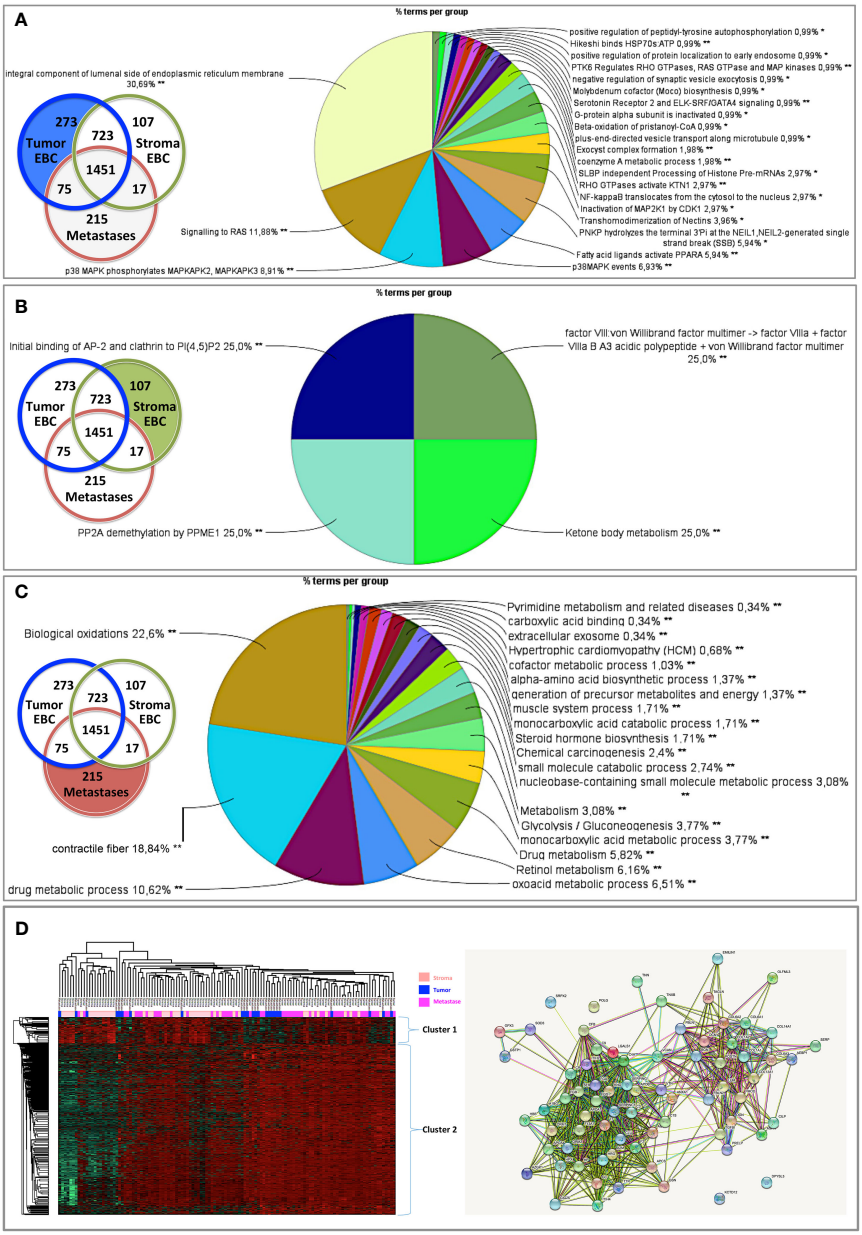

FIGURE 6 | Biological processes enriched from proteins specifically found in **(A)** primary tumors, **(B)** stroma, or **(C)** metastases. Proteins differentially expressed in **(D)** primary tumors, stroma and metastases were analyzed using a multiple sample test ANOVA with a p<0.01 and represented in a heat map (on the left) identifying 2 clusters separating the stroma (Cluster 1) from the primary tumor and the metastases (Cluster 2). The String networks of the clusters are shown on the bottom right Analyses were performed with Cytoscape, ClueGo and String; proportions of processes in %. *p<0.05; **p<0.01.

and profile specific tumor subpopulations in luminal breast cancers for clonal theranostic applications. This unsupervised and label-free technology characterized the tumors conventional proteome along with the mutated and alternative proteomes, at a clonal level, to identify candidate druggable targets. Our MS imaging and microproteomic technology offers the advantage of identifying proteomic clones *in situ* on intact tumors. In MALDI MSI, the signal intensities are recorded for analytes at specific x,y coordinates of the tissue section in their native states. MSI produces images of the scanned area where each pixel contains the MS spectrum at this location. In the present study, 204 spectra were generated by square millimeter. Spectra are high-dimensional vectors (typically in the order of 10^5 dimensions), making MSI data similar to hyperspectral images. The spectrum produced by MSI at a given location represents a signature of the molecules present at this location. This proteomic signature was

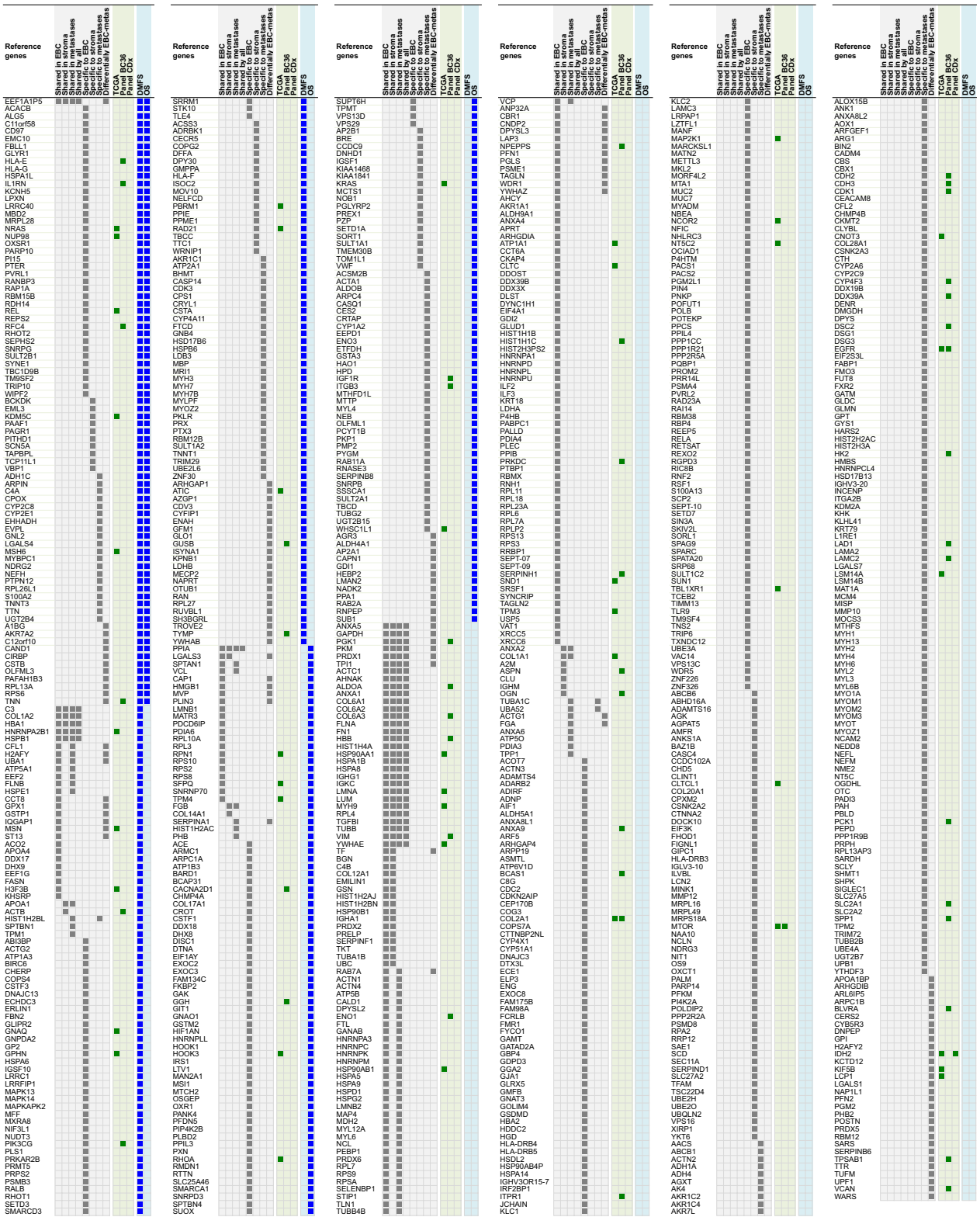

FIGURE 7 | Proteins shared, specific or differentially expressed in the clonal proteome dataset (in grey). 892 proteins are indicated with their reference gene. Proteins also found in TCGA, BC360 or CDx datasets are indicated in green. Genes associated with DMFS or OS using publically available databases are shown in blue. EBC, early breast cancer; DMFS, distant metastases free survival; OS, overall survival.

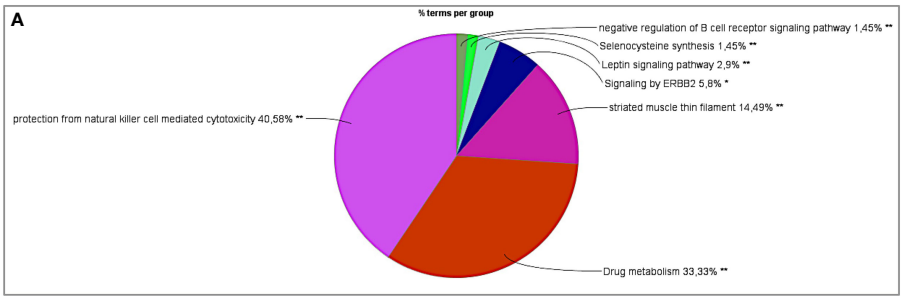

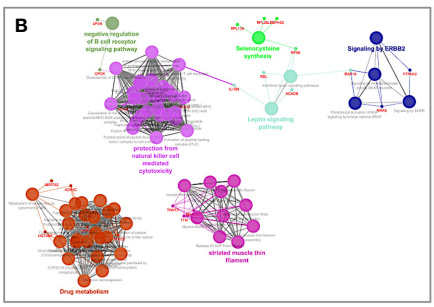

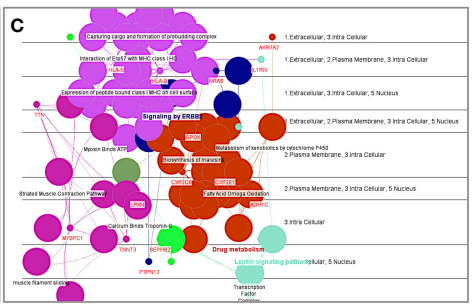

D

Reference gene	Shared in EBC	Shared in RPDmis	Shared in metastases	Shared by all	Specific to EBC	Specific to stroma	Specific to metastases	Differentially EBC-metas	Target protein	Target class	Drug	ATC drug category	Antitumor activity in breast cancer
ANXA1									Annexin A1	Cytosolic other	betamethasone	Alimentary tract and metabolism	–
GAPDH									Glyceraldehyde-3-phosphate dehydrogenase liver	Enzyme	adenosine	Cardiovascular system	–
HSP90AA1									Heat shock protein HSP 90-alpha	Cytosolic other	famotidine	Alimentary tract and metabolism	Parshad et al. 2005; Parshad et al. 2002
HSPA9									Heat shock cognate 71 kDa protein	Unclassified	adenosine triphosphate		–
AHCY									Adenosylhomocysteinase	Enzyme	adenosine	Cardiovascular system	–
AKR1A1									Alcohol dehydrogenase [NADP(+)]	Enzyme	epalrestat		Wu et al. 2017
FASN									Fatty acid synthase	Enzyme	cerulenin		Vasquez-Martin et al. 2007; Hu et al. 2011; Jeong et al. 2012
GSTP1									Glutathione S-transferase P	Enzyme	clomipramine	Nervous system	Rossi et al. 2014
LDHA									L-lactate dehydrogenase A chain	Enzyme	adenosine phosphate		–
PPIB									Peptidyl-prolyl cis-trans isomerase B	Enzyme	ciclosporin		Helgason et al. 2006
PPIA									Peptidyl-prolyl cis-trans isomerase A	Enzyme	ciclosporin		Helgason et al. 2006
TUBB									Tubulin beta chain	Structural	colchicine	Musculo-skeletal system	Wang et al. 2017; Urbaniak et al. 2020; Sun et al. 2016
TUBB4B									Tubulin beta-4B chain	Structural	anhydrovinblastine	Antineoplastic agents	Barni et al. 1994; Martin et al. 2007
ATP1A1									Sodium/potassium-transporting ATPase	Transporter	acetyldigitoxin	Cardiovascular system	Saxe Einbond et al. 2010; Kulkarni etal. 2017
HSP90B1									Endoplasmin	Membrane other	adenosine triphosphate		–
ECE1									Endothelin-converting enzyme 1	Enzyme	racecadotril	Alimentary tract and metabolism	–
SETD7									Histone-lysine N-methyltransferase SETD7	Unclassified	cyproheptadine	Respiratory system	Takemoto et al. 2016
CYP51A1									Lanosterol 14-alpha demethylase	Enzyme	bifonazole	Dermatologicals	Egbuta et al. 2014
GAK									Cyclin-G-associated kinase	Kinase	dasatinib	Antineoplastic agents	Park et al. 2012; Scher et Somlo 2013
MAPK14									Mitogen-activated protein kinase 14	Kinase	benzbromarone	Musculo-skeletal system	Tadjuidje et al. 2012
MAPKAPK2									MAP kinase-activated protein kinase 2	Kinase	adenosine triphosphate		–
POLB									DNA polymerase beta	Enzyme	cytarabine	Antineoplastic agents	Mrugala et al. 2019; Jaeckle et al. 2001
STK10									Serine/threonine-protein kinase 10	Kinase	dasatinib	Antineoplastic agents	Park et al. 2012; Scher et Somlo 2013
TPMT									Thiopurine S-methyltransferase	Enzyme	azathioprine	Immunosuppressants	Menna et al. 2009
ACE									Angiotensin-converting enzyme	Enzyme	racecadotril	Alimentary tract and metabolism	–
CACNA2D1									Voltage-dependent calcium channel subunit alpha-2/delta-1	Ion channel	amlodipine	Cardiovascular system	Lee et al. 2016; Zhang et al. 2011; Taylor et al. 1992
MAP2K1									Dual specificity mitogen-activated protein kinase kinase 1	Kinase	dasatinib	Antineoplastic agents	Park et al. 2012; Scher et Somlo 2013
TLR9									Toll-like receptor 9	Membrane receptor	alexidine		–
SAE1									SUMO-activating enzyme	Enzyme	benserazide		–
PIK4CA									Phosphatidylinositol 4-kinase, PI4K	Kinase	adenine		–
SCN5A									Sodium channel protein type 5 subunit alpha	Unclassified	amiodarone	Cardiovascular system	Chauffert et al. 1987
MINK1									Misshapen-like kinase 1	Kinase	dasatinib	Antineoplastic agents	Park et al. 2012; Scher et Somlo 2013
MTOR									Serine/threonine-protein kinase mTOR	Kinase	dasatinib	Antineoplastic agents	Park et al. 2012; Scher et Somlo 2013
AOX1									Aldehyde oxidase	Enzyme	amitriptyline	Nervous system	–
FABP1									Fatty acid-binding protein, liver	Unclassified	bezafibrate	Alimentary tract and metabolism	–
PYGM									Glycogen phosphorylase, muscle form	Enzyme	caffeine	Nervous system	Rosendahl et al. 2015; Niknafs 2011; Machado et al. 2020; Al-Ansari et al. 2014
ABCB1									Multidrug resistance protein 1	Transporter	acrivastine	Respiratory system	–
AKR1C1									Aldo-keto reductase family 1 member C1	Enzyme	benzbromarone	Musculo-skeletal system	Tadjuidje et al. 2012
AKR1C2									Aldo-keto reductase family 1 member C2	Enzyme	flufenamic acid	Musculo-skeletal system	Li et al. 2020
ALOX15B									Arachidonate 15-lipoxygenase, type II	Enzyme	chloroxine		–
CYP1A2									Cytochrome P450 1A2	Enzyme	methoxsalen	Dermatologicals	Takeuchi et al. 2006
CYP2C9									Cytochrome P450 2C9	Enzyme	amiodarone	Cardiovascular system	Chauffert et al. 1987
SLC2A1									Solute carrier family 2, facilitated glucose transporter member 1	Transporter	colforsin daropate		–
TUBB2B									Tubulin beta-2B chain	Structural	colchicine	Musculo-skeletal system	Wang et al. 2017; Urbaniak et al. 2020; Sun et al. 2016
EGFR									Epidermal growth factor receptor	Kinase	astemizole	Respiratory system	Garcia-Quiroz et al. 2012 and 2014 and 2019; Jakhar et al. 2016
ITGA2B									Integrin alpha-IIb/beta-3	Adhesion	eptifibatide	Blood and blood forming organs	Kononczuk et al. 2015
GLO1									Lactoylglutathione lyase	Enzyme	acemetacin	Musculo-skeletal system	–
TTR									Transthyretin	Secreted	aceclofenac	Musculo-skeletal system	Garg et al. 2017

FIGURE 8 | Analyses of the proteins from the clonal proteome associated both with DMFS and OS, showing **(A)** enrichment, **(B)** networks analysis, **(C)** cerebral layout of cellular distribution, and **(D)** their druggability. In the table, targets with a known drug-target interaction are in dark green, those with a less known interaction are in green, and those with limited data are in yellow. The target class, matching drug name, ATC classification and reported antitumor activity in breast cancer are indicated. *$p < 0.05$; **$p < 0.01$.

used to provide a label free unbiased method to map and visualize tumor functional heterogeneity and perform directed proteomic profiling on selected tumor subpopulations. This label free method is a strength compared to multiplex technics that require few selected markers (23). This makes the MSI-microproteomics technology particularly suited to discovery. So far, relevant candidate tumor targets for drug development are sought mainly among tumor genomic alterations because of their putative role as oncogenic drivers and in drug resistance. Implementation of this concept in the clinic has yielded mitigated benefit for patients (87). Moreover, the majority of oncogenic mutations are not druggable (88). Target inference from bioinformatic analyses based on genomic data may not provide knowledge precise enough about the functional state of the tumor and its diversity to identify relevant targets. Searching candidate targets among proteins circumvents these limitations. The performance and usefulness of the MSI-microproteomic technology was previously reported in solid tumors such as

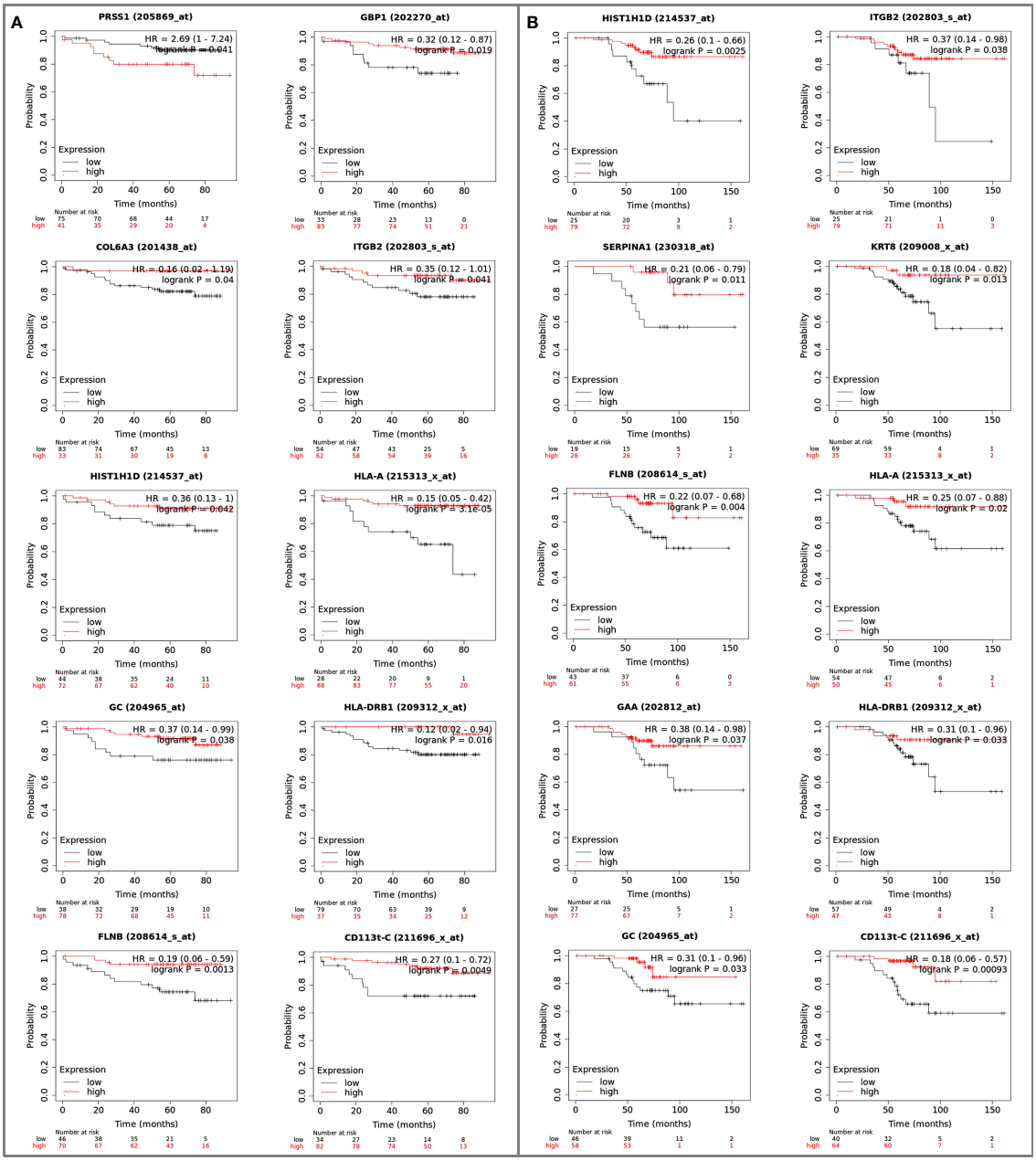

FIGURE 9 | Reference genes of the mutated proteins identified in the clonal proteome dataset associated with breast cancer **(A)** DMFS or **(B)** OS. The breast cancer Kaplan-Meier plotter tool was used to run multiple reference gene testing in publically available estrogen receptor positive and HER2 negative cohorts. A logrank p<0.05 was considered significant. DMFS, distant metastases free survival; HR, hazard ratio; OS, overall survival.

ovarian cancer or gliomas to help finding novel biomarkers or refining diagnosis classification (29, 30). Additionally, MSI-microproteomics tumor subpopulation scale allowed a successful identification of specific tumor stroma proteins. This is a significant advantage given the involvement of the tumor microenvironment in drug response (88), contrary to single cell methods, which cannot analyze intercellular communications in their intact microenvironment.

The clonal proteome showed a rich landscape of proteins and biological processes compared to genomic or transcriptomic datasets. The overlap with TCGA data and transcriptomic panels was limited and a distinct distribution of biological processes was observed in enrichment analyses. The clonal proteomic dataset provided more information on enzymatic and metabolic processes. A study by Patel et al. reporting on a computational assessment of drug targets showed that enzymes

TABLE 3 | Anticancer drugs identified through the clonal proteome that are under clinical investigation in breast cancer patients for repositioning.

Drug name	Protein targets	Reference genes	Trial status	Phase 1 trials	Phase 1/2 trials	Phase 2 trials	Phase 3 trials or other
afatinib	Cyclin-G-associated kinase Serine/threonine-protein kinase 10 STE20-like serine/threonine-protein kinase Mitogen-activated protein kinase 14	GAK STK10 SLK MAPK14	Completed Ongoing	NCT01649271 NCT03878524	NCT01441596; NCT01594177 NCT02768337	 NCT04158947; NCT02465060	
apatinib	Tyrosine-protein kinase CSK	CSK	Completed Ongoing	 NCT03075462		NCT01176669; NCT01653561; NCT02878057; NCT03394287 NCT02768415; NCT03254654; NCT03775928; NCT03982485; NCT04303741; NCT03580395	 NCT04335006; NCT03475589
belinostat	Histone deacetylase 1,2,3,4,5,6,7,8,9,10,11	HDAC1,2,3,4,5,6,7,8,9,10,11	Completed Ongoing	NCT00413322 NCT04315233; NCT04703920			
bendamustine	Histone deacetylase 1,2,3,6,8,10	HDAC1,2,3,6,8,10	Completed	NCT00661739	NCT00834678	NCT01891227	
bortezomib	Proteasome subunit alpha type-1 Prothrombin Cathepsin G Chymase Proteasome subunit beta type-1/-5/-2 Nuclear factor NF-kappa-B complex 26S proteasome non-ATPase regulatory subunit 1	PSMA1 F2 CTSG CMA1 PSMB1/2/5 NFKB1 PSMD1	Completed Ongoing	NCT00620295; NCT00622674; NCT00667641 NCT03878524		NCT00025584; NCT00028639 NCT01142401	
bosutinib	ALK tyrosine kinase receptor Angiopoietin-1 receptor Bcr/Abl fusion protein Dual specificity mitogen-activated protein kinase kinase 1/2 Ephrin type-A receptor 2 Epidermal growth factor receptor Hepatocyte growth factor receptor Histone deacetylase 1,2,3,4,5,6,7,8,9,10,11 Macrophage colony-stimulating factor 1 receptor Mast/stem cell growth factor receptor Kit Non-receptor tyrosine-protein kinase TYK2 Platelet-derived growth factor receptor alpha/beta	ALK TEK ABL1 MAP2K1/2 EPHA2 EGFR MET HDAC1,2,3,4,5,6,7,8,9,10,11 CSF1R KIT TYK2 PDGFRA/B PRKCD RET SRC ERBB2/4 FLT3 ROCK1/2 ABL1, BTK, FYN, HCK, ITK, JAK2, JAK3, LCK, LYN, YES1	Completed	NCT00759837			

(Continued)

TABLE 3 | Continued

Drug name	Protein targets	Reference genes	Trial status	Phase 1 trials	Phase 1/2 trials	Phase 2 trials	Phase 3 trials or other
	Protein kinase C delta type Proto-oncogene tyrosine-protein kinase receptor Ret Proto-oncogene tyrosine-protein kinase Src Receptor tyrosine-protein kinase erbB-2/-4 Receptor-type tyrosine-protein kinase FLT3 Rho-associated protein kinase 1/2 Tyrosine-protein kinase ABL1, BTK, FYN, HCK, ITK, JAK2, JAK3, LCK, LYN, YES1						

Their known protein targets are indicated along with the identification number of the clinical trials (NCT number) and the trials phase.

TABLE 4 | Non-anticancer drugs identified through the clonal proteome that are under clinical investigation in breast cancer patients for repurposing.

Drug ATC class	Drug name	Protein targets	Reference genes	Trial status	Phase 1 trials	Phase 2 trials	Phase 3/4 or other
Alimentary tract and metabolism	calcitriol	Vitamin D3 receptor Vitamin D 25-hydroxylase 25-hydroxyvitamin D-1 alpha hydroxylase, mitochondrial Vitamin D-binding protein	VDR CYP2R1 CYP27B1 GC	Ongoing		NCT01293682	
Alimentary tract and metabolism	doxycycline	72 kDa type IV collagenase	MMP2	Completed Ongoing	 NCT03435952	NCT01847976 NCT02874430	
Alimentary tract and metabolism	lansoprazole	Microtubule-associated protein tau	MAPT	Ongoing		NCT04188119	
Alimentary tract and metabolism	omeprazole	Cytochrome P450 1A2 Cytochrome P450 2C9 Multidrug resistance protein 1	CYP1A2 CYP2C9 ABCB1	Completed Ongoing	NCT01596647 NCT02950259	 NCT02595372	
Alimentary tract and metabolism	sulfasalazine	Caspase-1 Mitogen-activated protein kinase 1 Acetyl-CoA acetyltransferase, mitochondrial Carbonic anhydrase 1, 2 Cyclooxygenase	CASP1 MAPK1 ACAT1 CA1, CA2 PTGS1	Ongoing		NCT03847311	
Antiinfectives for systemic use	itraconazole	Lanosterol 14-alpha demethylase	CYP51A1	Completed Ongoing	 NCT04712396		NCT00798135
Antiinfectives for systemic use	ritonavir	Cytochrome P450 2C9 Multidrug resistance protein 1	CYP2C9 ABCB1	Completed	NCT01009437		
Antiparasitic products, insecticides and repellents	hydroxychloroquine	Toll-like receptor 9	TLR9	Ongoing	NCT03774472	NCT03032406; NCT04523857	
Antiparasitic products, insecticides and repellents	suramin	DNA-dependent protein kinase catalytic subunit Protein arginine N-methyltransferase 1	PRKDC PRMT1	Completed	NCT00003038; NCT00054028		

(Continued)

TABLE 4 | Continued

Drug ATC class	Drug name	Protein targets	Reference genes	Trial status	Phase 1 trials	Phase 2 trials	Phase 3/4 or other
Blood and blood forming organs	apixaban	Prothrombin Coagulation factor X	F2 F10	Completed	NCT03083782		
Cardiovascular system	amlodipine	Voltage-dependent L-type calcium channel subunit alpha-1D/-1C Voltage-dependent calcium channel gamma-1 subunit Alpha-2A adrenergic receptor 5-hydroxytryptamine receptor 6 Alpha-2C adrenergic receptor Sodium-dependent dopamine transporter Carbonic anhydrase 1 Aldehyde oxidase Voltage-dependent T-type calcium channel subunit alpha-1H Alpha-1D adrenergic receptor Potassium channel subfamily K member 2 Alpha-1A adrenergic receptor Alpha-1B adrenergic receptor Voltage-dependent calcium channel subunit alpha-2/delta-1	CACNA1D/C CACNG1 ADRA2A HTR6 ADRA2C SLC6A3 CA1 AOX1 CACNA1H ADRA1D KCNK2 ADRA1A ADRA1B CACNA2D1	Ongoing	NCT02834403		
Cardiovascular system	atorvastatin	3-hydroxy-3-methylglutaryl-coenzyme A reductase Nuclear receptor subfamily 1 group I member 3 Cytochrome P450 3A4 Histone deacetylase 1,2,6	HMGCR NR1I3 CYP3A4 HDAC1,2,6	Completed Ongoing	NCT01980823	NCT00816244 NCT03872388	
Cardiovascular system	digoxin	Sodium/potassium-transporting ATPase Signal transducer and activator of transcription 3	ATP1A1 STAT3	Completed Ongoing	NCT00650910; NCT04094519 NCT03928210	NCT01763931	
Cardiovascular system	indomethacin	Prostaglandin G/H synthase 1 Aldo-keto reductase family 1 member C4/C2 Lactoylglutathione lyase Multidrug resistance protein 1	PTGS1 AKR1C4/AKR1C2 GLO1 ABCB1	Ongoing	NCT02950259		
Cardiovascular system	lidocaine	Sodium channel protein type 5 subunit alpha	SCN5A	Completed		NCT02839668	
Cardiovascular system	losartan	Cytochrome P450 2C9 Angiotensin-converting enzyme Multidrug resistance protein 1	CYP2C9 ACE ABCB1	Ongoing	NCT03878524		
Cardiovascular system	propranolol	Cytochrome P450 1A2 Multidrug resistance protein 1	CYP1A2 ABCB1	Ongoing		NCT01847001	

(Continued)

TABLE 4 | Continued

Drug ATC class	Drug name	Protein targets	Reference genes	Trial status	Phase 1 trials	Phase 2 trials	Phase 3/4 or other
Dermatologicals	tacrolimus	Peptidyl-prolyl cis-trans isomerase FKBP1A Peptidyl-prolyl cis-trans isomerase FKBP10 Serine/threonine-protein kinase mTOR Splicing factor 3B subunit 3 Serine/threonine-protein phosphatase 2B catalytic subunit alpha isoform Peptidyl-prolyl cis-trans isomerase FKBP5	FKBP1A FKBP10 MTOR SF3B3 PPP3CA FKBP5	Completed	NCT03083782		
Dermatologicals	tretinoin	Mitogen-activated protein kinase 1	MAPK1	Ongoing	NCT03878524		
Dermatologicals	ketoconazole	Aldehyde oxidase Lanosterol 14-alpha demethylase Multidrug resistance protein 1	AOX1 CYP51A1 ABCB1	Ongoing	NCT03796273		
Genito urinary system and sex hormones	celecoxib	Carbonic anhydrase 2 Prostaglandin G/H synthase 1 Carbonic anhydrase 1/9 Mitogen-activated protein kinase 14	CA2 PTGS1 CA1 - CA9 MAPK14	Completed	NCT00070057; NCT01425476	NCT00006381; NCT00056082; NCT00201773; NCT00291694; NCT01695226	NCT00525096; NCT02429427
				Ongoing	NCT01881048; NCT03599453; NCT03878524; NCT04081389	NCT04348747	
Genito urinary system and sex hormones	mifepristone	Mitogen-activated protein kinase 14	MAPK14	Completed	NCT01493310; NCT02046421		NCT02651844
				Ongoing		NCT01898312; NCT02788981; NCT03225547	
Genito urinary system and sex hormones	sildenafil	cGMP-specific 3',5'-cyclic phosphodiesterase	PDE5A	Completed	NCT01375699		
Musculo-skeletal system	nimesulide	Prostaglandin G/H synthase 1 Myeloperoxidase	PTGS1 MPO	Completed		NCT01500577	
Musculo-skeletal system	sulindac	72 kDa type IV collagenase Lactoylglutathione lyase	MMP2 GLO1	Completed	NCT00245024	NCT00039520	
Nervous system	modafinil	Cytochrome P450 1A2	CYP1A2	Completed			NCT00917748
Nervous system	disulfiram	Cytochrome P450 1A2 Amine oxidase [flavin-containing] A	CYP1A2 MAOA	Ongoing		NCT03323346; NCT04265274	
Nervous system	fluvoxamine	Cytochrome P450 1A2	CYP1A2	Completed	NCT01700270		
Nervous system	midazolam	Multidrug resistance protein 1	ABCB1	Completed	NCT00258050; NCT01596647; NCT03955939		
				Ongoing	NCT01296555; NCT01655225		
Nervous system	pregabalin	Voltage-dependent calcium channel subunit alpha-2/delta-1	CACNA2D1	Ongoing			NCT03216187
Nervous system	propofol	Prostaglandin G/H synthase 1	PTGS1 CYP2C9	Completed			NCT02005770; NCT02758249
Nervous system		Cytochrome P450 2C9 Carbonic anhydrase 1 Carbonic anhydrase 2	CA1 CA2	Ongoing			NCT01975064; NCT04074460

(Continued)

TABLE 4 | Continued

Drug ATC class	Drug name	Protein targets	Reference genes	Trial status	Phase 1 trials	Phase 2 trials	Phase 3/4 or other
Nervous system	valproic acid	Alcohol dehydrogenase [NADP(+)] Histone deacetylase 2 Succinate-semialdehyde dehydrogenase, mitochondrial Histone deacetylase 1	AKR1A1 HDAC2 ALDH5A1 HDAC1	Ongoing	NCT01552434		

The ATC category is indicated with the protein targets, the identification number of the clinical trials (NCT number) and the trials phase.

were the most frequent protein class and the most druggable (89). The clonal proteome revealed 41 exclusive metabolic pathways, most of them understudied in relation to breast cancer. This was of particular interest because tumor metabolic phenotype has been recognized as a hallmark of cancer and is involved in drug resistance (81). Transcriptomic panels were enriched with kinases or immune processes as expected. The discrepancy with TCGA data may be related to alternative splicing and post-translational modifications revealed by mass spectrometry analyses that cannot be predicted by genome databases. Although the bulk of targetable proteins identified might not be involved in driver oncogenic pathways to which cancer cells are addicted, focusing on common and cell type- or stage-specific proteins and processes might increase their relevance. The relevance of the protein targets was showed by the fact that a large number of proteins in the clonal proteome dataset was associated with breast cancer outcome and highlighted shared or specific biological processes of interest.

An additional strength of the present mass spectrometry technology relies on the detection of altered proteins, such as those originating from missense mutations or single nucleotide polymorphism missense mutations, and a newly recognized type of proteins named alternative proteins (or ghost proteins) because of their translation from alternative open reading frames. Although their functions cannot be predicted from their reference gene, their presence may reveal altered biological processes. Alternative proteins represent a vast class of proteins with still largely unknown biological functions, thus expanding the proteome complexity (90). This field of research offers exciting perspectives about the functions of these modified proteins related to cancer and their potential impact on drug target interactions.

Our study showed that a clonal proteomic analysis brought additional non-redundant molecular information. The proteins and pathways uniquely identified with this clonal approach may offer opportunities to identify novel drug targets. Drug development struggles with the molecular heterogeneity of tumor subpopulations, potentially leading to a differential target expression among cancer cells, which contributes to drug resistance. This has stimulated the development of multi-targeted therapeutic strategies (91, 92), facilitated by the fast expansion of the drug pipeline. Interestingly, a high proportion of the proteins in the clonal proteome dataset were druggable, with interactions with a variety of drug classes, either antineoplastic agents or non-anticancer drugs. We showed that many of these drugs, both antineoplastic agents and non-anticancer drugs, were already under clinical investigation for breast cancer treatment. This underlines the clinical relevance of using this approach for clone-tailored strategies of systematic high-throughput unbiased drug target screening for drug combination or repositioning (93). A significant number of proteins had partially or not yet known drug interactions, showing also the potential of our approach for discovery. Despite the recognition of breast cancer heterogeneity, technical limitations hampered the implementation of clonal theranostics in practice. MSI-microproteomics technology revealed more edges of breast cancer heterogeneity and bridges the technological gap to allow contemplating a paradigm shift from treating one main detectable tumor clone (with current technics) to strategies taking into account several functional clones. To tackle tumor complexity, system biology approaches are developing to reveal therapeutic opportunities associated with the multiple dimensions of cancer through integration of tumor genome, phenome and other omics data (94, 95). Accessing sufficient quantities of tumor tissue to perform all the omics analyses represents a technical challenge. Our technology uses only a limited amount of tumor tissue while maintaining the whole tissue section integrity allowing it to be re-used for additional experiments. For this reason and the large amount of data generated, the MSI-microproteomic technology is suited to multiomic strategies.

In conclusion, spatially resolved MSI-guided microproteomics is a unique tool to perform a label-free multidimensional proteomic characterization of intratumor heterogeneity for clone-tailored drug target screening. This new approach is adapted to drug target discovery and repurposing to achieve clonal theranostics. Moreover, it is applicable in routine clinical care and its scalability thanks to the speed of analysis of current and next generation mass spectrometry instruments, makes MSI-microproteomics integration to precision oncology tools foreseeable in a near future to implement clone-tailored therapies.

DATA AVAILABILITY STATEMENT

The datasets presented in this study can be found in online repositories. The names of the repository/repositories and accession number(s) can be found in the article/**Supplementary Material**.

ETHICS STATEMENT

The studies involving human participants were reviewed and approved by the local Research and Ethics Committee (Centre Oscar Lambret). The patients/participants provided their written informed consent to participate in this study.

AUTHOR CONTRIBUTIONS

NH wrote the manuscript original draft. NH designed the study. SA and NH performed the analyses. NH and DB selected and collected the breast cancer samples. Y-MR and DB performed histology and validated diagnostics. NH, SA, TC, IF, and MS analyzed the data. IF, MS, TC, and SA corrected the manuscript. NH, IF, and MS supervised the project and MS, IF, and NH provided the funding. All authors contributed to the article and approved the submitted version.

FUNDING

This work was funded by Inserm and Centre Oscar Lambret.

SUPPLEMENTARY MATERIAL

The Supplementary Material for this article can be found online at: https://www.frontiersin.org/articles/10.3389/fonc.2021.802177/full#supplementary-material

Supplementary Material 1 | TCGA database of mutations and CNV alterations in early and advanced breast cancers.

Supplementary Material 2 | BC360 panel gene list.

Supplementary Material 3 | CDx panel gene list.

Supplementary Material 4 | MALDI MSI of 52 cases of primary tumors showing the spatial proteomic heterogeneity of the tumors. In each sample vignette, the MALDI MS imaging is displayed with the histological HPS picture (upper left), the principal component analysis of the proteomic clones (upper right), the segmentation tree (middle right), and the spectra of the clones (bottom right).

Supplementary Material 5 | MALDI MSI of 24 cases of metastases showing the spatial proteomic heterogeneity of the tumors. In each sample vignette, the MALDI MS imaging is displayed with the histological HPS picture (upper left), the principal component analysis of the proteomic clones (upper right), the segmentation tree (middle right), and the spectra of the clones (bottom right).

Supplementary Material 6 | Number of total proteins identified according to **(A)** tissue types (bone n=3; liver n=5; nodes n=6; skin n=10) or **(B)** to the sampling method **(B)**, i.e. surgery (n=52), surgical biopsy (n=9) or fine needle core biopsy (n=15). Line in the middle of the box is the median, the upper and lower sides of the box represent the 75th and 25th percentiles respectively, and the outside lines are the extremes.

Supplementary Material 7 | Panther analysis of the clonal proteome landscape showing **(A)** the protein class distribution (in %), and **(B)** a comparison of the distribution between primary tumors and stroma (relative difference in % in blue) and between primary tumors and metastases (relative difference in % in red).

Supplementary Material 8 | Reference gene distribution across the four datasets (clonal proteome, TCGA, BC360, CDx).

Supplementary Material 9 | Targets interacting with anticancer drugs across the four datasets (clonal proteome, TCGA, BC360, CDx).

Supplementary Material 10 | String networks in stroma (cluster 1) and in primary tumors and metastases (cluster 2).

Supplementary Table 1 | Information concerning patients and type of tumors identified by the pathologist.

Supplementary Table 2 | References cited in **Table 2** and **Figure 8D**.

REFERENCES

1. Yates LR, Gerstung M, Knappskog S, Desmedt C, Gundem G, Van Loo P, et al. Subclonal Diversification of Primary Breast Cancer Revealed by Multiregion Sequencing. *Nat Med* (2015) 21:751–9. doi: 10.1038/nm.3886
2. Garraway LA, Jänne PA. Circumventing Cancer Drug Resistance in the Era of Personalized Medicine. *Cancer Discov* (2012) 2:214–26. doi: 10.1158/2159-8290.CD-12-0012
3. McDonald K-A, Kawaguchi T, Qi Q, Peng X, Asaoka M, Young J, et al. Tumor Heterogeneity Correlates With Less Immune Response and Worse Survival in Breast Cancer Patients. *Ann Surg Oncol* (2019) 26:2191–9. doi: 10.1245/s10434-019-07338-3
4. Pereira B, Chin S-F, Rueda OM, Vollan H-KM, Provenzano E, Bardwell HA, et al. The Somatic Mutation Profiles of 2,433 Breast Cancers Refines Their Genomic and Transcriptomic Landscapes. *Nat Commun* (2016) 7:11479. doi: 10.1038/ncomms11479
5. Greaves M, Maley CC. Clonal Evolution in Cancer. *Nature* (2012) 481:306–13. doi: 10.1038/nature10762
6. Williams MJ, Sottoriva A, Graham TA. Measuring Clonal Evolution in Cancer With Genomics. *Annu Rev Genomics Hum Genet* (2019) 20:309–29. doi: 10.1146/annurev-genom-083117-021712
7. Pogrebniak KL, Curtis C. Harnessing Tumor Evolution to Circumvent Resistance. *Trends Genet* (2018) 34:639–51. doi: 10.1016/j.tig.2018.05.007
8. Marine J-C, Dawson S-J, Dawson MA. Non-Genetic Mechanisms of Therapeutic Resistance in Cancer. *Nat Rev Cancer* (2020) 20:743–56. doi: 10.1038/s41568-020-00302-4
9. Gyanchandani R, Lin Y, Lin H-M, Cooper K, Normolle DP, Brufsky A, et al. Intratumor Heterogeneity Affects Gene Expression Profile Test Prognostic Risk Stratification in Early Breast Cancer. *Clin Cancer Res* (2016) 22:5362–9. doi: 10.1158/1078-0432.CCR-15-2889
10. Hennessy BT, Lu Y, Gonzalez-Angulo AM, Carey MS, Myhre S, Ju Z, et al. A Technical Assessment of the Utility of Reverse Phase Protein Arrays for the Study of the Functional Proteome in Non-Microdissected Human Breast Cancers. *Clin Proteomics* (2010) 6:129–51. doi: 10.1007/s12014-010-9055-y
11. Kim J, DeBerardinis RJ. Mechanisms and Implications of Metabolic Heterogeneity in Cancer. *Cell Metab* (2019) 30:434–46. doi: 10.1016/j.cmet.2019.08.013
12. Jackson HW, Fischer JR, Zanotelli VRT, Ali HR, Mechera R, Soysal SD, et al. The Single-Cell Pathology Landscape of Breast Cancer. *Nature* (2020) 578:615–20. doi: 10.1038/s41586-019-1876-x
13. Ståhl PL, Salmén F, Vickovic S, Lundmark A, Navarro JF, Magnusson J, et al. Visualization and Analysis of Gene Expression in Tissue Sections by Spatial Transcriptomics. *Science* (2016) 353:78–82. doi: 10.1126/science.aaf2403
14. Xia C, Fan J, Emanuel G, Hao J, Zhuang X. Spatial Transcriptome Profiling by MERFISH Reveals Subcellular RNA Compartmentalization and Cell Cycle-Dependent Gene Expression. *Proc Natl Acad Sci USA* (2019) 116:19490–9. doi: 10.1073/pnas.1912459116

15. Lee JH, Daugharthy ER, Scheiman J, Kalhor R, Ferrante TC, Terry R, et al. Fluorescent in Situ Sequencing (FISSEQ) of RNA for Gene Expression Profiling in Intact Cells and Tissues. *Nat Protoc* (2015) 10:442–58. doi: 10.1038/nprot.2014.191
16. Liu Y, Beyer A, Aebersold R. On the Dependency of Cellular Protein Levels on Mrna Abundance. *Cell* (2016) 165:535–50. doi: 10.1016/j.cell.2016.03.014
17. Gout J-F, Li W, Fritsch C, Li A, Haroon S, Singh L, et al. The Landscape of Transcription Errors in Eukaryotic Cells. *Sci Adv* (2017) 3:e1701484. doi: 10.1126/sciadv.1701484
18. Rapino F, Delaunay S, Rambow F, Zhou Z, Tharun L, De Tullio P, et al. Codon-Specific Translation Reprogramming Promotes Resistance to Targeted Therapy. *Nature* (2018) 558:605–9. doi: 10.1038/s41586-018-0243-7
19. García-Jiménez C, Goding CR. Starvation and Pseudo-Starvation as Drivers of Cancer Metastasis Through Translation Reprogramming. *Cell Metab* (2019) 29:254–67. doi: 10.1016/j.cmet.2018.11.018
20. Jewer M, Lee L, Leibovitch M, Zhang G, Liu J, Findlay SD, et al. Translational Control of Breast Cancer Plasticity. *Nat Commun* (2020) 11:2498. doi: 10.1038/s41467-020-16352-z
21. Chalmers ZR, Connelly CF, Fabrizio D, Gay L, Ali SM, Ennis R, et al. Analysis of 100,000 Human Cancer Genomes Reveals the Landscape of Tumor Mutational Burden. *Genome Med* (2017) 9:34. doi: 10.1186/s13073-017-0424-2
22. Santos R, Ursu O, Gaulton A, Bento AP, Donadi RS, Bologa CG, et al. A Comprehensive Map of Molecular Drug Targets. *Nat Rev Drug Discovery* (2017) 16:19–34. doi: 10.1038/nrd.2016.230
23. Giesen C, Wang HAO, Schapiro D, Zivanovic N, Jacobs A, Hattendorf B, et al. Highly Multiplexed Imaging of Tumor Tissues With Subcellular Resolution by Mass Cytometry. *Nat Methods* (2014) 11:417–22. doi: 10.1038/nmeth.2869
24. Schulz D, Zanotelli VRT, Fischer JR, Schapiro D, Engler S, Lun X-K, et al. Simultaneous Multiplexed Imaging of Mrna and Proteins With Subcellular Resolution in Breast Cancer Tissue Samples by Mass Cytometry. *Cell Syst* (2018) 6:25–36.e5. doi: 10.1016/j.cels.2017.12.001
25. Beechem JM. High-Plex Spatially Resolved RNA and Protein Detection Using Digital Spatial Profiling: A Technology Designed for Immuno-Oncology Biomarker Discovery and Translational Research. *Methods Mol Biol* (2020) 2055:563–83. doi: 10.1007/978-1-4939-9773-2_25
26. Fournier I, Wisztorski M, Salzet M. Tissue Imaging Using MALDI-MS: A New Frontier of Histopathology Proteomics. *Expert Rev Proteomics* (2008) 5:413–24. doi: 10.1586/14789450.5.3.413
27. Lemaire R, Tabet JC, Ducoroy P, Hendra JB, Salzet M, Fournier I. Solid Ionic Matrixes for Direct Tissue Analysis and MALDI Imaging. *Anal Chem* (2006) 78:809–19. doi: 10.1021/ac0514669
28. Lemaire R, Menguellet SA, Stauber J, Marchaudon V, Lucot J-P, Collinet P, et al. Specific MALDI Imaging and Profiling for Biomarker Hunting and Validation: Fragment of the 11S Proteasome Activator Complex, Reg Alpha Fragment, is a New Potential Ovary Cancer Biomarker. *J Proteome Res* (2007) 6:4127–34. doi: 10.1021/pr0702722
29. Delcourt V, Franck J, Leblanc E, Narducci F, Robin Y-M, Gimeno J-P, et al. Combined Mass Spectrometry Imaging and Top-Down Microproteomics Reveals Evidence of a Hidden Proteome in Ovarian Cancer. *EBioMedicine* (2017) 21:55–64. doi: 10.1016/j.ebiom.2017.06.001
30. Le Rhun E, Duhamel M, Wisztorski M, Gimeno J-P, Zairi F, Escande F, et al. Evaluation of non-Supervised MALDI Mass Spectrometry Imaging Combined With Microproteomics for Glioma Grade III Classification. *Biochim Biophys Acta Proteins Proteom* (2017) 1865:875–90. doi: 10.1016/j.bbapap.2016.11.012
31. Quanico J, Franck J, Cardon T, Leblanc E, Wisztorski M, Salzet M, et al. Nanolc-MS Coupling of Liquid Microjunction Microextraction for on-Tissue Proteomic Analysis. *Biochim Biophys Acta Proteins Proteom* (2017) 1865:891–900. doi: 10.1016/j.bbapap.2016.11.002
32. Fournier I, Day R, Salzet M. Direct Analysis of Neuropeptides by *in Situ* MALDI-TOF Mass Spectrometry in the Rat Brain. *Neuro Endocrinol Lett* (2003) 24:9–14.
33. Lemaire R, Desmons A, Tabet JC, Day R, Salzet M, Fournier I. Direct Analysis and MALDI Imaging of Formalin-Fixed, Paraffin-Embedded Tissue Sections. *J Proteome Res* (2007) 6:1295–305. doi: 10.1021/pr060549i
34. Wisztorski M, Lemaire R, Stauber J, Menguelet SA, Croix D, Mathé OJ, et al. New Developments in MALDI Imaging for Pathology Proteomic Studies. *Curr Pharm Des* (2007) 13:3317–24. doi: 10.2174/138161207782360672
35. Klein O, Strohschein K, Nebrich G, Oetjen J, Trede D, Thiele H, et al. MALDI Imaging Mass Spectrometry: Discrimination of Pathophysiological Regions in Traumatized Skeletal Muscle by Characteristic Peptide Signatures. *Proteomics* (2014) 14:2249–60. doi: 10.1002/pmic.201400088
36. Trede D, Kobarg JH, Oetjen J, Thiele H, Maass P, Alexandrov T. On the Importance of Mathematical Methods for Analysis of MALDI-Imaging Mass Spectrometry Data. *J Integr Bioinform* (2012) 9:189. doi: 10.1515/jib-2012-189
37. Alexandrov T, Becker M, Deininger S-O, Ernst G, Wehder L, Grasmair M, et al. Spatial Segmentation of Imaging Mass Spectrometry Data With Edge-Preserving Image Denoising and Clustering. *J Proteome Res* (2010) 9:6535–46. doi: 10.1021/pr100734z
38. Quanico J, Franck J, Dauly C, Strupat K, Dupuy J, Day R, et al. Development of Liquid Microjunction Extraction Strategy for Improving Protein Identification From Tissue Sections. *J Proteomics* (2013) 79:200–18. doi: 10.1016/j.jprot.2012.11.025
39. Cox J, Mann M. Maxquant Enables High Peptide Identification Rates, Individualized P.P.B.-Range Mass Accuracies and Proteome-Wide Protein Quantification. *Nat Biotechnol* (2008) 26:1367–72. doi: 10.1038/nbt.1511
40. Tyanova S, Temu T, Carlson A, Sinitcyn P, Mann M, Cox J. Visualization of LC-MS/MS Proteomics Data in Maxquant. *Proteomics* (2015) 15:1453–6. doi: 10.1002/pmic.201400449
41. Cox J, Neuhauser N, Michalski A, Scheltema RA, Olsen JV, Mann M. Andromeda: A Peptide Search Engine Integrated Into the Maxquant Environment. *J Proteome Res* (2011) 10:1794–805. doi: 10.1021/pr101065j
42. Cox J, Hein MY, Luber CA, Paron I, Nagaraj N, Mann M. Accurate Proteome-Wide Label-Free Quantification by Delayed Normalization and Maximal Peptide Ratio Extraction, Termed Maxlfq. *Mol Cell Proteomics* (2014) 13:2513–26. doi: 10.1074/mcp.M113.031591
43. Szklarczyk D, Franceschini A, Kuhn M, Simonovic M, Roth A, Minguez P, et al. The STRING Database in 2011: Functional Interaction Networks of Proteins, Globally Integrated and Scored. *Nucleic Acids Res* (2011) 39:D561–568. doi: 10.1093/nar/gkq973
44. Vizcaíno JA, Deutsch EW, Wang R, Csordas A, Reisinger F, Ríos D, et al. Proteomexchange Provides Globally Coordinated Proteomics Data Submission and Dissemination. *Nat Biotechnol* (2014) 32:223–6. doi: 10.1038/nbt.2839
45. Bonnet A, Lagarrigue S, Liaubet L, Robert-Granié C, Sancristobal M, Tosser-Klopp G. Pathway Results From the Chicken Data Set Using GOTM, Pathway Studio and Ingenuity Softwares. *BMC Proc* (2009) 3 Suppl 4:S11. doi: 10.1186/1753-6561-3-S4-S11
46. Yuryev A, Kotelnikova E, Daraselia N. Ariadne's Chemeffect and Pathway Studio Knowledge Base. *Expert Opin Drug Discov* (2009) 4:1307–18. doi: 10.1517/17460440903413488
47. Heberle H, Meirelles GV, da Silva FR, Telles GP, Minghim R. Interactivenn: A Web-Based Tool for the Analysis of Sets Through Venn Diagrams. *BMC Bioinf* (2015) 16:169. doi: 10.1186/s12859-015-0611-3
48. Mi H, Muruganujan A, Huang X, Ebert D, Mills C, Guo X, et al. Protocol Update for Large-Scale Genome and Gene Function Analysis With the PANTHER Classification System (V.14.0). *Nat Protoc* (2019) 14:703–21. doi: 10.1038/s41596-019-0128-8
49. Bindea G, Mlecnik B, Hackl H, Charoentong P, Tosolini M, Kirilovsky A, et al. Cluego: A Cytoscape Plug-in to Decipher Functionally Grouped Gene Ontology and Pathway Annotation Networks. *Bioinformatics* (2009) 25:1091–3. doi: 10.1093/bioinformatics/btp101
50. Flores MA, Lazar IM. Xman V2-a Database of Homo Sapiens Mutated Peptides. *Bioinformatics* (2020) 36:1311–3. doi: 10.1093/bioinformatics/btz693
51. Cardon T, Salzet M, Franck J, Fournier I. Nuclei of Hela Cells Interactomes Unravel a Network of Ghost Proteins Involved in Proteins Translation. *Biochim Biophys Acta Gen Subj* (2019) 1863:1458–70. doi: 10.1016/j.bbagen.2019.05.009
52. Sheils T, Mathias SL, Siramshetty VB, Bocci G, Bologa CG, Yang JJ, et al. How to Illuminate the Druggable Genome Using Pharos. *Curr Protoc Bioinf* (2020) 69:e92. doi: 10.1002/cpbi.92
53. Győrffy B, Lanczky A, Eklund AC, Denkert C, Budczies J, Li Q, et al. An Online Survival Analysis Tool to Rapidly Assess the Effect of 22,277 Genes on Breast Cancer Prognosis Using Microarray Data of 1,809 Patients. *Breast Cancer Res Treat* (2010) 123:725–31. doi: 10.1007/s10549-009-0674-9

54. Schug ZT, Peck B, Jones DT, Zhang Q, Grosskurth S, Alam IS, et al. Acetyl-Coa Synthetase 2 Promotes Acetate Utilization and Maintains Cancer Cell Growth Under Metabolic Stress. *Cancer Cell* (2015) 27:57–71. doi: 10.1016/j.ccell.2014.12.002
55. Yu L, Li K, Xu Z, Cui G, Zhang X. Integrated Omics and Gene Expression Analysis Identifies the Loss of Metabolite-Metabolite Correlations in Small Cell Lung Cancer. *Onco Targets Ther* (2018) 11:3919–29. doi: 10.2147/OTT.S166149
56. Vaughan RA, Gannon NP, Garcia-Smith R, Licon-Munoz Y, Barberena MA, Bisoffi M, et al. β-Alanine Suppresses Malignant Breast Epithelial Cell Aggressiveness Through Alterations in Metabolism and Cellular Acidity In Vitro. *Mol Cancer* (2014) 13:14. doi: 10.1186/1476-4598-13-14
57. Stewart A, Maity B, Fisher RA. Two for the Price of One: G Protein-Dependent and -Independent Functions of RGS6 *In Vivo*. *Prog Mol Biol Transl Sci* (2015) 133:123–51. doi: 10.1016/bs.pmbts.2015.03.001
58. Parczyk K, Schneider MR. The Future of Antihormone Therapy: Innovations Based on an Established Principle. *J Cancer Res Clin Oncol* (1996) 122:383–96. doi: 10.1007/BF01212877
59. Geck RC, Toker A. Nonessential Amino Acid Metabolism in Breast Cancer. *Adv Biol Regul* (2016) 62:11–7. doi: 10.1016/j.jbior.2016.01.001
60. Pickup KE, Pardow F, Carbonell-Caballero J, Lioutas A, Villanueva-Cañas JL, Wright RHG, et al. Expression of Oncogenic Drivers in 3D Cell Culture Depends on Nuclear ATP Synthesis by NUDT5. *Cancers (Basel)* (2019) 11. doi: 10.3390/cancers11091337
61. Ehmsen S, Pedersen MH, Wang G, Terp MG, Arslanagic A, Hood BL, et al. Increased Cholesterol Biosynthesis is a Key Characteristic of Breast Cancer Stem Cells Influencing Patient Outcome. *Cell Rep* (2019) 27:3927–3938.e6. doi: 10.1016/j.celrep.2019.05.104
62. Cai D, Wang J, Gao B, Li J, Wu F, Zou JX, et al. Rorγ is a Targetable Master Regulator of Cholesterol Biosynthesis in a Cancer Subtype. *Nat Commun* (2019) 10:4621. doi: 10.1038/s41467-019-12529-3
63. Simigdala N, Gao Q, Pancholi S, Roberg-Larsen H, Zvelebil M, Ribas R, et al. Cholesterol Biosynthesis Pathway as a Novel Mechanism of Resistance to Estrogen Deprivation in Estrogen Receptor-Positive Breast Cancer. *Breast Cancer Res* (2016) 18:58. doi: 10.1186/s13058-016-0713-5
64. Brown KK, Spinelli JB, Asara JM, Toker A. Adaptive Reprogramming of *De Novo* Pyrimidine Synthesis is a Metabolic Vulnerability in Triple-Negative Breast Cancer. *Cancer Discovery* (2017) 7:391–9. doi: 10.1158/2159-8290.CD-16-0611
65. Opolski A, Mazurkiewicz M, Wietrzyk J, Kleinrok Z, Radzikowski C. The Role of GABA-Ergic System in Human Mammary Gland Pathology and in Growth of Transplantable Murine Mammary Cancer. *J Exp Clin Cancer Res* (2000) 19:383–90.
66. Shkurnikov MY, Nechaev IN, Khaustova NA, Krainova NA, Savelov NA, Grinevich VN, et al. Expression Profile of Inflammatory Breast Cancer. *Bull Exp Biol Med* (2013) 155:667–72. doi: 10.1007/s10517-013-2221-2
67. Lampa M, Arlt H, He T, Ospina B, Reeves J, Zhang B, et al. Glutaminase is Essential for the Growth of Triple-Negative Breast Cancer Cells With a Deregulated Glutamine Metabolism Pathway and its Suppression Synergizes With Mtor Inhibition. *PloS One* (2017) 12:e0185092. doi: 10.1371/journal.pone.0185092
68. Kim D-H, Yoon H-J, Cha Y-N, Surh Y-J. Role of Heme Oxygenase-1 and its Reaction Product, Carbon Monoxide, in Manifestation of Breast Cancer Stem Cell-Like Properties: Notch-1 as a Putative Target. *Free Radic Res* (2018) 52:1336–47. doi: 10.1080/10715762.2018.1473571
69. Ifergan I, Assaraf YG. Molecular Mechanisms of Adaptation to Folate Deficiency. *Vitam Horm* (2008) 79:99–143. doi: 10.1016/S0083-6729(08)00404-4
70. Efimova EV, Takahashi S, Shamsi NA, Wu D, Labay E, Ulanovskaya OA, et al. Linking Cancer Metabolism to DNA Repair and Accelerated Senescence. *Mol Cancer Res* (2016) 14:173–84. doi: 10.1158/1541-7786.MCR-15-0263
71. Ferrer CM, Lynch TP, Sodi VL, Falcone JN, Schwab LP, Peacock DL, et al. O-Glcnacylation Regulates Cancer Metabolism and Survival Stress Signaling via Regulation of the HIF-1 Pathway. *Mol Cell* (2014) 54:820–31. doi: 10.1016/j.molcel.2014.04.026
72. Ferrer CM, Sodi VL, Reginato MJ. O-Glcnacylation in Cancer Biology: Linking Metabolism and Signaling. *J Mol Biol* (2016) 428:3282–94. doi: 10.1016/j.jmb.2016.05.028
73. Chiaradonna F, Ricciardiello F, Palorini R. The Nutrient-Sensing Hexosamine Biosynthetic Pathway as the Hub of Cancer Metabolic Rewiring. *Cells* (2018) 7. doi: 10.3390/cells7060053
74. Ma Z, Vosseller K. Cancer Metabolism and Elevated O-Glcnac in Oncogenic Signaling. *J Biol Chem* (2014) 289:34457–65. doi: 10.1074/jbc.R114.577718
75. Nie H, Yi W. O-Glcnacylation, a Sweet Link to the Pathology of Diseases. *J Zhejiang Univ Sci B* (2019) 20:437–48. doi: 10.1631/jzus.B1900150
76. Very N, Vercoutter-Edouart A-S, Lefebvre T, Hardivillé S, El Yazidi-Belkoura I. Cross-Dysregulation of O-Glcnacylation and PI3K/AKT/Mtor Axis in Human Chronic Diseases. *Front Endocrinol (Lausanne)* (2018) 9:602. doi: 10.3389/fendo.2018.00602
77. Makwana V, Ryan P, Patel B, Dukie S-A, Rudrawar S. Essential Role of O-Glcnacylation in Stabilization of Oncogenic Factors. *Biochim Biophys Acta Gen Subj* (2019) 1863:1302–17. doi: 10.1016/j.bbagen.2019.04.002
78. Singh A, Nunes JJ, Ateeq B. Role and Therapeutic Potential of G-Protein Coupled Receptors in Breast Cancer Progression and Metastases. *Eur J Pharmacol* (2015) 763:178–83. doi: 10.1016/j.ejphar.2015.05.011
79. Geck RC, Foley JR, Murray Stewart T, Asara JM, Casero RA, Toker A. Inhibition of the Polyamine Synthesis Enzyme Ornithine Decarboxylase Sensitizes Triple-Negative Breast Cancer Cells to Cytotoxic Chemotherapy. *J Biol Chem* (2020) 295:6263–77. doi: 10.1074/jbc.RA119.012376
80. Barupal DK, Gao B, Budczies J, Phinney BS, Perroud B, Denkert C, et al. Prioritization of Metabolic Genes as Novel Therapeutic Targets in Estrogen-Receptor Negative Breast Tumors Using Multi-Omics Data and Text Mining. *Oncotarget* (2019) 10:3894–909. doi: 10.18632/oncotarget.26995
81. Wang Y-P, Lei Q-Y. Perspectives of Reprogramming Breast Cancer Metabolism. *Adv Exp Med Biol* (2017) 1026:217–32. doi: 10.1007/978-981-10-6020-5_10
82. Kim H-Y, Lee K-M, Kim S-H, Kwon Y-J, Chun Y-J, Choi H-K. Comparative Metabolic and Lipidomic Profiling of Human Breast Cancer Cells With Different Metastatic Potentials. *Oncotarget* (2016) 7:67111–28. doi: 10.18632/oncotarget.11560
83. Strekalova E, Malin D, Weisenhorn EMM, Russell JD, Hoelper D, Jain A, et al. S-Adenosylmethionine Biosynthesis is a Targetable Metabolic Vulnerability of Cancer Stem Cells. *Breast Cancer Res Treat* (2019) 175:39–50. doi: 10.1007/s10549-019-05146-7
84. Surguchov A. Intracellular Dynamics of Synucleins: 'Here, There and Everywhere'. *Int Rev Cell Mol Biol* (2015) 320:103–69. doi: 10.1016/bs.ircmb.2015.07.007
85. Wang X, Wan J, Xu Z, Jiang S, Ji L, Liu Y, et al. Identification of Competitive Endogenous Rnas Network in Breast Cancer. *Cancer Med* (2019) 8:2392–403. doi: 10.1002/cam4.2099
86. Fan Y, Zhou X, Xia T-S, Chen Z, Li J, Liu Q, et al. Human Plasma Metabolomics for Identifying Differential Metabolites and Predicting Molecular Subtypes of Breast Cancer. *Oncotarget* (2016) 7:9925–38. doi: 10.18632/oncotarget.7155
87. Marquart J, Chen EY, Prasad V. Estimation of the Percentage of US Patients With Cancer Who Benefit From Genome-Driven Oncology. *JAMA Oncol* (2018) 4:1093–8. doi: 10.1001/jamaoncol.2018.1660
88. Beltran H, Eng K, Mosquera JM, Sigaras A, Romanel A, Rennert H, et al. Whole-Exome Sequencing of Metastatic Cancer and Biomarkers of Treatment Response. *JAMA Oncol* (2015) 1:466–74.
89. Patel MN, Halling-Brown MD, Tym JE, Workman P, Al-Lazikani B. Objective Assessment of Cancer Genes for Drug Discovery. *Nat Rev Drug Discov* (2013) 12:35–50. doi: 10.1038/nrd3913
90. Cardon T, Franck J, Coyaud E, Laurent EMN, Damato M, Maffia M, et al. Alternative Proteins are Functional Regulators in Cell Reprogramming by PKA Activation. *Nucleic Acids Res* (2020) 48:7864–82. doi: 10.1093/nar/gkaa277
91. Sicklick JK, Kato S, Okamura R, Schwaederle M, Hahn ME, Williams CB, et al. Molecular Profiling of Cancer Patients Enables Personalized Combination Therapy: The I-PREDICT Study. *Nat Med* (2019) 25:744–50. doi: 10.1038/s41591-019-0407-5
92. Al-Lazikani B, Banerji U, Workman P. Combinatorial Drug Therapy for Cancer in the Post-Genomic Era. *Nat Biotechnol* (2012) 30:679–92. doi: 10.1038/nbt.2284
93. Würth R, Thellung S, Bajetto A, Mazzanti M, Florio T, Barbieri F. Drug-Repositioning Opportunities for Cancer Therapy: Novel Molecular Targets

for Known Compounds. *Drug Discov Today* (2016) 21:190–9. doi: 10.1016/j.drudis.2015.09.017
94. Griffiths JI, Cohen AL, Jones V, Salgia R, Chang JT, Bild AH. Opportunities for Improving Cancer Treatment Using Systems Biology. *Curr Opin Syst Biol* (2019) 17:41–50. doi: 10.1016/j.coisb.2019.10.018
95. Kristensen VN, Lingjærde OC, Russnes HG, Vollan HKM, Frigessi A, Børresen-Dale A-L. Principles and Methods of Integrative Genomic Analyses in Cancer. *Nat Rev Cancer* (2014) 14:299–313. doi: 10.1038/nrc3721

Conflict of Interest: The authors declare that the research was conducted in the absence of any commercial or financial relationships that could be construed as a potential conflict of interest.

Publisher's Note: All claims expressed in this article are solely those of the authors and do not necessarily represent those of their affiliated organizations, or those of the publisher, the editors and the reviewers. Any product that may be evaluated in this article, or claim that may be made by its manufacturer, is not guaranteed or endorsed by the publisher.

frontiers in Oncology

ORIGINAL RESEARCH
published: 04 February 2022
doi: 10.3389/fonc.2022.829045

Construction and Validation of a Prognostic Risk Model for Triple-Negative Breast Cancer Based on Autophagy-Related Genes

Cheng Yan[1,2,3†], *Qingling Liu*[1†] *and Ruoling Jia*[1*]

[1] School of Pharmacy, Xinxiang University, Xinxiang, China, [2] Key Laboratory of Nano-Carbon Modified Film Technology of Henan Province, Xinxiang University, Xinxiang, China, [3] Diagnostic Laboratory of Animal Diseases, Xinxiang University, Xinxiang, China

OPEN ACCESS

Edited by:
San-Gang Wu,
First Affiliated Hospital of Xiamen University, China

Reviewed by:
Mingliang Zhang,
Shanghai Jiao Tong University, China
Daqian Xu,
Zhejiang University, China

***Correspondence:**
Ruoling Jia
jiaruolinggg@163.com

[†]These authors have contributed equally to this work

Specialty section:
This article was submitted to Breast Cancer, a section of the journal Frontiers in Oncology

Received: 04 December 2021
Accepted: 10 January 2022
Published: 04 February 2022

Citation:
Yan C, Liu Q and Jia R (2022) Construction and Validation of a Prognostic Risk Model for Triple-Negative Breast Cancer Based on Autophagy-Related Genes. Front. Oncol. 12:829045. doi: 10.3389/fonc.2022.829045

Background: Autophagy plays an important role in triple-negative breast cancer (TNBC). However, the prognostic value of autophagy-related genes (ARGs) in TNBC remains unknown. In this study, we established a survival model to evaluate the prognosis of TNBC patients using ARGs signature.

Methods: A total of 222 autophagy-related genes were downloaded from The Human Autophagy Database. The RNA-sequencing data and corresponding clinical data of TNBC were obtained from The Cancer Genome Atlas (TCGA) database. Differentially expressed autophagy-related genes (DE-ARGs) between normal samples and TNBC samples were determined by the DESeq2 package. Then, univariate Cox, least absolute shrinkage and selection operator (LASSO), and multivariate Cox regression analyses were performed. According to the LASSO regression results based on univariate Cox, we identified a prognostic signature for overall survival (OS), which was further validated by using the Gene Expression Omnibus (GEO) cohort. We also found an independent prognostic marker that can predict the clinicopathological features of TNBC. Furthermore, a nomogram was drawn to predict the survival probability of TNBC patients, which could help in clinical decision for TNBC treatment. Finally, we validated the requirement of an ARG in our model for TNBC cell survival and metastasis.

Results: There are 43 DE-ARGs identified between normal and tumor samples. A risk model for OS using CDKN1A, CTSD, CTSL, EIF4EBP1, TMEM74, and VAMP3 was established based on univariate Cox regression and LASSO regression analysis. Overall survival of TNBC patients was significantly shorter in the high-risk group than in the low-risk group for both the training and validation cohorts. Using the Kaplan–Meier curves and receiver operating characteristic (ROC) curves, we demonstrated the accuracy of the prognostic model. Multivariate Cox regression analysis was used to verify risk score as an independent predictor. Subsequently, a nomogram was proposed to predict 1-, 3-, and 5-year survival for TNBC patients. The calibration curves showed great accuracy of the

model for survival prediction. Finally, we found that depletion of EIF4EBP1, one of the ARGs in our model, significantly reduced cell proliferation and metastasis of TNBC cells.

Conclusion: Based on six ARGs (CDKN1A, CTSD, CTSL, EIF4EBP1, TMEM74, and VAMP3), we developed a risk prediction model that can help clinical doctors effectively predict the survival status of TNBC patients. Our data suggested that EIF4EBP1 might promote the proliferation and migration in TNBC cell lines. These findings provided a novel insight into the vital role of the autophagy-related genes in TNBC and may provide new therapeutic targets for TNBC.

Keywords: TNBC (triple-negative breast cancer), Autophagy, risk model, EIF4EBP1, prognosis

INTRODUCTION

Breast cancer is the most leading diagnosed cancer among women, with the fifth highest cancer mortality worldwide in 2020 (1). Triple-negative breast cancer (TNBC) is a subtype of breast cancer, which is defined by the lack in the expression of estrogen (ER), progesterone (PR), and HER2 receptors. TNBC takes up approximately 15%–20% of total breast cancers and is the second leading cause of cancer death among women worldwide (2). TNBC is characterized by high heterogeneity, early diagnosis difficulty, rapid metastasis, poor survival, and high recurrence rate (3). Statistics show that the 5-year survival rate of TNBC patients is <40% after diagnosis (4). Although various therapeutic approaches have been proposed for TNBC, the incidences and recurrence ratios of TNBC still remain unsatisfactory, especially for developed countries (5). Tumor–nodes–metastasis (TNM) stage and molecular subtypes have been widely used in the routine diagnosis and treatment of TNBC. However, traditional markers have limited sensitivity and specificity to precisely predict prognosis and design individualized treatment in TNBC patients. Therefore, it is imperative to establish new molecular biomarkers and prognostic models to further improve the effectiveness of treatment strategies for TNBC patients.

Autophagy is an important cellular catabolic process that maintains homeostasis by eliminating aggregated proteins and damaged organelles in eukaryotic cells (6). More and more studies showed that autophagy plays a paradoxical tumor-suppressive or tumor-promoting role in different contexts and stages of progression: it prohibits tumorigenesis in the early stage but supports various tumor growth in late stage (7). Recent evidence indicated that autophagy has a high vital function in tumorigenesis and metastasis of TNBC. Indeed, several reports have indicated that TNBC tumors exhibit a higher level of autophagy than other breast cancer subtypes (8–10). Knockdown of autophagy-related genes (LC3 and Beclin-1) inhibits autophagy and significantly reduces cell proliferation, colony formation, and migration and induces apoptosis in MDA-MB-231 and BT-549 TNBC cells (11). These findings have confirmed the importance of autophagy in TNBC and suggest that ARGs may serve as prognostic markers for TNBC. To our knowledge, there is no prognosis model of ARGs in TNBC that has been constructed to predict the prognosis of TNBC patients. Therefore, a novel prognostic model with ARGs for predicting survival in TNBC is highly needed.

In this study, we analyzed in detail the transcriptome and clinical data of TNBC obtained from The Cancer Genome Atlas (TCGA) database and built an ARGs-based prognosis model using univariate Cox regression and least absolute shrinkage and selection operator (LASSO) regression analysis. Then, the proposed model was validated by the test set. Finally, we knocked down the expression level of EIF4EBP1, one of the prognosis-related genes in our model, to explore its function in TNBC. This model may provide a new reference index for the stratification of prognosis risk and treatment strategy selection of TNBC patients. Meanwhile, therapeutic targeting of EIF4EBP1 may be a potential therapeutic strategy for TNBC.

METHODS

Data Acquisition

The Human Autophagy Database (HADb, http://www.autophagy.lu/index.html) can provide the entire set of human genes associated with autophagy (12). We collected 222 ARGs from HADB. In addition, the RNA-sequencing and corresponding clinical data of triple-negative breast cancer in TCGA were downloaded from the University of California, Santa Cruz (UCSC) XENA database (https://xena.ucsc.edu/). TNBC samples were selected using negative for "breast carcinoma estrogen receptor status," "breast carcinoma progesterone receptor status," and "lab procedure her2 neu *in situ* hybrid outcome type" as screening criteria. The microarray and corresponding clinical data of GSE58812 were downloaded from Gene Expression Omnibus (GEO) database (https://www.ncbi.nlm.nih.gov/geo/).

Identification of Differentially Expressed ARGs

Differential gene expression of ARGs (DE-ARGs) in 162 normal samples and 103 TNBC samples was carried out by the DESeq2 package. We set false discovery rate (FDR) <0.05 and $|\log_2$ fold change (FC)$|$ >1 as cutoff criteria to obtain DE-ARGs. Volcano plots of DE-ARGs were constructed with the OmicStudio tools (https://www.omicstudio.cn/tool); boxplots were plotted using

the ggplot2 R package, Heatmaps were obtained using Morpheus (https://software.broadinstitute.org/morpheu). Protein–protein interaction (PPI) networks were generated using the STRING website (https://string-db.org).

Functional Enrichment Analysis

We performed Gene Ontology (GO) and Kyoto Encyclopedia of Genes and Genomes (KEGG) biological process enrichment of the DE-ARGs by R statistical software including packages of "clusterProfiler", "org.Hs.eg.db", "enrichplot", "ggplot2", and "GOplot". An adjusted p-value <0.05 was considered statistically significant. Moreover, Gene Set Enrichment Analysis (GSEA) of TCGA and GEO was conducted to reveal the signaling pathways and biological processes between high- and low-risk groups in TNBC patients (http://software.broadinstitute.org/gsea/).

Identification of Prognostic Gene Signatures

We used the 103 TNBC samples from TCGA cohort as a training set. Univariate Cox regression analysis was performed on ARGs of train set to identify the association between the expression levels of the genes and patients' overall survival (OS) using the "survival" package (http://bioconductor.org/packages/survival/) in R 3.6.1. The hazard ratio (HR) and p-value of each gene were calculated. Genes with $p < 0.05$ were screened for further analysis. Later, we further used LASSO Cox regression to reduce the number of genes and eliminate collinearity between genes. Finally, we performed multivariate Cox regression analysis based on univariate Cox regression.

Construction and Validation of a Prognostic Model

According to the results of LASSO Cox regression, the risk scores of all samples were calculated according to the equation:

$$\text{risk score} = \sum_{j=1}^{n}(Coef_j \times Xj)$$

Coef refers to the regression coefficient of ARGs in LASSO Cox regression analysis, "X" is the expression value of the gene, and "n" is the number of prognostic ARGs. Using the median risk score as threshold, patients were divided into the high-risk group and low-risk group. We used the R package "survival" to assess differences in OS and obtain Kaplan–Meier survival plots. The receiver operating characteristic (ROC) curve was generated by the timeROC package to evaluate the prognostic ability of the model. Simultaneously, we used samples from GEO database as the validation set. We calculated risk scores for patients in the GEO cohort using the same formula of the train set. Then, we performed univariate and multivariate Cox regression analyses to investigate whether risk score was an independent prognostic factor for OS in TNBC patients in the train set. N, T, stage, and risk score were used as covariates. t-tests were used to test the correlation between risk score and clinicopathological factors. A p-value less than 0.05 ($p < 0.05$) was considered statistically significant.

The Construction of Nomogram and Calibration Curves

Nomogram and calibration plots were generated by using the "rms" package in R software. The nomogram was used to investigate the level of consistency between the actual and predicted probabilities. Calibration plot was used to predict 1-, 3-, and 5-year survival rates.

TNBC Cell Culture, Proliferation, Colony Formation, and Migration Assays

MDA-MB-231 and BT549 cells were cultured in Dulbecco's modified Eagle's medium (DMEM) medium. Two small inferring RNAs (siRNAs) were employed to knock down EIF4EBP1, and the sequences were as follows: siRNA1, 5′-GGG AGGTACCAGGATCATCTA-3′; siRNA2, 5′-GGAGGTAC CAGGATCATCTAT-3′. Cell proliferation of control and EIF4EBP1 knockdown cells was determined by CCK8 and Edu. Cells transfected with control or EIF4EBP1 siRNAs were seeded in six-well plates, and colonies were measured by crystal violet staining after 15 days culture. Transwell and wound healing assays were performed and quantified using control and EIF4EBP1 knockdown cells to determine cell migration.

RESULTS

Identification of DE-ARGs

Autophagy has been reported to contribute to TNBC progression. In this study, we intend to construct the prognosis model using ARGs signature for TNBCs. The overall experimental design in this study is indicated as a diagram (**Figure 1**). We first obtained the expression profiles containing 162 normal samples and 103 TNBC samples from TCGA database and gathered 222 ARGs from the HADb database. A total of 43 differentially expressed ARGs (DE-ARGs) were identified by comparing normal and tumor samples with the cutoff criteria of FDR <0.05 and $|\log_2 FC| > 1$. The volcano map (**Figure 2A**), box plots (**Figure 2C**), and heatmap (**Figure 2D**) demonstrated that 21 ARGs were significantly downregulated, while 22 ARGs were upregulated in TNBC patients. These DE-ARGs interacted with each other forming an autophagy network as measured by STRING (**Figure 2B**). Moreover, we observed that many mutations occur on these DE-ARGs in TNBCs (**Supplementary Figure 1**).

Enrichment Analysis of DE-ARGs

To determine the functional enrichment of DE-ARGs, we performed GO and KEGG enrichment analysis. We found that these 43 DE-ARGs were highly correlated to autophagy, process utilizing autophagic mechanism, and peptidyl serine modification in the term of biological process (BP). In the aspect of cellular components (CCs), these genes were enriched in the nuclear envelope, mitochondrial outer membrane, and organelle outer membrane. For the molecular functions (MFs),

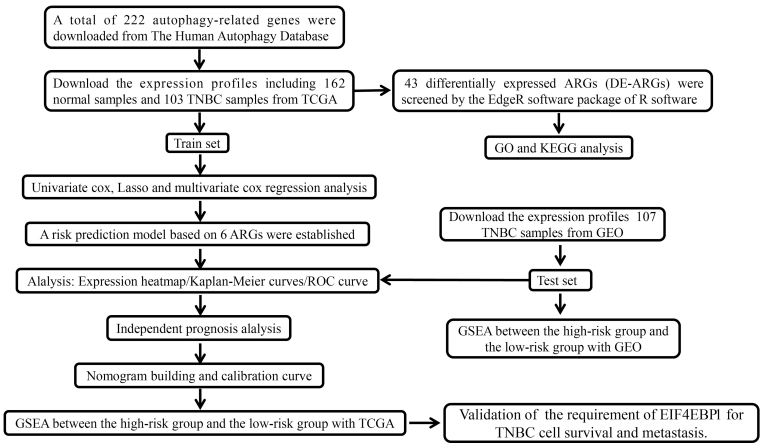

FIGURE 1 | The flowchart describing the experimental design to establish and validate the prognostic signature in the study.

these genes were mainly concentrated in ubiquitin protein ligase binding, ubiquitin-like protein ligase binding, and protein phosphatase (**Supplementary Figure 2A**). Moreover, KEGG enrichment analysis indicated that the DE-ARGs were involved in the signaling pathways such as autophagy animal (*Homo sapiens*), epidermal growth factor receptor (EGFR) tyrosine kinase inhibitor resistance and apoptosis (**Supplementary Figure 2B**). Overall, these data suggested that these ARGs play a role in other biological process in addition to autophagy.

Construction of a Prognostic ARG Signature of TNBC in the Train Set

To build the ARG prognostic model, we first analyzed the risk score of all ARGs in TNBC by performing univariate Cox regression analysis. Eight ARGs were screened out including seven potential risky genes and one potential protective gene (**Figure 3A**). Subsequently, we performed LASSO regression analysis on the basis of univariate Cox regression analysis (**Figures 3C, D**). Then, we constructed the prognostic ARG signature for OS using CDKN1A, CTSD, CTSL, EIF4EBP1, TMEM74, and VAMP3 by LASSO regression. Finally, we performed multivariate Cox regression analysis and screened out four ARGs including three potential risk genes and one potential protective gene (**Figure 3B**).

Next, we tested if the expression of these six ARGs was correlated with the prognosis of TNBCs. We found that the high expression of EIF4EBP1 ($p = 0.046$), CTSL ($p = 0.009$), and CTSD ($p = 0.07$) might indicate a worse prognosis. There were no statistical differences in the survival analyses of CDKN1A ($p = 0.362$), TMEM74 ($p = 0.107$), and VAMP3 ($p = 0.189$) (**Supplementary Figure 3**). Then, we want to validate whether this ARG signature can predict the OS of TNBC. We first divided TNBC patients into "high risk" ($n = 50$) and "low risk" ($n = 51$) group according to the threshold of the median risk score (**Figure 4A**). The risk score for each patient was calculated based on the formula: risk score = (0.246026 × CDKN1A) + (0.359130 × CTSD) + (0.234375 × CTSL) + (0.590736 × EIF4EBP1) + (−0.281261 × TMEM74) + (0.338378 × VAMP3). Patients were assigned to high-risk ($n = 50$) and low-risk groups ($n = 51$) according to the threshold of the median risk score. Patients with higher scores were more likely to have a poorer prognosis (**Figure 4C**). A heatmap was used to visualize differences in expression levels of the six ARGs between groups (**Figure 4D**). Survival curves further indicated that patients in the high-risk group showed a significantly lower probability of survival compared to low-risk group ($p < 0.05$) (**Figure 4B**). ROC analysis revealed that the area under the curves (AUCs) for 1-, 3-, and 5-year OS were 0.925, 0.866, and 0.784, respectively (**Figure 4E**). Principal component analysis indicated that the distribution patterns of high- and low-risk populations were different based on the train set (**Supplementary Figure 6A**). These data suggested that ARGs signature in our model could benefit the prognosis prediction of TNBCs.

Validation of the Risk Score of ARG Signature in a GEO Test Set

To further validate the prognostic and predictive role of ARGs signature, we employed another GEO cohort as a test set to calculate risk scores using the same formula used in the train set. The patients from the test set were divided into the high-risk group ($n = 34$) and low-risk group ($n = 73$) by the median value of the train set (**Figure 5A**), and the higher risk score predicted poorer prognosis in the patients (**Figure 5C**). A heatmap was presented to visualize the different expression levels of the six ARGs between test groups (**Figure 5D**). Similar to the train set, patients in the high-risk score group showed a poorer prognosis compared to the low-risk group in the test set ($p < 0.05$) (**Figure 5B**). Time-dependent ROC analysis showed that the prognostic accuracy of OS was 0.798 at 1 year, 0.564 at 3 years, and 0.696 at 5 years (**Figure 5E**). Principal component analysis indicated that the distribution patterns of high- and low-risk populations were different based on the test set (**Supplementary Figure 6B**).

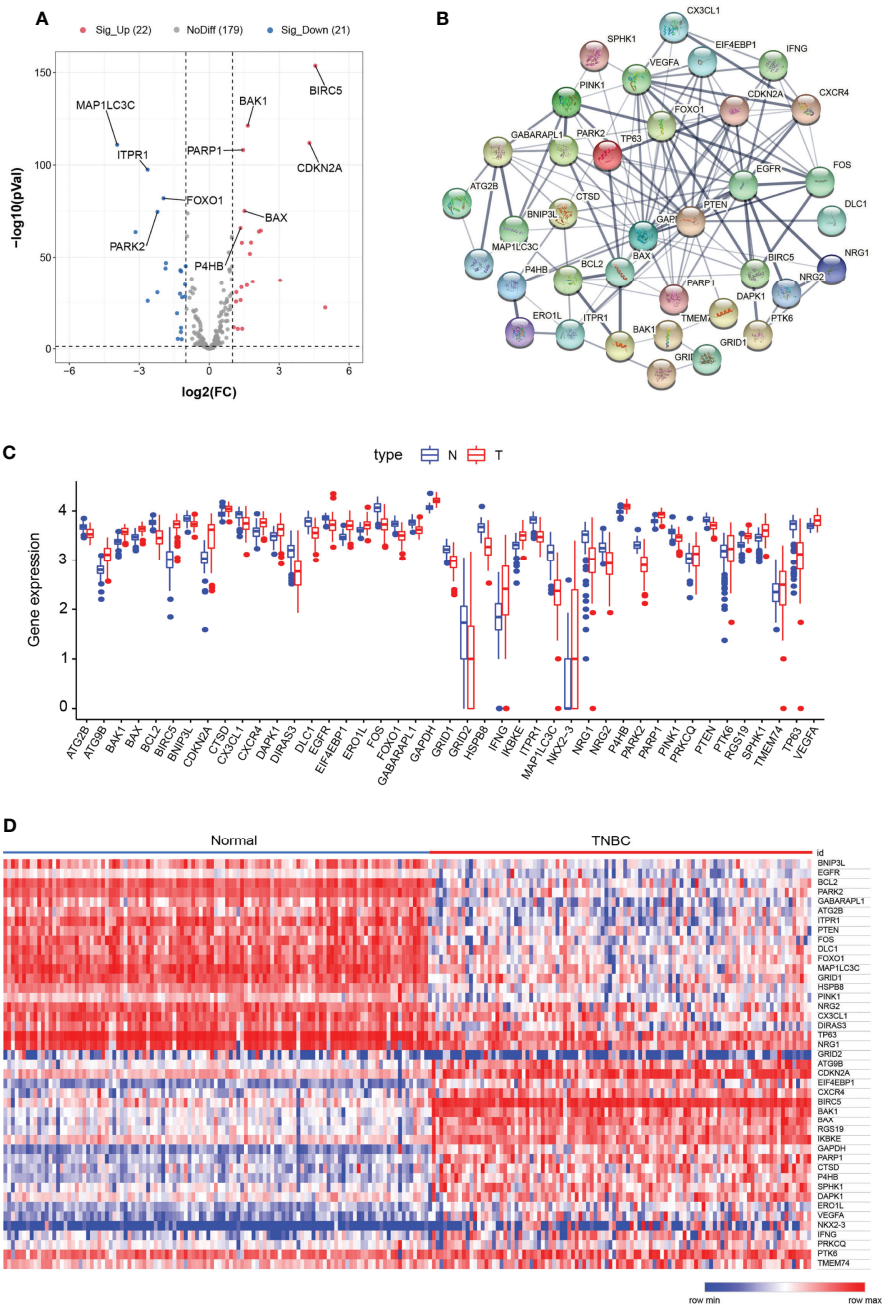

FIGURE 2 | Differentially expressed autophagy-related genes. **(A)** Volcano map showed differentially expressed genes between normal samples and TNBC samples. Red dots represent significantly upregulated genes, blue dots represent significantly downregulated genes, and gray dots represent ARGs with no difference. **(B)** Protein–protein interactions (PPI) network of ARGs using the STRING database. **(C)** Box plots showed gene expression values of ARGs. Blue represents normal samples, and red represents tumor samples. **(D)** Heatmap showed the expression levels of ARGs. The color scale represented the expression levels normalized by z-score.

Independent Prognostic Indicator of the Prognostic Risk Model

To confirm whether risk scores can be used as an independent predictor for TNBC patients' survival, we further performed univariate analysis in the training set. Univariate Cox regression analysis revealed that N, T, stage, and risk score were meaningful for predicting OS (**Figure 6A**). Subsequently, we performed a multivariate Cox regression analysis to verify risk score as an independent predictor ($p < 0.001$) (**Figure 6B**). Moreover, we identified that the expression of CTSD was significantly associated with stages ($p = 0.025$) (**Supplementary Figure 4A**) and T ($p = 0.031$) (**Supplementary Figure 4B**). These data demonstrated that

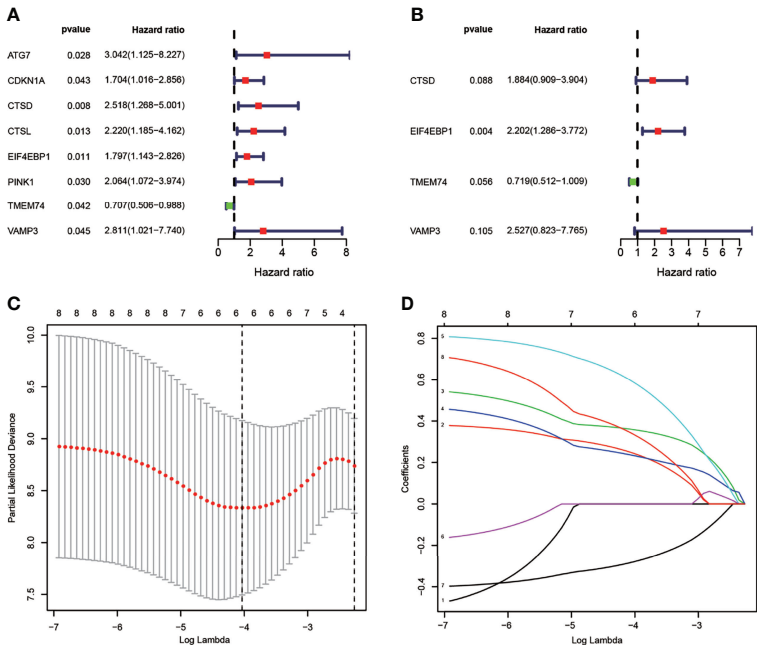

FIGURE 3 | Identification of ARGs with prognostic value in breast cancer. **(A)** Univariate Cox regression hazard model for the overall survival in TNBC. **(B)** Multivariate Cox regression hazard model for the overall survival in TNBC. **(C)** LASSO regression analysis of ARGs based on univariate Cox regression analysis. The horizontal axis represents the log value of the independent variable λ, whilst the vertical axis represents the partial likelihood deviance of the log value of each independent variable λ. **(D)** Coefficients were calculated for each lambda. Each line represents a gene confidence value.

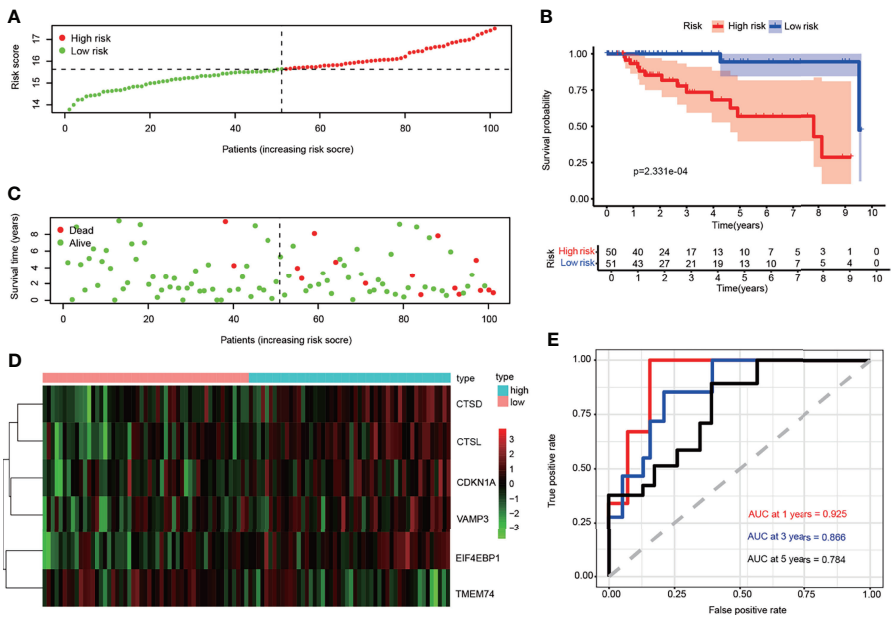

FIGURE 4 | Correlation between the risk score and overall survival in the train set. **(A)** The risk score stratified the TNBC patients into high-risk groups ("High" red line) and low-risk groups ("Low" green line). **(B)** Kaplan–Meier survival curves to show survival probability comparing the high-risk groups with low-risk group. **(C)** Comparison of survival time and survival status of patients in TNBC between high- and low-risk groups. Green plots for alive, red plots for dead. **(D)** Heatmap showing expression of the six genes screened from ARGs in TNBC. Blue color represents high-risk group, while pink color represents low-risk group. The color scale represented the expression levels normalized by z-score. **(E)** Time-dependent ROC curves for survival prediction by the risk score.

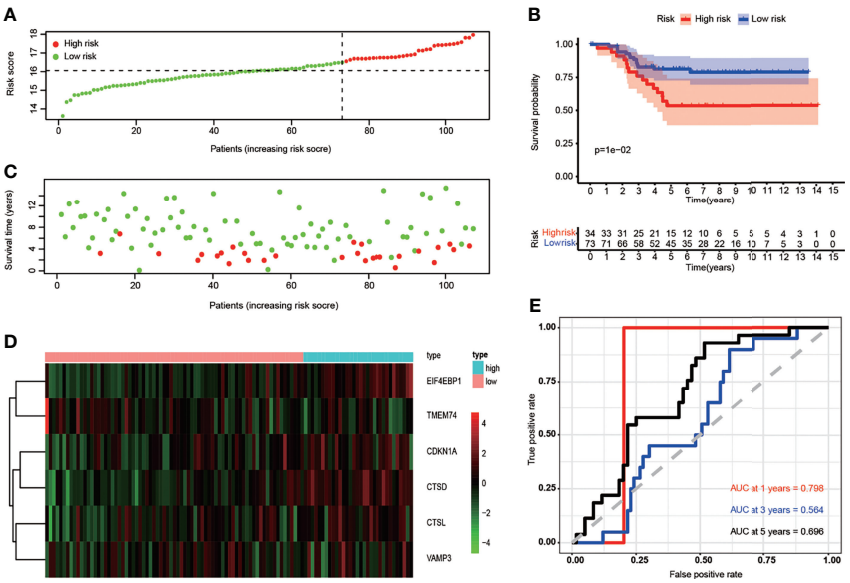

FIGURE 5 | Correlation between the risk score and overall survival in the test set. **(A)** The risk score stratified the TNBC patients into high-risk groups ("High" red line) and low-risk groups ("Low" green line). **(B)** Kaplan–Meier survival curves to show survival probability comparing the high-risk groups with low-risk group. **(C)** Survival time and survival status of patients in TNBC comparing high-risk group with low-risk group. Green plots for alive, red plots for dead. **(D)** Heatmap showing expression of the six genes screened from ARGs in TNBC. Blue color represents high group, while pink color represents low group. The color scale represented the expression levels normalized by z-score. **(E)** Time-dependent ROC curves for survival prediction by the risk score.

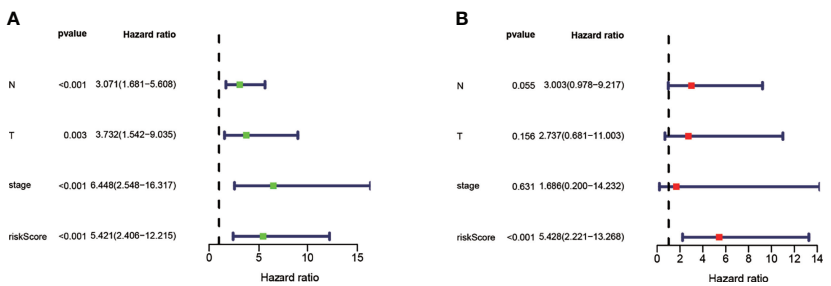

FIGURE 6 | Analysis of the risk scores as an independent prognostic indicator. **(A)** Univariate Cox regression analysis identified that N, T, stage, and risk score were significantly associated with OS prediction. **(B)** Multivariate Cox regression analysis identified that risk score was independent prognostic factor for TNBC.

our model could be a reliable prognostic predictor and biomarker in addition to known clinical classification.

Construction of the Nomogram and Performance Validation

To provide the clinician with a better quantitative method to predict prognosis of TNBC patient, we established a nomogram with multiple factors including N, T, stage, and risk score (**Figure 7A**). The nomogram was used to evaluate the survival probability of 1, 3, and 5 years. Nomograms showed a good performance with a high C-index of 0.764, suggesting that it could be served as an effective tool for the prognostic evaluation of patients with TNBC. In addition, we constructed calibration curves, which showed that the predicted and actual survival rates were in agreement with 1, 3, and 5 years (**Figures 7B–D**). Finally, we compared the predictive accuracy for TNBC between the nomogram and clinicopathological risk factors by the values of AUC. Our model's AUC value (AUC of 1-, 3-, and 5-year OS) was higher than the traditional prognostic scoring systems (**Figures 7E–G**). These findings revealed that the nomogram with our risk scores can precisely evaluate the OS in patients with TNBC.

Enrichment Analysis Between High- and Low-Risk Group

Finally, we performed GSEA between the high- and the low-risk group in TCGA and GSE58812 cohort, respectively, to further provide biological insight. We found that the enriched KEGG pathways of the high-risk group in TCGA cohort included apoptosis, Fc epsilon RI signaling pathway,

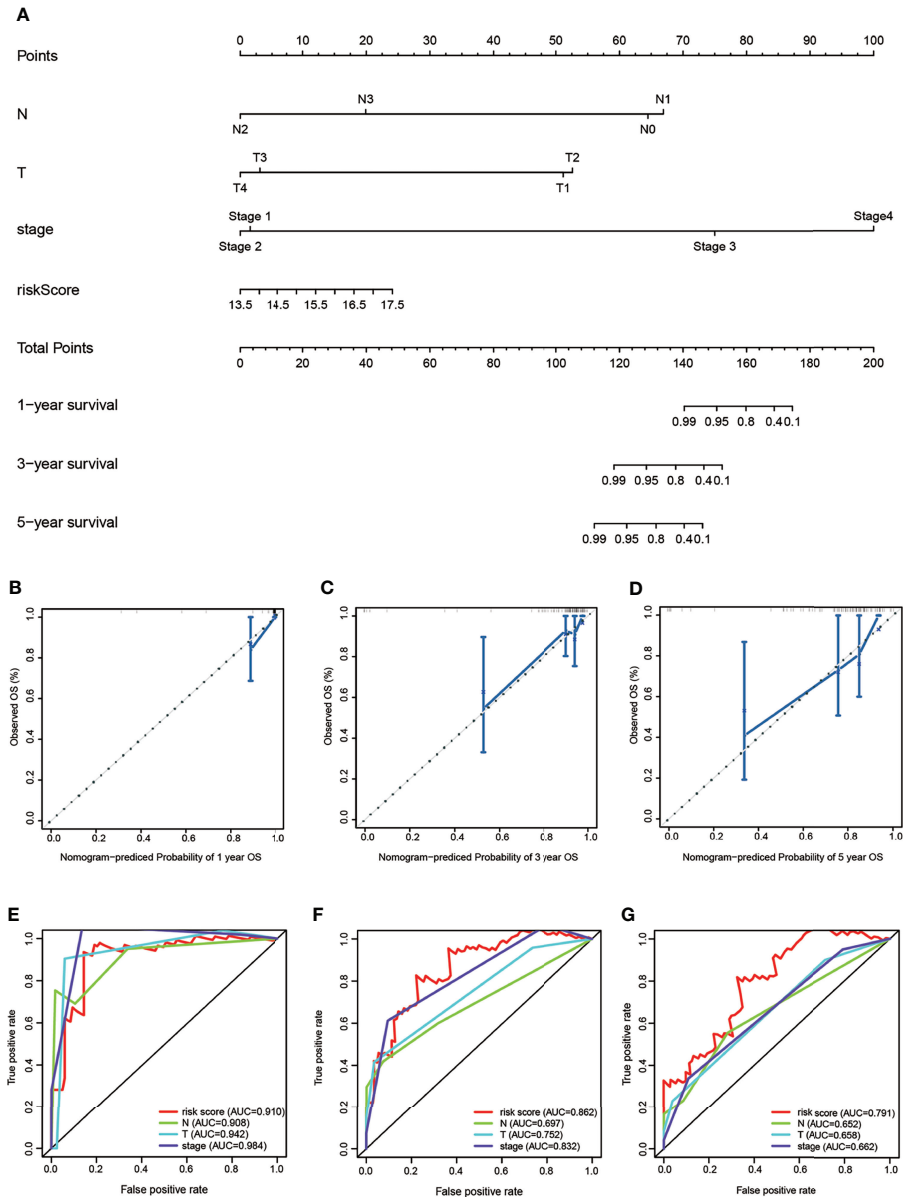

FIGURE 7 | The nomogram to predict overall survival of TNBC patients of TAGC cohort. **(A)** The nomogram for predicting survival proportion of patients in 1, 3-, and 5 years. **(B–D)** The calibration plots for predicting patient survival at 1, 3, and 5 years. **(E–G)** The ROC curve of OS for risk score, N, T, and stage at 1, 3, and 5 years.

glycosylphosphatidylinositol GPI anchor biosynthesis, lysosome, and olfactory transduction. Meanwhile, enriched KEGG pathways of low-risk group included protein export, RIG-I like receptor signaling pathway, RNA polymerase, taste transduction, and Toll-like receptor signaling pathway (**Supplementary Figure 5A**). In addition, KEGG enrichment pathway analysis of high-risk group in GSE58812 cohort indicated that the genes were enriched in ABC transporters, arginine and proline metabolism, lysosome, pathogenic *Escherichia coli* infection, and pentose phosphate pathway. KEGG enrichment pathways analysis of the low-risk group in GSE58812 cohort were mainly concentrated in the regulation of autophagy, RIG-I-like receptor signaling pathway, RNA degradation, spliceosome, and *Vibrio cholerae* infection (**Supplementary Figure 5B**).

Knockdown of EIF4EBP1 Inhibited TNBC Cell Proliferation and Migration

We next want to test the biological function of these ARGs in our model in TNBC. Among these six genes, the function of EIF4EBP1 in TNBC remains unknown. We knocked down EIF4EBP1 using two independent siRNAs in two TNBC cell

lines: MDA-MB-231 and BT549 (**Figure 8A**). Knockdown of EIF4EBP1 resulted in a dramatic decrease in cell growth and colony formation (**Figures 8B–D, F**). Edu staining showed that knockdown of eIF4EBP induced a significant decrease in proliferation (**Figures 8E, H**). In addition, EIF4EBP1 knockdown significantly impaired cell metastasis as measured by Transwell and wound healing assay (**Figures 8G, I–K**). Furthermore, we observed increased EIF4EBP1 expression in primary TNBC samples compared to adjacent normal tissues in collected three TNBC patients (**Figure 8L**). Based on the Human Protein Atlas database, the protein expression levels of EIF4EBP1 were evaluated by the CAB005032 antibody. Among 12 TNBC tissues examined, 6 cases had medium to high staining (4 medium and 8 high), while no cases had low staining.

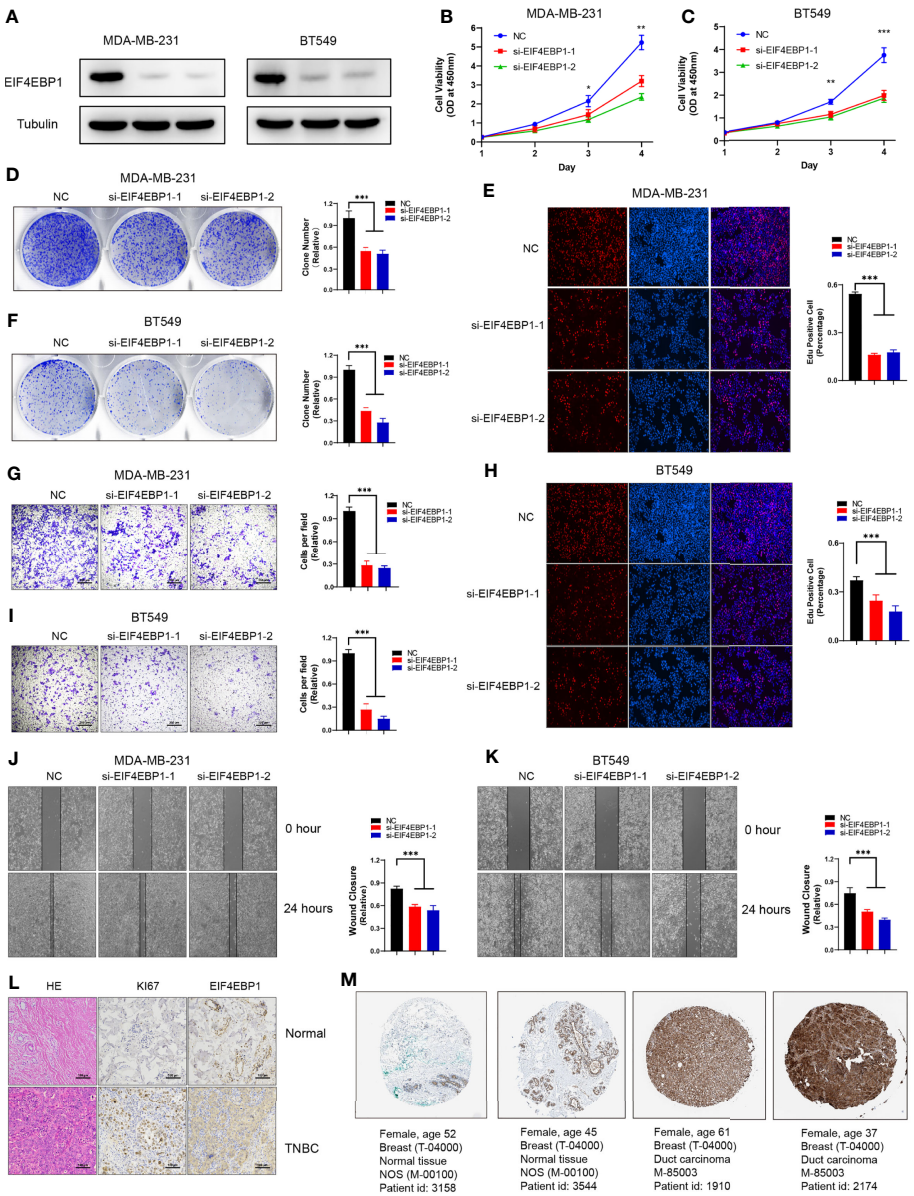

FIGURE 8 | EIF4EBP1 is required for TNBC cell survival and migration. **(A)** Western blot to show knockdown efficiency of EIF4EBP1 in MDA-MB-231 and BT549 cells by two independent siRNAs. **(B, C)** Cell proliferation of MDA-MB-231 cells **(B)** or BT549 cells **(C)** transfected with control or EIF4EBP1 siRNAs was measured by CCK8. **(D, F)** Colony formation of MDA-MB-231 cells or BT549 cells transfected with control or EIF4EBP1 siRNAs was measured by ImageJ. **(G, I)** Transwell assay to show the cell metastasis of control cells compared to EIF4EBP1 knockdown cells. **(E, H)** Edu assay to show the cell proliferation of control cells comparing to EIF4EBP1 knockdown cells. **(J, K)** Wound healing assay to show the cell migration of control cells compared to EIF4EBP1-depleted cells. **(L)** Representative images of HE staining, immunostaining of KI67, and EIF4EBP1 in primary TNBC samples versus normal samples. **(M)** Representative images of immunostaining of EIF4EBP1 in primary TNBC samples compared to normal tissues from the HPA database. All data are shown as mean ± SEM. *p < 0.05, **p < 0.01, ***p < 0.001 by one-way ANOVA.

Representative immunohistochemistry (IHC) image showed that EIF4EBP1 staining was higher in TNBC than in normal tissues (**Figure 8M**). Overall, these findings suggest a potential oncogenic role of EIF4EBP1 in TNBCs supporting the importance of our prognosis model in TNBCs.

DISCUSSION

TNBC is one of the most served malignant tumors among women in the world. Although <20% of all diagnosed breast cancer patients are triple-negative breast cancer, there are still 25%–40% of patients of the total breast cancer population with metastases, accounting for a disproportionate number of deaths from breast cancer (13). Due to the lack of targetable receptors, TNBC represents a clinically challenging endeavor. Currently, treating TNBC mainly includes adjuvant chemotherapy plus surgical resection for an early stage and adjuvant chemotherapy for an advanced stage. However, surgical resection may provide an unsatisfactory effect because of its highly invasive growth pattern and developed metastasis. Additionally, chemotherapy effects are diminished due to tumor heterogeneity. Even worse, TNBC is insensitive to the usual hormone therapies because of lack of hormone receptors expression. Therefore, it is essential to establish a novel biomarker to predict the prognosis and provide reliable treatment targets of TNBC.

Autophagy is a self-degradative process that is important for balancing sources of energy at critical times in the development and in response to cellular stress, which plays a dynamic tumor-suppressive or tumor-promoting role in different contexts and stages of cancer development (14). Expression of Beclin1 and LC3, key regulators of autophagy, are higher in TNBC cells compared to the other breast cancer subtypes, with the lowest expression in the stroma of TNBC (8). High LC3B expression is not only associated with lymph node and distant metastasis but also correlated with shorter survival in patients with triple-negative breast carcinoma (9). Moreover, knockdown of autophagy-related genes (LC3 and Beclin1) inhibits autophagy and significantly suppresses cell proliferation, colony formation, migration, and induced apoptosis in MDA-MB-231 and BT-549 TNBC cells (11). Similarly, silencing of ATG5, ATG7, and Beclin1 reduces the proliferation of different TNBC cell lines (15). These data strongly suggest that autophagy is essential to the survival of TNBC cells, indicating that therapeutic targeting of autophagy genes may be a potential therapeutic strategy for TNBC in breast cancer.

Recently, several prognostic factors have been identified in previous research with the aim of helping decision-making in pursuit of tailored individual care for TNBC patients. Yiduo Liu et al. screened four heterogeneous-related genes (FAM83B, KITLG, RBM24, and S100B) from 105 genes to construct a prognostic signature in the disease-free interval (DFI) of TNBC (16). Chao Li et al. identified a prognosis-related signature associated with energy metabolism including eight energy metabolism-associated genes (IL1RL2, FBLN7, CA3, PDE1B, SLURP1, CILP, AQP7, and TPSB) in triple-negative breast cancer (17). Ji Yeon Kim et al. obtained 13 immune-related genes to predict distant recurrence of early TNBC (18). Huan-Ming Hsu et al. unveiled six immunoglobulin genes as biomarkers in TNBC patients and explored the potential biomarkers of recurrence for TNBC (19). Fei Chen et al. identified nine steroid hormone-related genes as independent prognostic markers based on RNA-seq analysis in TNBC (20). To some degree, these models all showed better predicting ability than other clinicopathological factors and added prognostic value to the TNM staging system. Many studies have shown that autophagy plays an important role in prognosis of multiple cancers. However, to our knowledge, autophagy-related prognostic risk models have not been established for TNBC yet. It is of great significance to develop an autophagy-associated biomarker for TNBC prognosis prediction. In this study, we proposed that the prognostic risk model based on ARGs provided good prediction of prognosis for patients with TNBC, which may help clinical decision-making in pursuit of individual patient care.

In this study, we mined 43 DE-ARGs by comparing TNBC samples to normal samples. Subsequently, GO and KEGG pathways enrichment of these DE-ARGs revealed that some cancer-related signaling pathways were significantly enriched, such as autophagy, apoptosis, and HIF-1 signaling pathway. Through further univariate Cox regression and LASSO regression analysis, six ARGs (CDKN1A, CTSD, CTSL, EIF4EBP1, TMEM74, and VAMP3) were obtained. Finally, we established a prognostic signature based on the six ARGs to effectively predict the prognosis of TNBC patients.

Consistent with earlier research, these six ARGs have been reported to play multiple roles in various cancer types. A wide array of studies documented that CTSD promoted tumor growth, invasion, and metastatic dissemination in breast cancer (21–24). Wei Zhang et al. found that the CTSL expression levels in malignant ovarian tumors were significantly higher than in normal or benign tissues (25). Furthermore, Luosheng Zhang et al. also suggested that CTSL is involved in the proliferation and invasion of ovarian cancer cells (26). Some studies indicated that EIF4EBP1 is involved in the progression of various cancer types (including renal cell carcinoma, breast cancer) through regulating the transcription level of BRDT (27, 28). Kevin Luftman et al. investigated the function of VAMP3, and they found that silencing of VAMP3 could inhibit cancer metastasis (29). These results were consistent with our findings. Of note, data on the prognostic relevance of CDKN1A expression showed that increased expression of CDKN1A were associated with poor prognosis in esophageal, ovarian, prostate cancers, and gliomas (30–36). In contrast, some studies also indicated that low expression level of CDKN1A was correlated with better survival in cervical, gastric, cholangiocarcinoma, and ovarian cancers (37–39). These findings suggested the dual role of CDKN1A in cancer, which needs to be further explored. Interestingly, TMEM74 had been regarded as an oncogene in various cancers including liver cancer, lung cancer, breast cancer, colon cancer, cervical cancer, and hepatic carcinoma. Higher expression level of TMEM74

was associated with poorer survival, which was not consistent with our study (40). This could be due to the variation in genetic context in different cancer types. The high expression level of TMEM74 might play a protective role in TNBC, not in others.

This study needs to be expanded in the future, as the sample number of each cohort used is relatively small. Additionally, further studies are required to understand the role of ARGs in TNBC and its potential molecular mechanisms.

CONCLUSIONS

Based on six ARGs (CDKN1A, CTSD, CTSL, EIF4EBP1, TMEM74, and VAMP3), we developed a risk prediction model that can help clinical doctors effectively predict the survival status of TNBC patients. Our data suggested that EIF4EBP1 might promote the proliferation and migration in TNBC cell lines. These findings provided a novel insight into the vital role of the autophagy-related genes in TNBC and may provide new therapeutic targets for TNBC.

DATA AVAILABILITY STATEMENT

The original contributions presented in the study are included in the article/**Supplementary Material**. Further inquiries can be directed to the corresponding author.

ETHICS STATEMENT

The studies involving human participants were reviewed and approved by ethics committee of Xinxiang University. The patients/participants provided their written informed consent to participate in this study. Written informed consent was obtained from the individual(s) for the publication of any potentially identifiable images or data included in this article.

AUTHOR CONTRIBUTIONS

RJ designed the research and wrote the paper. CY and QL downloaded and analyzed the data. CY conducted the cell-culture-related experiment. All authors have agreed to the manuscript. All authors contributed to the article and approved the submitted version.

FUNDING

This work was supported by the Key Scientific and Technological Project of Henan Province (Grant No. 202102310416) and the Key Scientific Research Projects of Henan Colleges and Universities (Grant No. 21A310008).

ACKNOWLEDGMENTS

The authors thank the participants and staff of Xinxiang University for their contributions.

SUPPLEMENTARY MATERIAL

The Supplementary Material for this article can be found online at: https://www.frontiersin.org/articles/10.3389/fonc.2022.829045/full#supplementary-material

Supplementary Figure 1 | Mutation analysis of ARGs in TNBC in the TCGA database.

Supplementary Figure 2 | GO and KEGG enrichment analysis of DE-ARGs in TNBC. **(A)** DE-ARGs GO enrichment analysis. BP stands for biological process, CC stands for cellular component, MF stands for molecular function. **(B)** DE-ARGs KEGG enrichment analysis.

Supplementary Figure 3 | Kaplan-Meier curves of the selected six ARGs in the TCGA database were plotted.

Supplementary Figure 4 | The correlation between CTSD expression and clinicopathological variables. **(A)** The expression level of CTSD was reversely related to stage in TNBC. **(B)** The expression level of CTSD was reversely related to T stage in TNBC.

Supplementary Figure 5 | Gene set enrichment analysis (GSEA) identifies KEGG pathways associated with high-risk groups and low-risk groups in train set **(A)** and test set **(B)**.

Supplementary Figure 6 | Principal component analysis between high-risk groups and low-risk groups in train set **(A)** and test set **(B)**.

REFERENCES

1. Bray F, Ferlay J, Soerjomataram I, Siegel RL, Torre LA, Jemal A. Global Cancer Statistics 2018: GLOBOCAN Estimates of Incidence and Mortality Worldwide for 36 Cancers in 185 Countries. *CA Cancer J Clin* (2018) 68 (6):394–424. doi: 10.3322/caac.21492
2. DeSantis CE, Ma J, Gaudet MM, Newman LA, Miller KD, Goding Sauer A, et al. Breast Cancer Statistics, 2019. *CA Cancer J Clin* (2019) 69(6):438–51. doi: 10.3322/caac.21583
3. Scott LC, Mobley LR, Kuo TM, Il'yasova D. Update on Triple-Negative Breast Cancer Disparities for the United States: A Population-Based Study From the United States Cancer Statistics Database, 2010 Through 2014. *Cancer* (2019) 125(19):3412–7. doi: 10.1002/cncr.32207
4. Harbeck N, Gnant M. Breast Cancer. *Lancet* (2017) 389(10074):1134–50. doi: 10.1016/S0140-6736(16)31891-8
5. Peng F, Tang H, Liu P, Shen J, Guan X, Xie X, et al. Isoliquiritigenin Modulates miR-374a/PTEN/Akt Axis to Suppress Breast Cancer Tumorigenesis and Metastasis. *Sci Rep* (2017) 7(1):9022. doi: 10.1038/s41598-017-08422-y
6. Rabinowitz JD, White E. Autophagy and Metabolism. *Science* (2010) 330 (6009):1344–8. doi: 10.1126/science.1193497
7. Xia H, Green DR, Zou W. Autophagy in Tumour Immunity and Therapy. *Nat Rev Cancer* (2021) 21(5):281–97. doi: 10.1038/s41568-021-00344-2

8. Overgaard J, Yilmaz M, Guldberg P, Hansen LL, Alsner J. TP53 Mutation Is an Independent Prognostic Marker for Poor Outcome in Both Node-Negative and Node-Positive Breast Cancer. *Acta Oncol* (2000) 39(3):327–33. doi: 10.1080/028418600750013096
9. Zhao H, Yang M, Zhao J, Wang J, Zhang Y, Zhang Q. High Expression of LC3B Is Associated With Progression and Poor Outcome in Triple-Negative Breast Cancer. *Med Oncol* (2013) 30(1):475. doi: 10.1007/s12032-013-0475-1
10. Claude-Taupin A, Fonderflick L, Gauthier T, Mansi L, Pallandre JR, Borg C, et al. ATG9A Is Overexpressed in Triple Negative Breast Cancer and Its In Vitro Extinction Leads to the Inhibition of Pro-Cancer Phenotypes. *Cells* (2018) 7(12):248. doi: 10.3390/cells7120248
11. Hamurcu Z, Delibasi N, Gecene S, Sener EF, Donmez-Altuntas H, Ozkul Y, et al. Targeting LC3 and Beclin-1 Autophagy Genes Suppresses Proliferation, Survival, Migration and Invasion by Inhibition of Cyclin-D1 and uPAR/Integrin Beta1/Src Signaling in Triple Negative Breast Cancer Cells. *J Cancer Res Clin Oncol* (2018) 144(3):415–30. doi: 10.1007/s00432-017-2557-5
12. Singh SS, Vats S, Chia AY, Tan TZ, Deng S, Ong MS, et al. Dual Role of Autophagy in Hallmarks of Cancer. *Oncogene* (2018) 37(9):1142–58. doi: 10.1038/s41388-017-0046-6
13. Yao H, He G, Yan S, Chen C, Song L, Rosol TJ, et al. Triple-Negative Breast Cancer: Is There a Treatment on the Horizon? *Oncotarget* (2017) 8(1):1913–24. doi: 10.18632/oncotarget.12284
14. White E. The Role for Autophagy in Cancer. *J Clin Invest* (2015) 125(1):42–6. doi: 10.1172/JCI73941
15. Maycotte P, Gearheart CM, Barnard R, Aryal S, Mulcahy Levy JM, Fosmire SP, et al. STAT3-Mediated Autophagy Dependence Identifies Subtypes of Breast Cancer Where Autophagy Inhibition can be Efficacious. *Cancer Res* (2014) 74(9):2579–90. doi: 10.1158/0008-5472.CAN-13-3470
16. Liu Y, Teng L, Fu S, Wang G, Li Z, Ding C, et al. Highly Heterogeneous-Related Genes of Triple-Negative Breast Cancer: Potential Diagnostic and Prognostic Biomarkers. *BMC Cancer* (2021) 21(1):644. doi: 10.1186/s12885-021-08318-1
17. Li C, Li X, Li G, Sun L, Zhang W, Jiang J, et al. Identification of a Prognosisassociated Signature Associated With Energy Metabolism in Triplenegative Breast Cancer. *Oncol Rep* (2020) 44(3):819–37. doi: 10.3892/or.2020.7657
18. Kim JY, Jung HH, Sohn I, Woo SY, Cho H, Cho EY, et al. Prognostication of a 13-Immune-Related-Gene Signature in Patients With Early Triple-Negative Breast Cancer. *Breast Cancer Res Treat* (2020) 184(2):325–34. doi: 10.1007/s10549-020-05874-1
19. Hsu HM, Chu CM, Chang YJ, Yu JC, Chen CT, Jian CE, et al. Six Novel Immunoglobulin Genes as Biomarkers for Better Prognosis in Triple-Negative Breast Cancer by Gene Co-Expression Network Analysis. *Sci Rep* (2019) 9(1):4484. doi: 10.1038/s41598-019-40826-w
20. Chen F, Li Y, Qin N, Wang F, Du J, Wang C, et al. RNA-Seq Analysis Identified Hormone-Related Genes Associated With Prognosis of Triple Negative Breast Cancer. *J BioMed Res* (2020) 34(2):129–38. doi: 10.7555/JBR.34.20190111
21. Gemoll T, Epping F, Heinrich L, Fritzsche B, Roblick UJ, Szymczak S, et al. Increased Cathepsin D Protein Expression Is a Biomarker for Osteosarcomas, Pulmonary Metastases and Other Bone Malignancies. *Oncotarget* (2015) 6(18):16517–26. doi: 10.18632/oncotarget.4140
22. Park YJ, Kim EK, Bae JY, Moon S, Kim J. Human Telomerase Reverse Transcriptase (hTERT) Promotes Cancer Invasion by Modulating Cathepsin D *via* Early Growth Response (EGR)-1. *Cancer Lett* (2016) 370(2):222–31. doi: 10.1016/j.canlet.2015.10.021
23. Maynadier M, Farnoud R, Lamy PJ, Laurent-Matha V, Garcia M, Rochefort H. Cathepsin D Stimulates the Activities of Secreted Plasminogen Activators in the Breast Cancer Acidic Environment. *Int J Oncol* (2013) 43(5):1683–90. doi: 10.3892/ijo.2013.2095
24. Zhang M, Wu JS, Yang X, Pang X, Li L, Wang SS, et al. Overexpression Cathepsin D Contributes to Perineural Invasion of Salivary Adenoid Cystic Carcinoma. *Front Oncol* (2018) 8:492. doi: 10.3389/fonc.2018.00492
25. Zhang W, Wang S, Wang Q, Yang Z, Pan Z, Li L. Overexpression of Cysteine Cathepsin L Is a Marker of Invasion and Metastasis in Ovarian Cancer. *Oncol Rep* (2014) 31(3):1334–42. doi: 10.3892/or.2014.2967
26. Zhang L, Wei L, Shen G, He B, Gong W, Min N, et al. Cathepsin L Is Involved in Proliferation and Invasion of Ovarian Cancer Cells. *Mol Med Rep* (2015) 11(1):468–74. doi: 10.3892/mmr.2014.2706
27. Wan P, Chen Z, Zhong W, Jiang H, Huang Z, Peng D, et al. BRDT Is a Novel Regulator of Eif4ebp1 in Renal Cell Carcinoma. *Oncol Rep* (2020) 44(6):2475–86. doi: 10.3892/or.2020.7796
28. Rutkovsky AC, Yeh ES, Guest ST, Findlay VJ, Muise-Helmericks RC, Armeson K, et al. Eukaryotic Initiation Factor 4E-Binding Protein as an Oncogene in Breast Cancer. *BMC Cancer* (2019) 19(1):491. doi: 10.1186/s12885-019-5667-4
29. Luftman K, Hasan N, Day P, Hardee D, Hu C. Silencing of VAMP3 Inhibits Cell Migration and Integrin-Mediated Adhesion. *Biochem Biophys Res Commun* (2009) 380(1):65–70. doi: 10.1016/j.bbrc.2009.01.036
30. Sarbia M, Stahl M, zur Hausen A, Zimmermann K, Wang L, Fink U, et al. Expression of P21waf1 Predicts Outcome of Esophageal Cancer Patients Treated by Surgery Alone or by Combined Therapy Modalities. *Clin Cancer Res* (1998) 4(11):2615–23. doi: 10.1016/S0016-5085(00)81495-X
31. Ohashi R, Angori S, Batavia AA, Rupp NJ, Ajioka Y, Schraml P, et al. Loss of CDKN1A mRNA and Protein Expression Are Independent Predictors of Poor Outcome in Chromophobe Renal Cell Carcinoma Patients. *Cancers (Basel)* (2020) 12(2):465. doi: 10.3390/cancers12020465
32. Lin Y, Shen LY, Fu H, Dong B, Yang HL, Yan WP, et al. P21, COX-2, and E-Cadherin Are Potential Prognostic Factors for Esophageal Squamous Cell Carcinoma. *Dis Esophagus* (2017) 30(2):1–10. doi: 10.1111/dote.12522
33. Ferrandina G, Stoler A, Fagotti A, Fanfani F, Sacco R, De Pasqua A, et al. P21waf1/CIP1 Protein Expression in Primary Ovarian Cancer. *Int J Oncol* (2000) 17(6):1231–5. doi: 10.3892/ijo.17.6.1231
34. Baretton GB, Klenk U, Diebold J, Schmeller N, Lohrs U. Proliferation- and Apoptosis-Associated Factors in Advanced Prostatic Carcinomas Before and After Androgen Deprivation Therapy: Prognostic Significance of P21/WAF1/CIP1 Expression. *Br J Cancer* (1999) 80(3-4):546–55. doi: 10.1038/sj.bjc.6690390
35. Aaltomaa S, Lipponen P, Eskelinen M, Ala-Opas M, Kosma VM. Prognostic Value and Expression of P21(Waf1/Cip1) Protein in Prostate Cancer. *Prostate* (1999) 39(1):8–15. doi: 10.1002/(SICI)1097-0045(19990401)39:1<8::AID-PROS2>3.0.CO;2-N
36. Korkolopoulou P, Kouzelis K, Christodoulou P, Papanikolaou A, Thomas-Tsagli E. Expression of Retinoblastoma Gene Product and P21 (WAF1/Cip 1) Protein in Gliomas: Correlations With Proliferation Markers, P53 Expression and Survival. *Acta Neuropathol* (1998) 95(6):617–24. doi: 10.1007/s004010050848
37. Abbas T, Dutta A. P21 in Cancer: Intricate Networks and Multiple Activities. *Nat Rev Cancer* (2009) 9(6):400–14. doi: 10.1038/nrc2657
38. Lu X, Toki T, Konishi I, Nikaido T, Fujii S. Expression of P21waf1/CIP1 in Adenocarcinoma of the Uterine Cervix: A Possible Immunohistochemical Marker of a Favorable Prognosis. *Cancer* (1998) 82(12):2409–17. doi: 10.1002/(SICI)1097-0142(19980615)82:12<2409::AID-CNCR15>3.0.CO;2-T
39. Yu Y, Zhang M, Wang N, Li Q, Yang J, Yan S, et al. Epigenetic Silencing of Tumor Suppressor Gene CDKN1A by Oncogenic Long Non-Coding RNA SNHG1 in Cholangiocarcinoma. *Cell Death Dis* (2018) 9(7):746. doi: 10.1038/s41419-018-0768-6
40. Sun Y, Deng J, Xia P, Chen W, Wang L. The Expression of TMEM74 in Liver Cancer and Lung Cancer Correlating With Survival Outcomes. *Appl Immunohistochem Mol Morphol* (2019) 27(8):618–25. doi: 10.1097/PAI.0000000000000659

Conflict of Interest: The authors declare that the research was conducted in the absence of any commercial or financial relationships that could be construed as a potential conflict of interest.

frontiers in Oncology

ORIGINAL RESEARCH
published: 08 February 2022
doi: 10.3389/fonc.2022.816923

The COMT Genetic Factor Regulates Chemotherapy-Related Prospective Memory Impairment in Survivors With HER2–/+ Breast Cancer

Wen Li[†], *Qianqian Zhang*[†], *Yinlian Cai*[†], *Tingting Chen and Huaidong Cheng*[*]

Cancer Treatment Center, the Second Affiliated Hospital of Anhui Medical University, Hefei, China

Background: Previous findings indicated that polymorphism in gene catechol-O-methyltransferase (COMT) had been linked to chemotherapy-related cognitive impairment (CRCI). Nevertheless, the motivation of COMT polymorphisms in regulating cognitive impairment in breast cancer survivors with disparate status of human epidermal growth factor receptor 2 (HER2) was still vague.

Objective: The current research aimed to evaluate the regulation of the risk by COMT genotype on CRCI in breast cancer survivors with disparate status of HER2.

Methods: Breast cancer survivors (103 with HER2– and 118 with HER2+) underwent neuropsychological tests before and after chemotherapy, containing event- and time-based prospective memory (EBPM and TBPM). Three single-nucleotide polymorphisms (SNPs) were estimated by providing peripheral blood, containing COMT (rs165599, rs737865, and rs4680).

Results: The EBPM and TBPM performances was lower as compared with these before chemotherapy (z = –7.712, z = –2.403, respectively, $p < 0.01$). Furthermore, the EBPM and TBPM performances of HER2– group survivors were lower than those of HER2+ group survivors after chemotherapy (z = –7.181, $p < 0.01$; z = –2.205 $p < 0.05$, respectively). The survivors with COMT (rs165599) A/A genotype carriers had a meaningfully poorer chance of memory descend [dominant model: adjusted, OR = 2.21, CI (95%) = 1.156–4.225, $p = 0.016$] and showed better on TBPM test, relative to G/G genotype. Patients with the COMT (rs737865) A/G and G/G genotype showed protective function than the patients with the A/A and performed better on MMSE and TBPM tests.

Conclusion: The types of HER2 may be correlated to chemotherapy-related prospective memory impairments in breast cancer survivors. Furthermore, the COMT (rs165599, rs737865) polymorphisms were correlated to the risk of TBPM decline scores and possibly be a potential genetic identifying for increasing risk of CRCI in breast cancer patients with disparate status of HER2.

Keywords: catechol-O-methyltransferase (COMT), polymorphisms, chemotherapy, memory, human epidermal growth factor receptor 2 (HER2), breast cancer

OPEN ACCESS

Edited by:
San-Gang Wu,
First Affiliated Hospital of Xiamen University, China

Reviewed by:
Nian-Sheng Tzeng,
Tri-Service General Hospital, Taiwan
Manuel Pires Bicho,
University of Lisbon, Portugal

***Correspondence:**
Huaidong Cheng
chd1975ay@126.com

[†]*These authors have contributed equally to this work*

Specialty section:
This article was submitted to Breast Cancer, a section of the journal Frontiers in Oncology

Received: *17 November 2021*
Accepted: *12 January 2022*
Published: *08 February 2022*

Citation:
Li W, Zhang Q, Cai Y, Chen T and Cheng H (2022) The COMT Genetic Factor Regulates Chemotherapy-Related Prospective Memory Impairment in Survivors With HER2–/+ Breast Cancer. Front. Oncol. 12:816923. doi: 10.3389/fonc.2022.816923

INTRODUCTION

Breast cancer is the most familiar malignancy in Chinese women and the sixth main cause of cancer-related death (1). By the end of 2008, 169,452 new breast cancer cases were reported in China; 44,908 cases were related deaths (2). It is reported that 1 in 8–10 women in the United States will suffer from breast cancer during their lifetime (3). The incidence rate of breast cancer increased by about 0.3% every year from 2012 to 2016. On the contrary, the mortality rate decreased year by year, decreasing 40% from 1989 to 2017, which avoided the death of 375,900 breast cancer patients (4). Chemotherapy is one of the most main therapeutic methods for breast cancer; the 5-year survival rate of early breast cancer is close to 90%, which leads to a growing concern about the side effects of chemotherapy treatment (5). In addition to the common clinical side effects such as nausea, vomiting, bone marrow suppression, and hair loss, the impact of chemotherapy on cognitive function has attracted more and more attention in the world (6). A large body of evidence have reported that breast cancer patients experience a moderate to severe degree of cognitive impairment during or after chemotherapy (7–9). These cognitive function deficits involved memory, attention, information processing speed, executive function, and visual space function. This phenomenon is referred to as chemotherapy-related cognitive impairment (CRCI) (10). It is estimated that about 35%–70% of breast cancer patients develop CRCI after chemotherapy, which makes survivors unable to recover from pre-cancer life even after the end of treatment, having significant impact on their daily work and life and greatly reducing their quality of life (QOL) (11).

Prospective memory (PM) is outlined as the ability of remembering to carry out a purpose behavior at a convinced time or place in the future. It not only plays an important role in daily life but also an important part of advanced cognitive activities and is a key factor affecting the recovery of patients' cognitive function (12). PM was usually fallen into two groups: event-based PM (EBPM) and time-based PM (TBPM). Our previous studies found that patients with breast cancer had PM impairment after chemotherapy, especially significant deficit in EBPM (9).

Breast cancer is a highly heterogeneous malignancy; the most important research direction was concentrated in the field of molecular typing (13). The gene status of human epidermal growth factor receptor 2 (HER2) is important, which is key clinical–pathological characteristic for the prognosis recovery of breast cancer (14). There is an online comment that the main confusion in the CRCI study of breast cancer is its significant heterogeneity, as published in *CA: A Cancer Journal for Clinicians* (15). Our previous research findings simulated that heterogeneity among CRCI in breast cancer survivors with estrogen/progesterone receptor negative (ER–/PR–), showing significant damage on EBPM after chemotherapy (8). There was qualitative research that HER2 was crucial for the construction and maintenance in normal brain tissue (16). HER2 had been shown to be overexpressed in human intracranial tumors, such as gliomas, medulloblastomas, and meningiomas (17). Breast cancer with HER2+ had a higher risk of brain metastasis in comparison to those with the HER2– (18). However, the cognitive function impairment of breast cancer survivors with disparate status of HER2 after chemotherapy was still unclear.

Previous studies made known that COMT (rs4680, rs65599, and rs737865) was closely related to cognitive function (19). COMT gene played an important role in memory, executive control, response suppression, reward processing, decision analysis, and other cognitive processes through the regulation of dopaminergic concentration in the human brain (20, 21). Small et al. showed that breast cancer survivors who were COMT Val carriers were susceptible to cognitive deficits following chemotherapy (22). Furthermore, our previous studies had found that COMT (rs165599) gene was associated with retrospective memory (RM) in triple-negative breast cancer (TNBC) survivors (23). Recently, we found that COMT (rs737865) was correlated to EBPM in breast cancer patients with different hormonal receptor expression (24). However, the correlation between the chemotherapy-related PM impairment and the COMT polymorphisms in breast cancer patients with the disparate status of HER2 had not yet been illustrated.

In the current research, we attempt to survey the chemotherapy-related PM impairment in breast cancer survivors with different HER2 and clear cut the genetic features of COMT polymorphisms on CRCI in breast cancer patients with the disparate status of HER2 (HER2–, HER2+).

MATERIALS AND METHODS

Participants

A total of 221 breast cancer patients, who were recruited from 2014 to 2017 in the Department of Oncology, the Affiliated Second Hospital of Anhui Medical University, were assigned to HER2– (103 cases) or HER2+ group (118 cases).

The Research Ethics Committee of the Second Affiliated Hospital of Anhui Medical University, China, approved the research. Written informed consents were obtained from all participants before the research was conducted. Epidemiological data and blood samples were collected in accordance with ethical regulations.

All participants had exceeded 5 years of education and were all right handed. Inclusion criteria were as follows: (1) breast cancer was defined by immunohistochemical and pathological diagnosis and that positive of Her-2 was recorded as standard immunohistochemistry 3+ or ISH positive; (2) adriamycin, paclitaxel, cyclophosphamide, and fluorouracil were applied by standard chemotherapy regimen or combined with Herceptin-targeted therapy, based on chemotherapy, but no hormone therapy; (3) age and pathological type were not limited; (4) the participant could carry out normal daily activities, with Karnofsky performance status scale (KPS) scores ≥80; and (5) there are no communication barriers and could proceed with normal language communication. Exclusion criteria were as follows: (1) a history of radiotherapy and endocrine therapy;

(2) advanced cachexia; (3) metastatic encephaloma according to brain imaging examination; (4) anxiety, depression, paranoia, and other mental disorders; (5) medical history of alcohol or psychotropic drug dependence; and (6) clinical diagnose of dementia.

General Assessment of Cognitive

In accordance with the upward grouping of breast cancer survivors, a battery of cognitive tasks were performed within 1 month before chemotherapy and after six cycles of standard postoperative adjuvant chemotherapy. Mini-mental state examination (MMSE) was used to evaluate general cognitive functioning and the degree of intellect, containing seven aspects, presenting in time orientation, place orientation, immediate memory, attention and computational power, delayed memory, language, and visual space. The verbal fluency test (VFT) was reflected in the patient's ability to invoke certain kinds of things from the memory base, mainly measuring the ability of spontaneous language movement, where participants were required to speak out as many targets as they could remember in 1 min. The digit span test (DST) was applied to test patients' short-term memory, including in order and inverted order tests. Participants were required to reiterate the numbers by reading them out to the researchers. The total score corresponded to the number of the last correct character string retelling from the subjects.

Event-Based Prospective Memory Task

On each card of the 32 cards used, 12 high-frequency Chinese words were printed, of which 10 of 12 words belong to the first category (large category) and the spare two words belong to the second category (animal category). In the learning stage, the participants were required to say the two words pertaining to the small category that differed from the other 10 words on each card. The first two cards were for learning; the first card did not contain the target word, while the second one did. According to the instructions from the experimenter before the test, the target events for the PM task occurred on the 2th (exercise card), 6th, 11th, 16th, 21th, 25th, and 31th card, and each correct score was 1 point; all had 6 points. When the selected word was the target word (animal category), the participants were instructed to tap at the table. At the termination of card selection, they completed another task, that is, let the participants remember to leave their contact number (counted as 2 points). The highest scores of the event-based prospective memory (EBPM) tasks were 8 points.

Time-Based Prospective Memory Task

On each card of the 100 cards, 12 different two-digit numbers were printed. In the learning stage, participants were required to name the smallest and the largest numbers on each card. According to the instructions from experimenters before the task, when a specific goal time (i.e., at the time points of 5, 10, and 15 min after the beginning of the task), the participants were instructed to knock on the table: 2 points were endowed for responding within 10 s before and 10 s after each target time, and 1 point was endowed for responding within 30 s before and 30 s after each target time, with a topmost score of 6 points. The participant was told that the time can be checked through the clock placed 1 m away behind the subject's right shoulder. The clock was set to 0:0:0 at the beginning of the experiment, and the task was stopped when the clock indicated 17 min. The maximum score of time-based prospective memory (TBPM) was 6 points.

Genotyping

The peripheral blood (3–5 ml) of the subject was sampled into the sodium citrate anticoagulation blood tubes and reserved in the refrigerator at −80°C. Genomic DNA was picked up from the peripheral blood with blood genomic DNA Qiagen Kit (Shanghai Genesky Biotechnology Co., Ltd., http://biotech.geneskies.com), operated according to the instructions, and the extracted DNA was stored at −20°C. Genotyping was completed by Shanghai Genesky Biotechnology Co., Ltd. (Shanghai, China), utilizing the improved multiplex ligase detection reaction (iMLDR) technology. Different fluorescently labeled allele-specific oligonucleotide probe pairs were used to identify each SNP allele with high specificity. Nonspecific sequences of different lengths were introduced into the end of the ligation probe, and the ligation products were obtained by ligase chain reaction corresponding to the site. Then, the ligation products were amplified by PCR with fluorescent-labeled universal primers. The PCR-amplified products were separated by fluorescence capillary electrophoresis. Finally, GeneMapper 4.1 (Applied Biosystems, USA) was used to analyze the electropherogram; the genotyping success rate of each SNP locus was obtained. A sample accounting for 10% of the total DNA samples was randomly selected for duplicate tests for quality control.

Statistical Analysis

Statistical analysis was performed with a one-way ANOVA using SPSS software package (version 22.0, http://spss.en.softonic.com/; Chicago, IL, USA).The basic clinical data and neuropsychological tasks scores were compared between HER2– and HER2+ group. The two independent samples t-test and Mann–Whitney U-test were performed, respectively, for normal and non-normal distribution in continuous variable data. All results are presented in the forms of mean ± standard deviation (SD). Hardy–Weinberg equilibrium (HEW) was applied to analyze whether the distribution of genotype frequency of SNP loci conforms the genetic balance in two groups. In addition, the chi-square (χ^2) test was used to analyze the differences in alleles, genotype frequency, and other taxonomic variables between the two groups. Logistic regression was reported as the relative risk, odds ratio (OR), and 95% confidence interval (CI), evaluating the susceptible factors of cognitive impairment; a general genetic model (co-dominant, dominant, recessive, and additive models) to single SNP construes was covered, rectifying age, KPS, chemotherapy regimen, level of education, and pathological pattern. Binary logistic regression was applied to analyze the associations between COMT (rs165599 and rs737865) polymorphism and CRCI. A one-way ANOVA was used to

analyze the cognitive differences among different genotypes and genetic model (dominant and recessive models). All statistical results were two-tailed probability proofs, and the statistically significant standard was defined at $p < 0.05$.

RESULTS

The Basic Clinical Data for Research Objects

Table 1 has a total of 221 patients conformed to the inclusion criteria; among them, HER2− group included 103 patients, and HER2+ group included 118 patients. There was no striking difference in age (49.02 ± 10.95 vs. 48.56 ± 10.45), level of education (10.09 ± 3.63 vs. 10.10 ± 3.67), and KPS (82.91 ± 8.12 vs. 84.07 ± 7.76). Similarly, no significant differences were found for pathological patterns and cancer stages. In the HER2− group, 95 breast cancer patients were discriminated as non-special-type invasive ductal carcinoma (IDO-NOS), 3 breast cancer patients were discriminated as special-type invasive ductal carcinoma (IDO-S), and 5 patients were discriminated as microinvasive carcinoma (MIC). Similarly, in the HER2+ group, 112 breast cancer patients were discriminated as IDO-NOS, 1 breast cancer patients was identified as carcinoma *in situ* (CIS), and 5 breast cancer patient was identified as MIC. The percentages of stage I (3.9% and 5.9%, respectively) and stage II (52.4% and 48.3%, respectively) were found in breast cancer patients for the two groups. There was significant difference in chemotherapy regimen between the two groups ($\chi^2 = 32.101$, $p < 0.01$). The utilization rate of Trastuzumab accounted for about 23.7% in the HER2+ group.

General Assessment of Cognitive, EBPM, and TBPM Scores: Before and After Chemotherapy

Table 2 reveals that the MMSE was significantly lessened to 26.67 ± 1.64 after chemotherapy in comparison to that before chemotherapy (27.21 ± 1.59, $p < 0.01$). DST and VFT scores were also strikingly lessened from before (6.21 ± 0.71 and 11.43 ± 1.53, respectively) to after (5.79 ± 0.99, $p < 0.01$ and 9.93 ± 2.14, $p < 0.01$, respectively) chemotherapy. The EBPM and TBPM scores were significantly decreased after chemotherapy and manifested as 2.72 ± 0.98 vs. 1.84 ± 1.06 ($p < 0.01$), 4.95 ± 1.03 vs. 4.75 ± 0.92 ($p < 0.05$) and had a significant difference.

General Assessment of Cognitive, EBPM, and TBPM Scores: After Chemotherapy

Table 3 indicates the MMSE and TBPM scores of breast cancer patients in the HER2+ group after chemotherapy was raised (HER2−: 26.43 ± 1.65 vs. 4.62 ± 0.83; HER2+: 26.89 ± 1.60 vs.4.86 ± 0.98, p < 0.05). Significantly, the DST, VFT, and EBPM were raised in the HER2+ group and manifested as DST of 5.44 ± 0.97 vs. 6.09 ± 0.90, VFT of 9.10 ± 2.14 vs. 10.65 ± 1.86, and EBPM of 1.29 ± 1.13 vs. 2.32 ± 0.72 and had a significant difference ($p < 0.01$).

The Unit SNP Loci Analytical Results

The three SNPs of the COMT gene all conformed to Hardy–Weinberg equilibrium (HWE) for the two groups ($p > 0.05$). It indicated the SNP loci gene frequency distribution we chose from large randomly mating population.

Table 4 shows that the allelic distribution of COMT (rs165599 G vs. A; rs737865 A vs. G) were strikingly different between HER2− and HER2+ survivors ($p = 0.045$, $p = 0.012$, respectively). In **Table 5**, COMT rs165599 (co-dominant model: $\chi^2 = 6.909$, $p = 0.032$; dominant model: $\chi^2 = 6.042$, $p = 0.014$) and rs737865 (co-dominant model: $\chi^2 = 10.993$, $p = 0.004$; dominant model: $\chi^2 = 4.766$, $p = 0.029$; recessive model: $\chi^2 = 7.418$, $p = 0.006$) genotypic frequency distribution acted out strikingly different. Besides, logistic regression analysis results revealed that COMT rs165599 G/A genotypes [rectified, OR = 0.399, CI (95%) = 0.174–0.918, $p = 0.031$] had strikingly reduced occurrences of expanding cognitive descend than the patients with G/G. For the genetic model, the dominant model of rs165599 with G/A and A/A genotype [rectified, OR = 2.21, CI (95%) = 1.156–4.225, $p = 0.016$] could reduce the risk of cognitive decline. The A/G and G/G [rectified, OR = 0.178, CI (95%) = 0.054–0.579, $p = 0.004$; OR = 0.285, CI (95%) = 0.086–0.947, $p = 0.040$, respectively] genotype of the COMT rs737865 had strikingly lower odds of expanding cognitive descend than the patients with the A/A genotype. The rs737865 was discovered to strikingly enhance the venture of CRCI in the dominant model [rectified, OR = 1.999, CI (95%) = 1.139–3.509, $p = 0.016$] and recessive model [rectified, OR = 4.595, CI (95%) = 1.453–14.532, $p = 0.009$].When comparing the addictive models [rectified, OR = 0.769, CI (95%) = 0.450–1.408, $p = 0.433$], no significant correlations were established for COMT rs737865. There was no statistically striking difference in the locus of COMT rs4680 between the HER2− and HER2+ group.

The Correlation Analysis Between COMT (rs165599 and rs737865) Gene Polymorphisms and CRCI

As **Table 6** shows, the A/A genotype carriers of COMT rs165599 showed distinctly elevated scores on TBPM (4.94 ± 0.75 vs. 4.42 ± 0.71, $p < 0.05$) than G/G carriers in breast cancer patients with disparate status of HER2. Similarly, the G/G and A/G genotype carriers of COMT rs737865 represented higher scores on MMSE (HOM: 24.50 ± 2.38 vs. 26.88 ± 1.26, $p < 0.01$; HET: 25.87 ± 1.85 vs. 26.88 ± 1.26, $p < 0.01$, respectively) tests and TBPM (dominant model: 4.88 ± 0.71 vs. 4.45 ± 0.87, $p < 0.01$; HET: 4.89 ± 0.69 vs. 4.45 ± 0.87, $p < 0.01$, respectively) tests than A/A carriers.

DISCUSSION

The results of the current study revealed that, first, breast cancer survivors after chemotherapy had memory impairment on EBPM and TBPM compared to that before chemotherapy. Second, breast cancer patients with HER2− have poorer MMSE, DST, VFT, TBPM, and EBPM scores after

TABLE 1 | The basic clinical dates of breast cancer patients with HER2– and HER2+.

Items		Groups	
		A (n=103)	B (n=118)
Age (mean ± SD, year)		49.02 ± 10.95	48.56 ± 10.45
Education (mean ± SD, year)		10.09 ± 3.63	10.10 ± 3.67
KPS (mean ± SD, year)		82.91 ± 8.12	84.07 ± 7.76
Pathological patterns (%)	IDC-NOS	95 (92.2%)	112 (94.9%)
	IDC-S	3 (2.9%)	0
	CIS	0	1 (0.8%)
	MIC	5 (4.9%)	5 (4.2%)
Stages (%)	I	4 (3.9%)	7 (5.9%)
	II	54 (52.4%)	57 (48.3%)
	III	22 (21.4%)	18 (15.3%)
	IV	23 (22.3%)	36 (30.5%)
Chemotherapy regimen	PTX	6 (5.8%)	13 (11.0%)**
	Trastuzumab + chemotherapy	0	19 (16.1%)
	ADM	22 (21.4%)	28 (23.7%)
	PTX+ADM	75 (72.8%)	58 (49.2%)

***<0.01.*

KPS, Karnofsky performance status scale; IDC-NOS, non-special-type invasive ductal carcinoma of breast; IDC-S, special-type invasive ductal carcinoma of breast; CIS, carcinoma in situ; MIC, microinvasive carcinoma; PTX, pacliaxcl; ADM, adriamycin.

chemotherapy than that of patients with HER+. Third, there were significant differences on genotypes about COMT (rs165599 and rs737865) between HER– and HER+ groups; the A/A carriers of COMT rs165599 and the G/G and A/G carriers of COMT rs737865 performed more poorly than COMT (G/G, A/A, respectively) carriers on tests of TBPM in breast cancer patients with HER2–, and the COMT polymorphism may be an underlying genetic factor for the enhancement of the venture to chemotherapy-related PM impairment in breast cancer patients with disparate status of HER2. The results of this study are innovative in that they represent the first demonstration of a link between a risk factor for CRCI and COMT genotype in breast cancer patients with the disparate status of HER2.

Cancer patients will have a series of cognitive changes after chemotherapy, among which memory impairment was one of the main performances (25). Kanaskie et al. (26) believes that the changes in cognitive function are the side effects after chemotherapy for some breast cancer survivors, which include subtle changes in memory, attention, and executive function. Ibrahim et al. (27) found that Taxane-based cognitive impairment is more common in the areas of attention, executive function, and depression, and visual memory in breast cancer patients at 6 months or more after treatment. Andryszak et al. found that anthracycline-based adjuvant chemotherapy (AC) was associated with delayed memory deficits after chemotherapy, and about 19% of breast cancer patients deteriorated after treatment (28). Our previous study found that breast cancer patients mainly present with PM impairment after chemotherapy, especially EBPM deficits (9). Further research found that breast cancer patients with ER–/PR– performed worse on EBPM than those with ER+/PR+ after chemotherapy (8). In this study, 221 breast cancer patients were found to have a decline in cognitive function following chemotherapy, and in breast cancer patients with disparate expression of HER2, there exists an obvious difference in EBPM and TBPM after chemotherapy.

TABLE 2 | General assessment of cognitive before and after chemotherapy.

Task	Mean ± SD	
	Before chemotherapy (n=221)	After chemotherapy (n=221)
MMSE	27.21 ± 1.59	26.67 ± 1.64**
DST	6.21 ± 0.71	5.79 ± 0.99**
VFT	11.43 ± 1.53	9.93 ± 2.14**
EBPM	2.72 ± 0.98	1.84 ± 1.06**
TBPM	4.95 ± 1.03	4.75 ± 0.92*

**p < 0.05, **p < 0.01.*

MMSE, mini-mental state examination; DST, digit span test; VFT, verbal fluency test; EBPM, event-based prospective memory; TBPM, time-based prospective memory.

HER2 is a proto-oncogene, which can lead to resistance to tumor cells apoptosis and the proliferation tumor blood vessels and lymphatic vessels (29). HER2 was a prognostic factor, which was closely related to recurrence-free survival and overall survival; approximately 18–30% breast cancer patients shows high expression of HER2 (30). HER2-positive breast cancer patients can be assigned to luminal B (endocrine therapy responsive) or HER2 enriched (endocrine therapy unresponsive), according to their molecular subtypes (31). The combination of trastuzumab (the most widely used anti-HER2 drug) with chemotherapy resulted in significant improvement in the poor prognosis of early HER2+ breast cancer patients and reduced the recurrence risk and the mortality (32). With the application of trastuzumab, about 85% of HER2+ breast cancer patients were expected to survive for at least 10 years, and the prognosis of these patients has improved dramatically (33). Trastuzumab can prolong the survival time of breast cancer patients, but the research on the effect of anti-HER2 therapy on cognitive function is very rare and controversial, and the findings on the correlation between HER2 status and cognitive deficits are full of contradictions. Some studies showed that there was no correlation between cancer HER2 status and pre-adjuvant

TABLE 3 | General assessment of cognitive in HER2– and HER2+ groups after chemotherapy.

Task	Groups (mean ± SD)	
	Her2– (n=103)	Her2+ (n=118)
MMSE	26.43 ± 1.65	26.89 ± 1.60*
DST	5.44 ± 0.97	6.09 ± 0.90**
VFT	9.10 ± 2.14	10.65 ± 1.86**
EBPM	1.29 ± 1.13	2.32 ± 0.72**
TBPM	4.62± 0.83	4.86 ± 0.98*

*$p < 0.05$, **$p < 0.01$.
MMSE, mini-mental state; DST, digit span test; VFT, verbal fluency test; EBPM, event-based prospective memory; TBPM, time-based prospective memory.

therapy cognitive impairment in elderly breast cancer (>65 years of age) (34). On the contrary, Koleck et al. (35) found that the HER2-positive breast cancer patients were more likely to get poorer verbal, visual, and visual working memory performance compared to HER2-negative patients before adjuvant chemotherapy. One study found that the slight to significant deterioration of cognitive function was reported in breast cancer treatment following chemotherapy regimens containing trastuzumab (36). Lee et al. identified that chemo-brain was induced after trastuzumab treatment in an HER2-positive gastric cancer model, and atorvastatin could improve the cognitive impairment caused by trastuzumab (37). However, there were also findings indicating that the administration of subcutaneous trastuzumab can reduce the symptoms of nausea and vomiting caused by chemotherapy and had no negative impact on health-related quality of life (38). The incidence of suspected mild cognitive impairment was 28.6% in the trastuzumab plus chemotherapy group. It showed slightly better cognitive function than that with trastuzumab mono-therapy in HER2+ breast cancer (39). Until now, there is no report regarding CRCI in breast cancer with anti-HER2 therapy. In this study, breast cancer patients with HER2– have a more significant damage on neuropsychological tasks than patients with HER2+. This may be due to the improvement of cognitive function in patients with trastuzumab combined with chemotherapy. In the HER2– group, TNBC patients accounted 78.64%; the CRCI of this group was strikingly higher than that of the HER2+ group, which was consistent with our previous research (23).

The COMT gene was expressed throughout the brain, and its translation products played a key role in clearing catecholamines, such as dopamine, epinephrine, and norepinephrine (40). The expression level and product of COMT gene are affected by many factors. Breast cancer is a tumor closely associated with estrogen, and estrogen could downregulate the level of COMT gene, decreasing the activity of COMT enzyme (41). It has been found that estrogen inhibits COMT gene transcription *via* promoter reporter gene (42). Estrogen enhanced the promoters of DNMT3B, MBD2, and HDAC1 in breast cancer cells and reduced COMT transcription, resulting in increased DNA oxidative damage (43). Catecholestrogens were estradiol and estrone metabolites produced in breast cancer cells, and its derivatives could initiate estrogen receptor-mediated processes (44). The expression of COMT mRNA and protein was decreased by the proinflammatory cytokine tumor necrosis factor alpha (TNFα) in astrocytes, and neuroinflammation could be found in the recovery phase (45). There were at least eight different SNPs loci obtained on COMT gene, among which Val158Met locus had been studied the most frequently (46). COMT polymorphisms are manifested as a valine (Val or G) and methionine (Met or A) mutation at codon 158. The activity of the COMT enzyme with the Met carriers was three- to fourfold reduced than that with the Val carriers, increasing the dopaminergic concentration of synapses in the human brain (47). McIntosh et al. (48) found that the anterior cingulate cortex of Val homozygous carriers was significantly smaller than that of met carriers in schizophrenic patients; the altered brain structure could lead to cognitive impairment. COMT gene was widely expressed in the hippocampus and was associated with memory function (19, 49). Correa et al. (50) found that COMT SNPs were strikingly associated with attention, executive functions, and memory scores in patients with brain tumor. Matsuzaka et al. (51) showed the relationship between the two SNPs of the COMT (rs165599 and rs737865) and working memory; the cognition in schizophrenia patients may be modulated by COMT. Compared with healthy controls, breast cancer patients receiving chemotherapy had slower treatment speed and poorer executive function, while apolipoprotein E (APOE) and COMT gene polymorphisms were associated with cognitive impairment (52).Our previous research findings indicated that

TABLE 4 | Information about three genotyped SNPs loci of COMT gene in HER2– and HER2+ groups .

SNP	COMT		
	rs4680	rs165599	rs737865
CHR	22	22	22
Allele position	19951271	19956781	19930121
Ref allele	G	G	A
Alt allele	A	A	G
MAF	0.233	0.422	0.226
P for HWE	0.279	0.227	0.261
p*	0.648	0.045	0.012

SNP, single-nucleotide polymorphism; CHR, chromosome; Ref allele, loci alleles on the reference sequence; Alt allele, the other allele on the loci; MAF, minor allele frequency (data from 1000 Genomes); HWE, Hardy–Weinberg equilibrium, p-value for HWE in two groups.
**p-value for allele frequency differences between two groups.*

TABLE 5 | Genotype frequencies of SNPs of the COMT (rs4680, rs165599, and rs737865) genes between two groups.

SNP	Model	Genotype	Her2 (–)	Her2 (+)	p^a (χ^2)	Logistic regression	
						OR (95%CI)	p^b
rs4680	Co-dominant	G/G	63	65		–	–
		G/A	32	44	0.615	1.192 (0.409-3.478)	0.747
		A/A	8	9		1.597 (0.524-4.865)	0.410
	Dominant	G/A+A/A	40	53	0.361	1.233 (0.706-2.153)	0.461
		G/G	63	65			
	Recessive	A/A	8	9	0.969	0.752 (0.263-2.147)	0.594
		G/G+G/A	95	109			
	Addictive	–	–	–	–	0.732 (0.409-1.308)	0.292
rs165599	Co-dominant	G/G	33	21		–	–
		G/A	53	67	0.032	0.399 (0.174-0.918)	0.031
		A/A	17	30		0.84 (0.407-1.736)	0.638
	Dominant	G/A+A/A	70	97	0.014	2.21 (1.156-4.225)	0.016
		G/G	33	21			
	Recessive	A/A	17	30	0.106	1.511 (0.758-3.014)	0.241
		G/G+G/A	86	88			
	Addictive	–	–	–	–	0.72 (0.413-1.255)	0.246
rs737865	Co-dominant	A/A	60	52		–	–
		A/G	38	47	0.004	0.178 (0.054-0.579)	0.004
		G/G	4	19		0.285 (0.086-0.947)	0.040
	Dominant	A/G+G/G	42	66	0.029	1.999 (1.139-3.509)	0.016
		A/A	60	52			
	Recessive	G/G	4	19	0.006	4.595 (1.453-14.532)	0.009
		A/A+A/G	98	99			
	Addictive	–	–	–	–	0.769 (0.450-1.408)	0.433

[a]The χ^2 test of p-values for SNP polymorphisms distribution differences between Her2(–) and Her2(+) group.

[b]p-value for logistic regression analysis; odds ratio (the OR); 95% confidence interval (95%CI); models: various genetic models that were defined as 1 (MM + Mm) versus 0 (mm) for dominant; 1 (mm) versus 0 (MM + Mm) for recessive; and 0 (mm) versus 1 (Mm) versus 2 (MM) for additive and co-dominant (M and m represent major and minor alleles, respectively).

COMT (rs165599) was a risk-related genetic factor influencing CRCI in TNBC patients (23). Further study found that COMT (rs737865) was correlated with EBPM damage following chemotherapy in breast cancer with different expressions of hormone receptor (24). In this study, the A/A genotype carriers of COMT (rs165599) and G/G genotype carriers of COMT (rs737865) had higher scores on TBPM after chemotherapy and were genetic risks for CRCI in breast cancer with disparate expression of HER2.

Finally, limitations of this research should be recognized. First, this research only compared the changes in cognitive function in breast cancer patients with disparate expressions of

TABLE 6 | Comparison for neuropsychological performance of COMT (rs165599 and rs737865) genotypes and genetic model.

rs165599	Dominant		Recessive		HOM		HET	
	G/A+A/A vs. G/G		A/A vs. G/G+G/A		A/A vs. G/G		G/A vs. G/G	
MMSE	26.27 ± 1.72	26.76 ± 1.48	26.29 ± 1.65	26.45 ± 1.66	26.29 ± 1.65	26.76 ± 1.48	26.26 ± 1.76	26.76 ± 1.48
DST	5.42 ± 0.97	5.49 ± 0.98	5.56 ± 1.03	5.42 ± 0.96	5.56 ± 1.03	5.49 ± 0.98	5.38 ± 0.95	5.49 ± 0.98
VFT	8.87 ± 2.14	9.58 ± 2.09	9.35 ± 2.03	9.05 ± 2.17	9.35 ± 2.03	9.58 ± 2.09	8.72 ± 2.17	9.58 ± 2.09
EBPM	1.34 ± 1.17	1.18 ± 1.04	1.71 ± 1.36	1.21 ± 1.06	1.71 ± 1.36	1.18 ± 1.04	1.23 ± 1.09	1.18 ± 1.04
TBPM	4.71 ± 0.87	4.42 ± 0.71	4.94 ± 0.75	4.56 ± 0.84	4.94 ± 0.75	4.42 ± 0.71*	4.64 ± 0.90	4.42 ± 0.71
rs737865	**Dominant**		**Recessive**		**HOM**		**HET**	
	A/G+G/G vs. A/A		**G/G vs. A/A+A/G**		**G/G vs. A/A**		**A/G vs. A/A**	
MMSE	25.74 ± 1.91	26.88 ± 1.26**	24.50 ± 2.38	26.49 ± 1.59*	24.50 ± 2.38	26.88 ± 1.26**	25.87 ± 1.85	26.88 ± 1.26**
DST	5.52 ± 1.04	5.39 ± 0.92	5.25 ± 0.96	5.45 ± 0.97	5.25 ± 0.96	5.39 ± 0.92	5.55 ± 1.06	5.39 ± 0.92
VFT	8.93 ± 1.92	9.25 ± 2.29	8.75 ± 2.75	9.13 ± 2.13	8.75 ± 2.75	9.25 ± 2.29	8.89 ± 1.86	9.25 ± 2.29
EBPM	1.12 ± 1.09	1.43 ± 1.14	1.75 ± 1.50	1.29 ± 1.11	1.75 ± 1.50	1.43 ± 1.14	1.05 ± 1.04	1.43 ± 1.14
TBPM	4.88 ± 0.71	4.45 ± 0.87**	4.75 ± 0.96	4.62 ± 0.83	4.75 ± 0.96	4.45 ± 0.87	4.89 ± 0.69	4.45 ± 0.87**

**p < 0.05; **p < 0.01.*

MMSE, mini-mental state; DST, digit span test; VFT, verbal fluency test; EBPM, event-based prospective memory; TBPM, time-based prospective memory.

Models: Various genetic models that were defined as 1 (MM + Mm) versus 0 (mm) for dominant; 1 (mm) versus 0 (MM + Mm) for recessive; homozygote (HOM); heterozygote (HET).

HER2 before and after chemotherapy, lacking a healthy control group. Second, follow-up study was lacking. Cognitive impairments following chemotherapy may change in the later follow-up period. Thus, further research is needed. Third, the results were subjective memory impairment; further objective cognitive tests need to be clarified in future research. Fourth are the impacts of chemotherapy regimens. If some regimens had negative effects on cognitive function, but others did not, the effects of the former would be diluted and undetectable. Finally, the sample size in this research was small, and the numbers of breast cancer patients were scarce, therefore needing further supplement.

In a word, our study preliminarily found some differences in chemotherapy-related PM impairment and genetic polymorphisms in breast cancer patients with the disparate HER2. The heterogeneity of CRCI may be rectified by COMT (rs165599, rs737865) polymorphism, and this rectification may possibly show that COMT polymorphism is a risk leading to a lower memory performance in breast cancer patients with disparate HER2.

CONCLUSION

In brief, we conducted the discrepancy between chemotherapy-related PM impairment and genetic polymorphisms in patients with HER2–/+ breast cancer. The consequences indicated that the heterogeneity of CRCI may be regulated by COMT (rs165599 and rs737865), which may affect the CRCI in breast cancer with disparate status of HER2.

DATA AVAILABILITY STATEMENT

The datasets presented in this study can be found in online repositories. The names of the repository/repositories and accession number(s) can be found below: https://www.ncbi.nlm.nih.gov/, 111.

ETHICS STATEMENT

The studies involving human participants were reviewed and approved by the Research Ethics Committee of the Second Affiliated Hospital of Anhui Medical University. The patients/participants provided their written informed consent to participate in this study.

AUTHOR CONTRIBUTIONS

WL performed data collection, cognitive tests, EBPM and TBPM task, and blood collection. QZ and YC performed statistical analysis. TC performed data acquisition. HC designed the project and wrote the manuscript. All authors contributed to the article and approved the submitted version.

ACKNOWLEDGMENTS

This research was supported by the National Natural Science Foundation of China (No. 81872504).

REFERENCES

1. Wang X, Wang C, Guan J, Chen B, Xu L, Chen C. Progress of Breast Cancer Basic Research in China. *Int J Biol Sci* (2021) 17(8):2069–79. doi: 10.7150/ijbs.60631
2. Fan L, Strasser-Weippl K, Li JJ, St Louis J, Finkelstein DM, Yu KD, et al. Breast Cancer in China. *Lancet Oncol* (2014) 15(7):e279–89. doi: 10.1016/S1470-2045(13)70567-9
3. Harbeck N, Gnant M. Breast Cancer. *Lancet* (2017) 389(10074):1134–50. doi: 10.1016/S0140-6736(16)31891-8
4. DeSantis CE, Ma J, Gaudet MM, Newman LA, Miller KD, Goding Sauer A, et al. Breast Cancer Statistics, 2019. *CA: Cancer J Clin* (2019) 69(6):438–51. doi: 10.3322/caac.21583
5. Keetile NM, Osuch E, Lentoor AG. Chemotherapy-Related Subjective Cognitive Impairment in Breast Cancer Patients in Semi-Rural South Africa. *Health SA SA Gesondheid* (2021) 26:1605. doi: 10.4102/hsag.v26i0.1605
6. Huehnchen P, van Kampen A, Boehmerle W, Endres M. Cognitive Impairment After Cytotoxic Chemotherapy. *Neuro-Oncol Pract* (2020) 7(1):11–21. doi: 10.1093/nop/npz052
7. Hsu YH, Chen VC, Hsieh CC, Weng YP, Hsu YT, Hsiao HP, et al. Subjective and Objective Cognitive Functioning Among Patients With Breast Cancer: Effects of Chemotherapy and Mood Symptoms. *Breast Cancer* (2021) 28(1):236–45. doi: 10.1007/s12282-020-01168-y
8. Li W, Gan C, Lv Y, Wang S, Cheng H. Chemotherapy-Induced Prospective Memory Impairment in Breast Cancer Patients With Different Hormone Receptor Expression. *Medicine* (2017) 96(13):e6514. doi: 10.1097/MD.0000000000006514
9. Cheng H, Yang Z, Dong B, Chen C, Zhang M, Huang Z, et al. Chemotherapy-Induced Prospective Memory Impairment in Patients With Breast Cancer. *Psycho-Oncology* (2013) 22(10):2391–5. doi: 10.1002/pon.3291
10. de Ruiter MB, Reneman L, Kieffer JM, Oldenburg HSA, Schagen SB. Brain White Matter Microstructure as a Risk Factor for Cognitive Decline After Chemotherapy for Breast Cancer. *J Clin Oncol Off J Am Soc Clin Oncol* (2021) 39(35):3908–17. doi: 10.1200/JCO.21.00627
11. Runowicz CD, Leach CR, Henry NL, Henry KS, Mackey HT, Cowens-Alvarado RL, et al. American Cancer Society/American Society of Clinical Oncology Breast Cancer Survivorship Care Guideline. *J Clin Oncol Off J Am Soc Clin Oncol* (2016) 34(6):611–35. doi: 10.1200/JCO.2015.64.3809
12. Lin SZ, Wu YK, Su YA, Si TM. Prospective Memory in non-Psychotic First-Degree Relatives of Patients With Schizophrenia: A Meta-Analysis. *Neuropsychiatr Dis Treat* (2019) 15:1563–71. doi: 10.2147/NDT.S203729
13. Kurozumi S, Katayama A, Shirabe K, Horiguchi J, Rakha EA. Clinicopathological Utility of Human Epidermal Growth Factor Receptor 2 (HER2)-Heterogeneity for Next-Generation Treatments of Triple-Negative Breast Cancer. *Oncotarget* (2021) 12(22):2302–4. doi: 10.18632/oncotarget.28007
14. Li YL, Qin YC, Tang LY, Liao YH, Zhang W, Xie XM, et al. Patient and Care Delays of Breast Cancer in China. *Cancer Res Treat* (2019) 51(3):1098–106. doi: 10.4143/crt.2018.386
15. Barton MK. Cognitive Deficits are Usually Mild in Patients With Breast Cancer After Chemotherapy. *CA: Cancer J Clin* (2013) 63(1):3–4. doi: 10.3322/caac.21164
16. Waage IS, Vreim I. Torp SH. C-Erbb2/HER2 in Human Gliomas, Medulloblastomas, and Meningiomas: A Minireview. *Int J Surg Pathol* (2013) 21(6):573–82. doi: 10.1177/1066896913492196
17. Schmid RS, McGrath B, Berechid BE, Boyles B, Marchionni M, Sestan N, et al. Neuregulin 1-Erbb2 Signaling Is Required for the Establishment of Radial Glia and Their Transformation Into Astrocytes in Cerebral Cortex. *Proc Natl Acad Sci USA* (2003) 100(7):4251–6. doi: 10.1073/pnas.0630496100

18. Kennecke H, Yerushalmi R, Woods R, Cheang MC, Voduc D, Speers CH, et al. Metastatic Behavior of Breast Cancer Subtypes. *J Clin Oncol Off J Am Soc Clin Oncol* (2010) 28(20):3271–7. doi: 10.1200/JCO.2009.25.9820
19. Tougu P, Tulviste T, Veidebaum T, Harro J. Schoolchildren's Autobiographical Memory: COMT Gene Val(158)Met Polymorphism Effects on Emotional Content and Quality of First Memories. *Cogn Process* (2021). doi: 10.1007/s10339-021-01064-z
20. Wing VC, Tang YL, Sacco KA, Cubells JF, George TP. Effect of COMT Val (158)Met Genotype on Nicotine Withdrawal-Related Cognitive Dysfunction in Smokers With and Without Schizophrenia. *Schizophr Res* (2013) 150(2-3):602–3. doi: 10.1016/j.schres.2013.09.005
21. Favaro A, Clementi M, Manara R, Bosello R, Forzan M, Bruson A, et al. Catechol-O-Methyltransferase Genotype Modifies Executive Functioning and Prefrontal Functional Connectivity in Women With Anorexia Nervosa. *J Psychiatry Neurosci JPN* (2013) 38(4):241–8. doi: 10.1503/jpn.120068
22. Small BJ, Rawson KS, Walsh E, Jim HS, Hughes TF, Iser L, et al. Catechol-O-Methyltransferase Genotype Modulates Cancer Treatment-Related Cognitive Deficits in Breast Cancer Survivors. *Cancer* (2011) 117(7):1369–76. doi: 10.1002/cncr.25685
23. Cheng H, Li W, Gan C, Zhang B, Jia Q, Wang K. The COMT (Rs165599) Gene Polymorphism Contributes to Chemotherapy-Induced Cognitive Impairment in Breast Cancer Patients. *Am J Trans Res* (2016) 8(11):5087–97.
24. Li W, Zhao J, Ding K, Chao HH, Li CR, Cheng H, et al. Catechol-O-Methyltransferase Gene Polymorphisms and the Risk of Chemotherapy-Induced Prospective Memory Impairment in Breast Cancer Patients With Varying Tumor Hormonal Receptor Expression. *Med Sci Monitor Int Med J Exp Clin Res* (2020) 26:e923567. doi: 10.12659/MSM.923567
25. Oyovwi MO, Ben-Azu B, Edesiri TP, Victor E, Rotu RA, Ozegbe QEB, et al. Kolaviron Abates Busulfan-Induced Episodic Memory Deficit and Testicular Dysfunction in Rats: The Implications for Neuroendopathobiological Changes During Chemotherapy. *Biomed Pharmacother Biomed Pharmacother* (2021) 142:112022. doi: 10.1016/j.biopha.2021.112022
26. Kanaskie ML, Loeb SJ. The Experience of Cognitive Change in Women With Breast Cancer Following Chemotherapy. *J Cancer Survivorship Res Pract* (2015) 9(3):375–87. doi: 10.1007/s11764-014-0387-x
27. Ibrahim EY, Domenicano I, Nyhan K, Elfil M, Mougalian SS, Cartmel B, et al. Cognitive Effects and Depression Associated With Taxane-Based Chemotherapy in Breast Cancer Survivors: A Meta-Analysis. *Front Oncol* (2021) 11:642382. doi: 10.3389/fonc.2021.642382
28. Andryszak P, Wilkosc M, Zurawski B, Izdebski P. Verbal Memory in Breast Cancer Patients Treated With Chemotherapy With Doxorubicin and Cyclophosphamide. *Eur J Cancer Care* (2018) 27(1):e12749. doi: 10.1111/ecc.12749
29. Jinga DC, Jinga MR, Miron A, Noditi A, Blidaru A. Pathological Response and Survival After Neoadjuvant Therapy for Her-2 Positive Breast Cancer. *Chirurgia* (2021) 116(2 Suppl):91–7. doi: 10.21614/rurgia.116.2Suppl.S91
30. Cronin KA, Harlan LC, Dodd KW, Abrams JS, Ballard-Barbash R. Population-Based Estimate of the Prevalence of HER-2 Positive Breast Cancer Tumors for Early Stage Patients in the US. *Cancer Invest* (2010) 28 (9):963–8. doi: 10.3109/07357907.2010.496759
31. Harbeck N. Insights Into Biology of Luminal HER2 vs. Enriched HER2 Subtypes: Therapeutic Implications. *Breast* (2015) 24 Suppl 2:S44–8. doi: 10.1016/j.breast.2015.07.011
32. Daniels B, Kiely BE, Houssami N, Lord SJ, Dobbins T, Lu CY, et al. Survival Outcomes for Australian Women Receiving Trastuzumab for HER2-Positive Metastatic Breast Cancer Following (Neo)Adjuvant Trastuzumab: A National Population-Based Observational Study (2006-2014). *Br J Cancer* (2018) 118 (3):441–7. doi: 10.1038/bjc.2017.405
33. Kreutzfeldt J, Rozeboom B, Dey N, De P. The Trastuzumab Era: Current and Upcoming Targeted HER2+ Breast Cancer Therapies. *Am J Cancer Res* (2020) 10(4):1045–67.
34. Lange M, Giffard B, Noal S, Rigal O, Kurtz JE, Heutte N, et al. Baseline Cognitive Functions Among Elderly Patients With Localised Breast Cancer. *Eur J Cancer* (2014) 50(13):2181–9. doi: 10.1016/j.ejca.2014.05.026
35. Koleck TA, Bender CM, Sereika SM, Ryan CM, Ghotkar P, Brufsky AM, et al. Associations Between Pathologic Tumor Features and Preadjuvant Therapy Cognitive Performance in Women Diagnosed With Breast Cancer. *Cancer Med* (2017) 6(2):339–48. doi: 10.1002/cam4.964
36. Garcia-Sanchez J, Torregrosa MD, Cauli O. Cognitive Functions Under Anti-HER2 Targeted Therapy in Cancer Patients: A Scoping Review. *Endocrine Metab Immune Disord Drug Targets* (2021) 21(7):1163–70. doi: 10.2174/1871530320666200729153009
37. Lee S, Lee HJ, Kang H, Kim EH, Lim YC, Park H, et al. Trastuzumab Induced Chemobrain, Atorvastatin Rescued Chemobrain With Enhanced Anticancer Effect and Without Hair Loss-Side Effect. *J Clin Med* (2019) 8(2):234. doi: 10.3390/jcm8020234
38. Syrios J, Pappa E, Volakakis N, Grivas A, Alafis J, Manioudaki S, et al. Real-World Data on Health-Related Quality of Life Assessment in Patients With Breast Cancer Receiving Subcutaneous Trastuzumab. *Breast Cancer Basic Clin Res* (2018) 12:1178223418758031. doi: 10.1177/1178223418758031
39. Hagiwara Y, Sawaki M, Uemura Y, Kawahara T, Shimozuma K, Ohashi Y, et al. Impact of Chemotherapy on Cognitive Functioning in Older Patients With HER2-Positive Breast Cancer: A Sub-Study in the RESPECT Trial. *Breast Cancer Res Treat* (2021) 188(3):675–83. doi: 10.1007/s10549-021-06253-0
40. Bonetti L, Bruzzone SEP, Sedghi NA, Haumann NT, Paunio T, Kantojarvi K, et al. Brain Predictive Coding Processes Are Associated to COMT Gene Val158Met Polymorphism. *NeuroImage* (2021) 233:117954. doi: 10.1016/j.neuroimage.2021.117954
41. Jiang H. Human Catechol-O-Methyltransferase Down-Regulation by Estradiol. *Neuropharmacology* (2003) 45(7):1011–8. doi: 10.1016/s0028-3908(03)00286-7
42. Xie T, Ho SL, Ramsden D. Characterization and Implications of Estrogenic Down-Regulation of Human Catechol-O-Methyltransferase Gene Transcription. *Mol Pharmacol* (1999) 56(1):31–8. doi: 10.1124/mol.56.1.31
43. Wu Q, Odwin-Dacosta S, Cao S, Yager JD, Tang WY. Estrogen Down Regulates COMT Transcription *via* Promoter DNA Methylation in Human Breast Cancer Cells. *Toxicol Appl Pharmacol* (2019) 367:12–22. doi: 10.1016/j.taap.2019.01.016
44. Schutze N, Vollmer G, Tiemann I, Geiger M, Knuppen R. Catecholestrogens are MCF-7 Cell Estrogen Receptor Agonists. *J Steroid Biochem Mol Biol* (1993) 46(6):781–9. doi: 10.1016/0960-0760(93)90319-r
45. Tchivileva IE, Nackley AG, Qian L, Wentworth S, Conrad M, Diatchenko LB. Characterization of NF-kB-Mediated Inhibition of Catechol-O-Methyltransferase. *Mol Pain* (2009) 5:13. doi: 10.1186/1744-8069-5-13
46. Caldu X, Ottino-Gonzalez J, Sanchez-Garre C, Hernan I, Tor E, Sender-Palacios MJ, et al. Effect of the Catechol-O-Methyltransferase Val (158) Met Polymorphism on Theory of Mind in Obesity. *Eur Eating Disord Rev J Eating Disord Assoc* (2019) 27(4):401–9. doi: 10.1002/erv.2665
47. Vai B, Riberto M, Poletti S, Bollettini I, Lorenzi C, Colombo C, et al. Catechol-O-Methyltransferase Val(108/158)Met Polymorphism Affects Fronto-Limbic Connectivity During Emotional Processing in Bipolar Disorder. *Eur Psychiatry J Assoc Eur Psychiatrists* (2017) 41:53–9. doi: 10.1016/j.eurpsy.2016.10.002
48. McIntosh AM, Baig BJ, Hall J, Job D, Whalley HC, Lymer GK, et al. Relationship of Catechol-O-Methyltransferase Variants to Brain Structure and Function in a Population at High Risk of Psychosis. *Biol Psychiatry* (2007) 61(10):1127–34. doi: 10.1016/j.biopsych.2006.05.020
49. Laatikainen LM, Sharp T, Bannerman DM, Harrison PJ, Tunbridge EM. Modulation of Hippocampal Dopamine Metabolism and Hippocampal-Dependent Cognitive Function by Catechol-O-Methyltransferase Inhibition. *J Psychopharmacol* (2012) 26(12):1561–8. doi: 10.1177/0269881112454228
50. Correa DD, Satagopan J, Cheung K, Arora AK, Kryza-Lacombe M, Xu Y, et al. COMT, BDNF, and DTNBP1 Polymorphisms and Cognitive Functions in Patients With Brain Tumors. *Neuro-Oncology* (2016) 18(10):1425–33. doi: 10.1093/neuonc/now057
51. Matsuzaka CT, Christofolini D, Ota VK, Gadelha A, Berberian AA, Noto C, et al. Catechol-O-Methyltransferase (COMT) Polymorphisms Modulate Working Memory in Individuals With Schizophrenia and Healthy Controls. *Rev Bras Psiquiatria* (2017) 39(4):302–8. doi: 10.1590/1516-4446-2016-1987
52. Harrison RA, Rao V, Kesler SR. The Association of Genetic Polymorphisms With Neuroconnectivity in Breast Cancer Patients. *Sci Rep* (2021) 11(1):6169. doi: 10.1038/s41598-021-85768-4

Conflict of Interest: The authors declare that the research was conducted in the absence of any commercial or financial relationships that could be construed as a potential conflict of interest.

this article, or claim that may be made by its manufacturer, is not guaranteed or endorsed by the publisher.

frontiers in Oncology

ORIGINAL RESEARCH
published: 24 February 2022
doi: 10.3389/fonc.2022.804466

Co-Expression and Combined Prognostic Value of CSPG4 and PDL1 in *TP53*-Aberrant Triple-Negative Breast Cancer

Zhe-Yu Hu[1,2,3†], *Chanjuan Zheng*[4,5†], *Jianbo Yang*[1,6,7†], *Siyu Ding*[4,5], *Can Tian*[1,2,3], *Ning Xie*[1,2,3], *Lian Xue*[4,5], *Muyao Wu*[4,5], *Shujun Fu*[4,5], *Zhouzhou Rao*[4,5], *Matthew A. Price*[6], *James B. McCarthy*[6], *Quchang Ouyang*[1,2,3*], *Jizhen Lin*[7,8*] and *Xiyun Deng*[4,5*]

[1] Hunan Cancer Hospital and the Affiliated Cancer Hospital of Xiangya Medical School, Central South University, Changsha, China, [2] Department of Breast Cancer Medical Oncology, Hunan Cancer Hospital, Changsha, China, [3] Department of Breast Cancer Medical Oncology, the Affiliated Cancer Hospital of Xiangya Medical School, Central South University, Changsha, China, [4] Key Laboratory of Model Animals and Stem Cell Biology in Hunan Province, Department of Pathophysiology, Hunan Normal University School of Medicine, Changsha, China, [5] Key Laboratory of Translational Cancer Stem Cell Research, Hunan Normal University, Changsha, China, [6] Department of Laboratory Medicine and Pathology and Comprehensive Cancer Center, University of Minnesota, Minneapolis, MN, United States, [7] The Cancer Center, Union Hospital, Fujian Medical Center, Fuzhou, China, [8] Department of Otolaryngology, Cancer Center, University of Minnesota Medical School, Minnesota, MN, United States

OPEN ACCESS

Edited by:
San-Gang Wu,
First Affiliated Hospital of Xiamen University, China

Reviewed by:
Qingkun Song,
Capital Medical University, China
Juan Zhou,
Xiamen University, China

***Correspondence:**
Quchang Ouyang
oyqc1969@126.com
Jizhen Lin
linxx004@umn.edu
Xiyun Deng
dengxiyunmed@hunnu.edu.cn

[†]These authors have contributed equally to this work

Specialty section:
This article was submitted to Breast Cancer, a section of the journal Frontiers in Oncology

Received: 29 October 2021
Accepted: 31 January 2022
Published: 24 February 2022

Citation:
Hu Z-Y, Zheng C, Yang J, Ding S, Tian C, Xie N, Xue L, Wu M, Fu S, Rao Z, Price MA, McCarthy JB, Ouyang Q, Lin J and Deng X (2022) Co-Expression and Combined Prognostic Value of CSPG4 and PDL1 in TP53-Aberrant Triple-Negative Breast Cancer. Front. Oncol. 12:804466. doi: 10.3389/fonc.2022.804466

Background: In triple-negative breast cancer (TNBC), PDL1/PD1-directed immunotherapy is effective in less than 20% of patients. In our preliminary study, we have found CSPG4 to be highly expressed together with PDL1 in TNBCs, particularly those harboring *TP53* aberrations. However, the clinical implications of co-expressed CSPG4 and PDL1 in TNBCs remain elusive.

Methods: A total of 85 advanced TNBC patients treated in the Hunan Cancer Hospital between January 2017 and August 2019 were recruited. The expressions of CSPG4 and PDL1 in TNBC tissues were investigated using immunohistochemistry (IHC). The RNA-seq dataset from the TCGA-BRCA project was further used to analyze the mRNA expression of CSPG4 and PDL1 in *TP53*-aberrant TNBCs. Cox proportional hazards model and Kaplan–Meier curves with Logrank test was used to analyze the effects of CSPG4 and PDL1 on survival. TNBC cell lines were further used to investigate the molecular mechanism that were involved.

Results: *TP53* aberrations occurred in more than 50% of metastatic TNBCs and were related to higher tumor mutation burden (TMB). In TCGA-BRCA RNA-seq dataset analysis, both CSPG4 and PDL1 levels were high in TNBCs, especially in *TP53*-aberrant TNBCs. IHC assay showed nearly 60% of advanced TNBCs to be CSPG4-positive and about 25% to be both CSPG4-positive and PDL1-positive. The levels of CSPG4 and PDL1 were high in TNBC cell lines as revealed by flow cytometry and immunoblotting compared with non-TNBC cells. Univariate Cox regression analysis indicated that CSPG4 positivity was a significant risk factor for progression-free survival in metastatic TNBCs, with a hazard ratio (HR) of 2.26 ($P = 0.05$). KM curves with Logrank

test also identified high level of CSPG4 as a significant risk factor for overall survival in advanced breast cancers in TCGA-BRCA samples ($P = 0.02$). The immunoblotting assays showed that EMT-related pathways were involved in CSPG4-mediated invasion.

Conclusions: CSPG4 expression level is associated with PDL1 positivity in *TP53*-aberrant TNBC cells. Patients with CSPG4 expression have poor treatment response and poor overall survival. Co-expressed CSPG4 and PDL1 may have an important prognostic value and provide new therapeutic targets in TNBC patients. CSPG4 might mediate tumor invasion and PDL1 overexpression through EMT-related pathway.

Keywords: triple-negative breast cancer, *TP53* aberration, chondroitin sulfate proteoglycan 4, programmed cell death ligand 1, prognosis

INTRODUCTION

Breast cancer is the most common malignancy threatening the health of women around the world. Triple-negative breast cancer (TNBC) is characterized by negative expression of the hormone receptors [i.e., estrogen receptor (ER) and progesterone receptor (PR)] and the human epidermal growth factor receptor 2 (HER2), accounting for about 10–20% of all breast cancer cases. According to the St. Gallen consensus, the prognosis of TNBC is the worst among all subtypes of breast cancer (1). At present, single or combined chemotherapy is the mainstay of treatment for late-stage TNBC. However, after multiline chemotherapy, drug resistance occurs and the disease progresses rapidly. The median overall survival (OS) of patients with metastatic TNBC (mTNBC) is about 14.5 months (2), which is much shorter than that of luminal-type patients (42.9 months) and HER2-enriched patients (50.1 months). It is well known that the expression of PDL1 (also known as CD274) in breast cancer is associated with large tumor size, high grade, and high proliferation (3, 4). Although immune checkpoint inhibition using anti-PDL1 antibody, e.g., atezolizumab, in combination with chemotherapy has shown great promise in TNBC (5, 6), a majority of TNBC patients still do not benefit from PDL1-targeted immunotherapy. Therefore, challenges remain, particularly regarding the need for improvement of the therapeutic efficacy.

It has been demonstrated that *TP53* aberrations are prevalent in TNBC, with roughly 40–62% of patients having *TP53* aberrations, followed by *PIK3CA* aberrations in 10% of patients and aberrations of other genes, namely, *Rb1*, *PTEN*, *BRCA2*, *erbB2/3*, and *BRAF* in 7–9% of patients (7). Cancer cells with DNA damage induced by chemotherapy would be blocked by the p53 protein and enter the apoptosis program. The ATM/Chk2-p53 signaling pathway plays a critical role in cell cycle arrest, DNA repair and apoptosis induced by DNA-damaging agents (8). *TP53* aberrations are associated with poor treatment response and prognosis in breast cancers (9, 10). Breast cancer patients with *TP53* aberrations and particularly TNBC patients are more likely to be resistant to anti-cancer treatment (11–13). Gene abnormalities related to *TP53* aberrations in TNBC, such as 9p24.1 amplification and *PIK3CA* gene mutation, abnormal PI3K, ErbB1/EGFR, MUC1, Alix, and PARP-GSK3β signaling pathways, could alter immunogenicity (14–16) and are known to be associated with PDL1/PD1 abnormalities (17).

It has been demonstrated that chondroitin sulfate proteoglycan 4 (CSPG4), a scaffold protein composed of chondroitin sulfate and proteoglycan with multiple cancer-promoting functions, is overexpressed in TNBC (18). CSPG4 promotes tumor cell proliferation, angiogenesis, drug resistance, immune escape, and radiation resistance (19–21). CSPG4 binds to a variety of kinases and extracellular factors to mediate the activation of multiple signaling pathways (22). In TNBC, it has been demonstrated that CSPG4 binds to PDL1 on the cell surface. In our preliminary study, we found that CSPG4 and PDL1 are co-expressed in TNBC tissues. However, the clinical implications, i.e., the value of these co-expressed CSPG4 and PDL1 molecules as prognostic predictors in TNBC are not known.

As mentioned above, a majority of TNBC patients do not benefit from immune checkpoint-based immunotherapy. Therefore, increasing the sensitivity to immune checkpoint blockade through exploring new molecules, e.g., those that interact with the PDL1/PD1 axis, is an urgently unmet task. In this study, through next-generation sequencing and tumor mutation burden analysis, we found that CSPG4 was highly expressed together with PDL1 in TNBCs, particularly in those harboring *TP53* aberrations. We also investigated the clinical implications of CSPG4 and PDL1 in TNBC patients by analyzing on-line databases and found that co-expression of CSPG4 and PDL1 has important prognostic value in TNBCs. Overall, our study suggests that co-targeting CSPG4 and PDL1 in advanced TNBC might be a novel strategy to improve the therapeutic efficacy of PDL1-based immune checkpoint blockade.

METHODS

Study Design and Specimens

This study included 85 recurrent and mTNBC patients treated in the Hunan Cancer Hospital between January 2017 and August 2019. The inclusion criteria were: 1) pathologically confirmed diagnosis of breast cancer; 2) negative expression of ER and PR confirmed by immunohistochemistry (IHC); and 3) negative expression/amplification of HER2 confirmed by IHC/FISH. The

exclusion criteria were: 1) multiple primary tumors (≥2); and 2) no measurable invasive breast cancer tissue. The clinicopathological characteristics of the enrolled patients are listed in **Supplementary Table 1**. All molecular pathological data were confirmed by three experienced pathologists. This study was approved by the Ethics Committee of Hunan Cancer Hospital.

Next-Generation Sequencing and Tumor Mutation Burden Analysis

Among the 85 TNBC patients, 52 voluntarily received circulating tumor DNA (ctDNA) evaluations. Next-generation sequencing (NGS) of ctDNA samples was performed according to our previously published method (9). TMB, which was expressed as the somatic mutations per mega-base (Mb), was calculated from whole exome sequencing data or big gene panels (23, 24). TMB analysis interrogated single nucleotide variants (SNVs) and small INDELs with the variant allele frequency (VAF) ≥3%.

Transcriptome Profiling of TCGA-BRCA Dataset

This study firstly used the transcriptome dataset of the TCGA-BRCA project (RNA-seq dataset) from the cancer coordination dataset supported by the National Cancer Institute (NCI)—Cancer Genome Atlas. In the RNA-seq dataset, the gene expression level was recorded as the number of fragments per kilobase of exon model per million reads mapped (FPKM). More than 36,218 genes were identified in the HGNC (HUGO (Human Genome Organization) Gene Nomenclature Committee) database by using the Bioconductor "org.HS.eg.db" package.

TIMER Database Analysis

CSPG4 and PDL1 mRNA expression levels in different types of human cancers and subtypes of breast cancer were analyzed *via* the Tumor Immune Estimation Resource 2.0 (TIMER2.0) database (http://timer.cistrome.org/) (25). Box plots were generated by the Gene DE module to display the distributions of CSPG4 and PDL1 mRNA expression levels. The statistical significance computed by the Wilcoxon test was annotated by the number of stars (*P <0.05, **P <0.01, ***P <0.001).

Gene Set Enrichment Analysis

Functional enrichment was conducted using Gene Set Enrichment Analysis (GSEA) (https://www.gsea-msigdb.org/gsea/msigdb/index.jsp) to explore whether identified sets of genes showed significant differential expression between the high and low expression groups (26). Gene set permutations were conducted 1,000 times for each analysis. Gene sets with P <0.05 and false discovery rate (FDR) <0.25 were considered as enriched.

STRING Database Analysis

Search tool for retrieval of interacting genes/proteins (STRING) database was applied to evaluate the protein-protein interaction (PPI) network (27). The PPI network between CSPG4 or PDL1 and their correlated proteins was constructed by using the interaction database platform STRING v.11.0 (https://string-db.org/). The species was set to "*Homo sapiens*", and other parameters were set to default.

Immunohistochemical (IHC) Analysis

All tissue samples were stained with hematoxylin and eosin, and the presence of invasive breast cancer cells was confirmed by microscopic examination. The protein levels of PDL1 and CSPG4 were assessed by IHC. The IHC steps were as follows: 1) the sections were de-waxed and rehydrated with xylene and alcohol, respectively; 2) the sections were incubated with anti-PDL1 or anti-CSPG4 antibody at 4°C overnight, followed by horseradish peroxidase (HRP)-conjugated secondary antibody incubation and coloration; 3) the stained cells were analyzed microscopically and the positive rate of the stained tumor cells was quantified using the Image-Pro Plus software (Media Controlnetics, Maryland, USA).

According to the clinicopathological diagnostic criteria, PDL1 positivity was defined as the percentage of tumor cells or tumor-infiltrating lymphocytes (TILs) with membranous PDL1 expression ≥1% (28). The positive expression of CSPG4 was brownish yellow or brown and located in the membrane or cytoplasm. The expression level of CSPG4 was scored according to the staining density (no staining scored 0, light brown scored 1 and dark brown scored 2) and the percentage of positive cells (0% scored 0, 1–25% scored 1, 26–50% scored 2, 51–75% scored 3, and >75% scored 4). The total score of CSPG4 was a combination of the staining intensity and the percentage of positive cells, with a total score ≤3 and ≥4 defined as low and high expression, respectively (29).

CSPG4 Knockdown by CRISPR/CAS9 in TNBC SUM149 Cells

The guide RNAs used to make the CSPG4-CRISPR cells were 5'-CGAGCGCGGCTCTGCTCCTG-3' and 5'-AGAGACC TGGAGACACCAGG-3'. Both guide RNA plasmids were co-transfected with a plasmid expressing the CAS9 enzyme (pT3.5 Caggs-FLAG-hCas9) and also two plasmids for puromycin and GFP selection, pcDNA-PB7 and pPB SB-CG-LUC-GFP (Puro) (+CRE). Mock cell line was transfected with selection plasmids only (pcDNA-PB7 and pPB SB-CG-LUC-GFP (Puro)(+CRE)) and selected by puromycin-containing medium (0.6 μg/ml). Single cell-derived colonies were expanded and screened by genomic PCR for the deletion of the CSPG4 gene using the primers 5'-GGGCCCTTTAAGAAGGTTGA-3' and 5'-GTTTTGACAGCCCAAACCAG-3'. Cell lines were further screened by immunoblotting and flow cytometry to verify the knockdown efficiency of the CSPG4 protein.

Immunoblotting

Immunoblotting was performed using our standard protocol as described (30). Briefly, cell lysates were prepared and separated on 7.5–12% SDS-polyacrylamide gels and transferred to polyvinylidenedifluoride (PVDF) membranes. The membranes were blocked with 5% milk blocking solution in TBST and incubated overnight at 4°C with the respective primary antibodies. After several washes with TBST, the membranes were subsequently incubated with HRP-conjugated secondary antibody and the signals were detected by the ECL substrate (ThermoScientific, Waltham, MA, USA).

Flow Cytometry

The cells were released in phosphate buffered saline (PBS)/ethylenediamine tetraacetic acid (EDTA) solution and washed 2 times with FACS buffer (RPMI medium supplemented with 1% goat serum and 5 mM HEPES). The cells were incubated with the indicated primary antibody for 45 min at 4°C, washed 3 times with FACS buffer, and then incubated with species-matched phycoerythrin-conjugated secondary antibody for 30 min at 4°C. The cells were analyzed on a BD Biosciences Accuri C6 Flow Cytometry System.

Colony Formation Assay

For 3D colony formation assay, a layer of 1% agarose in regular growth medium was pipetted into six well plates and allowed to solidify. The cells were resuspended in 6.75 ml regular growth medium at 5,000 cells/ml and incubated for 15 min at 37°C. 750 µl of 2% agarose was then added to the tubes, mixed thoroughly by pipetting, and 2 ml of cell suspension was pipetted into triplicate wells. The plates were placed at 4°C for 15 min to facilitate rapid polymerization of the agarose, and the wells overlaid with 2 ml growth medium and incubated at 37°C/5% CO_2 for 12 days. The medium was replaced every three days. The colonies were counted and the data were expressed as the average number (± s.e.m) of colonies from five fields/well from triplicate wells.

Cell Invasion Assay

The cells (2.5×10^4) in normal growth medium were added to the top chamber of triplicate wells of matrigel invasion chambers (8 µm, Corning, NY, USA), the bottom chambers filled with complete growth medium and cultured for 24 h at 37°C/5% CO_2. The remaining cells in the upper chamber were removed with a cotton swab and the invaded cells fixed and stained using Differential Quick Staining Kit (Electron Microscopy Sciences, Hatfield, PA, USA). The invaded cells were enumerated under a microscope at ×100 magnification from five random fields/well. The data shown are the average number (± s.e.m) of invaded cells from five fields/well from 3 combined experiments. Statistical significance was determined using Students t-test.

Co-Immunoprecipitation Assay

For co-immunoprecipitation experiments, the cells were lysed on ice with IP buffer (20 mM Tris–HCl, pH 7.5, 150 mM NaCl, 1 mM Na_2EDTA, 1 mM EGTA, 1% Nonidet P-40, 2.5 mM sodium pyrophosphate,1 mM glycerophosphate, 1 mM Na_3O_4, 1 µg/ml leupetin, 1 mM PMSF) and the insoluble materials were removed by centrifugation. The lysates were pre-cleared with protein A/G Sepharose beads (Amersham Pharmacia, Piscataway, NY) for 30 min at 4°C. The lysates were incubated with each antibody overnight at 4°C, and the immunocomplexes collected by incubation with protein A/G-Sepharose beads for 1 h at 4°C. The immunocomplexes were washed three times with lysis buffer at 4°C and the bead-associated proteins resolved by SDS-PAGE.

Statistical Analysis

To analyze the demographic and clinicopathological parameters, categorical and continuous variables were expressed as counts (percentages) and mean ± s.d., respectively. In order to compare the differences of symmetrical distribution between continuous variables, t-test was used. Kaplan–Meier (KM) analysis and bilateral Logrank test were used to evaluate the effect of CSPG4 expression on OS. Patients without OS information were censored at the last follow-up date. Cox proportional hazards model was used to evaluate the risk factors for the treatment outcomes, which was expressed as hazard ratio (HR) and 95% confidence interval (CI). All statistical analyses were performed using SAS 9.4 software (SAS Institute Inc., NC, USA) and R 3.6.2 (https://www.r-project.org). All hypothesis tests were two-sided. The significance level was 0.05, and the marginal significance level was 0.15.

RESULTS

TP53 Aberrations Increase Tumor Mutation Burden in TNBCs

We have previously demonstrated that more than 30% of metastatic breast cancers had *TP53* aberrations (9). In this study, NGS analysis on ctDNA revealed that about 52% (27/52) of mTNBCs had *TP53* aberrations (**Figure 1A**). The gene aberrations and pathway enrichment in *TP53*-aberrant and *TP53* wild-type mTNBCs showed distinct genetic landscapes. mTNBCs with gene aberrations in Notch, MAPK, cell adhesion, PI3K, and Hedgehog pathways were strongly associated with *TP53* aberrations (**Figures 1B, C**).

It has been demonstrated that high tumor mutation burden (TMB) is an important predictor for the treatment outcomes of PDL1 inhibition in lung cancer (31, 32) and colorectal carcinoma (33). Here, we found that *TP53*-aberrant metastatic breast cancers had significantly higher TMB than *TP53* wild-type metastatic breast cancers (median: 5.00 muts/Mb *vs* 1.44 muts/Mb; $P = 0.004$) (**Figure 1D**). In addition, *TP53*-aberrant mTNBCs had significantly higher TMB than *TP53* wild-type mTNBCs (median: 5.56 muts/Mb *vs* 1.00 muts/Mb; $P = 0.0001$) (**Figure 1E**). This trend was not significant in non-TNBCs (**Supplementary Figure 1**).

In addition, our previous study has suggested *TP53* aberrations to be a significant risk factor for PFS in metastatic breast cancer (9). In this study, KM curves derived from the TCGA-BRCA dataset showed that advanced breast cancer patients with *TP53* aberrations had poorer OS, compared with patients with wild-type *TP53* ($P = 0.0484$) (**Figure 1F**). These results suggest that *TP53* aberrations could lead to genomic instability and significantly increased tumor mutation loads in mTNBCs, which might be associated with the poor clinical outcomes in TNBC.

CSPG4 and PDL1 Are Highly Expressed in *TP53*-Aberrant TNBCs

Since higher TMB is a predictor of the efficacy of PDL1-targeted immunotherapy in cancer, we speculated that the increased *TP53* aberrations would lead to increased expression of PDL1 in TNBC. To this end, we analyzed the mRNA expression levels of PDL1 in human cancers using the TIMER2.0 database.

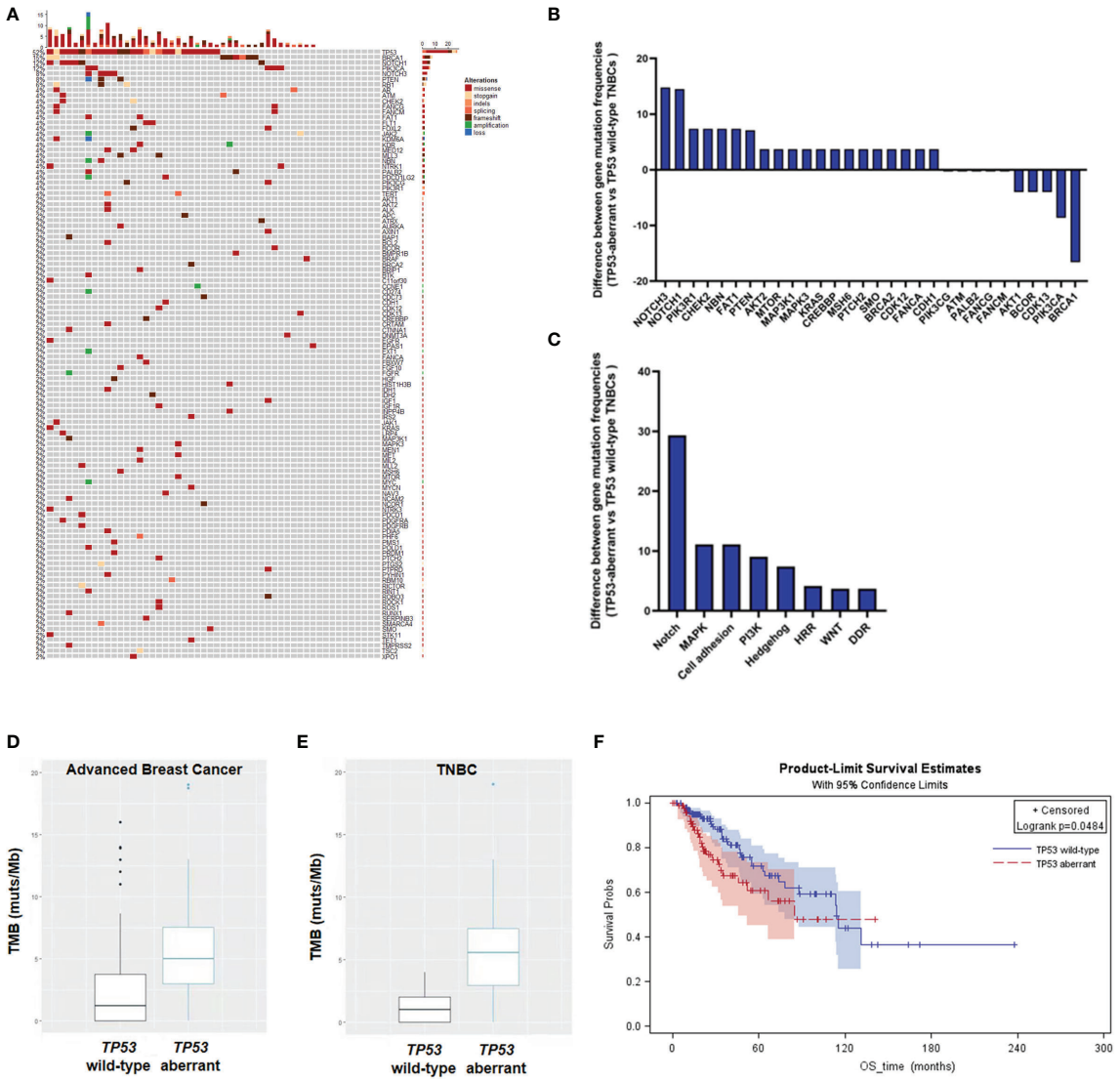

FIGURE 1 | Heatmap and KM curves of *TP53* alterations and tumor mutation burden (TMB) in TNBCs. **(A)** Heatmap of *TP53* alterations in mTNBCs. **(B)** Difference of gene mutation frequencies between *TP53*-aberrant and *TP53* wild-type mTNBCs. **(C)** Difference of signaling pathways between *TP53*-aberrant and *TP53* wild-type mTNBCs. **(D, E)** Difference of TMB between *TP53*-aberrant and *TP53* wild-type metastatic breast cancer **(D)** and TNBC patients **(E)**. **(F)** KM curves for overall survival (OS) between *TP53*-aberrant and *TP53* wild-type breast cancer patients.

Indeed, the mRNA level of PDL1 was higher in basal-like breast cancer (BLBC)/TNBC than luminal-type breast cancer (**Figure 2A**). Because of the inefficiency of PDL1-targeted immunotherapy in most TNBC patients and the major role for CSPG4 has been shown to be overexpressed in TNBC, we though co-expression we investigated the status of CSPG4 in TNBC in this study. The high expression level of CSPG4 in TNBC was confirmed through analyzing the TCGA-BRCA dataset, showing that CSPG4 expression was higher in BLBC/TNBC than other subtypes of breast cancer (**Figure 2B**).

To further assess the role of *TP53* aberrations in the expression of CSPG4 and PDL1, we analyzed the transcriptome profile of breast cancers in the TCGA database. As shown in **Figure 2C**, PDL1 was significantly higher in *TP53*-aberrant TNBCs compared with *TP53* wild-type TNBCs (median: 1.29 *vs* 0.86, $P = 0.01$). As for CSPG4, there was an obvious trend of increased level in *TP53*-aberrant TNBCs compared with *TP53* wild-type TNBCs (median: 3.60 *vs* 3.29, $P = 0.47$), although the difference was not statistically significant (**Figure 2D**). These findings suggest that *TP53* aberrations might be associated with the increased TMB level and high expression of CSPG4 and PDL1 in mTNBCs and that CSPG4 might be used as an alternative or supplementary target for the therapeutic intervention in TNBC.

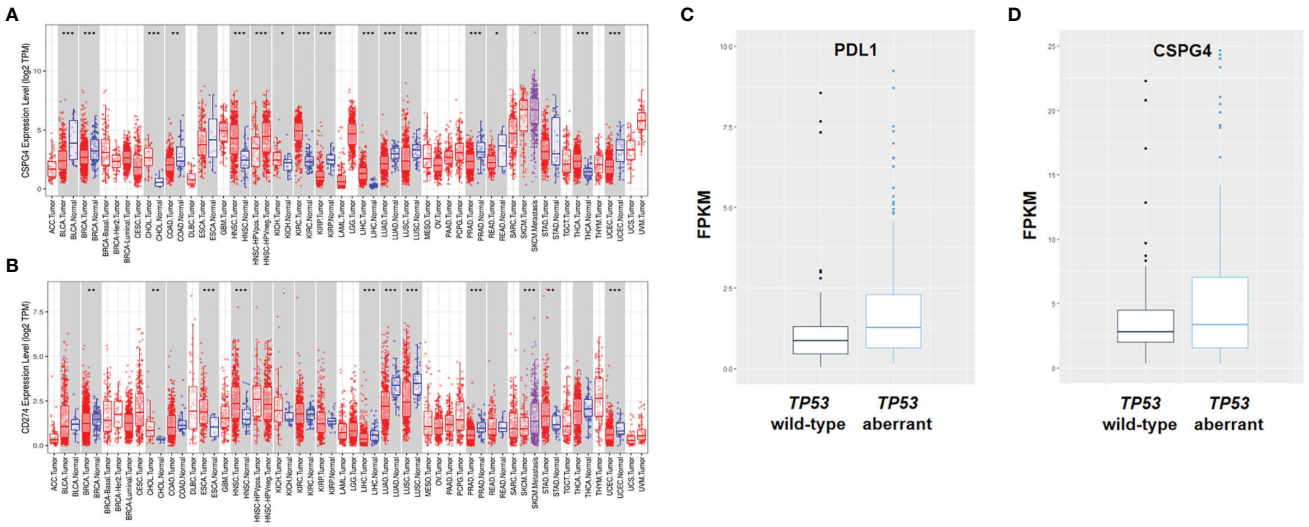

FIGURE 2 | Expression of PDL1 and CSPG4 in different types of human cancers and subtypes of breast cancer. **(A, B)** The expression levels of human PDL1 **(A)** and CSPG4 **(B)** in different tumor types and subtypes of breast cancer analyzed using the TIMER2.0 database. **(C, D)** The expression levels of PDL1 **(C)** and CSPG4 **(D)** between *TP53*-aberrant and *TP53* wild-type TNBC patients. $^{*}P < 0.05$, $^{**}P < 0.01$, $^{***}P < 0.001$.

CSPG4 and PDL1 Are Highly Correlated in Advanced TNBC Tissues and TNBC Cell Lines

Considering the important role of CSPG4 and PDL1 in malignant proliferation, metastasis and immunosuppression and their over-expression in *TP53*-aberrant TNBCs, we further examined the expression levels of CSPG4 and PDL1 in tissue samples from advanced TNBCs using IHC staining. IHC assays demonstrated that the positive rate of CSPG4 and PDL1 in advanced TNBC samples were about 60 and 35%, respectively. We further asked whether CSPG4 was associated with PDL1 expression in TNBC. Interestingly, we found a majority of TNBC patients with high CSPG4 expression also had high PDL1 expression. **Figure 3A** shows representative TNBC cases who had low levels of both PDL1 and CSPG4 (left) and high levels of both PDL1 and CSPG4 (right). Quantification of the IHC results revealed that the percentage of $CSPG4^{high}$ TNBC patients (CSPG4 expression score ≥4) was higher in PDL1-positive patients than PDL1-negative patients (50% *vs* 34%, $P = 0.144$) (**Figure 3B**). Compared with PDL1-negative TNBCs, PDL1-positive TNBC samples had significantly higher CSPG4 expression level (scores) (3.09 *vs* 1.96, $P = 0.0368$) (**Figure 3C**). These findings suggest that CSPG4 and PDL1 were highly co-expressed in TNBC tissues.

To further investigate the expression of PDL1 and CSPG4 in TNBC cells, we analyzed their protein levels in several breast cancer cell lines by immunoblotting and flow cytometry. **Figure 3D** shows that, compared with ER-positive MCF-7 cells, TNBC cell lines SUM149, MDA-MB 231 and HS578T had significantly higher PDL1 levels. As shown in **Figure 3E**, compared with ER-positive (T47D and MCF-7) and HER2-positive (SK-BR-3) cell lines, the expression of CSPG4 was significantly higher in TNBC cell lines SUM149, MDA-MB 231, and HS578T. All these TNBC cells examined so far had *TP53* mutations. For example, MDA-MB-231 cells had *TP53* p.P72R mutation (34); SUM149 cells had *TP53* p.M237I mutation (35); HS578T cells had *TP53* V157F mutation (36). Furthermore, the TNBC cell line HS578T that had the highest level of PDL1 (**Figure 3D**) also had the highest level of CSPG4 (**Figure 3E**). These findings suggest that both CSPG4 and PDL1 were highly expressed and the expression of these two proteins was positively correlated in TNBC cells.

Co-Expression of CSPG4 and PDL1 Has Important Prognostic Value in TNBCs

In TNBC samples, both univariate and multivariate Cox regression analyses were performed to evaluate the risk factors for progression-free survival (PFS) in advanced TNBCs. As shown in **Figure 4**, in univariate and multivariate Cox regression analyses, the hazard of progression for PDL1-positive patients was 1.28 times and 1.12 times, respectively, higher than PDL1-negative patients (95% CI: 0.54–3.00, univariate; 0.45–2.79, multivariate), but not statistically significant. However, the progression of CSPG4-positive patients was significantly higher than that of CSPG4-negative patients, with an HR of 2.26 (95% CI: 1.01–5.03, $P = 0.05$) and 2.06 (95% CI: 1.02–4.15, $P = 0.05$), respectively, in univariate and multivariate Cox regression analyses. Therefore, both univariate and multivariate Cox regression analyses indicate that CSPG4 positivity is an important adverse prognostic factor for advanced TNBC.

The effect of CSPG4 in conjugation with PDL1 overexpression on patient survival was further analyzed in advanced breast cancers by using the TCGA-BRCA database.

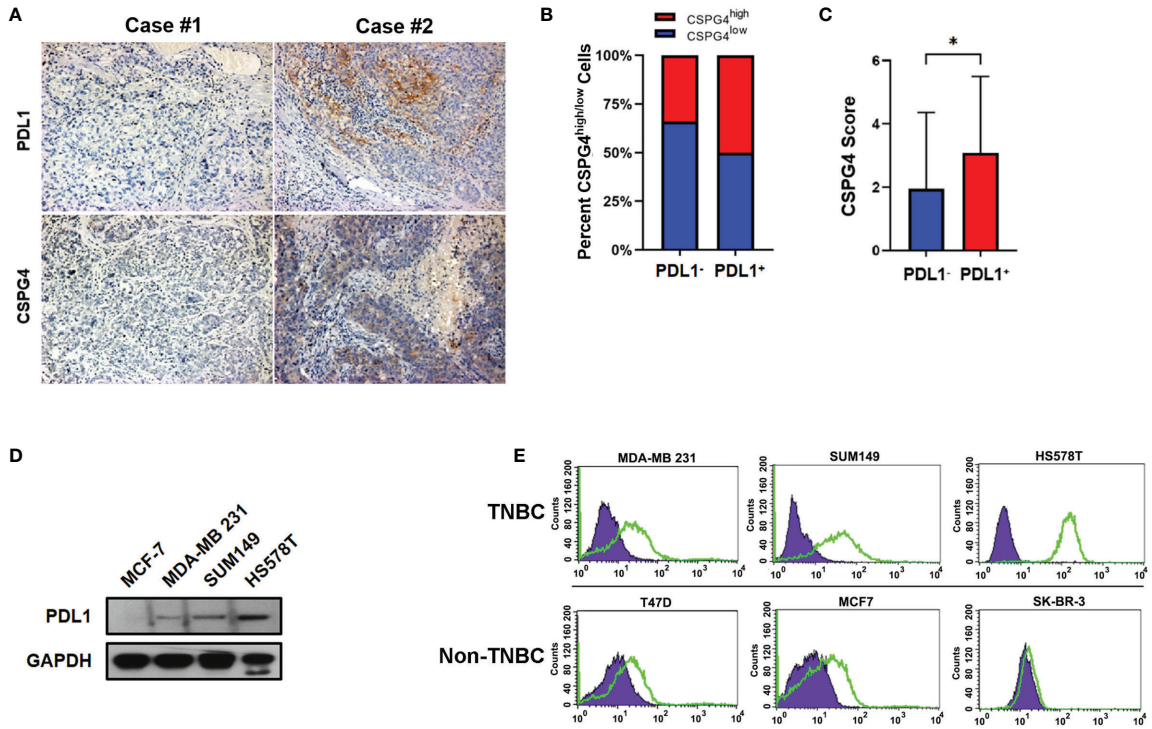

FIGURE 3 | Expression of PDL1 and CSPG4 in advanced TNBC tissues and breast cancer cell lines. **(A)** Representative IHC images of PDL1 and CSPG4 protein expression in advanced TNBC tissues. The upper-left and upper-right panels show PDL1^{-} and PDL1^{+} tissue, respectively; and the lower-left and lower-right panels show CSPG4^{-} and CSPG4^{+} tissue, respectively. Original magnification: ×400. **(B)** Bar plot comparing the percentage of CSPG4^{high} tissues in PDL1^{-} and PDL1^{+} advanced TNBC samples. **(C)** Bar plot comparing the staining score of CSPG4 in PDL1^{-} and PDL1^{+} advanced TNBC samples. **(D)** PDL1 expression in breast cancer cell lines detected by immunoblotting assay. **(E)** CSPG4 expression in breast cancer cell lines detected by flow cytometry. (Purple area represents isotype-matched antibody staining; Green area represents CSPG4 staining). *P < 0.05.

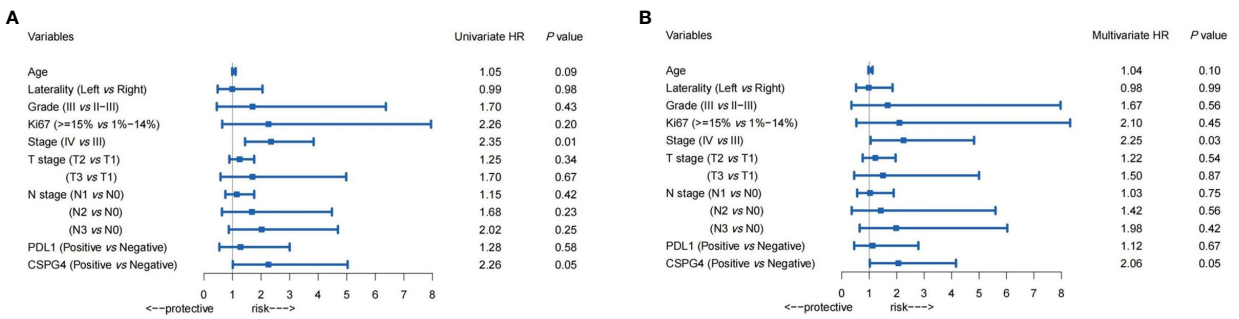

FIGURE 4 | Prognostic value of PDL1, CSPG4, and clinicopathological variables in advanced TNBCs. Univariate **(A)** and Multivariate **(B)** Cox regression analysis showed the hazard ratios (HRs) (with 95% CI) of PDL1, CSPG4, and clinicopathological variables on progression-free survival (PFS) in advanced TNBCs.

The higher expression of CSPG4 was correlated with poorer OS (P = 0.0216) (**Figure 5A**). However, PDL1 high level did not show significant risk to OS; instead, PDL1 high level was a marginally protective factor for OS (P = 0.0702) (**Figure 5B**). When combined with PDL1, CSPG4 high level was still a significant risk factor for OS. Among the PDL1^{high} advanced breast cancers, CSPG4 high level was a significant risk factor for poor OS (P = 0.0493) (**Figure 5C**). Among the PDL1^{low} advanced breast cancers, CSPG4 high level was also a marginally significant risk factor for poor OS (P = 0.0730) (**Figure 5D**). These results suggest that co-expression of CSPG4 and PDL1 had important prognostic value in advanced breast cancers.

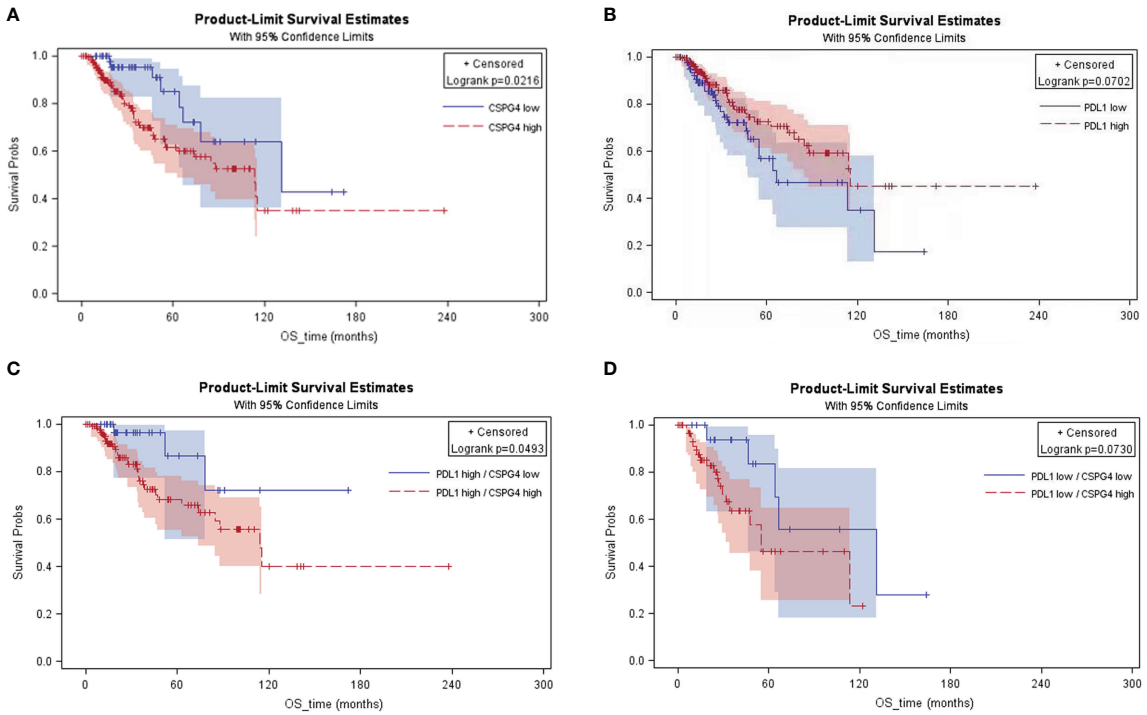

FIGURE 5 | KM curves of the advanced breast cancer patients with different expression levels of CSPG4 and PDL1 on overall survival. **(A)** Survival rate between CSPG4^{high} and CSPG4^{low} advanced breast cancer patients. **(B)** Survival rate between PDL1^{high} and PDL1^{low} advanced breast cancer patients. **(C)** Survival rate between CSPG4^{high} and CSPG4^{low} patients in PDL1^{high} advanced breast cancer patients. **(D)** Survival rate between CSPG4^{high} and CSPG4^{low} patients in PDL1^{low} advanced breast cancer patients.

EMT-Related Pathways Are Enriched in TNBCs With High Expression of CSGP4 and PDL1

In order to screen the potential biological pathways that were related with the expression of CSPG4/PDL1 in TNBC, we performed GSEA comparing between the high and low CSPG4 and PDL1 expression groups. Gene sets with P <0.05 and FDR <0.25 were considered as significantly enriched. As shown in **Figure 6**, EMT-related pathways, namely, focal adhesion, extracellular matrix receptor interaction, extracellular matrix disassembly, extracellular matrix assembly, regulation of actin cytoskeleton were all significantly enriched in TNBC with CSPG4^{high} expression. In TNBC with PDL1^{high} expression, cell adhesion molecules were also significantly enriched (**Supplementary Figure 2**). To further investigate the relationship between CSPG4 or PDL1 and EMT, we constructed a PPI network between these two proteins and their correlated proteins by using the STRING v.11.0. As shown in **Supplementary Figure 3**, we found close correlations between CSPG4 and the EMT-related proteins, namely, SDC1, HSPG2, ITGB1, etc. PDL1 was also correlated with EMT-related proteins, namely, PTPN11, PXN, VAV1, etc. (**Supplementary Figure 4**). These data provide a functional link between CSPG4 expression and the EMT-related pathways.

In order to further investigate the effect of CSPG4 on the EMT phenotype in TNBC cells, we knocked down CSPG4 expression using the CRISPR/CAS9 technology. As shown in **Figure 7A**, by using CRISPR/CAS9-mediated gene silencing, we successfully suppressed the CSPG4 level in TNBC SUM149 cells, and constructed SUM149-CSPG4-CRISPR-B4 and SUM149-CSPG4-CRISPR-D7 cell lines. In these SUM149-CSPG4-knockdown cells, the colony formation capability was significantly inhibited (**Figure 7B**). Both SUM149-CSPG4-CRISPR cell lines had significantly lower number of invasive cells and lower invasive distance (**Figures 7C, D**).

Because EGFR/ERK1/2 signaling is important for the regulation of EMT-related markers, we examined the status of the EGFR/ERK1/2 signaling pathway in CSPG4-silenced TNBC cells. We found that both phosphorylated EGFR and phosphorylated ERK1/2 were inhibited in SUM149-CSPG4-knockdown cells (**Figure 8A**). The EMT markers Claudin-1, N-Cadherin, and β-Catenin were significantly inhibited (**Figure 8B**). EMT is reported to drive immune-suppression *via* the Zeb1 transcription factor, which induces the expression of PDL1 on these invading cells (37). We thus also checked the level of PDL1 in CSPG4-knockdown cells. **Figure 8C** showed that the expression of PDL1 was significantly inhibited in SUM149-CSPG4-knockdown cells. These findings suggested that CSPG4 might mediate PDL1 through EGFR/ERK1/2/EMT markers pathway in TNBC cells.

DISCUSSION

Since high TMB associated with the prevalent *TP53*-aberrations is an important predictor for the treatment outcomes of PDL1 blockade in cancer, immunotherapy becomes a potential option

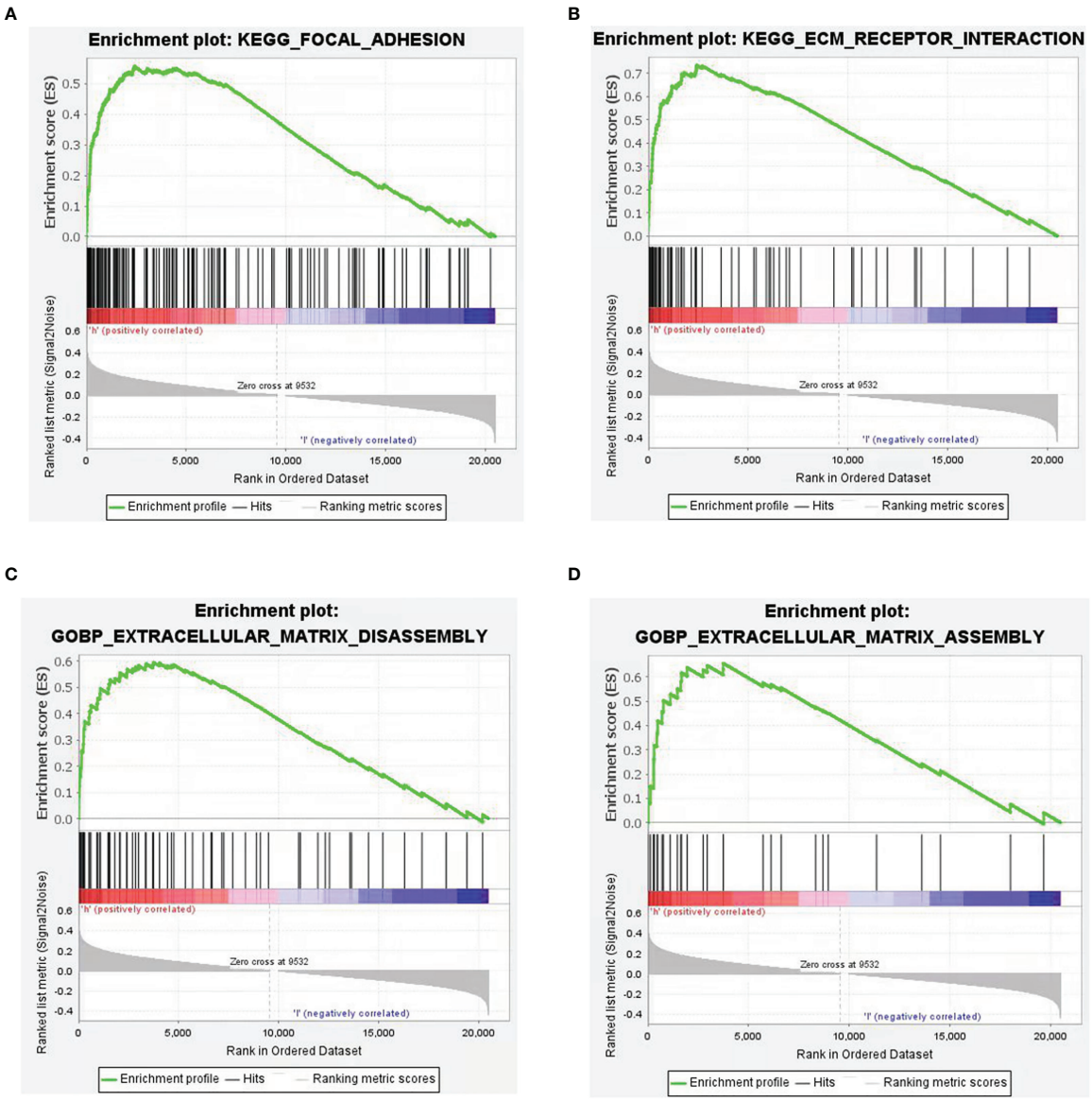

FIGURE 6 | Gene Set Enrichment Analysis (GSEA) according to CSPG4 expression level in TNBCs. **(A–D)** Significant enrichment plots of EMT-related pathways in CSPG4^{high} TNBCs using GSEA, namely, focal adhesion **(A)**, extracellular matrix receptor interaction **(B)**, extracellular matrix disassembly **(C)**, extracellular matrix assembly **(D)**.

in TNBCs. However, despite the clinical benefits of PDL1/PD1 blockade in some TNBC patients, therapy resistance remains a significant challenge for further clinical application of PDL1/PD1-targeted immunotherapy. Therefore, other therapeutic targets are worth exploring, at least, in the context of enhancing the therapeutic efficacy of immune checkpoint inhibition. In this study, we found that CSPG4 was upregulated and co-expressed with PDL1 in TNBCs and that the high expression of CSPG4 was a significant prognostic factor for poor PFS and OS in advanced TNBCs. CSPG4 thus might provide a new target that can be coupled with and enhance the efficacy of PDL1/PD1-directed immunotherapy for TNBC.

As a scaffold protein, CSPG4 may not only bind to a variety of kinases and extracellular factors to mediate the activation of multiple signaling pathways (22), but also interacts with PDL1 on the surface of TNBC cells. In addition, CSPG4 might be able to induce PDL1 expression through the SNAI1/SIRT3 pathway (38). SNAI1 and ZEB1 upregulated PDL1 by binding directly to E-boxes in PDL1 promoter region (39). In addition, by stabilizing SNAIL and inhibiting AXIN2, SIRT1 upregulates PDL1 by enhancing the binding of beta-catenin/TCF to PDL1 promoter region (40). Consistent with above research findings, we found that the knockdown of CSPG4 could significantly inhibit the phosphorylated-EGFR and beta-catenin, and thus

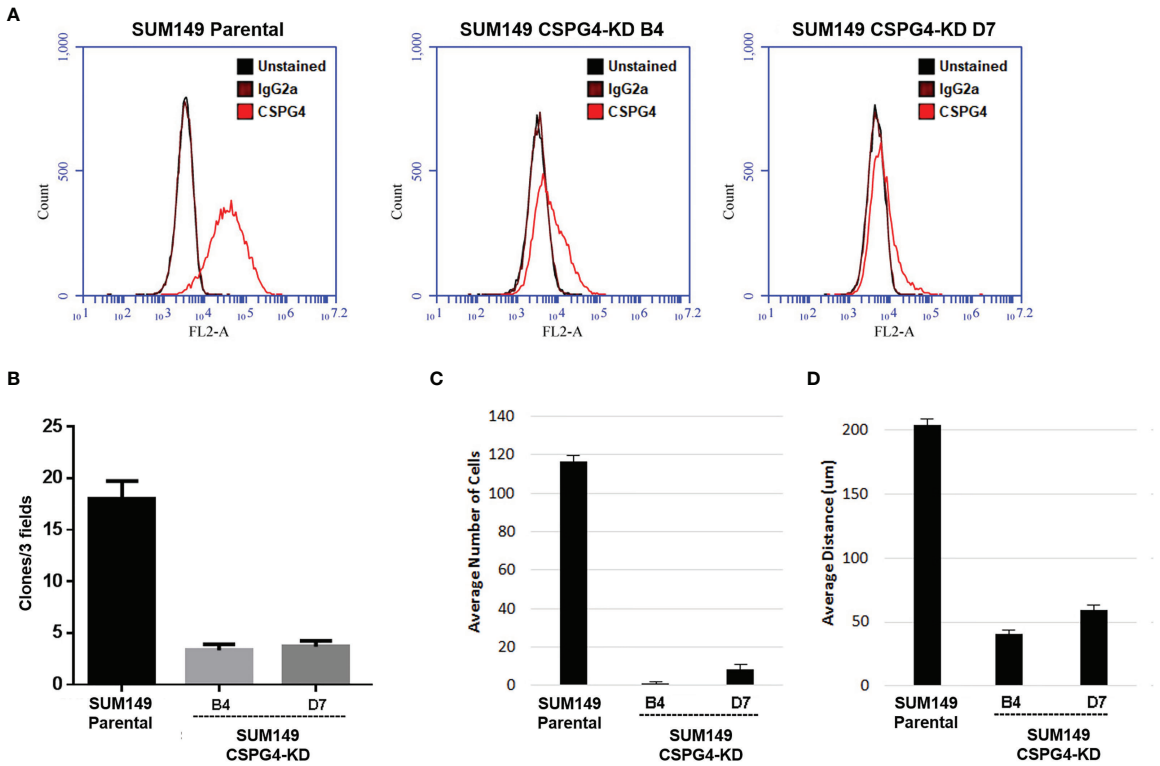

FIGURE 7 | CSPG4 knockdown changes several EMT markers, implicating to reverse the mesenchymal phenotype. **(A)** Establishment of CSPG4-knockdown breast cancer cell lines B4 and D7 using CRISPR/CAS9 technology. **(B–D)** Colony formation numbers **(B)**, invasive cell numbers **(C)**, and the invasive distance **(D)** in established CSPG4-knockdown cell lines.

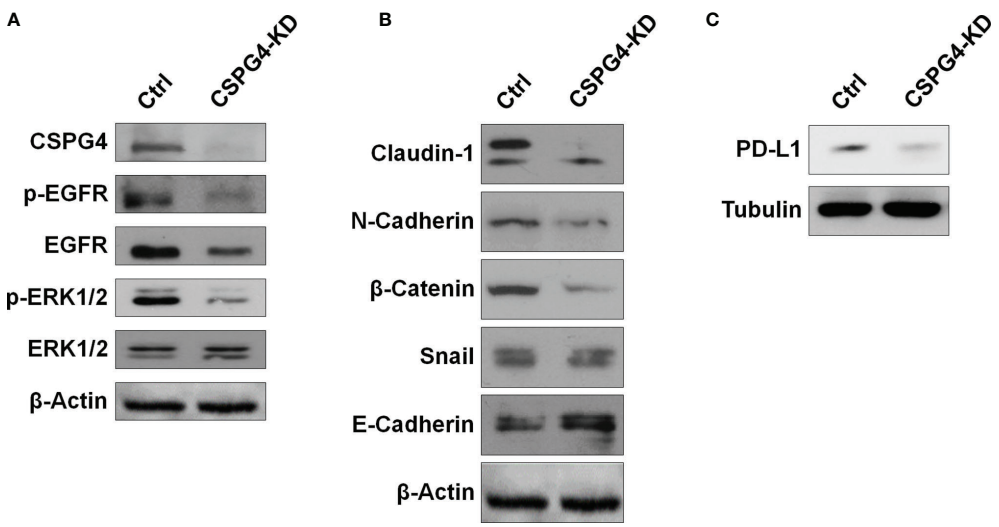

FIGURE 8 | CSPG4 knockdown affects EGFR and ERK1/2 activation and PDL1 expression. The protein levels of phosphorylated and unphosphorylated EGFR and ERK1/2 **(A)**, EMT markers **(B)**, and PDL1 **(C)** in CSPG4-knockdown SUM149 cells.

suppressed PDL1 level in TNBC cells. Based on these findings, we supposed that CSPG4 overexpression facilitated PDL1 expression through EMT-related pathways.

In survival analysis, we found CSPG4 to be a significant risk factor for poor response to 1st-line chemotherapy in advanced TNBCs. High expression of CSPG4 promotes tumor cell proliferation, angiogenesis, immune escape, and therapy resistance (21). We found that high level of CSPG4 was also a significant risk factor for OS in advanced breast cancers, suggesting a critical role for CSPG4 in determining the outcomes of advanced breast cancers. However, how CSPG4 leads to adverse clinical outcomes of advanced breast cancers is still not known and will be an interesting topic to investigate. Interestingly, we found that knocking down of CSPG4 by CRIPR/CAS9-mediated gene silencing led to downregulation of PDL1 (data not shown), suggesting a mechanistic link between these two cell surface molecules. Further studies will be needed to elucidate through which intracellular signaling pathway(s) CSPG4 is linked to PDL1, thus impacting the clinical outcomes of advanced TNBCs.

As TNBC-specific cell surface antigens, CSPG4 and PDL1 have a potential targeted therapeutic value. Because of their potential molecular mechanism of interaction, targeting either molecule may not achieve complete tumor regression, highlighting the necessity of co-targeting both molecules. Our results justify CSPG4 as a valid therapeutic target that might be used in conjugation with PDL1-targeted strategy in TNBC. This study will provide clues and call for further exploring the therapeutic value of CSPG4 and PDL1 in TNBC.

DATA AVAILABILITY STATEMENT

The original contributions presented in the study are included in the article/**Supplementary Material**. Further inquiries can be directed to the corresponding authors.

ETHICS STATEMENT

This study was approved by the ethics committee of Hunan Cancer Hospital with the approval number of kyjj-2019-014. The author declares that he has received ethical recognition. The authors declare that they have obtained ethical approval and patients consent to participate. The patients/participants provided their written informed consent to participate in this study.

AUTHOR CONTRIBUTIONS

ZH, CZ, JY, SD and CT performed the experiments. NX, LX, MW and SF collected and analyzed the data. ZH, CZ and JY drafted the manuscript. ZR, MP and JM reviewed the manuscript. QO, JL and XD conceived and designed the research. All authors listed have made a substantial, direct, and intellectual contribution to the work and approved it for publication.

FUNDING

This work was supported by the National Natural Science Foundation of China (81872167, 82173374, 82103342), the Key Grant of Research and Development in Hunan Province (2018SK2124, 2020DK2002), the Natural Science Foundation of Hunan (2020JJ8064, 2019JJ50360, 2019JJ40193, 2020JJ5386), the Hunan Provincial Health Commission Project (B2019089, C2019070), and the Changsha Science and Technology Project (kq2004125).

SUPPLEMENTARY MATERIAL

The Supplementary Material for this article can be found online at: https://www.frontiersin.org/articles/10.3389/fonc.2022.804466/full#supplementary-material

REFERENCES

1. Vasconcelos I, Hussainzada A, Berger S, Fietze E, Linke J, Siedentopf F, et al. The St. Gallen Surrogate Classification for Breast Cancer Subtypes Successfully Predicts Tumor Presenting Features, Nodal Involvement, Recurrence Patterns and Disease Free Survival. *Breast* (2016) 29:181–5. doi: 10.1016/j.breast.2016.07.016. doi:S0960-9776(16)30126-6 [pii].
2. Grinda T, Antoine A, Jacot W, Blaye C, Cottu PH, Dieras V, et al. Evolution of Overall Survival and Receipt of New Therapies by Subtype Among 20 446 Metastatic Breast Cancer Patients in the 2008-2017 ESME Cohort. *ESMO Open* (2021) 6(3):100114. doi: 10.1016/j.esmoop.2021.100114
3. Muenst S, Schaerli AR, Gao F, Daster S, Trella E, Droeser RA, et al. Expression of Programmed Death Ligand 1 (PD-L1) is Associated With Poor Prognosis in Human Breast Cancer. *Breast Cancer Res Treat* (2014) 146(1):15–24. doi: 10.1007/s10549-014-2988-5
4. Ali HR, Glont SE, Blows FM, Provenzano E, Dawson SJ, Liu B, et al. PD-L1 Protein Expression in Breast Cancer is Rare, Enriched in Basal-Like Tumours and Associated With Infiltrating Lymphocytes. *Ann Oncol* (2015) 26(7):1488–93. doi: 10.1093/annonc/mdv192
5. Schmid P, Adams S, Rugo HS, Schneeweiss A, Barrios CH, Iwata H, et al. Atezolizumab and Nab-Paclitaxel in Advanced Triple-Negative Breast Cancer. *N Engl J Med* (2018) 379(22):2108–21. doi: 10.1056/NEJMoa1809615
6. Schmid P, Salgado R, Park YH, Munoz-Couselo E, Kim SB, Sohn J, et al. Pembrolizumab Plus Chemotherapy as Neoadjuvant Treatment of High-Risk, Early-Stage Triple-Negative Breast Cancer: Results From the Phase 1b Open-Label, Multicohort KEYNOTE-173 Study. *Ann Oncol* (2020) 31(5):569–81. doi: 10.1016/j.annonc.2020.01.072
7. Shah SP, Roth A, Goya R, Oloumi A, Ha G, Zhao Y, et al. The Clonal and Mutational Evolution Spectrum of Primary Triple-Negative Breast Cancers. *Nature* (2012) 486(7403):395–9. doi: 10.1038/nature10933
8. Knappskog S, Chrisanthar R, Lokkevik E, Anker G, Ostenstad B, Lundgren S, et al. Low Expression Levels of ATM may Substitute for CHEK2 /TP53 Mutations Predicting Resistance Towards Anthracycline and Mitomycin Chemotherapy in Breast Cancer. *Breast Cancer Res* (2012) 14(2):R47. doi: 10.1186/bcr3147
9. Hu ZY, Xie N, Tian C, Yang X, Liu L, Li J, et al. Identifying Circulating Tumor DNA Mutation Profiles in Metastatic Breast Cancer Patients With Multiline Resistance. *EBioMedicine* (2018) 32:111–8. doi: 10.1016/j.ebiom.2018.05.015
10. Takahashi S, Fukui T, Nomizu T, Kakugawa Y, Fujishima F, Ishida T, et al. TP53 Signature Diagnostic System Using Multiplex Reverse Transcription-Polymerase Chain Reaction System Enables Prediction of Prognosis of Breast Cancer Patients. *Breast Cancer* (2021) 28(6):1225–34. doi: 10.1007/s12282-021-01250-z
11. Geisler S, Borresen-Dale AL, Johnsen H, Aas T, Geisler J, Akslen LA, et al. TP53 Gene Mutations Predict the Response to Neoadjuvant Treatment With

5-Fluorouracil and Mitomycin in Locally Advanced Breast Cancer. *Clin Cancer Res* (2003) 9(15):5582–8.
12. Andersson J, Larsson L, Klaar S, Holmberg L, Nilsson J, Inganas M, et al. Worse Survival for TP53 (P53)-Mutated Breast Cancer Patients Receiving Adjuvant CMF. *Ann Oncol* (2005) 16(5):743–8. doi: 10.1093/annonc/mdi150
13. Li J, Yang L, Gaur S, Zhang K, Wu X, Yuan YC, et al. Mutants TP53 P.R273H and P.R273C But Not P.R273G Enhance Cancer Cell Malignancy. *Hum Mutat* (2014) 35(5):575–84. doi: 10.1002/humu.22528
14. Blackley EF, Loi S. Targeting Immune Pathways in Breast Cancer: Review of the Prognostic Utility of TILs in Early Stage Triple Negative Breast Cancer (TNBC). *Breast* (2019) 48(Suppl 1):S44–8. doi: 10.1016/S0960-9776(19)31122-1
15. Gao C, Li H, Liu C, Xu X, Zhuang J, Zhou C, et al. Tumor Mutation Burden and Immune Invasion Characteristics in Triple Negative Breast Cancer: Genome High-Throughput Data Analysis. *Front Immunol* (2021) 12:650491. doi: 10.3389/fimmu.2021.650491
16. Chen H, Chong W, Yang X, Zhang Y, Sang S, Li X, et al. Age-Related Mutational Signature Negatively Associated With Immune Activity and Survival Outcome in Triple-Negative Breast Cancer. *Oncoimmunology* (2020) 9(1):1788252. doi: 10.1080/2162402X.2020.1788252
17. Lehmann BD, Bauer JA, Chen X, Sanders ME, Chakravarthy AB, Shyr Y, et al. Identification of Human Triple-Negative Breast Cancer Subtypes and Preclinical Models for Selection of Targeted Therapies. *J Clin Invest* (2011) 121(7):2750–67. doi: 10.1172/JCI45014
18. Wang X, Osada T, Wang Y, Yu L, Sakakura K, Katayama A, et al. CSPG4 Protein as a New Target for the Antibody-Based Immunotherapy of Triple-Negative Breast Cancer. *J Natl Cancer Inst* (2010) 102(19):1496–512. doi: 10.1093/jnci/djq343
19. Pluschke G, Vanek M, Evans A, Dittmar T, Schmid P, Itin P, et al. Molecular Cloning of a Human Melanoma-Associated Chondroitin Sulfate Proteoglycan. *Proc Natl Acad Sci USA* (1996) 93(18):9710–5. doi: 10.1073/pnas.93.18.9710
20. Nicolosi PA, Dallatomasina A, Perris R. Theranostic Impact of NG2/CSPG4 Proteoglycan in Cancer. *Theranostics* (2015) 5(5):530–44. doi: 10.7150/thno.10824
21. Cooney CA, Jousheghany F, Yao-Borengasser A, Phanavanh B, Gomes T, Kieber-Emmons AM, et al. Chondroitin Sulfates Play a Major Role in Breast Cancer Metastasis: A Role for CSPG4 and CHST11 Gene Expression in Forming Surface P-Selectin Ligands in Aggressive Breast Cancer Cells. *Breast Cancer Res* (2011) 13(3):R58. doi: 10.1186/bcr2895
22. Yang J, Price MA, Neudauer CL, Wilson C, Ferrone S, Xia H, et al. Melanoma Chondroitin Sulfate Proteoglycan Enhances FAK and ERK Activation by Distinct Mechanisms. *J Cell Biol* (2004) 165(6):881–91. doi: 10.1083/jcb.200403174.jcb.200403174
23. Chalmers ZR, Connelly CF, Fabrizio D, Gay L, Ali SM, Ennis R, et al. Analysis of 100,000 Human Cancer Genomes Reveals the Landscape of Tumor Mutational Burden. *Genome Med* (2017) 9(1):34. doi: 10.1186/s13073-017-0424-2. 10.1186/s13073-017-0424-2 [pii].
24. Budczies J, Allgauer M, Litchfield K, Rempel E, Christopoulos P, Kazdal D, et al. Optimizing Panel-Based Tumor Mutational Burden (TMB) Measurement. *Ann Oncol* (2019) 30(9):1496–506. doi: 10.1093/annonc/mdz205
25. Li T, Fu J, Zeng Z, Cohen D, Li J, Chen Q, et al. TIMER2.0 for Analysis of Tumor-Infiltrating Immune Cells. *Nucleic Acids Res* (2020) 48(W1):W509–14. doi: 10.1093/nar/gkaa407
26. Subramanian A, Tamayo P, Mootha VK, Mukherjee S, Ebert BL, Gillette MA, et al. Gene Set Enrichment Analysis: A Knowledge-Based Approach for Interpreting Genome-Wide Expression Profiles. *Proc Natl Acad Sci USA* (2005) 102(43):15545–50. doi: 10.1073/pnas.0506580102
27. Szklarczyk D, Gable AL, Lyon D, Junge A, Wyder S, Huerta-Cepas J, et al. STRING V11: Protein-Protein Association Networks With Increased Coverage, Supporting Functional Discovery in Genome-Wide Experimental Datasets. *Nucleic Acids Res* (2019) 47(D1):D607–13. doi: 10.1093/nar/gky1131
28. Yeong J, Tan T, Chow ZL, Cheng Q, Lee B, Seet A, et al. Multiplex Immunohistochemistry/Immunofluorescence (mIHC/IF) for PD-L1 Testing in Triple-Negative Breast Cancer: A Translational Assay Compared With Conventional IHC. *J Clin Pathol* (2020) 73(9):557–62. doi: 10.1136/jclinpath-2019-206252
29. Geldres C, Savoldo B, Hoyos V, Caruana I, Zhang M, Yvon E, et al. T Lymphocytes Redirected Against the Chondroitin Sulfate Proteoglycan-4 Control the Growth of Multiple Solid Tumors Both *In Vitro* and *In Vivo*. *Clin Cancer Res* (2014) 20(4):962–71. doi: 10.1158/1078-0432.CCR-13-2218
30. Zheng C, Yan S, Lu L, Yao H, He G, Chen S, et al. Lovastatin Inhibits EMT and Metastasis of Triple-Negative Breast Cancer Stem Cells Through Dysregulation of Cytoskeleton-Associated Proteins. *Front Oncol* (2021) 11:656687. doi: 10.3389/fonc.2021.656687
31. Chen Y, Liu Q, Chen Z, Wang Y, Yang W, Hu Y, et al. PD-L1 Expression and Tumor Mutational Burden Status for Prediction of Response to Chemotherapy and Targeted Therapy in Non-Small Cell Lung Cancer. *J Exp Clin Cancer Res* (2019) 38(1):193. doi: 10.1186/s13046-019-1192-1. 10.1186/s13046-019-1192-1 [pii].
32. Rizvi NA, Hellmann MD, Snyder A, Kvistborg P, Makarov V, Havel JJ, et al. Cancer Immunology. Mutational Landscape Determines Sensitivity to PD-1 Blockade in Non-Small Cell Lung Cancer. *Science* (2015) 348(6230):124–8. doi: 10.1126/science.aaa1348
33. Goodman AM, Sokol ES, Frampton GM, Lippman SM, Kurzrock R. Microsatellite-Stable Tumors With High Mutational Burden Benefit From Immunotherapy. *Cancer Immunol Res* (2019) 7(10):1570–3. doi: 10.1158/2326-6066.CIR-19-0149
34. Salvianti F, Rotunno G, Galardi F, De Luca F, Pestrin M, Vannucchi AM, et al. Feasibility of a Workflow for the Molecular Characterization of Single Cells by Next Generation Sequencing. *Biomol Detect Quantif* (2015) 5:23–9. doi: 10.1016/j.bdq.2015.07.002
35. Giordano A, Liu Y, Armeson K, Park Y, Ridinger M, Erlander M, et al. Polo-Like Kinase 1 (Plk1) Inhibition Synergizes With Taxanes in Triple Negative Breast Cancer. *PloS One* (2019) 14(11):e0224420. doi: 10.1371/journal.pone.0224420
36. Marzec KA, Lin MZ, Martin JL, Baxter RC. Involvement of P53 in Insulin-Like Growth Factor Binding Protein-3 Regulation in the Breast Cancer Cell Response to DNA Damage. *Oncotarget* (2015) 6(29):26583–98. doi: 10.18632/oncotarget.5612
37. Guo Y, Lu X, Chen Y, Rendon B, Mitchell RA, Cuatrecasas M, et al. Zeb1 Induces Immune Checkpoints to Form an Immunosuppressive Envelope Around Invading Cancer Cells. *Sci Adv* (2021) 7(21):eabd7455. doi: 10.1126/sciadv.abd7455
38. Wang S, Li J, Xie J, Liu F, Duan Y, Wu Y, et al. Programmed Death Ligand 1 Promotes Lymph Node Metastasis and Glucose Metabolism in Cervical Cancer by Activating Integrin Beta4/SNAI1/SIRT3 Signaling Pathway. *Oncogene* (2018) 37(30):4164–80. doi: 10.1038/s41388-018-0252-x
39. Noman MZ, Van Moer K, Marani V, Gemmill RM, Tranchevent LC, Azuaje F, et al. CD47 Is a Direct Target of SNAI1 and ZEB1 and its Blockade Activates the Phagocytosis of Breast Cancer Cells Undergoing EMT. *Oncoimmunology* (2018) 7(4):e1345415. doi: 10.1080/2162402X.2017.1345415
40. Yang M, Li Z, Tao J, Hu H, Li Z, Zhang Z, et al. Resveratrol Induces PD-L1 Expression Through Snail-Driven Activation of Wnt Pathway in Lung Cancer Cells. *J Cancer Res Clin Oncol* (2021) 147(4):1101–13. doi: 10.1007/s00432-021-03510-z

Conflict of Interest: The authors declare that the research was conducted in the absence of any commercial or financial relationships that could be construed as a potential conflict of interest.

Publisher's Note: All claims expressed in this article are solely those of the authors and do not necessarily represent those of their affiliated organizations, or those of the publisher, the editors and the reviewers. Any product that may be evaluated in this article, or claim that may be made by its manufacturer, is not guaranteed or endorsed by the publisher.

frontiers in Oncology

ORIGINAL RESEARCH
published: 04 March 2022
doi: 10.3389/fonc.2022.831507

Expression Patterns of Ezrin and AJAP1 and Clinical Significance in Breast Cancer

Cong Xu[1], Feng Wang[1], Li Hao[1], Jing Liu[2,3,4], Benjie Shan[1], Shuhua Lv[5], Xinghua Han[1†], Yueyin Pan[1*†] and Yun Niu[2,3,4*†]*

[1] Department of Medical Oncology, The First Affiliated Hospital of University of Science and Technology of China (USTC), Division of Life Sciences and Medicine, University of Science and Technology of China, Hefei, China, [2] Tianjin Medical University Cancer Institute and Hospital, National Clinical Research Center of Cancer, Key Laboratory of Cancer Prevention and Therapy, Tianjin's Clinical Research Center for Cancer, Tianjin, China, [3] Key Laboratory of Breast Cancer Prevention and Therapy, Tianjin Medical University, Ministry of Education, Tianjin, China, [4] Department of Breast Cancer Pathology and Research Laboratory, Tianjin Medical University Cancer Institute and Hospital, Tianjin,China, [5] Department of Pathology, Tianjin Union Medical Center, Tianjin People's Hospital, Tianjin, China

OPEN ACCESS

Edited by:
San-Gang Wu, First Affiliated Hospital of Xiamen University, China

Reviewed by:
Concetta Saponaro, National Cancer Institute Foundation (IRCCS), Italy
Pranshu Sahgal, Dana–Farber Cancer Institute, United States

***Correspondence:**
Xinghua Han
hxhmail@ustc.edu.cn
Yueyin Pan
panyueyin@ustc.edu.cn
Yun Niu
yunniu0823@126.com

†These authors have contributed equally to this work and share last authorship

Specialty section:
This article was submitted to Breast Cancer, a section of the journal Frontiers in Oncology

Received: *08 December 2021*
Accepted: *02 February 2022*
Published: *04 March 2022*

Citation:
Xu C, Wang F, Hao L, Liu J, Shan B, Lv S, Han X, Pan Y and Niu Y (2022) Expression Patterns of Ezrin and AJAP1 and Clinical Significance in Breast Cancer. Front. Oncol. 12:831507. doi: 10.3389/fonc.2022.831507

Ezrin and adherens junction-associated protein 1 (AJAP1) are structural proteins which are involved in numerous human malignancies. However, little is known about the relationship between them in breast cancer. This study was set out to investigate the relationship between them and to further explore the mechanism of AJAP1-mediating cytoskeleton in breast cancer progression. Ezrin and AJAP1 expressions were detected in 377 samples of breast cancer by immunohistochemistry, and different expression patterns between AJAP1 and Ezrin with clinicopathological parameters were analyzed. Besides, univariate and multivariate Cox models were used to evaluate their prognostic potential. Enzyme-linked immunosorbent assay, Western blot, qRT-PCR, and phalloidin staining of F-actin were used to explore the relationship and the mechanism between AJAP1 and Ezrin in cytoskeleton arrangement. 377 cases of breast cancer results showed that AJAP1 expression was negatively related with histological grade and lymph node involvement and could be an independent prognosis marker of breast cancer. AJAP1 expression tended to be higher in the Ezrin-negative expression case. Patients with $AJAP1^{negative}$ and $Ezrin^{positive}$ expression had a worse prognosis ($p < 0.0001$) and shorter DFS ($p = 0.015$). More importantly, AJAP1 depletion increased the cell ability of F-actin formation through promoting Ezrin expression. AJAP1 depletion might mediate breast cancer malignancy potential through promoting Ezrin expression and cytoskeleton formation.

Keywords: AJAP1, Ezrin, adherens junction-associated 1, shrew-1, prognosis

Abbreviations: AJAP1, adherens junction-associated protein 1; IHC, immunohistochemistry; qRT-PCR, quantitative reverse-transcription polymerase chain reaction; ELISA, enzyme-linked immunosorbent assay; OS, overall survival; DFS, disease-free survival.

INTRODUCTION

Breast cancer, the leading cancer killer across the world, has been threatening women's health and its morbidity and mortality have increased recently (1). Tumor invasion and metastasis are two important reasons resulting in breast cancer development. Besides, cytoskeleton-associated proteins also play key roles in this process (2).

Adherens junction-associated protein 1 (AJAP1) is also named shrew-1; it was firstly found as a novel transmembrane protein of adherens junctions in epithelial cells (3, 4). AJAP1 has been proved as a tumor suppressor in glioma (5–7), hepatocellular carcinoma (8, 9), esophagus carcinoma (10), oligodendroglioma (11), and endometrial cancer (12). Especially in glioblastoma, AJAP1's role has been fully explored. For example, both Han et al. (7) and Yang et al. (5) testified that AJAP1 expression affected the cytoskeleton in glioblastoma and predicted poor prognosis. AJAP1 also participated in many transduction signals of cell–cell and cell–extracellular matrix related to cell motility, migration, and invasion ability. Our previous study verified that AJAP1 depletion promoted breast cancer progression by accelerating β-catenin nuclear transaction (13). However, data about the breast cancer are still scarce.

Ezrin is an important member of ERM (ezrin, radixin, and moesin) proteins, which is critical for structural stability and integrity maintenance (14). Recent studies show that Ezrin can act as a tumor metastasis regulator in invasion and metastasis of many types of cancer (15–18). Besides, it also mediates many cellular activities such as polarity, motility, adhesion, and survival which are associated with cancer development and progression (19, 20). Overexpression of Ezrin is seen as a tumor prognosis marker of several human cancers (21–26). In breast cancer, Ezrin also plays an instrumental role in mediating tumor progression and metastasis (27). However, more data on the mechanism of Ezrin in breast cancer need to be further explored.

The above data showed that both adherens junction-associated protein 1 (AJAP1) and Ezrin were structural proteins. In the current study, we first investigated the relationship between Ezrin and AJAP1 expression and then evaluated their prognosis accuracy in predicting prognosis of breast cancer patients. More importantly, these results might bring a new insight on the feedback loop of AJAP1 and Ezrin in breast cancer progression.

MATERIALS AND METHODS

Patients' Selection and Related Information

377 patients of breast cancer who underwent mastectomy and a diagnosis of invasive ductal carcinoma were made based on a histopathological evaluation between 2005 and 2006 at Tianjin Medical University Cancer Institute and Hospital. They were randomly selected, and all were informed with study information. None of them received preoperative treatment such as chemotherapy and radiotherapy. Besides, their clinicopathologic data were available. Patients of this cohort were female, and the age range is 27 to 82 years (median age is 51 years).

Immunohistochemistry and Evaluation

Immunohistochemistry assay was carried out as in our previous study (13). All primary antibodies included ER (ZETA, SP1; 1:200 dilution), PR (ZETA, SP2; 1:200 dilution), epidermal growth factor receptor 2 (HER2) (Invitrogen, Carlsbad, CA, USA, CB11; 1:100 dilution), Ki67 (Invitrogen, K-2; 1:100 dilution), AJAP1 (Abcam, Cambridge, MA, USA, ab205496, 1:100 dilution), and Ezrin (Santa Cruz Biotechnology, Dallas, TX, USA, sc-58758;1:200 dilution), respectively. Sections of normal breast tissue were processed simultaneously and served as positive controls for ER and PR. Similarly, HER2- and Ki67-positive breast cancer tissues were used as positive controls for HER2 and Ki67, respectively. Besides,AJAP1-positive glioma tissues represent AJAP1 positive, Ezrin-positive breast cancer tissues represent Ezrin positive. In addition, normal goat serum substituted primary antibodies as negative controls. Besides, we have also used positive and negative controls for each run. The AJAP1 and Ezrin score evaluation was based on the location of immunoreactivity, the percentage of stained cells. The percentage of positivity of the tumor was scored as "0" (no tumor cells), "1" (1%–25%), "2" (26%–50%), "3" (51%–75%), and "4" (75%–100%). The staining intensity of the positive tumor cells was scored as "0" (no staining), "1" (weak staining), "2" (moderate staining), and "3" (strong staining). Eventually, the multiplier of scores is as follows: 0–3 for negative expression, 4–12 for positive expression.

Follow-Up

All the patients had decent follow-up data which were obtained by medical records or telephone calls. The time of last follow-up was August 1, 2018. Follow-up time ranges from 85 to 144 months (average 104 months).

Cell Culture

T47D and MDA-MB-231 cell lines were obtained from the American Type Culture Collection (ATCC, Manassas, USA) for further study. They were cultured in RPMI-1640 medium (Gibco, Grand Island, NY, USA) with 10% FBS and 1% penicillin/streptomycin (HyClone, Logan, UT, USA) in a 5% CO_2 incubator at 37°C.

Western Blot

Total proteins were extracted by using RIPA with PMSF according to the manufacturer's protocol. An equal amount (30 μg) of samples was separated on 10% SDS-PAGE gels and transferred to PVDF membranes (Millipore, Burlington, MA, USA). Then, the membranes were blocked in 5% non-fat milk for 1 h. Eventually, these membranes were detected using the ECL detection Kit (Solarbio, Beijing, China) after incubating the primary antibodies including anti-AJAP1 (AJAP1; Abcam; ab205496,

rabbit secondary antibody) and anti-Ezrin (Ezrin; Santa Cruz Biotechnology, sc-58758, mouse secondary antibody).

Cell Transfection and Plasmids

The AJAP1 siRNAs and control plasmids are shown as in our previous study (13). T47D and MDA-MB-231 cells were transfected using FuGENE 6 according to the manufacturer's instruction.

Real-Time Quantitative RT-PCR

Total RNA was isolated from cell lines using TRIzol reagent (Invitrogen, Inc.) under the manufacturer's protocols. Then the RNA was reversed transcribed to cDNA using SuperScript Reverse Transcriptase (Takara, Shiga, Japan). Reactions were performed using the SYBR Green PCR Kit (Takara, Japan). GAPDH was used as an internal control. The mRNA expression folds were analyzed by $2^{-\Delta\Delta Ct}$. The primer sequences were as follows: Ezrin-forward: 5′-CGCTCTA AGGTTCTGCTCT-3′, Ezrin-reverse: 5′-TCCTGGGCAGACA CCTTCTTA-3′; GAPDH-forward: 5′-CTGGGCTACACT GAGCACC-3′, GAPDH-reverse: 5′-AAGTGGTCGTTGAGGG CAATG-3′. Each experiment was conducted at least three times.

Phalloidin Staining of F-Actin

On the first day, stable cell lines were transferred to 24 wells. 24 hours later, they were fixed with paraformaldehyde for 10 min and permeabilized with 1 ml 0.2% of Triton X-100 for 10 min. After three times of PBS washing, samples were blocked with 1% of bovine serum albumin (BSA; Sigma-Aldrich, St. Louis, MO, USA) and incubated with 100 μl fluorescent phalloidin (Phalloidin-iFluor 488 Reagent, Abcam, ab176753) for 1 h, stained with DAPI for 10 min. Both of them were put in the dark environment at room temperature. After 3 times of PBS washing, cells were observed under a confocal microscope (Olympus, Center Valley, PA, USA).

Enzyme-Linked Immunosorbent Assay (ELISA)

The ELISA technique kit (Cusabio Biotech, Wuhan, China) was used to evaluate Ezrin expression in different AJAP1 expression groups according to the manufacturer's guidelines. Eventually, both of them were assessed using a spectrophotometer (Thermo Scientific, Waltham, MA, USA) at 450 nm.

Bioinformatics Analysis

StarBase V3.0 (https://www.ncbi.nlm.nih.gov/geo/) online databases were used to validate the potential relationship between AJAP1 and Ezrin in breast cancer. StarBase V3.0 is an open-source platform for studying the miRNA–ncRNA, miRNA–mRNA, ncRNA–RNA, RNA–RNA, RBP–ncRNA, and RBP–mRNA interactions from CLIP-seq, degradome-seq, and RNA–RNA interactome data. Besides, it also allows researchers to perform Pan-Cancer analysis on RNA–RNA and RBP–RNA interactions, as well as the survival and differential expression analysis of miRNAs, lncRNAs, pseudogenes, and mRNAs.

Then we also downloaded breast cancer datasets from the Cancer Genome Atlas (TCGA) project and used "R" software to analyze the potential relationship between AJAP1 and Ezrin expression.

Statistical Analysis

Statistical analyses were conducted using SPSS24.0 software. Clinicopathological parameters with the expression of two proteins were evaluated by the chi-square test and spearman test. Kaplan–Meier curves of DFS and OS were constructed. All data were shown as mean ± S.D. $p < 0.05$ was considered statistically significant.

RESULTS

Expression of Ezrin and AJAP1 in Breast Cancer

AJAP1 and Ezrin expressions were detected in 377 cases of breast cancer using immunohistochemistry (IHC) technology. Positive staining of Ezrin was mainly observed in the cytoplasm in the breast cancer tissue slides. Different staining intensities of Ezrin are demonstrated in **Figure 1A**. As our previous study reported (13), AJAP1 was mainly located in the cytoplasm, with little membrane staining. There are four different expression patterns between AJAP1 and Ezrin (**Figures 1B**–**E**). Thus, AJAP1-positive staining was observed in 213 (56.5%) cases of 377 breast cancer samples and Ezrin-positive staining occurred in 165 (43.77%) cases of 377 breast cancer tissue slides.

Correlation Between Ezrin and AJAP1 Expression With Clinicopathological Parameters

Next, the association between AJAP1 expression and Ezrin expression and the clinicopathological characteristics of breast cancer patients are shown in **Table 1**. It was obvious that AJAP1 expression was closely associated with histological grade ($p < 0.0001$) and lymph node ($p < 0.0001$). Meanwhile, Ezrin expression was more closely related with histological grade ($p = 0.004$) and lymph node ($p < 0.0001$). However, other clinicopathological parameters did not show any significant association with AJAP1 expression or Ezrin expression.

Different Expressional Patterns of AJAP1 and Ezrin With Clinicopathological Parameters

Table 2 shows that the different expressional patterns' results were inconsistent with the former results and they were also associated with lymph node ($p < 0.0001$) and histological grade ($p < 0.001$). Next, **Figure 2A** also shows that AJAP1 expression was also related with Ezrin expression. What is more, starBase v3.0 was utilized to reveal that AJAP1 expression was negatively related with Ezrin expression (**Figure 2B**). We also used Spearman test to analyze the relationship between AJAP1 and Ezrin. **Figure 2C** shows that AJAP1 was inversely related with Ezrin expression in

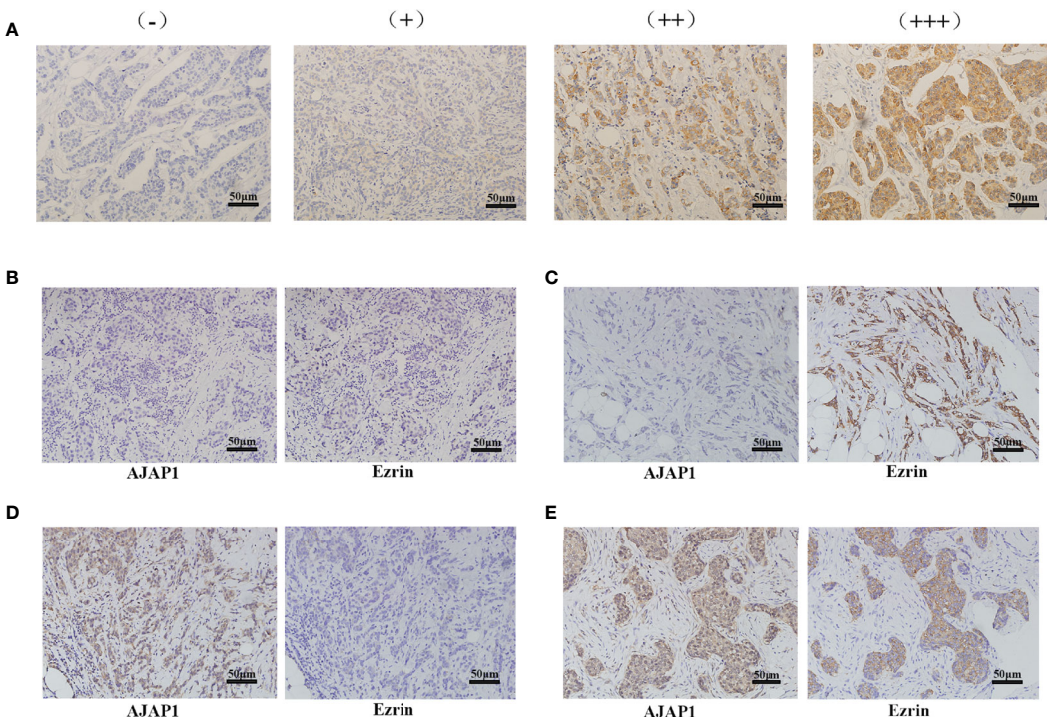

FIGURE 1 | Different expression of Ezrin and AJAP1 in breast cancer. **(A)** Different staining intensity of Ezrin in breast cancer (×100). **(B–E)** Series slides of Ezrin and AJAP1 expression in breast cancer tissue slides: **(B)** AJAP1 negative/Ezrin-negative (×100), **(C)** AJAP1-negative/Ezrin-positive (×100), **(D)** AJAP1-positive/Ezrin-negative (×100), **(E)** AJAP1-positive/Ezrin-positive (×100).

377 cases of breast cancer. The data of the TCGA dataset also identified this (**Figure 2D**).

Survival Analysis

Kaplan–Meier curves demonstrated that a high expression of AJAP1 showed a good prognosis and short disease progression (**Figure 3A**, OS: $p < 0.0001$; **Figure 3B**, DFS: $p = 0.003$). The OS and DFS curves showed that Ezrin expression was associated with shorter OS ($p = 0.008$, **Figure 3C**) and DFS ($p = 0.0043$, **Figure 3D**). The results of expression patterns with OS and DFS demonstrated that tumors with AJAP1-Ezrin+ expression exhibited the worst OS ($p < 0.0001$, **Figure 3E**) and shortest DFS ($p = 0.015$, **Figure 3F**) among four groups.

What is more, univariate analysis (**Table 3**) demonstrated that AJAP1-/Ezrin+ was a significant risk factor for unfavorable prognosis of OS ($p = 0.005$) and DFS ($p = 0.044$). Histological grade and lymph node metastasis also showed poor OS ($p < 0.0001$ and $p < 0.0001$, respectively) and short DFS ($p = 0.031$ and $p = 0.003$, respectively) among the four groups. Other factors did not have significant difference.

Multivariate analysis (**Table 4**) showed that AJAP1-Ezrin+, histological grade, and lymph node metastasis were risk factors for OS ($p = 0.021$, $p = 0.005$, and $p < 0.0001$). Additionally, none of the factors showed a significant difference.

Taken together, AJAP1-Ezrin+ was a potential risk factor for predicting breast cancer patients with poor prognosis.

Evaluation of Diagnostic Efficiency

Next, ROC curves and the area under the curve (AUC) were used to assess the accuracy of AJAP1 and Ezrin expressions as biomarkers for breast cancer diagnosis. Results demonstrated that AJAP1 AUC was 0.777 (95% confidence interval was 0.711–0.844, $p < 0.0001$) in different breast cancer patients and the optimal cutoff value was 0.528 (**Figure 4A**). Meanwhile, Ezrin's AUC was 0.610 (95% confidence interval was 0.507–0.714, $p = 0.045$) with the optical cutoff value of 0.329 (**Figure 4B**).

Next, the sensitivity and specificity of AJAP1 expression and Ezrin expression were calculated using AJAP1 expression 0.528 and Ezrin expression 0.329 as the cutoff. AJAP1 expression specificity and sensitivity were 0.561 and 0.767, respectively. As for Ezrin expression, the corresponding values were 0.9 and 0.628, respectively.

AJAP1 Affects the Cytoskeleton of Breast Cancer Cell by Mediating Ezrin Expression

The above results showed that AJAP1 expression was negatively related with Ezrin expression in breast cancer tissue slides. Besides, both AJAP1 and Ezrin were important molecules that maintained the cell structure and actin cytoskeleton. Next, the effect of changing the AJAP1 expression on the cytoskeleton of breast cancer cells was explored. Firstly, we conducted T47D cells with a knocked-down AJAP1 expression and MDA-MB-231 with an overexpressed AJAP1 expression. Results of the Western blot

TABLE 1 | AJAP1 and Ezrin expression with clinicopathological parameters in breast cancer patients.

Factor	AJAP1				*p*-value	Ezrin				*p*-value
	Positive		Negative			Positive		Negative		
	N	%	N	%		N	%	N	%	
All	213	56.50	164	43.50		165	43.77	212	56.23	
Age										
≤50	104	48.8	81	49.4	0.914	86	52.1	99	46.7	0.296
>50	109	51.2	83	50.6		79	47.9	113	53.3	
Menopausal status										
Premenopausal	115	54.0	87	53.0	0.856	97	58.8	105	49.5	0.074
Postmenopausal	98	46.0	77	47.0		68	41.2	107	50.5	
Tumor size										
T1	93	43.7	63	38.4	0.250	62	37.6	94	44.3	0.372
T2	102	47.9	79	48.2		83	50.3	98	46.2	
T3	18	8.5	22	13.4		20	12.1	20	9.4	
Histological grade										
1	53	24.9	16	9.8	<0.0001*	23	13.9	46	21.7	0.004*
2	117	54.9	83	50.6		81	49.1	119	56.1	
3	43	20.2	65	39.6		61	37.0	47	22.2	
Lymph node										
0	166	77.9	23	14.0	<0.0001*	56	33.9	133	62.7	<0.0001*
1–3	34	16.0	65	39.6		37	22.4	62	29.2	
4–9	9	4.2	50	30.5		45	27.3	14	6.6	
≥10	4	1.9	26	15.9		27	16.4	3	1.4	
ER										
Negative	82	38.5	66	40.2	0.731	67	40.6	81	38.2	0.636
Positive	131	61.5	98	59.8		98	59.4	131	61.8	
PR										
Negative	112	52.6	76	46.3	0.230	77	46.7	111	52.4	0.273
Positive	101	47.4	88	53.7		88	53.3	101	47.6	
Her-2										
Negative	161	75.6	122	74.4	0.790	119	72.1	164	77.4	0.244
Positive	52	24.4	42	25.6		46	27.9	48	22.6	
Ki67										
<20	48	22.5	28	17.1	0.190	33	20.0	43	20.3	0.946
≥20	165	77.5	136	82.9		132	80.0	169	79.7	
P53										
Negative	103	48.4	86	52.4	0.432	82	49.7	107	50.5	0.881
Positive	110	51.6	78	47.6		83	50.3	105	49.5	

**Difference was statistically significant.*

showed that AJAP1 depletion promoted Ezrin expression in T47D and upregulated AJAP1 exhibited the opposite results in MDA-MB-231 cells (**Figure 5A**). Then, qRT-PCR was also conducted to observe the RNA levels in cells with different expressions of AJAP1 (**Figure 5B**). It seemed that overexpressed AJAP1 can reduce the Ezrin RNA level and downregulation of AJAP1 increased the Ezrin RNA level, while when we overexpressed or knocked down Ezrin expression, it had no effect on AJAP1 (**Supplementary Figure S1**). Collectively, AJAP1 negatively mediated Ezrin expression in breast cancer cell lines. After that, the effect of changing the AJAP1 expression on the cytoskeleton of breast cancer cells was explored. The results of fluorescent staining of F-actin through phalloidin showed that AJAP1 depletion in T47D cells increased the amount of F-actin expression in the cytoskeleton filaments, which is demonstrated by a significant increase in fluorescent intensity compared with ShControl groups (**Figure 5C**). Consistently, ELISA assay showed a significant increase in Ezrin expression level after silencing AJAP1 expression in T47D cells (**Figure 5D**, top panel). Apart from this, overexpressed AJAP1 expression in MDA-MB-231 cells revealed contrasting results (**Figures 5C, D**). These experiments together suggested that AJAP1 suppressed actin expression by promoting Ezrin expression.

DISCUSSION

Tumor metastasis and invasion are a series of complex, multistep progression that depends on the dynamic motion of cell to cell and cell to extracellular matrix. Besides, the key factor is cytoskeleton-related proteins. Ezrin belongs to the ERM (ezrin–radixin–moesin) family, located on 6q25.2-q26 (17). Most studies also demonstrated that it was a tumor metastasis mediator (28). In breast cancer, many reports revealed Ezrin's different functions. Li et al. (29) revealed that upregulated Ezrin expression was positively related with lymph node involvement and proved that Ezrin could be a biomarker for predicting lymphatic metastasis of invasive ductal carcinoma. Consistent with their results, we showed that Ezrin

TABLE 2 | AJAP1/Ezrin expression and clinicopathological parameter in patients with breast cancer patients.

Factor	AJAP1+Ezrin+		AJAP1+/Ezrin-		AJAP1-/Ezrin+		AJAP1-/Ezrin-		*p* value
	N	%	N	%	N	%	N	%	
All	72	19.10	141	37.40	93	24.67	71	18.83	
Age									
≤50	38	52.8	66	46.8	48	51.6	33	46.5	0.773
>50	34	47.2	75	53.2	45	48.4	38	53.5	
Menopausal status									
Premenopausal	43	59.7	72	51.1	54	58.1	33	46.5	0.303
Postmenopausal	29	40.3	69	48.9	39	41.9	38	53.5	
Tumor size									
T1	29	40.3	64	45.4	33	35.5	30	42.3	0.663
T2	36	50.0	66	46.8	47	50.5	32	45.1	
T3	7	9.7	11	7.8	13	14.0	9	12.7	
Histological grade									
1	17	23.6	36	25.5	6	6.5	10	14.1	<0.0001*
2	37	51.4	80	56.7	44	47.3	39	54.9	
3	18	25.0	25	17.7	43	46.2	22	31.0	
Lymph node									
0	54	75.0	112	79.4	2	2.2	21	29.6	<0.0001*
1–3	10	13.9	24	17.0	27	29.0	38	53.5	
4–9	5	6.9	4	2.8	40	43.0	10	14.1	
≥10	3	4.2	1	0.7	24	25.8	2	2.8	
ER									
Negative	25	34.7	57	40.4	42	45.2	24	33.8	0.400
Positive	47	65.3	84	59.6	51	54.8	47	66.2	
PR									
Negative	33	45.8	79	56.0	44	47.3	32	45.1	0.320
Positive	39	54.2	62	44.0	49	52.7	39	54.9	
Her-2									
Negative	51	70.8	110	78.0	68	73.1	54	76.1	0.666
Positive	21	29.2	31	22.0	25	26.9	17	23.9	
Ki67									
<20	18	25.0	30	21.3	83.9	16.1	13	18.3	0.523
≥20	54	75.0	111	78.7	78	83.9	58	81.7	
P53									
Negative	35	48.6	68	48.2	47	50.5	39	54.9	0.818
Positive	37	51.4	73	51.8	46	49.5	32	45.1	

**Difference was statistically significant.*

expression was related with lymph node involvement and histological grade as well. As for breast cancer prognosis, high expression of Ezrin predicted poor OS and high DFS. Besides, David et al. (25) analyzed different locations of Ezrin and summarized that loss of Ezrin apical polarization was related with adverse tumor characteristics of breast cancer cells. Complete membrane staining of Ezrin was linked to high-grade, strong Her-2 and p-AKT expression. In this study, any significant relation between Ezrin expression and Her-2 expression had not been observed due to the limited number of samples. Moreover, silencing of Ezrin reduced the ability of breast cancer cell motion and invasion. Besides, many reports showed that estrogen E2, CD44, etc., mediated Ezrin to promote the malignant potential of breast cancer (30, 31). What is more, Ezrin is also related with breast cancer multidrug resistance (32, 33). It was found in the study that microparticles from breast cancer had tissue selectivity, that is to say, they only transferred resistance proteins to malignant breast cells. ERM protein family and cytoskeletal dynamic proteins may be one of the mechanisms for the multidrug resistance of microparticles from breast cancer (34).

Cell adhesion molecules are glycoproteins which link to the metastasis of tumor cells and that have been extensively studied in recent years. They are mainly distributed on the surface of the cell membrane, and their main function is to regulate the adhesion ability between cells and matrix. AJAP1 is a novel protein of adherens junction and has also been explored in 377 samples of breast cancer tissues. Our study found that the AJAP1-positive rate in 377 samples is 56.5% (213/377) and a low expression of AJAP1 also positively associated with histological grade and lymph node. AJAP1 expression was negatively associated with Ezrin expression including the prognosis function for breast cancer patients. A number of studies on AJAP1 vital function in a variety of types of cancer have attracted people's attention (5–12, 35–39). Moreover, our report provided the first document to explore the relationship between AJAP1 and Ezrin expression in breast cancer tissue slides and analyzed their expression with clinicopathological parameters.

During the past decades, many tools and markers were found to reflect the prognosis of breast cancer and created great advantage on

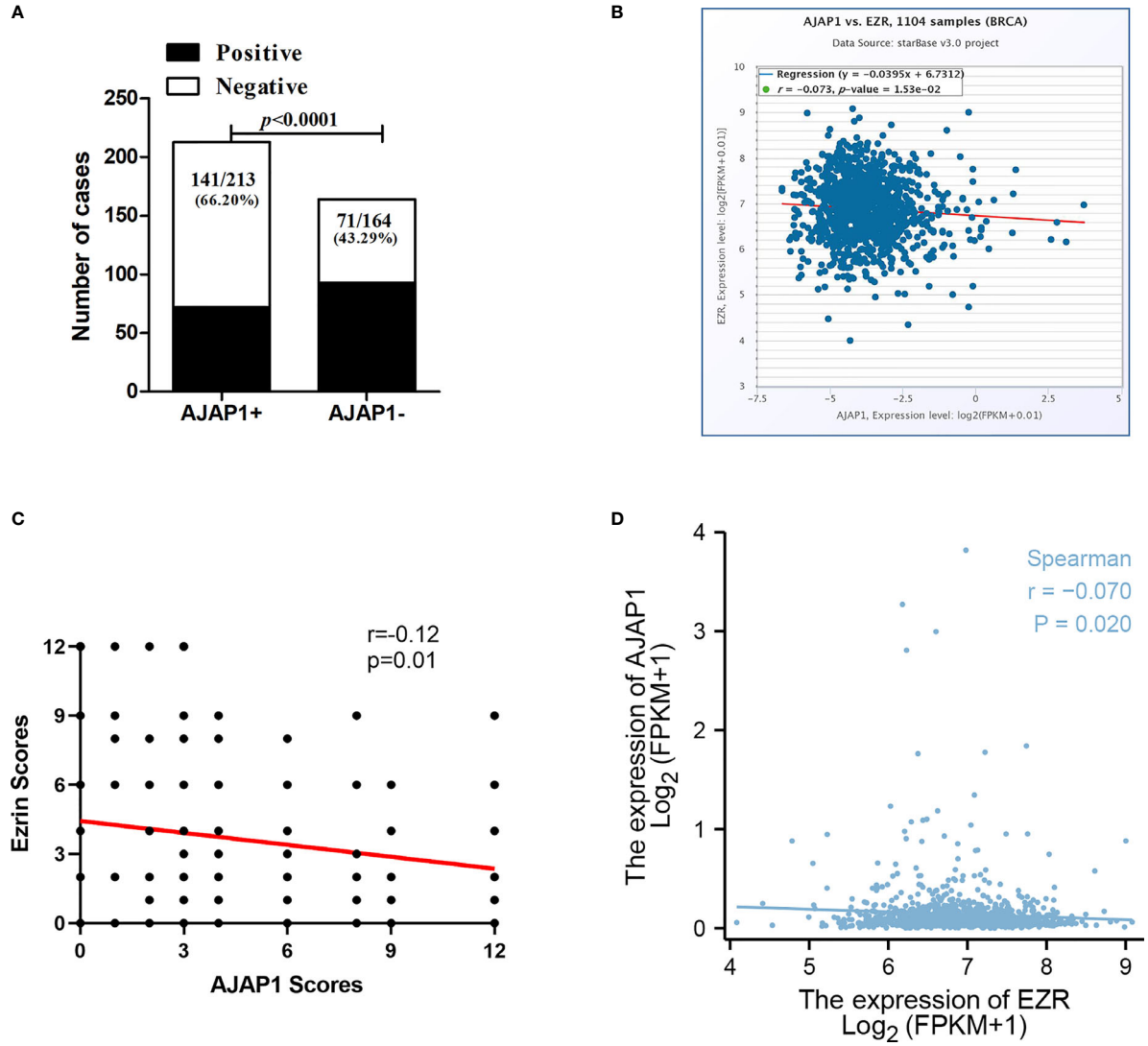

FIGURE 2 | AJAP1 expression is negatively correlated with Ezrin expression. **(A)** Number of cases of different Ezrin expression in AJAP1+ and AJAP1- samples. **(B)** Scatter plot analysis for the correlation between AJAP1 and Ezrin based on starBase v3.0. **(C)** Spearman test about the relationship between AJAP1 and Ezrin in 377 breast cancer cases. **(D)** Spearman analysis for the correlation between AJAP1 and Ezrin based on TCGA datasets.

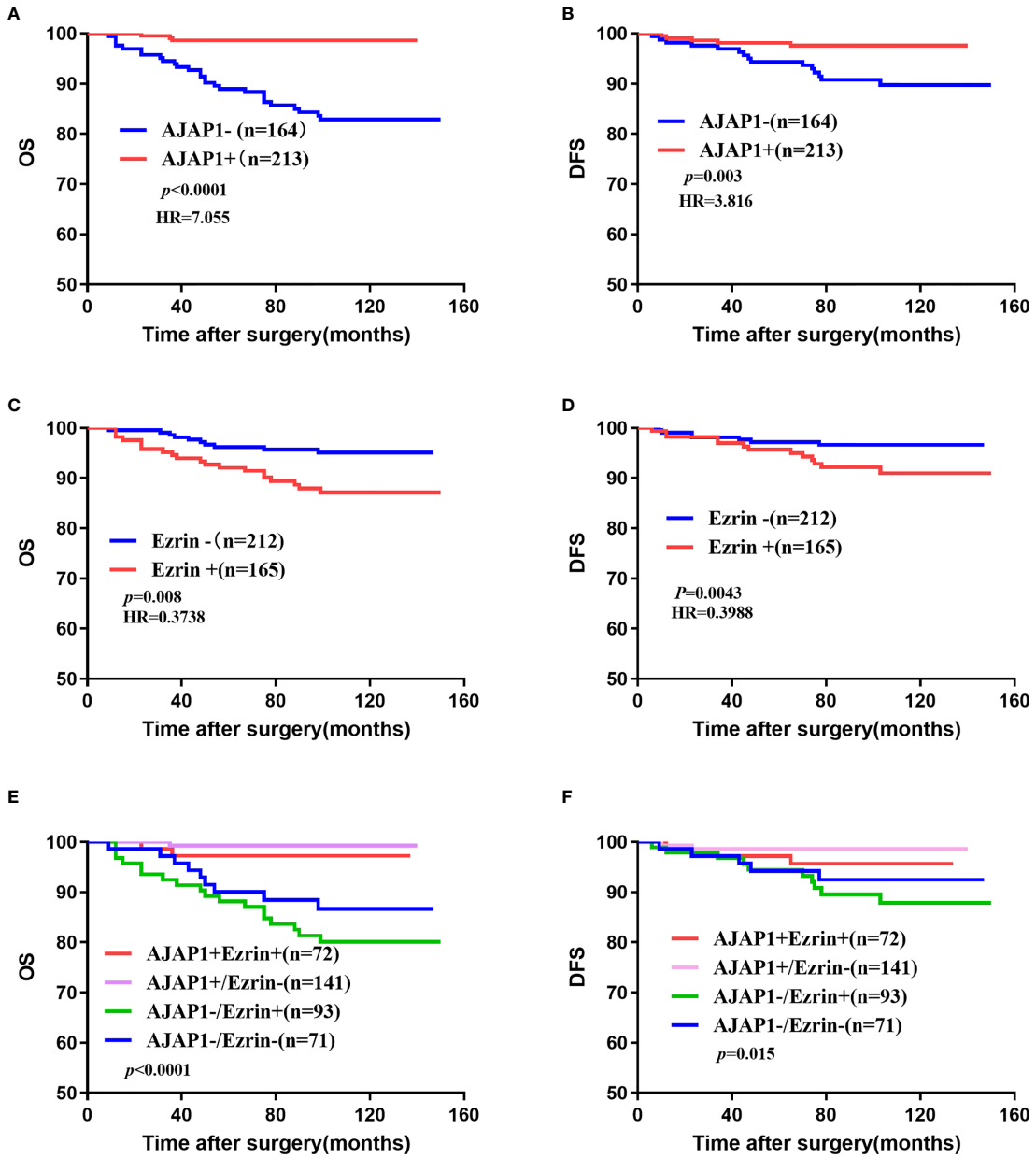

FIGURE 3 | Overall survival and disease-free survival of 377 cases of breast cancer. **(A, B)** OS **(A)** and DFS **(B)** of different AJAP1 expression. **(C, D)** OS **(A)** and DFS **(B)** of different Ezrin expression. **(E, F)** OS **(E)** and DFS **(F)** of different combination between AJAP1 and Ezrin expression.

daily clinical work (40–43). In our research, we found that AJAP1 expression was negatively linked with Ezrin expression and their combination can predict the prognosis of breast cancer. However, the ROC curve demonstrated that AJAP1 showed more accuracy to evaluate the OS status than Ezrin expression. Thus, the results for the combination of AJAP1 and Ezrin expression showed that $AJAP1^{negative}$ $Ezrin^{positive}$ tended to have a low OS. Meanwhile, univariate and multivariate analyses demonstrated that $AJAP1^{negative}Ezrin^{positive}$ was a potential risk factor for breast cancer patients' OS.

The proliferation of tumor cells depends on cytoskeletal recombination, formation of filamentous actin (actin) stress fibers, and increased cytoskeletal protein content. All of them may become the key to influencing the occurrence of cancer invasion and metastasis. Previous studies showed that AJAP1 controlled cell cytoskeleton to inhibit the tumor progression of glioma. Thus, we next examined the effect of AJAP1 act on the cytoskeleton. Here, in our study, we found that AJAP1 depletion can reduce the expression of F-actin. Besides, we also detected the level of Ezrin in AJAP1-silencing cells by ELISA and found

TABLE 3 | Univariate analysis of OS and DFS in breast cancer patients.

Factors	OS HR (95% CI)	*p*	DFS HR (95% CI)	*p*
AJAP1/Ezrin				
AJAP1+/Ezrin+	1		1	
AJAP1+/Ezrin-	0.219(0.047,1.015)	0.052	0.593(0.142,2.481)	0.474
AJAP1-/Ezrin+	0.052(0.007-0.414)	0.005*	0.186(0.036,0.959)	0.044*
AJAP1-/Ezrin-	1.533(0.689-3.414)	0.295	1.509(0.516,4.417)	0.452
Age				
≤50	1		1	
>50	1.286(0.624,2.647)	0.495	0.983(0.409,2.361)	0.969
Menopausal status				
Premenopausal	1		1	
Postmenopausal	1.160(0.567,2.372)	0.685	0.627(0.250,1.571)	0.319
Tumor size				
T1	0.540(0.205-1.420)	0.211	0.670(0.178,2.525)	0.670
T2	0.401(0.148,1.085)	0.072	0.672(0.182,2.484)	0.672
T3	1		1	
Histological grade				
1–2	1		1	
3	5.256(2.460,11.230)	<0.0001*	0.382(0.159,0.918)	0.031*
Lymph node				
Yes	10.255(4.563,23.046)	<0.0001*	3.723(1.548,8.954)	0.003*
No	1		1	
ER				
Positive	1		1	
Negative	0.873(0.610,1.250)	0.460	1.255(0.778,2.024)	0.353
PR				
Positive	1		1	
Negative	1.014(0.496,2.075)	0.969	2.049(0.925,6.269)	0.072
Her-2				
Positive	1		1	
Negative	1.711(0.824,3.554)	0.150	0.687(0.426,1.108)	0.123
Ki67				
<20	1		1	
≥20	2.714(1.002,7.353)	0.05	1.520(0.732,3.156)	0.261
P53				
Positive	1		1	
Negative	0.750(0.518,1.088)	0.129	0.802(0.512,1.254)	0.333

OS, overall survival; DFS, disease-free survival.
**Difference was statistically significant.*

TABLE 4 | Multivariate analysis of OS and DFS in breast cancer patients.

Factors	OS HR (95% CI)	*p*	DFS HR (95% CI)	*p*
AJAP1/Ezrin				
AJAP1+/Ezrin+	1			
AJAP1+/Ezrin-	0.250 (0.054,1.158)	0.076	0.612(0.146,2.562)	0.510
AJAP1-/Ezrin+	0.086(0.011,0.690)	0.021*	0.227(0.043,1.188)	0.079
AJAP1-/Ezrin-	0.851(0.375,1.932)	0.699	1.089(0.359,3.309)	0.880
Histological grade				
1–2	0.333(0.154,0.720)	0.005*	0.559(0.227,1.378)	0.206
3	1		1	
Lymph node				
Yes	1		1	
No	0.191(0.082,0.446)	<0.0001*	0.445(0.173,1.144)	0.093

OS, overall survival; DFS, disease-free survival.
**Difference was statistically significant.*

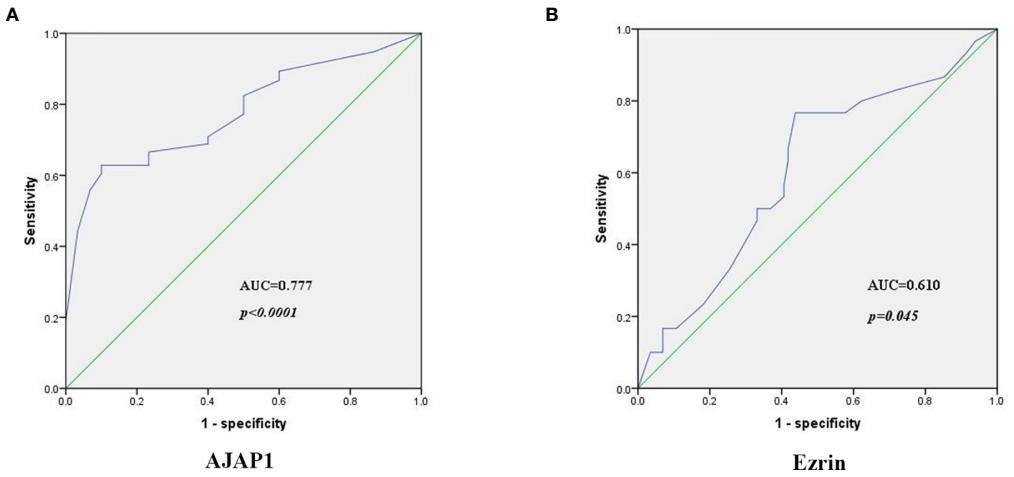

FIGURE 4 | The diagnosis power of AJAP1 **(A)** and Ezrin **(B)** expression in breast cancer patients.

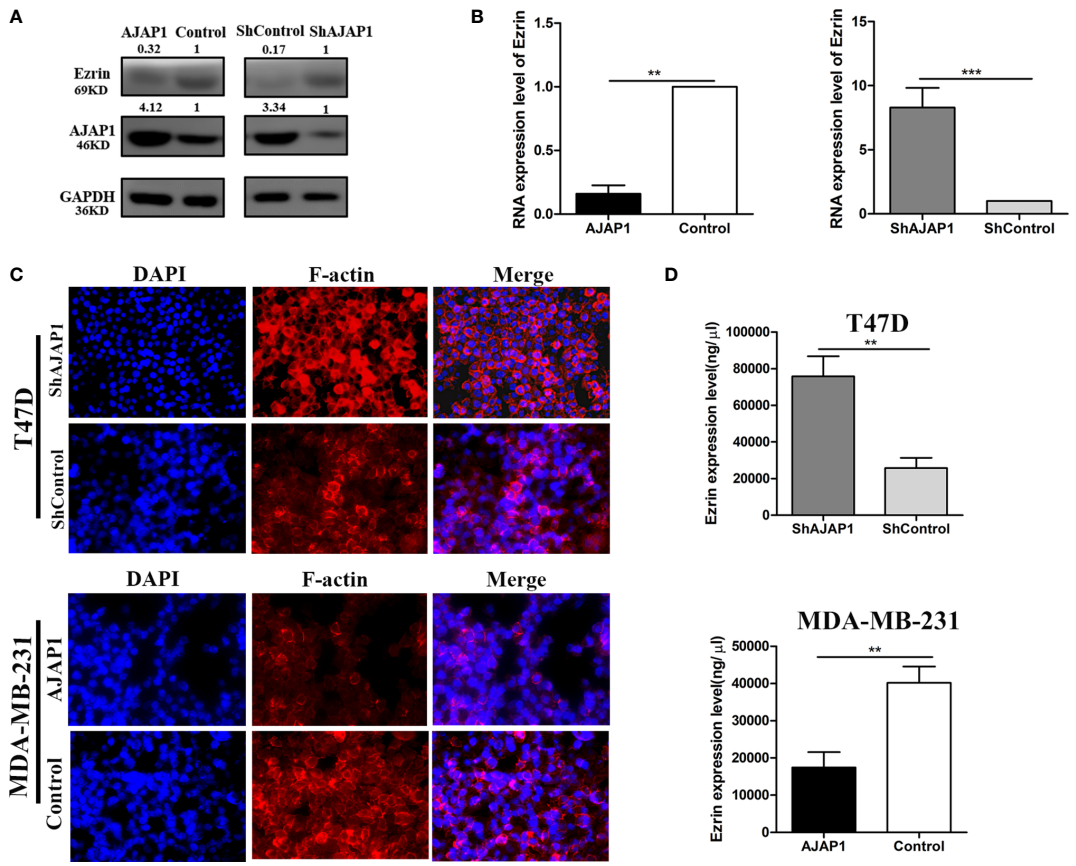

FIGURE 5 | AJAP1 inhibits cytoskeleton formation by reducing Ezrin expression. **(A)** Western blot results of Ezrin expression in AJAP1-overexpressed MDA-MB-231 cells and AJAP1-silenced T47D cells. **(B)** qRT-PCR results of Ezrin expression in AJAP1 overexpressed MDA-MB-231 cells and AJAP1-silenced T47D cells. **(C)** Fluorescent staining of F-actin by phalloidin in AJAP1 depletion T47D cells and AJAP1 overexpressed MDA-MB-231 cells. **(D)** The Ezrin level changes in different expression of AJAP1 stable cell lines by ELISA. Data were shown as mean ± SD. Each experiment was conducted at least three times $^{**}p < 0.01$, $^{***}p < 0.001$.

that downregulation of AJAP1 can reduce the Ezrin expression. Therefore, we presumed that AJAP1 may have prevented tumor malignant behavior by inhibiting Ezrin expression. However, the concrete mechanism needed to be explored in the future days.

To sum up, our research revealed that AJAP1 was low expressed in breast cancer and elucidated its potential pivotal biological role as well. Besides, we also demonstrated a new relationship between AJAP1 and Ezrin in mediating the cytoskeleton of breast cancer cells. However, further studies were needed to analyze the concrete pathway between AJAP1-mediated Ezrin activity in prohibiting breast cancer progression and related clinical therapeutic strategies.

DATA AVAILABILITY STATEMENT

The original contributions presented in the study are included in the article/**Supplementary Material**. Further inquiries can be directed to the corresponding authors.

ETHICS STATEMENT

This study was approved by the Tianjin Medical University Cancer Institute and Hospital, China, and has been performed in accordance with the ethical standards laid down in the 1975 Helsinki Declaration, revised in 2013. The patients/participants provided their written informed consent to participate in this study.

AUTHOR CONTRIBUTIONS

XHH,YYP and YN contributed equally to this work and shared last authorship. All authors contributed to the article and approved the submitted version.

FUNDING

This study was funded by the Key Research and Development Projects from Science and Technology Department of Anhui Province (1704a0802148 and 1804h08020259) and the Hefei Municipal Independent Innovation Policy "Borrowing and Transferring" Project (J2018Y01).

SUPPLEMENTARY MATERIAL

The Supplementary Material for this article can be found online at: https://www.frontiersin.org/articles/10.3389/fonc.2022.831507/full#supplementary-material

Supplementary Figure 1 | qRT-PCR results of AJAP1 expression in Ezrin overexpressed MDA-MB-231 cells and Ezrin-silenced T47D cells. N.S., no significance.

REFERENCES

1. Ginsburg O, Bray F, Coleman MP, Vanderpuye V, Eniu A, Kotha SR, et al. The Global Burden of Women's Cancers: A Grand Challenge in Global Health. *Lancet* (2017) 389(10071):847–60. doi: 10.1016/S0140-6736(16)31392-7
2. Meng W, Takeichi M. Adherens Junction: Molecular Architecture and Regulation. *Cold Spring Harbor Perspect Biol* (2009) 1(6):a002899. doi: 10.1101/cshperspect.a002899
3. Zeng L, Fee BE, Rivas MV, Lin J, Adamson DC. Adherens Junctional Associated Protein-1: A Novel 1p36 Tumor Suppressor Candidate in Gliomas (Review). *Int J Oncol* (2014) 45(1):13–7. doi: 10.3892/ijo.2014.2425
4. Bharti S, Handrow-Metzmacher H, Zickenheiner S, Zeitvogel A, Baumann R, Starzinski-Powitz A. Novel Membrane Protein Shrew-1 Targets to Cadherin-Mediated Junctions in Polarized Epithelial Cells. *Mol Biol Cell* (2004) 15(1):397–406. doi: 10.1091/mbc.e03-05-0281
5. Yang C, Li YS, Wang QX, Huang K, Wei JW, Wang YF, et al. EGFR/EGFRvIII Remodels the Cytoskeleton *via* Epigenetic Silencing of AJAP1 in Glioma Cells. *Cancer Lett* (2017) 403:119–27. doi: 10.1016/j.canlet.2017.06.007
6. Di C, Mladkova N, Lin J, Fee B, Rivas M, Chunsheng K, et al. AJAP1 Expression Modulates Glioma Cell Motility and Correlates With Tumor Growth and Survival. *Int J Oncol* (2018) 52(1):47–54. doi: 10.3892/ijo.2017.4184
7. Han L, Zhang KL, Zhang JX, Zeng L, Di CH, Fee BE, et al. AJAP1 is Dysregulated at an Early Stage of Gliomagenesis and Suppresses Invasion Through Cytoskeleton Reorganization. *CNS Neurosci Ther* (2014) 20(5):429–37. doi: 10.1111/cns.12232
8. Han J, Xie C, Pei T, Wang J, Lan Y, Huang K, et al. Deregulated AJAP1/beta-Catenin/ZEB1 Signaling Promotes Hepatocellular Carcinoma Carcinogenesis and Metastasis. *Cell Death Dis* (2017) 8(4):e2736. doi: 10.1038/cddis.2017.126
9. Qu W, Wen X, Su K, Gou W. MiR-552 Promotes the Proliferation, Migration and EMT of Hepatocellular Carcinoma Cells by Inhibiting AJAP1 Expression. *J Cell Mol Med* (2019) 23(2):1541–52. doi: 10.1111/jcmm.14062
10. Tanaka H, Kanda M, Koike M, Iwata N, Shimizu D, Ezaka K, et al. Adherens Junctions Associated Protein 1 Serves as a Predictor of Recurrence of Squamous Cell Carcinoma of the Esophagus. *Int J Oncol* (2015) 47(5):1811–8. doi: 10.3892/ijo.2015.3167
11. McDonald JM, Dunlap S, Cogdell D, Dunmire V, Wei Q, Starzinski-Powitz A, et al. The SHREW1 Gene, Frequently Deleted in Oligodendrogliomas, Functions to Inhibit Cell Adhesion and Migration. *Cancer Biol Ther* (2006) 5(3):300–4. doi: 10.4161/cbt.5.3.2391
12. Hotte K, Smyrek I, Starzinski-Powitz A, Stelzer EHK. Endogenous AJAP1 Associates With the Cytoskeleton and Attenuates Angiogenesis in Endothelial Cells. *Biol Open* (2017) 6(6):723–31. doi: 10.1242/bio.022335
13. Xu C, Liu F, Xiang G, Cao L, Wang S, Liu J, et al. Beta-Catenin Nuclear Localization Positively Feeds Back on EGF/EGFR-Attenuated AJAP1 Expression in Breast Cancer. *J Exp Clin Cancer Res: CR* (2019) 38(1):238. doi: 10.1186/s13046-019-1252-6
14. Ogihara T, Mizoi K, Kamioka H, Yano K. Physiological Roles of ERM Proteins and Transcriptional Regulators in Supporting Membrane Expression of Efflux Transporters as Factors of Drug Resistance in Cancer. *Cancers* (2020) 12(11):3352. doi: 10.3390/cancers12113352
15. Clucas J, Valderrama F. ERM Proteins in Cancer Progression. *J Cell Sci* (2014) 127(Pt 2):267–75. doi: 10.1242/jcs.133108
16. Hashimoto K, Hayashi R, Mukaigawa T, Yamazaki M, Fujii S. Concomitant Expression of Ezrin and HER2 Predicts Distant Metastasis and Poor Prognosis of Patients With Salivary Gland Carcinomas. *Hum Pathol* (2017) 63:110–9. doi: 10.1016/j.humpath.2017.02.017
17. Derouiche A, Geiger KD. Perspectives for Ezrin and Radixin in Astrocytes: Kinases, Functions and Pathology. *Int J Mol Sci* (2019) 20(15):3776. doi: 10.3390/ijms20153776

18. Song Y, Ma X, Zhang M, Wang M, Wang G, Ye Y, et al. Ezrin Mediates Invasion and Metastasis in Tumorigenesis: A Review. *Front Cell Dev Biol* (2020) 8:588801. doi: 10.3389/fcell.2020.588801
19. Bretscher A, Edwards K, Fehon RG. ERM Proteins and Merlin: Integrators at the Cell Cortex. *Nat Rev Mol Cell Biol* (2002) 3(8):586–99. doi: 10.1038/nrm882
20. Ponuwei GA. A Glimpse of the ERM Proteins. *J Biomed Sci* (2016) 23:35. doi: 10.1186/s12929-016-0246-3
21. Piao J, Liu S, Xu Y, Wang C, Lin Z, Qin Y, et al. Ezrin Protein Overexpression Predicts the Poor Prognosis of Pancreatic Ductal Adenocarcinomas. *Exp Mol Pathol* (2015) 98(1):1–6. doi: 10.1016/j.yexmp.2014.11.003
22. Horwitz V, Davidson B, Stern D, Trope CG, Tavor Re'em T, Reich R. Ezrin Is Associated With Disease Progression in Ovarian Carcinoma. *PloS One* (2016) 11(9):e0162502. doi: 10.1371/journal.pone.0162502
23. Zhang XQ, Chen GP, Wu T, Yan JP, Zhou JY. Expression and Clinical Significance of Ezrin in non–Small-Cell Lung Cancer. *Clin Lung Cancer* (2012) 13(3):196–204. doi: 10.1016/j.cllc.2011.04.002
24. Wang L, Lin GN, Jiang XL, Lu Y. Expression of Ezrin Correlates With Poor Prognosis of Nasopharyngeal Carcinoma. *Tumour Biol: J Int Soc Oncodevelopmental Biol Med* (2011) 32(4):707–12. doi: 10.1007/s13277-011-0171-8
25. Sarrio D, Rodriguez-Pinilla SM, Dotor A, Calero F, Hardisson D, Palacios J. Abnormal Ezrin Localization is Associated With Clinicopathological Features in Invasive Breast Carcinomas. *Breast Cancer Res Treat* (2006) 98(1):71–9. doi: 10.1007/s10549-005-9133-4
26. Li L, Wang YY, Zhao ZS, Ma J. Ezrin is Associated With Gastric Cancer Progression and Prognosis. *Pathol Oncol Res: POR* (2011) 17(4):909–15. doi: 10.1007/s12253-011-9402-y
27. Li N, Kong J, Lin Z, Yang Y, Jin T, Xu M, et al. Ezrin Promotes Breast Cancer Progression by Modulating AKT Signals. *Br J Cancer* (2019) 120(7):703–13. doi: 10.1038/s41416-019-0383-z
28. Bruce B, Khanna G, Ren L, Landberg G, Jirstrom K, Powell C, et al. Expression of the Cytoskeleton Linker Protein Ezrin in Human Cancers. *Clin Exp Metastasis* (2007) 24(2):69–78. doi: 10.1007/s10585-006-9050-x
29. Ma L, Zhang XH, Xing LX, Li YH, Wang XL, Wang YJ. Relationship of Ezrin Protein Expression to the Carcinogenesis and Prognosis of Infitrating Breast Ductal Carcinoma. *Zhonghua Zhong Liu Za Zhi Chinese J Oncol* (2008) 30 (4):279–83.
30. Pokharel D, Padula MP, Lu JF, Jaiswal R, Djordjevic SP, Bebawy M. The Role of CD44 and ERM Proteins in Expression and Functionality of P-Glycoprotein in Breast Cancer Cells. *Molecules* (2016) 21(3):290. doi: 10.3390/molecules21030290
31. Nam K, Oh S, Lee KM, Yoo SA, Shin I. CD44 Regulates Cell Proliferation, Migration, and Invasion *via* Modulation of C-Src Transcription in Human Breast Cancer Cells. *Cell Signalling* (2015) 27(9):1882–94. doi: 10.1016/j.cellsig.2015.05.002
32. Ma L, Liu YP, Geng CZ, Xing LX, Zhang XH. Low-Dose Epirubicin Inhibits Ezrin-Mediated Metastatic Behavior of Breast Cancer Cells. *Tumori* (2011) 97 (3):400–5. doi: 10.1177/030089161109700324
33. Li J, Tu Y, Wen J, Yao F, Wei W, Sun S. Role for Ezrin in Breast Cancer Cell Chemotaxis to CCL5. *Oncol Rep* (2010) 24(4):965–71. doi: 10.3892/or.2010.965
34. Jaiswal R, Luk F, Dalla PV, Grau GE, Bebawy M. Breast Cancer-Derived Microparticles Display Tissue Selectivity in the Transfer of Resistance Proteins to Cells. *PloS One* (2013) 8(4):e61515. doi: 10.1371/journal.pone.0061515
35. Zeng L, Kang C, Di C, Fee BE, Rivas M, Lin J, et al. The Adherens Junction-Associated Protein 1 is a Negative Transcriptional Regulator of MAGEA2, Which Potentiates Temozolomide-Induced Apoptosis in GBM. *Int J Oncol* (2014) 44(4):1243–51. doi: 10.3892/ijo.2014.2277
36. Schreiner A, Ruonala M, Jakob V, Suthaus J, Boles E, Wouters F, et al. Junction Protein Shrew-1 Influences Cell Invasion and Interacts With Invasion-Promoting Protein CD147. *Mol Biol Cell* (2007) 18(4):1272–81. doi: 10.1091/mbc.e06-07-0637
37. Resch E, Quaiser S, Quaiser T, Schneider G, Starzinski-Powitz A, Schreiner A. Synergism of Shrew-1's Signal Peptide and Transmembrane Segment Required for Plasma Membrane Localization. *Traffic* (2008) 9(8):1344–53. doi: 10.1111/j.1600-0854.2008.00765.x
38. Gross JC, Schreiner A, Engels K, Starzinski-Powitz A. E-Cadherin Surface Levels in Epithelial Growth Factor-Stimulated Cells Depend on Adherens Junction Protein Shrew-1. *Mol Biol Cell* (2009) 20(15):3598–607. doi: 10.1091/mbc.e08-12-1240
39. Cogdell D, Chung W, Liu Y, McDonald JM, Aldape K, Issa JP, et al. Tumor-Associated Methylation of the Putative Tumor Suppressor AJAP1 Gene and Association Between Decreased AJAP1 Expression and Shorter Survival in Patients With Glioma. *Chin J Cancer* (2011) 30(4):247–53. doi: 10.5732/cjc.011.10025
40. Zhou P, Zhang WW, Bao Y, Wang J, Lian CL, He ZY, et al. Chemotherapy and 21-Gene Recurrence Score Testing for Older Breast Cancer Patients: A Competing-Risks Analysis. *Breast* (2020) 54:319–27. doi: 10.1016/j.breast.2020.11.018
41. Yousefi H, Vatanmakanian M, Mahdiannasser M, Mashouri L, Alahari NV, Monjezi MR, et al. Understanding the Role of Integrins in Breast Cancer Invasion, Metastasis, Angiogenesis, and Drug Resistance. *Oncogene* (2021) 40 (6):1043–63. doi: 10.1038/s41388-020-01588-2
42. Baxevanis CN, Fortis SP, Perez SA. The Balance Between Breast Cancer and the Immune System: Challenges for Prognosis and Clinical Benefit From Immunotherapies. *Semin Cancer Biol* (2021) 72:76–89. doi: 10.1016/j.semcancer.2019.12.018
43. Place AE, Jin Huh S, Polyak K. The Microenvironment in Breast Cancer Progression: Biology and Implications for Treatment. *Breast Cancer Res: BCR* (2011) 13(6):227. doi: 10.1186/bcr2912

Conflict of Interest: The authors declare that the research was conducted in the absence of any commercial or financial relationships that could be construed as a potential conflict of interest.

frontiers in Oncology

ORIGINAL RESEARCH
published: 18 March 2022
doi: 10.3389/fonc.2022.825484

Systemic Deficiency of PTEN Accelerates Breast Cancer Growth and Metastasis

Jing Chen[1†], Jingjing Sun[2†], Qunfeng Wang[1†], Yanze Du[3], Jie Cheng[1], Juan Yi[1], Bei Xie[1], Suya Jin[1], Gang Chen[1], Lina Wang[1], Xiaoyuan Wang[1] and Hulai Wei[1]*

[1] Key Laboratory of Preclinical Study for New Drugs of Gansu Province, School of Basic Medical Sciences, Lanzhou University, Lanzhou, China, [2] Department of Clinical Laboratory, The First Hospital of Lanzhou University, Lanzhou, Gansu, China, [3] Department of Thoracic Surgery, Gansu Provincial Cancer Hospital, Lanzhou, China

Mutation or loss of the tumor suppressor gene *PTEN* or its functional status in tumor stromal cells may affect tumor occurrence, development, invasion, and metastasis, in which, however, the role of overall low PTEN expression, mutation, or deletion in the tumor-bearing host has rarely been reported. Breast cancer is a common highly invasive metastatic tumor. We therefore treated mouse breast cancer 4T1 cells with the specific PTEN inhibitor VO-OHpic to study the effects of PTEN suppression or deletion on malignant behavior *in vivo* and *in vitro*. VO-OHpic effectively inhibited PTEN gene/protein expression in 4T1 cells, accelerated cell proliferation, and enhanced cell migration and invasion. We also transplanted 4T1 cells with VO-OHpic-inhibited PTEN into mice to create orthotopic and metastatic breast cancer models. The proliferation of 4T1 cells in mouse mammary gland was increased and distant metastasis was enhanced, with metastatic foci in the lung, liver, and intestinal tract. In addition, injection of mice with VO-OHpic to inhibit PTEN in the overall microenvironment accelerated the proliferation of transplanted 4T1 cells and enhanced distant metastasis and the formation of metastatic tumors. Metastatic foci formed in the lung, liver, intestine, thymus, and brain, and PTEN levels in the organ/tissues were negatively associated with the formation of metastatic foci. Similarly, inoculation of PTEN-deficient 4T1 cells into systemic PTEN-inhibited mice further enhanced the orthotopic growth and distant metastasis of 4T1 breast cancer. VO-OHpic inhibition of PTEN in 4T1 cells was also associated with significantly increased phosphorylation of Akt and phosphoinositide 3-kinase (PI3K), suggesting that inhibition of PTEN could activate the PI3K-Akt pathway, as a key signaling pathway regulating cell proliferation and death. These results confirmed that functional loss or deletion of the tumor suppressor gene PTEN significantly enhanced the proliferation, invasion, and metastasis of 4T1 cells. Systemic decrease or deletion of PTEN in the organism or organ/tissue microenvironment was conducive to the proliferation of breast cancer cells *in situ* and distant metastasis. These results suggest that, as well the PTEN in cancer cells the systemic microenvironment PTEN intensely mediates the proliferation, invasion and metastasis of mouse breast cancer cells *via* regulating the PI3K-Akt signaling pathway.

Keywords: PTEN, 4T1 cell, multiplication, invasion, metastasis

OPEN ACCESS

Edited by:
San-Gang Wu,
First Affiliated Hospital of Xiamen University, China

Reviewed by:
Hailin Tang,
Sun Yat-sen University Cancer Center (SYSUCC), China
David Akhavan,
University of Kansas Medical Center, United States

****Correspondence:***
Hulai Wei
weihulai@lzu.edu.cn

[†]These authors have contributed equally to this work

Specialty section:
This article was submitted to Breast Cancer, a section of the journal Frontiers in Oncology

Received: *30 November 2021*
Accepted: *14 February 2022*
Published: *18 March 2022*

Citation:
Chen J, Sun J, Wang Q, Du Y, Cheng J, Yi J, Xie B, Jin S, Chen G, Wang L, Wang X and Wei H (2022) Systemic Deficiency of PTEN Accelerates Breast Cancer Growth and Metastasis. Front. Oncol. 12:825484. doi: 10.3389/fonc.2022.825484

INTRODUCTION

Breast cancer is the most common malignant tumor in women, with the highest morbidity and mortality rates (1, 2). Its incidence and mortality are currently increasing year by year, with a trend towards younger patients (1–3). According to the latest data released by the China National Cancer Center in 2019, breast cancer accounted for 7.74% of all malignant tumors and 2.99% of the total mortality in China in 2015. The incidence of breast cancer in China (7.7%) is higher than that worldwide (5.8%), with about 304,000 new cases each year (4). Invasion and distant metastasis are the main causes of death due to breast cancer, accounting for >90% of breast cancer-related deaths. The main target organs of breast cancer metastasis are the lungs, liver, bone, lymph nodes, and brain (4–8). Numerous studies have shown that breast cancer metastatic ability depends not only on the characteristics of the cancer itself, but also on the tumor microenvironment and interactions between tumor cells and the tumor microenvironment, with the target organ microenvironment having a strong influence on the fate of the cancer cells and the formation of metastatic carcinoma (7–11). We therefore propose that the primary tumor microenvironment regulates the proliferation, invasion, and metastatic characteristics of breast cancer cells, while the fate of those cells depends on the microenvironment of the distant metastatic target organs. Invasion and metastasis of breast cancer cells currently presents a problem in treating breast cancer patients and inhibiting or blocking these processes is key to the effective prevention and treatment of breast cancer.

The invasion and metastasis of breast cancer cells is a multi-gene, multi-stage process involving the activation of oncogene mutations and inactivation of tumor suppressor genes (7–9). Phosphatase and tensin homolog (*PTEN*) is a tumor suppressor gene with dual protein phosphatase and lipid phosphatase activities discovered in 1997, which is second only to *P53* (10, 11). *PTEN* is widely involved in cell proliferation, differentiation, adhesion, migration, metastasis, and apoptosis, as well as in the cell cycle, energy metabolism, genome stability, and other processes (10–14). Previous studies have confirmed that *PTEN* mutation and functional loss play a key role in the occurrence, development, and metastasis of malignant tumors (13–15).

PTEN abnormalities in breast cancer cells are mainly caused by deletion mutation, abnormal promoter DNA methylation, and abnormal degradation or functional loss of PTEN protein expression (10, 13–18). Loss of heterozygosity of *PTEN* has been reported in about 40%–50% of breast cancer patients, and about 5%–10% of patients with breast cancer have *PTEN* mutations, most commonly frameshift mutations, resulting in PTEN functional loss (13, 15, 18). *PTEN* inactivation is mainly attributed to somatic mutations, including missense and nonsense mutations, single- or double-allele deletions at *PTEN* gene loci, resulting in PTEN protein degradation and post-translational changes as a result of epigenetic silencing *via* promoter methylation (13–17, 19). Similarly, PTEN function may be regulated by post-translational modifications, such as phosphorylation, acetylation, oxidation, monoubiquitination, and polyubiquitination (10–13, 15–20). Most studies on the role of PTEN in the invasion and metastasis of breast cancer and other malignant tumors have focused on the functional changes of PTEN in the tumor cells themselves and have ignored the effects on the overall function of tumor-bearing hosts, and the effects of target organ-specific PTEN on tumor cell invasion, distant metastasis, and colonization (21–23).

The embryo-lethality of homozygous *PTEN* knockout makes it difficult to prepare a *PTEN* full-gene knockout mouse model, and only conditional or heterozygous knockouts models can be produced (23, 24), making it difficult to analyze the effect of the overall PTEN status of tumor-bearing hosts on breast cancer proliferation and metastasis. Current studies on the relationship between PTEN in the tumor microenvironment and the invasion and metastasis of breast cancer and other malignant tumors are mostly limited to examining the effect of PTEN expression in the primary tumor microenvironment on the proliferation, invasion, and metastasis of tumor cells *in situ* (9–11, 18, 22–25). However, few studies have considered the effect of the host itself, especially regarding the functional state of PTEN in the microenvironment of the metastatic target organ, on the ability of the metastatic breast cancer cells to colonize, proliferate, and form metastatic foci in the organ, and the mutual adaptation of cells in the target organ microenvironment and metastatic breast cancer cells.

We therefore investigated the effects of the PTEN-specific inhibitor VO-OHpic in BALB/c mice and in the derived breast cancer 4T1 cells, to determine the effects of PTEN on the proliferation, migration, and invasion of 4T1 cells and their ability to form distant metastases *in vivo*. We also investigated the effects of PTEN levels in the host mouse or target organ microenvironment on the colonization and survival of metastatic breast cancer cells in the target organs and on the formation of metastatic cancers. We aimed to clarify the mechanism by which the functional status of PTEN in the whole host/metastatic organ microenvironment determines the fate of metastatic breast cancer cells, and to explore strategies to reduce the invasion and metastasis of breast cancer by enhancing PTEN levels in tumor-bearing organisms.

MATERIALS AND METHODS

Reagents and Cells

Dulbecco's Modified Eagle Medium (Gibco BRL, MD, USA), fetal bovine serum (BI Biotechnology, Kibbutz Beit Haemek, Israel), TRIzol reagent (Invitrogen Penrose, Auckland, New Zealand), RIPA protein lysate BCA protein concentration assay kits, and Crystal violet solution were all from Solebro (Beijing, China). Rabbit anti-PTEN polyclonal antibody, mouse anti-phospho (Ser-473 cat no: 3257-100)-, rabbit anti-Akt polyclonal antibody (3247–100) were purchased from Biovision Inc. (CA, USA). Rabbit anti- PI3 Kinase p85 (Tyr-467, cat no: GTX132597)-, PI3 Kinase p85 alpha (GTX111068) polyclonal antibody were from GeneTex (Texas, USA). Color pre-dyed Marker was obtained from Thermo Scientific (MA, USA), Prime Script™ RT Reagent Kit with gDNA Eraser and SYBR Premix Ex Taq were from TaKaRa Bio (Dalian, China), and VO-OHpic and luciferin were from Sigma–Aldrich (Darmstadt, Germany).

Mouse breast cancer 4T1 cells and luciferase gene-labeled mouse breast cancer 4T1 cells (4T1-luc) were provided by the Laboratory of Medical Laboratory Zoology, School of Basic Medicine, Lanzhou University. The cells were routinely cultured in complete culture medium containing 10% fetal bovine serum.

Xenograft Mouse Model

Balb/c mice (female, 5–6 weeks old, body weight 20 ± 2 g) maintained in a specific-pathogen-free (SPF) animal room were purchased from the Experimental Animal Center of Lanzhou University (production license number: SCXK (GAN) 2018-0002; use license number: SYXK (GAN) 2018-0002). The management, care, and ethical welfare of the experimental animals were all in accordance with the Guiding Suggestions on the Ethical Review of Experimental Animal Welfare (GB/T 35892-2018) issued by the Ministry of Science and Technology of China.

Cell Viability Assay

MTT Colorimetric Assay

4T1 cells were inoculated into 96-well plates at a density of 0.6×10^5 cells/mL, and then cultured at 37°C until they adhered to the plate. 200 or 500 nmol/L VO-OHpic were then added for 4 h. The culture medium was then replaced without VO-OHpic for a further 24–72 h, and 10 μl MTT (5 mg/mL) was added to each well for the last 4 h. After continuous culture for 4 h, 10% sodium dodecyl sulfate (SDS) 100 μl per well was added and incubated overnight at 37°C. The absorbance value (λ=570 nm) was determined by enzyme-linked immunoassay (Powerwave X plate reader Omega Bio−Tek, Inc., Norcross, GA, USA) to calculate the proliferation rate or proliferation inhibition rate of 4T1 cells.

Clonogenicity Assay

Normally cultured 4T1 cells were inoculated into 6-well plates at a density of 5×10^3 cells/ml. After the cells attached to the well, 200 or 500 nmol/L VO-OHpic was added to the cells for 30 min–4 h. The supernatant was then discarded, and 2 ml complete medium was added followed by further culture for 72 h. The supernatant was discarded again, and the cells were fixed with 100% methanol for 30 min, stained with 0.1% crystal violet for 30 min, washed with water, and dried at room temperature, and cell proliferation was observed by light microscopy (original magnification, ×10).

Real Time Quantitative Reverse Transcription-Polymerase Chain Reaction (RT-PCR)

Target cells were collected, and total RNA was extracted using TRIzol. Samples were reverse transcribed using a Prime Script™ RT Reagent Kit with gDNA Eraser (Perfect Real Time; Takara), according to the manufacturer's instructions, with 5× gDNA Eraser Buffer to obtain the first cDNA strand. The cDNA was then amplified using a Prime Script reverse transcriptase kit (Takara Bio, Inc.) according to the following protocol: 70°C for 30 min, 37°C for 15 min, and 95°C for 5 min. For PCR, cDNA was mixed with SYBR Premix Ex Taq and subjected to 40 cycles of denaturing at 95°C for 5 s and annealing at 60°C for 30 s. The following primers for PCR were designed and synthesized by Takara Bio, Inc. and analyzed by Rotor-Gene 6.0 using the comparative domain value method: β−actin forward, 5'-TGCTCCTCCTGAGCGCAAGTA-3' and reverse, 5′-CCAC ATCTGCTGGAAGGTGGA-3′; and PTEN forward, 5′-CTCCTCTACTCCATTCTTCCC-3′ and reverse, 5′-ACTCCCACCAATGAACAAAC-3′

Cell Invasion and Migration

The ability of target cells to penetrate synthetic basement membranes was assessed using a Matrigel−Boyden chamber (BD Biosciences, NJ, USA). The transwell compartment was placed in a 24-well plate filled with complete medium and cells were collected and seeded into the wells at a density of 5×10^3 cells per well, in serum−free medium. After incubation for 36 h, the compartment was removed, cells above the synthetic membranes were wiped off with cotton swabs, and the lower side of the compartment was fixed in 4% paraformaldehyde for 30 min–1 h, and then stained with 0.1% crystal violet at room temperature for 30 min. Cells that crossed the membranes were observed and imaged using an optical microscope (Olympus IX81, Japan). Cell migration ability was assessed as for the invasion assay, except for the absence of Matrigel.

Cell Scratch Assay

4T1 cells were plated in 6-well plates at 0.6×10^5 cells per well. The next day, the cells were treated with 200 or 500 nmol/L VO-OHpic, respectively, for 30 min–4 h. The medium was then replaced with complete culture medium without VO-OHpic, and a straight line was drawn across the middle of the adherent cell layer using a 200 μl pipette tip. Imaging was performed under an optical microscope at 0 h and after incubation for 24 h, to calculate the cell-migration rate.

Cell Cycle Analysis

After treatment of 4T1 cells with 200 or 500 nmol/L VO-OHpic, respectively, for 30 min–4 h, the cells were collected, washed with phosphate-buffered saline (PBS), blended gently, and suspended in 70%–75% cold ethanol overnight at −20°C, washed with PBS, and 500 μl propidium iodide dye was added to each tube for dark staining for 30 min. The distribution of cell cycle phases was determined by flow cytometry (ACEA NovoCyte, Jiangsu, China).

Western Blotting

Protein expression was determined by western blotting. Proteins from cells were isolated and dissolved with RIPA lysis buffer and their concentration levels were determined using the BCA method (Solarbio, Beijing, Chian). The proteins (30 μg) were subsequently separated by 10% SDS−polyacrylamide gel electrophoresis and transferred onto polyvinylidene difluoride membranes (Millipore, MA, USA), and blocked with 5% nonfat milk at room temperature for 1 h. After washing three times with PBS−Tween−20 for 5 min, the membranes were probed with

primary antibodies at 4°C overnight. As for immunodetection, the membranes were incubated at room temperature with horseradish peroxidase-conjugated secondary antibody for 1 h and subsequently observed and analyzed using an Amersham Enhanced Chemiluminescence system (GE Healthcare Life Sciences, Beijing, Chian).

Mouse Homograft Tumor Model

We established mouse orthotopic and metastatic tumor models by inoculation of 4T1-luc breast cancer cells into the breast fat pad or caudal vein of female Balb/c mice (8 weeks old, body weight 20 ± 2 g), and observed the tumor cell growth and metastasis by small-animal imaging (IVIS Lumina II, Caliper Life Science, Cold Spring Harbor, USA). To create an orthotopic model, 4T1–luc cells (2×10^6/ml) were treated with 0, 200, or 500 nmol/L VO-OHpic, respectively, for 2 h *in vitro* to inhibit PTEN expression, and then inoculated into the breast fat pad, or mice were injected intraperitoneally with 10 or 20 μg/kg VO-OHpic, and 4T1–luc cells (2×10^6/ml) were then inoculated directly into the fat pad. 4T1–luc cells treated as above were also injected into the tail vein of female Balb/c mice to establish a metastatic model. All the model mice were raised under SPF conditions and observed regularly.

The formation of *in situ* and metastatic tumors in the above animal models were observed using a small-animal imaging system at 7, 15, and 21 days after inoculation, respectively. The mice were sacrificed humanely at the end of the experiment, and the *in situ* tumor masses, as well as tumors in the lungs, liver, intestines, and kidneys, were isolated, and the tumors and organs were observed by imaging. Some fresh tissues were also used for RNA and protein extraction to detect the expression of related genes.

This animal experiment program was reviewed and approved by the Laboratory Animal Science and Technology Management Committee of the School of Basic Medicine of Lanzhou University (Approval Number: LZUSBMS-EAAC-2018-009), in accordance with the Ministry of Science and Technology of the People's Republic of China on the Guiding Opinion on the Treatment of Laboratory Animals and the national standard "Laboratory Animal Welfare Ethics Review Guide" (GB/T 35892-2018).

Immunohistochemical (IHC) Assay

The following IHCs, according to manufacturers' protocols were performed: Freshly isolated tissues were fixed with formalin and embedded with paraffin, cut into 4–5 μm slices, and fixed on slides with a polylysine coating. The slides were deparaffinized in xylene followed by graded ethanols (100%, 95%, 70%, 50%), and finally washed in cold running water. Endogenous peroxidase was removed using 0.5% hydrogen peroxide in methanol solution, and antigen blocking was carried out using 5% bovine serum albumin, following antigen retrieval in a pressure cooker using a thermally-induced method that the slides were put into an autoclaver containing medlar buffer, heated for 5 minutes, and then cooled in cold water to repair epitopes in citrate buffer (pH 6). Slides were incubated with primary antibodies at different dilution ratios to determine the optimal concentrations. The slides were then washed and treated with a secondary antibody. Incubations with antibody (Rabbit anti-PTEN, Cell Signalling, Massachusetts, USA) was carried out in a humidified box to avoid drying. After incubation with the secondary antibodies, the slides were washed with PBS, covered with freshly prepared DAB color solution, and then washed again with water, followed by hematoxylin staining, clearing, drying, and mounting. The immunohistochemical stains were evaluated by two pathologists with consensus.

Statistical Analysis

All data were analyzed using SPSS version 22.0 (SPSS, Inc., Chicago, IL, USA) and the statistical results were presented as mean ± standard deviation. Multi-factor comparisons between samples were performed using two–way analysis of variance followed by a Newman–Keuls *post hoc* test. All experiments were repeated at least three times. $P<0.05$ was considered to indicate a significant difference, and error bars were used to represent the standard error of the mean.

RESULTS

Inhibition of PTEN Expression by VO-OHpic Increased Proliferation of 4T1 Breast Cancer Cells

Treatment of mouse-derived breast cancer 4T1 cells with 200 or 500 nmol/L VO-OHpic for 1–4 h inhibited PTEN mRNA and protein levels, with particularly notable effects after treatment for 2–4 h, especially for PTEN protein (**Figures 1A, B**).

After treatment of 4T1 cells with different concentrations of VO-OHpic for 4 h and culture for 24–72 h, MTT colorimetry showed that 10–800 nmol/L VO-OHpic increased the proliferation activity of 4T1 cells. However, when the concentration of VO-OHpic increased to 1000 nmol/L, the enhancing effect on cell proliferation gradually began to weaken, ultimately leading to inhibition of cell proliferation (**Figure 1C**).

We treated 4T1 cells with 200 or 500 nmol/L VO-OHpic for 0.5–4 h, followed by removal of VO-OHpic and inoculation of the cells into 6-well plates for routine culture. After regular observation, the cells were stained with 0.1% crystal violet to count the number of cell colonies. The number of 4T1 cell colonies was significantly increased after treatment with 200 and 500 nmol/L VO-OHpic, especially after treatment for 2–4 h (**Figure 1D**).

We also detected the cell cycle phase distribution by flow cytometry and showed that the proportion of S phase cells increased to varying degrees, with the most obvious increases of 9.43% and 7.46% at 2 and 4 h, respectively, compared with the control cells (**Figure 1E**), suggesting that VO-OHpic promoted the proliferation of 4T1 cells by inhibiting PTEN.

Inhibition of PTEN Expression Enhanced Migration and Invasion of 4T1 Cells

Both 200 and 500 nmol/L VO-OHpic treatment for 30 min-4 h increased the migration rate of 4T1 breast cancer cells and accelerated scratch healing, especially after 2–4 h, according to

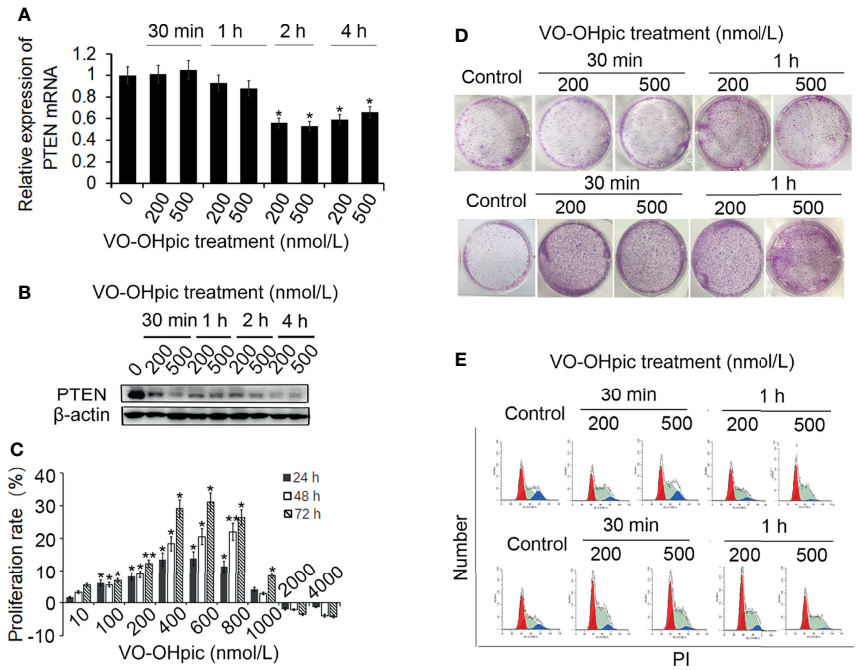

FIGURE 1 | Effects of VO-OHpic on proliferation of 4T1 cells by inhibiting *PTEN* gene expression. 4T1 cells were treated with 200 or 500 nmol/L VO-OHpic for 0.5–4 h and PTEN mRNA expression was detected by real-time quantitative RT-PCR **(A)**, and PTEN protein expression was detected by western blotting **(B)**. **(C)** Effects of different concentrations of VO-OHpic for 4 h on proliferation activity of 4T1 cells. **(D)** Effects of VO-OHpic on cell colony formation and cell cycle phase distribution in 4T1 cells **(E)** after 0.5–4 h treatment. *P<0.05, **P<0.01 compared with the control group.

the cell scratch test (**Figure 2A**). Treatment with 200 or 500 nmol/L VO-OHpic for 30 min–4 h also enhanced the number of 4T1 cells crossing the compartment membrane in transwell assays (**Figure 2B**). These results suggest that inhibition of PTEN expression and activity in mouse breast cancer 4T1 cells by VO-OHpic significantly enhanced their invasion and migration

PTEN Inhibition Activated PI3K-Akt Signaling Pathway in 4T1 Cells

The PTEN/PI3K/Akt pathway is an important signal-regulation pathway in the body. PTEN can negatively regulate the PI3K/Akt signaling pathway and participate in the physiological and pathological activities of cell proliferation, differentiation and maturation, apoptosis, cycle arrest, invasion, and migration (15, 25, 26). PTEN protein levels in 4T1 cells were inhibited by 200 and 500 nmol/L VO-OHpic to different degrees, while levels of PI3K, p-PI3K, Akt, and p-Akt were significantly increased (**Figure 2C**). These results suggest that inhibition of PTEN promoted the proliferation, migration, and invasion of 4T1 cells by activating the PI3K-Akt pathway.

Inhibition of PTEN Expression in 4T1 Cells Enhanced Orthotopic Growth and Distant Metastasis *In Vivo*

PTEN was inhibited in 4T1-luc cells by treatment with 200 or 500 nmol/L VO-OHpic for 2 h (**Figures 3A, B**), and the cells were then inoculated into Balb/c mice to establish an orthotopic breast cancer tumor model, or into the tail vein to establish a model of breast cancer metastasis. Tumor growth and metastasis were observed using an IVIS. PTEN function was inhibited in 4T1-luc cells, and the growth rate was faster than that of tumors created by normal PTEN cells, the mean sizes of *in situ* mammary tumors in mice increased from 0.44×0.37 cm^2 (length×width) of control group to 1.59×1.68 cm^2 (200 nmol/L) and 1.86×1.72 cm^2 (500 nmol/L), respectively (**Figures 3C–E**). Organ metastases, including lung, liver, kidney, intestine, bladder, thymus, and ovary metastases, were also significantly increased in mice injected with 4T1-luc cells treated with the above concentrations of VO-OHpic, and tumor bioluminescence was significantly enhanced (**Figures 3F–H**).

The PTEN Loss of Host Systemic Microenvironment Enhanced the *In Vivo* Growth and Distant Metastasis of 4T1 Breast Cancer Cells

PTEN gene levels in the lungs, liver, intestine, ovary, bladder, and other organs were significantly decreased following intraperitoneal injection of 10 or 20 μg/kg VO-OHpic for 1 h (**Figure 4A**). Routine cultured 4T1-luc cells were inoculated into Balb/c mice to establish *in situ* and metastasis breast tumor models. Observation by small-animal *in vivo* imaging showed that inhibition of PTEN *in vivo* increased the growth of mouse breast tumors *in situ*, with increased mean length×width from 0.82×1.01 cm^2 of control group to 1.41×1.63 cm^2 (10 μg/kg) and

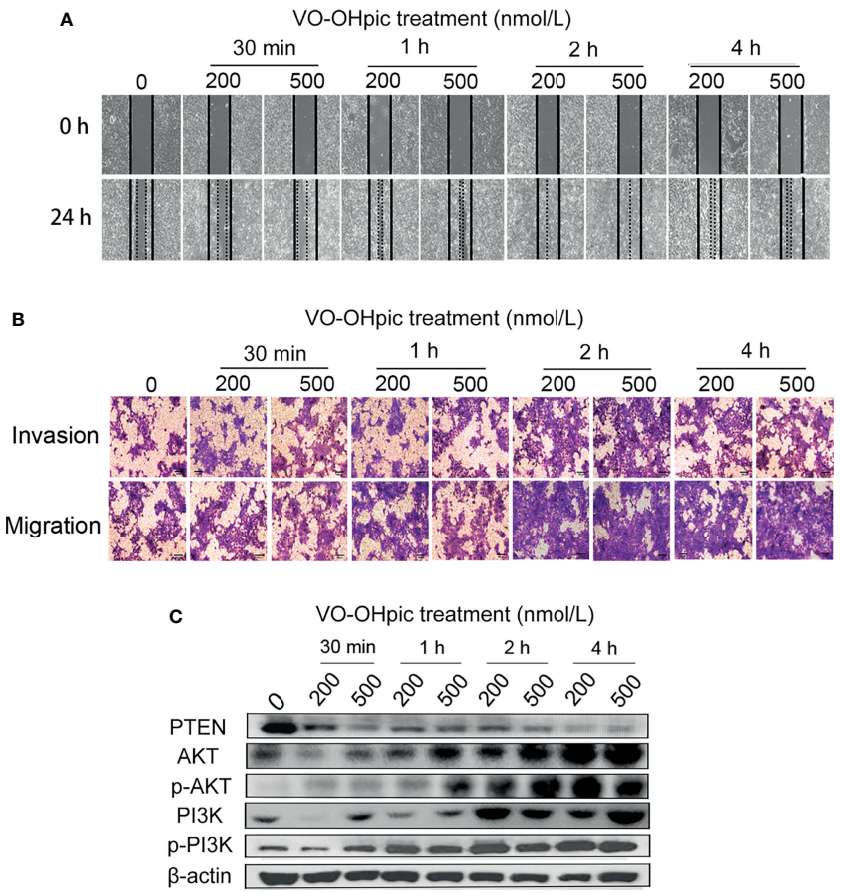

FIGURE 2 | Effect of inhibition of PTEN expression on migration and invasion of 4T1 cells. 4T1 cells were treated with 200 or 500 nmol/L VO-OHpic for 0.5–4 h and their migration and invasion abilities were then detected by cell scratch and transwell assays. **(A)** Cell scratch healing map. **(B)** Observation of cell migration and invasion by the transwell method (original magnification, 100×), and effect of intracellular PTEN on cell proliferation activity **(C)**.

1.89×1.97 cm^2 (20 μg/kg), respectively (**Figures 4B–D**), and increased tumor metastasis in distant organs. Bioluminescence of metastatic foci was significantly enhanced (**Figures 4E–G**).

PTEN-Inhibited 4T1 Breast Cancer Cells in a Systemic PTEN-Deficient Host Microenvironment Showed Greater Proliferation and Metastasis Potential

Balb/c mice treated with 20 μg/kg VO-OHpic by intraperitoneal injection for 1 h were inoculated with 4T1-luc cells treated with 200 or 500 nmol/L VO-OHpic to establish *in situ* and metastasis breast cancer models, respectively. Proliferation of breast tumors (**Figures 5A, B**) and distant metastases (**Figures 5C, D**) were significantly increased in mice treated with PTEN inhibition *in vivo* and simultaneous inoculation of PTEN-deficient 4T1-luc cells, compared with mice treated with cellular or *in vivo* PTEN inhibition alone (**Figures 5A–D**). Notably PTEN inhibition by intraperitoneal injection of VO-OHpic *in vivo* resulted in larger *in situ* breast tumors, more metastatic organs, and faster growth of transplanted tumors (**Figures 5C, D**, **Table 1**). Immunohistochemical detection showed that organs with more obvious tumor metastasis and faster tumor growth, such as the lung, liver, and intestine, had lower PTEN protein expression levels (**Figure 5E**), while PTEN expression was not significantly changed in the spleen, kidney, and other organs with less metastatic tumor proliferation. These results suggest that inhibition of intracellular PTEN promoted the rapid proliferation of tumor cells, while PTEN inhibition in mouse organs also promoted the colonization and rapid growth of tumor cells in the corresponding organs. Thus PTEN-deficient breast cancer cells were more likely to show accelerated growth and metastases to distant organs if PTEN activity in the body was low.

DISCUSSION

Breast cancer is a malignant mammary epithelial tumor. Although local breast cancer is rarely fatal, breast tumor cells shed and spread easily throughout the body *via* the blood and

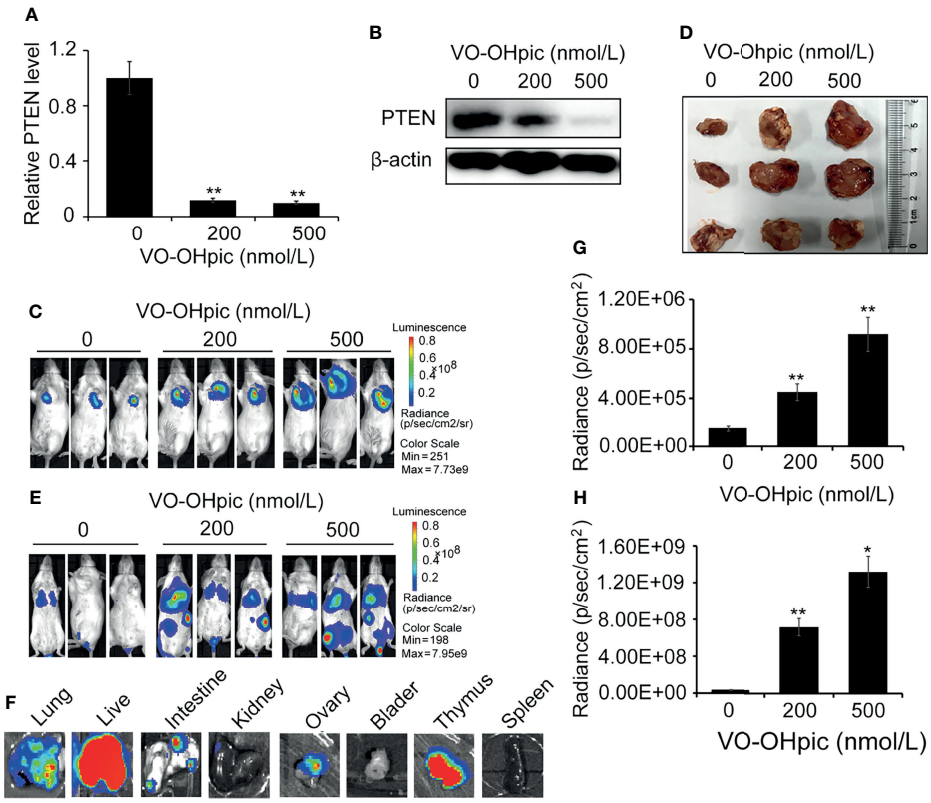

FIGURE 3 | Inhibition of PTEN promoted the growth of orthotopic breast tumors and organ metastases and colonization in mice. PTEN gene **(A)** and protein **(B)** levels in 4T1-luc cells were decreased after treatment with 200 or 500 nmol/L VO-OHpic for 2 h. The above cells were inoculated into the breast fat pad of Balb/c mice to establish an *in situ* tumor model **(C)** and dissected tumor tissues were imaged at 10 days **(D)**. Tumor metastasis models **(F)** were established by injection of the above cells *via* the tail vein, and visceral tumor metastasis was observed at 14 days. Cellular PTEN inhibition by VO-OHpic significantly increased the counts of bioluminescent photons *in situ* breast tumors **(E)** and visceral metastases **(G)**. **(H)** Bioluminescence of some visceral metastases. Compared with 0 nmol/L VO-OHpic group, $^{*}P<0.05$, $^{**}P<0.01$.

lymph circulation, resulting in various potentially lethal metastatic tumors.

The *PTEN* gene is widely involved in the regulation of important signaling pathways including the PI3K/Akt/mTOR, FAK/p130cas, and ERK/MAPK signaling pathways (15, 25–27), and is one of the most important tumor suppressor genes identified to date. Its main functions include inhibiting cell adhesion and migration, inducing cell apoptosis, blocking the cell cycle and cell proliferation, inhibiting the generation of new blood vessels, DNA repair, and regulating normal embryo development, aging, and metabolism (10, 18, 26–29). Abnormal expression or function of PTEN has been closely related to the occurrence and development of various malignant tumors, including endometrial, prostate, liver cancer, colorectal, breast, bladder, stomach, and lung cancers and leukemia (10–14, 19, 20, 22–25). PTEN expression is significantly reduced in many malignant tumors compared with paracancerous tissues/normal cells, especially in highly invasive, highly metastatic, and poorly differentiated cancers, most of which demonstrate *PTEN* mutations or deletions (10–14, 19, 20, 22–25). Migration and invasion abilities are significantly enhanced in tumor cells with *PTEN* deletions or mutations (10–14, 23–29). In addition, PTEN promotes the proliferation, invasion, and metastasis of breast cancer cells, and PTEN levels in metastatic breast cancer cells are much lower than in localized cancer cells (9, 13, 15, 18, 19). However, most studies of the relationship between the tumor suppressor gene *PTEN* and malignant tumors have focused on changes in the expression and function of tumor suppressor genes in the tumor cells themselves, while few reports have considered the effects of the expression and function of tumor suppressor genes such as *PTEN* in the host as a whole, on tumor cell invasion, metastasis, or colonization. In the current study, we treated murine 4T1 breast cancer cells with the highly effective PTEN inhibitor VO-OHpic, and showed that VO-OHpic effectively inhibited PTEN gene and protein expression levels, accompanied by significantly enhanced cell proliferation and increased colony-forming ability, altered the cell cycle distribution, and increased the proportion of S phase cells, suggesting that the rapid proliferation of 4T1 cells might be related to decreased expression or activity of PTEN in the cells.

PI3K is an intracellular phosphatidylinositol kinase with serine/threonine kinase activity (25–28). Its key downstream effector molecule Akt is also a serine/threonine protein kinase. Activation of PI3K promotes the growth and invasion of tumor

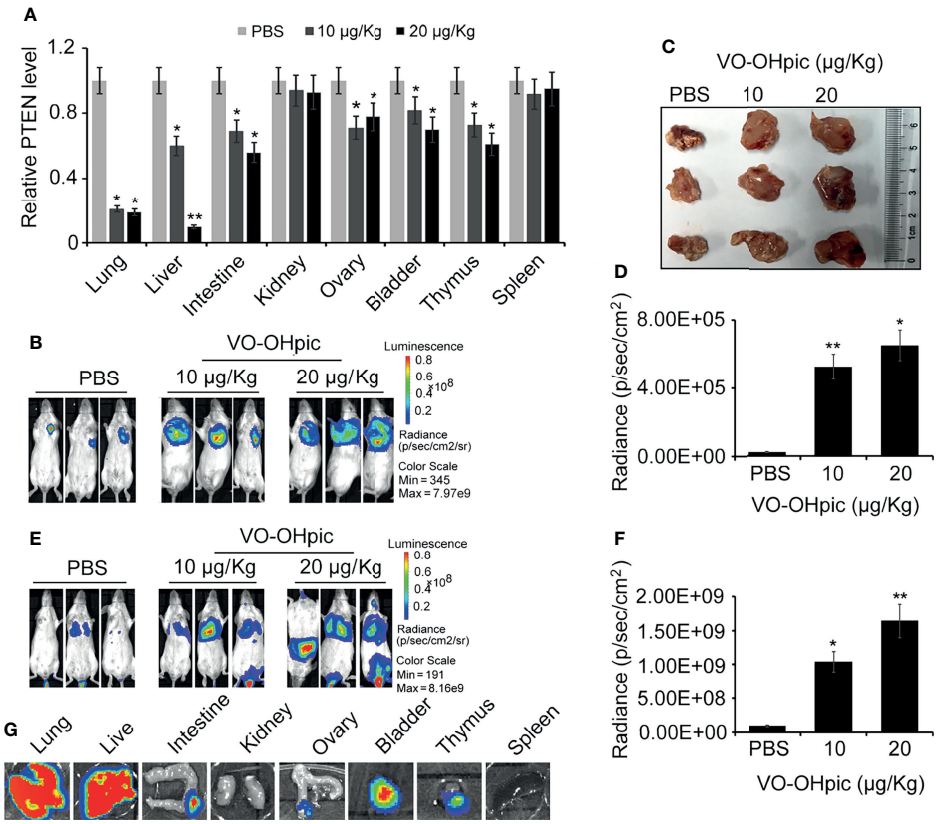

FIGURE 4 | Inhibition of PTEN in mice promoted the metastasis and proliferation of 4T1-luc cells in mice. Expression levels of PTEN mRNA in some organs of Balb/c mice were affected by intraperitoneal injection of 10 or 20 μg/kg VO-OHpic for 1 h, as detected by real-time PCR **(A)**. Routine cultured 4T1-luc cells were inoculated into the breast fat pad of mice treated as above to establish an *in situ* tumor model and tumor formation was observed at 10 days using an IVIS **(B)**. Some exfoliated tumor tissues *in situ* were imaged **(C)**. A metastatic breast cancer model was established by injecting 4T1-luc cells into the tail vein **(E)**. PTEN inhibition by intraperitoneal injection of VO-OHpic *in vivo* significantly increased the counts of bioluminescent photons *in situ* breast tumors **(D)** and visceral metastases **(F)**. Bioluminescence of metastatic tumors in organs including the lung, liver, and intestine were observed using an IVIS **(G)**. Compared with control group, $^{*}P<0.05$, $^{**}P<0.01$.

cells *in vivo* by inactivating various effector molecules to regulate the cell cycle, promote blood vessel growth, and activate cell migration and other related procedures (25–28). The current results showed that inhibition of PTEN gene and protein expression by VO-OHpic significantly accelerated the rate of healing of cell scratches in 4T1 cells. Moreover, the ability of cells to pass through the transwell compartment membrane was enhanced, and the number of cells reaching the lower chamber through the Matrigel was thus significantly increased. These results indicated that the proliferation activity of PTEN-deficient cells was greatly increased, and intercellular adhesion, invasion, and migration were also significantly enhanced. PTEN negatively regulates the classical PI3K/Akt signaling pathway, inhibits cell proliferation, and promotes cell apoptosis. PTEN protein blocks the PI3K/Akt signaling pathway by causing dephosphorylation of the 3' phosphoric acid of phospha tidylinositol-3, 4, 5-triphosphate, thus maintaining the relative stability of PI3K activity and thereby regulating normal cell growth and apoptosis. In addition, the PI3K/Akt signaling pathway is an important pathway regulating a series of physiological and pathological phenomena, such as cell differentiation, maturation, proliferation, and apoptosis. Deletion of the *PTEN* gene in many primary and metastatic tumors leads to uncontrolled continuous signaling of the PI3K/Akt pathway, which in turn stimulates the cells to keep multiplying. Treatment of 4T1 cells with 200 or 500 nmol/L VO-OHpic effectively inhibited PTEN gene and protein expression in 4T1 cells, and significantly up-regulated expression levels of intracellular Akt, p-Akt, PI3K, and p-PI3K proteins. These results indicate that PTEN protein plays a key role in the negative regulation of the PI3K/Akt signaling pathway. Notably PTEN expression in 4T1 cells was significantly decreased after treatment with VO-OHpic for 1–4 h. Activation of the PTEN/PI3K/Akt signaling pathway significantly enhanced cell proliferation, invasion, and migration, consistent with the results of previous studies.

In this study, we established orthotopic xenograft and metastatic breast tumor models by transplantation of 4T1 cells into BALB/c mice and observed the effects of VO-OHpic interventions using small-animal imaging technology.

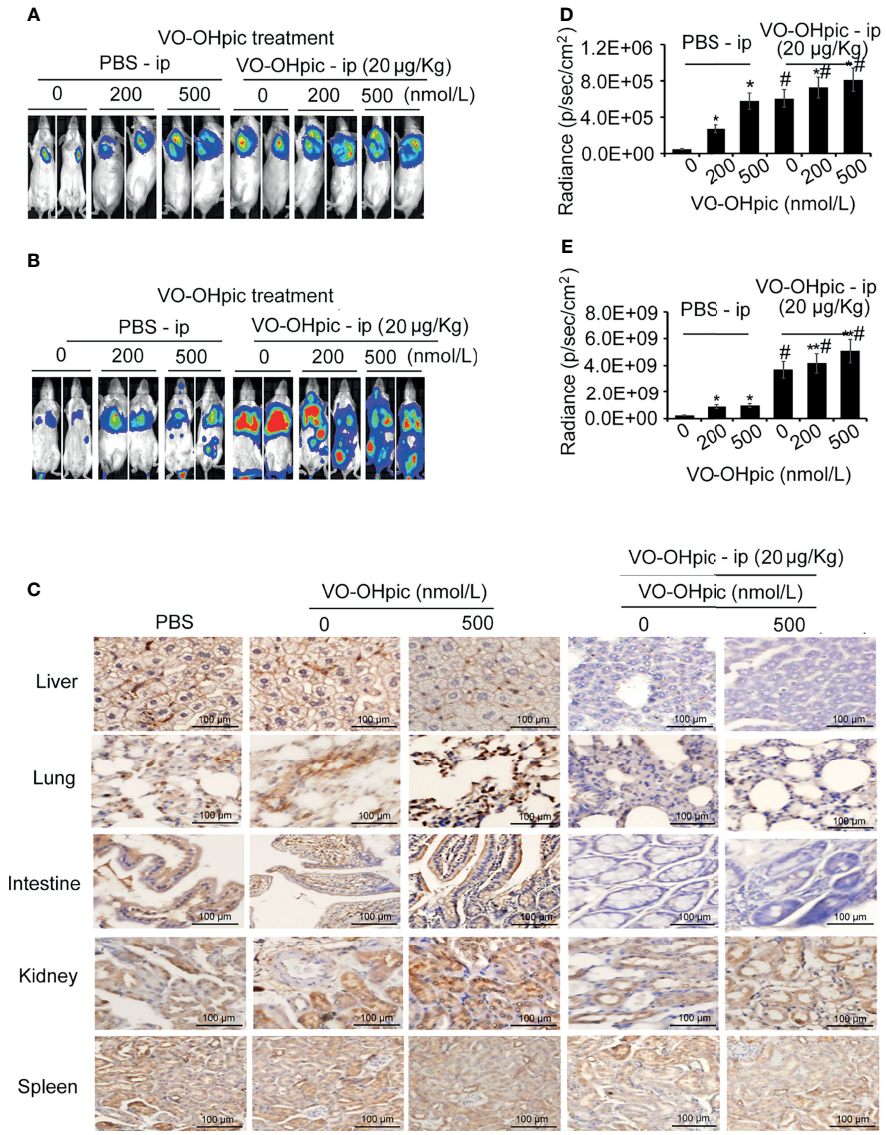

FIGURE 5 | PTEN-deficient breast cancer cells showed greater proliferation and metastasis potential in hosts with low PTEN function. 4T1-luc cells treated with VO-OHpic were inoculated *via* the breast fat pad or tail vein into Balb/c mice intraperitoneally injected with VO-OHpic, to establish a local model **(A)** and an organ metastasis model **(C)**. Flux intensity of breast tumors *in situ* **(B)** and distant metastases **(D)** were significantly increased in mice treated with PTEN inhibition *in vivo* and simultaneous inoculation of PTEN-deficient 4T1-luc cells, compared with mice treated with cellular or *in vivo* PTEN inhibition alone. PTEN protein expression levels in the lung, liver, intestine, and kidney were observed by immunohistochemistry under light microscopy (original magnification, 20×) **(E)**. Compared with 0 nmol/L VO-OHpic group, $^{*}P<0.05$, $^{**}P<0.01$. Compared to PBS - ip group, $^{\#}P<0.01$.

Inhibition of PTEN at the cellular level *in vitro* or direct inhibition of PTEN *in vivo* by intraperitoneal injection of VO-OHpic led to rapid growth of orthotopic transplanted tumors in mice, with general trends towards faster tumor growth and more liver, lung, intestine, bladder, and other distant metastases in line with increasing concentrations of VO-OHpic, including up to almost 100% of lung metastases. Further detection of PTEN gene and protein expression levels in the transplanted tumors and some organs showed that larger transplanted tumors were associated with lower PTEN expression levels. PTEN expression levels in liver, lung, and intestinal tissues, which are prone to metastasis, were significantly inhibited after intraperitoneal injection of VO-OHpic, especially in liver and lung tissues, with intraperitoneal injection of 20 μg/kg VO-OHpic reducing PTEN expression to about 10%–19% of that in the normal control group. Notably, intraperitoneal injection directly inhibited PTEN expression in the internal organs, with lower organ levels associated with a higher metastasis rate, wide implantation area, and fast proliferation of metastatic tumors in the corresponding organs. While the changes in PTEN gene and protein levels in the kidney and spleen were not significant, no colonization or growth of tumor cells generally occurs in these

TABLE 1 | Organic metastases of PTEN-inhibited and -uninhibited B16 cells in wild and PTEN-deficient Balb/c mice.

Mouse viscera		Mice / PBS ip			Mice / VO-OHpic ip (20 μg/kg)		
		4T1 / VO-OHpic (nmol/L)			4T1 / VO-OHpic(nmol/L)		
		0	200	500	0	200	500
Liver	NMT	0	3	6	0	3	5
	MTD (L×W cm^2)		0.32×0.3	0.8×0.52	0.4×0.5	1.23×0.77	1.1×1.4
Lung	NMT	5	8	10	3	10	10
	MTD (L×W cm^2)	0.14×0.17	0.3×0.17	0.93×0.7	0.4×0.38	1.41×1.25	1.35×1.5
Intestine	NMT	1	2	5	0	6	8
	MTD (L×W cm^2)		0.33×0.3	0.8×1.3		1.3×1.2	1.4×1.1
Kidney	NMT	0	0	0	0	1	0
	MTD (L×W cm^2)					0.3×0.4	
Spleen	NMT	0	0	0	0	0	0
	MTD (L×W cm^2)						
Thymus	NMT	0	0	0		2	3
	MTD (L×W cm^2)					0.3×0.1	0.2×0.2
Bladder	NMT	0	0	0		1	2
	MTD (L×W cm^2)					0.2×0.1	0.2×0.2
Ovary	NMT	0	0	0		2	3
	MTD (L×W cm^2)					0.3×0.17	0.29×0.25

Mean tumor diameter (MTD), L (long), W (wide).
The number of metastatic tumors of mice (NMT).

organs, suggesting that the expression and function of the tumor suppressor gene *PTEN* in the tumor-bearing host itself, especially in the microenvironment of the organ, directly affects the invasion, metastasis, colonization, and proliferation of tumor cells. These results demonstrate that a metastatic tumor microenvironment is one in which tumor cells can directly contact, grow, and survive. It can provide essential nutrients and energy for tumor growth, but also enables the metastatic tumor cells to adapt to the new dynamic microenvironment and participate in regulating the signaling pathways related to tumor development. The tumor microenvironment thus aids the growth and proliferation of tumor cells, as well as further invasion and metastasis.

The role of PTEN in tumor-microenvironment cells and its effect on tumor cells have received great attention in recent years. About 25% of patients with breast cancer had loss of PTEN expression in stromal fibroblasts (29–32). Clinical studies also suggested that patients with breast, prostate, pancreatic, and endometrial cancers with PTEN-deficient stromal fibroblasts had a poor prognosis (22, 23, 25, 29–31, 33). Inactivation of *PTEN* in mouse breast stromal fibroblasts accelerated the malignant transformation of breast epithelial cells, and *PTEN* knockout in stromal fibroblasts promoted extracellular matrix remodeling, tumor angiogenesis, proliferation, invasion, metastasis, and other events, and mediated therapeutic resistance in mice with breast cancer (30, 31). Previous studies suggested that the severity and tissue selectivity of the disease in tumor cells and the tumor microenvironment were determined by PTEN protein level rather than *PTEN* gene mutation. Slight changes in PTEN protein levels can have major impacts on oncogenic signaling pathways, and its sensitivity is tissue-specific.

We inhibited the expression and activity of PTEN in host organs by intraperitoneal injection of VO-OHpic. Both local proliferation and distant metastases were significantly enhanced, and the ability of tumor cells to metastasize in each organ was related to the PTEN level in the organ. These results suggest that a low level or deletion of PTEN in the microenvironment of metastatic target organs promotes the colonization by metastatic breast cancer cells and the formation of metastatic tumors. However, use of the chemical inhibitor VO-OHpic to inhibit systemic PTEN in mice may be associated with problems related to the non-specific unexpected effects of chemical substances and persistence of effects. It is therefore necessary to determine the detailed effects of PTEN on breast cancer metastasis in relation to the host as a whole and the organ tissue microenvironment, and to establish a mouse model of complete *PTEN* knockout. However, it is difficult to establish such a model due to the embryo-lethal nature of *PTEN* total knockout, and only tissue- or organ-specific conditional knockout strategies can be adopted (27). However, if *PTEN* is knocked out in only one or several specific tissues or organs, normal expression of *PTEN* in the other tissues, including immune system cells, will affect the microenvironment of the knocked-out tissues and organs, thus affecting the reliability of the conclusions. We aim to conduct future studies to explore targeted ways of solving these problems, to clarify the molecular mechanism by which *PTEN* regulates the co-evolution of metastatic cancer cells and the metastatic microenvironment, and to establish a strategy to reduce the invasion and metastasis of breast cancer cells by enhancing the function of tumor suppressor genes in tumor-bearing organisms.

The current findings showed that decremental loss of *PTEN* expression and activity in the host by *in vivo* injection of VO-OHpic significantly enhanced the growth of orthotopic breast cancer and its metastasis to distant organs, with the metastasis intensity in each organ being negatively related to the PTEN expression level in the organ. These facts suggest that a systemic loss of or decrease of PTEN in the microenvironment of metastatic target organs promotes the implantation of metastatic breast cancer cells and the formation of metastatic tumors. However, the *in vivo* use of the chemical PTEN inhibitor

VO-OHpic may have unexpected non-specific chemical effects, as well as causing persistent inhibition. The ideal strategy for investigating the precise effect of PTEN in the microenvironment of specific tissues or organ or in the body as a whole on the metastasis of breast cancer would involve the creation of a conventional knockout mouse model; however, this is not possible because of the embryo-lethality of systemic *PTEN* knockout. Thus only tissue- or organ-specific conditional knockout strategies have been available to date; however, *PTEN* knockout in only one or several specific tissues or organs may be affected by PTEN from non-knockout tissues or organs, especially the immune system, with potential implications for the reliability of the study conclusions. We are conducting ongoing studies to explore targeted methods or models for elucidating the mechanisms by which PTEN regulates the co-evolution of metastatic cancer cells and the metastatic microenvironment, and to find an effective means of preventing the invasion and metastasis of human breast cancer cells *via* systemic elevation of tumor suppressor gene function in the tumor-bearing host.

DATA AVAILABILITY STATEMENT

The raw data supporting the conclusions of this article will be made available by the authors, without undue reservation.

ETHICS STATEMENT

The animal study was reviewed and approved by Laboratory Animal Science and Technology Management Committee of the School of Basic Medicine of Lanzhou University.

AUTHOR CONTRIBUTIONS

All authors listed have made a substantial, direct, and intellectual contribution to the work and approved it for publication.

FUNDING

This work was mainly supported by Natural Science Fund of Gansu province, China (20JR5RA269, 20JR5RA281 and 18JR3RA291) and National Natural Science Foundation of China (NO. 31701206).

ACKNOWLEDGMENTS

We thank International Science Editing (http://www.internationalscienceediting.-com) for editing this manuscript.

REFERENCES

1. Philip JM, Glynis W, Erika D. Breast Cancer Screening and Diagnosis in the 21st Century Within the U.K. *Post Reprod Health* (2015) 21(3):105–11. doi: 10.1177/2053369115594954
2. Agnieszka K, Marzena K, Katarzyna S, Agnieszka B, Dariusz S, Bożena K, et al. Primary and Secondary Prevention of Breast Cancer. *Ann Agric Environ Med* (2017) 24(4):549–53. doi: 10.26444/aaem/75943
3. Wei Y, Lv J, Guo Y, Bian Z, Gao M, Du H, et al. Soy Intake and Breast Cancer Risk: A Prospective Study of 300,000 Chinese Women and a Dose-Response Meta-Analysis. *Eur J Epidemiol* (2020) 35(6):567–78. doi: 10.1007/s10654-019-00585-4
4. Breast Cancer Expert Committee of National Cancer Quality Control Center; Breast Cancer Expert Committee of China Anti-Cancer Association and Cancer Drug Clinical Research Committee of China Anti-Cancer Association. Guidelines for Clinical Diagnosis and Treatment of Advanced Breast Cancer in China (2020 Edition). *Zhonghua Zhong Liu Za Zhi* (2020) 42(10):781–97. doi: 10.3760/cma.j.cn112152-20200817-00747
5. Liang YR, Zhang HW, Song XJ, Yang QF. Metastatic Heterogeneity of Breast Cancer: Molecular Mechanism and Potential Therapeutic Targets. *Semin Cancer Biol* (2020) 60:14–27. doi: 10.1016/j.semcancer.2019.08.012
6. Yousefi M, Nosrati R, Salmaninejad A, Dehghani S, Shahryari A, Saberi A. Organ-Specific Metastasis of Breast Cancer: Molecular and Cellular Mechanisms Underlying Lung Metastasis. *Cell Oncol (Dordr)* (2018) 41 (2):123–40. doi: 10.1007/s13402-018-0376-6
7. Lah TT, Novak M, Breznik B. Brain Malignancies: Glioblastoma and Brain Metastases. *Semin Cancer Biol* (2020) 60:262–73. doi: 10.1016/j.semcancer.2019.10.010
8. Tahara RK, Brewer TM, Theriault RL, Ueno NT. Bone Metastasis of Breast Cancer. *Adv Exp Med Biol* (2019) 1152:105–29. doi: 10.1007/978-3-030-20301-6_7
9. Alzubi MA, Turner TH, Olex AL, Sohal SS, Tobin NP, Recio SG, et al. Separation of Breast Cancer and Organ Microenvironment Transcriptomes in Metastases. *Breast Cancer Res* (2019) 21(1):36. doi: 10.1186/s13058-019-1123-2
10. Aquila S, Santoro M, Caputo A, Panno ML, Pezzi V, De Amicis F. The Tumor Suppressor PTEN as Molecular Switch Node Regulating Cell Metabolism and Autophagy: Implications in Immune System and Tumor Microenvironment. *Cells* (2020) 9(7):1725. doi: 10.3390/cells9071725
11. Mitra S, Lauss M, Cabrita R, Choi J, Zhang T, Isaksson K, et al. Analysis of DNA Methylation Patterns in the Tumor Immune Microenvironment of Metastatic Melanoma. *Mol Oncol* (2020) 14(5):933–50. doi: 10.1002/1878-0261.12663
12. Furnari FB, Lin H, Huang HJ, Cavenee WK. Growth Suppression of Glioma Cells by PTEN Requires a Functional Phosphatase Catalytic Domain. *Proc Natl Acad Sci USA* (1997) 94(23):12479–84. doi: 10.1073/pnas.94.23.12479
13. Li J, Yen C, Liaw D, Podsypanina K, Bose S, Wang SI, et al. PTEN, a Putative Protein Tyrosine Phosphatase Gene Mutated in Human Brain, Breast and Prostate Cancer. *Science* (1997) 275(5308):1943–7. doi: 10.1126/science.275.5308.1943
14. Worby CA, Dixon JE. PTEN. *Annu Rev Biochem* (2014) 83:641–69. doi: 10.1146/annurev-biochem-082411-113907
15. Xing Y, Lin NU, Maurer MA, Chen H, Mahvash A, Sahin A, et al. Phase II Trial of AKT Inhibitor MK-2206 in Patients With Advanced Breast Cancer Who Have Tumors With PIK3CA or AKT Mutations, and/or PTEN Loss/PTEN Mutation. *Breast Cancer Res* (2019) 21(1):78–12. doi: 10.1186/s13058-019-1154-8
16. Jasphin SS, Desai D, Pandit S, Gonsalves NM, Nayak PB, Iype A. Immunohistochemical Expression of Phosphatase and Tensin Homolog in Histologic Gradings of Oral Squamous Cell Carcinoma. *Contemp Clin Dent* (2016) 7(4):524–8. doi: 10.4103/0976-237X.194111
17. Lapthanasupkul P, Klongnoi B, Mutirangura A, Kitkumthorn N. Investigation of PTEN Promoter Methylation in Ameloblastoma. *Med Oral Patol Oral Cir Bucal* (2020) 25(4):e481–7. doi: 10.4317/medoral.23498
18. Li K, Li GD, Sun LY, Li XQ. PTEN and SHIP: Impact on Lymphatic Metastasis in Breast Cancer. *J Cancer Res Ther* (2018) 14(Supplement):S937–41. doi: 10.4103/0973-1482.193894
19. Momozawa Y, Iwasaki Y, Parsons MT, Kamatani Y, Takahashi A, Tamura C, et al. Germline Pathogenic Variants of 11 Breast Cancer Genes in 7,051 Japanese Patients and 11,241 Controls. *Nat Commun* (2018) 9(1):4083. doi: 10.1038/s41467-018-06581-8
20. Bubien V, Bonnet F, Brouste V, Hoppe S, Barouk-Simonet E, David A, et al. High Cumulative Risks of Cancer in Patients With PTEN Hamartoma

Tumour Syndrome. *J Med Genet* (2013) 50(4):255–63. doi: 10.1136/jmedgenet-2012-101339
21. Abdulkareem IH, Blair M. Phosphatase and Tensin Homologue Deleted on Chromosome 10. *Niger Med J* (2013) 54(2):79–86. doi: 10.4103/0300-1652.110033
22. Zhang P, Chen JH, Guo XL. New Insights Into PTEN Regulation Mechanisms and Its Potential Function in Targeted Therapies. *BioMed Pharmacother* (2012) 66(7):485–90. doi: 10.1016/j.biopha.2012.04.004
23. Thies KA, Lefler JE, Leone G, Ostrowski MC. PTEN in the Stroma. *Cold Spring Harb Perspect Med* (2019) 9(10):a036111. doi: 10.1101/cshperspect.a036111
24. Yan M, Wang Y, Wong CW, Or PM, Wong KL, Li L, et al. PTEN PDZ-Binding Domain Suppresses Mammary Carcinogenesis in the MMTV-PyMT Breast Cancer Model. *Cancer Lett* (2018) 28:430. doi: 10.1016/j.canlet.2018.05.012
25. Chen H, Zhou L, Wu X, Li R, Wen J, Sha J, et al. The PI3K/AKT Pathway in the Pathogenesis of Prostate Cancer. *Front Biosci (Landmark Ed)* (2016) 21:1084–91. doi: 10.2741/4443
26. Bi X, Lv X, Liu D, Guo H, Yao G, Wang L, et al. METTL3-Mediated Maturation of miR-126-5p Promotes Ovarian Cancer Progression *via* PTEN-Mediated PI3K/Akt/mTOR Pathway. *Cancer Gene Ther* (2021) 28(3-4):335–49. doi: 10.1038/s41417-020-00222-3
27. Alzahrani AS. PI3K/Akt/mTOR Inhibitors in Cancer: At the Bench and Bedside. *Semin Cancer Biol* (2019) 59:125–32. doi: 10.1016/j.semcancer.2019.07.009
28. Rodgers SJ, Ferguson DT, Mitchell CA, Ooms LM. Regulation of PI3K Effector Signalling in Cancer by the Phosphoinositide Phosphatases. *Biosci Rep* (2017) 37(1):BSR20160432. doi: 10.1042/BSR20160432
29. Suda T, Oba H, Takei H, Kurosumi M, Hayashi S, Yamaguchi Y. ER-Activating Ability of Breast Cancer Stromal Fibroblasts Is Regulated Independently of Alteration of TP53 and PTEN Tumor Suppressor Genes. *Biochem Biophys Res Commun* (2012) 428(2):259–63. doi: 10.1016/j.bbrc.2012.10.035
30. Jones CE, Hammer AM, Cho Y, Sizemore GM, Cukierman E, Yee LD, et al. Stromal PTEN Regulates Extracellular Matrix Organization in the Mammary Gland. *Neoplasia* (2019) 21(1):132–45. doi: 10.1016/j.neo.2018.10.010
31. Lin JJ, Fan JJ, Ge XJ, Sha HB. PAG1 Stimulates Proliferation and Metastasis of Nasopharyngeal Carcinoma Through Downregulating PTEN. *Eur Rev Med Pharmacol Sci* (2020) 24(21):11096–104. doi: 10.26355/eurrev_202011_23596
32. Shiovitz S, Korde LA. Genetics of Breast Cancer: A Topic in Evolution. *Ann Oncol* (2015) 26(7):1291–9. doi: 10.1093/annonc/mdv022
33. Kapusta P, Dulińska-Litewka J, Totoń-Żurańska J, Borys A, Konieczny PS, Wołkow PP, et al. Dysregulation of Transcription Factor Activity During Formation of Cancer-Associated Fibroblasts. *Int J Mol Sci* (2020) 21(22):8749. doi: 10.3390/ijms21228749

Conflict of Interest: The authors declare that the research was conducted in the absence of any commercial or financial relationships that could be construed as a potential conflict of interest.

Publisher's Note: All claims expressed in this article are solely those of the authors and do not necessarily represent those of their affiliated organizations, or those of the publisher, the editors and the reviewers. Any product that may be evaluated in this article, or claim that may be made by its manufacturer, is not guaranteed or endorsed by the publisher.

frontiers in Oncology

ORIGINAL RESEARCH
published: 21 March 2022
doi: 10.3389/fonc.2022.821334

Verification and Validation of a Four-Gene Panel as a Prognostic Indicator in Triple Negative Breast Cancer

Mamta Pariyar[1,2], *Rick F. Thorne*[1,3], *Rodney J. Scott*[1,2,4] *and Kelly A. Avery-Kiejda*[1,2]*

[1] School of Biomedical Sciences and Pharmacy, College of Health, Medicine and Wellbeing, University of Newcastle, Callaghan, NSW, Australia, [2] Hunter Medical Research Institute, New Lambton Heights, NSW, Australia, [3] Translational Research Institute, Henan Provincial People's Hospital, Academy of Medical Science, Zhengzhou University, Zhengzhou, China, [4] NSW Health Pathology, John Hunter Hospital, New Lambton Heights, NSW, Australia

Triple negative breast cancer (TNBC) is a highly aggressive subtype with a high rate of metastasis, early distant recurrence and resistance to therapy leading to worse survival than other breast cancer subtypes. There are no well-established biomarkers that can determine women who will do better and those who are likely to have poorer outcomes with TNBC, nor are there targeted therapies. Thus, the identification of prognostic and/or predictive biomarkers will enable tailored therapies based on their likelihood of disease outcomes and may prevent over- and under-diagnosis. Previous studies from our laboratory have identified four genes (ANP32E, DSC2, ANKRD30A and IL6ST/gp130) that are specific to TNBC and were associated with lymph node metastasis (LNmets), the earliest indicator of tumor progression *via* distal spread. This study aimed to validate these findings using absolute quantitation by digital droplet PCR (ddPCR) and to determine relationships with clinicopathological features and survival. Our analysis confirmed all four genes displayed significant expression differences between TNBC cases and non-TNBC cases. Moreover, low IL6ST expression was significantly associated with grade 3 disease, hormone receptor negativity and earlier age at diagnosis; low ANKRD30A expression was associated with tumor size; and high ANP32E expression was significantly associated with grade and the number of positive lymph nodes. Individually, three of the four genes were associated with relapse-free survival in TNBC and in combination, all four genes were significantly associated with TNBC survival, but not in hormone receptor-positive cases. Collectively our results suggest that the four genes may have utility in TNBC prognostication.

Keywords: triple negative breast cancer (TNBC), metastasis, gene expression, ddPCR, prognostic

OPEN ACCESS

Edited by:
San-Gang Wu,
First Affiliated Hospital of Xiamen University, China

Reviewed by:
Victoria Seewaldt,
City of Hope, United States
Anuraag Shrivastav,
University of Winnipeg, Canada

***Correspondence:**
Kelly A. Avery-Kiejda
kelly.kiejda@newcastle.edu.au

Specialty section:
This article was submitted to Breast Cancer, a section of the journal Frontiers in Oncology

Received: *24 November 2021*
Accepted: *25 February 2022*
Published: *21 March 2022*

Citation:
Pariyar M, Thorne RF, Scott RJ and Avery-Kiejda KA (2022) Verification and Validation of a Four-Gene Panel as a Prognostic Indicator in Triple Negative Breast Cancer. Front. Oncol. 12:821334. doi: 10.3389/fonc.2022.821334

INTRODUCTION

Triple negative breast cancer (TNBC) is one of the most aggressive subtypes due to it not being amenable to targeted therapies including Tamoxifen and Herceptin (trastuzumab) and it is associated with rapid metastasis, higher risk of recurrence and poorer survival outcomes, when compared to receptor positive breast cancer subtypes (1, 2). Because of the lack of targeted

treatment, the current treatment options are limited to chemotherapy and surgery. There are no well-established prognostic biomarkers in TNBC that can be used in disease prognosis. Therefore, identification of prognostic biomarkers to improve treatment regimens and that can potentially be targets for therapy in this breast cancer subtype are urgently required.

Previous studies from our laboratory have identified four genes that are differentially expressed in invasive ductal carcinoma (IDCs) compared to normal adjacent tissues (NATs) in TNBC as well as being differentially expressed in TNBC compared to non-TNBC. These results were validated in two independent cohorts, including a large cohort sourced from The Cancer Genome Atlas (TCGA) using the same method (cDNA microarrays) (3). Ankyrin repeat domain 30A (*ANKRD30A*) and interleukin 6 signal transducer (*IL6ST*) were downregulated in TNBC compared to non-TNBC, whereas desmocollin-2 (*DSC2*) and acidic nuclear phosphoprotein 32 family member E (*ANP32E*) were upregulated in TNBC compared to non-TNBC. *ANKRD30A* is a breast differentiation antigen responsible for protein-protein interactions and other cellular functions (4). *IL6ST* also known as glycoprotein 130 (gp130) is a signal transducer for the interleukin family of cytokines such as IL6, CNTF, LIF and OSM; and an activator of JAK/STAT and MAPK/PI3K/ERK signaling pathways (5). *DSC2* is one of the main components of desmosomes, which aid in cell-cell attachments as well as play a key role in cell growth and apoptosis (6). *ANP32E* is a histone chaperone that has the ability to strip H2A.Z away from DNA, allowing chromatin remodeling and thus altering gene expression (7). Although some of these genes have been implicated in other types of breast cancer, the relationship of these genes to prognosis in TNBC is currently unknown. Moreover, our previous results need to be verified using a different method in order to move these results forward to the clinic.

Amplification by digital droplet PCR (ddPCR) offers several advantages over conventional qRT-PCR; it can be used to calculate the absolute concentration of cDNA in a sample without the need for any standards, as the cDNA within a sample is partitioned into thousands of droplets, amplified and counted directly by Poisson statistics. Because of the sample partitioning and endpoint quantitation used in ddPCR, PCR amplification is independent of reaction efficiency as well as being less susceptible to Taqman polymerase inhibitors compared to that in qPCR in which PCR amplification is dependent on the concentration of inhibitors in the entire sample. Thus ddPCR provides accurate, precise and reproducible data (8, 9) and also can be used for low concentration samples with increased precision (10). Moreover, ddPCR can be utilized to perform multiplexing to detect more than one target in the reaction, reducing the time and cost of the experiment (11).

The aim of this study was to verify the differential expression of *ANKRD30A*, *IL6ST*, *DSC2* and *ANP32E* in TNBC compared to NATs and between TNBC and non-TNBC using an independent method (ddPCR) and to define their relationship with clinicopathological features and survival outcomes. We have shown that these genes were significantly different between TNBC cases and non-TNBC cases. Individually, three of the four genes were associated with relapse-free survival in TNBC and when combined, the four genes were significantly associated with survival in TNBC, but not in hormone receptor-positive cases. Thus, *ANKRD30A*, *IL6ST*, *DSC2* and *ANP32E* may represent novel prognostic markers for the TNBC subtype.

MATERIALS AND METHODS

Cohorts

Two cohorts were used in this study. The first cohort consisted of a total of 28 invasive ductal carcinomas of the TNBC subtype, with 13 matched LNmets and 2 unmatched LNmets as well as 8 matched normal adjacent tissue (NAT) and 1 unmatched NAT. All samples were formalin fixed paraffin embedded (FFPE) and obtained by 1.5mm punch biopsy from the archives of NSW Health Pathology, John Hunter Hospital, Newcastle, Australia. This cohort has been described previously (3). Areas of IDC, LNmet and NAT were identified and confirmed by a pathologist. The clinical characteristics of the patients used in this study are shown in **Table 1**.

A second cohort with a total of 13 TNBCs and 105 non-TNBCs for comparisons with a non-TNBC cohort. The samples were fresh frozen IDC and were provided by the Australian Breast Cancer Tissue Bank (Westmead, NSW, Australia), which have been previously described (12). The cohort characteristics are described in **Table 2**.

This study complies with the Helsinki Declaration with ethical approval from the Hunter New England Human Research Ethics Committee (Approval number: 09/05/20/5.02). In accordance with the National Statement on Ethical Conduct in Research Involving Humans, a waiver of consent was granted for cases from NSW Health Pathology, whilst all other cases have consented to their tissue and clinical information being used for research.

TABLE 1 | Clinical characteristics of 28 TNBC samples of the first cohort.

Variable	n (%)
Age (years)	
Median (Range)	55 (36-84)
<40	2 (7.1%)
40-50	9 (32.1%)
>50	17 (60.7%)
Grade	
1 or 2	5 (17.8%)
3	23 (82.1%)
Tumour size (mm)	
median	28
≤28	15 (53.5%)
>28	13 (46.4%)
No. of positive lymph nodes	
0	13 (46.4%)
1-3	11 (39.2%)
>3	3 (10.7%)
	LN status of 1 case is unavailable.

TABLE 2 | Clinical characteristics of 118 (TNBC and non-TNBC) samples of the second cohort.

Variable	n (%)
Age years	
Median (Range)	56 (28-90)
<40	12 (10.1%)
40-50	36 (30.5%)
>50	70 (59.3%)
Grade	
1 or 2	59 (50%)
3	59 (50%)
Tumour size (mm)	
median	25
≤25	65 (55.0%)
>25	53 (44.9%)
No. of positive lymph nodes	
0	52 (44.0%)
1-3	46 (38.9%)
>3	20 (16.9%)
ER	
Positive	93 (78.8%)
Negative	25 (21.1%)
PR	
Positive	86 (72.8%)
Negative	32 (27.1%)
HER2	
Positive	18 (15.2%)
Negative	99 (83.8%)
	HER2 status of 1 case is unavailable
TNBC	
Yes	13 (11.0%)
No	105 (88.9%)

RNA Extraction and Quantification

RNA extraction of the whole biopsy samples was previously described (13). All samples were stored at -80°C. These were quantitated before cDNA synthesis using the Qubit™ RNA BR (broad range) Assay Kit. The extracted FFPE DNA stored at -20°C was quantitated using the Qubit® dsDNA HS Assay Kit.

Reverse Transcription

Either 75ng RNA from fresh frozen tissues or 125 ng RNA from FFPE tissues was used for cDNA synthesis, the latter amount increased to counter the highly degraded nature of the RNA in FFPE samples. cDNA synthesis was performed as using the High-Capacity cDNA Reverse Transcription Kit (Life Technologies, Mulgrave, VIC, Australia) to generate complementary DNA (cDNA) according to the manufacturers' instructions.

Digital Droplet PCR (ddPCR)

A total reaction volume of 25 µl was prepared according to the manufacturers' instructions (Bio-Rad). The amount of cDNA added to the PCR reaction depended on whether it was extracted from fresh frozen or FFPE tissues, due to the differing amplification efficiencies: 12.5 ng cDNA equivalent to RNA input from FFPE tissues was used in the reaction; while 3.75 ng cDNA equivalent to RNA input that had been reverse transcribed from fresh frozen tissues was used. TaqMan Gene Expression Assays (Life Technologies) for *ANKRD30A* (Hs00369567_m1), *IL6ST* (Hs00174360_m1), *ANP32E* (Hs01064731_m1) and *DSC2* (Hs00951428_m1) were used for digital droplet PCR. Droplets were generated in an Automated Droplet QX200 Generator (1864101, Bio-Rad) according to the manufacturers' instructions. PCR amplification of the cDNA within the droplets was performed using the C1000 thermal cycler (Bio-Rad) according to the manufacturers' instructions.

After PCR amplification of the target cDNA within the droplets, the sample plate was placed in the droplet reader (QX200 Droplet Reader, 1864003, Bio-Rad) which counts each droplet individually using a fluorescent detection system which is set to detect FAM or HEX/VIC and classifies them as positive or negative droplets based on endpoint fluorescent amplitude. Positive droplets containing at least one copy of the target cDNA molecule have an increased fluorescence compared to negative droplets. The number of positive and negative droplets read by droplet reader was then used by Quantasoft software (Bio-Rad) to calculate the absolute quantity of DNA per sample in copies/µl where it first determines the fraction of positive droplets and after combination with a Poisson algorithm, provides the original concentration of the target template. Based on Poisson statistics, the average copies (of target) per droplet (CPD) was calculated as: $CPD = -\ln(1-p)$; where p = fraction of positive droplet. CPD can then be converted into the concentration of target (copies/µl) in the initial sample as shown below:

$$Concentration\ (copies/\mu L) = CPD/V^{droplet};$$

where $V^{droplet}$ is the average droplet volume (μL).

Statistical Analysis

All statistical analysis was performed using GraphPad Prism 7 (San Diego, California, USA). The normality of the distribution was tested using the D'Agostino & Pearson normality test. As some of the groups were not normally distributed, a Kruskal-Wallis test was used to determine if differences in the expression of *DSC2*, *ANP32E* and *IL6ST* were statistically significant between unmatched groups. A two-tailed Mann Whitney test was used to assess if there was a statistically significant difference in the expression of *DSC2*, *ANP32E, IL6ST* and *ANKRD30A* between two groups. To assess if the differential expression was associated with clinical features including age, tumor size, grade and lymph node positivity, a chi-squared test was used. A p value ≤ 0.05 was considered to be statistically significant.

Kaplan-Meier (KM) Plotter Database Analysis

KM plotter is a publicly available online database with gene expression and survival information data downloaded from Gene Expression Omnibus (GEO), European genome-phenome Archive (EGA) and The Cancer Genome Atlas (TCGA). This database was used to perform relapse free survival analysis in TNBC and non-TNBC cases. Each gene of interest was entered into the database to obtain KM survival curves plots and number at risk. The following probe IDs were used for this analysis: *ANKRD30A* (223864_at), *IL6ST* (204863_s_at, 204864_s_at, 211000_s_at, 212195_at, 212196_at), *DSC2* (204750_s_at, 204751_x_at, 226817_at) and

ANP32E (208103_s_at, 221505_at). A total of 255 TNBC cases in the database were available for RFS analysis on *ANP32E* and IL6ST, while only 161 TNBC cases were available for RFS analysis with the *DSC2* and *ANKRD30A* microarray probes. No gene expression microarray data for *DSC2* and *ANKRD30A* were available in the rest of the 94 TNBC samples. The automatically generated best cut-off (more accurate than median) was chosen to classify the expression of genes into high and low values. The best cut-off provided in the KM plotter is the best performing cut-off with the most statistically significant p-value (Cox regression analysis) from all the possible cut-offs computed automatically by the database between the lower and upper quartiles. The publicly available microarray datasets including E-MTAB-365, E-TABM-43 and GSE (Gene Expression Omnibus Series) in the software were selected to generate the Kaplan-Meier plots in this study. A log rank p-value of 0.05 was considered statistically significant. The hazard ratio, 95% confidence interval and number at risk were obtained using the database.

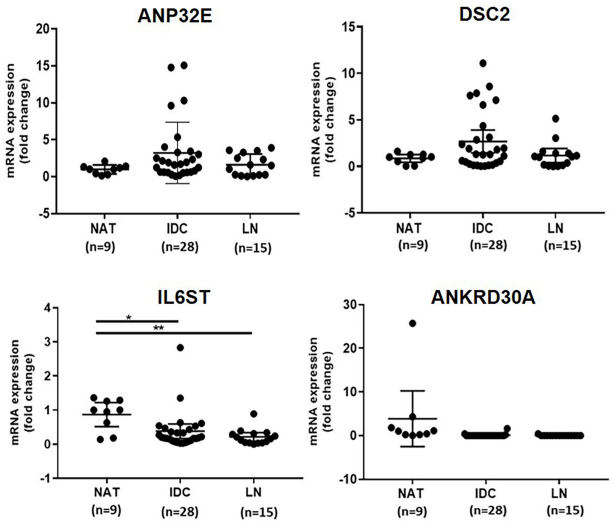

FIGURE 1 | Verification of differential expression of *ANP32E, DSC2, IL6ST* and *ANKRD30A* genes at the mRNA level in tumour compared to normal tissue in the first cohort. The mRNA expression of *ANP32E, DSC2, IL6ST* and *ANKRD30A* genes obtained as copies per µl using ddPCR. Results show the fold change expression of four genes in IDCs and LNmets compared to NATs. Values are presented as the median ± interquartile range. A Kruskal-Wallis test followed by Dunn's test for multiple comparisons was performed to determine the statistical significance of the expression. A p value ≤ 0.05 was considered significant. Asterisks in the figure represents statistical significance (*p ≤ 0.05; **p ≤ 0.01). NAT, Normal adjacent tissue; IDC, Invasive ductal carcinoma and LNmet, Lymph node metastasis.

RESULTS

Verification of Differential mRNA Expression of ANP32E, DSC2, IL6ST and ANKRD30A Between Normal and Tumour Samples by ddPCR

The mRNA expression of *ANP32E*, *DSC2*, *IL6ST* and *ANKRD30A* was quantified using ddPCR to verify the differential mRNA expression of these genes in IDC (n = 28) compared to NAT (n = 9) as well as LNmets (n = 15). This was performed in the first cohort, which was previously used for gene expression analysis in a recent publication by our group (3). The sample number used in this study varied from the numbers in the previous study as some samples were excluded due to the low RNA amount. In concordance with our previous findings (3), the expression of *IL6ST* was significantly downregulated in IDCs (median fold change = -0.2) and LNmets (median fold change = -0.2) compared to NATs (p=0.0171 and 0.0020, respectively). The expression of *DSC2* (median fold change = 1.3) and *ANP32E* (median fold change = 1.8) were upregulated in IDCs compared to NATs, however, the increase in expression was not statistically significant (p = 0.4537, p = 0.1743, respectively) (**Figure 1**). Additionally, the expression of these genes was increased in LNmets when compared to NAT (median fold change for *ANP32E* = 1.5), but this difference was not significant (p ≥ 0.999 and 0.9864, respectively). *ANKRD30A* showed very low to no expression in IDCs and LNmets compared to NATs and was undetectable in the majority of samples (**Figure 1**).

Verification of Differential mRNA Expression of ANP32E, DSC2, IL6ST and ANKRD30A Between TNBC and Non-TNBC by ddPCR

Next, the differential expression of ANP32E, DSC2, IL6ST and ANKRD30A in TNBC compared to non-TNBC was verified using digital droplet PCR. For this analysis, 13 TNBC and 105 non-TNBC samples (second cohort) were used. This was to confirm the differential expression of these genes identified in our previous study at the mRNA level using a different method. In concordance with our previous finding (3), ANP32E (median fold change = 2.1) and DSC2 (median fold change = 3.5) were significantly upregulated in TNBC compared to non-TNBC (p = 0.0009, p<0.0001, respectively), whereas IL6ST (median fold change = -0.2) and ANKRD30A (median fold change = 0.00) were significantly downregulated in TNBC compared to non-TNBC (p <0.0001, p < 0.0001, respectively) (**Figure 2**).

Association of mRNA Expression of ANP32E, DSC2 and IL6ST With Clinicopathological Features

To assess whether the mRNA expression of *ANP32E*, *DSC2* and *IL6ST* in TNBC were correlated with clinicopathological features, a chi-square test was performed for all genes except *ANKRD30A* (due to the low number of samples with detectable expression) in relation to age, grade, tumor size, and number of positive lymph nodes. The samples were divided into high (n = 14), and low (n = 14) mRNA expression based on the median expression of each gene within the first cohort. However, the differential mRNA expression of *DSC2*, *ANP32E* and *IL6ST* genes showed no correlation with the clinical characteristics in the first cohort (**Table 3**).

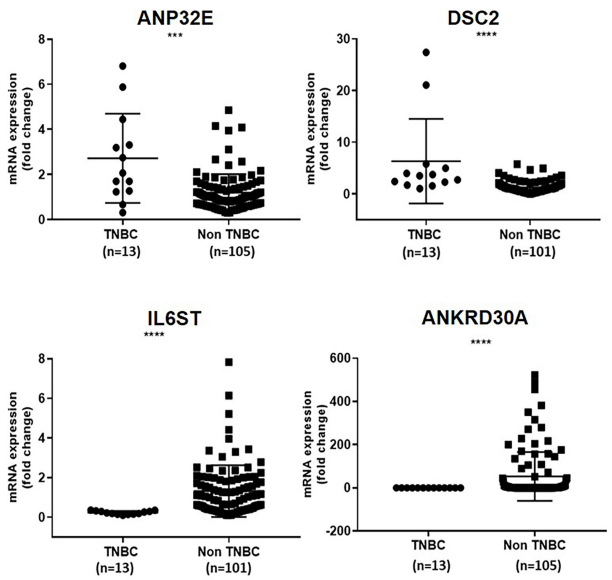

FIGURE 2 | Verification of differential expression of *ANP32E, DSC2, IL6ST* and *ANKRD30A* genes in TNBC compared to non-TNBC at the mRNA level in the second cohort. The mRNA expression of *ANP32E, DSC2, IL6ST* and *ANKRD30A* genes obtained as copies per µl using ddPCR. Results are shown as fold change expression of target genes in TNBC compared to non-TNBC. Values are presented as the median ± interquartile range. A Mann Whitney test was used to determine the statistical significance of the expression in TNBC. A p value ≤ 0.05 was considered significant. Asterisks in the figure represent statistical significance (***p ≤ 0.001, ****p ≤ 0.0001).

In the second cohort, which contained both receptor positive and negative IDC cases, a chi-square test was performed to determine whether the high or low mRNA expression of the four genes was associated with age, grade, tumor size, number of positive lymph nodes, hormone receptor positivity and TNBC status. *ANP32E* was significantly associated with grade (p = 0.0017), number of positive lymph nodes (p = 0.0304); and ER, PR and TNBC status (p = 0.0282, 0.0384 and 0.0081, respectively). *DSC2* expression was significantly associated with ER, PR and TNBC status (p = 0.001, 0.018 and 0.001, respectively). *IL6ST* expression showed a significant association with age (p = 0.05), tumor grade (p < 0.0001) as well as with ER, PR, HER2 and TNBC status (p < 0.0001, < 0.0001, 0.0033 and 0.0001, respectively). *ANKRD30A*

TABLE 3 | Association of ANP32E, DSC2 and IL6ST mRNA expression with clinicopathological features in TNBC cases from the first cohort.

Characteristic	ANP32E				DSC2				IL6ST			
	Total n=28	High n=14 (50%)	Low n=14 (50%)	P-value	Total n=28	High n=14 (50%)	Low n=14 (50%)	P-value	Total n=28	High n=14 (50%)	Low n=14 (50%)	P-value
Age (years)												
<40	2	1 (7)	1 (7)	0.466	2	0 (0)	2 (14)	0.338	2	1 (7)	1 (7)	0.919
40-50	9	6 (43)	3 (21)		9	5 (36)	4 (29)		9	4 (29)	5 (36)	
>50	17	7 (50)	10 (71)		17	9 (64)	8 (57)		17	9 (64)	8 (57)	
Grade												
1 or 2	4	1 (7)	3 (21)	0.280	4	2 (14)	2 (14)	>0.99	4	2 (14)	2 (14)	>0.99
3	24	13 (93)	11 (79)		24	12 (86)	12 (86)		24	12 (86)	12 (86)	
Tumour size (mm), median = 25												
≤25	13	5 (36)	8 (57)	0.256	13	7 (50)	6 (43)	0.705	13	6 (43)	7 (50)	0.705
>25	15	9 (64)	6 (43)		15	7 (50)	8 (57)		15	8 (57)	7 (50)	
No. of +ve LNs												
0	13	8 (57)	5 (36)	0.583	13	7 (50)	6 (43)	0.363	13	7 (50)	6 (43)	0.145
1-3	11	5 (36)	6 (43)		11	5 (36)	6 (43)		11	7 (50)	4 (29)	
>3	3	1 (7)	2 (14)		3	2 (14)	0 (0)		3	0 (0)	3 (21)	

Lymph node status of 1 case is unavailable.
Statistical analyses based on chi squared test. A p value of ≤ 0.05 was considered significant.

expression was significantly associated with tumor size, ER, PR and TNBC status (p = 0.0161, 0.0007, 0.0009, 0.0012, respectively) (**Table 4**).

Association of mRNA Expression of ANP32E, DSC2, IL6ST and ANKRD30A With Survival

Next, the impact of each of the four genes on survival was assessed after segmenting cases into high and low mRNA expression. Due to the low number of TNBC samples in the first and second cohorts, relapse-free survival (RFS) analysis was performed on the four genes in a larger cohort of TNBC cases using the KM plotter online database, which contains expression values from publicly available microarray data. A total of 255 TNBC cases in the database were available for RFS analysis on ANP32E and IL6ST, while only 161 TNBC cases were available for RFS analysis with the DSC2 and ANKRD30A microarray probes. No gene expression microarray data for DSC2 and ANKRD30A were available in the other 94 TNBC samples. High and low expression of these genes were split based on the automatically generated best cut-off value as described the methods. All the microarray probes that were specifically related to the gene of interest were selected. High expression of ANP32E (p = 0.0092) was significantly associated with decreased RFS while the high expression of DSC2 (p = 0.26) showed a non-significant trend of increased RFS. Low expression of IL6ST (p = 0.011) and ANKRD30A (p = 0.027) was significantly associated with decreased RFS (**Figure 3**).

To determine if the combined expression of the four gene panel was associated with survival, relapse free survival analysis of the four gene panel including ANKRD30A, IL6ST, ANP32E and DSC2 was performed using the KM plotter database in both TNBC and non-TNBC samples. For this, the mean expression of the four genes was selected for survival curve analysis with inverted expression of the two low expressed genes: ANKRD30A and IL6ST and not inverted for the two highly expressed genes: ANP32E and DSC2 in both TNBC and non-TNBC samples. A total of 161 TNBC cases and 467 non-TNBC cases was available for four gene panel survival analysis in the KM plotter database. High expression of the four gene panel was significantly associated with low RFS compared to its low expression in TNBC. In contrast, the differential expression of

TABLE 4 | Association of *ANP32E, DSC2, IL6ST* and *ANKRD30A* mRNA expression with clinicopathological features in breast cancer cases from the second cohort.

Characteristics	ANP32E				DSC2				IL6ST				ANKRD30A			
	Total n=118	High n=59 (50%)	Low n=59 (50%)	P-value	Total n=114	High n=57 (50%)	Low n=57 (50%)	P-value	Total n=114	High n=57 (50%)	Low n=57 (50%)	P-value	Total n=118	High n=59 (50%)	Low n=59 (50%)	P-value
Age (years)																
<40	12	5 (8)	7 (12)	0.458	12	5 (9)	7 (12)	0.348	12	2 (4)	10 (18)	**0.05**	12	4 (7)	8 (14)	0.260
40-50	36	21 (36)	15 (25)		35	21 (37)	14 (25)		34	18 (32)	16 (28)		36	16 (27)	20 (34)	
>50	70	33 (56)	37 (63)		67	31 (54)	36 (63)		68	37 (65)	31 (54)		70	39 (66)	31 (53)	
Grade																
1 or 2	59	21 (36)	38 (64)	**0.002**	58	24 (42)	34 (60)	0.061	57	40 (70)	17 (30)	**<0.000**	59	34 (58)	25 (42)	0.098
3	59	38 (64)	21 (36)		56	33 (58)	23 (40)		57	17 (30)	40 (70)		59	25 (42)	34 (58)	
Tumour size (mm), median = 25																
≤25	65	28 (47)	37 (63)	0.097	62	31 (54)	31 (54)	0.999	62	34 (60)	28(49)	0.259	65	39 (66)	26 (44)	**0.016**
>25	53	31 (53)	22 (37)		52	26 (46)	26 (46)		52	23 (40)	29 (51)		53	20 (34)	33 (56)	
No. of +ve lymph nodes																
0	52	21 (36)	31 (53)	**0.030**	49	23 (40)	26 (46)	0.486	49	25 (44)	24 (42)	0.116	52	26 (44)	26 (44)	0.866
1-3	46	30 (51)	16 (27)		46	26 (46)	20 (35)		45	26 (46)	19 (33)		46	24 (41)	22 (37)	
>3	20	8 (14)	12 (20)		19	8 (14)	11 (19)		20	6 (11)	14 (25)		20	9 (15)	11 (19)	
ER																
positive	93	44 (75)	49 (83)	**0.028**	90	38 (67)	52 (91)	**0.001**	89	57 (100)	32 (56)	**<0.000**	93	54 (92)	39 (66)	**0.000**
Negative	25	18 (31)	7 (12)		24	19 (33)	5 (9)		25	0 (0)	25 (44)		25	5 (8)	20 (34)	
PR																
positive	86	38 (64)	48 (81)	**0.038**	85	37 (65)	48 (84)	**0.018**	83	53 (93)	30 (53)	**<0.000**	86	51 (86)	35 (59)	**0.000**
negative	32	21 (36)	11 (19)		29	20 (35)	9 (16)		31	4 (7)	27 (47)		32	8 (14)	24 (41)	
HER2																
Positive	18	10 (17)	8 (14)	0.636	18	10 (18)	8 (14)	0.607	17	3 (5)	14 (25)	**0.003**	18	7 (12)	11 (19)	0.324
Negative	99	49 (83)	50 (85)		96	47 (82)	49 (84)		96	54 (95)	42 (74)		99	51 (86)	48 (81)	
TNBC																
Yes	13	11 (19)	2 (3)	**0.008**	13	12 (21)	1 (2)	**0.001**	13	0 (0)	13 (23)	**0.000**	13	1 (2)	12 (20)	**0.001**
NO	105	48 (81)	57 (97)		101	45 (79)	56 (98)		101	57 (100)	44 (77)		105	58 (98)	47 (80)	

HER2 status of 1 case is unavailable.
Statistical analyses based on chi squared test. A p value of ≤ 0.05 was considered significant.
The values in bold are significant (p < 0.05).

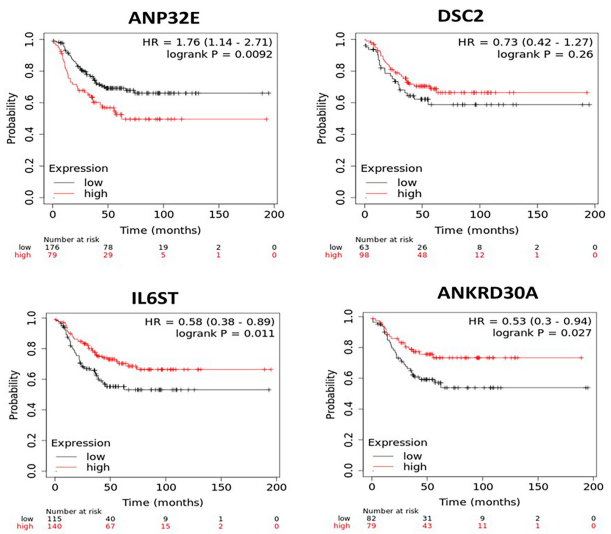

FIGURE 3 | Kaplan-Meier survival curves for patients with high or low mRNA expression of *ANP32E, DSC2, IL6ST* and *ANKRD30A* in TNBC samples. The survival analysis was performed in KM plotter using publicly available TNBC microarray data that is available within the database. TNBC samples in the KM plotter database were divided into high or low expression groups based on auto best cut-off expression value of each gene and compared by Kaplan-Meier survival analysis. A Log-rank p-value ≤ 0.05 was considered significant. HR, hazard ratio. The red curve represents high expression, and the black curve represents low expression of the indicated gene.

the 4-gene panel in non-TNBC cases (ER+/PR+/HER2+-) was not significantly associated with RFS (**Figure 4**).

To determine if the combined expression four gene panel was associated with survival, relapse free survival analysis was performed on the 6 TNBC subtypes (14). The four gene panel was associated with worse RFS (when compared to tumours in the low expression group), in the basal-like 1 and 2 (BL1, BL2) subtypes (HR=2.27, p=0.015; HR=2.52, p=0.013 respectively) and the mesenchymal subtype (HR=1.8; p=0.034). In contrast, this four gene panel was associated with better RFS in the luminal androgen receptor (LAR) subtype (HR=0.56, p=0.031) (**Figure 5**). Taken together, these results suggest that the four gene panel can predict distinct survival outcomes amongst the distinct TNBC subytpes, implying that this signature would be useful for most TNBC cases. However, it should be noted that the number of cases in these survival analyses is low, particularly in the mesenchymal stem-like and basal-like 2 subgroups, and should be interpreted with caution.

DISCUSSION

TNBC is a highly aggressive subtype of breast cancer with decreased survival rates compared to other subtypes of breast cancer (1, 2). Because of the absence of well-established prognostic and predictive biomarkers, there are no targeted treatment options available to improve patient survival. Previous studies from our laboratory have indicated that *ANKRD30A, IL6ST, ANP32E* and *DSC2* are differentially expressed in TNBC when compared to receptor positive disease, using cDNA microarrays. In this study, the expression of *ANKRD30A*, *IL6ST*, *ANP32E* and *DSC2* were analyzed using ddPCR to verify these results and to determine whether their expression was associated with clinical features and survival.

IL6ST/gp130 was significantly downregulated in IDCs and LNmets compared to NATs as well as in TNBC compared to non-TNBCs, verifying the results of our previous study (3). Additionally, its low expression level was significantly associated with grade 3 disease, hormone receptor negativity, earlier age at diagnosis and worse relapse free survival. Taken together, this implies that its downregulation may increase the

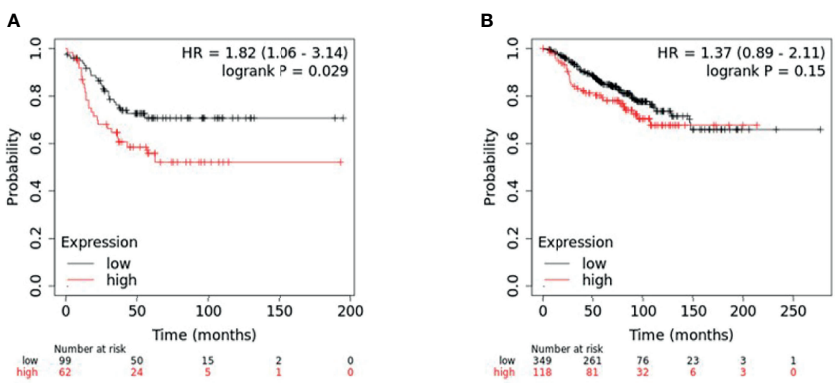

FIGURE 4 | KM plotter survival analysis for patients with differential expression of four-gene panel including *ANP32E, DSC2, IL6ST*, and *ANKRD30A*. Survival analysis was performed in KM plotter using publicly available microarray data that is available within the database. **(A)** TNBC samples (n = 161) and **(B)** non-TNBC (n = 467) were divided into high or low expression groups based on the median expression of the four-gene panel (with inverted expression of the two low expressed genes: ANKRD30A and IL6ST and not inverted for the two highly expressed genes: ANP32E and DSC2) and compared by Kaplan-Meier survival analysis. A Log-rank p-value ≤ 0.05 was considered significant. HR, hazard ratio. The red curve represents high expression, and the black curve represents low expression.

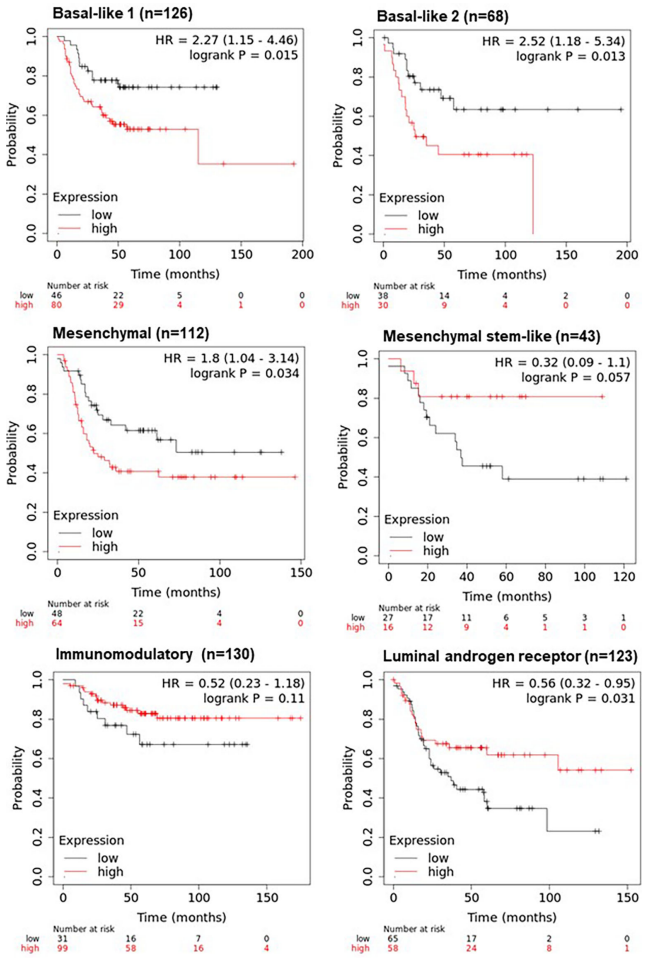

FIGURE 5 | KM plotter survival analysis of TNBC subtypes using the four-gene panel including *ANP32E*, *DSC2*, *IL6ST*, and *ANKRD30A*. Survival analysis was performed in KM plotter using publicly available microarray data that is available within the database according to the TNBC subtypes of basal-like 1, basal-like 2, mesenchymal, mesenchymal stem-like, immunomodulatory and the luminal androgen receptor subtype. Cases were divided into high or low expression groups based on the median expression of the four-gene panel (with inverted expression of the two low expressed genes: ANKRD30A and IL6ST and not inverted for the two highly expressed genes: ANP32E and DSC2) and compared by Kaplan-Meier survival analysis. A Log-rank p-value ≤ 0.05 was considered significant. HR, hazard ratio. The red curve represents high expression, and the black curve represents low expression.

aggressiveness of the disease and that its high expression is a marker of good prognosis in TNBC. Similar to this study, *IL6ST* has been shown to be downregulated in basal-like breast cancer compared to luminal A/B breast cancer subtypes and its lower expression was associated with poor overall survival in TNBC patients (15, 16). The loss of *IL6ST* is involved in pathways related to lymphovascular invasion in breast cancer patients (17) and its function has been associated with other physiologies such as myocardial and hematological development where embryos of mice deficient for *IL6ST* gradually die between 12.5 days post-coitum (18). *IL6ST* is known to be involved in the JAK/STAT pathway (19, 20) including the activation of *STAT3* and *STAT1*, as well as the PI3K/AKT and RAS/MAPK pathways. Therefore, its loss in TNBC may disrupt the JAK/STAT pathway resulting in transcriptional mis-regulation of associated genes and promoting tumor proliferation, migration and invasion. However, further study of *IL6ST* in a larger cohort is needed to understand its prognostic role in TNBC.

ANKRD30A showed significantly lower expression in TNBC compared to non-TNBC cases and its lower expression was associated with ER, PR status and tumor size; as well as worse RFS, suggesting a role in disease aggressiveness. Similar to the findings reported herein, another study have also found its downregulation in TNBC tissues (21, 22) and its expression was associated with ER status (23).Notably, *ANKRD30A* possesses an estrogen response element in the promoter region which may be regulated through estrogen receptor signaling (24), suggesting a possible mechanism for its low expression in TNBC. Additionally, the downregulation of Long Non-coding RNA LINC00993 (Long Intergenic Non-Protein Coding RNA 993) was significantly associated with the downregulated expression of the nearest coding gene, *ANKRD30A* in a microarray study of

TNBC (21). It should be noted that many genomic regions can be co-regulated. Hence, the association may well be coincidental rather than causative. Interestingly, the lncRNA LINC00993 was identified to act as a tumor suppressor in TNBC which suppresses the growth of tumor cells both *in vivo* and *in vitro* (25). *ANKRD30A* is classed as a transcription factor due to the presence of bZIPsite and bipartite nuclear localization signal motif, hence it may be involved in regulating the expression of LINC00993. Thus, this implies that downregulation of *ANKRD30A* may have a significant role in tumor progression in TNBC.

ANP32E was significantly upregulated in TNBC compared to non-TNBC. Furthermore, its high expression was significantly associated with grade, the number of positive lymph nodes and worse RFS. *ANP32E* knockdown has been shown to inhibit the proliferation, migration and metastasis of breast cancer cells (26). It has also been shown to be highly expressed in primary breast cancers with a high propensity of metastasizing to the lungs (27). One study showed that *ANP32E* promotes G1/S progression by increasing the expression of E2F1, thus inducing proliferation in TNBC cells (28). The same study also showed that *ANP32E* is highly expressed at protein level in TNBC cases compared to non-TNBC cell lines and tumors. Taken together, these data support a role for *ANP32E* in cancer progression. However, further studies in a larger cohort are needed to understand its prognostic role in TNBC.

DSC2 was significantly upregulated in TNBC compared to non-TNBC but was not associated with clinicopathological features or survival outcomes. Microarray gene expression analysis of 23 breast cancer metastases showed that the upregulation of *DSC2* expression may contribute to lung metastasis as a part of a 6-gene signature (27). Moreover, a study validated that the overexpression of five genes including *DSC2* worsens lung metastasis-free survival in geminin-overexpressing TNBC cells (29). In contrast, a reduction in *DSC2* expression has been identified in other cancer types such as colorectal, lung and esophageal squamous cell carcinoma (30–32). Conversely, a reduction in the expression of *DSC2* has been found in other cancers including colon cancer (33) and urothelial carcinoma tissues, where its downregulation was associated with rapid migration and invasion (34). Currently, there have been no other studies of *DSC2* expression and its role in TNBC.

Perhaps one of the most important findings was that when combined, the four-gene panel was strongly associated with RFS in TNBC, but not in hormone receptor positive breast cancers. Additionally, the four-gene panel provided a better survival curve discrimination when compared to each of the individual genes. The signature was further associated with RFS in 4/6 TNBC subtypes (**Figure 5**), indicating that this signature may be useful in predicting survival in the majority of TNBC cases. Interestingly, high expression of the gene panel was associated with better RFS in the LAR subtype, and worse RFS in the BL1, BL2 and mesenchymal subtypes. Given that xenografts developed from cell lines representative of these distinct subtypes show distinct responses to chemotherapeutic agents (14), the four gene panel defined in this study may have significant clinical utility, but these results would need to be validated in an independent cohort given the small sample size. Another key consideration is whether the mRNA expression of these four genes is correlated with their protein expression, the functional unit of the gene. There has been one published study showing that ANP32E is highly expressed at the mRNA and protein level in TNBC compared to non-TNBC tissues (28). However, for the other three genes, the correlation with protein expression has not been examined in breast cancer tissues to the best of our knowledge.

Taken together, these studies have verified the differential expression of *ANKRD30A, IL6ST, ANP32E* and *DSC2* in TNBC compared to non-TNBC and determined their association with clinical features and survival. Additionally, the four-gene panel may serve as a specific prognostic tool in TNBC management.

DATA AVAILABILITY STATEMENT

The raw data supporting the conclusions of this article will be made available by the authors, without undue reservation.

ETHICS STATEMENT

The studies involving human participants were reviewed and approved by Hunter New England Human Research Ethics Committee. The ethics committee waived the requirement of written informed consent for participation.

AUTHOR CONTRIBUTIONS

KA-K: conceptualization. MP and KA-K: data collection, curation, and methodology. MP and KA-K: writing—original draft preparation. MP, RT, RS, KA-K: review and editing. RT, RS, and KA-K: supervision. RS and KA-K: funding acquisition. All authors contributed to the article and approved the submitted version.

FUNDING

This work was funded by the National Breast Cancer Foundation and the Hunter Medical Research Institute, through donations from the Hunter Breast Cancer Foundation. MP was supported by a University Postgraduate Award. KA-K is supported by the Cancer Institute NSW (Career Development Fellowship; CDF181205).

ACKNOWLEDGMENTS

We would like to thank the Pathologist Dr. Ricardo Vilain for the validation of all tumor and normal tissue specimens used in this study, as well as Ms Sarah Nielsen and Dr. Mythily Mariasegaram for their assistance with archival specimens.

REFERENCES

1. Bauer KR, Brown M, Cress RD, Parise CA, Caggiano V. Descriptive Analysis of Estrogen Receptor (ER)-Negative, Progesterone Receptor (PR)-Negative, and HER2-Negative Invasive Breast Cancer, the So-Called Triple-Negative Phenotype: A Population-Based Study From the California Cancer Registry. *Cancer* (2007) 109(9):1721–8. doi: 10.1002/cncr.22618
2. Gonçalves HJr., Guerra MR, Duarte JR, Cintra VA, Fayer IV, Brum MT, et al. Survival Study of Triple-Negative and Non-Triple-Negative Breast Cancer in a Brazilian Cohort. *Clin Med Insights Oncol* (2018) 12:1179554918790563. doi: 10.1177/1179554918790563
3. Mathe A, Wong-Brown M, Morten B, Forbes JF, Braye SG, Avery-Kiejda KA, et al. Novel Genes Associated With Lymph Node Metastasis in Triple Negative Breast Cancer. *Sci Rep* (2015) 5(1):15832. doi: 10.1038/srep15832
4. Jäger D, Stockert E, Güre AO, Scanlan MJ, Karbach J, Jäger E, et al. Identification of a Tissue-Specific Putative Transcription Factor in Breast Tissue by Serological Screening of a Breast Cancer Library. *Cancer Res* (2001) 61(5):2055.
5. Reihmane D, Dela F. Interleukin-6: Possible Biological Roles During Exercise. *Eur J Sport Sci* (2014) 14(3):242–50. doi: 10.1080/17461391.2013.776640
6. Fang WK, Liao LD, Li LY, Xie YM, Xu XE, Zhao WJ, et al. Down-Regulated Desmocollin-2 Promotes Cell Aggressiveness Through Redistributing Adherens Junctions and Activating Beta-Catenin Signalling in Oesophageal Squamous Cell Carcinoma. *J Pathol* (2013) 231(2):257–70. doi: 10.1002/path.4236
7. Mao Z, Pan L, Wang W, Sun J, Shan S, Dong Q, et al. Anp32e, a Higher Eukaryotic Histone Chaperone Directs Preferential Recognition for H2A.Z. *Cell Res* (2014) 24(4):389–99. doi: 10.1038/cr.2014.30
8. Taylor SC, Laperriere G, Germain H. Droplet Digital PCR Versus qPCR for Gene Expression Analysis With Low Abundant Targets: From Variable Nonsense to Publication Quality Data. *Sci Rep* (2017) 7(1):2409. doi: 10.1038/s41598-017-02217-x
9. Dingle TC, Sedlak RH, Cook L, Jerome KR, et al. Tolerance of Droplet-Digital PCR vs Real-Time Quantitative PCR to Inhibitory Substances. *Clin Chem* (2013) 59(11):1670–2. doi: 10.1373/clinchem.2013.211045
10. Ma J, Li N, Guarnera M, Jiang F. Quantification of Plasma miRNAs by Digital PCR for Cancer Diagnosis. *Biomark Insights* (2013) 8:127–36. doi: 10.4137/BMI.S13154
11. Dobnik D, Štebih D, Blejec A, Morisset D, Žel J. Multiplex Quantification of Four DNA Targets in One Reaction With Bio-Rad Droplet Digital PCR System for GMO Detection. *Sci Rep* (2016) 6(1):35451. doi: 10.1038/srep35451
12. Avery-Kiejda KA, Morten B, Wong-Brown MW, Mathe A, Scott RJ. The Relative mRNA Expression of P53 Isoforms in Breast Cancer Is Associated With Clinical Features and Outcome. *Carcinogenesis* (2014) 35(3):586–96. doi: 10.1093/carcin/bgt411
13. Avery-Kiejda KA, Braye SG, Mathe A, Forbes JF, Scott RJ. Decreased Expression of Key Tumour Suppressor microRNAs Is Associated With Lymph Node Metastases in Triple Negative Breast Cancer. *BMC Cancer* (2014) 14:51. doi: 10.1186/1471-2407-14-51
14. Lehmann BD, Bauer JA, Chen X, Sanders ME, Chakravarthy AB, Shyr Y, et al. Identification of Human Triple-Negative Breast Cancer Subtypes and Preclinical Models for Selection of Targeted Therapies. *J Clin Invest* (2011) 121(7):2750–67. doi: 10.1172/JCI45014
15. Fertig EJ, Lee E, Pandey NB, Popel AS. Analysis of Gene Expression of Secreted Factors Associated With Breast Cancer Metastases in Breast Cancer Subtypes. *Sci Rep* (2015) 5(1):12133. doi: 10.1038/srep12133
16. Jia R, Weng Y, Li Z, Liang W, Ji Y, Liang Y, et al. Bioinformatics Analysis Identifies IL6ST as a Potential Tumor Suppressor Gene for Triple-Negative Breast Cancer. *Reprod Sci* (2021) 28(8):2331–41. doi: 10.1007/s43032-021-00509-2
17. Klahan S, Wong HS, Tu SH, Chou WH, Zhang YF, Ho TF, et al. Identification of Genes and Pathways Related to Lymphovascular Invasion in Breast Cancer Patients: A Bioinformatics Analysis of Gene Expression Profiles. *Tumour Biol* (2017) 39(6):1010428317705573. doi: 10.1177/1010428317705573
18. Yoshida K, Taga T, Saito M, Suematsu S, Kumanogoh A, Tanaka T, et al. Targeted Disruption of Gp130, a Common Signal Transducer for the Interleukin 6 Family of Cytokines, Leads to Myocardial and Hematological Disorders. *Proc Natl Acad Sci USA* (1996) 93(1):407–11. doi: 10.1073/pnas.93.1.407
19. Simpson RJ, Hammacher A, Smith DK, Matthews JM, Ward LD. Interleukin-6: Structure-Function Relationships. *Protein Sci: Publ Protein Soc* (1997) 6(5):929–55. doi: 10.1002/pro.5560060501
20. Heinrich PC, Behrmann I, Müller-Newen G, Schaper F, Graeve L. Interleukin-6-Type Cytokine Signalling Through the Gp130/Jak/STAT Pathway. *Biochem J* (1998) 334(Pt 2):297–314. doi: 10.1042/bj3340297
21. Chen C, Li Z, Yang Y, Xiang T, Song W, Liu S. Microarray Expression Profiling of Dysregulated Long Non-Coding RNAs in Triple-Negative Breast Cancer. *Cancer Biol Ther* (2015) 16(6):856–65. doi: 10.1080/15384047.2015.1040957
22. Zombori T, Cserni G. Immunohistochemical Analysis of the Expression of Breast Markers in Basal-Like Breast Carcinomas Defined as Triple Negative Cancers Expressing Keratin 5. *Pathol Oncol Res* (2018) 24(2):259–67. doi: 10.1007/s12253-017-0246-y
23. Theurillat J-P, Zürrer-Härdi U, Varga Z, Storz M, Probst-Hensch NM, Seifert B, et al. NY-BR-1 Protein Expression in Breast Carcinoma: A Mammary Gland Differentiation Antigen as Target for Cancer Immunotherapy. *Cancer Immunol Immunother* (2007) 56(11):1723–31. doi: 10.1007/s00262-007-0316-1
24. Theurillat JP, Zürrer-Härdi U, Varga Z, Barghorn A, Saller E, Frei C, et al. Distinct Expression Patterns of the Immunogenic Differentiation Antigen NY-BR-1 in Normal Breast, Testis and Their Malignant Counterparts. *Int J Cancer* (2008) 122(7):1585–91. doi: 10.1002/ijc.23241
25. Guo S, Jian L, Tao K, Chen C, Yu H, Liu S. Novel Breast-Specific Long Non-Coding RNA LINC00993 Acts as a Tumor Suppressor in Triple-Negative Breast Cancer. *Front Oncol* (2019) 9(1325). doi: 10.3389/fonc.2019.01325
26. Li P, Xu T, Zhou X, Liao L, Pang G, Luo W, et al. Downregulation of miRNA-141 in Breast Cancer Cells Is Associated With Cell Migration and Invasion: Involvement of ANP32E Targeting. *Cancer Med* (2017) 6(3):662–72. doi: 10.1002/cam4.1024
27. Landemaine T, Jackson A, Bellahcene A, Rucci N, Sin S, Abad BM, et al. A Six-Gene Signature Predicting Breast Cancer Lung Metastasis. *Cancer Res* (2008) 68(15):6092–9. doi: 10.1158/0008-5472.CAN-08-0436
28. Xiong Z, Ye L, Zhenyu H, Li F, Xiong Y, Lin C, et al. ANP32E Induces Tumorigenesis of Triple-Negative Breast Cancer Cells by Upregulating E2F1. *Mol Oncol* (2018) 12(6):896–912. doi: 10.1002/1878-0261.12202
29. Sami E, Bogan D, Molinolo A, Koziol J, ElShamy WM. The Molecular Underpinning of Geminin-Overexpressing Triple-Negative Breast Cancer Cells Homing Specifically to Lungs. *Cancer Gene Ther* (2021). doi: 10.1038/s41417-021-00311-x
30. Kolegraff K, Nava P, Helms MN, Parkos CA, Nusrat A. Loss of Desmocollin-2 Confers a Tumorigenic Phenotype to Colonic Epithelial Cells Through Activation of Akt/β-Catenin Signaling. *Mol Biol Cell* (2011) 22(8):1121–34. doi: 10.1091/mbc.e10-10-0845
31. Fang W-K, Gu W, Li E-M, Wu Z-Y, Shen Z-Y, Shen J-H, et al. Reduced Membranous and Ectopic Cytoplasmic Expression of DSC2 in Esophageal Squamous Cell Carcinoma: An Independent Prognostic Factor. *Hum Pathol* (2010) 41(10):1456–65. doi: 10.1016/j.humpath.2010.04.003
32. Cui T, Chen Y, Yang L, Mireskandari M, Knösel T, Zhang Q, et al. Diagnostic and Prognostic Impact of Desmocollins in Human Lung Cancer. *J Clin Pathol* (2012) 65(12):1100. doi: 10.1136/jclinpath-2011-200630
33. Khan K, Hardy R, Haq A, Ogunbiyi O, Morton D, Chidgey M. Desmocollin Switching in Colorectal Cancer. *Br J Cancer* (2006) 95(10):1367–70. doi: 10.1038/sj.bjc.6603453
34. Hayashi T, Sentani N, Oue K, Anami N, Sakamoto S, Ohara J, et al. Desmocollin 2 Is a New Immunohistochemical Marker Indicative of Squamous Differentiation in Urothelial Carcinoma. *Histopathology* (2011) 59(4):710–21. doi: 10.1111/j.1365-2559.2011.03988.x

Conflict of Interest: The authors declare that the research was conducted in the absence of any commercial or financial relationships that could be construed as a potential conflict of interest.

this article, or claim that may be made by its manufacturer, is not guaranteed or endorsed by the publisher.

frontiers in Oncology

ORIGINAL RESEARCH
published: 24 March 2022
doi: 10.3389/fonc.2021.782383

Prognostic Evaluation of Metastasis-Related Lymphocyte/Monocyte Ratio in Stage Ⅰ-Ⅲ Breast Cancer Receiving Chemotherapy

Zihan Zhang[1†], Qian Lin[2†], Yi Chen[1†], Chenlin Su[1], Wuye Lin[1], Daoyu Wei[1], Litu Zhang[1,3] and Haizhou Liu[1,3]*

[1] Department of Research, Guangxi Medical University Cancer Hospital, Nanning, China, [2] Development Planning Office, Guangxi Medical University , Nanning, China, [3] Department of Research, Guangxi Cancer Molecular Medicine Engineering Research Center, Nanning, China

Purpose: This study aims to clarify the prognostic significance of metastasis-related indicators in peripheral blood in stage I-III breast cancer (BC).

Methods: The clinicopathological data of 938 breast cancer patients and 509 benign breast disease patients were retrospectively analyzed, and fasting blood samples were collected before treatment. Univariate and multivariate regression analyses were used to evaluate factors related to metastasis risk and prognosis. The Kaplan-Meier method was used to generate survival curves, and the log-rank test was used to measure differences in survival between groups.

Results: Use the cut-off value (3.433) of LMR, the logistic regression analysis revealed that high carbohydrate antigen 153 (CA153), carbohydrate antigen 125 (CA125), carcinoembryonic antigen (CEA), killer T cell level, and low lymphocyte to monocyte ratio (LMR) level were significantly associated with BC distant metastasis. In contrast, LMR>=3.433 (HR: 0.409, 95%CI: 0.193–0.867, P = 0.020), Th/Tc ratio >=1.946 (HR: 0.378, 95% CI: 0.158–0.904, P =0.029) is regarded as a protective factor in the multivariate cox analyses. LMR is an independent prognostic factor for DFS in HER2-negative BC patients.

Conclusion: Peripheral blood parameters play an important role in predicting distant metastasis and prognosis of BC patients. As a potential marker, LMR can predict the metastasis and prognosis of patients with stage I-III BC.

Keywords: breast cancer, predictive factor, lymphocyte/monocyte ratio, inflammatory biomarkers, prognostic

OPEN ACCESS

Edited by:
San-Gang Wu,
First Affiliated Hospital of Xiamen University, China

Reviewed by:
Sweety Gupta,
All India Institute of Medical Sciences, Rishikesh, India
Maria Helena Ornellas,
Universidade Estadual do Rio de Janeiro, Brazil

****Correspondence:***
Haizhou Liu
liuhaizhou@gxmu.edu.cn

[†]These authors have contributed equally to this work

Specialty section:
This article was submitted to Breast Cancer, a section of the journal Frontiers in Oncology

Received: *24 September 2021*
Accepted: *17 December 2021*
Published: *24 March 2022*

Citation:
Zhang Z, Lin Q, Chen Y, Su C, Lin W, Wei D, Zhang L and Liu H (2022) Prognostic Evaluation of Metastasis-Related Lymphocyte/Monocyte Ratio in Stage Ⅰ-Ⅲ Breast Cancer Receiving Chemotherapy. Front. Oncol. 11:782383. doi: 10.3389/fonc.2021.782383

INTRODUCTION

Breast cancer (BC) is the most common cancer in women and the leading cause of cancer death among them. In both sexes combined, female BC (11.6% of all cases) is the second most widely diagnosed cancer in 20 regions of the world (1). Curative surgical treatment of local BC patients and pathological sampling of lymph nodes are the first steps in treatment in the traditional sense (2). However, in the current treatment, neoadjuvant chemotherapy before surgery has been considered the preferred strategy for operable or non-operable BC (3). Recurrence or metastasis may occur in these treated BC patients, but we lack effective and reliable predictive biomarkers to guide risk stratification before treatment (4, 5). However, these studies' results are still inconsistent in the efficacy of risk estimation among various tumors, and it is difficult to find accurate estimates of BC diagnosis and metastasis.

Immune function is an important prognostic factor of BC. It is involved in tumorigenesis, progression, and metastasis (6). Platelet to lymphocyte ratio (PLR), lymphocyte to monocyte ratio (LMR), neutrophil to lymphocyte ratio (NLR) in tumors, including BC, shows its diagnostic and prognostic value (7–9). We observed changes in the ratio of neutrophils, lymphocytes, and monocytes in peripheral blood during the tumor immunity response (10, 11). In these studies, the percentage of NLR is associated with a poor tumor prognosis (12). Changes in the ratio of LMR and PLR also reflect that the balance between the adaptive immune system and the innate immune system is broken, and the body lacks anti-tumor activity (13, 14)

Currently, research shows that the lymphocyte to monocyte ratio (LMR) can be used as a biomarker for BC detection and monitoring (15, 16). More and more reports indicate that LMR is used in neoadjuvant chemotherapy for various tumors and is a powerful biomarker to verify the efficacy (17–19). All patients need to check the peripheral blood before treatment, and the indicators are cheap and easy to obtain.

Although some studies use the ROC curve based on DFS/OS to determine the LMR cut-off value (20), the DFS/OS outcome is sometimes too subjective and requires a lot of follow-up work, so the cut-off value of different studies is quite different. As we all know, patients with stage IV metastatic breast cancer generally have poor outcomes. Therefore, we used the blood parameters and cut-off ratio points determined by the ROC curve related to distant metastasis to retrospectively analyze the relationship between the survival status of BC patients after treatment and the LMR before treatment. We aim to explain the diagnosis value of these biomarkers as pre-treatment variables and test whether these biomarkers can also be used as post-treatment surveillance parameters.

Abbreviations: BC, breast cancer; EGFR, epidermal growth factor receptor; CEA, carcinoembryonic antigen; CA125, carbohydrate antigen 125; CA153, carbohydrate antigen 153; NK, natural killer; NEUT, neutrophile; LYMPH, lymphocyte; MONO, monocyte; PLT, platelet; NLR, neutrophil to lymphocyte ratio; LMR, lymphocyte to monocyte ratio; Th, helper T cell; Tc, killer T cell; Th/Tc ratio, helper T cell to killer T cell ratio; CTC, circulating tumor cells; ROC, receiver operating characteristic; LASSO, the minor absolute shrinkage, and selection operator; PFS, progression-free survival; CI, confidence interval; OR, odds ratio; AUC, the area under curve; HR, hazard ratio.

METHOD

Two Distinct Cohorts Composed the Comprehensive Study

Our study retrospectively collected data on patients who were treated at Guangxi Medical University from May 2018 to May 2020, the inclusion criteria as follows: 1) woman with BC or breast benign disease, which was confirmed by histology; 2) BC has to be primary; 3) the BC patients' clinical features, hematological indicators, and inflammatory biomarkers are complete, and 4) the breast benign disease patients' clinical features and hematological indicators are complete. The exclusion criteria were as follow: 1) patients with other malignant tumors; 2) patients who have acute or chronic hematologic disease, severe systemic infection, or autoimmune diseases; 3) the patients' clinical features and indicators required by the study are incomplete.

A total of 938 patients who received standard treatment and did not receive anticancer therapy before their surgery enrolled in the study. Patients were followed up for at least 0.5 months. The control cohort consisted of 509 female patients with benign breast diseases treated in our hospital. The laboratory medicine department carries out inflammatory biomarkers. This research was conducted in the Guangxi Medical University Cancer Hospital; this study followed the 2008 Declaration of Helsinki's ethical guidelines and our hospital code of ethics (LW2021086).

Data Collection

Participants' data is divided into three parts: clinical-pathological features, blood system indicators, and immunological indicators. The clinical pathological features included age, estrogen receptor (ER), progesterone receptor (PR), HER2, Ki-67, CK5-6, epidermal growth factor receptor (EGFR), TNM stage, location, and transfer area. The blood system indicators contained carcinoembryonic antigen (CEA), carbohydrate antigen 125 (CA125), carbohydrate antigen 153 (CA153) (21, 22), neutrophile, monocyte, platelet. Furthermore, the immunological indicators involved T cell, helper T cell (Th), killer T cell (Tc), natural killer (NK) cell, and B cell (23). All blood samples were collected before treatment. The prognosis was obtained through the follow-up department of this hospital and telephone.

Serum and Plasma Tumor-Related Markers

Before treatment, we collected 3ml of peripheral venous blood from all patients. Serum CEA, CA125, and CA153 were measured using an automatic chemiluminescence immunoassay system (SIEMENS ADVIA centaur; Siemens, Germany). NLR was the absolute neutrophil count/the total lymphocyte, LMR was the total lymphocyte/the absolute monocyte, and PLR was the total platelet count/the total lymphocyte count. These

parameters were analyzed from the peripheral blood cell count (DxH 800 hematology analyzer, Beckman Coulter). See **Supplementary** for the experimental methods of cellular immunology related indicators.

Statistical Analysis

The characteristics of BC patients and benign breast diseases were summarized and described. Frequency distribution represents categorical variables, whereas continuous variables are reported through the median and interquartile range. LMR, NLR, PLR, Th/Tc ratios were calculated from raw hematology indicators. Markers with disease and clinicopathological features were explored by Wilcoxon rank-sum test or Kruskal–Wallis test. The receiver operating characteristic (ROC) curve is built for selecting the optimal threshold and diagnostic accuracy of these continuous indicators. The least absolute shrinkage and selection operator (LASSO) (24) regression model and the multivariable logistic and Cox regression analysis were used to establish a convincing prediction model in BC patients. Disease-Free Survival (DFS) was the time between treatment start and disease recurrence or patient death due to disease progression. Survival difference analysis between groups used by log-rank test and display with the Kaplan-Meier plot. R-4.04 software was used for statistical analysis.

RESULT

Clinicopathological Features and Inflammatory Biomarkers

In this study, 938 BC patients and 509 benign breast disease patients were included after applying the conditions (**Figure 1A**),

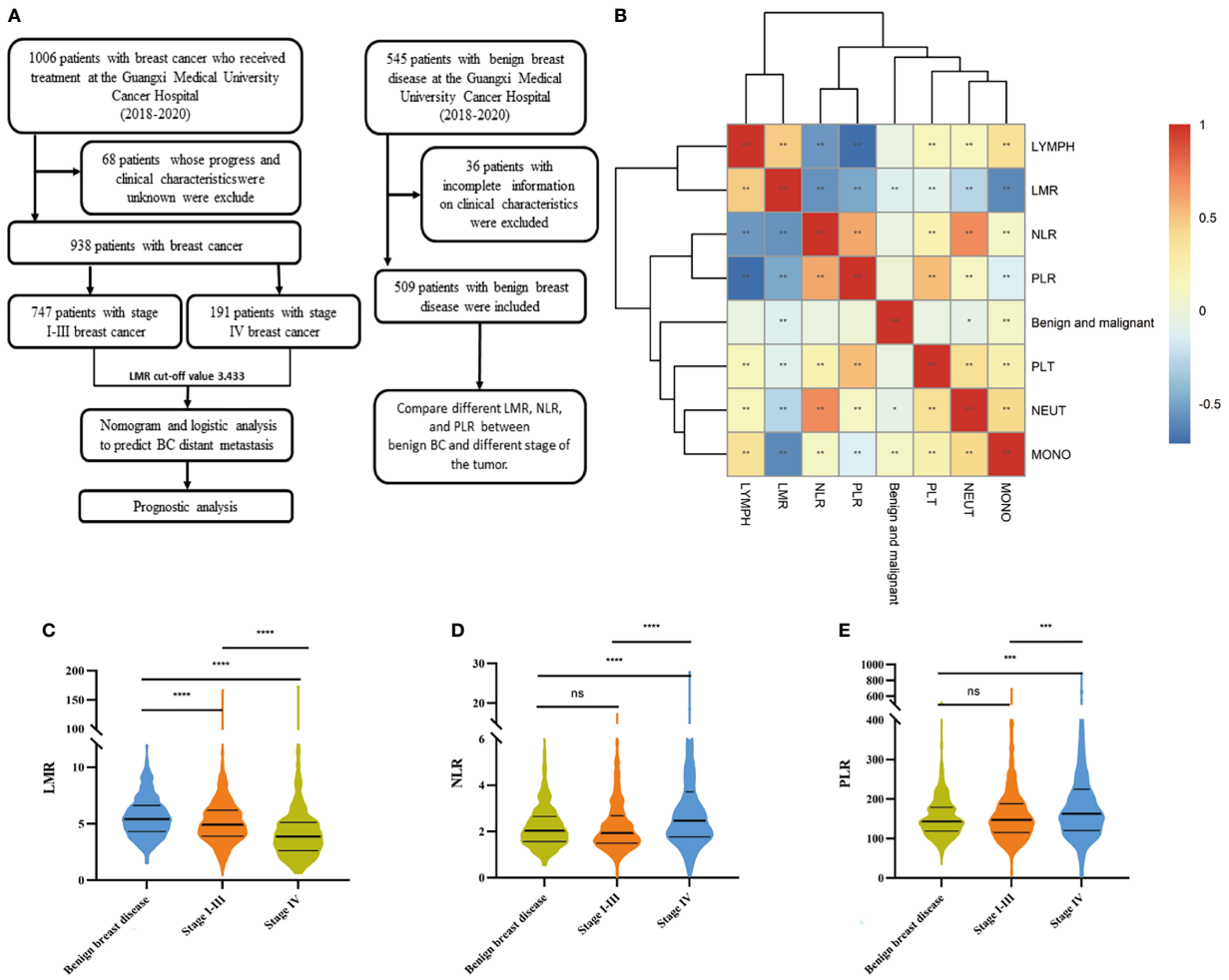

FIGURE 1 | Working mode and Distribution of LMR and other indicators in benign breast diseases and tumors. **(A)** The workflow of this study. **(B)** Visualization of the correlation matrix of hematology test indicators and benign and malignant tumors, showing that MONO, NRUT, and LMR are related to tumor malignancy. Boxplot of **(C)** LMR **(D)** NLR and **(E)** PLR in benign BC and different stages of the tumor. Differences between groups estimated by Mann–Whitney U as appropriate. (*P < 0.05, **P < 0.01, ***P < 0.001, ****P < 0.0001, ns P > 0.05).

and all participants were women. The median age of benign breast disease was 37 years, and the BC patients were 49 years. There were 747 patients diagnosed as stage I-III and 191 patients diagnosed as stage IV among BC patients.

PR-positive accounted for 67.70% of all BC patients, and ER-positive accounted for 71.32%. Of all BC patients 48.93% were HER2 positive, 12.90% CK5-6 positive, and 17.80% were EGFR positive. A further 82.94% of patients of Ki-67 were higher than 14%. Based on the above results, BC patients were identified as luminal A, luminal B, ERBB2, and triple-negative BC (10.13%, 66.31%, 12.69%, and 10.87%).

The median values of the NLR, PLR, LMR were 2.04 [1.56,2.86], 4.75 [3.66,6.08], 150.17 [116.71,194.76] in BC patients. the median values of the NLR, PLR, LMR were 2.04 [1.56,2.65], 5.42 [4.32,6.60], 143.65 [118.75,179.08] in benign breast disease patients. The patients' details are list in **Table 1**.

Compared With Benign Breast Disease and BC Patient Group in Inflammatory Biomarkers

The heat map shows that LMR is associated with benign breast disease and malignant BC (**Figure 1B**). Moreover, in the analyses of tumors benign and malignant, the level of LMR is highest in patients with benign breast disease. It gradually decreases in patients with stage I-III BC and stage IV BC, as shown in **Figure 1C** (P<0.01). The NLR and PLR gradually increased in patients with stage I-III BC and stage IV BC, but the difference between stage I-III BC patients and benign BC was not significant, as shown in **Figures 1D, E**.

Optimal Threshold of Inflammatory Biomarkers in BC

ROC curves were analyzed the optimal threshold and their diagnostic sensitivities and specificities drawn in **Figure 2** and **Table S1**. For the diagnosis of BC, we found that peripheral blood NLR, LMR, and PLR have a low diagnostic value (AUC<0.6) in BC with the threshold as 1.711, 5.239, and 237.011. When using one marker in BC distant metastasis, the best sensitivity was CEA (0.66), the best specificity was LMR with 0.846, and the highest Youden's index was CA153, respectively. Using the cut-off values in **Table S1**, we divided BC into high and low groups according to different markers for subsequent analysis.

Correlation Between Pre-Therapeutic Inflammatory Biomarkers With Clinicopathological Data

In **Figure 3A**, we initially compared the correlations between different markers and pathological data and traditional immune index, including Th, Tc, Bcell, etc. We found that LMR has no correlation with immune indicators, but it is related to metastasis and stage. At the first diagnosis, we divide BC patients into multiple groups based on demographic and clinical characteristics collected before receiving any treatment to assess differences in the baseline concentration of different markers. As shown in **Table S2**, most patients with advanced BC have high NLR, PLR, and low LMR ratios (p<0.001). The Kruskal–Wallis test of the TNM stage revealed that high PLR, NLR, and low LMR correlated with high T stage, lymph node metastasis, and distant metastasis, shown in **Figures 3B–D**.

The Predictive Value of Inflammatory Biomarkers for BC Distant Metastasis

To explore the diagnostic significance of high LMR before treatment for BC distant metastasis, we used five peripheral blood indicators to construct a nomogram to predict BC metastasis. These indicators are the smallest P values in multiple logistic regression (**Figure 4A**). First, based on 938 BC patients, we used LASSO and 10-fold cross-validation to screen out nine indicators (**Figure S1**), included Tcell, helper T cell, killer T cell, B cell, NLR, LMR, CEA, CA125, and CA153 (**Figure 4B**, lambda.min=0.006644068). To further verify the accuracy of the results, the univariate and multivariate logistic regression analysis among these above features is shown in **Table 2**. The model finally contains CA153 (OR=4.307, P<0.001), LMR (OR=0.375, P<0.001), CEA (OR=3.345, P<0.001), CA125 (OR=1.625, P=0.021), and killer T cell (OR=1.700, P=0.012). The BC metastasis risk nomogram's calibration curve, which use to predict a BC patient's risk of progressing to stage IV, shows excellent consistency (**Figure 4C**, AUC=0.8290404). The model was verified by bootstrapping (**Figure 4D**, C-index=0.829). The model decision curve analysis showed that using a nomogram to predict BC metastasis risk would benefit more than the scheme if the threshold probability of patients and doctors are >4% and <84% (**Figure 4E**), respectively.

Low LMR Indicated Poor Prognosis in Stage Ⅰ-Ⅲ BC

To explore the clinical significance of high LMR before treatment for BC, in our research cohort, the median follow-up period of 12 months (range: 0.5-24 months) of 747 stage I-III BC patients, 30 patients (4%) experienced disease recurrence or died (for any reason). **Table S1** determines the cut-off value of our grouping here. Univariate and multivariate Cox proportional hazards models conduct to investigate the relationship between clinical variables and DFS (**Figure 5A**). In the multivariate analysis, high LMR (HR=0.409, p=0.02) and Th/Tc ratio (HR=0.378, p=0.029) were independent prognostic factors of a protective factor in stage I-III BC. The time-dependent ROC curve analysis of LMR shows that the maximum AUC of our LMR in 6-24 months is 0.649 (**Figure S2**). We further analyze the distribution of risk levels, survival status, and survival time patterns of BC patients with different LMR (**Figures 5B**). Kaplan-Meier survival analyses performed on the stage I-III BC showed the DFS of BC patients with lower LMR values was worse than that of patients with higher LMR values (**Figures 5C**). We regret that no clinically valuable markers have been screened in either univariate or multivariate survival analysis in stage IV BC. The results show in **Table S3**.

Clinical Prognostic Evaluation of LMR in Different Molecular Subtypes of BC

We retrospectively analyzed the relationship between preoperative blood parameters and clinical outcomes after

TABLE 1 | Clinicopathological factors and baseline characteristics.

Characteristics	BC	Benign breast disease	*P*-value
Number of patients	938	509	
Age (years)			<0.01
Average (SD)	49.63 (11.07)	37.49 (11.91)	
Median (IQR)	49 (42,56)	37 (29,45)	
<45 years (%)	309 (32.94%)	375 (73.67%)	
≳ 45 to <55 years (%)	346 (36.89%)	92 (18.07%)	
≳ 55 years (%)	283 (30.17%)	42 (8.25%)	
T classification			
T_1T_2	671 (71.54%)	/	
T_3T_4	267 (28.46%)	/	
N classification			
N_0	410 (43.71%)	/	
$N_{1\text{-}3}$	528 (56.29%)	/	
M classification			
M_0	747 (79.64%)	/	
M_1	191 (20.36%)	/	
Clinical stage			
I/II	554 (59.06%)	/	
III/IV	384 (40.94%)	/	
Predictive factors			
Progesterone Receptor + (%)	635 (67.70%)	/	
Estrogen Receptor + (%)	669 (71.32%)	/	
HER2+ (%)	459 (48.93%)	/	
Ki_67≧14% (%)	778 (82.94%)	/	
CK5_6 + (%)	121 (12.90%)	/	
EGRF + (%)	167 (17.80%)	/	
Molecular subtypes			/
Luminal A	95 (10.13%)	/	/
Luminal B(HER2(-))	282 (30.06%)	/	/
Luminal B(HER2(+))	340 (36.25%)	/	/
ERBB2(HER2(+))	119 (12.69%)	/	/
Triple-negative	102 (10.87%)	/	/
Metastatic and relapse sites			
liver metastasis (%)	16 (1.71%)	/	/
lung metastasis (%)	3 (0.03%)	/	/
distant lymph node (%)	5 (0.05%)	/	/
others (%)	71 (7.57%)	/	/
multiple metastasis (%)	96 (10.23%)	/	/
CEA (median [IQR])	1.84 [1.22,3.07]	/	/
CA125 (median [IQR])	15.30 [10.10,24.98]	/	/
CA153 (median [IQR])	13.80 [8.10,22.80]	/	/
T cell (median [IQR])	67.50 [61.50,73.30]	/	/
Th (median [IQR])	39.40 [33.73,44.50]	/	/
Tc (median [IQR])	20.77 [16.70,25.58]	/	/
Th/Tc ratio(median [IQR])	1.90[1.44,2.50]	/	/
NK (median [IQR])	11.90 [8.40,17.00]	/	/
B cell (median [IQR])	12.33 [9.02,16.00]	/	/
NEUT(median [IQR])	**3.62 [2.85,4.64]**	**3.72 [2.92,4.78]**	**0.023**
LYMPH (median [IQR])	1.75 [1.40,2.12]	1.84 [1.53,2.11]	0.118
MONO (median [IQR])	**0.38 [0.30,0.46]**	**0.34 [0.28,0.42]**	**<0.01**
PLT (median [IQR])	259.00 [220.00,310.00]	268.00 [232.00,309.00]	0.139
NLR (median [IQR])	2.04 [1.56,2.86]	2.04 [1.56,2.65]	0.239
LMR (median [IQR])	**4.75 [3.66,6.08]**	**5.42 [4.32,6.60]**	**<0.01**
PLR (median [IQR])	150.17 [116.71,194.76]	143.65 [118.75,179.08]	0.603

Wilcoxon test. Bold values indicate significant differences.

EGRF, epidermal growth factor receptor; CEA, carcinoembryonic antigen; CA125, carbohydrate antigen 125; CA153, carbohydrate antigen 153; Th, helper T cell; Tc, killer T cell; NK, natural killer; NEUT, neutrophile; LYMPH, lymphocyte; MONO, monocyte; PLT, platelet; NLR, neutrophil-lymphocyte ratio; LMR, lymphocyte-monocyte ratio; PLR, platelet-lymphocyte ratio.

treatment in BC patients with different molecular subtypes. According to HR (ER, PR) expression, BC patients are divided into HR-positive (either ER, PR are positive for any term) and HR negative groups. Patients are divided into HER-2 positive and HER-2 negative groups according to HER-2 expression. In addition, we also discussed patients with triple-negative BC. Although in univariate analysis, LMR is a prognostic factor for DFS in HR-positive (p = 0.048), HR-negative (0.054), and HER2-negative (p = 0.007) BC patients, it is only an independent prognostic factor for DFS in HER2-negative BC patients (LMR,

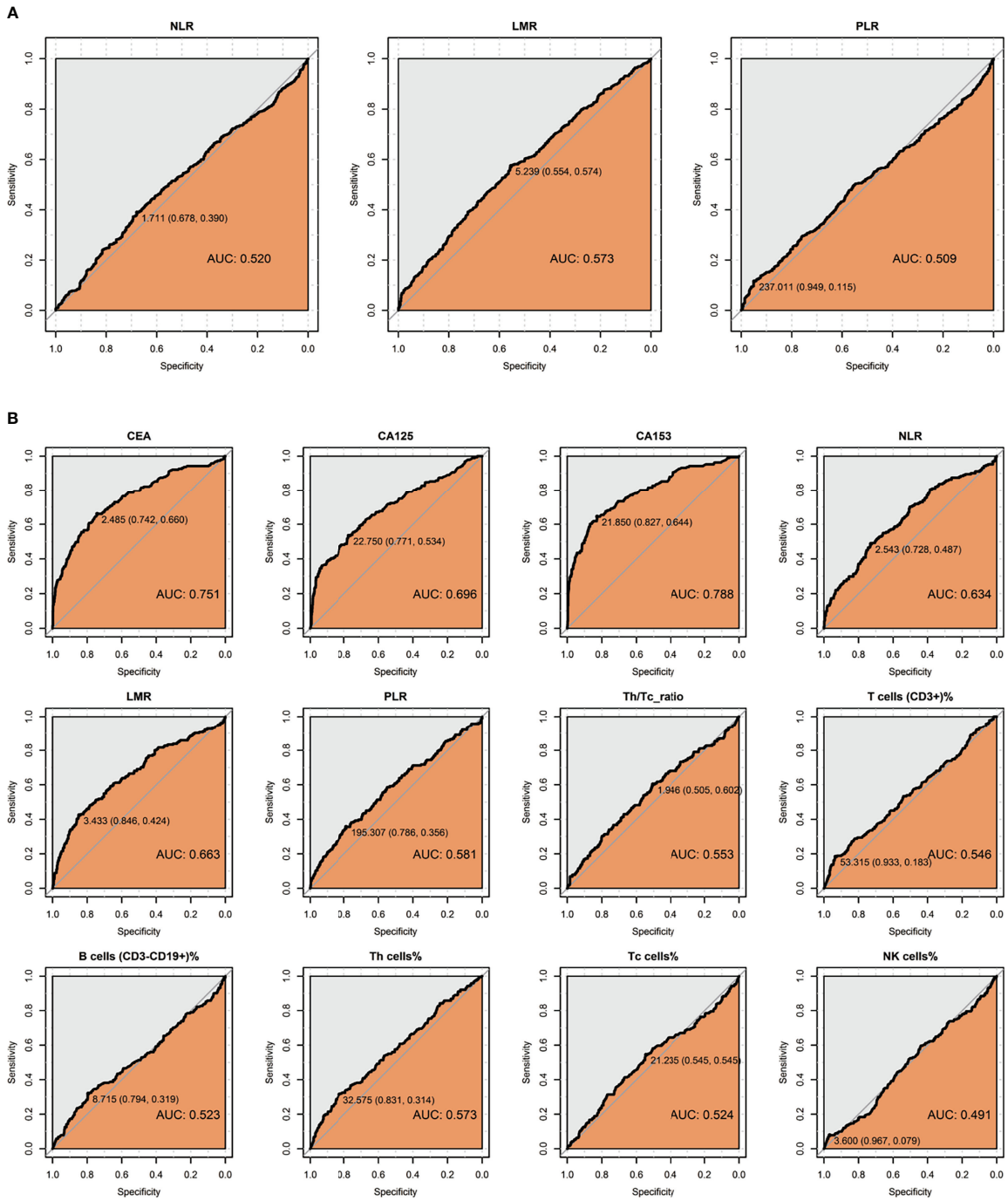

FIGURE 2 | ROC curve of peripheral blood indicators. **(A)** Perform ROC curve analysis on 1483 breast disease patients to select the best hematological index boundary value for distinguishing BC, including NLR, LMR, and PLR. **(B)** Performed on 938 BC patients to select the best cut-off value of hematological parameters for distinguishing patients with distant metastasis of BC, including CA153, CEA, CA125, NLR, LMR, PLR, Th cell%, Th/Tc radio, T cell%, Tc cell%, B cell%, NK cell%.

P = 0.022). We did not find any indicators as independent prognostic factors for DFS in patients with HR negative and triple-negative BC. The results are presented in **Table S4**. Using the cut-off values in **Table S1** divided stage I-III BC. The discrepancies in DFS stratified by the molecular subtypes were analyzed. The DFS of the high-LMR group was still better than the low LMR group, except for HR-positive and triple-negative subtypes (**Figure 6**).

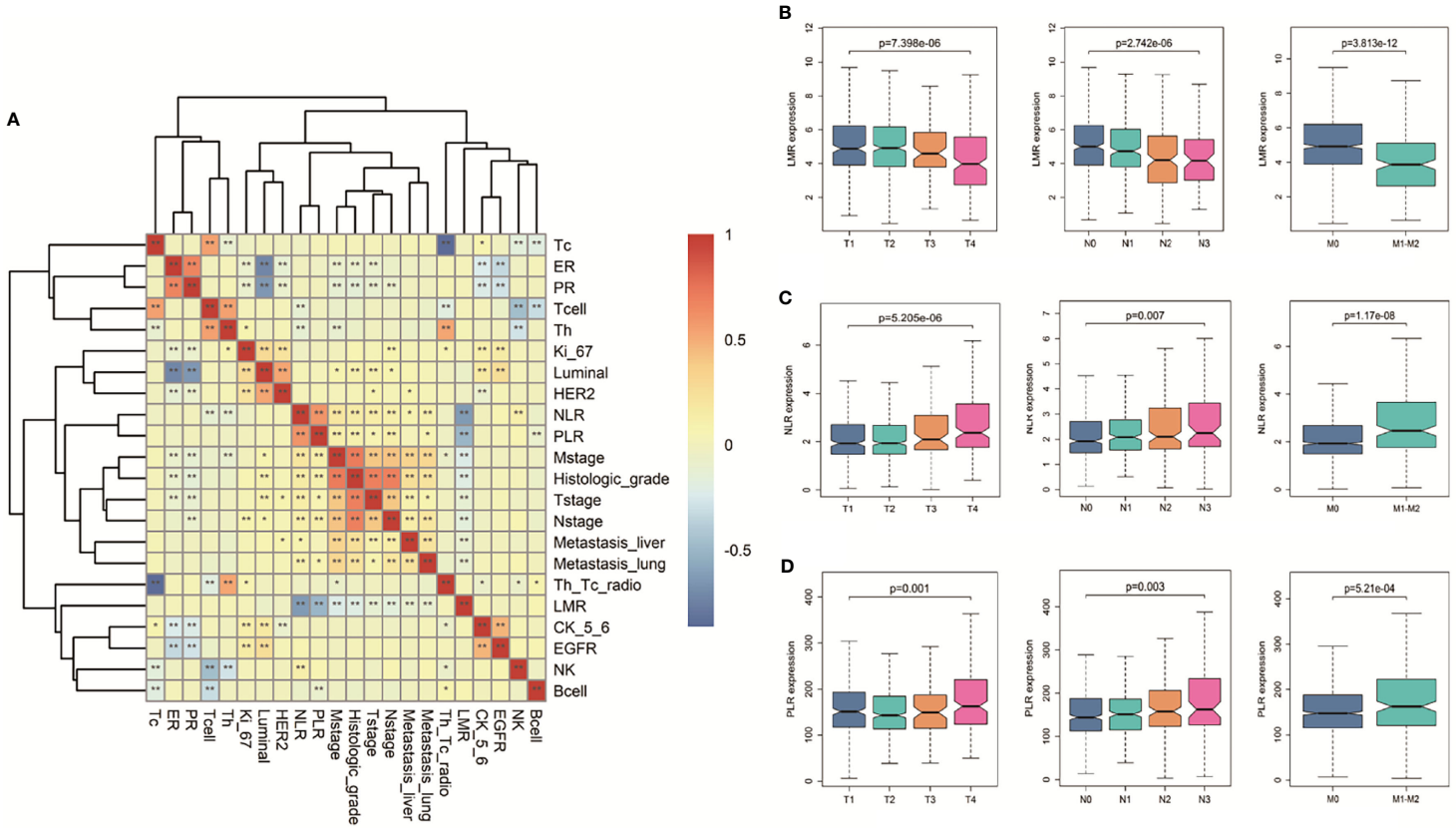

FIGURE 3 | Correlation between clinical indicators and hematological indicators. **(A)** The heat map of the correlation between clinical indicators and hematological indicators in BC. Different colors in the figure correspond to different correlation coefficients, and different significance levels are marked as *P < 0.05, **P < 0.01. **(B)** Boxplots of the significantly reduced LMR in the clinical TNM stage. Boxplots of elevated **(C)** NLR and **(D)** PLR in the clinical TNM setting. Differences between groups were estimated using the Kruskal–Wallis test.

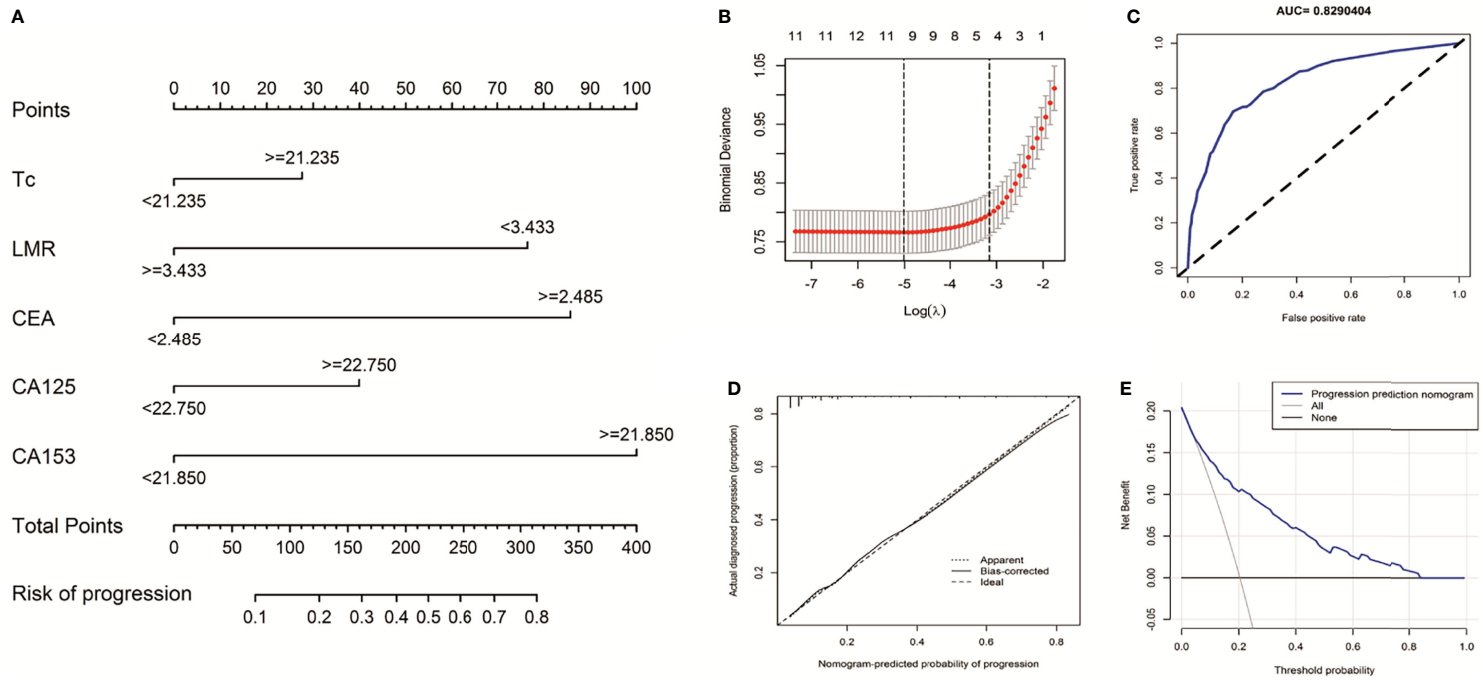

FIGURE 4 | Nomogram for prediction of BC metastasis risk. **(A)** shown is the Nomogram for predicting the risk of stage IV based on Multivariate logistic regression analysis in BC patients. **(B)** Selection results of the LASSO model. The partial likelihood deviance (binomial deviance) curve plot versus logλ. Dotted vertical lines draw at the optimal values by using the minimum criteria. **(C)** Plotted is a ROC curve for the independent validation cohort of the logistic regression model used in the Nomogram. The AUC is denoted, with the closer to 1, the better the model is. **(D)** the calibration plot gives the prediction performance of the proposed Nomogram in the discovery cohort, with the closer to the 45° line, the better the performance. **(E)** Decision curve analysis for the risk nomogram. The X-axis is the risk threshold probability that changes from 0 to 1, and the Y-axis is the calculated net benefit for a given threshold probability.

TABLE 2 | Univariate and multivariate logistic regression analysis predicts distant metastasis of BC.

	Univariate				Multivariate			
Profiles	**OR**	**95 (%) CI**		**p**	**OR**	**95 (%) CI**		**p**
CA153>=21.850	8.666	6.119	12.374	<0.001	4.307	2.863	6.499	<0.001
CEA>=2.485	5.564	3.971	7.863	<0.001	3.345	2.248	4.996	<0.001
LMR>=3.433	0.247	0.174	0.350	<0.001	0.375	0.227	0.618	<0.001
Tc>=21.235	1.431	1.041	1.972	0.028	1.700	1.130	2.577	0.012
CA125>=22.750	3.860	2.774	5.387	<0.001	1.625	1.073	2.444	0.021
Th/Tc ratio >=1.946	0.649	0.468	0.894	0.009				
Th>=32.575	0.443	0.310	0.638	<0.001				
Tcell>=53.315	0.320	0.201	0.512	<0.001				
PLR>=195.307	2.028	1.434	2.855	<0.001				
NLR>=2.543	2.543	1.835	3.526	<0.001				
NK>=3.6	0.406	0.212	0.804	0.008				
Bcell>=8.715	0.553	0.390	0.790	0.001				

CEA, carcinoembryonic antigen; CA125, carbohydrate antigen 125; CA153, carbohydrate antigen 153; NK, natural killer; NLR, neutrophil to lymphocyte ratio; PLR, platelet to lymphocyte ratio; LMR, lymphocyte to monocyte ratio; Th/Tc ratio, helper T cell to killer T cell ratio; CI, confidence interval; OR, odds ratio.

DISCUSSION

Compared with the pathological examination, detecting markers in whole blood after surgery has many advantages (25). The previous studies demonstrated that many clinical test indicators have diagnostic and prognostic functions in the diagnosis and metastasis of BC. A meta-analysis with 12,993 subjects showed that elevated serum CA153 or CEA was associated with poor overall and disease-free survival in BC patients (26). Serums CEA, CA199, CA125, CA153, and TPS can diagnose metastatic BC, and different combinations of tumor markers have varying diagnostic values (22).

The present study examined a cohort of 938 BC patients and 509 benign breast disease patients which investigated the association between peripheral blood NLR, LMR, PLR, and other traditional markers. Moreover, the role of these indicators on diagnosis and treatment effects in BC was explored. Our observations on NLR, LMR, and PLR are consistent with the research on multiple cancer types, including BC, in recent years (15, 16, 27–34).

Next, we analyzed the diagnostic accuracy of all indicators. Many previous studies have shown that the threshold is based on the prognosis or quartile of the analyzed cohort (35, 36). Our study used a pooled database of matched patients with stage I-III BC patients and stage IV BC patients. This strategy highlighted significantly higher CEA, CA153, CA125, and killer T cell values in stage I-III BC patients compared to stage IV BC patients. LMR had lower values in stage IV BC patients. It enabled us to compute a threshold based on diseases' progress and be different from the results obtained by benign disease patients as the control cohort. The obtained cut-offs for CEA, CA153, CA125, killer T cell, and LMR are slightly higher for those found in previous studies (CEA: 5 ng/ml, CA153: 31.3 U/ml, B cell%: literature range: 7%–23%, Th/Tc: literature range: 0.9-3.6, LMR: literature range: 3-5.5) (20, 30–32, 37–39). ROC analysis showed that the accuracy of a single marker for diagnosis of stage I-III BC patients and stage IV BC patients was not high (AUC <0.800). The combined use of CEA, CA153, CA125, killer T cell, and LMR can greatly enhance the diagnostic ability compared to using a single indicator, which indicates that this combination can better predict metastasis risk of BC (AUC =0.829).

Although many previous studies have reported the predictive utility of NLR, LMR, and PLR in treating BC patients, the results obtained are not consistent. Cho U's (40) reviewed 661 patients diagnosed with invasive BC from 1993 to 2011. In univariate analysis, high NLR, PLR, and low LMR are significantly associated with poor DSS and DFS. In multivariate analysis, only PLR is still considered as an independent predictor of prognosis. In gastrointestinal cancer, BC, and gynecological cancer, multivariate Cox regression analysis found that high expression of NLR was independently associated with decreased PFS (41). In a study of the effect of circulating blood lymphocyte subsets on the survival of patients with metastatic BC (MBC), Th cells was a negative independent predictor of PFS (hazard ratio [HR] = 0.538, 95% confidence interval [CI] = 0.313-0.926, P = 0.025) (42). Both Th and Tc increase and participate in the immune response. Tc cells are the key effector cell population that mediates effective anti-tumor immunity (43, 44). On the contrary, Th cells in the tumor have a negative prognostic effect on the prognosis of BC patients.

The degree of tumor malignancy is related to non-specific inflammation. Inflammatory mediators can cause abnormal proliferation and deterioration of tumor cells (45). This study used metastatic BC with a high degree of malignancy to divide the cut-off value of LMR and other hematological indicators. It used this value to find effective markers to predict the risk of distant metastasis and stage I- III BC prognosis. Although different cut-off values were selected, consistent with our research is that LMR predicts the efficacy and prognosis of BC patients (16, 20, 46). However, relevant research reports also have different results. The clinical prognostic effect of PLR in BC is better than that of LMR (47).

We followed up a larger BC cohort and included tumor proliferation, cellular immunity, and inflammatory factors before treatment compared with other studies. We were surprised to find that the Th/Tc (CD4:CD8) ratio is an independent prognostic factor for stage I- III BC. Th/Tc ratio repeatedly reports being associated with lymph node metastasis and the prognosis of triple-negative BC (44, 48–52).

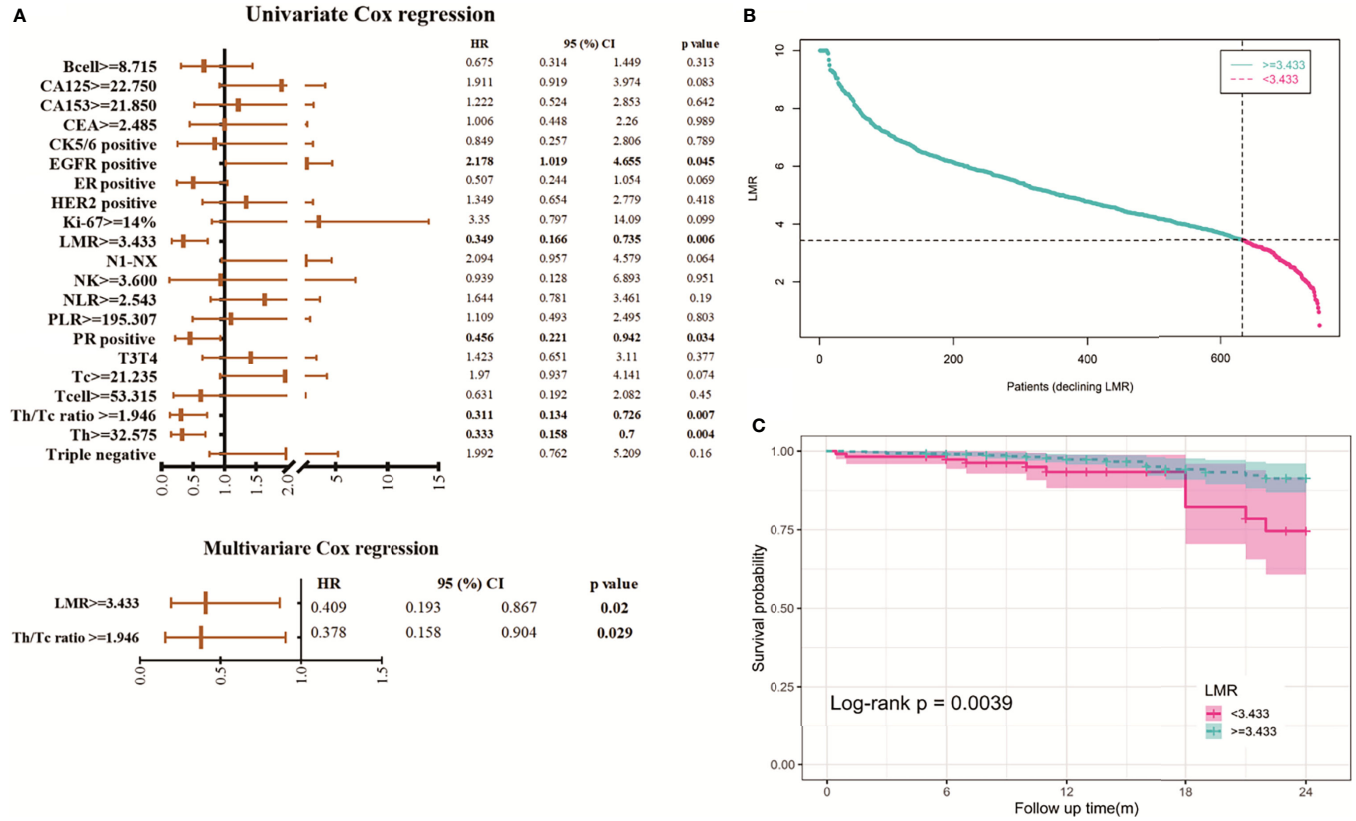

FIGURE 5 | Assessment of the prognostic risk model of LMR and clinical features in stage I-III BC. **(A)** Univariate and multivariate analyses of the clinical characteristics and LMR with the DFS. **(B)** Distribution of LMR risk score for the stage I-III BC. **(C)** Kaplan-Meier survival curves of the DFS of patients in the different LMR groups for stage I-III BC.

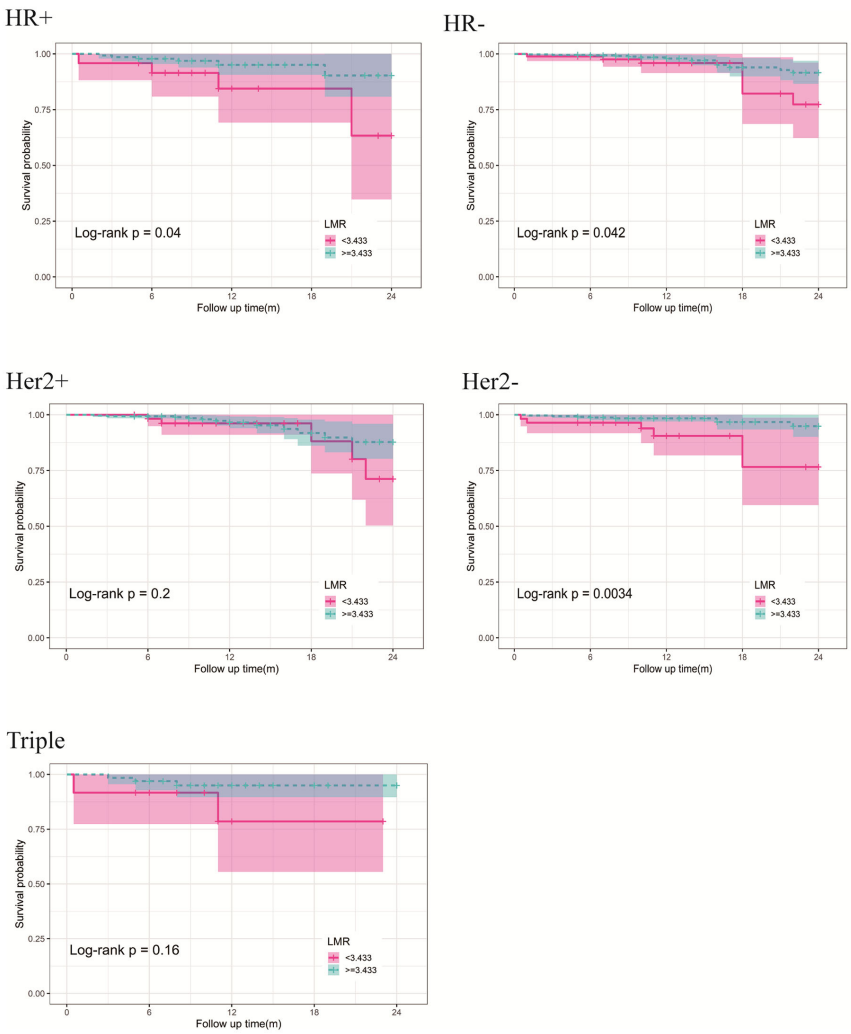

FIGURE 6 | Kaplan-Meier curves of DFS differences stratified by the molecular subtypes between the high- and low-LMR groups in the stage I-III BC.

However, this study has limitations. First of all, the patients enrolled in this study are single-center, which lacks the universality of the results. Second, due to the limited follow-up data, detailed treatment factors did not include in the analysis (including neoadjuvant chemotherapy, immunotherapy, and surgical methods), which may affect the accuracy of the results. Third, because there is no epidemiological investigation of patients, the level of peripheral blood markers may be affected by surgical methods and accompanying diseases. Finally, this study may help better understand the relationship between different types of whole blood markers and BC progress.

CONCLUSIONS

The prognosis of BC recurrence and metastasis is poor, and there is an urgent need for easily available predictors. This study found that low LMR and Th/Tc ratios in stage I- III BC indicate poor prognosis. Additionally, LMR combined with other indicators (CEA, CA153, CA125, and Tc cell%) can enhance the predictive value of BC distant metastasis. Although CEA, CA153, CA125, NLR, PLR, and other factors are not independent prognostic indicators of DFS, the values of NLR and PLR are related to TNM staging. CEA, CA153, and CA125 can independently predict metastasis, suggesting that other markers still have clinical significance. We hope this research can help doctors treat BC patients.

DATA AVAILABILITY STATEMENT

The original contributions presented in the study are included in the article/**Supplementary Material**. Further inquiries can be directed to the corresponding author.

ETHICS STATEMENT

The studies involving human participants were reviewed and approved by Guangxi Medical University Cancer Hospital Ethics Committee. The patients/participants provided their written informed consent to participate in this study.

AUTHOR CONTRIBUTIONS

HL and LZ designed the study. ZZ, YC, WL, DW and CS performed the experiments. HL and ZZ analyzed the data. ZZ and QL wrote the manuscript. All authors approved the manuscript.

FUNDING

This study support by grants from the Scientific Research & Technical Development Project of Qingxiu District, Nanning City, Guangxi Province (No. 2017036; No. 2016051). The Guangxi Scientific Research and Technical Planning Project (Grant No. Guike AB19110018). Self-funded scientific research project of Guangxi Zhuang Autonomous Region Health Committee (Grant No. 20191022).

ACKNOWLEDGMENTS

Thanks, the Guangxi Cancer Hospital Biological Resource Bank for providing the samples.

SUPPLEMENTARY MATERIAL

The Supplementary Material for this article can be found online at: https://www.frontiersin.org/articles/10.3389/fonc.2021.782383/full#supplementary-material

REFERENCES

1. Bray F, Ferlay J, Soerjomataram I, Siegel RL, Torre LA, Jemal A. Global Cancer Statistics 2018: GLOBOCAN Estimates of Incidence and Mortality Worldwide for 36 Cancers in 185 Countries. *CA Cancer J Clin* (2018) 68:394–424. doi: 10.3322/caac.21492
2. Anglade F, Miller J. U. Can Pathology Diagnostic Services for Cancer be Stratified and Serve Global Health? *Wiley Online Libr* (2020) 126:2431–8. doi: 10.1002/cncr.32872
3. Montemurro F, Nuzzolese I, Ponzone R. Neoadjuvant or Adjuvant Chemotherapy in Early Breast Cancer? *Expert Opin Pharmacother* (2020) 21:1071–82. doi: 10.1080/14656566.2020.1746273
4. Gupta G, Lee CD, Guye ML, vanSciver RE, MP L, Lafever AC, et al. Unmet Clinical Need: Developing Prognostic Biomarkers and Precision Medicine to Forecast Early Tumor Relapse, Detect Chemo-Resistance and Improve Overall Survival in High-Risk Breast Cancer. *Ann Breast Cancer Ther* (2020) 4:48. doi: 10.36959/739/525
5. Batis N, Brooks JM, Payne K, Sharma N, Nankivell P, Mehanna H. Lack of Predictive Tools for Conventional and Targeted Cancer Therapy: Barriers to Biomarker Development and Clinical Translation. *Adv Drug Deliv Rev* (2021) 176:113854. doi: 10.1016/J.ADDR.2021.113854
6. Yang QK, Su YN, Wang W, Wang N, Yao ZX, Zhang XJ. CONUT Score or/and Peripheral Blood CD4+/CD8+ Ratio-Based Web Dynamic Nomograms to Predict the Individualized Survival of Patients With Advanced Osteosarcoma. *Cancer Manag Res* (2020) 12:4193–208. doi: 10.2147/CMAR.S251814
7. Xia WK, Liu ZL, Shen D, Lin QF, Su J, Mao WD. Prognostic Performance of Pre-Treatment NLR and PLR in Patients Suffering From Osteosarcoma. *World J Surg Oncol* (2016) 14:127. doi: 10.1186/s12957-016-0889-2
8. Yersal Ö, Çetinkünar S, Aktimur R, Aziret M, Özdas S, Erdem H, et al. Neutrophil/lymphocyte and Platelet/Lymphocyte Ratios are Not Different Among Breast Cancer Subtypes. *Asian Pac J Cancer Prev* (2017) 18:2227–31. doi: 10.22034/APJCP.2017.18.8.2227
9. Gerratana L, Basile D, Toffoletto B, Bulfoni M, Zago S, Magini A, et al. Biologically Driven Cut-Off Definition of Lymphocyte Ratios in Metastatic Breast Cancer and Association With Exosomal Subpopulations and Prognosis. *Sci Rep* (2020) 10(1):7010. doi: 10.1038/s41598-020-63291-2
10. Roxburgh CSD, McMillan DC. Role of Systemic Inflammatory Response in Predicting Survival in Patients With Primary Operable Cancer. *Futur Oncol* (2010) 6:149–63. doi: 10.2217/fon.09.136
11. Viganó A, Bruera E, Jhangri GS, Newman SC, Fields AL, Suarez-Almazor ME. Clinical Survival Predictors in Patients With Advanced Cancer. *Arch Intern Med* (2002) 160:861–8. doi: 10.1001/archinte.160.6.861
12. Bartlett EK, Flynn JR, Panageas KS, Ferraro RA, Jessica JM, Postow MA, et al. High Neutrophil-to-Lymphocyte Ratio (NLR) is Associated With Treatment Failure and Death in Patients Who Have Melanoma Treated With PD-1 Inhibitor Monotherapy. *Cancer* (2020) 126:76–85. doi: 10.1002/cncr.32506
13. Mandaliya H, Jones M, Oldmeadow C, Nordman IIC. Prognostic Biomarkers in Stage IV non-Small Cell Lung Cancer (NSCLC): Neutrophil to Lymphocyte Ratio (NLR), Lymphocyte to Monocyte Ratio (LMR), Platelet to Lymphocyte Ratio (PLR) and Advanced Lung Cancer Inflammation Index (ALI). *Transl Lung Cancer Res* (2019) 8:886–94. doi: 10.21037/tlcr.2019.11.16
14. Goto W, Kashiwagi S, Asano Y, Takada K, Takahashi K, Hatano T, et al. Predictive Value of Lymphocyte-to-Monocyte Ratio in the Preoperative Setting for Progression of Patients With Breast Cancer. *BMC Cancer* (2018) 18(1):1137. doi: 10.1186/s12885-018-5051-9
15. Gilmore N, Mohile S, Lei L, Culakova E, Mohamed M, Magnuson A, et al. The Longitudinal Relationship Between Immune Cell Profiles and Frailty in Patients With Breast Cancer Receiving Chemotherapy. *Breast Cancer Res* (2021) 23(1):19. doi: 10.1186/S13058-021-01388-W
16. Ma Y, Zhang J, Chen X. Lymphocyte-To-Monocyte Ratio is Associated With the Poor Prognosis of Breast Cancer Patients Receiving Neoadjuvant Chemotherapy. *Cancer Manag Res* (2021) 13:1571. doi: 10.2147/CMAR.S292048
17. Gong J, Jiang H, Shu C, Hu MQ, Huang Y, Liu Q, et al. Prognostic Value of Lymphocyte-to-Monocyte Ratio in Ovarian Cancer: A Meta-Analysis. *J Ovarian Res* (2019) 12(1):51. doi: 10.1186/S13048-019-0527-Z
18. Hutterer GC, Stoeckigt C, Stojakovic T, Jesche J, Eberhard K, Pummer K, et al. Low Preoperative Lymphocyte-Monocyte Ratio (LMR) Represents a Potentially Poor Prognostic Factor in Nonmetastatic Clear Cell Renal Cell Carcinoma. *Urol Oncol Semin Orig Investig* (2014) 32:1041–8. doi: 10.1016/J.UROLONC.2014.04.001
19. Stotz M, Szkandera J, Stojakovic T, Siedel J, Samonigg H, Kornprat P, et al. The Lymphocyte to Monocyte Ratio in Peripheral Blood Represents a Novel Prognostic Marker in Patients With Pancreatic Cancer. *Clin Chem Lab Med* (2015) 53:499–506. doi: 10.1515/CCLM-2014-0447
20. Zenan H, Zixiong L, Zhicheng Y, Mei H, Xiongbin Y, Tiantian W, et al. Clinical Prognostic Evaluation of Immunocytes in Different Molecular Subtypes of Breast Cancer. *J Cell Physiol* (2019) 234:20584–602. doi: 10.1002/JCP.28662
21. Wu SG, He ZY, Zhou J, Sun JY, Li FY, Lin Q, et al. Serum Levels of CEA and CA15-3 in Different Molecular Subtypes and Prognostic Value in Chinese Breast Cancer. *Breast* (2014) 23(1):88-93. doi: 10.1016/j.breast.2013.11.003
22. Wang W, Xu X, Tian B, Wang Y, Du L, Sun T, et al. The Diagnostic Value of Serum Tumor Markers CEA, CA19-9, CA125, CA15-3, and TPS in Metastatic

Breast Cancer. *Clin Chim Acta* (2017) 470:51–5. doi: 10.1016/j.cca.2017.04.023
23. Nelson MA, Ngamcherdtrakul W, Luoh SW, Yantasee W. Prognostic and Therapeutic Role of Tumor-Infiltrating Lymphocyte Subtypes in Breast Cancer. *Cancer Metastasis Rev* (2021) 40(2):519–36. doi: 10.1007/s10555-021-09968-0
24. McEligot AJ, Poynor V, Sharma R, Panangadan A. Logistic Lasso Regression for Dietary Intakes and Breast Cancer. *Nutrients* (2020) 12:1–14. doi: 10.3390/NU12092652
25. Liskova A, Samec M, Koklesova L, Giordano FA, Kubatka P, Golubnitschaja O. Liquid Biopsy is Instrumental for 3PM Dimensional Solutions in Cancer Management. *J Clin Med* (2020) 9:1–38. doi: 10.3390/jcm9092749
26. Li X, Dai D, Chen B, Tang H, Xie X, Wei W. Clinicopathological and Prognostic Significance of Cancer Antigen 15-3 and Carcinoembryonic Antigen in Breast Cancer: A Meta-Analysis Including 12,993 Patients. *Dis Markers* (2018) 2018:9863092. doi: 10.1155/2018/9863092
27. Ataş H, Korukluoğlu B, Özdemir BA, Yakşi N, Saylam B, Tez M. Diagnostic Value of Modified Systemic Inflammation Score for Prediction of Malignancy in Patients With Indeterminate Thyroid Nodules. *Am J Surg* (2021) 221:117–21. doi: 10.1016/J.AMJSURG.2020.08.002
28. Nakamoto S, Ikeda M, Kubo S, Yamamoto M, Yamashita T, Notsu A. Systemic Immunity Markers Associated With Lymphocytes Predict the Survival Benefit From Paclitaxel Plus Bevacizumab in HER2 Negative Advanced Breast Cancer. *Sci Rep* (2021) 11(1):6328. doi: 10.1038/S41598-021-85948-2
29. Yamazaki H, Iwasaki H, Suganuma N, Toda S, Masudo K, Nakayama H, et al. Inflammatory Biomarkers and Dynamics of Neutrophil-to-Lymphocyte Ratio in Lenvatinib Treatment for Anaplastic Thyroid Carcinoma. *Gland Surg* (2021) 10:852–60. doi: 10.21037/GS-20-871
30. Cho A, Untersteiner H, Fitschek F, Khalaveh F, Pruckner P, Pavo N, et al. The Clinical Relevance of Laboratory Prognostic Scores for Patients With Radiosurgically Treated Brain Metastases of non-Pulmonary Primary Tumor. *J Neurooncol* (2021) 153:497–505. doi: 10.1007/S11060-021-03788-6
31. Wang J, Zhang F, Jiang F, Hu L, Chen J, Wang Y. Distribution and Reference Interval Establishment of Neutral-to-Lymphocyte Ratio (NLR), Lymphocyte-to-Monocyte Ratio (LMR), and Platelet-to-Lymphocyte Ratio (PLR) in Chinese Healthy Adults. *J Clin Lab Anal* (2021) 35(9):e23935. doi: 10.1002/JCLA.23935
32. Gupta V, Chaudhari V, Shrikhande SV, Bhandare MS. Does Preoperative Serum Neutrophil to Lymphocyte Ratio (NLR), Platelet to Lymphocyte Ratio (PLR), and Lymphocyte to Monocyte Ratio (LMR) Predict Prognosis Following Radical Surgery for Pancreatic Adenocarcinomas? Results of a Retrospective Study. *J Gastrointest Cancer* (2021). doi: 10.1007/S12029-021-00683-1
33. Mei J, Sun X-Q, Lin W-P, Li S-H, Lu L-H, Zou J-W, et al. Comparison of the Prognostic Value of Inflammation-Based Scores in Patients With Hepatocellular Carcinoma After Anti-PD-1 Therapy. *J Inflamm Res* (2021) 14:3879–90. doi: 10.2147/JIR.S325600
34. Yu D, An G, Yao J. Lymphocyte-To-Monocyte Ratio Combined With CA19-9 for Predicting Postoperative Recurrence of Colorectal Cancer in Patients With Diabetes. *J Clin Lab Anal* (2021) 35(9):e23944. doi: 10.1002/JCLA.23944
35. Hu C, Bai Y, Li J, Zhang G, Yang L, Bi C, et al. Prognostic Value of Systemic Inflammatory Factors NLR, LMR, PLR and LDH in Penile Cancer. *BMC Urol* (2020) 20(1):57. doi: 10.1186/s12894-020-00628-z
36. Meng X, Chang Q, Liu Y, Chen L, Wei G, Yang J, et al. Determinant Roles of Gender and Age on SII, PLR, NLR, LMR and MLR and Their Reference Intervals Defining in Henan, China: A Posteriori and Big-Data-Based. *J Clin Lab Anal* (2018) 32(2):e22228. doi: 10.1002/jcla.22228
37. Song X, Liang B, Wang C, Shi S. Clinical Value of Color Doppler Ultrasound Combined With Serum CA153, CEA and TSGF Detection in the Diagnosis of Breast Cancer. *Exp Ther Med* (2020) 20:1822–8. doi: 10.3892/etm.2020.8868
38. Chen R, Jiang C, Zhu Q, You S, Li Y, Li S, et al. Combining the Tumor Abnormal Protein Test With Tests for Carcinoembryonic Antigens, Cancer Antigen 15-3, and/or Cancer Antigen 125 Significantly Increased Their Diagnostic Sensitivity for Breast Cancer. *Med (Baltimore)* (2020) 99:e21231. doi: 10.1097/MD.0000000000021231
39. Raheem AR, Abdul-Rasheed OF, Al-Naqqash MA. The Diagnostic Power of Circulating Micro Ribonucleic Acid 34a in Combination With Cancer Antigen 15-3 as a Potential Biomarker of Breast Cancer. *Saudi Med J* (2019) 40:1218–26. doi: 10.15537/smj.2019.12.24712
40. Cho U, Park HS, Im SY, Yoo YC, Jung JH, Suh YJ, et al. Prognostic Value of Systemic Inflammatory Markers and Development of a Nomogram in Breast Cancer. *PLoS One* (2018) 13(7):e0200936. doi: 10.1371/journal.pone.0200936
41. Marra A, Criscitiello C, Morganti S, Viale G, Zagami P, Nicolò E, et al. Baseline Blood Parameters as Predictive Biomarkers of Immunotherapy Efficacy in Solid Tumors. *J Clin Oncol* (2020) 38:e15147–7. doi: 10.1200/jco.2020.38.15_suppl.e15147
42. Yang J, Xu J, E Y, Sun T. Predictive and Prognostic Value of Circulating Blood Lymphocyte Subsets in Metastatic Breast Cancer. *Cancer Med* (2019) 8 (2):492-500. doi: 10.1002/cam4.1891
43. Huang Y, Ma C, Zhang Q, Ye J, Wang F, Zhang Y, et al. CD4+ and CD8+ T Cells Have Opposing Roles in Breast Cancer Progression and Outcome. *Oncotarget* (2015) 6:17462–78. doi: 10.18632/oncotarget.3958
44. Ghalib NN, Nasrullayeva GM, Qaziyev AY, Al-Ali Jawad KH. T- Lymphocyte Subset (CD4 /CD8) Ratios of Breast Cancer Patients in Basra-Iraq and Baku-Azerbaijan. *Asian Pac J Cancer Prev* (2016) 17:175–7. doi: 10.7314/APJCP.2016.17.S3.175
45. Xie H-Y, Shao Z-M, Li D-Q. Tumor Microenvironment: Driving Forces and Potential Therapeutic Targets for Breast Cancer Metastasis. *Chin J Cancer* (2017) 36:36. doi: 10.1186/S40880-017-0202-Y
46. Peng Y, Chen R, Qu F, Ye Y, Fu Y, Tang Z, et al. Low Pretreatment Lymphocyte/Monocyte Ratio is Associated With the Better Efficacy of Neoadjuvant Chemotherapy in Breast Cancer Patients. *Cancer Biol Ther* (2020) 21:189–96. doi: 10.1080/15384047.2019.1680057
47. Yao M, Liu Y, Jin H, Liu X, Lv K, Wei H, et al. Prognostic Value of Preoperative Inflammatory Markers in Chinese Patients With Breast Cancer. *Onco Targets Ther* (2014) 7:1743–52. doi: 10.2147/OTT.S69657
48. Jafarian AH, Tasbandi A, Gilan H, Sheikhi M, Roshan NM. Evaluation of CD30/CD4/CD8 in Triple-Negative Invasive Ductal Carcinoma of Breast in Association With Clinicopathological Prognostic Factors. *Indian J Pathol Microbiol* (2018) 61:500–4. doi: 10.4103/IJPM.IJPM_67_18
49. Rad FR, Ajdary S, Omranipour R, Alimohammadian MH, Hassan ZM. Comparative Analysis of CD4+ and CD8+ T Cells in Tumor Tissues, Lymph Nodes and the Peripheral Blood From Patients With Breast Cancer. *Iran BioMed J* (2015) 19:35–44. doi: 10.6091/IBJ.1289.2014
50. Jagtap SV. Evaluation of CD4+ T-Cells and CD8+ T-Cells in Triple-Negative Invasive Breast Cancer. *Indian J Pathol Microbiol* (2018) 61:477–8. doi: 10.4103/IJPM.IJPM_201_18
51. Solis-Castillo LA, Garcia-Romo GS, Diaz-Rodriguez A, Reyes-Hernandez D, Tellez-Rivera E, Rosales-Garcia VH, et al. Tumor-Infiltrating Regulatory T Cells, CD8/Treg Ratio, and Cancer Stem Cells are Correlated With Lymph Node Metastasis in Patients With Early Breast Cancer. *Breast Cancer* (2020) 27:837–49. doi: 10.1007/S12282-020-01079-Y
52. Wang K, Shen T, Siegal GP, Wei S. The CD4/CD8 Ratio of Tumor-Infiltrating Lymphocytes at the Tumor-Host Interface has Prognostic Value in Triple-Negative Breast Cancer. *Hum Pathol* (2017) 69:110–7. doi: 10.1016/J.HUMPATH.2017.09.012

Conflict of Interest: The authors declare that the research was conducted in the absence of any commercial or financial relationships that could be construed as a potential conflict of interest.

frontiers | Frontiers in Oncology

ORIGINAL RESEARCH
published: 03 May 2022
doi: 10.3389/fonc.2022.809715

An Initial Evaluation of Human Plasma cMLC-1: A Potential Protein Biomarker for Trastuzumab-Induced Cardiotoxicity, Breast Cancer Screening and Progression

Ling Yu[1,2†], Read Allen[3†], Lin Jia[1†], Ting Sun[1], Steven J. Isakoff[3], Marielle Scherrer-Crosbie[4], Allison M. Kehlmann[3], Hui Zheng[5], Amy Ly[6], Charlotte S. Walmsley[3], Katherine Hesler[3], Ava N. Varasteh[3], Christopher J. Pinto[3], Daniel E. McLoughlin[3], Wenjin Wu[7] and Xinhui Wang[1]*

[1] Division of Gastrointestinal and Oncologic Surgery, Department of Surgery, Massachusetts General Hospital, Harvard Medical School, Boston, MA, United States, [2] Key Laboratory of Luminescence Analysis and Molecular Sensing, Ministry of Education, School of Materials and Energy, Southwest University, Chongqing, China, [3] Termeer Center for Targeted Therapies, Massachusetts General Hospital Cancer Center, Boston, MA, United States, [4] Perelman Center for Advanced Medicine, Cardiovascular Medicine Division, The Hospital of the University of Pennsylvania, Philadelphia, PA, United States, [5] Biostatistics Center, Massachusetts General Hospital, Harvard Medical School, Boston, MA, United States, [6] Department of Pathology, Massachusetts General Hospital, Harvard Medical School, Boston, MA, United States, [7] Division of Monoclonal Antibodies, Office of Biotechnology Products, Office of Pharmaceutical Science, Center for Drug Evaluation and Research, U.S. Food and Drug Administration, Bethesda, MD, United States

OPEN ACCESS

Edited by:
San-Gang Wu,
First Affiliated Hospital of Xiamen University, China

Reviewed by:
Carlos Martinez-Perez,
Medical Research Council Institute of Genetics and Molecular Medicine (MRC), United Kingdom
Juan Zhou,
Xiamen University, China

***Correspondence:**
Xinhui Wang
xwang30@mgh.harvard.edu

[†]These authors have contributed equally to this work

Specialty section:
This article was submitted to Breast Cancer, a section of the journal Frontiers in Oncology

Received: 05 November 2021
Accepted: 21 March 2022
Published: 03 May 2022

Citation:
Yu L, Allen R, Jia L, Sun T, Isakoff SJ, Scherrer-Crosbie M, Kehlmann AM, Zheng H, Ly A, Walmsley CS, Hesler K, Varasteh AN, Pinto CJ, McLoughlin DE, Wu W and Wang X (2022) An Initial Evaluation of Human Plasma cMLC-1: A Potential Protein Biomarker for Trastuzumab-Induced Cardiotoxicity, Breast Cancer Screening and Progression. Front. Oncol. 12:809715. doi: 10.3389/fonc.2022.809715

Background: Trastuzumab is a targeted therapy for human epidermal growth factor receptor 2 (HER2)-positive breast cancer. However, trastuzumab-induced cardiotoxicity (TIC) has been reported when trastuzumab is administered to patients as a single agent or combined with anthracycline. Currently no means for detecting the early onset of TIC such as a protein biomarker is available. In this regard and based on promising results from a preliminary animal study, the potential of cardiac myosin light chain 1(cMLC-1) as a biomarker to predict TIC, screen patients for breast cancer and monitor tumor progression in breast cancer patients was evaluated.

Methods: Archived plasma samples collected before and after trastuzumab treatment at various fixed time points from 15 $HER2^+$ patients with or without cardiotoxicity, recently collected plasma samples from 79 breast cancer patients (40 $HER2^+$, 39 $HER2^-$), and 46 healthy donors were analyzed for cMLC-1 levels using an enzyme-linked immunosorbent assay (ELISA).

Results: An elevated plasma cMLC-1 level was found to be associated with TIC in 3 out of 7 (43%) trastuzumab-treated $HER2^+$ breast cancer patients. However, this study provided an opportunity for us to study plasma cMCL-1 levels in breast cancer patients. It was demonstrated that elevated plasma cMCL-1 is associated with breast cancer. The cutoff cMLC-1 concentration is estimated to be 44.99 ng/mL with a sensitivity of 59.49% (95%CI: 48.47%-69.63%) and specificity of 71.74% (95%CI: 57.45% -82.68%). We also found a noticeable but not significantly more elevated plasma cMCL-1 level in $HER2^-$ than

in HER2$^+$ breast cancer patients with the given sample sizes. As a result, improved sensitivity of 79.49% (95%CI: 64.47%-89.22%) with the specificity of 63.04% (95% CI:48.60%-75.48%) were obtained for cMLC-1 to predict HER2$^-$ breast cancer with the cutoff at 37.17 ng/mL. Moreover, this study determined that cMLC-1 level was significantly higher in patients with metastatic breast cancer than in patients with non-metastatic breast cancer.

Conclusions: While the analysis of cMLC-1 levels in the plasma of a limited number of trastuzumab-treated HER2$^+$ breast cancer patients failed to fully support its identification as a blood protein biomarker for predicting TIC, additional analyses of plasma cMLC-1 levels did significantly establish its correlations with breast cancer and disease progression. Our findings shed light on and filled, to some extent, the gap of knowledge of the potential of cMLC-1 as a blood protein biomarker for screening breast cancer and monitoring disease progression of breast cancer.

Keywords: cardiac myosin light chain 1(cMLC-1), biomarkers, trastuzumab-induced cardiotoxicity, breast cancer screening, breast cancer progression

BACKGROUND

Breast cancer (BC) is one of the most common malignancies in the United States, with over 280,000 new cases expected in 2021 (1). Approximately one in five women diagnosed with breast cancer worldwide will have an aggressive form of the disease with human epidermal growth factor receptor 2 (HER2) gene amplification or protein overexpression, known as HER2$^+$ subtype (2). Trastuzumab (Herceptin®) is a humanized monoclonal antibody specifically targeting HER2 that is used to treat both early- and late-stage HER2$^+$ breast cancer. When started before or after surgery to treat early disease, the drug is administered every 21 days for a total of one year. For advanced breast cancer, treatment is typically given as long as the patient continues to derive clinical benefit (3). Trastuzumab is typically prescribed as a single agent or in combination with standard chemotherapy regimens such as anthracyclines. However, trastuzumab treatment is associated with cardiac dysfunction, which manifests as a decrease in left ventricular ejection fraction (LVEF) and heart failure (4–6). Trastuzumab-induced cardiotoxicity (TIC) has been reported to occur in up to 7% of patients when trastuzumab was used as a single agent (7). When combined trastuzumab with an anthracycline, however, cardiotoxicity increases dramatically to up to 27% of patients (7).

Alarmingly, a decrease in LVEF has even been detected in asymptomatic breast cancer patients administered trastuzumab. Early identification of breast cancer patients for left ventricular dysfunction following trastuzumab therapy is essential for early initiation of cardioprotective measures. A blood-based biomarker for TIC would be better as an ongoing surveillance strategy than the current system of echocardiographic LVEF measurement to reveal TIC. However, to date, no such biomarker has been identified and validated for clinical use. Previous studies focused mainly on evaluating the potential of troponins I and T, brain natriuretic peptide (BNP), N-terminal pro b-type natriuretic peptide (NT-proBNP) and high-sensitivity C-reactive protein (hs-CRP) as blood protein biomarkers to predict TIC. Sawaya et al. revealed an association between troponin I (TnI) (also known as cardiac troponin I) levels at 3 months post-treatment with trastuzumab and development of cardiotoxicity at 6 months (8). Later, Onitilo et al. reported that elevated hs-CRP, but not BNP or troponin I, predicted decreased LVEF with a sensitivity of 92.9% but with a specificity of only 45.7%. With such a high false positives rate, this assay does not reliably predict toxicity (9). Recently, Zardavas et al. found that baseline (before trastuzumab treatment) troponin I and T levels were elevated in 13.6% (56 of 412) and 24.8% (101 of 407) patients, respectively, and that these measurements were associated with a significantly increased risk of reduced LVEF (10). While these findings are encouraging, these efforts indicate that the search for better biomarkers for early prediction and identification of TIC must continue. Troponin I is considered as a sensitive and specific biomarker in the diagnosis of myocardial infarction. However, it is not sensitive and specific for the diagnosis of early stage of TIC (11). Cardiac myosin light chain-1 (cMLC-1, also known as myosin essential

Abbreviations: AUC, area under the curve; BC, breast cancer; BNP, brain natriuretic peptide; CEA, carcinoembryonic antigen; CI, confidence intervals; cMLC-1, cardiac myosin light chain 1; CK, creatine kinase; CREC, Cardiac Review and Evaluation Committee for Trastuzumab; ELC, essential light chain; ELISA, enzyme-linked immunosorbent assay; ER, estrogen-receptor; FISH, Fluorescent *In Situ* Hybridization; HER2, epidermal growth factor receptor 2; HRP, horseradish peroxidase; hs-CRP, high-sensitivity C-reactive protein; IHC, immunohistochemistry; LVEF, left ventricular ejection fraction; NT-proBNP, N-terminal pro b-type natriuretic peptide; OD, optical density; PR, progesterone-receptor; ROC, receiver operator characteristic; SD, standard deviation; TIC, Trastuzumab-induced cardiotoxicity; TnI, Troponin-I.

light chain (ELC)), is encoded by the MYL3 gene and is a part of the myosin complex that plays an important role in cardiac muscle contraction (11, 12). Impaired integrity of damaged or injured cardiomyocytes leads to release of cMLC-1 from the myocardium into circulation (13–15). Past studies have shown that circulating cMLC-1 protein was elevated in patients a few hours after acute myocardial infarction, and peaked on days 2 to 4 post infarction (16, 17). In addition, when serum levels of cMLC-1 and creatine kinase (CK) were measured in serial samples from 49 patients with acute myocardial infarction, the results suggested that serum cMLC-1 is a better marker than CK in predicting LVEF changes (18).Thus, we investigated the possibility of cMLC-1 as a potential biomarker for TIC in mice. Using echocardiography, we found that trastuzumab significantly reduced LVEF (11). Importantly, this reduced LVEF was associated with elevated levels of serum cMLC-1 in mice (11). The initial objective of this study was to evaluate for the first time the potential of cMLC-1 as a blood biomarker for TIC in breast cancer patients using plasma samples collected from $HER2^+$ breast cancer patients, who had been treated with trastuzumab and either developed cardiotoxicity or did not. In turn, this effort led to analyses of cMLC-1 plasma levels as a prognostic indicator of breast cancer as well as disease progression in breast cancer patients.

MATERIALS AND METHODS

Patients

Archived human plasma samples (n=15) were collected at multiple time points from a relatively homogenous patient population. The cohort consisted of women with newly diagnosed breast cancer administered anthracyclines followed by taxanes and trastuzumab. Approximately 50% of these patients (7/15) were selected because they had developed TIC and another ~50% of these patients (8/15) were selected because they had not developed TIC for this study. This experimental design did not involve in any way the incidence of TIC (**Tables 1**, **2**). Cardiotoxicity was defined using the Cardiac Review and Evaluation Committee for Trastuzumab (CREC) criteria as a decrease of more than 10% in the echocardiographic LVEF to a value of less than 55%. The women had been monitored every 3 months. The plasma samples had been collected and banked under the Massachusetts General Hospital Institutional Review Board (IRB protocol 2006P000886).

TABLE 1 | Comparisons of plasma cMLC-1 levels at different time points in trastuzumab-treated BC patients.

Patient	Time	Mean	*p* value
#1	baseline *vs.* 3-month	55.05 ± 6.37 *vs.* 65.32 ± 2.72	0.230
#1	baseline *vs.* 6-month	55.05 ± 6.37 *vs.* 75.57 ± 7.07	0.010
#2	baseline *vs.* 3-month	17.60 ± 1.10 vs. 27.95 ± 3.38	0.050
#2	baseline *vs.* 6-month	17.60 ± 1.10 vs. 23.77 ± 4.02	0.140
#3	baseline *vs.* 3-month	0.57 ± 0.74 *vs.* 110.09 ± 26.94	0.001
#3	baseline *vs.* 6-month	0.57 ± 0.74 *vs.* 91.63 ± 15.36	0.002
#3	3-month *vs.* 6-month	110.09 ± 26.94 *vs.* 91.63 ± 15.36	0.264
#3	6-month *vs.* 9-month	91.63 ± 15.36 *vs.* 51.16 ± 0.64	0.059
#4	baseline *vs.* 6-month	18.19 ± 1.45 *vs.* 20.49 ± 2.02	0.076
#4	3-month *vs.* 6-month	12.96 ± 0.61 *vs.* 20.49 ± 2.02	0.035
#5	baseline *vs.* 3-month	26.57 ± 5.33 *vs.* 18.42 ± 1.81	0.148
#5	baseline *vs.* 6-month	26.57 ± 5.33 *vs.* 27.67 ± 1.13	0.410
#5	3-month *vs.* 6-month	18.42 ± 1.81 *vs.* 27.67 ± 1.13	0.024
#5	3-month *vs.* 9-month	18.42 ± 1.81 *vs.* 24.88 ± 1.41	0.053

TABLE 2 | Comparisons of plasma cMLC-1 levels before and 3-month after trastuzumab treatment in BC patients.

Patient	Baseline	3-month	*p* value	Diagnosed Cardiotoxicity
#1	55.05 ± 6.37	65.32 ± 2.72	0.230	NO
#2	17.60 ± 1.10	27.95 ± 3.38	0.050	NO
#3	0.57 ± 0.74	110.09 ± 26.94	0.001	YES
#4	18.19 ± 1.45	12.96 ± 0.61	0.040	YES
#5	26.27 ± 5.33	18.42 ± 1.81	0.148	NO
#6	209.40 ± 31.11	298.70 ± 67.75	0.083	YES
#7	78.82 ± 3.65	42.38 ± 0.61	0.005	YES
#8	14.35 ± 0.11	119.40 ± 0.09	9.42E-07	NO
#9	33.24 ± 3.56	28.67 ± 0.25	0.164	YES
#10	0.22 ± 0.10	1.04 ± 0.75	0.194	NO
#11	89.48 ± 13.69	39.76 ± 2.82	0.035	NO
#12	72.18 ± 5.82	60.25 ± 6.88	0.158	NO
#13	48.96 ± 5.56	55.61 ± 8.05	0.283	NO
#14	100.10 ± 28.01	79.08 ± 19.40	0.217	YES
#15	60.54 ± 17.20	174.60 ± 49.23	0.018	YES

For the additional studies detailed in this report, patients with $HER2^+$ (n=40) and $HER2^-$ (n=39) breast cancer were recruited from the Massachusetts General Hospital Cancer Center between March 2018 and January 2020 (**Tables 3**, **4**). Based on existing clinical guidelines (19), $HER2^+$ was defined as ≥2.0 amplification of HER2 by Fluorescent *In Situ* Hybridization (FISH) as noted on the pathology report from the date of original diagnosis, or as 2-3+ by immunohistochemistry (IHC) if FISH was not available. Patients who were receiving trastuzumab as standard therapy were also included in the $HER2^+$ cohort, even if IHC and FISH did not meet the criteria. Relevant clinical data such as clinicopathological characteristics and treatment history were extracted from electronic medical records. All studies were approved by the Dana Farber/Harvard Cancer Center Institutional Review Board (IRB protocol 13-416). Patients provided written informed consent for data collection, blood collection, and downstream analysis. Plasma samples from healthy donors (n=46) were obtained commercially (Innovative Research, 46430 Peary Court, Novi, MI 48377).

Plasma Collection

Blood samples (10 mL) were collected in cfDNA BCT tubes (Streck Inc., La Vista, NE, USA) at an arbitrary time point coinciding with the patients' clinical visits. Samples were stored ambient for up to 7 days and were centrifuged at 1000 x g for 15 min at 2-8°C. In one instance, plasma was previously isolated from whole blood by double centrifugation at 1,600 x g for 10 min followed by 3,000 x g for 10 min. The resulting plasma was frozen at -80°C, and later thawed for analysis.

Measurement of cMLC-1 by ELISA

A sandwich ELISA was performed using the human cMLC-1 ELISA kit from MyBioSource (Cat# MBS2506936, San Diego, CA, USA) according to the protocol provided. Each plasma sample was 1:10 diluted with 2% BSA/PBS and then added into anti-cMLC-1 antibody pre-coated wells and incubated at 37°C for 1.5 h. The plasma samples were then decanted. Next, 100 µL of biotinylated anti-cMLC-1 detection antibody working solution was added to each well, and incubated for 1 h at 37°C. After decanting the solution, the wells were washed with the provided washing buffer 3 times. One hundred µL of horseradish peroxidase conjugated avidin (HRP-avidin) working solution was added to each well, and incubated for 30 min at 37°C. The non-bound HRP-avidin was removed by washing with the buffer 5 times. To generate the colorimetric signal, 90 µL of substrate reagent was added to each well. After incubation for 15 min, the enzymatic reaction was stopped with 50 µL stop solution. The optical density (OD) of each well was measured with a microplate reader (Epoch, BioTeck Instrument, Winooski, VT, USA) at a wavelength of 450 nm. In the same test, serial concentrations of standard cMLC-1 working solution (provided in the kit)

TABLE 3 | Patient demographics and characteristics.

Characteristic	Patients		
	$HER2^+$ N= 40 Number (%)	$HER2^-$ N= 39 Number (%)	Total n = 79 Number (%)
Demographic characteristics			
Age (years, m+/-s)	54.5 (+/-12.7)	59.1 (+/-9.6)	56.9 (+/-11.39)
Race			
Black	2 (5%)	1 (2.6%)	3 (3.8%)
Asian	1 (2.5%)	1 (2.6%)	2 (2.5%)
White	33 (82.5%)	36 (92.3%)	69 (87.3%)
Other	3 (7.5%)	0	3 (3.8%)
Not stated	1 (2.5%)	1(2.6%)	2 (2.5%)
Treatment history			
Radiation treatment			
Yes	28 (70.0%)	32 (82.1%)	60 (75.9%)
No	12 (30.0%)	7 (17.9%)	19 (24.1%)
Trastuzumab at blood collection			
Yes	34 (85.0%)	–	–
No	6 (15.0%)	–	–
Other type of therapy at blood col.			
CDK4/6 (single or in combo)	1 (2.5%)	21 (53.8%)	22 (27.8%)
PIK3CA/mTOR (single or in combo)	1 (2.5%)	8 (20.5%)	9 (11.4%)
Chemotherapy	3 (7.5%)	3 (7.7%)	6 (7.6%)
Immunotherapy	0	1 (2.6%)	1 (1.3%)
Targeted therapy	1 (2.5%)	5 (12.8%)	6 (7.6%)
Endocrine therapy (single agent)	0	5 (12.8%)	5 (6.3%)

TABLE 4 | Patient clinicopathologic features.

Clinicopathologic features	Patients		
	$HER2^+$ N = 40 Number (%)	$HER2^-$ N = 39 Number (%)	Total n = 79 Number (%)
ER			
Positive	33 (82.5%)	34 (87.2%)	67 (84.8%)
Negative	7 (17.5%)	5 (12.8%)	12 (15.2%)
PR			
Positive	23 (57.5%)	29 (74.4%)	52 (65.8%)
Negative	17(42.5%)	10 (25.6%)	27 (34.2%)
Metastatic			
Yes	22 (55%)	30 (76.9%)	52 (65.8%)
No	18 (45%)	9 (23.1%)	27 (34.2%)
Histology grade			
Grade 1	–	7 (17.9%)	7 (8.9%)
Grade 2	8 (20.0%)	16 (41.0%)	24 (30.4%)
Grade 2-3	4 (10.0%)	–	4 (5.1%)
Grade 3	23 (57.5%)	11 (28.2%)	34 (43.0%)
Unknown	5 (12.5%)	5 (12.8%)	10 (12.6%)
Invasive histologic type			
Ductal	31 (77.5%)	30 (76.9%)	61 (77.2%)
Lobular	4 (10.0%)	7 (17.9%)	11 (13.9%)
Mixed	5 (12.5%)	2 (5.1%)	7 (8.9%)
Lymph node invasion			
Yes	23 (57.5%)	26 (66.7%)	49 (62.0%)
No	15 (37.5%)	9 (23.1%)	24 (30.4%)
Unknown	2 (5.0%)	4 (10.2%)	6 (7.6%)
Lymphovascular invasion			
Yes	32 (80.0%)	13 (33.3%))	45 (57.0%)
No	6 (15.0%)	22 (56.4%)	28 (35.4%)
Unknown	2 (5.0%)	4 (10.3%)	6 (7.6%)

were included. A four-parameter logistic curve on log-log equation was followed to draw the calibration curve. In each experiment, the standard cMLC-1 protein and all plasma samples were tested in duplicate.

To establish an appropriate detection method, each plasma sample undiluted and at 2-fold dilutions was tested to confirm that its cMLC-1 concentration was within the detectable range of the ELISA kit (0.625 to 40 ng/mL). Based on this titration experiment, a 1:10 dilution of plasma samples was found to be optimal for detection of cMLC-1 concentrations that fit well within the standard curve. The calibration curve following a four-parameter logistic curve on log-log equation was: $y = A^2 + (A_1 - A_2)/(1+(x/x_0)\ p)$, where $A_1 = 0.051$, $A_2 = 6.401$, $x_0 = 96.859$, $p = 0.887$, $R^2 = 0.996$. All the plasma samples were tested at least 2 times with a duplicate of each sample, and the concentration of cMLC-1 was calculated according to the calibration equation.

Statistical Analysis

Paired samples were compared with the paired *t* test. Area under the curve (AUC) was used to evaluate the clinical performance of the tests, and estimates of sensitivity, specificity, and predictive values were calculated and reported with 95% confidence intervals (CI). The medians of foci intensity distributions were tested with the Mann-Whitney U test. One-way ANOVA was used for multiple samples. Data are expressed as mean ± SD of the number of biological replicates indicated in each figure legend. Values of $p < 0.05$ were considered significant.

RESULTS

Plasma cMLC-1 Levels of Trastuzumab-Treated Breast Cancer Patients

To investigate if the association of reduced LVEF and elevated cMLC-1 that we previously noted in mice was clinically relevant in humans, archived plasma samples obtained from breast cancer patients (n=5) administered anthracyclines followed by taxanes and trastuzumab were analyzed for cMLC-1. The archived samples had been collected at multiple time points (baseline, 3, 6, and 9 months). Of the five patients, patients #3 and #4 developed cardiotoxicity. Compared to baseline, cMLC-1 increased in patient #3, but not in patient #4 nor the three patients, #1, #2 and #5, who did not develop TIC (**Figure 1**; **Table 1**). It is worth nothing that, unlike the huge difference of cMLC-1 between 0 and 3 months in patient #3, the changes of cMLC-1 were small between 3 and 6 months in patients #1, #4 and #5. Additionally, there was no change between 3 and 6 months in patient #2, or between 6 and 9 months in any of the 5 patients (**Figure 1A**; **Table 1**). Thus, we decided to test samples from an additional 10 patients (total n=15). These archived plasma samples were collected from these patients at baseline (prior

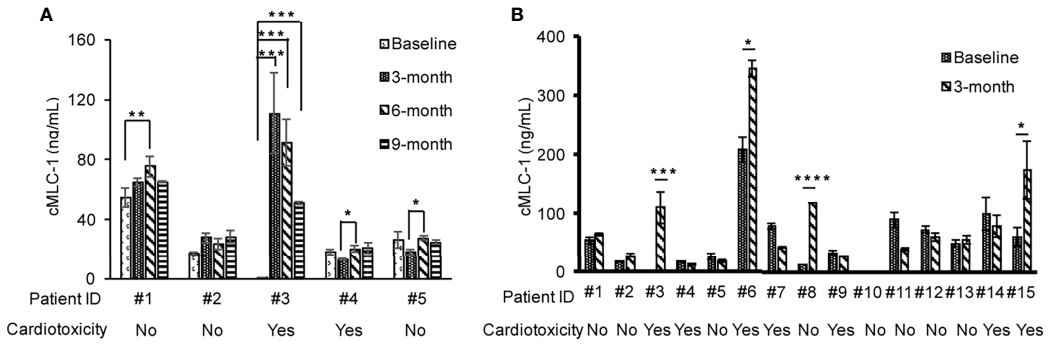

FIGURE 1 | Profile of plasma cMLC-1 levels in trastuzumab-treated breast cancer patients with or without cardiotoxicity. Plasma samples were collected at multiple time points as indicated. Each plasma sample was diluted 1:10 and tested in duplicate to determine cMLC-1 concentration by ELISA. The mean ± SD of cMLC-1 in each sample is shown. Baseline: before trastuzumab treatment; 3, 6 and 9 months: time points after trastuzumab treatment **(A)**. A total of 15 paired-plasma samples collected at before (baseline) and after 3-months trastuzumab treatment were measured for cMLC-1 **(B)**. The mean ± SD of cMLC-1 in each sample is shown. The paired Student -t test was used to analyze the differences. *p<0.05; **p <0.01; ***p <0.005 and ****p <0.001.

trastuzumab treatment) and at 3 months after initiation of trastuzumab treatment. Five of 10 patients in this cohort developed TIC. Therefore, of the combined total of 15 trastuzumab-treated patients, seven developed TIC, eight did not. The 3-month plasma cMLC-1 measurements were significantly higher than baseline in 3 of the 7 TIC patients, #3, #6 and #15 (3/7, 43%) (**Figure 1B**; **Table 2**). However, only one of the 8 non-TIC patients, #8 (1/8, 13%) had a higher cMLC-1 level at 3 months compared to baseline (**Figure 1B**; **Table 2**). Although this difference was noticeable and indicative, but due to the small sample size, our current available data are not conclusive to support an association between elevated cMLC-1 plasma levels and TIC in trastuzumab-treated breast cancer patients. However, the presented data provide a basis suggesting that the possibility of using plasma cMLC-1 as a biomarker for TIC should be further investigated and validated in a larger cohort of patients with and without cardiotoxicity following trastuzumab treatment.

Elevated Plasma cMCL-1 Is Associated With Breast Cancer

There are currently no blood-based biomarkers approved for the detection of breast cancer. In establishing a reliable assay to measure cMLC-1 protein in plasma, we observed that cMLC-1 levels were significantly higher in samples obtained from breast cancer patients (n=20) than from normal donors (n=10). To validate this finding, cMLC-1 levels in plasma samples obtained from additional 59 patients (total n=79) and 36 normal donors (total n=46) were determined. The final results established that the cMLC-1 level was significantly higher in plasma of patients with breast cancer than in normal donors (63.18 ± 55.31 ng/mL *vs.* 37.61 ± 35.39 ng/mL, p=0.0006) (**Figure 2A**). The receiver operator characteristic (ROC) curve analysis of breast cancer ($HER2^-$ and $HER2^+$) *vs*. normal donors determined area under curve (AUC) value of the logistic regression is 0.6791 (p=0.0009). It shows the cutoff cMLC-1 concentration is at 44.99 ng/mL for detecting breast cancer with a sensitivity of 59.49% (95%CI: 48.47%-69.63%) and specificity of 71.74% (95%CI: 57.45% -82.68%) (**Figure 2B**). It is also noteworthy that cMLC-1 did not vary across age or race groups in normal donors (**Figures 2C–E**) or in patients (**Figures 2F, G**; **Table 3**). Collectively, this finding suggests cMLC-1 may be a novel potential biomarker combined with other methods and/or biomarkers for breast cancer screening.

cMCL-1 Plasma Levels in $HER2^-$ and $HER2^+$ BC Patients

Next, we analyzed and compared plasma cMCL-1 to determine if it is a potential biomarker for subtyping breast cancer. Interestingly, it was determined that $HER2^-$ patients (n=39) had a noticeable, but not significant, increase in their cMLC-1 plasma level compared to $HER2^+$ patients (n=40) (73.22 ± 55.88 ng/mL *vs.* 56.67 ± 52.34 ng/mL, p=0.0578) (**Figure 3A**). Compared to normal donors, however, $HER2^-$ patients had a significant 2.0-fold higher level of cMLC-1 (73.22 ± 55.88 ng/mL *vs.* 37.61 ± 35.39 ng/mL, p<0.0001) (**Figure 3B**). As a result, an improved sensitivity of 79.49% (95% CI: 64.47%-89.22%) with the specificity of 63.04% (95%CI:48.60%-75.48%) was for cMLC-1 to predict $HER2^-$ breast cancer with the cutoff at 37.17 ng/mL. In line with this finding, cMLC-1 plasma level in $HER2^+$ patients was noticeable, but not significant, higher compared to that of normal donors (56.67 ± 52.34 ng/mL *vs.* 37.61 ± 35.39 ng/mL, p=0.0549) (**Figure 3C**). ROC curve analysis of $HER2^-$ *vs.* normal donors determined AUC value of the logistic regression is 0.7480 (p<0.0001) (**Figure 3D**). Subsequently, we compared cMLC-1 levels among the 4 major molecular subtypes of BC patients (n=79): Luminal A (estrogen-receptor $(ER)^+$ or progesterone-receptor $(PR)^+$, $HER2^-$, n=35), Luminal B (ER^+ or PR^+, $HER2^+$, n=34), HER2-enriched (ER^-, PR^-, $HER2^+$, n=6) and triple negative breast cancer (TNBC) (ER^-, PR^- and $HER2^-$, n=4) (20, 21). It was found no significant difference among the 4 subtypes (**Figure 3E**). However, we should interpret the results with caution since

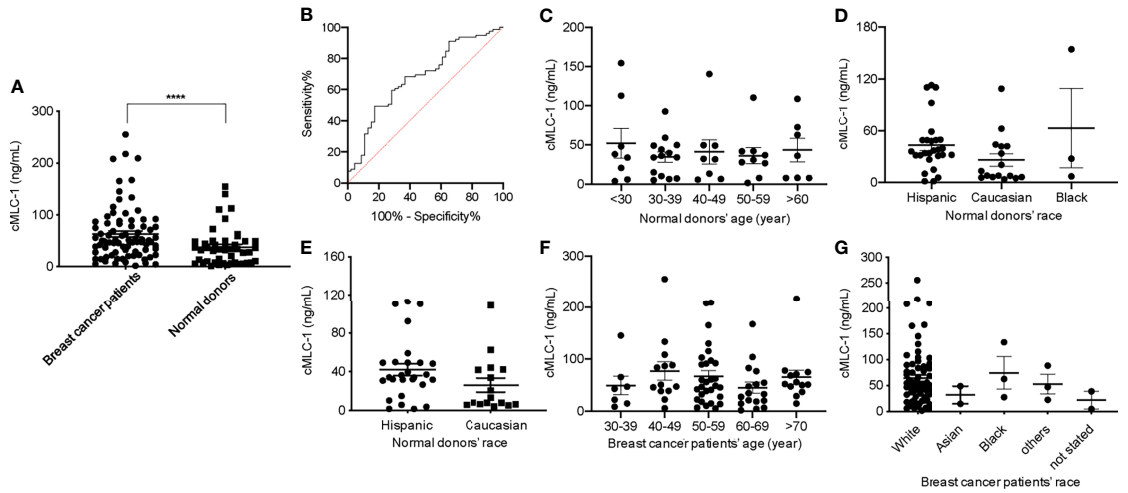

FIGURE 2 | Plasma cMLC-1 level was significantly higher in breast cancer patients than normal healthy women. Each plasma sample was 1:10 diluted and tested twice in duplicate to determine cMLC-1 concentration by ELISA. The mean ± SD of cMLC-1 in breast cancer patients (n=79) *vs.* normal donors (n=46) is shown. The Mann-Whitney U test was used to analyze the difference. ****p=0.0006 **(A)**. The receiver operator characteristic (ROC) graph of the logistic regression result was calculated by GraphPad Prism 8 to determine the relationship between sensitivity and specificity. The cutoff of cMLC-1 at (or higher) 49.55 ng/mL was chosen to reach a sensitivity of 59.49% **(B)**. To determine the impact of age and race factors on cMLC-1 level, plasma samples from all normal donors of different ages and races (n=46) were analyzed and compared. The one-way ANOVA was used for differences among all indicated groups of age (p=0.8630) **(C)** and of race (p=0.138) **(D)**. To ensure the data were accurate, cMLC-1 between "Hispanic" and "Caucasian" were analyzed by the Mann-Whitney U test (p=0.0988) **(E)** without the "black" group given its small size of samples. Plasma samples from all patients of different ages and races (n=79) were analyzed and compared. The one-way ANOVA was used to test differences among all indicated groups of age (p=0.4767) **(F)** and of race (p=0.7079) **(G)**.

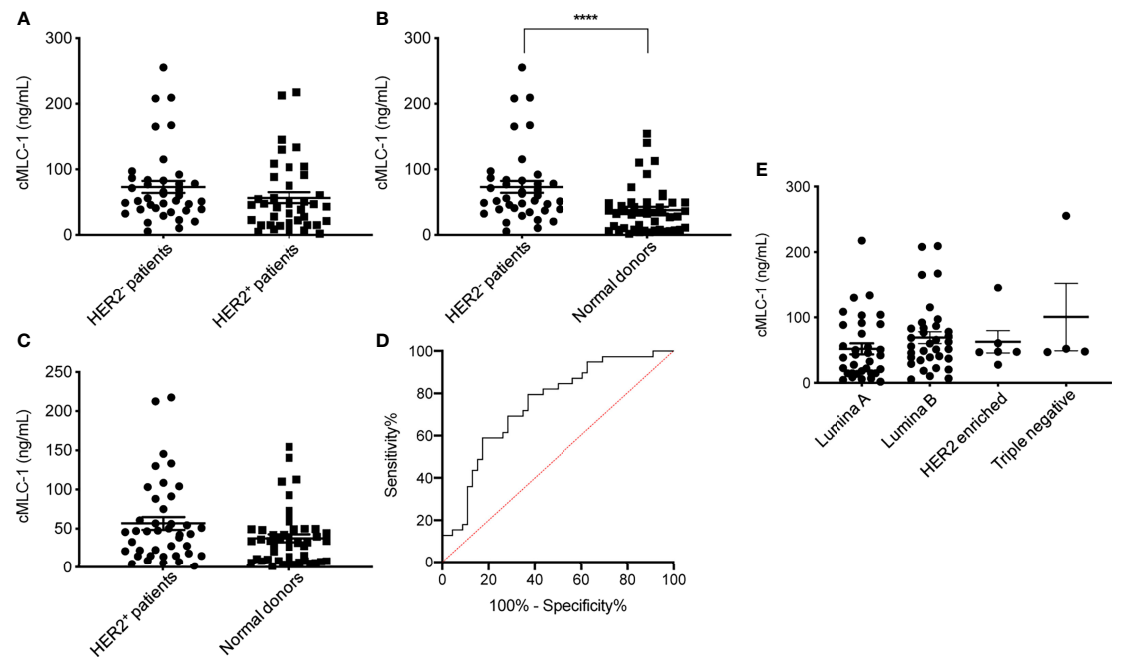

FIGURE 3 | Plasma cMLC-1 levels in HER2$^-$, HER2$^+$ and different molecule subtypes of breast patients. The mean ± SD of cMLC-1 in HER2$^-$ (n=39) *vs.* HER2$^+$ (n=40) is shown (p=0.0578) **(A)**. Plasma cMLC-1 was much higher in HER2$^-$ patients than in normal donors(n=46) (****$p < 0.0001$) **(B)**; plasma cMLC-1 was noticeable but not significantly higher in HER2$^+$ patients than in normal donors (p=0.0549) **(C)**. The Mann-Whitney U test was used to analyze the above differences between every two groups. ROC curve analysis determined area under curve (AUC) value of the logistic regression is 0.7480 (p<0.0001), indicating cMLC-1 at (or higher) the cutoff of 37.17 ng/mL could predict HER2$^-$ breast cancer **(D)**. The means ± SD of cMLC-1 in each subtype of Luminal A (n=35), Luminal B (n=34), HER2 enriched (n=6) and triple negative (n=4) breast cancer patients were analyzed and compared using the one-way ANOVA test (p=0.2864) **(E)**.

the sample sizes in HER2-enriched and TNBC are too small, which reduces the power of the study, to get a conclusive statistical analysis.

Plasma cMCL-1 Is a Potential Biomarker for Breast Cancer Progression

We then wanted to assess if cMCL-1 levels differ in patients with or without metastasis. As shown in **Table 4**, 52 out of 79 patients (65.8%) analyzed had metastatic disease. We found that cMLC-1 level was higher in patients with metastatic breast cancer than in patients with early or locally advanced breast cancer, or non-metastatic breast cancer (75.96 ± 59.85 ng/mL *vs.* 43.41 ± 34.26 ng/mL, p=0.0072) (**Figure 4A**). Although it is highly unlikely, this finding may be somewhat affected by the fact that more metastatic BC patients (30/52, 57.7%) were $HER2^-$ with high cMLC-1 levels, while less metastatic BC patients (22/52, 42.3%) were $HER2^+$ with comparatively lower cMLC-1 levels (**Table 4).** No significant difference was noted in the cMLC-1 plasma level of metastatic (n=30) versus non-metastatic (n=9) $HER2^-$ patients (78.68 ± 60.78 ng/mL *vs.* 54.99 ± 28.54 ng/mL, p=0.3657) (**Figure 4B**), while $HER2^+$ patients with metastatic disease (n=22) had a significantly higher level of cMLC-1 than non-metastatic $HER2^+$ patients (n=18) (72.26 ± 58.37 ng/mL *vs.* 37.62 ± 35.57 ng/mL, p=0.0204) (**Figure 4C**). Our results indicate that the cMLC-1 level may be associated with the progression of disease and may serve as a potential biomarker for metastasis as well as monitoring response to therapy.

Plasma cMCL-1 Level and Additional Clinicopathological Characteristics of Patients

Next, we investigated if cMCL-1 level was associated with additional clinicopathological characteristics collected from patients at the time of diagnosis/treatment. First, plasma cMCL-1 level was compared among 69/79 patients with known histologic grade 1 (n=7), 2 (n=24), 2-3 (n=4) or 3 (n=34), and no difference was found (**Figure 5A**; **Table 4**). Second, plasma cMCL-1 level was compared among cohorts of patients with different histologic types, i.e., ductal (n=61), lobular (n=11), and mixed (n=7), and no difference was found (**Figure 5B**; **Table 4**). Third, plasma cMCL-1 level was compared between known lymph node positive (n=49) *vs.* negative (n=24) cohorts and no difference was found (63.54 ± 52.48 ng/mL *vs.* 53.23 ± 50.64 ng/mL, p=0.3163) (**Figure 5C**; **Table 4**). Lastly, plasma cMCL-1 level was compared between patients with known lymphovascular invasion (LVI) (n=19) *vs.* without LVI (n= 54) and no difference was found (70.08 ± 55.48 ng/mL *vs.* 56.65 ± 50.41 ng/mL, p=0.2730) (**Figure 5D**; **Table 4**).

Plasma cMCL-1 Levels Are Stable at -80°C Over Time

To evaluate the stability of cMLC-1 in archived plasma samples over time, plasma samples kept at -80°C storage for 12, 19 and 24 months were analyzed for this marker. The levels of cMCL-1 were consistent across all time points tested for specimens from a given breast cancer patient or normal donor. Representative data are shown (**Figure 6**), and indicate that cMLC-1 in plasma samples stored at -80°C is stable for at least 2 years. Its long-term stability will facilitate its use as a biomarker and in other clinical studies.

DISCUSSION

The initial results of this research indicated that cMLC-1 plasma levels were elevated with respect to baseline in 4/15 trastuzumab treated breast cancer patients studied. Of these four patients, three did but one did not develop TIC. Due to its small sample size, however, this analysis did not validate cMLC-1 as a biomarker for early detection and prediction of TIC. Consequently, the current

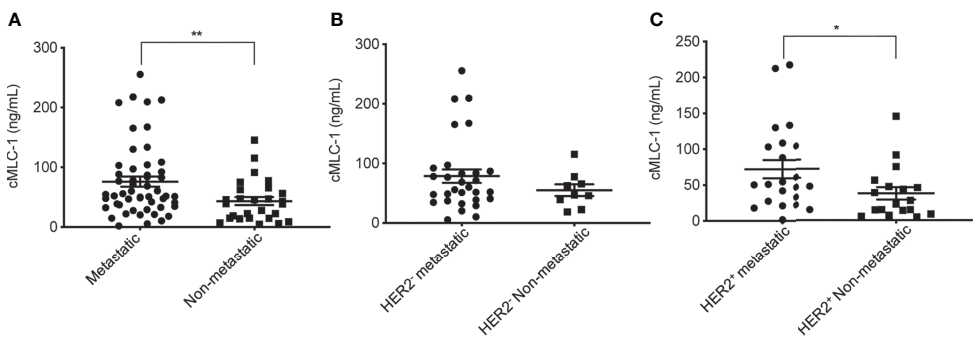

FIGURE 4 | Plasma cMCL-1 was higher in metastatic than non-metastatic breast cancer patients. The means ± SD of cMLC-1 in metastatic (n=52) *vs.* non-metastatic patients (n=27) are shown (**p=0.0069) **(A)**. Plasma cMLC-1 was not significantly different in $HER2^-$ metastatic (n=30) *vs.* non-metastatic patients (n=9) (p=0.3657) **(B)**. Plasma cMLC-1 was higher in $HER2^+$ metastatic (n=22) *vs.* non-metastatic patients (n=18) (*p=0.0204) **(C)**. The Mann-Whitney U test was used to analyze the above differences between every two groups.

data does not support our hypothesis that elevated cMCL-1 plasma levels are indicative of TIC. Nevertheless, our data suggests it is worthy to further test this hypothesis employing a larger cohort of patients to assess its clinical significance. For future studies, sample collection should be timed within the 3 month period (i.e. 1-week, 2-week, 1-, 2- and 3- months post-treatment with trastuzumab) in order to validate cMLC-1 as a biomarker for early detection or prediction of TIC (16, 17). It is also worthy to point out that plasma cMLC-1 may serve as a cardiotoxicity marker but not specifically for TIC based on previous study results (16–18).

To date, the most effective means of early detection and screening for breast cancer involves mammography, a technique that has been approved and widely practiced since the 1980s (22). Though mammography has undoubtedly improved outcomes for women with breast cancer—research estimates at least a 50% mortality reduction since becoming standard practice—this method is imperfect and presents its own challenges (23). Yearly mammograms are recommended starting at age 40, which is often too late for women with some of the more aggressive forms of breast cancer. Additionally, due to the nature of the exam and the frequency at which it is required, attendance rates among women for their yearly mammograms vary, suggesting an additional layer of more accessible screening measures may help close the gap (24). Finally, the false positive rate for mammography is alarmingly high. In the U.S., the 10-year false positive rate is 30%, and 50% of all women will receive a false positive result at some point (24). The ideal solution for breast cancer screening is a blood-based biomarker that can complement or replace the flawed practice of mammography to overcome its shortcomings. A blood test is generally far easier to schedule, better tolerated by patients, and can be integrated into a routine clinical visit. Additionally, a blood test can be justifiably introduced earlier than age 40, as it will be less expensive for payers.

Currently, no blood biomarkers for breast cancer diagnosis or screening have been approved for clinical use. Our data suggest that elevated cMLC-1 (79 patients consisting of ~50% each of $HER2^-$ and $HER2^+$) *vs.* 46 normal donors, p=0,0006) may be a potential candidate as a biomarker for initial and/or combinational screening of women under 40 who are at high risk for breast cancer (**Figure 2**). It is noteworthy that plasma cMCL-1 might be more sensitive in predicting $HER2^-$ breast cancer as cMLC-1 is noticeably but not significantly higher in $HER2^-$ than $HER2^+$ patients (**Figure 3**). However, since cMLC-1 levels are higher in both $HER2^-$ (p<0.0001) and $HER2^+$ patients (p=0.0549) compared to normal donors, although the latter difference did not reach a statistically significant level with the given small sample size, we anticipate that a larger sample size would result in a narrower 95% confidence interval for sensitivity and specificity to predict breast cancer, regardless of HER2 status.

Importantly, plasma cMLC-1 levels are correlated with disease progression; it is higher in metastatic (n=52) than in non-metastatic

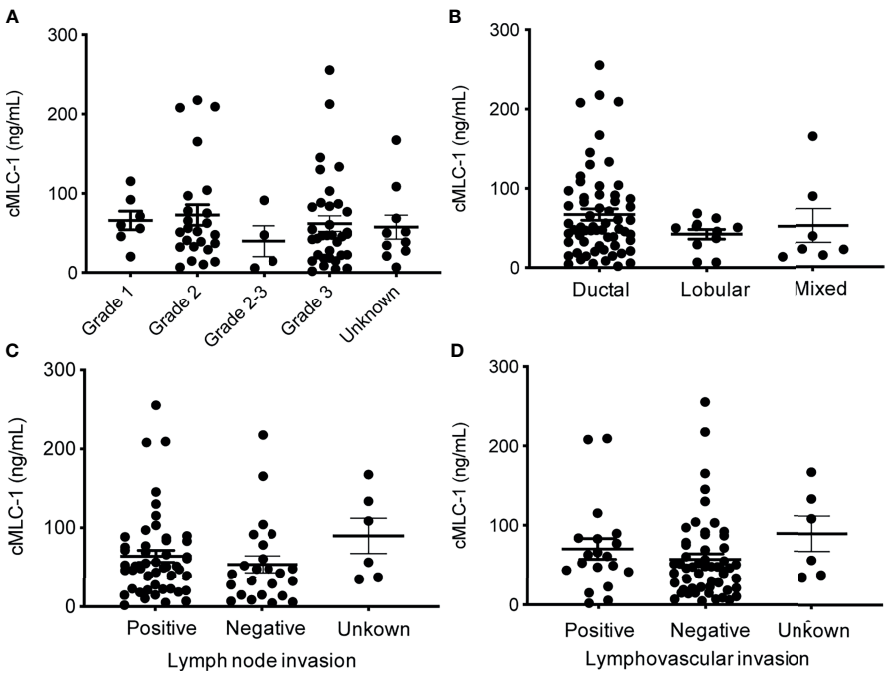

FIGURE 5 | Plasma cMCL-1 levels in breast cancer patient sub-cohorts divided by various clinicopathological features. The means ± SD of plasma cMLC-1 levels in groups of histology grade [Grade 1 (n=7), Grade 2 (n=24), Grade 2-3 (n=4), Grade 3 (n=34), unknown (n=10)] (p=0.8233) **(A)**; in ductal (n=61), lobular (n=11), and mixed histology characters (n=7) (p= 0.3169) **(B)** are shown. The means ± SD of cMLC-1 levels in patients with lymph node (+) (n=49), lymph node (–) (n=24), unknown (n=6) (p=0.3163) **(C)**; and in patients with lymphovascular invasion (+) (n=19), without (–) (n=54), unknown (n=6) (p=0.2730) **(D)** are shown. The one-way ANOVA was used to test differences among all indicated multiple groups.

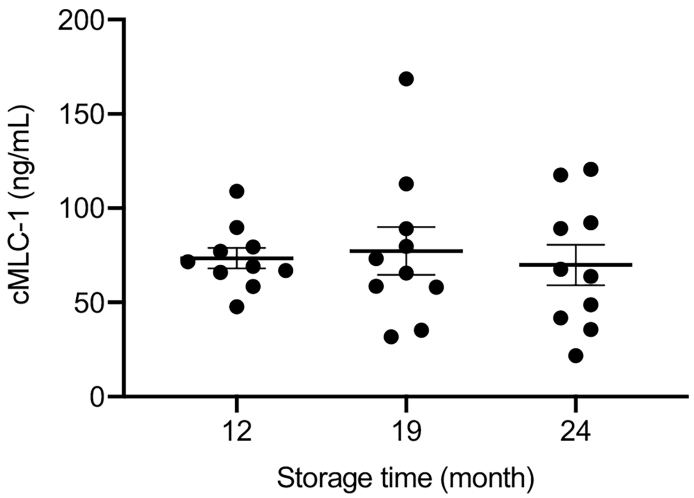

FIGURE 6 | Stability of cMCL-1 in plasma stored at -80°C. Plasma cMLC-1 levels were repeatedly tested in samples from breast cancer patients and normal donors. Representative data using the same set of normal donors samples (n=10) stored at -80°C for 12, 19 and 24 months are shown. The one-way ANOVA was used to test the difference (p=0.8737).

(n=27) breast cancer patients (75.96 ± 59.85 ng/mL *vs.* 43.41 ± 34.26 ng/mL, p=0.0072) (**Figure 4A**). It is also noticeable that a lack of significant difference was found in the cMLC-1 plasma level of metastatic (n=30) versus non-metastatic (n=9) $HER2^-$ patients (p=0.3657) (**Figure 4B**), while a significantly higher level of cMLC-1 was found in metastatic (n=22) than non-metastatic (n=18) $HER2^+$ patients (p=0.0237) (**Figure 4C**). The data on cMCL-1 level in $HER2^-$ patients in relation to metastasis must be explained with caution since the sample size of non-metastatic $HER2^-$ patients is small (n=9). In contrast, the data on cMCL-1 level in $HER2^+$ patients in relation to metastasis seems to be more convincing due to bigger sample sizes from both cohorts used for the statistical analysis. In addition, no association of plasma cMCL-1 was established with either any of the 4 major molecular subtypes of breast cancer or any of the additional clinicopathological characteristics of patients analyzed, including age, race, histologic grade, invasive histologic types, breast cancer spread to lymph node (+ *vs.* -) or LVI (+ *vs.* -) (**Figure 5**). Again, these preliminary data must be interpreted cautiously since the small number of plasma samples from each sub-cohort was examined. This is the limitation of this study. Despite the limitation, our overall data on elevated plasma cMCL-1 found in breast cancer patients vs. normal donors as well as in metastatic vs. non-metastatic breast cancer patients provided valuable information on the first attempt to assess cMCL-1 as a potential biomarker for disease screening and therapy monitoring. The method described here to detect plasma cMLC-1 is fast and easy. Moreover, we demonstrated that plasma cMLC-1 is stable over time after storing in -80°C freezers for at least 2 years (**Figure 6**). We acknowledge that the sample sizes are seemed small for our sub-aim studies between cohorts, i.e., $HER2^-$ (n=39) *vs.* $HER2^+$ (n=40), metastatic (n=52) *vs.* non-metastatic (n=27). However, the aim of these additional analyses was not to identify and validate plasma cMLC-1 as an ultimate biomarker but to explore the potential for a promising biomarker to decide whether an enlarged study is worthwhile to pursue (25). Therefore, besides having presented our statistical analysis-based conclusions, here we provided all detailed information regarding the technical and statistical analysis methods for our colleagues who may have a large number of archived patient samples to validate our study results timely. We believe our initial data as they stand now would serve as a first stepping stone and new idea to facilitate and attract more studies from the research field to evaluate the potential of cMLC-1 as a biomarker for breast cancer screening and disease progression.

CONCLUSION

The results of this investigation provide a sound basis for the novel and exciting further investigation of cMLC-1 as a blood protein biomarker for screening breast cancer, evaluating disease progression, monitoring treatment response and predicting TIC. Furthermore, our study highlights the need to define the mechanisms(s) of how and why plasma cMLC-1 is elevated in breast cancer patients.

DATA AVAILABILITY STATEMENT

The raw data supporting the conclusions of this article will be made available by the authors, without undue reservation.

ETHICS STATEMENT

All studies were approved by the Massachusetts General Hospital Institutional Review Board (IRB protocol 2006P000886) and the Dana Farber/Harvard Cancer Center Institutional Review Board

(IRB protocol 13-416). Patients provided written informed consent for data collection, blood collection, and downstream analysis. The patients/participants provided their written informed consent to participate in this study. Written informed consent was obtained from the individual(s) for the publication of any potentially identifiable images or data included in this article.

AUTHOR CONTRIBUTIONS

XW, WW, SI, and MS-C conceived the study and designed the experiments. LJ, LY, and TS carried out the experiments. RA, AK, CW, KH, and AV collected patient sample collection and provided de-identified patient information. CP and DM supported the patient sample collection. RA, AK, and LJ analyzed and organized patient information. LY, RA, LJ, HZ, and AL analyzed the data. XW, LY, and RA interpreted the data. XW, LY, RA, and HZ wrote the manuscript. All the authors read and approved the submitted manuscript.

FUNDING

This work was supported by grants 1R30FD006290-01 U.S. Food & Drug Administration (XW), R01CA226981-01A1 (XW), the FDA Office of Women's Health Research Science Program Award (Project ID: 750912CDR, WW), China scholarship council (No. 201906995004, LY), Susan G. Komen for the Cure (SCM) and NIH/NHLBI R01HL130539 (SCM).

ACKNOWLEDGMENTS

We are grateful to our patients for their contributions to this research work.

REFERENCES

1. *Cancer Facts & Figures 2021*. Available at: https://www.cancer.org/research/cancer-facts-statistics/all-cancer-facts-figures/cancer-facts-figures-2021.html.
2. Wolff AC, Hammond ME, Hicks DG, Dowsett M, McShane LM, Allison KH, et al. Recommendations for Human Epidermal Growth Factor Receptor 2 Testing in Breast Cancer: American Society of Clinical Oncology/College of American Pathologists Clinical Practice Guideline Update. *J Clin Oncol* (2013) 31(31):3997–4013. doi: 10.1200/JCO.2013.50.9984
3. Denduluri N, Chavez-MacGregor M, Telli ML, Eisen A, Graff SL, Hassett MJ, et al. Selection of Optimal Adjuvant Chemotherapy and Targeted Therapy for Early Breast Cancer: ASCO Clinical Practice Guideline Focused Update. *J Clin Oncol* (2018) 36(23):2433–43. doi: 10.1200/JCO.2018.78.8604
4. Telli ML, Witteles RM. Trastuzumab-Related Cardiac Dysfunction. *J Natl Compr Cancer Netw* (2011) 9(2):243–9. doi: 10.6004/jnccn.2011.0019
5. Bowles EJA, Wellman R, Feigelson HS, Onitilo AA, Freedman AN, Delate T, et al. Risk of Heart Failure in Breast Cancer Patients After Anthracycline and Trastuzumab Treatment: A Retrospective Cohort Study. *J Natl Cancer Inst* (2012) 104(17):1293–305. doi: 10.1093/jnci/djs317
6. DeCara JM. Early Detection of Chemotherapy-Related Left Ventricular Dysfunction. *Curr Cardiol Rep* (2012) 14(3):334–41. doi: 10.1007/s11886-012-0256-z
7. Seidman A, Hudis C, Pierri MK, Shak S, Paton V, Ashby M, et al. Cardiac Dysfunction in the Trastuzumab Clinical Trials Experience. *J Clin Oncol* (2002) 20(5):1215–21. doi: 10.1200/JCO.2002.20.5.1215
8. Sawaya H, Sebag IA, Plana JC, Januzzi JL, Ky B, Cohen V, et al. Early Detection and Prediction of Cardiotoxicity in Chemotherapy-Treated Patients. *Am J Cardiol* (2011) 107(9):1375–80. doi: 10.1016/j.amjcard.2011.01.006
9. Onitilo AA, Engel JM, Stankowski RV, Liang H, Berg RL, Doi SA. High-Sensitivity C-Reactive Protein (Hs-CRP) as a Biomarker for Trastuzumab-Induced Cardiotoxicity in HER2-Positive Early-Stage Breast Cancer: A Pilot Study. *Breast Cancer Res Treat* (2012) 134(1):291–8. doi: 10.1007/s10549-012-2039-z
10. Zardavas D, Suter TM, Van Veldhuisen DJ, Steinseifer J, Noe J, Lauer S, et al. Role of Troponins I and T and N-Terminal Prohormone of Brain Natriuretic Peptide in Monitoring Cardiac Safety of Patients With Early-Stage Human Epidermal Growth Factor Receptor 2-Positive Breast Cancer Receiving Trastuzumab: A Herceptin Adjuvant Study Cardiac Marker Substudy. *J Clin Oncol* (2017) 35(8):878–84. doi: 10.1200/JCO.2015.65.7916
11. ElZarrad MK, Mukhopadhyay P, Mohan N, Hao E, Dokmanovic M, Hirsch DS, et al. Trastuzumab Alters the Expression of Genes Essential for Cardiac Function and Induces Ultrastructural Changes of Cardiomyocytes in Mice. *PloS One* (2013) 8(11):e79543. doi: 10.1371/journal.pone.0079543
12. Shi Q, Li RK, Mickle DA, Jackowski G. Analysis of the Upstream Regulatory Region of Human Ventricular Myosin Light Chain 1 Gene. *J Mol Cell Cardiol* (1992) 24(11):1221–9. doi: 10.1016/0022-2828(92)93089-3
13. Stejskal D, Lacnak B, Andelova K, Skvarilova M, Bartek J. MCL-1 (Myosin Light Chains-1) in Differential Diagnosis of Dyspnea. *BioMed Pap Med Fac Univ Palacky Olomouc Czech Repub* (2005) 149(1):89–91. doi: 10.5507/bp.2005.010
14. Hansen MS, Stanton EB, Gawad Y, Packer M, Pitt B, Swedberg K, et al. Relation of Circulating Cardiac Myosin Light Chain 1 Isoform in Stable Severe Congestive Heart Failure to Survival and Treatment With Flosequinan. *Am J Cardiol* (2002) 90(9):969–73. doi: 10.1016/S0002-9149(02)02663-2
15. Goto T, Takase H, Toriyama T, Sugiura T, Sato K, Ueda R, et al. Circulating Concentrations of Cardiac Proteins Indicate the Severity of Congestive Heart Failure. *Heart* (2003) 89(11):1303–7. doi: 10.1136/heart.89.11.1303
16. Katus HA, Yasuda T, Gold HK, Leinbach RC, Strauss HW, Waksmonski C, et al. Diagnosis of Acute Myocardial Infarction by Detection of Circulating Cardiac Myosin Light Chains. *Am J Cardiol* (1984) 54(8):964–70. doi: 10.1016/S0002-9149(84)80126-5
17. Mair J, Thome-Kromer B, Wagner I, Lechleitner P, Dienstl F, Puschendorf B, et al. Concentration Time Courses of Troponin and Myosin Subunits After Acute Myocardial Infarction. *Coron Artery Dis* (1994) 5(10):865–72.
18. Isobe M, Nagai R, Ueda S, Tsuchimochi H, Nakaoka H, Takaku F, et al. Quantitative Relationship Between Left Ventricular Function and Serum Cardiac Myosin Light Chain I Levels After Coronary Reperfusion in Patients With Acute Myocardial Infarction. *Circulation* (1987) 76(6):1251–61. doi: 10.1161/01.CIR.76.6.1251
19. Wolff AC, Hammond MEH, Allison KH, Harvey BE, Mangu PB, Bartlett JMS, et al. Human Epidermal Growth Factor Receptor 2 Testing in Breast Cancer: American Society of Clinical Oncology/College of American Pathologists Clinical Practice Guideline Focused Update. *J Clin Oncol* (2018) 36 (20):2105–22. doi: 10.1200/JCO.2018.77.8738
20. Tang P, Tse GM. Immunohistochemical Surrogates for Molecular Classification of Breast Carcinoma: A 2015 Update. *Arch Pathol Lab Med* (2016) 140(8):806–14. doi: 10.5858/arpa.2015-0133-RA
21. Vuong D, Simpson PT, Green B, Cummings MC, Lakhani SR. Molecular Classification of Breast Cancer. *Virchows Arch* (2014) 465(1):1–14. doi: 10.1007/s00428-014-1593-7
22. Coleman C. Early Detection and Screening for Breast Cancer. *Semin Oncol Nurs* (2017) 33(2):141–55. doi: 10.1016/j.soncn.2017.02.009
23. Cady B, Michaelson JS. The Life-Sparing Potential of Mammographic Screening. *Cancer* (2001) 91(9):1699–703. doi: 10.1002/1097-0142(20010501)91:9<1699::AID-CNCR1186>3.0.CO;2-W
24. Loberg M, Lousdal ML, Bretthauer M, Kalager M. Benefits and Harms of Mammography Screening. *Breast Cancer Res* (2015) 17:63. doi: 10.1186/s13058-015-0525-z

25. Al-Mekhlafi A, Becker T, Klawonn F. Sample Size and Performance Estimation for Biomarker Combinations Based on Pilot Studies With Small Sample Sizes. *Commun Stat - Theor M* (2020) 49:1–15. doi: 10.1080/03610926.2020.1843053

Conflict of Interest: The authors declare that the research was conducted in the absence of any commercial or financial relationships that could be construed as a potential conflict of interest.

Publisher's Note: All claims expressed in this article are solely those of the authors and do not necessarily represent those of their affiliated organizations, or those of the publisher, the editors and the reviewers. Any product that may be evaluated in this article, or claim that may be made by its manufacturer, is not guaranteed or endorsed by the publisher.

frontiers | Frontiers in Oncology

ORIGINAL RESEARCH
published: 30 June 2022
doi: 10.3389/fonc.2022.804868

The NFAT3/RERG Complex in Luminal Breast Cancers Is Required to Inhibit Cell Invasion and May Be Correlated With an Absence of Axillary Lymph Nodes Colonization

Lucie Coillard[1], *Frédéric Guaddachi*[1], *Maëlle Ralu*[1], *Eva Brabencova*[2], *Christian Garbar*[2], *Armand Bensussan*[1], *Morgane Le Bras*[1], *Jacqueline Lehmann-Che*[1,3] *and Sébastien Jauliac*[1]*

[1] Université de Paris, Research Saint Louis Institute (IRSL), Institut National de la Santé et de la Recherche Médicale, Human Immunology Pathophysiology Immunotherapy (INSERM HIPI) U976, Paris, France, [2] Department of Biopathology, Centre Régional de Lutte Contre le Cancer, Institut Godinot, Reims, France, [3] Molecular Oncology Unit, Assistance Publique-Hôpitaux de Paris (AP-HP), Hôpital Saint Louis, Paris, France

Luminal breast cancers represent 70% of newly diagnosed breast cancers per annum and have a relatively good prognosis compared with triple-negative breast cancers. Luminal tumors that are responsive to hormonal therapy are particularly associated with a favorable prognosis. Nonetheless, the absolute number of metastatic relapses in luminal cancers is larger than in triple-negative breast cancers. A better understanding of the biology of luminal cancers, control of metastases formation, and identification of predictive markers of their evolution are therefore still necessary. In this context, we previously disclosed the key role of NFAT3 in regulating luminal breast cancer invasion. We have now identified a specific inhibitory region, in the C-terminal part of NFAT3, required for the inhibition of invasion of the human luminal breast cancer cell line T-47D. Indeed, we showed that this 85 amino acid C-terminal region acts as a dominant negative form of NFAT3 and that its overexpression in the T-47D cell line led to increased cell invasion. Mechanistically, we have revealed that this region of NFAT3 interacts with the small Ras GTPase RERG (RAS like estrogen regulated growth inhibitor) and shown that RERG expression is required for NFAT3 to impede T-47D cell invasion. We have validated the association of NFAT3 with RERG in human luminal breast cancer tissues. We have shown an increase of the quantity of the NFAT3/RERG complexes in patients without axillary lymph node colonization and therefore proposed that the detection of this complex may be a non-invasive marker of axillary lymph node colonization.

Keywords: breast cancer, NFAT3/c4, RERG, invasion, lymph nodes metastasis

OPEN ACCESS

Edited by:
San-Gang Wu,
First Affiliated Hospital of Xiamen University, China

Reviewed by:
Juan Zhou,
Xiamen University, China
Jun Wang,
Sichuan University, China

***Correspondence:**
Sébastien Jauliac
sebastien.jauliac@inserm.fr

Specialty section:
This article was submitted to Breast Cancer, a section of the journal Frontiers in Oncology

Received: *29 October 2021*
Accepted: *25 May 2022*
Published: *30 June 2022*

Citation:
Coillard L, Guaddachi F, Ralu M, Brabencova E, Garbar C, Bensussan A, Le Bras M, Lehmann-Che J and Jauliac S (2022) The NFAT3/RERG Complex in Luminal Breast Cancers Is Required to Inhibit Cell Invasion and May Be Correlated With an Absence of Axillary Lymph Node Colonization. Front. Oncol. 12:804868. doi: 10.3389/fonc.2022.804868

INTRODUCTION

Breast cancer is still a major cause of cancer-related death in women. This morbidity often relies on the potency of the breast tumors to develop distant metastases. One of the characteristics of breast cancers is their high molecular heterogeneity (1) where classically, the triple-negative subtype has a worse prognosis compared to the luminal one. This poor prognosis is directly related to the high rate of metastases formation in triple-negative tumors. However, even if the luminal subtype has a relatively good prognosis, it is the most frequently diagnosed and represents a proportion of 70% of all identified breast cancers. Because of this overrepresentation, the absolute number of metastatic relapses in luminal cancers is larger than in triple-negative breast cancers. Indeed, as recently shown by Maaren et al. (2), in ten-year recurrences, the number of patients with metastases represents 10% of the luminal subtype whereas this number falls to 4% for the other subtypes. There is therefore a real need for predictive tools to distinguish between luminal tumors that will be more susceptible to metastasize and those that will not metastasize. These predictive tools associated with other clinicopathological parameters would be valuable assets for decisions concerning optimal treatment. Moreover, elucidating the mechanisms of action of pro- or anti-metastatic factors expressed in different breast cancer subtypes would be a useful approach to potentially identify new targetable pro- or anti-oncogenic pathways.

In this context, our group identified that the isotypes of the NFAT transcription factors family are differentially expressed between breast cancer subtypes and have opposite effects on metastatic dissemination. Indeed, NFAT1 (NFATc2) exerts a pro-invasive function and is mainly expressed in the triple-negative subtype, whereas NFAT3 (NFATc4) has anti-invasive properties, limiting the aggressiveness of primary NFAT3-expressing luminal breast cancer cells (3–6). Additionally, we recently showed that NFAT3-expressing cells can produce anti-tumoral and anti-metastatic NFAT3-directed extracellular vesicles (7). Considering the high amino acid sequence homology between NFAT1 and NFAT3, it is puzzling that these two isotypes have clearly opposed effects on tumor growth and metastasis formation. Unraveling the origins and molecular mechanisms of their antagonistic functions in breast cancer could be a key contribution to better understand their respective roles in tumor progression. The most obvious reason for these specific functions may rely upon their abilities to interact with specific protein partners. Indeed, many NFAT protein partners with a direct role on isotype function have been reported (8–11). Apart from their specific functions in breast cancer, the differential expression of NFAT1 in the triple-negative subtype and of NFAT3 in luminal cancers opens the possibility that these factors may be potential prognostic markers with NFAT3 protein expression for tumors that will not generate distant metastasis.

Among these putative prognostic markers, RERG (12), a growth-inhibitory gene highly expressed in luminal breast cancer, was correlated with the estrogen-regulated longest survival of luminal breast cancer patients (13) without metastases.

Here, we report that NFAT3 specifically interacts, at least *via* its last 85 C-terminal amino acids, with RERG in the luminal breast cancer cell line T-47D. This interaction is functional and is required for NFAT3 to inhibit the invasion of this breast cancer luminal cell line. We confirmed the presence of this association in luminal breast cancer tissues from patients. Finally, we report that tumors with axillary lymph nodes (ALN) colonization (N+) had fewer detectable NFAT3/RERG complexes compared to those without ALN infiltration (N0). Together these results provide new insights in the anti-tumoral effects of NFAT3 and its association with RERG and also highlight the potential value of the detection of the NFAT3/RERG association in luminal breast tumor patients as an indicator of the ALN status.

MATERIALS AND METHODS

Cell Lines

T-47D and NIH3T3 cell lines were obtained from the ATCC. All cell lines were validated as mycoplasma negatives by PCR and grown in an Roswell Park Memorial Institute medium (RPMI) 1640 medium (T-47D) plus 10% fetal bovine serum (PAN BIOTECH) or in high-glucose (4.5 g/L) Dulbecco's Modified Eagle Medium (DMEM) (NIH3T3) plus 10% newborn calf serum (PAN BIOTECH) and were maintained in a 5% CO_2 incubator at 37°C.

Antibodies and Reagents

Antibodies used in the study were α-HA (Roche Cat# 11867423001, RRID: AB_390918), α-NFAT3 [(Sigma-Aldrich Cat# HPA031641, RRID: AB_10600826), for Proximity Ligation Assay (PLA)], α-RERG (Sigma-Aldrich Cat# SAB1403408, RRID: AB_10737054, for PLA), α-pan cytokeratin (Sigma-Aldrich Cat# F3418, RRID: AB_259536); α-actin (Thermo Fisher Scientific Cat# MA5-15739, RRID: AB_10979409), α-NFAT3 (Thermo Fisher Scientific Cat# PA1-021, RRID: AB_2267268, for Western blot); α-RERG (Proteintech Cat# 10687-1-AP, RRID: AB_2253772, for Western blot); α-HA (Abcam Cat# ab18181, RRID: AB_444303, For PLA). ReadyTector α-Mouse-HorseRadish Peroxidase (HRP) #720 500 and α-Rabbit-HRP #730 500 were from Candor. Lipofectamine 2000 #11668019 from Thermofisher Scientific; Dharmafect 1 #T-2001-03 and siNFAT3 #D-009584-07, siRERG #L-0082004; siCtl #D-001810-10 and # D-001210-01 were from Horizon.

Plasmids and Generation of NFAT3 Expression Constructs

All the deletion mutants generated by PCR were cloned into the pcDNA3.1 (+) vector with the Hemagglutinin (HA) epitope for NFAT3, NFAT3-85C, ΔNFAT3, ΔNFAT3-85c, and NFAT3-Cter and verified by sequencing. The plasmid pCS2-(n)-β-galactosidase has been described previously (3). The pTRIP plasmid was provided to us by P. Charneaux (Institut Pasteur, Paris, France), the ReMTH plasmids by Sonyang Z. (Sun Yat-sen University, Canton, China) the Venus construct by A. Miyawaki (Riken, Tokyo, Japan), and RERG expression vector by C.M. Perou (University of North Carolina, Chapel Hill, North Carolina, USA).

Western Blot

Whole cell lysates were obtained by boiling $0.5.10^6$ cells in the reducing Laemmli sample buffer. The lysates were resolved by SDS-PAGE and probed with α-NFAT3 #PA1-021,1:1,000 diluted in ReadyTector α-Rabbit-HRP; α-actin, 1:2,500 in ReadyTector α-Mouse-HRP; α-RERG, 1:1,000 in ReadyTector α-Rabbit-HRP. Revelation with α-HA was followed by incubation with Goat α-Rat IgG secondary antibody at room temperature. All primary incubations were performed overnight at 4°C.

Retrovirus-Based Complementation Assay

The RePCA screen was carried out as described previously (14) with the T-47D cell line infected with the lentivirus pTRIP stably expressing the fusion of the N-terminal part of Venus fused to the C-terminal part of NFAT3 (VNN-N3Cter) infected with the ReMTH-VC (retrovirus-based molecular) retrovirus containing the C-terminal part of Venus upstream of a splice donor site in the 3 open reading frames. The infected cells were selected by treatment with puromycin, and the fluorescent ones were sorted individually by Fluorescence Activated Cell Sorter (FACS). Total RNA from sorted cells was extracted with TRIzol (Ambion, Austin, Texas, USA). Reverse transcription was performed with the Superscript II kit (Life Technologies, Eugene, Oregon, USA) and random primers containing the T7 tag (5′-TAATACGACTCACTATAGGGNNNNNNN-3′). The complementary DNA (cDNA) was amplified by PCR with a primer hybridizing to the C-terminal part of Venus (5'-CCACTACCTGAGCTACCAGTCC-3') and a T7 primer (5'-GCGCTAATACGACTCACTATAGGG-3'). The PCR products were gel purified and sequenced and identified by Basic Local Alignment Search Tool (BLAST).

Invasion Assays, Immunofluorescence, and Proximity Ligation Assay

Invasion assays were performed essentially as previously described (5). For immunofluorescence and PLA, cells were grown on coverslips in 24-well plates and transfected with the relevant siRNA or plasmids. Approximately 48 h after transfection, cells were labeled for PLA. Slides were fixed in 4% paraformaldehyde for 15 min, washed 3 times in PBS 100 mM glycine, and permeabilized for 10 min in PBS Triton 0.2%. Saturation for non-specific binding was carried out in the blocking buffer [PBS, 5% Bovine Albumin Serum (BSA)] for 45 min at room temperature. Then, the slides were incubated with α-NFAT3 (1:200) and α-RERG, (1:50) or α-HA (# ab18181, 1:500) in the blocking buffer overnight at 4°C. The following day, slides were washed and incubated with the Plus and Minus probes of the Duolink kit (#DUO92101, Sigma-Aldrich) diluted in the blocking buffer. The kit was used as indicated by the manufacturer. The same protocol was followed for the frozen tissues following addition, after the last washes of the Duolink reaction, of an α-pan cytokeratin coupled to Fluorescein IsoThioCyanate (FITC) (1:100) in the blocking buffer overnight at 4°C. The α-pan cytokeratin allowed us to identify the breast epithelial carcinoma cells. The following day, slides were washed and mounted with a Fluoromount G medium (SouthernBiotech, Homewood, Alabama, USA).

Microscope Image Acquisition

Cell lines: Fluorescence images were captured using a Microscope Axio Imager.D2 equipped with a Plan Apochromat 63X N.A.1.4 oil immersion objective: room temperature with an AxioCamMR3 and the Axiovision acquisition software.

Tissues: Fluorescence images were acquired by confocal microscopy on a Zeiss LSM 800 confocal laser microscope (Zeiss) using a Plan Apochromat 63X N.A.1.4 oil immersion objective using the ZEN software (Zeiss). For both cell lines and tissues, both the control and the sample images were acquired using the same settings. The settings of acquisition were optimized to avoid the saturation of signals. PLA dots were counted using the particle analysis function of ImageJ for both cell lines and tissues. For the cell lines, the number of nuclei were counted manually and the PLA index was obtained by dividing the number of PLA dots by the number of the nuclei. For tissues, in order to minimize bias, as the coalescence of the nuclear signal prevented accurate counting of the nuclei in cytokeratin-positive cells, we manually measured with ImageJ the DAPI-positive surface of the cytokeratin-positive cells. Consequently, the index of PLA for the tissues was obtained by dividing the number of PLA dots by the surface of the nuclei of cytokeratin-positive cells.

Human Luminal Breast Cancer Tissues

All the tissue ER+ samples (N+ and N0) had been flash-frozen between 2011 to 2014 and were stored at -80°C. Frozen tissue specimens were collected from the Biobank of the biopathology department of Godinot Institute, Reims, France, for 21 luminal breast cancer patients with ALN colonization [n=10: 2014 (2), 2013 (4), 2012 (1), 2011 (3)] or without [n=11: 2014 (2), 2013 (4), 2012 (3), 2011 (2)]. We included all available ER+ breast primary tumor tissues without selection. All patients gave informed written consent. The research was approved by the Ethics Committee of Saint Louis Hospital and the Godinot Institute.

Statistical Analysis

The error bars in the graphical data represent the means ± SEM. When relevant, p-values were obtained by an unpaired, two-tailed Student's t-test using GraphPad Prism software (GraphPad Software Inc., La Jolla, CA, USA).

RESULTS

The Last 85 C-Terminal Amino Acids of NFAT3 Are Required to Inhibit Cell Invasion

NFAT1 and NFAT3 amino acid sequences are highly homologous in the central region containing the NHR and the RHR domains, while they show an isotype specificity in the first 100 N-terminal and the last 200 C-terminal amino acids (**Figure 1A**). We thus hypothesized that the specific function of the pro-invasive (NFAT1) (3, 5, 6) or anti-invasive (NFAT3) (4, 7) capacity could be linked to these unique regions. We chose to specifically focus on the NFAT3 anti-invasive capacity as we have already shown that deleting its first 374 amino acids to

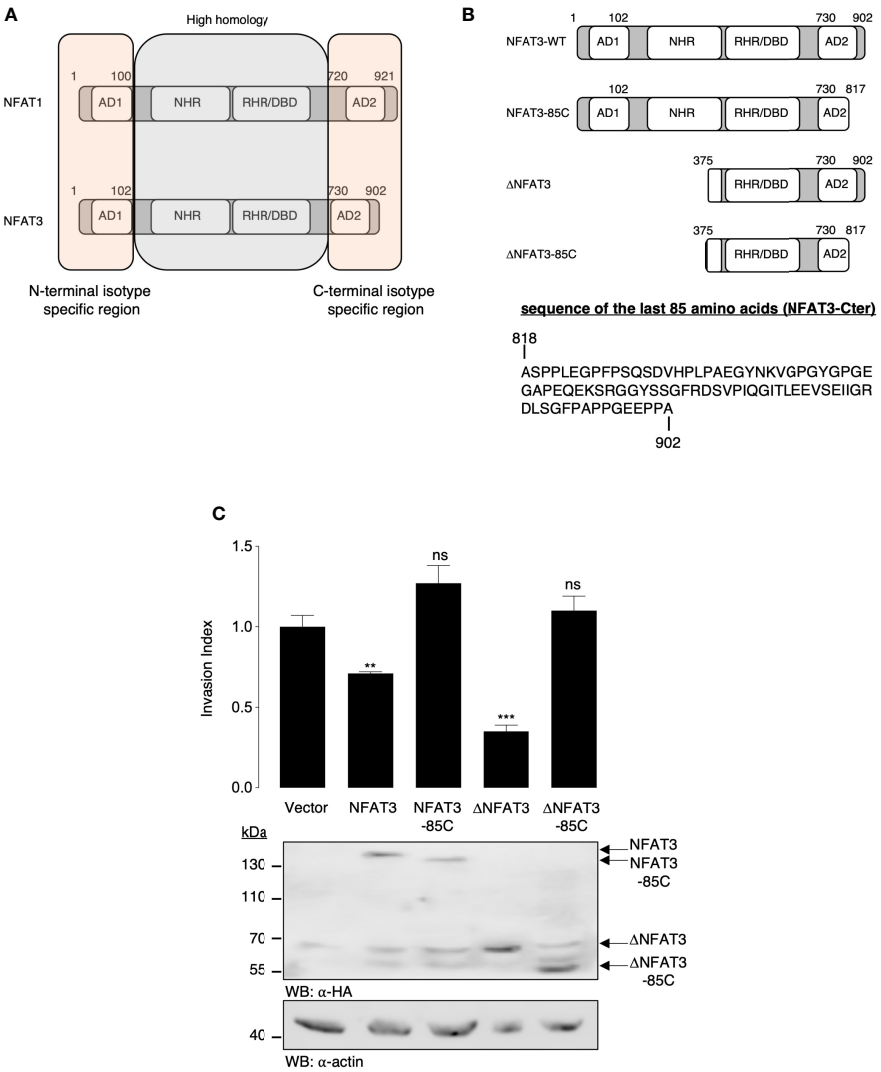

FIGURE 1 | The last 85 C-terminal amino acids of NFAT3 are required for the inhibition of cell invasion. **(A)** Schematic representation of the homologous and isotype-specific regions of human NFAT1 and NFAT3 with the activation domains (ADs), the NFAT homology domain (NHR), the Rel homology domain (RHR), and the DNA-binding domain (DBD). **(B)** Schematic representation of the NFAT3, NFAT3-85C, ΔNFAT3, and ΔNFAT3-85C constructs used in the study and the sequence of the last 85 amino acids of NFAT3 (NFAT3-Cter). **(C)** T-47D cells were transiently transfected with either a vector encoding the HA epitope fused to NFAT3, NFAT3-85C, ΔNFAT3, or ΔNFAT3-85C or with the empty vector (Vector). The following day, transfected cells were subjected to an *in vitro* invasion assay for 24 h. All data are shown as the mean of two independent experiments ± SEM (n=2 biological replicates; 3 technical replicates for each experiment, **p<0.005, ***p< 0.0001, ns, non specific relative to the vector-transfected cells). Whole cell lysates were revealed by α-HA and normalized by revelation with an α-actin.

generate the ΔNFAT3 deletion mutant did not prevent its anti-invasive function (4). Accordingly, we suggested that the anti-invasive activity of NFAT3 might rely on its C-terminal region. To validate this hypothesis, we generated C-terminal truncated NFAT3 and ΔNFAT3 mutants (**Figure 1B**) and determined that the last 85 C-terminal amino acids were required for both NFAT3- and ΔNFAT3-inhibited cell invasion as shown in **Figure 1C**. We did not identify any specific domains in the NFAT3-Cter. The last 85 C-terminal amino acids, lacking specific functional domains, were referred to as NFAT3-Cter for the rest of the study.

Overexpression of NFAT3-Cter Is Sufficient to Increase Breast Cancer Cell Invasion

To elucidate the mechanisms underlying the requirement for the inhibitory NFAT3-Cter region (NFAT3-Cter), we overexpressed this region in T-47D cells and evaluated their invasive capacity. The overexpression of the NFAT3-Cter did not inhibit breast cancer cell invasion but significantly increased it compared to the cells transfected with the empty vector (**Figure 2A**). We then hypothesized that the overexpressed NFAT3-Cter region could have a dominant negative effect on the endogenous NFAT3.

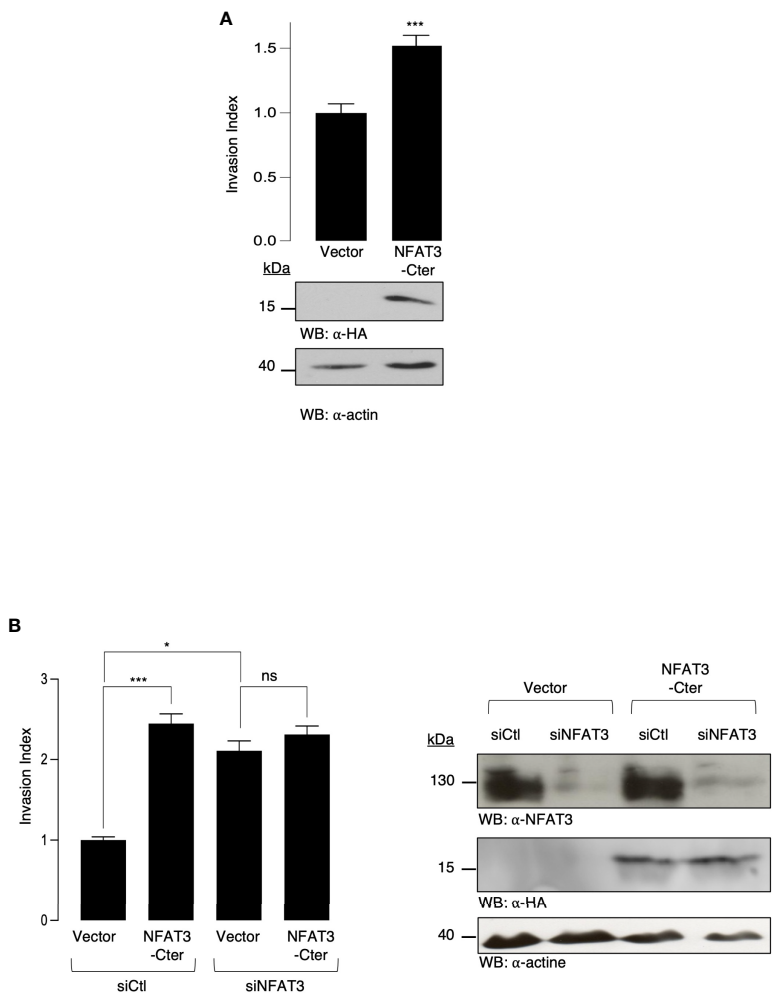

FIGURE 2 | NFAT3-Cter acts as a dominant negative form of endogenous NFAT3. **(A)** T-47D cells were transiently transfected with either a vector encoding the HA epitope fused to NFAT3-Cter or with the empty vector (Vector). The following day, transfected cells were subjected to an *in vitro* invasion assay for 24 h. All data are shown as the mean of three independent experiments ± SEM (n=3 biological replicates; 3 technical replicates for each experiment; *p<0.005). Whole cell lysates were revealed by α-HA and normalized by revelation with α-actin. **(B)** T-47D cells were transiently cotransfected with either an siRNA control (siCtl) or an siRNA targeting the endogenous NFAT3 (siNFAT3) in combination with either a vector encoding the HA epitope fused to NFAT3-Cter or with the empty vector (Vector). Approximately 48 h later, transfected cells were subjected to an *in vitro* invasion assay for 24 h. The mean of three independent experiments ± SEM is shown (n=3 biological replicates; 3 technical replicates for each experiment; *p<0,05, ***p<0,001, ns, non-specific). Whole cell lysates were revealed by α-HA and α-NFAT3 and normalized by revelation with α-actin.

Indeed, the results presented in **Figure 2B** indicate that the depletion of the endogenous NFAT3 protein by a specific siRNA prevented the increased invasion induced by the NFAT3-Cter region. Altogether, these results suggested that the pro-invasive function of the NFAT3-Cter region behaved as a dominant negative form of NFAT3.

Identification of RERG as an NFAT3-Cter Interacting Protein

Dominant negative constructs generally act on endogenous proteins by modulating their association with other factors. Therefore, we hypothesized that the overexpression of NFAT3-Cter reduced available inhibitory co-factors, required to impede cell invasion, and are usually associated with the endogenous NFAT3 C-terminal region. To identify these cofactors, we performed a retrovirus-based complementation assay (RePCA) screen as described by Ding et al. (14). The bait was the NFAT3-Cter region fused to the N-terminal half of the Green Fluorescent Protein (GFP). T-47D cells were stably infected by a lentivirus containing this bait. The resulting stable clones were then infected with a retrovirus carrying a vector containing the half C-terminal of the GFP cloned upstream of a splice donor site (prey). The resulting green cells indicated that the NFAT3-Cter region interacted with the prey. GFP-positive cells were sorted, and genomic DNA was extracted and sequenced. BLAST analysis was performed to identify interacting proteins. Among the

different proteins, we identified a fusion of the GFP C-terminal half with the second exon of RERG (data not shown). We chose to focus on the association of RERG with NFAT3 because previous studies have associated RERG expression with better survival in luminal breast cancer patients (13) and revealed its capacity to inhibit cell invasion (15). To confirm the potential association of the endogenous NFAT3 and RERG in T-47D cells, we performed PLA assays after the downregulation of either NFAT3 or RERG, using specific siRNAs. Both siRNAs against NFAT3 and RERG were competent to reduce protein expression compared with a control siRNA (**Figure 3A**, left panel). In cells transfected with a control siRNA, we observed red dots, indicating the association of NFAT3 with RERG (**Figure 3A**, (a) and index PLA). This signal was reduced in cells transfected with either the NFAT3 or the RERG siRNA (**Figure 3A**, (b, c) and index PLA), underlining the specificity of this association. Moreover, we showed that the deletion of the NFAT3-Cter region was insufficient to prevent NFAT3 association with endogenous RERG (**Figure 3B**, (c) and index PLA). These results indicate that NFAT3 and RERG are associated in T-47D cells, with NFAT3-Cter being dispensable for this association. This suggests that other regions of NFAT3 may participate with the NFAT3-Cter region in this association.

NFAT3 Requires RERG to Suppress Breast Cancer Cell Invasion

As previously reported in other models (16, 17), we confirmed that the overexpression of RERG inhibits cell invasion (**Figure 3C**) and that the siRNA-mediated downregulation of RERG enhanced the invasion **(Figure 3D)**. To determine the functional role of RERG binding to the last 85 amino acids of NFAT3, we tested whether NFAT3 was dependent on RERG to inhibit cell invasion. To do so, we cotransfected T-47D cells with either a control siRNA (siCtl) or an RERG siRNA (siRERG) along with either a control empty vector (Vector) or the active deletion mutant of NFAT3 (ΔNFAT3). The results presented in **Figure 3E** show that ΔNFAT3 was no longer able to inhibit breast cancer cell invasion when endogenous RERG was downregulated. These results, alongside those obtained from the PLA experiments, demonstrate that the presence of RERG and its association with NFAT3 *via* the Cter region is mandatory for NFAT3 to impede breast cancer cell invasion. This revealed the functional association between NFAT3 and RERG in the T-47D luminal breast cancer cell line.

NFAT3/RERG Interaction Is Increased in Luminal Breast Cancer Tissues and Correlated With the Absence of Axillary Lymph Node Colonization

We further validated the NFAT3 interaction with RERG by PLA assays (**Figure 4A**) in luminal breast cancer tissues (**Figure 4C**) obtained from patients with (10 patients) or without (11 patients) distant ALN metastases at diagnosis. This association was present in almost all the luminal breast cancer tissues tested so far, at different levels, independently of the N0 or N+ status of the patients (data not shown). Remarkably, the number of NFAT3/RERG complexes was statistically increased in tissues from patients with no ALN colonization (N0) compared with patients with ALN colonization (N+) (**Figures 4A, B**). These results suggest that the detection of NFAT3/RERG complex may constitute a new prognostic marker of the absence of ALN colonization.

DISCUSSION

The recurrence of luminal breast cancer subtypes generally occurs later than the recurrence of triple- negative cancers. This therapeutic situation underlines the urgency of improving both our knowledge of the fundamental mechanisms regulating breast cancer cell invasion/metastases and the discovery of additional prognostic markers. Such progress could eventually enhance the pathological complete response (pCR) by a patient-tailored treatment and individualized follow-up.

In this context, we have previously uncovered the anti-invasive role of NFAT3 in luminal breast cancer (4) and shown that extracellular vesicles (EVs) produced by NFAT3-expressing luminal breast cancer cells were competent to prevent tumor growth and restrain metastases spreading in a murine triple- negative breast cancer model (7). Regarding the expression and function of NFAT isotypes in breast cancer, we have highlighted that NFAT3 and NFAT1 had absolutely opposed effects on breast cancer cell invasion, NFAT3 being anti-invasive and NFAT1 pro-invasive (3–6). These last observations were puzzling since NFAT3 and NFAT1 are highly homologous in terms of amino acid sequence.

In the present study, we aimed to understand the structural requirements for NFAT3 to impede breast cancer cell invasion. Therefore, we focused our attention on the N- and C-terminal sequences of NFAT1 and NFAT3 that had isotype specificity (**Figure 1A**) and identified a specific region of 85 amino acids, in the C-terminal part of NFAT3, required for the inhibition of cell invasion of the human luminal breast cancer cell line T-47D. Numerous studies have shown that the NFAT factors interact with multiple cofactors to modulate their functions (8–11, 18–26). Indeed, because of the dominant negative effect of the last 85 amino acid C-terminal of NFAT3 on the invasive capacity of this luminal breast cancer cell line, we hypothesized co-factor binding to this specific region to inhibit cell invasion and revealed its association with RERG. We confirmed that this NFAT3/RERG complex, *via* the NFAT3-Cter region, was functional and necessary for NFAT3 to impede invasion in the human luminal T-47D breast cancer cell line. Future studies will reveal whether this is also the case in other luminal breast cancer cell lines than T-47D. RERG is a growth-inhibitory gene highly expressed in luminal breast cancer (12) and is associated with the longest survival of luminal breast cancer patients (13) without metastases. Some studies have reported that RERG is an inhibitor of the MAPK/ERK pathway (15), a pathway implicated in breast cancer cell migration (27, 28). However, further investigations are required to study the potential role of the ERK pathway in the anti-invasive effect of NFAT3.

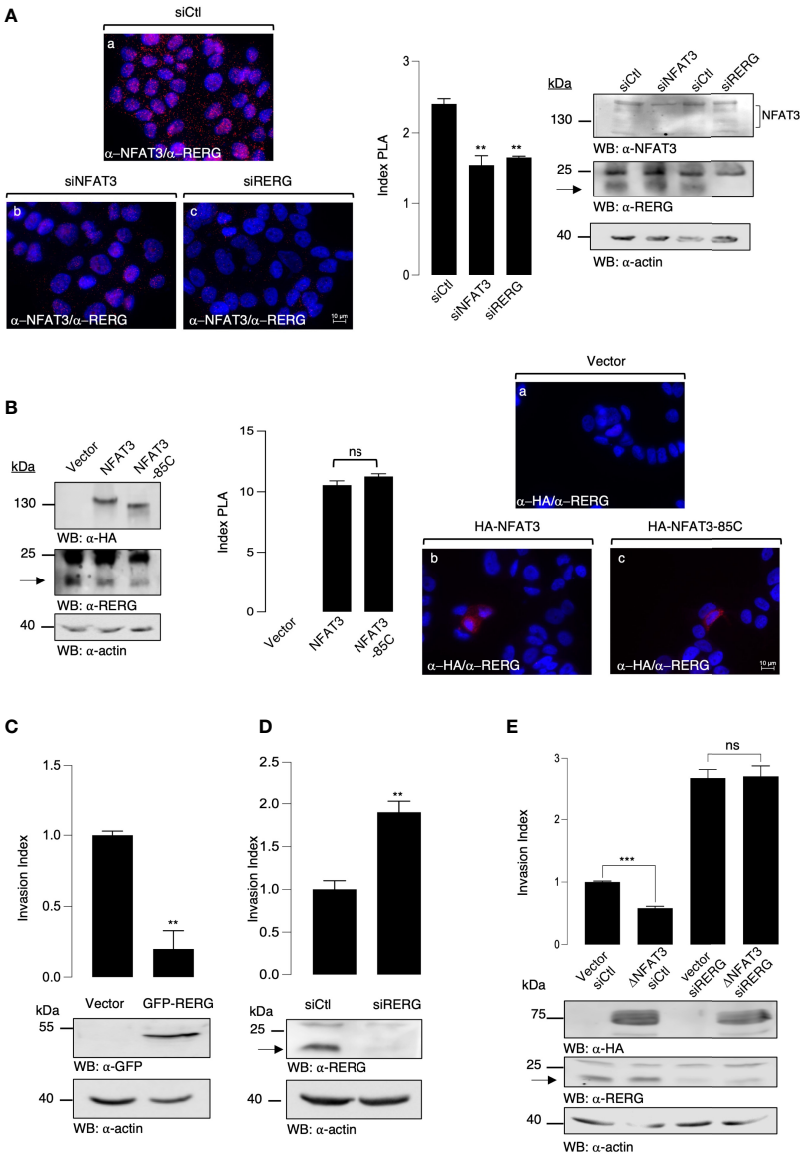

FIGURE 3 | NFAT3 is associated with RERG in T-47D cells to suppress breast cancer cell invasion. **(A)** T-47D cells were grown on coverslips and transfected with either an siRNA control (siCtl), a siRNA targeting the endogenous NFAT3 (siNFAT3), or the endogenous RERG (siRERG). Approximately 48 h after transfection PLA assays were performed on the transfected cells with the anti-NFAT3 and the anti-RERG (α-NFAT3/α-RERG) (a-c). Index of PLA was obtained by analyzing ten random fields for each condition, all data are shown as the mean of three independent experiments ± SEM (n=3 biological replicates; 3 technical replicates for each experiment; **p<0.005, ***p<0,001, ns, nonspecific). Whole cell lysates were revealed by α-NFAT3 and α-RERG and normalized by comparison with an α-actin. **(B)** T-47D cells were grown on coverslips and transfected with either the empty vector or a vector encoding the HA epitope fused to either NFAT3 or NFAT3-85C. Approximately 24 h after transfection, PLA assays were performed on the transfected cells with the α-HA and α-RERG (a-c). Index of PLA was obtained by analyzing fifteen random fields for each condition; all data are shown as the mean of three independent experiments ± SEM (n=3 biological replicates; 10 random fields for each condition; ns = non-specific). Whole cell lysates were revealed by α-HA and α-RERG and normalized by revelation with an α-actin. **(C)** T-47D cells were transiently transfected with either a vector encoding the GFP protein fused to RERG or with the empty vector (Vector). The following day, transfected cells were subjected to an *in vitro* invasion assay for 24 h. Data are shown as the mean of three independent experiments ± SEM (n=3 biological replicates; 3 technical replicates for each experiment; ***p<0.001). Whole cell lysates were revealed by α-GFP and normalized by revelation with α-actin. **(D)** T-47D cells were transiently transfected with either an siRNA control (siCtl) or an siRNA targeting the endogenous RERG (siRERG). Approximately 48 h after the transfected cells were subjected to an *in vitro* invasion assay for 24 h, all data are shown as the mean of three independent experiments ± SEM (n=3 biological replicates; 3 technical replicates for each experiment; ***p<0.001, ns, non-specific). Whole cell lysates were revealed by α-RERG and normalized by revelation with α-actin. **(E)** T-47D cells were transiently co-transfected with either an siRNA control (siCtl) or an siRNA targeting the endogenous RERG (siRERG) in combination with either a vector encoding the HA epitope fused to ΔNFAT3 or with the empty vector (Vector). Approximately 48 h later, the transfected cells were subjected to an *in vitro* invasion assay for 24 h. Data are shown as the mean of three independent experiments ± SEM (n=3 biological replicates; 3 technical replicates for each experiment; ***p<0.001, ns, non-specific). Whole cell lysates were revealed by α-HA and α-RERG and normalized by revelation with α-actin.

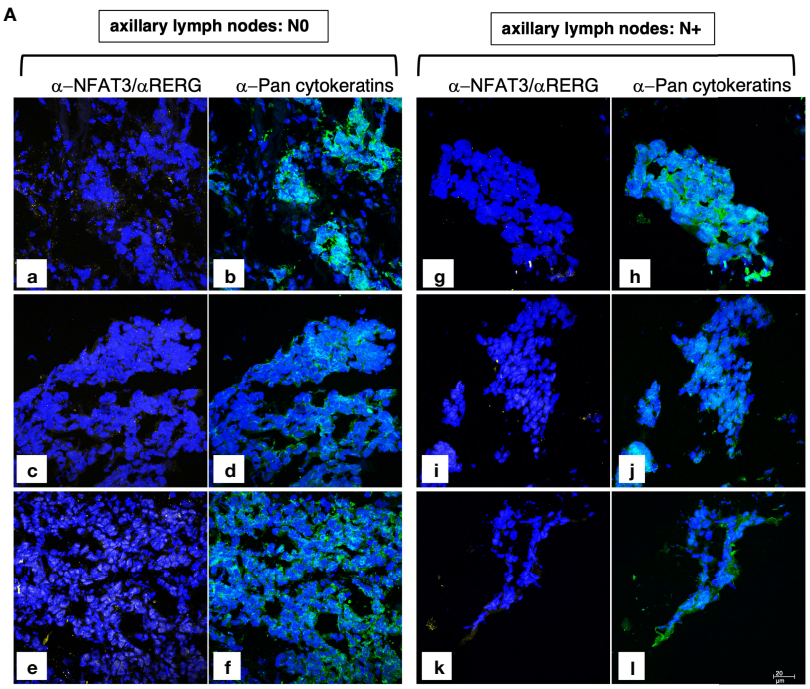

B

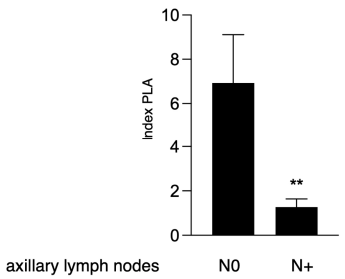

C

Characteristics of the population

Characteristics	Patients (%)
Total	21
Age at diagnosis (year)	
- Mean	62
- Range	(47-78)
% ER (IHC staining, positive if >10%)	
- Mean	95
- Range	50-100
% PR	
- Mean	80
- Range	10-100
% Ki67	
- Mean	26
- Range	4-70
Histological grade	
- 1	2 (9.5)
- 2	11 (52.4)
- 3	8 (38.1)
Her2	
- 0	19 (90.5)
- 1+	1 (4.75)
- 3+	1 (4.75)
Axillary lymph nodes metastases	
- No	11 (52.4)
- Yes	10 (47.6)

FIGURE 4 | NFAT3/RERG interaction is increased in luminal breast cancer tissues and is correlated with the absence of ALN colonization. **(A)** Frozen luminal breast cancer sections from patients who developed ALN colonization (N+; a-f) or not (N0; g-l) were incubated with α-NFAT3 and α-RERG followed by PLA assays (yellow dots) and labeling with α-pan cytokeratin coupled to FITC. Data from 6 representative patient slides out of 21 are shown. **(B)** Index of PLA was obtained by analyzing 2 random fields for the 21 slides; data are shown as mean ± SEM (**p<0,005). **(C)** Characteristics of the patients used for microscopy.

Importantly, we validated the association of NFAT3 with RERG in luminal breast cancer tissues from patients and disclosed that a higher amount of this complex, in the primary tumor, was observed in patients lacking axillary lymph node colonization. Axillary lymph node colonization remains a strong prognostic factor for predicting prognosis in breast cancer patients (29, 30). Thus, our study suggests that detection of NFAT3/RERG complex in the primary tumor could be a new prognostic marker of the absence of ALN colonization. Further studies with a larger cohort of patients will be necessary to definitively confirm the potential use of the NFAT3/RERG association as a valuable non-invasive indicator of the ALN status.

DATA AVAILABILITY STATEMENT

The original contributions presented in the study are included in the article/**Supplementary Material** Further inquiries can be directed to the corresponding author.

ETHICS STATEMENT

The studies involving human participants were reviewed and approved by Ethics Committee of Saint Louis Hospital, Ethics Committee of the Godinot Institute. The patients/participants provided their written informed consent to participate in this study.

AUTHOR CONTRIBUTIONS

SJ and LC contributed to conception and design of the study. SJ, LC, FG, and MR performed the experiments. AB organized the access for the breast cancer tissues. EB and CG provided the breast cancer tissues. SJ wrote the first draft of the manuscript. LC, ML, JL, and MR wrote sections of the manuscript. All authors contributed to manuscript revision, read, and approved the submitted version.

FUNDING

Fondation ARC pour la Recherche sur le Cancer: PJA 20131200039 and Groupements des Entreprises Française dans la lutte contre le Cancer (GEFLUC).

ACKNOWLEDGMENTS

We thank Nuala Mooney for checking the English. We thank the IRSL Technology Platform for their technical assistance. This work was supported by Gefluc and ARC Foundation grants.

SUPPLEMENTARY MATERIAL

The Supplementary Material for this article can be found online at: https://www.frontiersin.org/articles/10.3389/fonc.2022.804868/full#supplementary-material

REFERENCES

1. Guedj M, Marisa L, de A, Reynies, Orsetti B, Schiappa R, et al. A Refined Molecular Taxonomy of Breast Cancer. *Oncogene* (2012) 31:1196–206. doi: 10.1038/onc.2011.301
2. Maaren MC, Munck L, Strobbe LJA, Sonke GS, Westenend PJ, Smidt ML, et al. Ten-Year Recurrence Rates for Breast Cancer Subtypes in the Netherlands: A Large Population-Based Study. *Int J Cancer* (2019) 144:263–72. doi: 10.1002/ijc.31914
3. Jauliac S, López-Rodriguez C, Shaw LM, Brown LF, Rao A, Toker A. The Role of NFAT Transcription Factors in Integrin-Mediated Carcinoma Invasion. *Nat Cell Biol* (2002) 4:540–4. doi: 10.1038/ncb816
4. Fougère M, Gaudineau B, Barbier J, Guaddachi F, Feugeas J-P, Auboeuf D, et al. NFAT3 Transcription Factor Inhibits Breast Cancer Cell Motility by Targeting the Lipocalin 2 Gene. *Oncogene* (2010) 29. doi: 10.1038/onc.2009.499
5. Gaudineau B, Fougère M, Guaddachi F, Lemoine F, de la Grange P, Jauliac S. Lipocalin 2, the TNF-Like Receptor TWEAKR and its Ligand TWEAK Act Downstream of NFAT1 to Regulate Breast Cancer Cell Invasion. *J Cell Sci* (2012) 125:4475–86. doi: 10.1242/jcs.099879
6. Yoeli-Lerner M, Yiu GK, Rabinovitz I, Erhardt P, Jauliac S, Toker A. Akt Blocks Breast Cancer Cell Motility and Invasion Through the Transcription Factor NFAT. *Mol Cell* (2005) 20. doi: 10.1016/j.molcel.2005.10.033
7. de Camargo LCB, Guaddachi F, Bergerat D, Ourari N, Coillard L, Parietti V, et al. Extracellular Vesicles Produced by NFAT3-Expressing Cells Hinder Tumor Growth and Metastatic Dissemination. *Sci Rep* (2020) 10:8964. doi: 10.1038/s41598-020-65844-x
8. Bodor J, Bodorova J, Gress RE. Suppression of T Cell Function: A Potential Role for Transcriptional Repressor ICER. *J Leukocyte Biol* (2000) 67:774–9. doi: 10.1002/jlb.67.6.774
9. Avni O, Lee D, Macian F, Szabo SJ, Glimcher LH, Rao A. TH Cell Differentiation Is Accompanied by Dynamic Changes in Histone Acetylation of Cytokine Genes. *Nat Immunol* (2002) 3:643–51. doi: 10.1038/ni808
10. Wu Y, Borde M, Heissmeyer V, Feuerer M, Lapan AD, Stroud JC, et al. FOXP3 Controls Regulatory T Cell Function Through Cooperation With NFAT. *Cell* (2006) 126:375–87. doi: 10.1016/j.cell.2006.05.042
11. Molkentin JD, Lu J-R, Antos CL, Markham B, Richardson J, Robbins J, et al. Olson En. *A Calcineurin-Dependent Transcriptional Pathway Cardiac Hypertrophy Cell* (1998) 93:215–28. doi: 10.1016/s0092-8674(00)81573-1
12. Finlin BS, Gau C-L, Murphy GA, Shao H, Kimel T, Seitz RS, et al. RERG Is a Novel Ras-Related, Estrogen-Regulated and Growth-Inhibitory Gene in Breast Cancer. *J Biol Chem* (2001) 276:42259–67. doi: 10.1074/jbc.m105888200
13. Habashy HO, Powe DG, Glaab E, Ball G, Spiteri I, Krasnogor N, et al. RERG (Ras-Like, Oestrogen-Regulated, Growth-Inhibitor) Expression in Breast Cancer: A Marker of ER-Positive Luminal-Like Subtype. *Breast Cancer Res Tr* (2011) 128:315–26. doi: 10.1007/s10549-010-1073-y
14. Ding Z, Liang J, Lu Y, Yu Q, Songyang Z, Lin S-Y, et al. A Retrovirus-Based Protein Complementation Assay Screen Reveals Functional AKT1-Binding Partners. *Proc Natl Acad Sci* (2006) 103:15014–9. doi: 10.1073/pnas.0606917103
15. Zhao W, Ma N, Wang S, Mo Y, Zhang Z, Huang G, et al. RERG Suppresses Cell Proliferation, Migration and Angiogenesis Through ERK/NF-κb Signaling Pathway in Nasopharyngeal Carcinoma. *J Exp Clin Canc Res* (2017) 36:88. doi: 10.1186/s13046-017-0554-9
16. Ho J-Y, Hsu R-J, Liu J-M, Chen S-C, Liao G-S, Gao H-W, et al. MicroRNA-382-5p Aggravates Breast Cancer Progression by Regulating the RERG/Ras/ERK Signaling Axis. *Oncotarget* (2017) 8:22443–59. doi: 10.18632/oncotarget.12338
17. Huang L, Tang X, Shi X, Su L. miR-532-5p Promotes Breast Cancer Proliferation and Migration by Targeting RERG. *Exp Ther Med* (2019) 19:400–8. doi: 10.3892/etm.2019.8186
18. Macián F, López-Rodríguez C, Rao A. Partners in Transcription: NFAT and AP-1. *Oncogene* (2001) 20:2476–89. doi: 10.1038/sj.onc.1204386
19. Ho I-C, Hodge MR, Rooney JW, Glimcher LH. The Proto-Oncogene C-Maf Is Responsible for Tissue-Specific Expression of Interleukin-4. *Cell* (1996) 85:973–83. doi: 10.1016/s0092-8674(00)81299-4
20. Bert AG, Burrows J, Hawwari A, Vadas MA, Cockerill PN. Reconstitution of T Cell-Specific Transcription Directed by Composite NFAT/Oct Elements. *J Immunol* (2000) 165:5646–55. doi: 10.4049/jimmunol.165.10.5646
21. Hodge MR, Chun HJ, Rengarajan J, Alt A, Lieberson R, Glimcher LH. NF-AT-Driven Interleukin-4 Transcription Potentiated by NIP45. *Science* (1996) 274:1903–5. doi: 10.1126/science.274.5294.1903
22. Rengarajan J, Mowen KA, McBride KD, Smith ED, Singh H, Glimcher LH. Interferon Regulatory Factor 4 (IRF4) Interacts With NFATc2 to Modulate Interleukin 4 Gene Expression. *J Exp Med* (2002) 195:1003–12. doi: 10.1084/jem.20011128
23. Carneiro FRG, Ramalho-Oliveira R, Mognol GP, Viola JPB. Interferon Regulatory Factor 2 Binding Protein 2 Is a New NFAT1 Partner and Represses Its Transcriptional Activity. *Mol Cell Biol* (2011) 31:2889–901. doi: 10.1128/mcb.00974-10
24. Decker EL, Skerka C, Zipfel PF. The Early Growth Response Protein (EGR-1) Regulates Interleukin-2 Transcription by Synergistic Interaction With the Nuclear Factor of Activated T Cells. *J Biol Chem* (1998) 273:26923–30. doi: 10.1074/jbc.273.41.26923

25. Yang XY, Wang LH, Chen T, Hodge DR, Resau JH, DaSilva L, et al. Activation of Human T Lymphocytes Is Inhibited by Peroxisome Proliferator-Activated Receptor γ (Pparγ) Agonists Pparγ Co-Association With Transcription Factor NFAT. *J Biol Chem* (2000) 275:4541–4. doi: 10.1074/jbc.275.7.4541
26. Musarò A, McCullagh KJA, Naya FJ, Olson EN, Rosenthal N. IGF-1 Induces Skeletal Myocyte Hypertrophy Through Calcineurin in Association With GATA-2 and NF-Atc1. *Nature* (1999) 400:581–5. doi: 10.1038/23060
27. Krueger JS, Keshamouni VG, Atanaskova N, Reddy KB. Temporal and Quantitative Regulation of Mitogen-Activated Protein Kinase (MAPK) Modulates Cell Motility and Invasion. *Oncogene* (2001) 20:4209–18. doi: 10.1038/sj.onc.1204541
28. Irie HY, Pearline RV, Grueneberg D, Hsia M, Ravichandran P, Kothari N, et al. Distinct Roles of Akt1 and Akt2 in Regulating Cell Migration and Epithelial–Mesenchymal Transition. *J Cell Biol* (2005) 171:1023–34. doi: 10.1083/jcb.200505087
29. Michaelson JS, Silverstein M, Sgroi D, Cheongsiatmoy JA, Taghian A, Powell S, et al. The Effect of Tumor Size and Lymph Node Status on Breast Carcinoma Lethality. *Cancer* (2003) 98:2133–43. doi: 10.1002/cncr.11765
30. de Boer M, van Dijck JAAM, Bult P, Borm GF, Tjan-Heijnen VCG. Breast Cancer Prognosis and Occult Lymph Node Metastases, Isolated Tumor Cells, and Micrometastases. *Jnci J Natl Cancer Inst* (2010) 102:410–25. doi: 10.1093/jnci/djq008

Conflict of Interest: *The authors declare that the research was conducted in the absence of any commercial or financial relationships that could be construed as a potential conflict of interest.*

Publisher's Note: All claims expressed in this article are solely those of the authors and do not necessarily represent those of their affiliated organizations, or those of the publisher, the editors and the reviewers. Any product that may be evaluated in this article, or claim that may be made by its manufacturer, is not guaranteed or endorsed by the publisher.

frontiers | Frontiers in Oncology

TYPE Correction
PUBLISHED 30 August 2022
DOI 10.3389/fonc.2022.1016189

OPEN ACCESS

APPROVED BY
Frontiers Editorial Office, Frontiers Media SA, Switzerland

*CORRESPONDENCE
Sébastien Jauliac
sebastien.jauliac@inserm.fr

SPECIALTY SECTION
This article was submitted to Breast Cancer, a section of the journal Frontiers in Oncology

RECEIVED 11 August 2022
ACCEPTED 12 August 2022
PUBLISHED 30 August 2022

CITATION
Coillard L, Guaddachi F, Ralu M, Brabencova E, Garbar C, Bensussan A, Le Bras M, Lehmann-Che J and Jauliac S (2022) Corrigendum: The NFAT3/RERG complex in luminal breast cancers is required to inhibit cell invasion and may be correlated with an absence of axillary lymph nodes colonization.
Front. Oncol. 12:1016189.
doi: 10.3389/fonc.2022.1016189

Corrigendum: The NFAT3/RERG complex in luminal breast cancers is required to inhibit cell invasion and may be correlated with an absence of axillary lymph nodes colonization

Lucie Coillard[1], Frédéric Guaddachi[1], Maëlle Ralu[1], Eva Brabencova[2], Christian Garbar[2], Armand Bensussan[1], Morgane Le Bras[1], Jacqueline Lehmann-Che[1,3] and Sébastien Jauliac[1]*

[1]Université de Paris, Research Saint Louis Institute (IRSL), Institut National de la Santé et de la Recherche Médicale, Human Immunology Pathophysiology Immunotherapy (INSERM HIPI) U976, Paris, France, [2]Department of Biopathology, Centre Régional de Lutte Contre le Cancer, Institut Godinot, Reims, France, [3]Molecular Oncology Unit, Assistance Publique-Hôpitaux de Paris (AP-HP), Hôpital Saint Louis, Paris, France

KEYWORDS

breast cancer, NFAT3/c4, RERG, invasion, lymph nodes metastasis

A Corrigendum on

The NFAT3/RERG complex in luminal breast cancers is required to inhibit cell invasion and may be correlated with an absence of axillary lymph nodes colonization

by Coillard L, Guaddachi F, Ralu M, Brabencova E, Garbar C, Bensussan A, Le Bras M, Lehmann-Che J and Jauliac S (2022). *Front. Oncol.* 12:804868. doi: 10.3389/fonc.2022.804868

In the published article, there was an error in the abstract. NFAT3/REG should be replaced by NFAT3/RERG.

A correction has been made to **Abstract**. The corrected sentence appears below:

"We have shown an increase of the quantity of the NFAT3/RERG complexes in patients without axillary lymph node colonization and therefore proposed that the detection of this complex may be a non-invasive marker of axillary lymph node colonization."

The authors apologize for this error and state that this does not change the scientific conclusions of the article in any way. The original article has been updated.

Publisher's note

Advantages of publishing in Frontiers

OPEN ACCESS
Articles are free to read for greatest visibility and readership

FAST PUBLICATION
Around 90 days from submission to decision

HIGH QUALITY PEER-REVIEW
Rigorous, collaborative, and constructive peer-review

TRANSPARENT PEER-REVIEW
Editors and reviewers acknowledged by name on published articles

Frontiers
Avenue du Tribunal-Fédéral 34
1005 Lausanne | Switzerland

Visit us: www.frontiersin.org
Contact us: frontiersin.org/about/contact

REPRODUCIBILITY OF RESEARCH
Support open data and methods to enhance research reproducibility

DIGITAL PUBLISHING
Articles designed for optimal readership across devices

FOLLOW US
@frontiersin

IMPACT METRICS
Advanced article metrics track visibility across digital media

EXTENSIVE PROMOTION
Marketing and promotion of impactful research

LOOP RESEARCH NETWORK
Our network increases your article's readership